

PROBING NEW PHYSICS IN WEAK DECAYS
AND
FLAVOUR-CHANGING PROCESSES

A Thesis

Submitted to the
Tata Institute of Fundamental Research, Mumbai
for the degree of Doctor of Philosophy
in Physics

by
Debjyoti Bardhan

DEPARTMENT OF THEORETICAL PHYSICS
TATA INSTITUTE OF FUNDAMENTAL RESEARCH
MUMBAI
August 2017

DECLARATION

This thesis is a presentation of my original research work. Wherever contributions of others are involved, every effort is made to indicate this clearly, with due reference to the literature, and acknowledgement of collaborative research and discussions. The work was done under the guidance of Professor Sreerup Raychaudhuri, at the Tata Institute of Fundamental Research, Mumbai.


[Debjyoti Bardhan]

In my capacity as supervisor of the candidate's thesis, I certify that the above statements are true to the best of my knowledge.


[Sreerup Raychaudhuri]

Date: 10.08.2017

*To the bravest person I've ever known,
my mother ...*

ACKNOWLEDGEMENTS

It is my utmost pleasure to express my deepest gratitude to my PhD advisor Prof. Sreerup Raychaudhuri, who has patiently and kindly guided my course through the graduate years. He has offered me advice both on academic and non-academic matters.

The person whom I am most indebted to is my mother, the person behind every little bit of my achievements. I have witnessed her struggle through the years, all the while making sure that I got the best of everything. It is impossible, with the extent of my lexicon at any rate, to express the respect and thankfulness that I wish to express towards her.

My sincere thanks must go to my senior and collaborator Dr. Diptimoy Ghosh. Although for most of my graduate years in TIFR, he was abroad for his postdoctoral studies, our collaboration, online via remote voice and video chat services like Skype, has been a great learning experience for me. In the same breath, I have to mention Dr. Pritibhajan Byakti, another collaborator of mine. Both have been constant sources of good conversation on a variety of topics and reliable providers of important advice. It has been a privilege working with such kind and knowledgeable seniors. Apart from them, I am also fortunate enough to collaborate with Dr. Amit Chakraborty who introduced me to the newest techniques in collider physics. Collaboration with Dr. Monalisa Patra was also a learning experience for me. I wish to also thank Dr. Sabyasachi Chakraborty for all the wonderful discussions, several of which have been over a glass of tea.

No period of stay in TIFR, my alma mater, could be completely described without mentioning several faculty members with whom one is bound to develop deep and intricate bonds through a variety of ways. I have thoroughly enjoyed the courses offered by Prof. Shiraz Minwalla, Prof. Amol Dighe, Prof. Mustansir Barma, Prof. Mandar Deshmukh, Prof. Sunil Mukhi, Prof. Rajeev Bhalerao, Prof. H.M Antia, Prof. Deepak Dhar, Prof. Gautam Mandal and Prof. Sreerup Raychaudhuri. I feel privileged to have interacted with each and many more for extended lengths of time. Special mention must be made of Prof. Sourendu Gupta, Prof. Rajeev Gavai, Dr. Tuhin Roy, Dr. Basudeb Dasgupta and Dr. Tridib Sadhu. Although I have never attended a course by them, I have gained immensely from conversations.

The department would be adrift if it were not for the wonderful people working at the department office and handling the computer network. The office is smoothly manned by Mr. Raju Bathija, Mr. Rajendra Pawar, Mr. Mohan Shinde, Mr. Aniket Surve and Mr. Girish Ogale, who have often taken the burden of the paperwork off my shoulders and onto their own. As for the computer section in the department, no amount of praise can suffice for Mr. Ajay Salve and Mr. Kapil Ghadiali. They are absolute stalwarts in their work and I have greatly benefitted from their expertise.

I am also extremely lucky to have had wonderful seniors, with whom I have had such beautiful memories. There are too many to name, but I can readily recall a few. A very dear senior was Dr. Sayan Chakraborti, who was brilliant enough to get into Harvard as a Fellow and courageous enough to leave the field of astronomy when he stopped enjoying it. I can similarly

name Dr. Shamashis Sengupta, who piqued my interest in a variety of things, right from photography to movies. I cannot possibly miss mentioning Dr. Nilay Kundu, who was the protective elder brother for me here. I can similarly mention Dr. Umesh Vijayshankar, Dr. Naveen Yadav, Dr. Kabir Ramola, Dr. Padmanaath Nair, Dr. Sambudhha Sanyal, Dr. Prithvi Narayan, Dr. Jyotirmoy Bhattacharyya, Dr. Nikhil Karthik, Dr. Sachin Jain and Dr. Swastik Bhattacharyya. Special mention must be made of Dr. Sayantan Sharma, Dr. Sanmay Ganguly and Dr. Gouranga Kole, all very dear seniors to me.

The years in TIFR have been kind to allow me to foster several lasting friendships. I count among them a close group of friends comprising Nairit, Soureek, Atreyee, Khadiza, Ritam, Subhodeep, Rickmoy and Chitrak. We often wonder how fortunate we have been to find oddballs as our individual selves all huddled up under a single roof. Besides other things, I have to thank Nairit for getting me interested in photography, which has become a primary hobby of mine. I must make special mention of Parul Tomar, with whom I became very good friends quite fast and in unlikely ways. It is not often that one is as sure of anything in life as the fact that these friendships will last for a lifetime.

I must mention Priti Gupta, Subhrangshu Sarkar, Ram Dewanjee, Aritra Biswas, Jayita Lahiri, Abhirup Ghosh and Krishnendu Gope among my contemporaries with whom I have had lots of fond memories. From among my juniors, I wish to name Sarbajaya, Ashish, Sarath, Manibrata, Tousik, Disha, Anirban, Chandroday, Indranil, Abhisek, Sounak, Sumeru, Ahana, Yogesh, Sayani, Anupama and Sarath for the same. An exhaustive list is too long to provide, so I will just curtail it here.

One of the most important activities I was involved in in TIFR was science popularization and outreach. Huge thanks must go to Prof. Arnab Bhattacharya and Mr. Surendra Kulkarni for deeming me fit to be a part of the committee. We have had plenty of collaborative projects, all in an effort to take science to the masses, both within Mumbai and outside it. I will cherish the experiences and the memories. In the course, I have met wonderful people and gotten to know acquaintances better. In this regard, I would like to express my gratitude to Kiran Pavaskar, whom I count as one of my closest friends and a close confidant, who, being in theatre arts, has introduced me to the wonderful world of performing arts. I would also like to mention Anusheela Chatterjee and Vidur Sabharwal, with whom I have collaborated on several Outreach programs, a collaboration which has been absolutely joyful.

This acknowledgement would be incomplete without the mention of a few people who have always backed my decisions in the past, constantly standing by me through thick and thin. In this regard, my deepest respect and gratitude to Mrs. Suparna Majumdar, Mrs. Sabari Paul and Dr. Subhro Chatterjee, all teachers in school who have showered me with a lot of affection and have been constant sources of encouragement.

Finally, I would like to thank all those whose jobs have made my stay in TIFR an absolute pleasure. Physics Subject Board secretary, Mr. Girish Ogale, and the staff of the University Cell, especially Ms. Alka Bhoir and Ms. Bindu Jose have ensured that all my official documents stayed in order. Right from the kind people in the medical and the travel section, to

central office staff, people managing the security, those in the library and the photography department, those in charge of the hostels and canteen, and those who have always helped me with finances, they are the ones who keep the cogs of the institute turning, without any fanfare.

Contents

1	The Standard Model	1
1.1	Introduction	1
1.2	Gauge Symmetries in the Standard Model	2
1.2.1	The Gauge Principle	2
1.2.2	Abelian Symmetry : QED	2
1.2.3	Non-Abelian Symmetry : QCD	4
1.2.4	Electroweak Symmetry	6
1.3	Electroweak Symmetry-Breaking	8
1.3.1	Gauge Boson Masses	8
1.3.2	The Higgs Mechanism	11
1.4	Construction of the Standard Model	12
1.4.1	Gauge interactions of fermions	12
1.4.2	Chiral Fermions	13
1.4.3	Fermion Masses	15
1.4.4	Flavour Mixing	16
1.4.5	Absence of FCNCs	17
1.4.6	CP Violation	18
1.4.7	Global Symmetries in the SM	19
1.5	Flavour Changing Processes in the SM Quark Sector	20
2	Beyond the Standard Model	23
2.1	New Physics beyond the Standard Model	23
2.2	Shortcomings of the Standard Model	23
2.2.1	Problems in the Classical Structure of the SM	24
2.2.2	Standard Model as a Quantum Field Theory	29
2.2.3	Phenomenological Problems	33
2.3	Beyond Standard Model Physics	43
2.3.1	Hierarchy Problem	43
2.3.2	Parity Violation	48
2.3.3	Spontaneous CP Violation	50

2.3.4	Strong CP Problem and Peccei-Quinn symmetry	50
2.3.5	Fermion Mass Models	52
2.3.6	Neutrino Masses	53
2.4	Grand Unified Theories	53
2.5	Supersymmetry	57
2.5.1	SUSY breaking	58
2.5.2	The Higgs Sector in the MSSM:	61
2.5.3	Mixing between SUSY particles	62
2.5.4	R-parity and its violation	64
2.5.5	Decay of SUSY particles	64
3	Flavour-changing Decays of Top Quarks	67
3.1	Introduction : FCNC portal to new physics	67
3.2	Generic FCNC Decays of the top quark in a toy model	71
3.3	FCNC decays of the top quark in the SM	77
3.4	FCNC decays of the top quark in the cMSSM	78
3.5	Beyond the MFV paradigm : R-parity violation	84
3.6	Summary and Conclusions	89
4	A closer look at the R_D and R_{D^*} anomalies	93
4.1	Introduction	93
4.2	Operator basis	95
4.3	Observables	97
4.4	$\bar{B} \rightarrow D$ form factors	98
4.5	$\bar{B} \rightarrow D^*$ form factors	101
4.6	Expressions for a_ℓ^D , b_ℓ^D and c_ℓ^D for $\bar{B} \rightarrow D\ell\bar{\nu}_\ell$	102
4.7	Expressions for $a_\ell^{D^*}$, $b_\ell^{D^*}$ and $c_\ell^{D^*}$ for $\bar{B} \rightarrow D^*\ell\bar{\nu}_\ell$	104
4.8	Results	105
4.8.1	Explaining R_D alone	105
4.8.2	Explaining R_{D^*} alone	108
4.8.3	Explaining R_D and R_{D^*} together	110
4.9	Summary	112
5	Bottom squarks in B-number violating MSSM	113
5.1	Introduction	113
5.2	The R-parity violating MSSM	114
5.3	The Simplified Model Spectrum and Simulation	116
5.4	Leptonic Final State	119
5.4.1	Cut-based Analysis	119
5.4.2	Multivariate Analysis	122
5.5	The Hadronic Final State	126
5.5.1	Multivariate Analysis	128
5.5.2	Results	131

5.6	Summary and Outlook	133
6	The Sgoldstino as a 750 GeV diphoton resonance	137
6.1	Introduction	137
6.2	Generalities	139
6.2.1	Theoretical framework	139
6.2.2	Explaining the excess	141
6.3	Ordinary gauge mediation	141
6.3.1	Possibility of larger λ	145
6.3.2	Estimate of the mass of \mathcal{S}	146
6.4	Extra Ordinary Gauge Mediation	147
6.5	Way out?	149
6.5.1	D -term contribution to the gaugino mass	149
6.5.2	Metastable SUSY breaking	150
6.5.3	Quark anti-quark initiated production of the sgoldstino	152
6.6	Conclusion	154
7	Conclusion	157
A	FCNC Processes in the SM: CP Violation	161
A.1	CKM Matrix and Unitarity Triangles	161
A.2	Oscillations of Neutral Mesons: Formalism	164
A.3	Measuring CP Violation: Formalism	164
A.4	Measuring CP violation in Mesons	167
B	FCNC Decays of the Top Quark	171
B.1	Toy model amplitudes	171
B.1.1	The decay $t \rightarrow c + H$	171
B.1.2	The decay $t \rightarrow c + Z$	173
B.2	SM and cMSSM amplitudes	175
B.2.1	The decay $t \rightarrow c + H$	175
B.2.2	The decay $t \rightarrow c + Z$	180
B.3	RPV-MSSM amplitudes	185
B.3.1	The decay $t \rightarrow c + H$	185
B.3.2	The decay $t \rightarrow c + Z$	186
C	The R_D and R_{D^*} Anomalies	189
C.1	Full expressions for a_ℓ^D , b_ℓ^D and c_ℓ^D	189
C.2	Full expressions for $a_\ell^{D^*}$, $b_\ell^{D^*}$ and $c_\ell^{D^*}$	190
C.3	Contribution of the Tensor operator $\mathcal{O}_{\text{TL}}^{cbl}$	194
C.3.1	$\bar{B} \rightarrow D\tau\bar{\nu}_\tau$	194
C.3.2	$\bar{B} \rightarrow D^*\tau\bar{\nu}_\tau$	194
C.4	$\text{SU}(3)_C \times \text{SU}(2)_L \times \text{U}(1)_Y$ gauge invariance	196

C.5	RG Running of Wilson Coefficients	196
D	The Sgoldstino as a 750 GeV candidate	201
D.1	Calculation of the partial decay widths	201
D.1.1	$\phi \rightarrow \gamma\gamma$	201
D.1.2	$a \rightarrow \gamma\gamma$	202
D.1.3	$\phi \rightarrow ZZ$	203
D.1.4	$a \rightarrow ZZ$	204
D.2	Calculation of $\mathcal{A}_{\text{LHC energy}}^{ii}$	205
D.2.1	Production by gluon fusion	205
D.2.2	Production by quarks	206
D.3	Calculation of the sgoldstino mass	207
D.3.1	Diagrammatic calculation	208
D.3.2	Coleman-Weinberg potential	210
D.3.3	Tree level sgoldstino mass	211
D.4	Calculation of the gaugino mass	212
	Bibliography	215

Synopsis

Introduction

The Standard Model (SM) of strong and electroweak interactions, despite its great success in explaining experimental data, is known to have many shortcomings as a final theory, and it is widely expected that discovery of New Physics (NP) beyond the SM is around the corner. However, we do not have a clear idea where the NP may be expected to show up. It is, therefore, necessary at this stage to investigate all possibilities in order to be prepared if and/or when the NP is actually found. This thesis investigates some signals which are not expected in the SM, but are predicted in NP models. Most of these signals are small effects which require more running of the LHC and similar machines before an observable effect can be expected.

This synopsis of the thesis work is organised as follows.

1. Flavour Changing Neutral Current (FCNC) Decays of the Top Quark, as a probe of NP in high energy collider machines;
2. A closer look at the deviations from the SM predictions in the measured values of R_D and R_{D^*} , and their possible explanations in a model-independent fashion;
3. Predictions for LHC searches for an sbottom LSP in a model with R-parity-violating supersymmetry (SUSY);
4. Investigating the sgoldstino as a possible candidate for the (now defunct) diphoton excess reported at the LHC in December 2015, showing that it was unlikely to have been a correct explanation.

The thesis will be organised to contain a brief review of the motivation and major ideas for NP, and then to elaborate on the above ideas in the successive chapters.

FCNC Decays of the Top Quark

The top quark is the heaviest fundamental particle discovered and, unlike other quarks in the SM, it decays before hadronising. Since low energy QCD effects can be neglected for the top quark to a high degree of accuracy, the decay is essentially an electroweak process.

The top quark decays into a b -quark and a W -boson most of the time, but very rarely also decays into an up-type quark, like a c or a u -quark, associated with a neutral boson like a Z or a Higgs boson. These rare decay modes have very small SM branching ratios (BRs) ($\sim 10^{-15}$) and are far beyond the detection capabilities of the LHC, which can optimistically probe a maximum BR of 10^{-5} . We can study the different methods of suppression because of which the BR in the SM is so small; conversely, we can think about a scenario by which the BR can be enhanced. An enhanced BR can be detected at the LHC easily because the tiny SM BR won't affect the signal.

In Ref. [1], we discuss the different mechanisms of suppression that lead to the tiny branching ratios of these FCNC processes. They are:

- The Glashow–Iliopoulos–Maiani (GIM) suppression in these decays
- The Minimal Flavour Violation (MFV) framework which leads to a hierarchy of the values of the CKM matrix elements
- The smallness of the weak coupling constant

TOY MODEL:

In order to study the effects of these modes of suppression in detail, we consider a toy model where, apart from the quarks and the Higgs (H), there is a flavour changing charged scalar field denoted by ω . The interaction Lagrangian is given by:

$$\mathcal{L}_{int} = \xi \omega^+ \omega^- H + \sum_{i,j=1}^3 (\eta V_{ij} \bar{u}_{iL} d_{jR} \omega^+ + h.c.) \quad (0.0.1)$$

where the parameter ξ controls the strength of the coupling between ω and the Higgs.

A similar Lagrangian can be written down for a theory with a Z boson, instead of the Higgs. This is a theoretical laboratory for studying the effects of relaxing each mode of suppression, one at a time.

The effects on the amplitude can be summarised as follows:

- GIM Mechanism: The unitarity of the CKM matrix leads to this mode of suppression [30]. The matrix element for a process in which one quark q changes to another quark q' of the same charge can be written as

$$M_{qq'} = \sum_{i=1}^3 V_{qi}^* V_{q'i} A(x_i, M_W) = \sum_{i=1}^3 \lambda_i A(x_i, M_W) \quad (0.0.2)$$

where $x_i = m_i^2/M_W^2$ carries the generation information, M_W is the scale of the charged current interaction and $\lambda_i = V_{qi}^* V_{q'i}$ is the CKM factor. This can be expanded as

$$A(x_i, M_W) = A_0(M_W) + x_i A'_i(M_W) + \frac{1}{2} x_i^2 A''_i(M_W) + \dots \quad (0.0.3)$$

Now, putting this back in Eqn. 0.0.2 and using the fact that $\sum_i \lambda_i = 0$, due to the unitarity of the CKM matrix, it can be seen that the dominant term is actually not proportional to A_0 , but to $x_i A'_i$. This gives us a suppression of x_i in the amplitude. For the top to charm decay, $x_i \sim x_b \sim m_b^2/M_W^2 \sim 10^{-3}$, leading to a suppression of $\sim 10^{-6}$ in the decay width.

- The MFV framework [3] means that the CKM matrix has a strong hierarchy in the values of its elements as we proceed from the diagonal to the off-diagonal elements. In our case of a top decay to a charm, the dominant CKM factor involved is $V_{tb}^* V_{cb} \sim 0.04$. An alternative prescription, which preserves unitarity but doesn't have the hierarchy seen here, can be constructed. For example, we might have

$$V = \begin{pmatrix} 1 & 0 & 0 \\ 0 & \cos \theta & \sin \theta \\ 0 & -\sin \theta & \cos \theta \end{pmatrix} \quad (0.0.4)$$

The dominant CKM element here is $\lambda_3 = \sin \theta \cos \theta = \frac{1}{2} \sin 2\theta$, which can take up a maximum value of 0.5, as opposed to the 0.04 in the previous case.

- Finally, the weak coupling constant is rather small in magnitude and we can think upon a new physics model which can have large couplings. As these values are restricted by the requirements of perturbation theory, we can get a modest enhancement of ~ 7 .

The effect on the amplitude is summarised in Fig. 1.

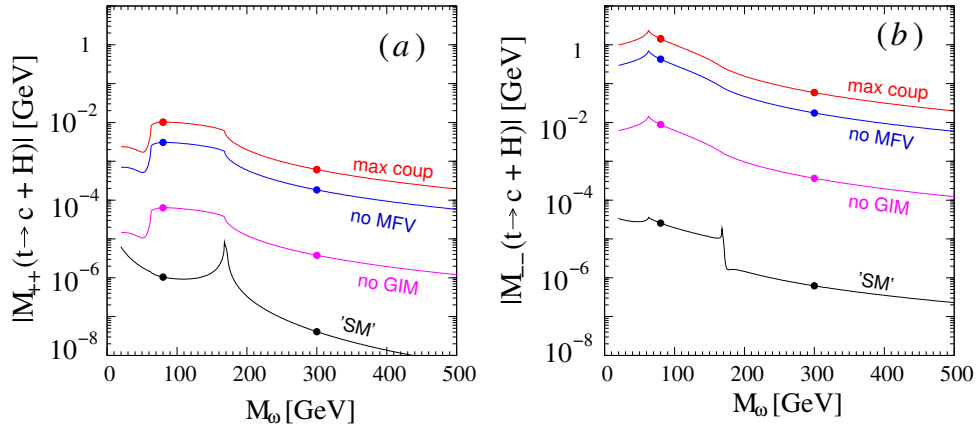


Figure 1: The absolute value of the two helicity amplitudes and how the relaxation of the different suppression factors enhances the amplitude. The subscript of \mathcal{M} , plotted on the y-axis, denotes the helicity of the charm and the top.

The overall enhancement in the amplitude is then $10^3 \times 25 \times 7 \sim 1.75 \times 10^5$ and thus, in the branching ratio, it is a factor of $\sim 3 \times 10^{10}$.

IN DIFFERENT MODELS:

Standard Model:

The SM BR, which is subject to all these suppression mechanisms, is calculated to be 5×10^{-15} . If all the three suppression mechanisms can be invalidated, one can hope to reach a BR of 10^{-5} .

cMSSM:

In the constrained Minimal SuperSymmetric Model (cMSSM) (see in review [167]), given by the four parameters - $m_{1/2}$, m_0 , A_0 and $\tan\beta$ - apart from $\text{sgn } \mu$, there exist charged Higgs bosons which naturally violate the GIM mechanism. However, the four parameters are constrained by various experimental inputs, most notably the Higgs boson mass. The effect of various constraints can be seen in the left panel of Fig. 2. The effect of these constraints is to raise the mass of the charged Higgs bosons in the theory, which is instrumental in suppressing the amplitude significantly. Thus, any enhancement gained by GIM-breaking is offset by the heavy charged Higgs in the theory. Furthermore, the cMSSM does not go beyond the MFV framework and the enhancement due to the coupling is also not very large. Overall, the cMSSM enhancement doesn't exceed $\sim 10^4$, leading to branching ratio $\sim 10^{-11}$ at best. This is illustrated in the right panel of Fig. 2.

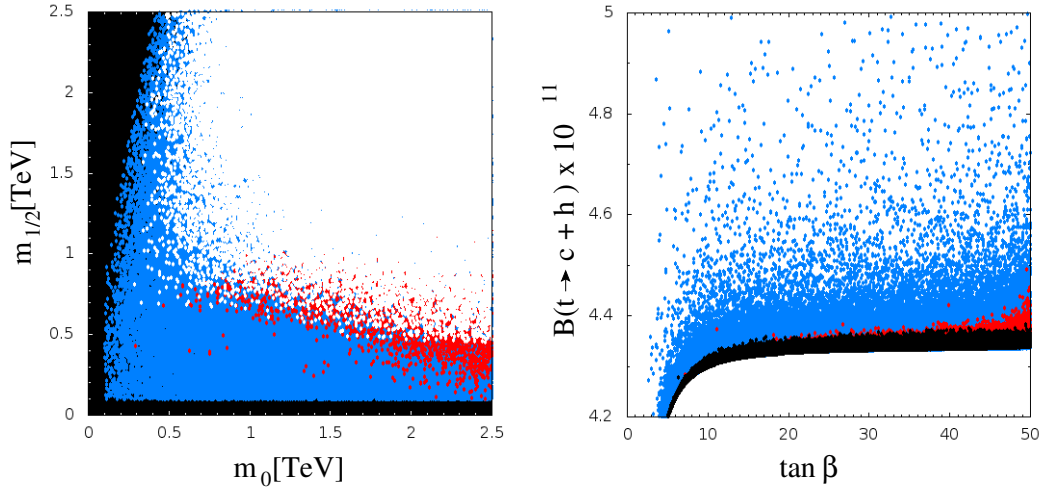


Figure 2: The cMSSM parameter space spanned by $m_{1/2}$ - m_0 . The black points are excluded from theoretical considerations, like unstable vacuum, tachyonic states etc. The blue points are excluded by the Higgs mass constraint, while the red points are excluded from flavour constraints. The plot on the right is the branching ratio for these points, where the colours are the same, except that the white (allowed) points on the left correspond to the black points on the right.

RPV SUSY:

SUSY models which break R -parity [318] are particularly interesting in this context for several reasons: firstly, there is no unitary CKM-like mixing matrix, thus there is no GIM suppression; secondly, there is no MFV framework to subscribe to either, and thus there is no off-diagonal

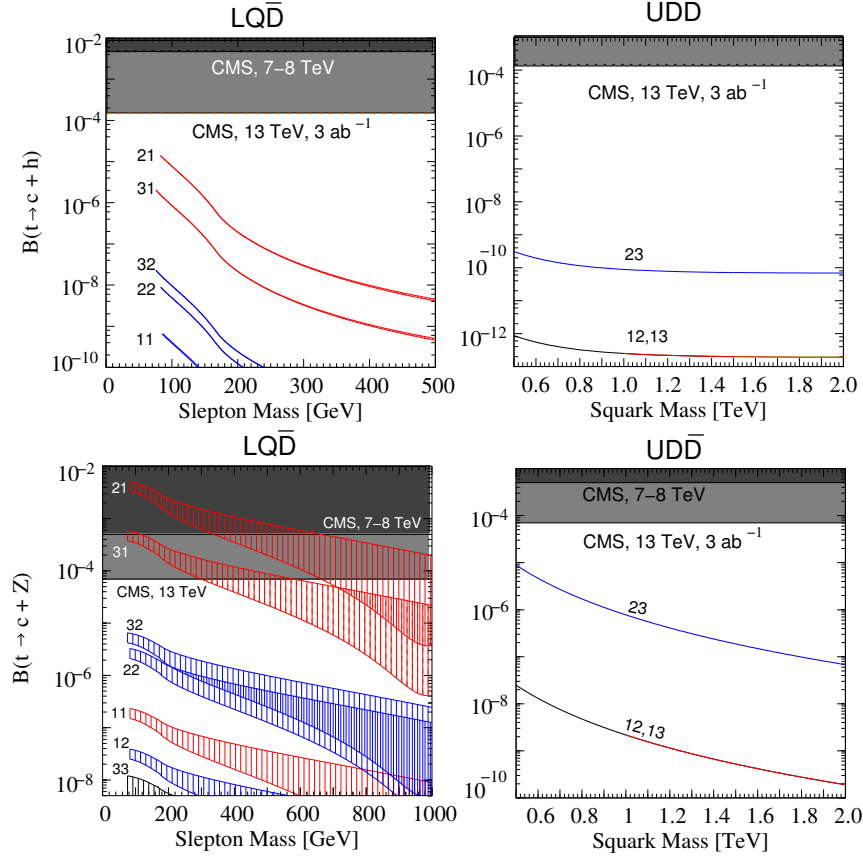


Figure 3: Illustrating the variation in the branching ratios $B(t \rightarrow c + h_0)$ (upper panels) and $B(t \rightarrow c + Z_0)$ (lower panels) with increase in the sfermion masses. For the panels on the left, which show branching ratios proportional to $(\lambda_{i2k}\lambda_{i3k})^2$ with the values of ik marked next to each curve, the mass of the slepton e_{Li} is plotted along the abscissa, and the mass of the squark \tilde{d}_{Rk} is responsible for the thickness of the lines in the upper panel and the hatched region in the lower panel. For the panels on the right, which show branching ratios proportional to $(\lambda_{2jk}\lambda_{3jk})^2$ with the values of jk marked next to each curve, the mass of the squark \tilde{d}_{Rk} is plotted along the abscissa. The dark (light) grey shaded regions represent the experimental bounds (discovery limits) from the LHC, operating at 7 – 8 TeV (13 TeV, projected)

hierarchy; thirdly, several of the R -parity violating couplings can be rather large, as most low-energy constraints are invalidated by the large values to which the sfermion masses have been pushed up by LHC data. As a result, all three of the SM suppression mechanisms are violated and we may expect full enhancement of the BR as explained above.

The RPV superpotential is given as:

$$\hat{W}_{\mathcal{R}_p} = \sum_{i,j,k=1}^3 \left(\frac{1}{2} \lambda_{ijk} \hat{L}_i \hat{L}_j \hat{E}_k^c + \lambda'_{ijk} \hat{L}_i \hat{Q}_j \hat{D}_k^c + \lambda''_{ijk} \hat{U}_i^c \hat{D}_j^c \hat{D}_k^c \right) \quad (0.0.5)$$

where a hat ($\hat{}$) represents a superfield. \hat{L} and \hat{Q} are SU(2) doublet superfields, while \hat{E} , \hat{U} and \hat{D} are singlets. The LQD term (second term) and the UDD term (third term) on the right are relevant to the analysis. The LQD term violates lepton number (L) and the UDD term violates baryon number (B). We can only consider one set of couplings at a time, but not both together, since that would lead to rapid proton decay. We carried out a thorough update

of the RPV couplings applicable to our case and found that the most promising products were of the form $\lambda'_{i2k}\lambda'_{i3k}$ or $\lambda''_{2jk}\lambda''_{3jk}$ with each of i, j, k running over 1, 2, 3

As shown in Fig. 3, the results are rather encouraging for the $t \rightarrow cZ$ decays, where the projected experimental limits would actually constrain the model.

The most important feature of this work is that it provides a clear rule of thumb for determining if any NP model can provide observable signals.

SINGLE TOP PRODUCTION:

An extension of this analysis which we feel to be worthwhile is studying the production of single top quarks in an e^+e^- collider. In the SM, this occurs purely at the one-loop level, and though the contributing Feynman diagrams would include a box diagram in addition to triangle diagrams, the suppression factors (as explained above) would all be very strong. In the context of RPV-SUSY, where these suppression factors are evaded, we find that the largest contributions to this will come from tree-level diagrams containing the products $\lambda'_{13k}\lambda'_{1jk}$, where $j = 1, 2$ and $k = 1, 2, 3$. These have been studied in the Ref. [6]. However, there exist several other products where the contribution is only at the one-loop level (triangle as well as box diagrams) and here the fact that RPV model evade all the suppression factors may, in fact, lead to observable signals or extended discovery limits, as the case may be.

The theoretical calculations for this analysis have been completed, and the numerical computations are under way.

A Closer look at R_D and R_{D^*}

Flavour changing processes via charged currents have been widely studied, especially in the b quark sector. B -meson factories have diligently built up a huge repository of measurements of the different quantities related to the decay and this is a sector where the SM has been very stringently tested. One of the interesting processes measured is the decay of the B -meson to a D -meson and a lepton-neutrino pair. Two channels have been studied in this regard - the $B \rightarrow D$ decay and the $B \rightarrow D^*$ decay. Theoretical calculations of branching ratios for these processes with different leptons in the final state are fraught with uncertainties arising from errors in the different quantities involved in the decay, like the CKM matrix element V_{cb} . A ratio of the branching ratios is more useful as such quantities simply cancel and provides us with a cleaner observable. Two such quantities are R_D and R_{D^*} , defined as follows:

$$R_{D^{(*)}} = \frac{\mathcal{B}(B \rightarrow D^{(*)}\tau\bar{\nu}_\tau)}{\mathcal{B}(B \rightarrow D^{(*)}l\bar{\nu}_l)} \quad (0.0.6)$$

where $l = e, \mu$. However, when experimental measurements of these two quantities, viz. $R_D = 0.397 \pm 0.028$ and $R_{D^*} = 0.316 \pm 0.019$ [358] are compared with the theoretical predictions from the Standard Model (SM), $R_D = 0.300 \pm 0.011$ and $R_{D^*} = 0.254 \pm 0.004$, we find deviations of 1.9σ and 3.3σ for R_D and R_{D^*} respectively. The combined discrepancy for the two is quite large $\sim 4\sigma$. We consider the exciting possibility that this might be a signal for

new physics¹ and we perform a model-independent analysis of the process using all relevant six-dimensional operators in [8].

Apart from R_D and R_{D^*} per se, the other observables of interest are the binned values of R_D and R_{D^*} , the polarisation, P_τ^D and $P_\tau^{D^*}$, of the final state τ lepton and the forward-backward asymmetry in the two processes, \mathcal{A}_{FB}^D and $\mathcal{A}_{FB}^{D^*}$. The definitions of all the observables are given below:

$$\text{Integrated } R_{D^{(*)}} : R_{D^{(*)}} = \frac{\mathcal{B}(B \rightarrow D^{(*)} \tau \bar{\nu}_\tau)}{\mathcal{B}(B \rightarrow D^{(*)} \ell \bar{\nu}_\ell)} \quad (0.0.7)$$

$$\text{Binned } R_{D^{(*)}} : R_{D^{(*)}}[q^2 \text{ bin}] = \frac{\mathcal{B}(B \rightarrow D^{(*)} \tau \bar{\nu}_\tau)[q^2 \text{ bin}]}{\mathcal{B}(B \rightarrow D^{(*)} \ell \bar{\nu}_\ell)[q^2 \text{ bin}]} \quad (0.0.8)$$

$$\text{Tau Polarisation} : P_\tau^{D^{(*)}} = \frac{\Gamma_\tau^{D^{(*)}}(+)-\Gamma_\tau^{D^{(*)}}(-)}{\Gamma_\tau^{D^{(*)}}(+)+\Gamma_\tau^{D^{(*)}}(-)} \quad (0.0.9)$$

$$\text{FB Asymmetry} : \mathcal{A}_{FB}^{D^{(*)}} = \frac{\int_0^{\pi/2} d\theta \frac{d\Gamma_\tau^{D^{(*)}}}{d\theta} - \int_{\pi/2}^\pi d\theta \frac{d\Gamma_\tau^{D^{(*)}}}{d\theta}}{\int_0^{\pi/2} d\theta \frac{d\Gamma_\tau^{D^{(*)}}}{d\theta} + \int_{\pi/2}^\pi d\theta \frac{d\Gamma_\tau^{D^{(*)}}}{d\theta}} \quad (0.0.10)$$

The branching ratio $\mathcal{B}(B \rightarrow D^{(*)} \ell \bar{\nu}_\ell) \equiv \mathcal{B}_\ell^{D^{(*)}}$ can be written as

$$\frac{d^2 \mathcal{B}_\ell^{D^{(*)}}}{dq^2 d(\cos \theta)} = \mathcal{N} |p_{D^{(*)}}| \left(a_\ell^{D^{(*)}} + b_\ell^{D^{(*)}} \cos \theta + c_\ell^{D^{(*)}} \cos^2 \theta \right) \quad (0.0.11)$$

$$\mathcal{B}_\ell^{D^{(*)}} = \int dq^2 \mathcal{N} |p_{D^{(*)}}| \left(2a_\ell^{D^{(*)}} + \frac{2}{3} c_\ell^{D^{(*)}} \right) \quad (0.0.12)$$

where

$$\mathcal{N} = \frac{\tau_B G_F^2 |V_{cb}|^2 q^2}{256 \pi^3 M_B^2} \left(1 - \frac{m_\ell^2}{q^2} \right)^2 \quad \text{and} \quad |p_{D^{(*)}}| = \frac{\sqrt{\lambda(M_B^2, M_{D^{(*)}}^2, q^2)}}{2M_B}$$

where $\lambda(a, b, c) = a^2 + b^2 + c^2 - 2(ab + bc + ca)$ and θ is the angle between the lepton and $D^{(*)}$ -meson in the lepton-neutrino centre-of-mass frame. While a recent measurement of $P_\tau^{D^*}$ has been reported by BELLE for the first time (although with large errors) [275], none of the other quantities have been experimentally measured as yet.

The decay amplitude for the process can be factorised into two parts – the hadronic part and the leptonic part. The hadronic part of the decay amplitude cannot be calculated exactly and is parametrised using form factors. These form factors are calculated in some theoretical and numerical framework and, in this work, we choose to simply borrow those results already available in the literature.

THE OPERATOR BASIS:

The effective six-dimensional operators for $b \rightarrow c \ell \bar{\nu}_\ell$ used for the analysis respect the SM gauge symmetry. This restricts the set of relevant operators to

¹It is worth noting that a recent measurement the BELLE collaboration [275] of $R_{D^*} = 0.276 \pm 0.034_{-0.026}^{+0.029}$ is consistent with the SM value. However, the error bars are quite large compared to the other results.

$$\begin{aligned}
\mathcal{O}_{VL}^{cb\ell} &= [\bar{c} \gamma^\mu b][\bar{\ell} \gamma_\mu P_L \nu] & \mathcal{O}_{PL}^{cb\ell} &= [\bar{c} \gamma_5 b][\bar{\ell} P_L \nu] \\
\mathcal{O}_{AL}^{cb\ell} &= [\bar{c} \gamma^\mu \gamma_5 b][\bar{\ell} \gamma_\mu P_L \nu] & \mathcal{O}_{TL}^{cb\ell} &= [\bar{c} \sigma^{\mu\nu} b][\bar{\ell} \sigma_{\mu\nu} P_L \nu] \\
\mathcal{O}_{SL}^{cb\ell} &= [\bar{c} b][\bar{\ell} P_L \nu]
\end{aligned} \tag{0.0.13}$$

The set of Wilson Coefficients (WCs), denoted by $C_{VL}^{cb\ell}$ etc., corresponding to these operators, are defined at the renormalization scale $\mu = m_b$. Note that in the SM, $C_{VL}^{cb\ell} = -C_{AL}^{cb\ell} = 1$ and all others are zero. Any NP model would predict deviation from these values. In the initial analysis, we neglect the tensorial contributions since it is difficult to build a microscopic model with such interactions. (For the study of tensor operators in this case, refer to the Appendix of Ref. [8]).

FORM FACTORS:

- For $B \rightarrow D$ decay: The non-zero hadronic matrix elements for $\bar{B} \rightarrow D$ transition are parametrised as

$$\begin{aligned}
\langle D(p_D, M_D) | \bar{c} \gamma^\mu b | \bar{B}(p_B, M_B) \rangle &= F_+(q^2) \left[(p_B + p_D)^\mu - \frac{M_B^2 - M_D^2}{q^2} q^\mu \right] \\
&+ F_0(q^2) \frac{M_B^2 - M_D^2}{q^2} q^\mu \\
\langle D(p_D, M_D) | \bar{c} b | \bar{B}(p_B, M_B) \rangle &= F_0(q^2) \frac{M_B^2 - M_D^2}{m_b - m_c} \\
\langle D(p_D, M_D) | \bar{c} \sigma^{\mu\nu} b | \bar{B}(p_B, M_B) \rangle &= -i(p_B^\mu p_D^\nu - p_B^\nu p_D^\mu) \frac{2F_T(q^2)}{M_B + M_D} \\
\langle D(p_D, M_D) | \bar{c} \sigma^{\mu\nu} \gamma_5 b | \bar{B}(p_B, M_B) \rangle &= \varepsilon^{\mu\nu\rho\sigma} p_{B\rho} p_{D\sigma} \frac{2F_T(q^2)}{M_B + M_D}
\end{aligned} \tag{0.0.14}$$

Numerical values for the form factors $F_0(q^2)$ and $F_+(q^2)$ have been computed in a lattice framework [314]. The axial vector and the pseudoscalar matrix elements are zero from symmetry considerations and thus only the WCs C_{VL}^τ and C_{SL}^τ contribute to this decay.

- For $B \rightarrow D^*$ decay: The non-zero hadronic matrix elements for $\bar{B} \rightarrow D^*$ transition are

parametrised as

$$\begin{aligned}
\langle D^*(p_{D^*}, M_{D^*}) | \bar{c} \gamma_\mu b | \bar{B}(p_B, M_B) \rangle &= i \varepsilon_{\mu\nu\rho\sigma} \epsilon^{\nu*} p_B^\rho p_{D^*}^\sigma \frac{2V(q^2)}{M_B + M_{D^*}} \\
\langle D^*(p_{D^*}, M_{D^*}) | \bar{c} \gamma_\mu \gamma_5 b | \bar{B}(p_B, M_B) \rangle &= 2M_{D^*} \frac{\epsilon^*.q}{q^2} q_\mu A_0(q^2) \\
&\quad + (M_B + M_{D^*}) \left[\epsilon_\mu^* - \frac{\epsilon^*.q}{q^2} q_\mu \right] A_1(q^2) \\
&\quad - \frac{\epsilon^*.q}{M_B + M_{D^*}} \left[(p_B + p_{D^*})_\mu - \frac{M_B^2 - M_{D^*}^2}{q^2} q_\mu \right] A_2(q^2) \\
\langle D^*(p_{D^*}, M_{D^*}) | \bar{c} \gamma_5 b | \bar{B}(p_B, M_B) \rangle &= -\epsilon^*.q \frac{2M_{D^*}}{m_b + m_c} A_0(q^2) \quad (0.0.15) \\
\langle D^*(p_{D^*}, M_{D^*}) | \bar{c} \sigma_{\mu\nu} b | \bar{B}(p_B, M_B) \rangle &= -\varepsilon_{\mu\nu\alpha\beta} \left[-\epsilon^{\alpha*} (p_{D^*} + p_B)^\beta T_1(q^2) \right. \\
&\quad \left. + \frac{M_B^2 - M_{D^*}^2}{q^2} \epsilon^{*\alpha} q^\beta (T_1(q^2) - T_2(q^2)) \right. \\
&\quad \left. + 2 \frac{\epsilon^*.q}{q^2} p_B^\alpha p_{D^*}^\beta \left(T_1(q^2) - T_2(q^2) - \frac{q^2}{M_B^2 - M_{D^*}^2} T_3(q^2) \right) \right] \\
\langle D^*(p_{D^*}, M_{D^*}) | \bar{c} \sigma_{\mu\nu} q^\nu b | \bar{B}(p_B, M_B) \rangle &= -2\varepsilon_{\mu\nu\rho\sigma} \epsilon^{*\nu} p_B^\rho p_{D^*}^\sigma T_1(q^2)
\end{aligned}$$

While no lattice calculation exists at the present for the form factors in this case, these have been calculated in a Heavy Quark Effective Theory (HQET) framework [313]. In this case, symmetry dictates that the scalar current is zero and thus there is no contribution to the decay width from C_{SL}^τ .

It is important to note that the two processes depend on different sets of WCs: while C_{VL}^τ and C_{SL}^τ contribute to the $B \rightarrow D$ decay process, C_{VL}^τ , C_{AL}^τ and C_{PL}^τ contribute $B \rightarrow D^*$. This leads us to postulate that R_D and R_{D^*} are theoretically independent measurements and allow for separate explanations.

EXPLAINING R_D ALONE:

The quantities a_ℓ^D , b_ℓ^D and c_ℓ^D (in Eqn. 0.0.11) can be calculated for a particular helicity of the final state lepton using the helicity amplitude approach. Since only C_{VL}^τ and C_{SL}^τ are relevant, we can separately plot R_D as a variation of the two WCs and note the range of values for which it satisfies the experimental constraints. In this analysis, one of them is varied, the other is held constant at its SM value. The results are given in Table 1 and plotted in Fig. 4, where the red (brown) band corresponds to the 1σ (2σ) uncertainty on the experimental measurement.

EXPLAINING R_{D^*} ALONE:

We can carry out a similar treatment for the case of $B \rightarrow D^*$ decay. In this case, three WCs - C_{VL}^τ , C_{AL}^τ and C_{PL}^τ - contribute. The plots of R_{D^*} as a function of the different WCs are given in Fig. 5. As before, the 1σ (2σ) bands are indicated by the red (brown) bands.

In Table 2, the prediction for the binned R_{D^*} is given, as are those for $P_\tau^{D^*}$ and $\mathcal{A}_{FB}^{D^*}$. Except for an imprecise measurement of $P_\tau^{D^*}$, no measurement for any of the other quantities exists.

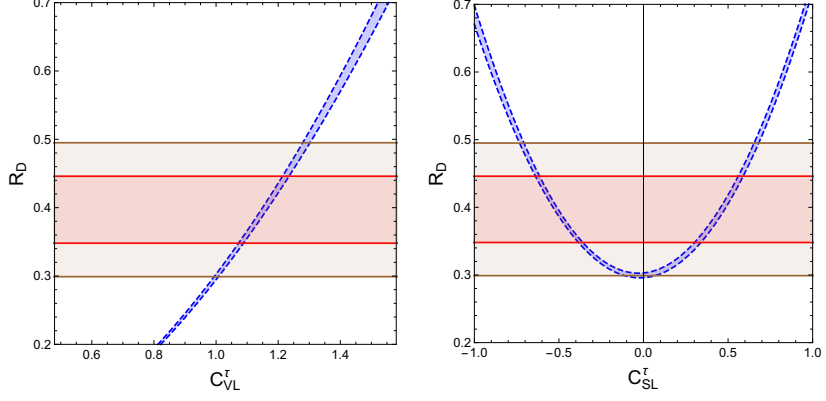


Figure 4: The dependence of R_D with respect to the variation of the WCs C_{VL}^τ (left) and C_{SL}^τ (right).

		SM	$\mathbf{C_{VL}}$ ($\mathbf{C_{SL} = 0}$)	$\mathbf{C_{SL}}$ ($\mathbf{C_{VL} = 1}$)
	1σ range of the WC		[1.073, 1.222]	$[-0.656, -0.342]$ [0.296, 0.596]
	$P_\tau(D)$	[0.313, 0.336]	[0.313, 0.336]	[0.408, 0.556]
	\mathcal{A}_{FB}^D	$[-0.361, -0.358]$	$[-0.361, -0.358]$	$[-0.168, -0.022]$ $[-0.450, -0.428]$
R_D [bin]	$[m_\tau^2 - 5] \text{ GeV}^2$	[0.154, 0.158]	[0.178, 0.236]	[0.161, 0.181]
	$[5 - 7] \text{ GeV}^2$	[0.578, 0.593]	[0.665, 0.888]	[0.626, 0.752]
	$[7 - 9] \text{ GeV}^2$	[0.980, 1.003]	[1.127, 1.505]	[1.125, 1.502]
	$[9 - (M_B - M_D)^2] \text{ GeV}^2$	[1.776, 1.823]	[2.049, 2.741]	[2.294, 3.669]

Table 1: The values of the WCs consistent with the 1σ experimental range for R_D are shown in the second row. The subsequent rows show the predictions for $P_\tau(D)$, \mathcal{A}_{FB}^D and R_D in four q^2 bins for the WC ranges shown in the second row.

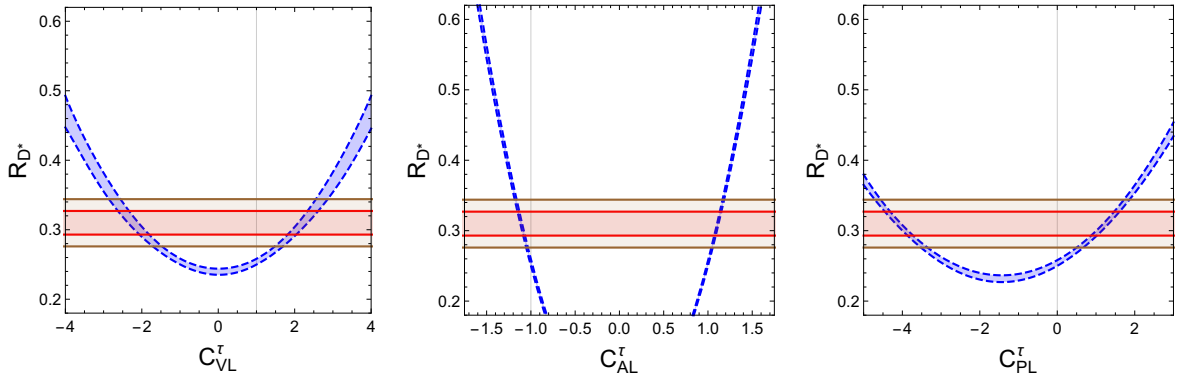


Figure 5: The dependence of R_{D^*} with respect to the variation of the WCs C_{VL}^τ (left), C_{AL}^τ (middle) and C_{PL}^τ (right). A thin vertical line shows the SM values of the WCs.

		SM	$\mathbf{C_{VL}}$ $\mathbf{C_{AL,PL} = -1, 0}$	$\mathbf{C_{AL}}$ $\mathbf{C_{VL,PL} = 1, 0}$	$\mathbf{C_{PL}}$ $\mathbf{C_{VL,AL} = 1, -1}$
	Range in WC		[1.856, 2.569]	[-1.149, -1.073]	[0.890, 1.583]
	$P_\tau(D^*)$	[-0.505, -0.490]	[-0.530, -0.509]	[-0.505, -0.488]	[-0.322, -0.144]
	$\mathcal{A}_{FB}^{D^*}$	[0.050, 0.078]	[0.191, 0.297]	[0.028, 0.062]	[-0.078, -0.007]
R_{D^*} [bin]	$[m_\tau^2 - 5] \text{ GeV}^2$	[0.103, 0.105]	[0.120, 0.140]	[0.116, 0.132]	[0.124, 0.148]
	$[5 - 7] \text{ GeV}^2$	[0.331, 0.336]	[0.387, 0.457]	[0.373, 0.425]	[0.390, 0.465]
	$[7 - 9] \text{ GeV}^2$	[0.475, 0.479]	[0.535, 0.613]	[0.535, 0.613]	[0.534, 0.610]
	$[9 - (M_B - M_{D^*})^2] \text{ GeV}^2$	[0.554, 0.556]	[0.577, 0.619]	[0.621, 0.710]	[0.571, 0.611]

Table 2: The values of the WCs consistent with the 1σ experimental range for R_{D^*} are shown in the second row. We only show the ranges that are closest to the SM values of the WCs. The subsequent rows show the predictions for $P_\tau(D^*)$, $\mathcal{A}_{FB}^{D^*}$ and R_{D^*} in four q^2 bins for the WC ranges shown in the second row.

We can combine the predictions for the binned R_{D^*} restricted to the highest q^2 bin, $P_\tau^{D^*}$

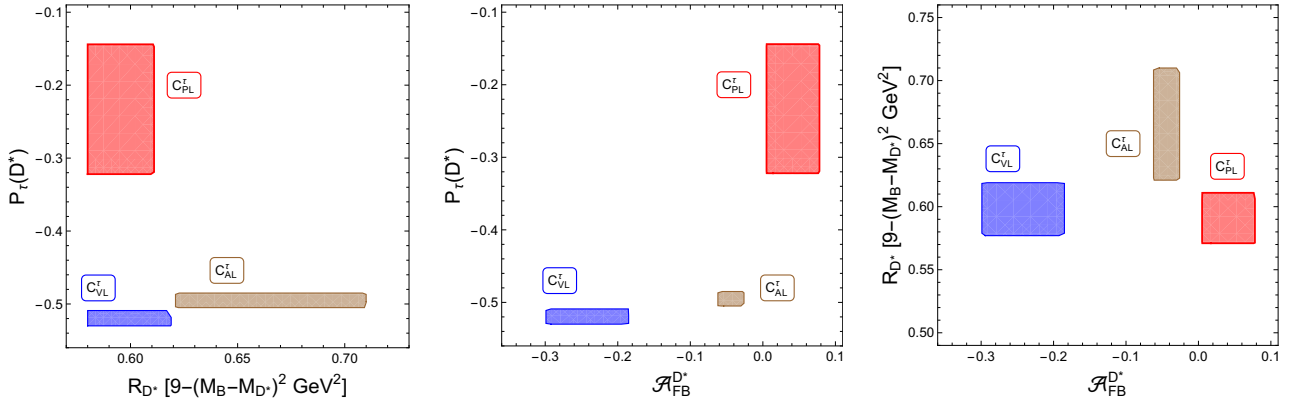


Figure 6: The predictions for $P_\tau^{D^*}$, R_{D^*} in the last bin and $\mathcal{A}_{FB}^{D^*}$ are shown in three different planes for the ranges of the three WCs C_{VL}^T , C_{AL}^T and C_{PL}^T .

and $\mathcal{A}_{FB}^{D^*}$ to construct three planes. When plotted in these three planes, the regions of the allowed values of the WCs all separate out nicely as shown in Fig. 6. A future measurement of any two of these three observables would help in restricting us to a particular region, thus limiting the scope of any NP model.

We have thus set up a framework in which any NP model can be studied vis-a-vis its predictions for $B \rightarrow D\ell\nu_\ell$ and $B \rightarrow D^*\ell\nu_\ell$, and the results compared directly with the experimental measurements.

Collider search for sbottom LSP in a SUSY model with baryonic R -parity violation

While the majority of SUSY search analyses assume the conservation of the adhoc \mathbb{Z}_2 symmetry called R -parity, defined as $R = (-1)^{3B+L+2S}$ with B , L and S being the baryon number, lepton number and spin of the particle respectively, it is also possible for the symmetry to be violated (see section 2). Conservation of R -parity implies that SUSY particles will be pair produced and heavy SUSY particles will decay into an odd number of lighter SUSY particles. Violation of R -parity allows SUSY particles to decay to a pair of SM fermions. This leads to a radical difference in the final state signatures - while the R -parity conserving scenario typically leads to large missing transverse energy (\cancel{E}_T) in the final state, an R -parity violating (RPV) scenario might produce final states with very little \cancel{E}_T . This departure also permits us to evade some of the most stringent bounds from direct searches, which are generally made assuming the conservation of R -parity.

In Ref. [12], we perform a collider analysis of the lighter SUSY partner of the bottom quark, the sbottom – which also happens to be the Lightest Supersymmetric Particle (LSP) in our chosen spectrum – decaying to a top quark and a light d-type quark through baryon number violating couplings. The final states with either the top quark decaying leptonically or hadronically can be :

- $2\ell\ell' + b\bar{b} + \text{jets} + \cancel{E}_T$ ($\ell, \ell' = e, \mu$);
- $1\ell + b\bar{b} + \text{jets} + \cancel{E}_T$;
- $0\ell + b\bar{b} + \text{jets} + \cancel{E}_T$

The RPV superpotential is given in Eqn. (0.0.5) and we need to choose only the baryon-number violating terms, viz. the UDD terms with λ'' couplings. The Lagrangian is given by:

$$\mathcal{L}_{UDD} = -\frac{1}{2}\lambda''_{ijk} \left(\tilde{u}_{iR}^* \bar{d}_{jR} d_{kL}^c + \tilde{d}_{kR}^* \bar{u}_{iR} d_{jL}^c + \tilde{d}_{jR}^* \bar{u}_{iR} d_{kL}^c \right) \quad (0.0.16)$$

For the decay of the sbottom, to a top quark and a d-type quark, only certain λ''_{ijk} need to be non-zero. For example, one of j, k must be 3 and $i = 3$ because there needs to be a t-quark in the final state. Thus, we can have either λ''_{313} (giving $\tilde{b}_1 \rightarrow t + d$) or λ''_{323} (giving $\tilde{b}_1 \rightarrow t + s$). We shall only consider one of these two couplings to be non-zero so as to avoid the problem of large FCNCs.

The relevant dominant background processes which provide similar final state signatures are $t\bar{t} + \text{jets}$ (upto 2), $t\bar{t}b\bar{b}$, $t\bar{t}Z$, $t\bar{t}W$ and $t\bar{t}H$. For the case with hadronic final states, the QCD multijet background becomes the most dominant background.

We have used MADGRAPH [359] to generate the different sets of signal and background events at the partonic level. It is interfaced with PYTHIA8 [14] for parton showering and hadronisation. The events are then passed through DELPHES [362] in order to simulate the detector response. The signals events are samples of sbottom pairs of different masses. We set 6 benchmark

points BP-1 to BP-6, with BP-1 at $m_{\tilde{b}} = 500$ GeV and each benchmark point being an increment of 100 GeV over the previous one, finally ending up at $m_{\tilde{b}} = 1$ TeV for BP-6.

LEPTONIC FINAL STATE:

For the leptonic final state, we perform a cut-based analysis and then follow it up with a multivariate analysis, implemented through the Toolkit for Multivariate Analysis (TMVA) using the ROOT framework [16].

Cut-based Analysis:

For the cut-based analysis, we demand the following:

- **C1** : At least one lepton in the final state
- **C2** : More than four jets in the final state
- **C3** : Leading non b-tagged jet having $p_T > 250$ GeV in the final state
- **C4** : Second leading non b-tagged jet in the final state having $p_T > 150$ GeV
- **C5** : A large value for the scalar p_T sum of all visible particles (H_T). Demand that $H_T > 1000$ GeV, where

$$H_T = \sum_{i=e,\mu,j,\gamma} |\vec{p}_T(i)|. \quad (0.0.17)$$

- **C6** : The value of $M_{T_2} > 360$ GeV, which is defined as [17]

$$M_{T_2}(\vec{p}_T^{\mathcal{V}1}, \vec{p}_T^{\mathcal{V}2}, \vec{p}_T) = \min_{\vec{p}_T^{\mathcal{A}1} + \vec{p}_T^{\mathcal{A}2} = \vec{p}_T} \left[\max \left\{ M_T(\vec{p}_T^{\mathcal{V}1}, \vec{p}_T^{\mathcal{A}1}), M_T(\vec{p}_T^{\mathcal{V}2}, \vec{p}_T^{\mathcal{A}2}) \right\} \right] \quad (0.0.18)$$

where, $\vec{p}_T^{\mathcal{A}1}$ and $\vec{p}_T^{\mathcal{A}2}$ are two hypothetical subdivisions of the total missing transverse momentum, \vec{p}_T . In general, the transverse mass $M_T(\vec{p}_1, \vec{p}_2)$ of the (\vec{p}_1, \vec{p}_2) system is defined as

$$M_T(\vec{p}_1, \vec{p}_2) = \sqrt{m_1^2 + 2|\vec{p}_1||\vec{p}_2|(1 - \cos\phi)} \quad (0.0.19)$$

where $p_1^2 = m_1^2$, the invisible particle is assumed to be massless and ϕ is the azimuthal angle between the \vec{p}_1 and \vec{p}_2 vectors.

The result of the cut-based analysis is given in Table 3. The significance is calculated for a particular luminosity (\mathcal{L}) by the following formula:

$$\mathcal{S}_{\mathcal{L}} = \frac{\sigma_S \mathcal{L}}{\sqrt{\sigma_S \mathcal{L} + \sigma_B \mathcal{L}}} \quad (0.0.20)$$

where $\sigma_{S(B)}$ is the surviving cross-section for the signal (background) after the cut-flow.

Multivariate Analysis:

We performed the multivariate analysis using Toolkit for Multivariate Analysis (TMVA) implemented in the ROOT framework. The variables we use to carry out the analysis are:

$$(p_T)_{j1}, (p_T)_{j2}, (p_T)_{j3}, (p_T)_{j4}, (p_T)_{bj1}, (p_T)_{bj2}, H_T, \cancel{E}_T, \text{nJets and } M_{T_2}$$

Cuts	$t\bar{t} + jets$	$t\bar{t}b\bar{b}$	$t\bar{t}Z$	$t\bar{t}H$	$t\bar{t}W$	BP1 (500)	BP2 (600)	BP3 (700)	BP4 (800)	BP5 (900)	BP6 (1000)
Initial	8.32×10^5	1.72×10^4	874	509	645	519	175	67.0	28.3	12.9	6.15
After cuts:	757	13.9	5.48	1.61	1.93	17.43	10.85	5.62	2.73	1.29	0.575
$\mathcal{S}@300\text{fb}^{-1}$						10.7	6.68	3.47	1.69	0.80	0.36

Table 3: The surviving cross-section for the different processes entire series of cuts. The numbers in the brackets for the different benchmark points indicate the sbottom mass corresponding to the respective benchmark point and are in GeV.

where $(p_T)_{ji}$ refers to the p_T of the i^{th} non-b tagged jet and $(p_T)_{bji}$ refers to the p_T of the i^{th} b-tagged jet. The analysis was carried out with default values of the TMVA parameters, and we achieve a reach greater than in the cut-based case. The results are summarised in Table 4.

	BP-1	BP-2	BP-3	BP-4	BP-5	BP-6
$m_{\tilde{b}_1}$ (GeV)	500	600	700	800	900	1000
BDT cut	0.165	0.185	0.262	0.245	0.270	0.335
$\mathcal{S} = \frac{S}{\sqrt{S+B}}$	17.8	7.9	4.9	2.2	1.3	0.9

Table 4: Signal significances for the benchmark points with the choice of BDT cuts with $\mathcal{L} = 300 \text{ fb}^{-1}$ of luminosity.

It is clear from Table 4 that the exclusion bounds for the sbottom can be extended to beyond 800 GeV using MVA at a luminosity of 300 fb^{-1} .

HADRONIC FINAL STATE:

For the hadronic final state, in the absence of a lepton to tag on, our analysis is organised around tagging a top jet. In order to construct jets, we avail of the particle information from the **EFlow** branch of the **DELPHES** generated **ROOT** file. We use **FASTJET** [363] to construct fat jets of $R = 1.8$ using the anti-kT algorithm [19] after demanding that $p_T > 30 \text{ GeV}$ and $|\eta| < 3$. Jets with $p_T > 200 \text{ GeV}$ are reclustered using the Cambridge-Aachen (C/A) [20] algorithm, using $R = 1.8$, and passed through to **HEPTopTagger** [21] for top tagging. We select only those events with at least one tagged top for further analysis. Tops are tagged with an efficiency of $\sim 30\%$.

We employ jet grooming techniques to get rid of soft and large angle radiations, along with underlying events. In this analysis, we use Jet Trimming [22] as our preferred grooming technique. This technique uses two independent parameters - R_{trim} and p_T^{frac} . The algorithm gets rid of large angle radiation by constraining all the constituents of the fat jet to lie within a smaller jet radius R_{trim} and of soft radiation by keeping only those constituents whose $p_T > p_T^{\text{frac}} \cdot p_T^{\text{jet}}$, where p_T^{jet} is the p_T of the input fat jet. We use $R_{\text{trim}} = 0.4$ and $p_T^{\text{frac}} = 1\%$. The final state jets are classified into three categories - top jets (tagged by the top tagger),

Variable	Definition
1. nlJet	The number of light jets in the event
2. nbJet	The number of b-tagged jets in the event
3. ntJet	The number of top-tagged jets in the event
4. $(p_T)_{j_1}$	p_T of the hardest non-top tagged jet
5. $(p_T)_{j_2}$	p_T of the second hardest non-top jet
6. $(p_T)_{j_t^{(1)}}$	p_T of the hardest top tag jet
7. H_T	scalar sum of the p_T of all the jets
8. m_{tj}	the invariant mass of the top and jet system
9. m_{jets}	the invariant mass of all the other jets
10. $\Delta M = m_{tj} - m_{\text{jets}} $	the mass difference of the two reconstructed invariant masses
11. $\rho = \frac{(p_T)_{j_t^{(1)}}}{(p_T)_{j_\ell^{(1)}}}$	Ratio of the hardest top-jet p_T and light jet p_T
12. $\tau_{21} = \tau_2/\tau_1$	Ratio of the Nsubjettiness variables
13. $\tau_{31} = \tau_3/\tau_1$	Ratio of the Nsubjettiness variables
14. $\tau_{32} = \tau_3/\tau_2$	Ratio of the Nsubjettiness variables
15. $\Phi(t, j)$	Azimuthal angle separation between the top jet and hardest light jet.

Table 5: List of all the variables used in the multivariate analysis.

b-tagged jets (tagged using a p_T dependent b-tagging efficiency function) and light jets (those which are neither top nor b-tagged jets).

For this section, we just consider QCD multijets and $t\bar{t}$ + jets as the background, as these overwhelm all other background processes. The variables used in the multivariate analysis are given in Table 5.

	QCD	$t\bar{t}$ + jets	BP-1 (500)	BP-2 (600)	BP-3 (700)	BP-4 (800)	BP-5 (900)	BP-6 (1000)
σ_0 (fb)	1.87×10^7	8.32×10^5	5.19×10^2	1.75×10^2	67.0	28.3	12.9	6.15
$\sigma_{\text{top tag}}$ (fb)	2.65×10^6	9.52×10^4	1.66×10^2	57.8	22.6	9.75	4.52	2.23
$\mathcal{S} = \frac{S}{\sqrt{S+B}}$			3.50	1.21	0.57	0.32	0.20	0.16

Table 6: Showing the initial cross-section (σ_0) and surviving cross-section after at least one top is tagged ($\sigma_{\text{top tag}}$) for the background and all the signal benchmarks. The QCD multijet sample is generated after a cut on the H_T variable of 800 GeV and cut of 100 GeV on the p_T of the two hardest jets.

Trimmed jets are particularly important for the reconstruction of the sbottom. The reconstruction is done only for those events with four or more jets. The reconstruction is done by taking two mass functions. One takes into account the top-tagged jet and a light jet to calculate the invariant mass of the system, m_{tj} . The other mass function is done by taking all the other jets and constructing their invariant mass, m_{jets} . The process is iterated over all the light jets such that the difference between these two masses ($\Delta M = |m_{tj} - m_{\text{jets}}|$) is minimised and the corresponding values of m_{tj} and m_{jets} are used in the MVA.

Apart from the reconstructed masses, we also use n-subjettiness variables [385], since the

QCD multijets are not expected to have a definite substructure, unlike the jets from the sbottoms.

The results for the hadronic case, however, are not very encouraging. In Table (6), besides the initial and the top tagged cross-sections, the results of the TMVA are also shown. For discovery, the leptonic channel remains the more promising channel. It might also be interesting to consider a fusion of these two analysis techniques, with semi-leptonic final states, but we have restricted ourselves only to the separate analyses in this work.

Investigating the sgoldstino as a possible candidate for the diphoton excess

Discovery through direct searches has always been the Holy Grail of progress in particle physics, especially in the context of a hadronic collider like the LHC. Since the LHC hasn't yet thrown up any signs of a new particle, there was a lot of excitement in the community when one of the most tantalising signals in recent times was announced near the end of 2015. Both the CMS and ATLAS collaborations reported an excess in the diphoton channel at $\sim 750\text{GeV}$, prompting an explosion of papers discussing possible explanations. Various ideas competed for attention: one of the most intriguing ones involved the sgoldstino. The sgoldstino is the supersymmetric scalar partner of the goldstino, the fermion produced when global SUSY is spontaneously broken. The explanation was proposed by several different groups [405–408, 418], all using an effective theory approach.

We studied the impact of the existence of such a scalar in the context of the Gauge Mediation (GM) framework, in which SUSY breaking in the hidden sector is communicated to the visible sector at a high scale by gauge interactions carried by messenger particles. These messengers are charged under both the SM gauge group as well as the hidden sector quantum numbers. Our analysis in Ref. [29] led us to conclude that under scrutiny, several theoretical aspects affect the viability of the model in its minimal form.

In order to parametrise the effect of SUSY breaking in the visible sector, it is assumed that it happens due to the F component of a chiral superfield X in the hidden sector acquiring a VEV. This breaking effect is then communicated to the visible sector through messenger gauge fields with the following effective Lagrangian

$$\mathcal{L} = -\frac{c_1}{2M_1} \int d^2\theta \hat{X} \hat{W}^{1\alpha} \hat{W}_\alpha^1 - \frac{c_2}{2M_2} \int d^2\theta \hat{X} \hat{W}^{2\alpha A} \hat{W}_\alpha^{2A} - \frac{c_3}{2M_3} \int d^2\theta \hat{X} \hat{W}^{3\alpha A} \hat{W}_\alpha^{3A} + H.c \quad (0.0.21)$$

where the superscripts $\{1,2,3\}$ refer to the gauge groups $U(1)$, $SU(2)$ and $SU(3)$ respectively, α is the spinor index and A runs over the field components in the adjoint representation. The masses $\{M_1, M_2, M_3\}$ set the mass scale of the messenger fields. The superfields \hat{X} and \hat{W}_α^A

are written in terms of the ordinary fields as:

$$\hat{X} = \mathcal{S}(y) + \sqrt{2}\theta\xi(y) + \theta^2 F_x(y) \quad (0.0.22)$$

$$= \frac{1}{\sqrt{2}}\{\phi(y) + i\alpha(y)\} + \sqrt{2}\theta\xi(y) + \theta^2 F_x(y) \quad (0.0.23)$$

$$\hat{W}_\alpha^A = -i\lambda_\alpha^A(y) + D^A(y)\theta_\alpha - (\sigma^{\mu\nu}\theta)_\alpha F_{\mu\nu}^A(y) - \theta^2 \sigma_{\alpha\dot{\beta}}^\mu D_\mu(y) \lambda^{\dagger A\dot{\beta}}(y) \quad (0.0.24)$$

The Majorana masses of the gauginos are given by:

$$m_i = c_i \frac{\langle F_x \rangle}{M_i} \quad (0.0.25)$$

The total cross-section of the diphoton production via the resonance \mathcal{S} (assuming small decay width) is given by :

$$\sigma_{\gamma\gamma}(\sqrt{s}) = \sigma_{pp \rightarrow \mathcal{S}}(\sqrt{s}) \text{Br}(\mathcal{S} \rightarrow \gamma\gamma) \quad (0.0.26)$$

$$= \sum_i \mathcal{A}^{ii}(\sqrt{s}) \Gamma(\mathcal{S} \rightarrow p_i p_i) \frac{\Gamma(\mathcal{S} \rightarrow \gamma\gamma)}{\Gamma_{\mathcal{S}}} \quad (0.0.27)$$

where $\{p_i, p_i\}$ refers to the initial state partons, $\{g, g\}$, $\{\bar{u}, u\}$ etc, $\Gamma_{\mathcal{S}}$ is the width of the sgoldstino and the numerical values of the quantities $\mathcal{A}^{ii}(\sqrt{s})$ can be calculated from the parton distribution functions at a particular energy. We require that $\sigma_{\gamma\gamma}(\sqrt{s} = 13 \text{ TeV})$ be in the range of 3 – 8 fb in order to explain the excess.

FORMALISM:

We work in the Ordinary Gauge Mediation (OGM) framework [30]. Apart from the chiral superfield \hat{X} , whose scalar and auxiliary components both get vevs, there are N_5 pairs of vector-like messenger fields $\{\Phi_i, \tilde{\Phi}_i\}$ ($i = 1, N_5$), which transform under $\mathbf{5} + \bar{\mathbf{5}}$ of $SU(5)$. The superpotential is given by

$$\hat{W}_{OGM} = \lambda_{ij} \hat{X} \hat{\Phi}_i \hat{\Phi}_j \quad (0.0.28)$$

We can diagonalise λ_{ij} by independently rotating the $\{\hat{\Phi}_i, \hat{\Phi}_j\}$ pair, without affecting the Kähler potential. The Dirac mass of the fermions in each pair of messengers is $m_F^i = \lambda_i \langle \mathcal{S} \rangle$, while the complex scalars have squared masses $m_{i\pm}^2 = \lambda_i^2 \langle \mathcal{S} \rangle^2 \pm \lambda_i \langle F_x \rangle$. The gaugino masses are generated at one loop and are given by:

$$m_a = \frac{\alpha_a}{4\pi} \sum_{i=1}^{N_5} d_i^a \frac{\lambda_i \langle F_x \rangle}{m_F^i} g(x_i) \quad (a = 1, 2, 3) \quad (0.0.29)$$

where a is the gauge group label, $x_i = \lambda_i \langle F_x \rangle / (m_F^i)^2$ and d_i is the Dynkin index for the representation ($d_i = 1$ for $SU(5)$, which is our case). The function $g(x)$ is given by:

$$g(x) = \frac{1}{x^2} [(1+x)\text{Ln}(1+x) + (1-x)\text{Ln}(1-x)] \quad (0.0.30)$$

Assuming that all the $\lambda_i = \lambda$ (equal couplings), we get

$$m_a = \frac{\alpha_a}{4\pi} \kappa m_F N_5 g(\kappa) \quad (0.0.31)$$

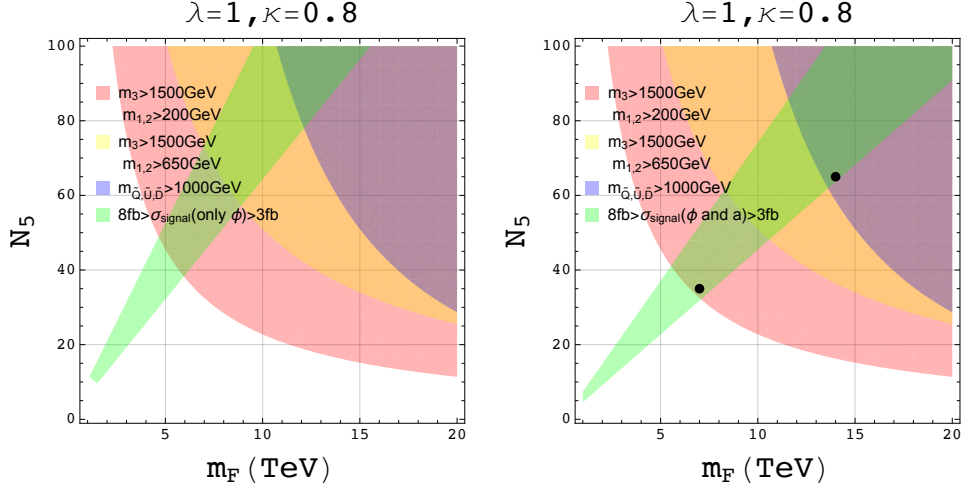


Figure 7: Allowed region in the OGM parameter space that successfully explains the signal and satisfies LHC bounds on squark and gaugino masses. While in the left panel the contribution from only ϕ (the scalar) is considered, the right panel takes into account both ϕ (scalar) and a (pseudoscalar) contributions. The black dots in the plot on the right hand side are referenced in the caption of Fig. 8.

where $\kappa = \lambda \langle F_x \rangle / m_F^2$, which can never exceed 1 (since otherwise one of the complex scalar masses squared becomes negative). The decay width of the sgoldstino to the pair of photons is given by:

$$\Gamma_{\gamma\gamma} = \Gamma(\phi \rightarrow \gamma\gamma) = \frac{1}{2\pi} \left[\frac{m_\phi^4}{4} \left(\frac{c_1}{M_1} c_W^2 + \frac{c_2}{M_2} s_W^2 \right)^2 \right] \quad (0.0.32)$$

For the excess to be satisfied, we require that:

$$\mathcal{A}_{13}^{gg} \frac{\Gamma_{gg} \Gamma_{\gamma\gamma}}{\Gamma_{gg} + \Gamma_{\gamma\gamma} + \Gamma_{ww} + \Gamma_{zz} + \Gamma_{z\gamma}} \gtrsim 3 \text{ fb} \quad (0.0.33)$$

Considering gluon fusion as the dominant mode of production, using this requirement, we consider various aspects of the model - among them, the number of messenger pairs needed, the running of the coupling constant and mass of \mathcal{S} .

NUMBER OF MESSENGERS:

We have three free parameters - m_F , $\langle F_x \rangle$ or κ , and N_5 . Taking $N_5 = 1$, we find that imposing Eqn. (0.0.33), gives us

$$m_F \lesssim 175 \text{ GeV} \quad (0.0.34)$$

The mass of the messengers can be raised by raising the number of messengers. Choosing $\kappa = 0.8$, a reasonable value, we can plot the region on the $m_F - N_5$ plane which can explain the signal as well as evade the LHC bounds on squark and gaugino masses. This is shown in Fig 7.

Taking into account all collider constraints, it is seen that we would need a very large number of messenger fields (≥ 60). In itself, this is not a problem but with so many messenger fields, the running of the $SU(3)$ gauge coupling hits the Landau pole at quite low energy scales ~ 50 TeV. This is shown in Fig. 8.

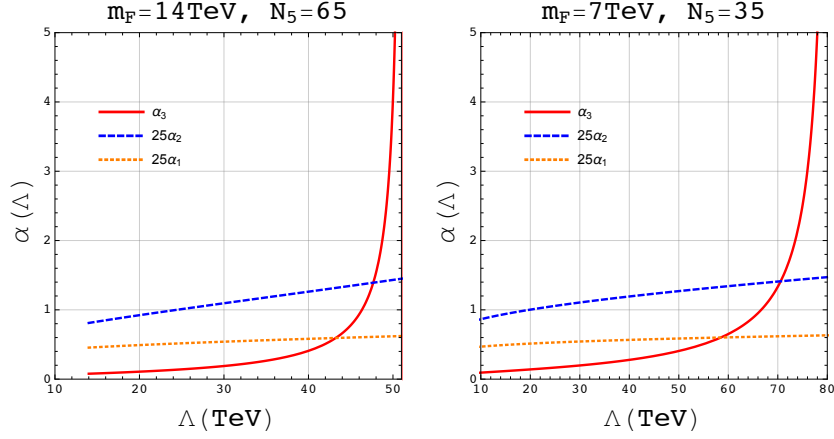


Figure 8: RG running of the SM gauge couplings above m_F for the two representative sets of values of $\{m_F, N_5\}$ shown as black dots in Fig. 7. The values of the couplings at the scale m_F is obtained using the SM evolution from M_Z to 2 TeV and the MSSM evolution from 2 TeV to m_F .

MASS OF SGOLDSTINO:

The fermion component of X - the goldstino - is exactly massless at tree-level (and even at one-loop level). The scalar component also remains massless at tree-level, but can get mass through quantum corrections at one-loop. The total mass of the sgoldstino can arise from messenger contributions added to any possible contribution from the hidden sector. The messenger contribution to the mass squared can be calculated to be

$$\Pi(p^2 = 0) = - \left(\frac{\lambda}{g_3^2} \right)^2 \left(4\pi \sqrt{\frac{5}{N_5}} F(\kappa) \right)^2 m_g^2 \quad (0.0.35)$$

where

$$F(x) = \sqrt{-G(x)/g(x)^2}; \quad G(x) = \frac{1}{x^2} [(2+x)\text{Ln}(1+x) + (2-x)\text{Ln}(1-x)]$$

and $g(x)$ is as defined in Eqn. 0.0.30.

This is manifestly negative and much larger in magnitude than the squared gluino mass. With the LHC constraining the gluino to very high masses (~ 1.8 TeV), a large contribution from the hidden sector is required to stabilise the potential and end up with ~ 750 GeV mass, a deeply uncomfortable fact for the minimal model. We see, therefore, that if the sgoldstino explanation of the 750 GeV diphoton excess - or any similar signal - is to be valid, we would have a model with rather improbable features. One can conclude, therefore, that this is unlikely to be an explanation of the observed signal. Our conclusion was, in a sense, vindicated, when it turned out that the observed signal was a mere statistical fluctuation and not a genuine scalar resonance.

Summary

This thesis work has invoked four different NP threads with the common factor being that they all predict signals at colliders at levels which are not currently observable, but would become so after sufficient running of the machines in question if the underlying NP model is correct. In the process, several detailed computations have been performed, and numerical analyses have been carried out keeping in mind the most currently available experimental data and constraints arising from them. We have also used some of the state-of-the-art techniques in the theoretical and computational analyses and in that sense, these represent the most up-to-date analyses of the processes in question.

Bibliography

- [1] D. Bardhan, G. Bhattacharyya, D. Ghosh, M. Patra and S. Raychaudhuri, Phys. Rev. D **94**, no. 1, 015026 (2016)
- [2] S. L. Glashow, J. Iliopoulos and L. Maiani, Phys. Rev. D **2**, 1285 (1970).
- [3] A. J. Buras, Acta Phys. Polon. B **34**, 5615 (2003) [hep-ph/0310208].
- [4] S. P. Martin, Adv. Ser. Direct. High Energy Phys. **21**, 1 (2010) [Adv. Ser. Direct. High Energy Phys. **18**, 1 (1998)] [hep-ph/9709356].
- [5] R. Barbier *et al.*, Phys. Rept. **420**, 1 (2005)
- [6] M. Chemtob and G. Moreau, Phys. Rev. D **61** (2000) 116004
- [7] Y. Amhis *et al.* [Heavy Flavor Averaging Group (HFAG)], arXiv:1412.7515 [hep-ex]
- [8] D. Bardhan, P. Byakti and D. Ghosh, JHEP **1701**, 125 (2017)
- [9] A. Abdesselam *et al.*, arXiv:1608.06391 [hep-ex].
- [10] J. A. Bailey *et al.* [MILC Collaborations], Phys. Rev. D **89**, no. 11, 114504 (2014)
- [11] I. Caprini, L. Lellouch and M. Neubert, Nucl. Phys. B **530**, 153 (1998)
- [12] D. Bardhan, A. Chakraborty, D. Choudhury, D. K. Ghosh and M. Maity, arXiv:1611.03846 [hep-ph]
- [13] J. Alwall *et al.*, JHEP **1407**, 079 (2014)
- [14] T. Sjostrand, S. Mrenna and P. Z. Skands, Comput. Phys. Commun. **178**, 852 (2008) doi:10.1016/j.cpc.2008.01.036 [arXiv:0710.3820 [hep-ph]]
- [15] J. de Favereau *et al.* [DELPHES 3 Collaboration], JHEP **1402**, 057 (2014) [arXiv:1307.6346 [hep-ex]]; J. Alwall *et al.*, JHEP **1407**, 079 (2014) [arXiv:1405.0301 [hep-ph]].

- [16] A. Hoecker, P. Speckmayer, J. Stelzer, J. Therhaag, E. von Toerne, and H. Voss, “TMVA: Toolkit for Multivariate Data Analysis,” PoS A CAT 040 (2007) [physics/0703039].
- [17] C. G. Lester and D. J. Summers, Phys. Lett. B **463**, 99 (1999) [hep-ph/9906349]; A. Barr, C. Lester and P. Stephens, J. Phys. G **29**, 2343 (2003) [hep-ph/0304226].
- [18] M. Cacciari, G. P. Salam and G. Soyez, Eur. Phys. J. C **72** (2012) 1896 [arXiv:1111.6097 [hep-ph]].
- [19] M. Cacciari, G. P. Salam and G. Soyez, JHEP **0804**, 063 (2008) [arXiv:0802.1189 [hep-ph]].
- [20] Y. L. Dokshitzer, G. D. Leder, S. Moretti and B. R. Webber, JHEP **9708**, 001 (1997) [hep-ph/9707323].
- [21] T. Plehn, M. Spannowsky, M. Takeuchi and D. Zerwas, JHEP **1010**, 078 (2010) [arXiv:1006.2833 [hep-ph]].
- [22] D. Krohn, J. Thaler and L. T. Wang, JHEP **1002**, 084 (2010) [arXiv:0912.1342 [hep-ph]].
- [23] J. Thaler and K. Van Tilburg, JHEP **1103**, 015 (2011) doi:10.1007/JHEP03(2011)015 [arXiv:1011.2268 [hep-ph]].
- [24] B. Bellazzini, R. Franceschini, F. Sala and J. Serra, JHEP **1604**, 072 (2016)
- [25] C. Petersson and R. Torre, Phys. Rev. Lett. **116**, no. 15, 151804 (2016)
- [26] S. V. Demidov and D. S. Gorbunov, JETP Lett. **103**, no. 4, 219 (2016)
- [27] J. A. Casas, J. R. Espinosa and J. M. Moreno, Phys. Lett. B **759**, 159 (2016)
- [28] R. Ding, Y. Fan, L. Huang, C. Li, T. Li, S. Raza and B. Zhu, Int. J. Mod. Phys. A **31**, no. 26, 1650151 (2016)
- [29] D. Bardhan, P. Byakti, D. Ghosh and T. Sharma, JHEP **1606**, 129 (2016)
- [30] P. Meade, N. Seiberg and D. Shih, Prog. Theor. Phys. Suppl. **177**, 143 (2009) doi:10.1143/PTPS.177.143 [arXiv:0801.3278 [hep-ph]].

List of Publications

PAPERS INCLUDED THIS THESIS:

1. *Detailed analysis of flavor-changing decays of top quarks as a probe of new physics at the LHC*
Debjyoti Bardhan, Gautam Bhattacharyya, Diptimoy Ghosh, Monalisa Patra, Sreerup Raychaudhuri
[Phys.Rev. D 94, 015026 (2016)]
2. *The 750 GeV diphoton resonance as an sgoldstino: a reappraisal*
Debjyoti Bardhan, Pritibhajan Byakti, Diptimoy Ghosh, Tarun Sharma
[JHEP 1606 (2016) 129]
3. *A closer look at the R_D and R_{D^*} anomalies*
Debjyoti Bardhan, Pritibhajan Byakti, Diptimoy Ghosh
[JHEP **1701**, 125 (2017)]
4. *Search for the bottom squarks in the baryonic R -parity violating MSSM*
Debjyoti Bardhan, Amit Chakraborty, Debajyoti Choudhury, Dilip Kumar Ghosh, Manas Maity
[arXiv:1611.03846 [hep-ph]] (To appear in PRD)

PAPERS NOT INCLUDED THIS THESIS:

1. *Radion Candidate for the LHC Diphoton Resonance*
Debjyoti Bardhan, Disha Bhatia, Amit Chakraborty, Ushoshi Maitra, Sreerup Raychaudhuri, Tousik Samui
[arXiv:1512.06674 [hep-ph]]
2. *Role of Tensor operators in R_K and R_{K^*}*
Debjyoti Bardhan, Pritibhajan Byakti, Diptimoy Ghosh
[arXiv:1705.09305 [hep-ph]] (Accepted in PLB)

Chapter 1

The Standard Model

1.1 Introduction

The Standard Model (SM) of particle physics is the central framework on which the study of elementary particles is currently based. It purports to answer the age-old question of what everything is made up of. With the SM, we have a viable theory encompassing three of the four fundamental interactions and all the elementary particles discovered so far.

There are two classes of elementary particles – fermions and bosons. Fermions, e.g. electrons, are spin- $\frac{1}{2}$ particles obeying the Pauli Exclusion principle, thereby following Fermi-Dirac statistics. Bosons, e.g. photons, are integer-spin particles which follow the Bose-Einstein statistics. While fermions appear to be the building blocks of matter, bosons are responsible for mediating the fundamental interactions.

The four fundamental interactions are the electromagnetic force, the weak (nuclear) force, the strong (nuclear) force and gravity. The first three are explained by the SM, while gravity is as yet explained only classically by the theory of General Relativity. Extensive attempts are being made to construct a quantum theory of gravity. All these interactions are believed to be mediated by integer spin particles – the three forces of the SM by spin-1 particles, viz. the photon and the W and Z bosons, while gravity is thought to be mediated by a spin-2 particle, viz. the graviton. The nature of all these interactions is understood in terms of certain underlying symmetries, which may or may not be partially broken. The mathematical tool employed to describe these symmetries is group theory.

The three interactions are described by three distinct groups corresponding to gauge symmetries. Electromagnetism is described by the Abelian gauge group $U(1)_Y$, while the non-Abelian groups $SU(2)_L$ and $SU(3)_C$ describe weak and strong interactions respectively. In this construction, the fermions belong to the fundamental representation of the groups and the gauge bosons are placed in the adjoint representation. The strength of interaction between these particles are fixed by the different charges these particles carry under the different

gauge groups.

In this chapter, we review the general gauge principle, along with the different gauge symmetries mentioned above. We then enlist the particle content of the SM and the charges of each under the different gauge groups before taking a brief look at the phenomenon of spontaneous symmetry breaking and the Higgs mechanism. This is followed by a discussion on global symmetries of the SM and finally by the different flavour changing processes, both via neutral and charged currents. Natural units ($\hbar = 1$ and $c = 1$) are used throughout.

1.2 Gauge Symmetries in the Standard Model

1.2.1 The Gauge Principle

A physical system described by multiple degrees of freedom can have several mathematically-equivalent descriptions. A transformation between two such equivalent descriptions is called a *symmetry transformation*. There are of two kinds, viz. *spacetime symmetries*, where the transformation is of the spacetime coordinates (the most general case is the Poincarè symmetry), and *internal symmetries*, where the transformation is of other degrees of freedom. Symmetry transformations governed by parameters that are spacetime-independent are called *global*; if the transformation parameters are functions of space-time they are *local*. Gauge symmetries are internal symmetries in a classical field theory involving specific redefinitions of the fields and can be both global and local.

The *gauge principle* is a postulate that every fundamental interaction is described by an action S which is invariant under some gauge transformations, i.e. by a *gauge theory*. Nöther's theorem then tells us that there must be associated conserved currents and charges. Historically, it was the discovery of these conservation laws which led to the development of gauge theories.

1.2.2 Abelian Symmetry : QED

Quantum Electrodynamics (QED) is the description of electromagnetic interactions of a Dirac fermion (typically the electron) by a gauge theory with a $U(1)_{\text{em}}$ symmetry. Fermions such as electrons, are charged under this $U(1)_{\text{em}}$ group i.e. they belong to its fundamental representation. Photons belong to the adjoint representation of the $U(1)_{\text{em}}$ gauge group. Gauge symmetry then dictates the form of the interactions between the spinor and bosonic fields, as follows.

The free electron Lagrangian is given by

$$\mathcal{L}_e = \bar{\psi}(x) (\gamma^\mu \partial_\mu - m) \psi(x) \quad (1.2.1)$$

where $\psi(x)$ is the electron spinor field. This term is evidently symmetric under a global $U(1)_{\text{em}}$ transformation (or a phase change)

$$\psi(x) \rightarrow \psi'(x) = \exp(-ie\theta)\psi(x) \quad (1.2.2)$$

where e is the gauge charge (in this case electric charge) of the fermion. Making this transformation local, i.e. taking the parameter of the transformation as $\theta = \theta(x)$, we have

$$\psi'(x) = \exp\{-ie\theta(x)\}\psi(x) \quad (1.2.3)$$

and the Lagrangian is no longer gauge symmetric since under this transformation, for we get

$$\bar{\psi}(x)\partial_\mu\psi(x) \rightarrow \bar{\psi}'(x)\partial_\mu\psi'(x) = \bar{\psi}(x)\partial_\mu\psi(x) - ie\bar{\psi}(x)\partial_\mu\theta(x)\psi(x) \quad (1.2.4)$$

To restore gauge invariance, we replace the derivative ∂_μ with a gauge-covariant derivative D_μ such that $D_\mu\psi(x)$ transforms as

$$D_\mu\psi(x) \rightarrow [D_\mu\psi(x)]' = e^{-ie\theta(x)}D_\mu\psi(x)$$

where $D_\mu = \partial_\mu + ieA_\mu(x)$ where we introduce a vector *gauge field* $A_\mu(x)$. Gauge invariance is then satisfied if $A_\mu(x)$ transforms as

$$A_\mu(x) \rightarrow A'_\mu(x) = A_\mu(x) + \frac{1}{e}\partial_\mu\theta(x) \quad (1.2.5)$$

The new gauge invariant Lagrangian is then

$$\mathcal{L}_{\text{eA}} = \bar{\psi}(x)i\gamma^\mu D_\mu\psi(x) - m\bar{\psi}(x)\psi(x) = \mathcal{L}_{\text{e}} + \mathcal{L}_{\text{int}} \quad (1.2.6)$$

where the covariant derivative term has automatically provided an interaction term between the spinor field $\psi(x)$ and the bosonic field $A_\mu(x)$ of the form

$$\mathcal{L}_{\text{int}} = -eJ^\mu(x)A_\mu(x)$$

where $J^\mu(x) = \bar{\psi}(x)\gamma^\mu\psi(x)$ is the Nöther current corresponding to the gauge symmetry.

The $U(1)_{\text{em}}$ -symmetric Lagrangian will also contain a kinetic term for the gauge field $A_\mu(x)$ which is given by

$$\mathcal{L}_{\text{A}} = -\frac{1}{4}F^{\mu\nu}(x)F_{\mu\nu}(x) \quad (1.2.7)$$

with a *field strength tensor*

$$F_{\mu\nu} = \partial_\mu A_\nu(x) - \partial_\nu A_\mu(x) = -\frac{i}{e}[D_\mu, D_\nu]$$

This is the minimal form required to preserve both gauge and Lorentz invariance. The full QED Lagrangian is now given by

$$\begin{aligned} \mathcal{L}_{\text{QED}} &= \mathcal{L}_{\text{e}} + \mathcal{L}_{\text{A}} + \mathcal{L}_{\text{int}} \\ &= \bar{\psi}(x)(\gamma^\mu\partial_\mu - m)\psi(x) - \frac{1}{4}F^{\mu\nu}(x)F_{\mu\nu}(x) - e\bar{\psi}(x)\gamma^\mu\psi(x)A_\mu(x) \end{aligned} \quad (1.2.8)$$

Gauge invariance not only determines the form of the Lagrangian and the interaction terms, it also precludes a mass term for the gauge field A_μ since a mass term of the form

$$\mathcal{L}_{\text{m}} = M_A^2 A^\mu(x)A_\mu(x)$$

is not gauge invariant. Further, there are no self-coupling terms for the A_μ field in the classical Lagrangian. Such terms can, however, arise at higher orders in a quantum field theory.

1.2.3 Non-Abelian Symmetry : QCD

This construction of a gauge theory can be repeated for the non-Abelian gauge group $SU(3)_C$, as follows. We first consider a Dirac fermion field $\Psi(x)$ in the fundamental (triplet) representation of $SU(3)_C$, i.e. having a *colour* quantum number 1. This can be written

$$\Psi = \begin{pmatrix} \psi_1 \\ \psi_2 \\ \psi_3 \end{pmatrix} \quad (1.2.9)$$

where the spacetime dependence is henceforth not indicated explicitly. This will have a Dirac adjoint

$$\bar{\Psi} = \left(\bar{\psi}_1 \quad \bar{\psi}_2 \quad \bar{\psi}_3 \right) . \quad (1.2.10)$$

This is really a triplet of mass-degenerate fermions ψ_1 , ψ_2 and ψ_3 carrying the third component of colour $+1$, 0 and -1 respectively. For the free Lagrangian analogous to Eqn. 1.2.6 for this colour triplet Ψ is

$$\mathcal{L}_\Psi = \bar{\Psi} (\gamma^\mu \partial_\mu - m) \Psi \quad (1.2.11)$$

where expansion of the mass term makes the mass-degeneracy of the ψ_1 , ψ_2 and ψ_3 fields explicit.

Now, under an $SU(3)_C$ transformation, with the strong coupling constant g_s replacing the electromagnetic e , we have

$$\Psi \rightarrow \Psi' = \exp \left(-ig_s \vec{\mathbb{T}} \cdot \vec{\theta} \right) \Psi = \mathbb{U}(\vec{\theta}) \Psi \quad (1.2.12)$$

where $\vec{\theta} = (\theta_1, \theta_2, \dots, \theta_8)$ are the $SU(3)_C$ transformation parameters, and $\mathbb{T}^a = \frac{1}{2}\lambda^a$ ($a = 1, 2, \dots, 8$) are the $SU(3)_C$ generators, with the λ^a being Gell-Mann matrices. For the Dirac adjoint, we will have

$$\bar{\Psi} \rightarrow \bar{\Psi}' = \bar{\Psi} \mathbb{U}^\dagger(\vec{\theta}) \quad (1.2.13)$$

It is simple to see that if the $\vec{\theta}$ are independent of spacetime, then the Lagrangian of Eqn. 1.2.11 will be invariant under global $SU(3)_C$ transformations. If, however, $\vec{\theta} = \vec{\theta}(x)$, then the kinetic term transforms as

$$\bar{\Psi} \gamma^\mu \partial_\mu \Psi \rightarrow \bar{\Psi}' \gamma^\mu \partial_\mu \Psi' = \bar{\Psi} \gamma^\mu \partial_\mu \Psi + \bar{\Psi} \gamma^\mu \mathbb{U}^\dagger(\vec{\theta}) \left[\partial_\mu \mathbb{U}(\vec{\theta}) \right] \Psi \quad (1.2.14)$$

and the second term on the right would break the gauge symmetry.

As before, gauge invariance can be restored by replacing the simple derivative ∂_μ by a covariant derivative

$$\partial_\mu \rightarrow \mathbb{D}_\mu = \mathbb{I} \partial_\mu - ig_s \vec{\mathbb{T}} \cdot \vec{G}_\mu \quad (1.2.15)$$

where the $\vec{G}_\mu = (G_\mu^1, G_\mu^2, \dots, G_\mu^8)$ are the 8 vector gauge fields (gluons) in the adjoint representation of $SU(3)_C$ and \mathbb{I} denotes the 3×3 unit matrix. Gauge invariance then demands

$$\vec{\mathbb{T}} \cdot \vec{G}'_\mu = \mathbb{U}(\vec{\theta}) \vec{\mathbb{T}} \cdot \vec{G}_\mu \mathbb{U}^\dagger(\vec{\theta}) - \frac{i}{g_s} [\partial_\mu \mathbb{U}(\vec{\theta})] \mathbb{U}^\dagger(\vec{\theta}) \quad (1.2.16)$$

Under infinitesimal transformations, i.e. $\theta^a \rightarrow 0$, we have

$$\mathbb{U}(\vec{\theta}, \theta_Y) = 1 - ig_s \vec{\mathbb{T}} \cdot \vec{\theta}_\mu$$

and the gluon fields transform as

$$G_\mu^{a'} = G_\mu^a - \frac{1}{g_s} \partial_\mu \theta^a + f^{abc} \theta^b G_\mu^c \quad (1.2.17)$$

where

$$[\mathbb{T}^a, \mathbb{T}^b] = i f^{abc} \mathbb{T}^c \quad (1.2.18)$$

with f^{abc} being the structure functions of the group.

We can now write a gauge-invariant Lagrangian as

$$\mathcal{L}_{\Psi G} = \bar{\Psi} (\gamma^\mu \mathbb{D}_\mu - m) \Psi = \mathcal{L}_\Psi - g_s \bar{\Psi} \gamma^\mu \vec{\mathbb{T}} \cdot \vec{G}_\mu \Psi \quad (1.2.19)$$

i.e. as in the Abelian case, the gauge symmetry enforces an interaction of the form

$$\mathcal{L}_{\text{int}} = -g_s \bar{\Psi} \gamma^\mu \vec{\mathbb{T}} \cdot \vec{G}_\mu \Psi \quad (1.2.20)$$

The gauge-kinetic term can now be written using the same prescription as in the Abelian case, i.e.

$$\mathcal{L}_G = -\frac{1}{12} \text{Tr} \left[\left(\vec{\mathbb{T}} \cdot \vec{G}^{\mu\nu} \right) \left(\vec{\mathbb{T}} \cdot \vec{G}_{\mu\nu} \right) \right] \quad (1.2.21)$$

where

$$\vec{\mathbb{T}} \cdot \vec{G}_{\mu\nu} = -\frac{i}{g_s} [\mathbb{D}_\mu, \mathbb{D}_\nu] \quad (1.2.22)$$

which yields

$$G_{\mu\nu}^a = \partial_\mu G_\nu^a - \partial_\nu G_\mu^a - ig_s f^{abc} G_\mu^b G_\nu^c$$

using the Lie algebra in Eqn. 1.2.18.

Thus, finally, the $\text{SU}(3)_C$ -invariant Lagrangian has the form

$$\begin{aligned} \mathcal{L}_{\text{QCD}} &= \mathcal{L}_\Psi + \mathcal{L}_G + \mathcal{L}_{\text{int}} \\ &= \bar{\Psi} (\gamma^\mu \partial_\mu - m) \Psi - \frac{1}{12} \text{Tr} \left[\left(\vec{\mathbb{T}} \cdot \vec{G}^{\mu\nu} \right) \left(\vec{\mathbb{T}} \cdot \vec{G}_{\mu\nu} \right) \right] - g_s \bar{\Psi} \gamma^\mu \vec{\mathbb{T}} \cdot \vec{G}_\mu \Psi \end{aligned} \quad (1.2.23)$$

It is worth mentioning two important points of difference with the Abelian case, viz.

1. In the Abelian case, at the lowest order, there is no self-interaction of the photon field A_μ , whereas the G_μ^a have mutual cubic and quartic interactions arising from the f^{abc} term in Eqn. 1.2.23.
2. While in the $\text{U}(1)_{\text{em}}$ case, the charge can be chosen at will, this is not possible for the $\text{SU}(3)_C$ case. For if we try to rescale the generators to $\alpha \mathbb{T}^a$, then Eqn. 1.2.18 would enforce $\alpha = 1$. The $\text{SU}(3)$ colour charge is thus universal and this property manifests itself as the universal nature of strong interactions.

As in the Abelian case, it is not possible to construct a mass term for the gauge bosons, for the form

$$\mathcal{L}_m = M_G^2 \vec{G}^\mu \cdot \vec{G}_\mu \quad (1.2.24)$$

would not be gauge invariant. Thus, the eight gluons in QCD are all massless.

1.2.4 Electroweak Symmetry

We now describe the extension of the gauge principle to the theory of weak interactions, constructing in the process a unifying framework for the electromagnetic and weak interactions. This is known as the *electroweak theory* of Glashow, Salam and Weinberg (GSW). The gauge group here is $SU(2) \times U(1)_Y$, with $U(1)_Y$ being different from $U(1)_{\text{em}}$. The construction of this non-Abelian theory is very similar to that of QCD.

In a toy version of the model (where both chiralities are equivalent), we first consider a Dirac fermion field $\Psi(x)$ in the fundamental (doublet) representation of $SU(2)$, i.e. having a *weak isospin* of $\frac{1}{2}$,

$$\Psi = \begin{pmatrix} \psi_1 \\ \psi_2 \end{pmatrix} \quad (1.2.25)$$

with a Dirac adjoint

$$\bar{\Psi} = \begin{pmatrix} \bar{\psi}_1 & \bar{\psi}_2 \end{pmatrix}. \quad (1.2.26)$$

Once again, these are really a pair of mass-degenerate fermions ψ_1 and ψ_2 carrying the third component of isospin $+\frac{1}{2}$ and $-\frac{1}{2}$ respectively.

Now, under an $SU(2) \times U(1)_Y$ transformation

$$\Psi \rightarrow \Psi' = \exp \left(-ig\vec{\tau} \cdot \vec{\theta} - ig'Y\eta\theta_Y \right) \Psi(x) = \mathbb{U}(\vec{\theta}, \theta_Y) \Psi \quad (1.2.27)$$

where $\vec{\theta} = (\theta_1, \theta_2, \theta_3)$ and θ_Y are the $SU(2)$ and $U(1)_Y$ transformation parameters respectively defining the unitary transformation matrix $\mathbb{U}(\vec{\theta}, \theta_Y)$. We denote the $SU(2)$ generators as $\tau^a = \frac{1}{2}\sigma^a$ ($a = 1, 2, 3$), where the σ^a are the Pauli spin matrices, while $\eta = \frac{1}{2}\mathbb{I}$ is the $U(1)_Y$ generator for the doublet with \mathbb{I} denoting the 2×2 unit matrix and Y the *weak hypercharge* of the doublet. Once again

$$\bar{\Psi} \rightarrow \bar{\Psi}' = \bar{\Psi} \mathbb{U}^\dagger(\vec{\theta}, \theta_Y) \quad (1.2.28)$$

for the Dirac adjoint. Now, the free Lagrangian analogous to Eqn. 1.2.6 for the fermion doublet Ψ is

$$\mathcal{L}_\Psi = \bar{\Psi} (\gamma^\mu \partial_\mu - m) \Psi \quad (1.2.29)$$

This Lagrangian is again invariant under a global transformation, but if $\vec{\theta} = \vec{\theta}(x)$ and $\theta_Y = \theta_Y(x)$, then the kinetic term transforms as

$$\bar{\Psi} \gamma^\mu \partial_\mu \Psi \rightarrow \bar{\Psi}' \gamma^\mu \partial_\mu \Psi' = \bar{\Psi} \gamma^\mu \partial_\mu \Psi + \bar{\Psi} \gamma^\mu \mathbb{U}^\dagger(\vec{\theta}, \theta_Y) \left[\partial_\mu \mathbb{U}(\vec{\theta}, \theta_Y) \right] \Psi \quad (1.2.30)$$

i.e. the gauge invariance is lost. As before, we then replace the simple derivative ∂_μ by a covariant derivative

$$\partial_\mu \rightarrow \mathbb{D}_\mu = \mathbb{I} \partial_\mu - ig\vec{\tau} \cdot \vec{W}_\mu - ig'Y\eta B_\mu \quad (1.2.31)$$

where the $\vec{W}_\mu = (W_\mu^1, W_\mu^2, W_\mu^3)$ and B_μ are the vector gauge fields in the adjoint representation of $SU(2) \times U(1)_Y$. Denoting

$$g\mathbb{A}_\mu = g\vec{\tau} \cdot \vec{W}_\mu + g'Y\eta B_\mu$$

so that

$$\mathbb{D}_\mu = \mathbb{I}\partial_\mu - ig\mathbb{A}_\mu$$

gauge invariance now demands

$$\mathbb{A}'_\mu = \mathbb{U}(\vec{\theta}, \theta_Y) \mathbb{A}_\mu \mathbb{U}^\dagger(\vec{\theta}, \theta_Y) - \frac{i}{g} [\partial_\mu \mathbb{U}(\vec{\theta}, \theta_Y)] \mathbb{U}^\dagger(\vec{\theta}, \theta_Y) \quad (1.2.32)$$

Under infinitesimal transformations, i.e. $\theta^a, \theta_Y \rightarrow 0$, we have

$$\mathbb{U}(\vec{\theta}, \theta_Y) = 1 - ig\vec{\tau} \cdot \vec{\theta}_\mu - ig'Y\eta\theta_Y$$

and the gauge fields transform as

$$W_\mu^{a'} = W_\mu^a - \frac{1}{g} \partial_\mu \theta^a + \epsilon^{abc} \theta^b W_\mu^c \quad B'_\mu = B_\mu - \frac{1}{g'Y} \partial_\mu \theta_Y \quad (1.2.33)$$

We can now write a gauge-invariant Lagrangian as

$$\mathcal{L}_{\Psi\mathbb{A}} = \bar{\Psi} (\gamma^\mu \mathbb{D}_\mu - m) \Psi = \mathcal{L}_\Psi - g \bar{\Psi} \gamma^\mu \mathbb{A}_\mu \Psi \quad (1.2.34)$$

i.e. we have an interaction term of the form

$$\mathcal{L}_{\text{int}} = -g \bar{\Psi} \gamma^\mu \mathbb{A}_\mu \Psi = -\bar{\Psi} \gamma^\mu \left(g\vec{\tau} \cdot \vec{W}_\mu + g'Y\eta B_\mu \right) \Psi \quad (1.2.35)$$

The gauge-kinetic term can now be written using the same prescription as in the Abelian case, i.e.

$$\mathcal{L}_\mathbb{A} = -\frac{1}{8g^2} \text{Tr} \left[\left(g\vec{\tau} \cdot \vec{F}^{\mu\nu} + g'Y\eta B^{\mu\nu} \right) \left(g\vec{\tau} \cdot \vec{F}_{\mu\nu} + g'Y\eta B_{\mu\nu} \right) \right] \quad (1.2.36)$$

where

$$g\vec{\tau} \cdot \vec{F}_{\mu\nu} + g'Y\eta B_{\mu\nu} = -i [\mathbb{D}_\mu, \mathbb{D}_\nu] \quad (1.2.37)$$

which yields

$$\begin{aligned} F_{\mu\nu}^a &= \partial_\mu W_\nu^a - \partial_\nu W_\mu^a - ig\epsilon^{abc} W_\mu^b W_\nu^c \\ B_{\mu\nu} &= \partial_\mu B_\nu^a - \partial_\nu B_\mu^a \end{aligned} \quad (1.2.38)$$

using the Lie algebra

$$[\tau^a, \tau^b] = i\epsilon^{abc} \tau^c \quad [\eta, \tau^a] = 0 \quad (1.2.39)$$

Thus, finally, the $\text{SU}(2) \times \text{U}(1)_Y$ Lagrangian has the form

$$\begin{aligned} \mathcal{L}_{\text{GSW}} &= \mathcal{L}_\Psi + \mathcal{L}_\mathbb{A} + \mathcal{L}_{\text{int}} \\ &= \bar{\Psi} (\gamma^\mu \partial_\mu - m) \Psi \\ &\quad - \frac{1}{8g^2} \text{Tr} \left[\left(g\vec{\tau} \cdot \vec{F}^{\mu\nu} + g'Y\eta B^{\mu\nu} \right) \left(g\vec{\tau} \cdot \vec{F}_{\mu\nu} + g'Y\eta B_{\mu\nu} \right) \right] \\ &\quad - g \bar{\Psi} \gamma^\mu \left(g\vec{\tau} \cdot \vec{W}_\mu + g'Y\eta B_\mu \right) \Psi \end{aligned} \quad (1.2.40)$$

As in the case of colour, the $\text{SU}(2)$ charge is universal and this manifests itself as the universal nature of weak interactions. And once again, a mass term for the gauge bosons

$$\mathcal{L}_m = M_W^2 \vec{W}^\mu \cdot \vec{W}_\mu + M_B^2 B^\mu B_\mu \quad (1.2.41)$$

would not be gauge invariant. Thus the four gauge bosons in this toy model — $W_\mu^1, W_\mu^2, W_\mu^3$ and B_μ — are all massless.

1.3 Electroweak Symmetry-Breaking

Though the gauge principle provides a good description of electrodynamics (QED) and of strong interactions (QCD), weak interactions require the vector bosons to be massive, to account for (a) the short-range nature of the weak interactions, and (b) the success of the effective four-fermion theory of Fermi. In fact, the weak bosons are known to have very large masses, which cannot be explained by having *approximate* gauge symmetries in the same spirit as we have approximate flavour symmetries. Thus, to explain these large masses, we require to invoke the phenomenon of *spontaneous symmetry-breaking* for the electroweak sector. This refers to the phenomenon in which the ground state of a system does not share the symmetry of the Lagrangian (\mathcal{L}_S). Thus, if U is some symmetry transformation, then for a spontaneously broken system

$$U\mathcal{L}_S U^{-1} = \mathcal{L}_S \quad (1.3.1)$$

but

$$U|0\rangle \neq |0\rangle \quad (1.3.2)$$

where $|0\rangle$ is the ground state of the system. Classic examples, known from condensed matter theory, are the Heisenberg ferromagnet and the Ginzburg -Landau theory of superconductivity. From our knowledge of these, we can easily infer that near the ground state, such a system undergoes a *phase transition* from a configuration with the symmetry, to one without the symmetry – with consequent changes in the physical behaviour.

In this section we describe how the electroweak symmetry based on the $SU(2) \times U(1)_Y$ group is spontaneously broken to yield a physically-viable theory.

1.3.1 Gauge Boson Masses

To break the $SU(2) \times U(1)_Y$ symmetry, we need to add to the theory with a fermion doublet and gauge bosons, a further doublet of complex scalars, i.e. another isospin- $\frac{1}{2}$ object

$$S(x) = \begin{pmatrix} s^+(x) \\ s^0(x) \end{pmatrix} = \frac{1}{\sqrt{2}} \begin{pmatrix} s_1 + is_2 \\ s_3 + is_4 \end{pmatrix} \quad (1.3.3)$$

where s^+ and s^0 are complex scalar fields which can be written in terms of real scalar fields s_1, s_2, s_3 and s_4 . The hypercharge of this doublet is $Y = +1$.

As in the case of the fermion, we can write a free Lagrangian for this scalar doublet in the form

$$\mathcal{L}_\Phi = (\mathbb{D}^\mu S)^\dagger (\mathbb{D}_\mu S) - M^2 S^\dagger S \quad (1.3.4)$$

with

$$\mathbb{D}_\mu = \partial_\mu - ig\vec{\tau} \cdot \vec{W}_\mu - ig'\eta B_\mu \quad (1.3.5)$$

where $\eta = \frac{1}{2}\mathbb{I}$ as before. The only difference from En. 1.2.31 is that we have put $Y = 1$.

The above Lagrangian has a local $SU(2) \times U(1)_Y$ symmetry and the gauge bosons are massless as before. There is no scope for spontaneous symmetry-breaking with this Lagrangian. We, therefore, modify it to the form

$$\mathcal{L}_V = (\mathbb{D}^\mu S)^\dagger (\mathbb{D}_\mu S) + \mu^2 S^\dagger S - \lambda (S^\dagger S)^2 \quad (1.3.6)$$

where $\mu^2, \lambda > 0$. The μ^2 term can no longer be called a mass term, for such a mass would be tachyonic and therefore, non-physical. Thus, these two interaction terms can be combined into a *scalar potential*

$$V(S) = -\mu^2 S^\dagger S + \lambda (S^\dagger S)^2 \quad (1.3.7)$$

and the Lagrangian written as

$$\mathcal{L}_V = (\mathbb{D}^\mu S)^\dagger (\mathbb{D}_\mu S) - V(S) \quad (1.3.8)$$

The vacuum will correspond to the minimum of this scalar potential, which will clearly be at

$$\langle S^\dagger S \rangle = \frac{\mu^2}{2\lambda} \equiv \frac{v^2}{2} \quad (1.3.9)$$

i.e.

$$\langle s_1^2 \rangle + \langle s_2^2 \rangle + \langle s_3^2 \rangle + \langle s_4^2 \rangle = v^2 \quad (1.3.10)$$

This is the surface of a four-sphere in the Euclidean space of ϕ 's, all points of which are potential minima, i.e. vacua of the quantum field theory. However, only one point on this surface can be the physical vacuum. We now note that the Lagrangian, too, has a global $SO(4)$ invariance corresponding to rotations in the Euclidean space of s 's, which is known as *reparametrisation invariance*. We exploit this to ensure that the physical vacuum falls on the s_3 axis, i.e.

$$\langle s_3 \rangle = v \quad \langle s_1 \rangle = \langle s_2 \rangle = \langle s_4 \rangle = 0$$

or

$$\langle S \rangle = \frac{1}{\sqrt{2}} \begin{pmatrix} 0 \\ v \end{pmatrix} \quad (1.3.11)$$

The global $SO(4)$ broken by this choice of axes is actually a subgroup of the $SU(2)$ gauge group, and hence, this choice of vacuum breaks the gauge symmetry. This is, therefore, a case of spontaneous symmetry-breaking.

We now define a new set of scalars in the neighbourhood of the vacuum by

$$\varphi_3 = s_3 - v \quad \varphi_i = s_i \quad \text{for } i = 1, 2, 4 \quad (1.3.12)$$

so that

$$\Phi = S - \langle S \rangle = \begin{pmatrix} \varphi^+(x) \\ \varphi^0(x) \end{pmatrix} = \frac{1}{\sqrt{2}} \begin{pmatrix} \varphi_1 + i\varphi_2 \\ \varphi_3 + i\varphi_4 \end{pmatrix} \quad (1.3.13)$$

The Lagrangian for the scalar field now becomes

$$\mathcal{L}_V = [\mathbb{D}^\mu (\Phi + \langle S \rangle)]^\dagger [\mathbb{D}_\mu (\Phi + \langle S \rangle)] - V(\Phi) \quad (1.3.14)$$

where

$$V(\Phi) = -\mu^2(\Phi + \langle S \rangle)^\dagger(\Phi + \langle S \rangle) + \lambda[(\Phi + \langle S \rangle)^\dagger(\Phi + \langle S \rangle)]^2 \quad (1.3.15)$$

Of particular interest in this case are the terms in Eqn. 1.3.14 of the form

$$\begin{aligned} \mathcal{L}_m &= [\mathbb{D}^\mu \langle S \rangle]^\dagger \mathbb{D}_\mu \langle S \rangle \\ &= \langle S \rangle^\dagger \left(ig\vec{\tau} \cdot \vec{W}^\mu + ig'\eta B^\mu \right) \left(-ig\vec{\tau} \cdot \vec{W}_\mu - ig'\eta B_\mu \right) \langle S \rangle \end{aligned} \quad (1.3.16)$$

which are easily recognised as mass terms for the W and B bosons. These are now permitted because the gauge symmetry has been broken by the vacuum.

The gauge boson mass term now expands to

$$\begin{aligned} \mathcal{L}_m &= \frac{1}{8}g^2v^2(W_{1\mu}W_1^\mu + W_{2\mu}W_2^\mu) \\ &+ \frac{1}{8}v^2 \begin{pmatrix} W_3^\mu & B^\mu \end{pmatrix} \begin{pmatrix} g^2 & -gg' \\ gg' & g'^2 \end{pmatrix} \begin{pmatrix} W_{3\mu} \\ B_\mu \end{pmatrix} \end{aligned} \quad (1.3.17)$$

We can now define physical fields

$$\begin{aligned} W_\mu^+ &= \frac{1}{\sqrt{2}}(W_\mu^1 - iW_\mu^2) \\ W_\mu^- &= \frac{1}{\sqrt{2}}(W_\mu^1 + iW_\mu^2) \\ Z_\mu &= W_\mu^3 \cos \theta_W + B_\mu \sin \theta_W \\ A_\mu &= -W_\mu^3 \sin \theta_W + B_\mu \cos \theta_W \end{aligned} \quad (1.3.18)$$

where $\tan \theta_W = g'/g$. In terms of these, the mass terms reduce to

$$\mathcal{L}_m = M_W^2 W^{+\mu} W_\mu^- + \frac{1}{2} M_Z^2 Z^\mu Z_\mu \quad (1.3.19)$$

with

$$M_W = \frac{gv}{2} \quad M_Z = \frac{gv}{2 \cos \theta_W}$$

We note that the A_μ field still has zero mass, and we identify it as the photon. Moreover, we can define a ‘ ρ parameter’ (often called Veltman parameter) [20]:

$$\rho = \frac{M_W^2}{M_Z^2 \cos^2 \theta_W} = 1 \quad (1.3.20)$$

which is a prediction of this pattern of symmetry breaking. The covariant derivative in Eqn. 1.3.5 can now be written in terms of these fields

$$\mathbb{D}_\mu = \partial_\mu - ig(\tau_+ W_\mu^+ + \tau_- W_\mu^-) + ig \cos \theta_W \tau_Z Z_\mu + ig \sin \theta_W Q A_\mu \quad (1.3.21)$$

and the electroweak generators as

$$\tau_\pm = \frac{1}{\sqrt{2}}(\tau_1 \pm i\tau_2) \quad \tau_Z = \tau_3 - \eta \tan^2 \theta_W \quad Q = \tau_3 + \eta = \tau_3 + \frac{1}{2}\mathbb{I} \quad (1.3.22)$$

Identification of the photon with A_μ implies that $g \sin \theta_W = e$ and Q is the generator of $SU(2)_{\text{em}}$. In general, it will also contain the Y quantum number and its eigenvalues will be $i_3 + \frac{Y}{2}$. This justifies the charge assignments of s^+ and s^0 at the beginning of this section.

1.3.2 The Higgs Mechanism

Expansion of the scalar potential in Eqn.1.3.15 leads to a form

$$V(\Phi) = \frac{1}{4}\lambda v^4 - v(\mu^2 - \lambda v^2)\varphi_3 - \frac{1}{2}(\mu^2 - \lambda v^2)(\varphi_1^2 + \varphi_2^2 + \varphi_3^2 + \varphi_4^2) + \lambda v^2\varphi_3^2 + \dots \quad (1.3.23)$$

where the ellipsis denotes cubic and quartic interaction terms. We can now drop the constant term (except for cosmological considerations) and note that since $v^2 = \mu^2/2\lambda$, the potential simplifies to

$$V(\Phi) = \lambda v^2\varphi_3^2 + \dots \quad (1.3.24)$$

The Lagrangian will now contain a mass term of the correct sign for the φ_3 scalar, of the form

$$\mathcal{L}_m(\varphi_3) = \frac{1}{2}M_3^2\varphi_3^2 \quad (1.3.25)$$

where $M_3 = \sqrt{2}\mu$. This massive scalar is known as the *Higgs boson*. However, the φ_1 , φ_2 and φ_3 bosons, which are massless, also appear in the Lagrangian. These are known as *Goldstone bosons* and we do not have any experimental evidence for such massless scalar particles. However, it turns out that these are actually unphysical degrees of freedom of the theory and can be easily eliminated. To see this, we note that the initial scalar doublet could have been parametrised in polar form as

$$S(x) = \frac{1}{\sqrt{2}} \exp\left(\frac{i}{v}\vec{\tau} \cdot \vec{\xi}(x)\right) \begin{pmatrix} 0 \\ v + H(x) \end{pmatrix} \quad (1.3.26)$$

where $\vec{\xi} = (\xi_1, \xi_2, \xi_3)$ is a triplet of scalar fields and H is another scalar field. Clearly we will have

$$\langle \xi_1 \rangle = \langle \xi_2 \rangle = \langle \xi_3 \rangle = \langle H \rangle = 0$$

to be consistent with En. 1.3.11. Expanding the exponential in the neighbourhood of the vacuum (i.e. $\xi^a \ll v$) enables us to identify $H = \varphi_3$.

Now, since we are going to break the gauge symmetry anyway, we can initially exploit the unbroken symmetry to make a local gauge transformation

$$\begin{aligned} S \rightarrow S' &= \frac{1}{\sqrt{2}} \mathbb{U}(\vec{\theta}, \theta_Y) S \\ &= \frac{1}{\sqrt{2}} \mathbb{U}(\vec{\theta}, \theta_Y) \exp\left(\frac{i}{v}\vec{\tau} \cdot \vec{\xi}(x)\right) \begin{pmatrix} 0 \\ v + H(x) \end{pmatrix} \end{aligned} \quad (1.3.27)$$

where the parameters $\vec{\theta}, \theta_Y$ are chosen to make

$$\mathbb{U}(\vec{\theta}, \theta_Y) \exp\left(\frac{i}{v}\vec{\tau} \cdot \vec{\xi}(x)\right) = \mathbb{I}$$

Using the form of Eqn. 1.2.27, it is easy to check that this choice of gauge parameters is just

$$\vec{\theta}(x) = \frac{1}{gv}\vec{\xi}(x) \quad \theta_Y = 0 \quad (1.3.28)$$

This choice defines the so-called *unitary gauge*. In this gauge, we have

$$S' = \frac{1}{\sqrt{2}} \begin{pmatrix} 0 \\ v + H(x) \end{pmatrix} \quad (1.3.29)$$

Thus, in this gauge, which is the physically interpretable gauge, we have a massive Higgs scalar, but no Goldstone scalars. The degrees of freedom represented by the ξ^a fields in the unbroken theory reappear as the longitudinal modes of the massive gauge bosons W^\pm, Z . In the broken theory, therefore the Goldstone bosons must be regarded as mere gauge artefacts, and they therefore can be removed by an appropriate gauge choice – as we have shown. This feature of the electroweak symmetry is known as the *Higgs mechanism*.

We can now combine the Lagrangian of a fermion doublet Ψ with that of the Higgs doublet Φ to obtain a toy version of the GSW electroweak model. In the next section, we show how this is built upon to get the SM.

1.4 Construction of the Standard Model

1.4.1 Gauge interactions of fermions

The gauge interactions of a fermion doublet with weak isospin Y are given by Eqn. 1.2.35, which can be combined with eqn. 1.3.22 to write

$$\mathcal{L}_{\text{int}} = \bar{\Psi} \gamma^\mu [g (\tau_+ W_\mu^+ + \tau_- W_\mu^-) + g \cos \theta_W \tau_Z Z_\mu + e Q A_\mu] \Psi \quad (1.4.1)$$

For this representations, the electroweak generators can be calculated from Eqn. 1.3.22 as

$$\begin{aligned} \tau_+ &= \frac{1}{\sqrt{2}} \begin{pmatrix} 0 & 1 \\ 0 & 0 \end{pmatrix} \\ \tau_- &= \frac{1}{\sqrt{2}} \begin{pmatrix} 0 & 0 \\ 1 & 0 \end{pmatrix} \\ \tau_Z &= \frac{1}{\cos^2 \theta_W} \begin{pmatrix} 1 - q_1 \sin^2 \theta_W & 0 \\ 0 & -(1 + q_2 \sin^2 \theta_W) \end{pmatrix} \\ Q &= \begin{pmatrix} q_1 & 0 \\ 0 & q_2 \end{pmatrix} \end{aligned}$$

where $q_1 = \frac{1+Y}{2}$ and $q_2 = \frac{-1+Y}{2}$. Plugging these into En. 1.4.1 leads to

$$\mathcal{L}_{\text{int}} = \mathcal{L}_{\text{cc}} + \mathcal{L}_{\text{nc}} + \mathcal{L}_{\text{em}} \quad (1.4.2)$$

where the three terms on the right are given by

$$\begin{aligned} \mathcal{L}_{\text{cc}} &= \frac{g}{\sqrt{2}} (\bar{\psi}_1 \gamma^\mu \psi_2 W_\mu^+ + \bar{\psi}_2 \gamma^\mu \psi_1 W_\mu^-) \\ \mathcal{L}_{\text{nc}} &= \frac{g}{\cos \theta_W} (1 - q_1 \sin^2 \theta_W) \bar{\psi}_1 \gamma^\mu \psi_1 Z_\mu - \frac{g}{\cos \theta_W} (1 + q_2 \sin^2 \theta_W) \bar{\psi}_2 \gamma^\mu \psi_2 Z_\mu \\ \mathcal{L}_{\text{em}} &= e q_1 \bar{\psi}_1 \gamma^\mu \psi_1 A_\mu + e q_2 \bar{\psi}_2 \gamma^\mu \psi_2 A_\mu \end{aligned} \quad (1.4.3)$$

and are known as the *charged current*, *neutral current* and *electromagnetic* interactions respectively. The last of these, is identical with the case of QED discussed above if we put $q = -1$ for the electron field.

1.4.2 Chiral Fermions

In the 1950's it was established [8–10, 12–14] that weak interactions violate parity maximally. This is best expressed in the language of gauge theory as a statement that the W^\pm -bosons interact only with the left-chiral components of fermion fields and not with their right-chiral components. It is thus appropriate to attach a subscript ‘L’ (for left) and call the symmetry group $SU(2)_L \times U(1)_Y$. Under $SU(2)_L$, the left-handed fermions form doublets and the right-handed fermions are singlets. Thus, we denote a pair of fermions as

$$\Psi_L = \begin{pmatrix} \psi_{1L} \\ \psi_{2L} \end{pmatrix} \quad \psi_{1R} \quad \psi_{2R} \quad (1.4.4)$$

where, in general, $\psi_L = \frac{1}{2}(1 - \gamma_5)\psi$ and $\psi_R = \frac{1}{2}(1 + \gamma_5)\psi$. We have already seen that the pattern of electroweak symmetry-breaking leads us to identify the electric charge $q = i_3 + Y/2$, where the i_3 and Y are the weak isospin and weak hypercharge assignments of a field. Since $i_3 = \pm\frac{1}{2}$ for the left-handed fields and $i_3 = 0$ for the right handed fields, it follows that they must have different Y assignments so that the electric charge can be the same. The interactions in Eqn. 1.4.3 can then be rewritten in the more realistic form

$$\begin{aligned} \mathcal{L}_{cc} &= \frac{g}{2\sqrt{2}} [\bar{\psi}_{1L}\gamma^\mu\psi_{2L}W_\mu^+ + \bar{\psi}_{2L}\gamma^\mu\psi_{1L}W_\mu^-] \\ \mathcal{L}_{nc} &= \frac{g}{4\cos\theta_W} [(1 - 4q_1\sin^2\theta_W)\bar{\psi}_{1L}\gamma^\mu\psi_{1L}Z_\mu - (1 + 4q_2\sin^2\theta_W)\bar{\psi}_{2L}\gamma^\mu\psi_{2L}Z_\mu] \\ &\quad - \frac{2g\sin^2\theta_W}{\cos\theta_W} [q_1\bar{\psi}_{1R}\gamma^\mu\psi_{1R}Z_\mu + q_2\bar{\psi}_{2R}\gamma^\mu\psi_{2R}Z_\mu] \\ \mathcal{L}_{em} &= e [q_1\bar{\psi}_1\gamma^\mu\psi_1A_\mu + q_2\bar{\psi}_2\gamma^\mu\psi_2A_\mu] \end{aligned} \quad (1.4.5)$$

We note that since both the chiralities have the same electric charge, the electromagnetic current is of parity-conserving form, whereas the charged and neutral currents are manifestly parity-violating.

Thus far, we have discussed only a toy model with a non-specific fermion doublet. In the SM, however, we have two classes of chiral fermions, with the left-handed doublets denoted as

$$L_L = \begin{pmatrix} \nu_{\ell L} \\ \ell_L \end{pmatrix} \quad Q_L = \begin{pmatrix} u_L \\ d_L \end{pmatrix} \quad (1.4.6)$$

while e_R , u_R and d_R denote the right-handed singlet fields. The ℓ and ν_ℓ are the *lepton* and its *neutrino*, while the u and d are a pair of *quarks*. To get the correct charge assignments for leptons, we choose $Y = -1$ and for quarks, we choose $Y = \frac{1}{3}$. These values of Y must be taken into account when writing the covariant derivatives in the electroweak Lagrangian. We have also seen that strong interactions are described by the $SU(3)_C$ group, where the

interactions respect parity, i.e. they are the same for right- and left-handed quarks. Leptons do not carry the colour charge and are unaffected by strong interactions. Thus, the gauge quantum number assignments of the leptons and quarks are as summarised in Table 1.1.

	Left-Handed Fields				Right-Handed Fields			
		$SU(3)_C$	$SU(2)_L$	$U(1)_Y$		$SU(3)_C$	$SU(2)_L$	$U(1)_Y$
Quarks	$Q_L = \begin{pmatrix} u_L \\ d_L \end{pmatrix}$	3	2	$+\frac{1}{3}$	u_R d_R	3 3	1 1	$+\frac{4}{3}$ $-\frac{2}{3}$
Leptons	$L_L = \begin{pmatrix} \nu_{\ell L} \\ \ell_L \end{pmatrix}$	1	2	-1	e_R ν_R	1 0	1 0	-2 0

Table 1.1: The fermion content of the SM along with their charges under the different direct product gauge groups.

It is worth mentioning at this stage itself that normally there is no right-handed neutrino in the minimal SM, as such a particle would be a singlet under all the SM gauge groups. However, after the discovery of neutrino oscillations, naive extensions of the SM do have a right-handed neutrino. In this discussion, however, it will not be considered further.

In the unbroken phase of the electroweak model, all these fermions are massless, since a fermion mass term

$$\mathcal{L}_m^{(f)} = m\bar{\psi}\psi = m(\bar{\psi}_L\psi_R + \bar{\psi}_R\psi_L)$$

will clearly break the gauge symmetry, as ψ_L and ψ_R transform differently under $SU(2)_L$. Fermion masses, then, must arise from the spontaneous symmetry-breaking, for which they must interact with the scalars of the theory. The simplest way to achieve this is to introduce Yukawa-like operators of the form $\bar{\psi}\psi\phi$ in the Lagrangian. This is discussed in the next section. However, at this point it may be noted that in the unbroken phase of the electroweak model, all the particles are massless – the gauge bosons because of gauge symmetry, the scalars because the quadratic term is tachyonic and the fermions from a combination of parity violation and gauge symmetry. It follows that *all* particle masses arise from the spontaneous breaking of electroweak symmetry.

Though this is not demanded by any symmetry arguments, the SM has three copies or generations of the leptons and quarks, each with the same representation and charges as described above. In the gauge symmetric phase of the SM, the three generations are identical to each other; it is only after the introduction of the Higgs scalar and the breaking of gauge symmetry that the generations become non-degenerate in terms of mass. We thus have up (u), down (d), strange (s), charm (c), bottom (b) and top (t) quarks respectively, in increasing order of mass. These can be arranged in three families of weak-isopin doublets and singlets

$$\begin{pmatrix} u_L \\ d_L \end{pmatrix}; \quad \begin{pmatrix} c_L \\ s_L \end{pmatrix}; \quad \begin{pmatrix} t_L \\ b_L \end{pmatrix}; \quad u_R; \quad d_R; \quad c_R; \quad s_R; \quad t_R; \quad b_R \quad (1.4.7)$$

We must remember that each of these fields is a colour triplet. Thus, if we count all quantum numbers, there are 18 quarks in all.

Similarly, there are three generations of leptons – electrons, muons and tau leptons – along with their respective neutrino partners, which can also be arranged as

$$\begin{pmatrix} \nu_{eL} \\ e_L \end{pmatrix}; \quad \begin{pmatrix} \nu_{\mu L} \\ \mu_L \end{pmatrix}; \quad \begin{pmatrix} \nu_{\tau L} \\ \tau_L \end{pmatrix}; \quad e_R; \quad \mu_R; \quad \tau_R \quad (1.4.8)$$

These are colour singlets and hence there are just 3 leptons and 3 neutrinos.

To get the full particle content of the SM, now, we must add on the 8 gluons, the 4 electroweak bosons and the massive Higgs boson, making a total of 37 fields in all. Often this count is given as 25 if the differently-coloured quarks are not considered distinct.

1.4.3 Fermion Masses

It has been mentioned in the previous section that fermion masses must be generated through spontaneous symmetry-breaking through Yukawa-like interactions between the fermions and the Higgs scalars. Since there are three generations, the most general gauge-invariant interactions have the form

$$\mathcal{L}_{Sf} = y_{ij}^d \bar{Q}_{Li}^{(0)} S d_{Rj}^{(0)} + y_{ij}^u \bar{Q}_{Li}^{(0)} \tilde{S} u_{Rj}^{(0)} + y_{ij}^\ell \bar{L}_{Li}^{(0)} S e_{Rj}^{(0)} + \text{H.c.} \quad (1.4.9)$$

where $\tilde{S} = -i\tau_2 S^*$ is the charge conjugate of the S doublet and summation is implied over the generation indices $i, j = 1, 2, 3$. These generation indices are intended as follows $u_1 = u$, $u_2 = c$, $u_3 = t$ and so on. The Yukawa couplings y_{ij}^d , y_{ij}^u and y_{ij}^ℓ then form a set of three 3×3 complex matrices, i.e. 54 real parameters in all. However, most of them are not measurable, as is shown below. The superscript ‘(0)’ is a reminder that these fermion fields (gauge basis) are not the physical fields, which will be defined presently. It is also relevant to mention that there is no term of the form $y_{ij}' \bar{L}_{Li} \tilde{S} \nu_{Rj}$ because of the absence of the ν_{Rj} ’s, at least in this discussion.

Once the electroweak symmetry is broken, the scalar field must be shifted $S = \Phi + \langle S \rangle$ and this leads to

$$\mathcal{L}_{Sf} = \mathcal{L}_{\text{Yuk}} + \mathcal{L}_{\text{m}}^{(f)} \quad (1.4.10)$$

where

$$\mathcal{L}_{\text{Yuk}} = y_{ij}^d \bar{Q}_{Li}^{(0)} \Phi d_{Rj}^{(0)} + y_{ij}^u \bar{Q}_{Li}^{(0)} \tilde{\Phi} u_{Rj}^{(0)} + y_{ij}^\ell \bar{L}_{Li}^{(0)} \Phi e_{Rj}^{(0)} + \text{H.c.} \quad (1.4.11)$$

are the Yukawa interactions and

$$\mathcal{L}_{\text{m}}^{(f)} = y_{ij}^d \bar{Q}_{Li}^{(0)} \langle S \rangle d_{Rj}^{(0)} + y_{ij}^u \bar{Q}_{Li}^{(0)} \langle \tilde{\Phi} \rangle u_{Rj}^{(0)} + y_{ij}^\ell \bar{L}_{Li}^{(0)} \langle S \rangle e_{Rj}^{(0)} + \text{H.c.} \quad (1.4.12)$$

is the mass term for the fermions. This expands to

$$\begin{aligned} \mathcal{L}_{\text{m}}^{(f)} &= \frac{y_{ij}^d v}{\sqrt{2}} \bar{d}_{Li}^{(0)} d_{Rj}^{(0)} + \frac{y_{ij}^u v}{\sqrt{2}} \bar{u}_{Li}^{(0)} u_{Rj}^{(0)} + \frac{y_{ij}^\ell v}{\sqrt{2}} \bar{\ell}_{Li}^{(0)} \ell_{Rj}^{(0)} + \text{H.c.} \\ &= M_{ij}^d \bar{d}_{Li}^{(0)} d_{Rj}^{(0)} + M_{ij}^u \bar{u}_{Li}^{(0)} u_{Rj}^{(0)} + M_{ij}^\ell \bar{\ell}_{Li}^{(0)} \ell_{Rj}^{(0)} + \text{H.c.} \end{aligned} \quad (1.4.13)$$

These mass matrices \mathbb{M}^u , \mathbb{M}^d and \mathbb{M}^ℓ , can always be diagonalised by bi-unitary transformations of the form

$$\begin{aligned}\mathbb{M}_D^u &= \mathbb{V}_L^u \mathbb{M}^u \mathbb{V}_R^{u\dagger} = \text{diag.} (m_u, m_c, m_t) \\ \mathbb{M}_D^d &= \mathbb{V}_L^d \mathbb{M}^d \mathbb{V}_R^{d\dagger} = \text{diag.} (m_d, m_s, m_b) \\ \mathbb{M}_D^\ell &= \mathbb{V}_L^\ell \mathbb{M}^\ell \mathbb{V}_R^{\ell\dagger} = \text{diag.} (m_e, m_\mu, m_\tau)\end{aligned}\quad (1.4.14)$$

Thus, Eqn. 1.4.13 becomes

$$\begin{aligned}\mathcal{L}_m^{(f)} &= \bar{d}_{Li}^{(0)} (V_L^d)_{ik} M_{kl}^d (V_R^{d\dagger})_{lj} d_{Rj}^{(0)} + \bar{u}_{Li}^{(0)} (V_L^u)_{ik} M_{kl}^u (V_R^{u\dagger})_{lj} u_{Rj}^{(0)} + \bar{\ell}_{Li}^{(0)} (V_L^\ell)_{ik} M_{kl}^\ell (V_R^{\ell\dagger})_{lj} e_{Rj}^{(0)} + \text{H.c.} \\ &= \bar{d}_{Li} (M_D^d)_{ij} d_{Rj} + \bar{u}_{Li} (M_D^u)_{ij} u_{Rj} + \bar{\ell}_{Li} (M_D^\ell)_{ij} e_{Rj} + \text{H.c.} \\ &= m_i^d \bar{d}_i d_i + m_i^u \bar{u}_i u_i + m_i^\ell \bar{\ell}_i \ell_i\end{aligned}\quad (1.4.15)$$

where we define physical fermion fields (mass basis) by

$$\begin{aligned}d_{Li} &= (V_L^d)_{ij} d_{Lj}^{(0)} & d_{Ri} &= (V_R^d)_{ij} d_{Rj}^{(0)} \\ u_{Li} &= (V_L^u)_{ij} u_{Lj}^{(0)} & u_{Ri} &= (V_R^u)_{ij} u_{Rj}^{(0)} \\ \ell_{Li} &= (V_L^\ell)_{ij} \ell_{Lj}^{(0)} & \ell_{Ri} &= (V_R^\ell)_{ij} \ell_{Rj}^{(0)}\end{aligned}\quad (1.4.16)$$

and the m_i^u , m_i^d and m_i^ℓ are the mass eigenvalues listed in Eqn. 1.4.14.

1.4.4 Flavour Mixing

It is important to note that the gauge boson-fermion interactions listed in Eqn. 1.4.5 are for fermions in the gauge basis, denoted above by the superscript '(0)'. To get realistic interactions, we require to rewrite them in the physical or mass basis, and this leads to the phenomenon of flavour-mixing in the SM.

We first consider the charged current interactions, which, in the gauge basis, have the form

$$\begin{aligned}\mathcal{L}_{cc} &= \frac{g}{\sqrt{2}} \left[\bar{u}_{Li}^{(0)} \gamma^\mu d_{Li}^{(0)} W_\mu^+ + \bar{\nu}_{Li}^{(0)} \gamma^\mu \ell_{Li}^{(0)} W_\mu^+ \right] + \text{H.c.} \\ &= \frac{g}{\sqrt{2}} \left[\bar{u}_{Li} (\mathbb{V}_L^u)_{ik} \gamma^\mu (\mathbb{V}_L^d)_{jk}^* d_{Lj} W_\mu^+ + \bar{\nu}_{Li}^{(0)} \gamma^\mu (\mathbb{V}_L^\ell)_{ji}^* \ell_{Lj} W_\mu^+ \right] + \text{H.c.}\end{aligned}\quad (1.4.17)$$

In the above, we have the freedom to redefine physical neutrino fields as

$$\nu_{Li} = (\mathbb{V}_L^\ell)_{ij} \nu_{Lj}^{(0)} \quad (1.4.18)$$

since there was no neutrino mass matrix, but there is no more freedom in the case of the quark fields. Accordingly, Eqn. 1.4.17 assumes the form

$$\mathcal{L}_{cc} = \frac{g}{\sqrt{2}} \left[V_{ij} \bar{u}_{Li} \gamma^\mu d_{Lj} W_\mu^+ + \bar{\nu}_{Li} \gamma^\mu \ell_{Lj} W_\mu^+ \right] + \text{H.c.} \quad (1.4.19)$$

where

$$\mathbb{V} = \mathbb{V}_L^u \mathbb{V}_L^{d\dagger} \quad (1.4.20)$$

is the Cabibbo-Kobayashi-Maskawa matrix, or *CKM matrix*. Since this is non-diagonal, it follows that charged current interactions can have quarks of different generations (and hence flavours), with interaction strengths proportional to the off-diagonal elements of the CKM matrix. This phenomenon is referred to as *flavour-mixing* in the charged current sector of the electroweak Lagrangian. It is important to note that there is no reason to suppose that $\mathbb{V}_L^u = \mathbb{V}_L^d$, which would make the charged currents diagonal and remove flavour mixing from the SM. At the same time, there is no *a priori* reason compelling $\mathbb{V}_L^u \neq \mathbb{V}_L^d$, for no principle would be violated by such a choice. Thus, all that we can say is that the SM can nicely accommodate flavour mixing, but not that it predicts flavour-mixing. The fact that $\mathbb{V}_L^u \neq \mathbb{V}_L^d$ is something which we must – and do – infer from empirical evidences.

1.4.5 Absence of FCNCs

When we turn to the neutral current, i.e. the current coupling to the Z boson, we have, in the gauge basis,

$$\begin{aligned}
\mathcal{L}_{\text{nc}} &= \frac{g}{4 \cos \theta_W} \left[\left(1 - \frac{8}{3} \sin^2 \theta_W\right) \bar{u}_{Li}^{(0)} \gamma^\mu u_{Li}^{(0)} Z_\mu - \left(1 - \frac{4}{3} \sin^2 \theta_W\right) \bar{d}_{Li}^{(0)} \gamma^\mu d_{Li}^{(0)} Z_\mu \right] \\
&+ \frac{g}{4 \cos \theta_W} \left[\bar{\nu}_{Li}^{(0)} \gamma^\mu \nu_{Li}^{(0)} Z_\mu - (1 - 4 \sin^2 \theta_W) \bar{\ell}_{Li}^{(0)} \gamma^\mu \ell_{Li}^{(0)} Z_\mu \right] \\
&- \frac{2g \sin^2 \theta_W}{\cos \theta_W} \left[\frac{2}{3} \bar{u}_{Ri}^{(0)} \gamma^\mu u_{Ri}^{(0)} Z_\mu - \frac{1}{3} \bar{d}_{Ri}^{(0)} \gamma^\mu d_{Ri}^{(0)} Z_\mu - \bar{\ell}_{Ri}^{(0)} \gamma^\mu \ell_{Ri}^{(0)} Z_\mu \right] \\
&= \frac{g}{4 \cos \theta_W} \left[\left(1 - \frac{8}{3} \sin^2 \theta_W\right) \bar{u}_{Li} (\mathbb{V}_L^u)_{ik} \gamma^\mu (\mathbb{V}_L^u)^*_{jk} u_{Lj} Z_\mu \right. \\
&\quad \left. - \left(1 - \frac{4}{3} \sin^2 \theta_W\right) \bar{d}_{Li} (\mathbb{V}_L^d)_{ik} \gamma^\mu (\mathbb{V}_L^d)^*_{jk} d_{Lj} Z_\mu \right] \\
&+ \frac{g}{4 \cos \theta_W} \left[\bar{\nu}_{Lj} (\mathbb{V}_L^\ell)_{ji} \gamma^\mu (\mathbb{V}_L^\ell)^*_{ki} \nu_{Lk} Z_\mu - (1 - 4 \sin^2 \theta_W) \bar{\ell}_{Lj} (\mathbb{V}_L^\ell)_{ji} \gamma^\mu (\mathbb{V}_L^\ell)^*_{ki} \ell_{Lk} Z_\mu \right] \\
&- \frac{2g \sin^2 \theta_W}{\cos \theta_W} \left[\frac{2}{3} \bar{u}_{Ri} (\mathbb{V}_R^u)_{ik} \gamma^\mu (\mathbb{V}_R^u)^*_{jk} u_{Rj} Z_\mu - \frac{1}{3} \bar{d}_{Ri} (\mathbb{V}_R^d)_{ik} \gamma^\mu (\mathbb{V}_R^d)^*_{jk} d_{Rj} Z_\mu \right. \\
&\quad \left. - \bar{\ell}_{Rj} (\mathbb{V}_R^\ell)_{ji} \gamma^\mu (\mathbb{V}_R^\ell)^*_{ki} \ell_{Rk} Z_\mu \right] \\
&= \frac{g}{4 \cos \theta_W} \left[\left(1 - \frac{8}{3} \sin^2 \theta_W\right) \bar{u}_{Lj} \gamma^\mu u_{Lj} Z_\mu - \left(1 - \frac{4}{3} \sin^2 \theta_W\right) \bar{d}_{Lj} \gamma^\mu d_{Lj} Z_\mu \right] \\
&+ \frac{g}{4 \cos \theta_W} \left[\bar{\nu}_{Lj} \gamma^\mu \nu_{Lj} Z_\mu - (1 - 4 \sin^2 \theta_W) \bar{\ell}_{Lj} \gamma^\mu \ell_{Lj} Z_\mu \right] \\
&- \frac{2g \sin^2 \theta_W}{\cos \theta_W} \left[\frac{2}{3} \bar{u}_{Rj} \gamma^\mu u_{Rj} Z_\mu - \frac{1}{3} \bar{d}_{Rj} \gamma^\mu d_{Rj} Z_\mu - \bar{\ell}_{Rj} \gamma^\mu \ell_{Rj} Z_\mu \right] \tag{1.4.21}
\end{aligned}$$

using the unitary property of the \mathbb{V} matrices. Thus, there are no flavour-changing neutral currents (FCNCs) in the SM. This can be expressed in words by saying that physical fermions of the same charge are *aligned*, whereas those of dissimilar charges are not aligned, with the off-diagonal part of the CKM matrix being a measure of the degree of mis-alignment.

We also have the electromagnetic currents

$$\begin{aligned} \mathcal{L}_{\text{em}} = e \left[\frac{2}{3} \bar{u}_{Li}^{(0)} \gamma^\mu u_{Li}^{(0)} A_\mu + \frac{2}{3} \bar{u}_{Ri}^{(0)} \gamma^\mu u_{Ri}^{(0)} A_\mu - \frac{1}{3} \bar{d}_{Li}^{(0)} \gamma^\mu d_{Li}^{(0)} A_\mu - \frac{1}{3} \bar{d}_{Ri}^{(0)} \gamma^\mu d_{Ri}^{(0)} A_\mu \right. \\ \left. - \bar{\ell}_{Li}^{(0)} \gamma^\mu \ell_{Li}^{(0)} A_\mu - \bar{\ell}_{Ri}^{(0)} \gamma^\mu \ell_{Ri}^{(0)} A_\mu \right] \end{aligned} \quad (1.4.22)$$

which also remains diagonal in flavour as the chiral fermions in every current are aligned. Similar arguments show that scalar currents coupling to the Higgs boson are also similarly diagonal. Thus, we conclude that there are no flavour- changing neutral currents (vector, scalar or electromagnetic) in the SM at the tree level. We note that this a firm prediction of the SM, and not just a feature which can be accommodated. At the one-loop and higher levels, however, FCNC's can appear through intermediate charged currents and this has been observed in many experiments.

1.4.6 CP Violation

In the electromagnetic Lagrangian, there are three discrete symmetries, viz. charge conjugation (C), parity (P) and time reversal (T), and therefore, all product transformations like CP and CPT are also symmetries. In fact, it can be shown from very general field theoretic considerations that CPT is a symmetry of the action, except in pathological exceptions constructed for that specific purpose. This is known as the CPT theorem.

In the weak interactions, however, we have seen that parity P is not conserved. Since particles are taken to antiparticles by charge conjugation C , and antiparticles have opposite parity, it was initially thought that CP is conserved in the weak interactions. In 1964, however, it was discovered that CP is violated in neutral kaon decays.

If we write the SM Lagrangian in the form

$$\mathcal{L}_{\text{SM}} = \mathcal{L}_{\text{gauge}}(e, g_2, g_s) + \mathcal{L}_\Phi(\mu, \lambda) + \mathcal{L}_Y(m_f, \mathbb{V}_{CKM}) + \mathcal{L}_{\text{g-f}}(\xi) + \mathcal{L}_{\text{FP}}(\xi) \quad (1.4.23)$$

in the R_ξ gauge, with m_f generically denoting all the fermion masses, and the last two terms denoting the gauge-fixing and ghost terms required for quantisation. Then, under a CP transformation,

$$\begin{aligned} \mathcal{L}_{\text{SM}} &\rightarrow (CP) \mathcal{L}_{\text{SM}} (CP)^\dagger \\ &= \mathcal{L}_{\text{gauge}}(e, g_2, g_s) + \mathcal{L}_\Phi(\mu, \lambda) + \mathcal{L}_Y(m_f, \mathbb{V}_{CKM}^\dagger) + \mathcal{L}_{\text{gf}}(\xi) + \mathcal{L}_{\text{FP}}(\xi) \end{aligned} \quad (1.4.24)$$

where every term is invariant except the Yukawa term, where, in general $\mathbb{V}_{CKM}^\dagger \neq \mathbb{V}_{CKM}$. Once again, we do not know this *a priori*, so all that we can say is that CP violation can be accommodated in the SM by having nonzero phase(s) in the CKM matrix. The fact that $\mathbb{V}_{CKM}^\dagger \neq \mathbb{V}_{CKM}$ is something which we must – and do – infer from empirical evidences.

If we consider the Lagrangian for QCD in Eqn. (1.2.24), it can be easily seen that it is invariant under CP . However, there is no known principle which can prevent us from adding a term

which violates the CP symmetry, viz.

$$\mathcal{L}_{CP} = -\frac{\Theta}{16\pi^2} F_{\mu\nu}^a \tilde{F}^{a\mu\nu} \quad (1.4.25)$$

where $\tilde{F}^{a\mu\nu} = \frac{1}{2}\epsilon^{\mu\nu\rho\sigma} F_{\rho\sigma}^a$ and Θ is a free parameter. This term contributes to the neutron electric dipole momenta (NEDM) and thus experiments measuring NEDM can put bounds on the value of Θ . The current bound on Θ is so stringent that many believe that the value is actually zero, which leaves us with a fine-tuning problem. This is known as the *strong-CP problem*. We return to this in Chapter 2.

1.4.7 Global Symmetries in the SM

Besides the discrete spacetime symmetries C , P and T mentioned above, the SM has a large group of continuous global symmetries [25, 26], which are termed *accidental symmetries*, since they follow from the construction of the SM Lagrangian, rather than from any fundamental principle. Let us consider the fermion sector first. The global symmetry, in the absence of Yukawa matrices ($y = 0$), is

$$G_{\text{global}}^{(y=0)} = U(3)_Q \times U(3)_U \times U(3)_D \times U(3)_L \times U(3)_E \quad (1.4.26)$$

where each of the symmetry groups represent the flavour symmetry for the left-handed quarks (Q), the right-handed up-type quarks (U), the right-handed down-type quarks (D), the left-handed leptons (L) and the right-handed charged leptons (E).

Considering just the lepton sector

$$G_{\text{global}}^{\ell; (y=0)} = U(3)_L \times U(3)_E \quad (1.4.27)$$

The group $U(3)$ has 9 generators and thus $G_{\text{global}}^{\ell; (y=0)}$ has 18 generators. The Yukawa matrix in the lepton sector is a 3×3 complex matrix with 18 parameters (9 real and 9 imaginary). Non-zero Yukawa matrix elements break this symmetry to

$$U(3)_L \times U(3)_E \rightarrow U(1)_e \times U(1)_\mu \times U(1)_\tau \quad (1.4.28)$$

where each $U(1)$ corresponds to the lepton number for each generation. Thus, there are 3 unbroken generators and 15 broken generators. These broken generators allow us to rotate away a similar number of Yukawa parameters, thus leaving us with $18 - 15 = 3$ independent physical parameters, which can be readily identified with the masses of the electron, muon and tau. The rest are all absorbed in the lepton wavefunctions and do not appear in any physical process. What we are left with however, is three conserved quantum numbers L_e , L_μ and L_τ , which are the *lepton numbers*.

When we turn to the quark sector, we have

$$G_{\text{global}}^{q; (y=0)} = U(3)_Q \times U(3)_U \times U(3)_D \quad (1.4.29)$$

Thus $G_{\text{global}}^{q;(y=0)}$ has 27 generators. As before, the Yukawa matrices in the quark sector are 3×3 complex matrices with 36 parameters (18 real and 18 imaginary). Non-zero Yukawa matrix elements break this symmetry to

$$U(3)_Q \times U(3)_U \times U(3)_D \rightarrow U(1)_B \quad (1.4.30)$$

where $U(1)_B$ is the baryon number symmetry. The breaking leaves us with only one unbroken generator from the initial 27, meaning that there are 26 broken generators. These broken generators allow us to rotate away a similar number of Yukawa parameters, thus leaving us with $36 - 26 = 10$ independent physical parameters. Out of these 10, 6 are quark masses and the other 4 are parameters of the CKM matrix. 3 of the CKM parameters are angles and 1 is a phase. The discussion in the previous section then tells us that this phase is the only source of CP violation in the SM. It is noteworthy that this phase does not appear with less than three generations of quarks – the brilliant conclusion of Kobayashi and Maskawa in 1973 [28].

The Higgs sector also has a global ‘custodial’ symmetry. The orbit structure of the Higgs field after acquiring a vev is

$$s_1^2 + s_2^2 + s_3^2 + s_4^2 = v^2 \quad (1.4.31)$$

where $s_i, i = 1 \dots 4$ are the four components of the complex Higgs doublet S . This has a global $SO(3)$ symmetry, left over from the global $SO(4)$ of the Higgs field before electroweak symmetry breaking. Since the $SO(3)$ group is homomorphic to the $SU(2)$ group, the custodial symmetry group may be regarded as a global $SU(2)$, which survives even after symmetry-breaking. Various consequences of this custodial symmetry are discussed in Ref. [29].

1.5 Flavour Changing Processes in the SM Quark Sector

We have seen that flavour changes through charged-current processes happen at the tree level in the SM through the exchange of a charged W boson. In contrast, there are no flavour-changing neutral currents (FCNCs) at the tree level in the SM. However, as mentioned before, FCNCs can occur through quantum corrections involving one-loop diagrams and higher. Obviously, these effects would be weaker as they would be subject to the usual loop suppressions. A few charged and neutral current processes along with their SM branching ratios (BRs) are tabulated in Table 1.2. These experimental numbers make it obvious that flavour changing processes via charged currents have higher BRs compared to those via neutral current processes. However, it is to be noted that the difference in the BRs is absent if the process doesn’t involve any overall change in flavour, as in the decay of $J/\psi \rightarrow \mu^+ \mu^-$ given in Table 1.2, which has a much higher BR compared to seemingly similar processes listed in the table.

Neutral Currents		Charged Currents	
Process	BR	Process	BR
$B^0 \rightarrow X_s \gamma$	$(3.40 \pm 0.21) \times 10^{-4}$	$B \rightarrow X \mu \nu_\mu$	$(10.86 \pm 0.16)\%$
$B^0 \rightarrow K^0 \mu^+ \mu^-$	$(4.4 \pm 0.4) \times 10^{-7}$	$B_s^0 \rightarrow X \ell \nu_\ell$	$(10.5 \pm 0.8)\%$
$B_s \rightarrow \mu^+ \mu^-$	$(3.1 \pm 0.7) \times 10^{-9}$	$D^- \rightarrow K^0 \mu^+ \nu_\mu$	$(3.31 \pm 0.13)\%$
$J/\psi \rightarrow \mu^+ \mu^-$	$(5.96 \pm 0.03)\%$	$K^+ \rightarrow \mu^+ \nu_\mu$	$(63.55 \pm 0.11)\%$

Table 1.2: Some examples of neutral and charged current processes. All numbers are taken from the Particle Data Group [346].

It has also been mentioned above that all flavour-changing effects can be ultimately attributed to the off-diagonal elements in the CKM matrix. Charged currents are important for measuring these CKM matrix elements and this is summarised in Table 1.3.

CKM Element	Value	Process
$ V_{ud} $	0.9749 ± 0.0026	$\pi^+ \rightarrow \pi^0 e^+ \nu_e$
	$0.97425^{+0.00007}_{-0.00010}$	Average
$ V_{us} $	0.2220 ± 0.0025	$K \rightarrow \pi^0 e^+ \nu_e$
	0.2254 ± 0.0004	Average
$ V_{ub} $	0.00365 ± 0.00014	$B \rightarrow \pi \ell \bar{\nu}_\ell$
	0.00371 ± 0.00007	Average
$ V_{cd} $	0.214 ± 0.009	$D \rightarrow \pi \ell \bar{\nu}_\ell$
	0.2253 ± 0.0004	Average
$ V_{cs} $	0.997 ± 0.017	$D_s \rightarrow K \ell \nu_\ell$
	0.9734 ± 0.0001	Average
$ V_{cb} $	0.0422 ± 0.0008	$B \rightarrow D^* \ell \bar{\nu}_\ell$
	$0.0418^{+0.0003}_{-0.0007}$	Average

Table 1.3: Showing some of the charged current processes which are helpful in determining the CKM matrix elements. All the the values for the individual processes are taken from [31]. The averages are the latest values presented by CKMFitter [32].

For precise measurements, semileptonic decays are generally preferred. This is because in the fully hadronic decays, gluons can be exchanged between the initial and the final state, whereas this is absent in the case of the semileptonic case (as shown in Fig. 1.1). Thus there is less uncertainty due to QCD effects in the latter.

In addition to loop suppression, FCNC processes are also subject to the Glashow-Iliopoulos-Maiani (GIM) mechanism [30]. It originates from the unitarity of the CKM matrix and results in suppression of the amplitudes of FCNC processes by several orders of magnitude. This is discussed in detail in Chapter 3.

One of the most important experimental observations is the oscillation in neutral mesons. This was first observed in the Kaon system ($K^0 - \bar{K}^0$ oscillation) and now it has been measured in other systems like the D^0 and the B^0 mesons. In the light of the importance of these oscillations especially in the measurement of the amount of CP violation in each of these systems, it is worthwhile to take a formal look at neutral meson oscillations and how it is important in the measurement of CP violation. This is done in Appendix A.

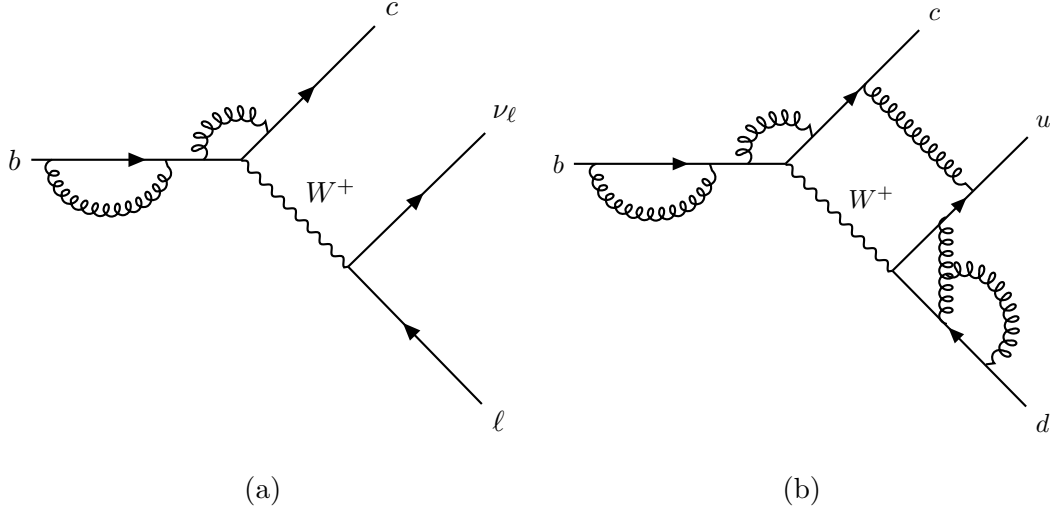


Figure 1.1: Showing possible gluon exchanges which explain why the semi-leptonic decay in (a) has less QCD effects than the fully hadronic one in (b).

The initial and final states of neutral current decays can either be up-type quarks or down-type quarks. The presence of a loop in the decay dictates that all quarks of the opposite type contribute in the loop. Since the top is much more massive than any of the other quarks, even being several times as massive of the b quark, the heaviest down-type quark, neutral currents for b-mesons, for example $B^0 \rightarrow K^0$ decay, have very different decay widths compared to $t \rightarrow c$ decays, the up-type analogy.

Extensive experimental data have been gathered for neutral current decays in b - as well as s - mesons. These are considered fertile hunting grounds for New Physics (NP) as any NP particle would contribute in the loop and enhance the matrix element. Again, semileptonic decays are preferred as they suffer from less QCD uncertainties. NP searches can also be carried out in the top FCNCs. Since the top quark doesn't hadronize, it is protected from much of the QCD effects. Furthermore, the top FCNC decay to a charm quark and a Z or a Higgs boson has an extremely small branching ratio in the SM ($\sim 10^{-15}$), which makes it conducive for NP searches as any enhancement of the signal can be easily distinguished from the tiny SM contribution. The $t \rightarrow cH$ and $t \rightarrow cZ$ decays are studied in great detail in Chapter 3. In recent times, there have been a lot of attention devoted to processes like $B \rightarrow D\ell\nu_\ell$ and $B \rightarrow D^*\ell\nu_\ell$ since experimental observations seem to show violation in lepton universality. In particular, the two ratios R_D and R_{D^*} defined as

$$R_{D^{(*)}} = \frac{\text{Br}(B \rightarrow D^{(*)}\tau\nu_\tau)}{\text{Br}(B \rightarrow D^{(*)}\ell\nu_\ell)}; \quad \ell = e, \mu \quad (1.5.1)$$

are shown to deviate from the theoretical SM values. We discuss this anomaly in detail in Chapter 4.

General references used for writing this chapter are [38], [39], [40], [41] and [37]. More specific references have been cited as and when relevant.

Beyond the Standard Model

2.1 New Physics beyond the Standard Model

The Standard Model, despite its somewhat ad hoc structure, has been amazingly successful in explaining the results of practically all terrestrial experiments conducted till date, with the exception of a few small anomalies of questionable permanence. With the possible exception of General Relativity, no other modern theory has enjoyed such a long and uninterrupted run of success. Nevertheless, despite all these successes, the SM fails to provide satisfactory explanations to a number of questions. These, and speculations about their solutions, form the substance of the present discussion.

This chapter is divided into three main parts. The first part is devoted to the problems and perceived shortcomings of the Standard Model. In the second part, a few of the better-known new physics (NP) solutions to some of these problems are elaborated. The third part discusses the most popular NP structure within which many of these can be solved. viz., supersymmetry.

2.2 Shortcomings of the Standard Model

In the previous chapter we have seen how the fundamental interactions can be described by gauge theories. These work nicely for electromagnetic and strong interactions, but in order to get a valid theory for the weak interactions, we require to combine it with electromagnetism in a unified theory, and then introduce a scalar potential with $\lambda\phi^4$ interactions, as well as put in parity violation by hand and then utilise the scope for flavour and CP violation. Because these disconnected ideas have been thrown in for purely phenomenological reasons to create the electroweak model, purists have always felt that the SM is not a final theory, but an effective low-energy limit of a more complete theory, which may be manifest at higher energies. Some of these NP ideas are discussed in the next section, but here we introduce

some of the well-known deficiencies of the SM. These can be grouped into (a) problems in the classical structure of SM, (b) problems in the quantum mechanical structure of the SM, and (x) phenomenological problems with the SM.

2.2.1 Problems in the Classical Structure of the SM

The structural problems with the classical version are

- A. Accidental symmetries leading to conservation of baryon (B) and lepton (L) number,
- B. Maximal parity violation,
- C. The flavour problem(s),
- D. The origin of spontaneous symmetry-breaking.

Each item is discussed below.

A. Accidental B & L conservation

Once the SM Lagrangian has been fully constructed in accordance with the principles of gauge invariance and renormalisability, it turns out to have a set of residual global symmetries which are not demanded by any fundamental principle. Two of these accidental symmetries are baryon number (B) and (total) lepton number (L). Gauge-invariant operators which break these symmetries do not appear in the SM because, given the SM field content, the simplest constructions are of mass dimension greater than 4, and therefore non-renormalisable. For example, the simplest L -violating operator has dimension five and is of the form $(L\phi)^2$, while the simplest B -violating operator has dimension six and is of the form $(QQ)(QL)$. Misiak *et al.* [42] list the relevant six-dimensional operators as

L Violating	$\mathcal{O}_{\nu\nu} = (\tilde{\phi}^\dagger l_p) C (\tilde{\phi}^\dagger l_r)$
B Violating	$\mathcal{O}_{duq} = \varepsilon^{\alpha\beta\gamma} \varepsilon_{jk} \left[(d_p^\alpha)^T C u_r^\beta \right] \left[(q_s^{\gamma j})^T C l_t^k \right]$ $\mathcal{O}_{qqu} = \varepsilon^{\alpha\beta\gamma} \varepsilon_{jk} \left[(q_p^{\alpha j})^T C q_r^{\beta k} \right] \left[(u_s^\gamma)^T C e_t \right]$ $\mathcal{O}_{qqq} = \varepsilon^{\alpha\beta\gamma} \varepsilon_{jn} \varepsilon_{km} \left[(q_p^{\alpha j})^T C q_r^{\beta k} \right] \left[(q_s^{\gamma m})^T C l_t^n \right]$ $\mathcal{O}_{duu} = \varepsilon^{\alpha\beta\gamma} \left[(d_p^\alpha)^T C u_r^\beta \right] \left[(u_s^\gamma)^T C e_t \right]$

Despite their ad hoc nature, these two accidental symmetries have stood up to a number of very rigorous tests. These fall in three categories:

1. $\Delta B = \Delta L = 1$; $\Delta(B-L) = 0$: The prototype search for this kind of B and L violation is the proton decay. If B and L were simultaneously violated, then the proton should decay through the process $p^+ \rightarrow \pi^0 e^+$. Proton decay searches started in the 1970s (including the pioneering Kolar gold mine experiment in India) and are continuing, but no decay has ever been recorded. The Kolar experiment gave a lower limit on the proton

lifetime of 3×10^{31} years [43]. This has since been improved greatly to a stringent lower bound of 1.6×10^{34} years by the SuperKamiokande collaboration [44] in Japan.

2. $\Delta B = 2$, $\Delta L = 0$; $\Delta(B - L) = 2$: An example of a process of this kind is $n - \bar{n}$ oscillations where n is a neutron. Several experiments are searching for signals of this oscillation, like SuperKamiokande [45]. Current lower bounds on the oscillation lifetime is 1.9×10^{32} years. (For a full review of experimental results, see Ref. [46].)
3. $\Delta B = 0$, $\Delta L = 2$; $\Delta(B - L) = -2$: This process is studied through the search for neutrinoless double beta decay (NDBD). It is being actively searched for by various groups around the world, including GERDA (which uses Germanium) and KamLAND (which uses Xenon). The current lower limit on the decay half-life from ^{76}Ge due to the GERDA experiment is $t^{1/2} \sim 2.2 \times 10^{25}$ years. (For a detailed review, see Ref. [47].)

While the listed experiments search for violation of total lepton number $L = \frac{1}{3}(L_e + L_\mu + L_\tau)$, there might be violation in the individual lepton flavours L_e, L_μ, L_τ . Such processes are allowed in the SM, but occur only at the loop level and are thus highly suppressed. Examples of such processes are $\mu \rightarrow e\gamma$ and $\tau \rightarrow 3e$. The former is being investigated at the MEG experiment which has observed an upper limit on the branching ratio, $\mathcal{B}(\mu^+ \rightarrow e^+\gamma) < 4.2 \times 10^{-13}$ [48]. The $\tau \rightarrow 3\mu$ process is being studied in Belle experiment [49].

Another manifestation of lepton flavour violation is in the neutrino sector, where the three neutrino fields ν_e, ν_μ and ν_τ , carrying L_e, L_μ and L_τ respectively can mix with each other. This is now established beyond doubt [50–53], though the exact mechanism is still unclear (see Section 2.3.2).

B. Maximal parity violation

In Chapter 1, Section 1.4.2, it was mentioned that parity is maximally violated in the SM. This is because the weak bosons $W_\mu^a (a = 1, 2, 3)$ — before spontaneous symmetry-breaking — interact exclusively with the left handed fermions and not at all with right handed ones, leading to a $V - A$ structure of the W_μ^\pm couplings. Though this is an experimentally well-established fact about weak interactions, there is nothing in the SM which explains a priori why it should be so. To take a contrary example, the $W_\mu^a (a = 1, 2, 3)$ could have coupled to both left- and right-chiral fermions with different strengths, and we would still have parity violation, though it would not be maximal. The SM accommodates the maximal nature of the parity-violation by setting the weak isospin of the right-chiral fermions to zero — this is done in a purely ad hoc manner, without any deeper insight. What makes the issue even more intriguing is that neither QED nor QCD violates parity at all, the theories being vectorlike.

C. Flavour Problem in the SM

The flavour sector of the SM is perhaps the one which contains the largest number of puzzles [54, 55]. They can be divided into the three segments described below.

1. *Number of fermion families:* As the couplings of the Z boson include an axial vector component, there will be one-loop diagrams in the quantum theory, leading to a chiral anomaly in the SM. It turns out that when this is summed over a full generation of quark and lepton doublets, the anomaly cancels. This is a beautiful feature of the SM about which we have no deeper insight than the fact that it happens. Thus, equality of the number of quark and lepton doublets is necessary for anomaly cancellation and we also know that at least three generations are needed for the existence of CP violation — which means that the SM does have the *minimal* structure needed for both these empirically-demanded features. However, there is no theoretical restriction on the existence of a larger number of generations than three. On the other hand, experimental evidence appears to tell us that there are only the three generations already known and no more [56]. The natural question to ask then is why we have *exactly* the minimal number (3) of families of quarks and leptons needed to make the SM work at both the classical and quantum levels. Does some deeper underlying feature manifest itself in this apparent parsimony of Nature?
2. *Hierarchy of quark and lepton masses:* The masses of charged fermions span a large number of scales, even apart from the neutrinos which are massless in the original version of the SM. If all the fermion masses are indeed provided by the Higgs mechanism — for which we have increasingly sound empirical evidence (see, e.g., Fig. 13 in [57]) — the magnitudes of the Yukawa couplings will have a correspondingly large hierarchy, varying from that of the electron ($y_e \sim 10^{-4}$) to that of the top quark ($y_t \sim 1$). The origins of such a steep hierarchy are completely unknown.

If we include neutrino masses, and assume they come from the same mechanism as those of the other fermions, the largest Yukawa coupling would be of the order of $y_\nu \sim 10^{-13}$, which is so much smaller than the top quark Yukawa coupling that it is widely believed that there is some suppression mechanism at work, or that, alternatively, neutrinos acquire their masses through some other mechanism altogether. Either hypothesis takes us beyond the SM.

3. *Hierarchy in the CKM matrix:* As Table 1.3 makes clear, the CKM matrix is nearly a unit matrix; the off-diagonal elements are quite small compared to the diagonal elements. All that the theory requires, however, is that the CKM matrix should be unitary. If the CKM matrix is parametrised as

$$\mathbb{V}_{CKM} = \begin{pmatrix} c_{12}c_{13} & s_{12}c_{13} & s_{13}e^{-i\delta^{CP}} \\ -s_{12}c_{23} - c_{12}s_{23}s_{13}e^{i\delta^{CP}} & c_{12}c_{23} - s_{12}s_{23}s_{13}e^{i\delta^{CP}} & s_{23}c_{13} \\ s_{12}s_{23} - c_{12}c_{23}s_{13}e^{i\delta^{CP}} & -c_{12}s_{23} - s_{12}c_{23}s_{13}e^{i\delta^{CP}} & c_{23}c_{13} \end{pmatrix} \quad (2.2.1)$$

where $s_{ij} = \sin \theta_{ij}$, $c_{ij} = \cos \theta_{ij}$ and δ^{CP} is the CKM phase, then experimental data can be combined to get

$$\theta_{12} \simeq 13.0^\circ \quad \theta_{23} \simeq 2.3^\circ \quad \theta_{13} \simeq 0.2^\circ \quad \delta^{CP} \simeq 70^\circ \quad (2.2.2)$$

It is clear that the mixing between generations is generically small and there is a strong hierarchy here too, with the third generation having small mixing with the second and almost vanishing mixing with the first. On the other hand, the CP -violating phase is large. However, a basis-independent measure of CP -violation is not the phase per se, but a combination of CKM elements known as the Jarlskog invariant, which is defined by

$$\begin{aligned} J_{CP} &= \text{Im} (V_{ik}^* V_{jk} V_{il} V_{jl}^*) \quad (i, j, k, l = 1, 2, 3) \\ &= \cos \theta_{13} \sin 2\theta_{12} \sin 2\theta_{23} \sin 2\theta_{13} \sin \delta^{\text{CP}} \end{aligned} \quad (2.2.3)$$

Given the values of θ_{ij} in Eqn. 2.2.2, this is

$$J_{CP} \simeq 3.2 \times 10^{-5} \sin \delta^{\text{CP}} \quad (2.2.4)$$

as opposed to a possible maximum value $J_{CP} \simeq 0.71 \sin \delta$ when the mixing is maximal, i.e. $\theta_{12} = \theta_{23} = \theta_{13} = 45^\circ$. The main issue here is that we have no idea why these angles are small. This is especially interesting since the CP phase $\delta^{\text{CP}} \simeq \mathcal{O}(1)$ [346] which means that the amount of CP violation is heavily screened in the SM by the small mixing angles in the CKM matrix.

If we permit for flavour-mixing in the lepton sector, which can happen if neutrinos have masses generated by the Higgs mechanism in the same way as quarks, then there will be a mixing matrix in the lepton sector exactly like the CKM matrix, and this is known as the Pontecorvo-Maki-Nakagawa-Sakata matrix, or PMNS matrix [58, 59]. In contrast to the CKM matrix, the PMNS matrix has large off-diagonal terms, which might be considered ‘natural’ since there is no strong hierarchy in the different mixing parameters. This underlines the non-canonical character of quark mixing.

Finally, we recall that the SM simply postulates the existence of the CP violating phase δ^{CP} without prescribing any source for it.

D. Origin of Spontaneous Symmetry Breaking (SSB)

The SM contains the Higgs field which allows gauge symmetry to be broken spontaneously by acquiring a non-zero vacuum expectation value (vev). This is because the Higgs potential is written as

$$V(S) = -\mu^2 S^\dagger S + \lambda (S^\dagger S)^2 \quad (2.2.5)$$

and the values

$$-\mu^2 \simeq 7.8 \times 10^3 \text{ GeV}^2 \quad \lambda \simeq 0.065 \quad (2.2.6)$$

are simply grafted on by hand, in order to get the correct values for the measured masses of the W^\pm and H^0 bosons. Negativity of the coefficient of the $S^\dagger S$ term is crucial to have symmetry-breaking and this is just what the SM does not even try to explain.

A possible quantum field-theoretic explanation for the shape of the potential was suggested by Coleman and Weinberg [60] in an Abelian theory as early as 1973. To adapt their work to

the SM, we can choose $\mu^2 = 0$ in Eqn. 2.2.5, leaving only the quartic interaction term. This itself is a special choice, of course, but vanishing of a term is generally easier to motivate than specific values such as those of Eqn. 2.2.6. The Coleman–Weinberg mechanism then generates an effective potential at one-loop, which can be computed as [61]

$$V_{\text{eff}}(H) = \frac{1}{4}\lambda H^4 + BH^4 \ln\left(\frac{H^2}{M^2}\right) \quad (2.2.7)$$

where M is a mass scale used to define the parameter λ , and the coefficient B is given by

$$\begin{aligned} B &= \left(\frac{\alpha}{8\sin^2\theta_W}\right)^2 \sum_i C_i(2J_i+1)(-1)^{2J_i} \frac{m_i^4}{M_W^4} \\ &= (4.22 \times 10^{-3})^2 \sum_i C_i(2J_i+1)(-1)^{2J_i} \frac{m_i^4}{M_W^4} \end{aligned} \quad (2.2.8)$$

where C_i counts the charge and colour, with the index i summing over vector bosons and fermions with mass m_i and spin J_i . This potential — known as the Coleman-Weinberg potential — for positive values of B , has a minimum at a non-zero value of H , which can be equated with its vacuum expectation value. Thus, spontaneous symmetry-breaking is generated by radiative corrections in the quantum field theory — an aesthetically pleasing result.

The Higgs mass can be calculated from the potential in Eqn. 2.2.7 as

$$M_H^2 = \frac{1}{2} \frac{d^2 V_{\text{eff}}}{dH^2} \Big|_{H=\langle H \rangle} = \left(\frac{\sqrt{2}M_W \sin\theta_W}{\pi\alpha} \right)^2 B \simeq (2243.2 \text{ GeV})^2 B \quad (2.2.9)$$

which, in combination with Eqn. 2.2.8 should yield a Higgs boson of mass in the ballpark of 10s of GeV, which makes the measured value around 125 GeV a not-impossible goal.

However, when we compute the sum in Eqn. 2.2.8, the B -term gets contributions from both bosons and fermions, but with different signs. For the Higgs mass squared to be positive, the mass of the top quark needs to be $m_t < 78 \text{ GeV}$. Since the top quark is known to be much heavier, the value of B is, in fact negative, and with negative B , the minimum shifts back to $\langle H \rangle = 0$.

Thus the Coleman-Weinberg mechanism fails to provide a correct explanation of spontaneous symmetry-breaking within the SM and we are forced back to assuming a nonzero negative coefficient of the $S^\dagger S$ term. The incorporation of more particles can ameliorate the effect of the top quark contribution in B , but that takes us beyond the SM. In fact, in supersymmetric models, the Coleman-Weinberg mechanism can be easily made to work because of the large number of heavy new particles in the theory.

We thus see that the construction of the SM involves making ad hoc choices of several parameters, and sometimes rather non-intuitive ones as well. This is a plainly unsatisfactory state of affairs and therefore a major motivation to seek a better theory.

2.2.2 Standard Model as a Quantum Field Theory

Apart from the above problems with its classical structure, the quantum field-theoretic version of the SM has its own set of problems, the chief of which are

- A. Hierarchy Problem and Naturalness;
- B. Metastability of Electroweak Vacuum;
- C. Axial Anomaly and Strong CP Problem.

Each item is discussed below.

A. Hierarchy Problem and Naturalness

As we have seen in the previous chapter, construction of the SM would not have been possible without the inclusion of elementary scalar fields, of which the Higgs boson is the empirical manifestation. The discovery of the Higgs boson by the CMS and ATLAS collaborations at the LHC [62, 63] and subsequent measurements of the Higgs boson decay probabilities (see, e.g., Fig. 13 in [57]) have more-or-less confirmed that the model of spontaneous symmetry-breaking in the SM is indeed the correct one. However, at 125 GeV, the mass of the Higgs boson is itself a puzzle, and the Higgs vacuum expectation value (vev) of 246 GeV and the masses of the W^\pm and Z bosons, to say nothing of the fermions, are all determined by this scale. The only other fundamental scales known are the QCD scale ($\Lambda_{\text{QCD}} \sim 200$ MeV) and the Planck scale $M_{\text{Pl}} = (G_N)^{-1/2} \simeq 10^{19}$ GeV, where G_N is Newton's gravitational constant. The extremely small ratio between the electroweak scale ($M_{\text{ew}} \sim 100$ GeV) and the Planck scale, while perfectly possible in a classical field theory, is untenable in its quantum field-theoretic version. This is a generic problem with quantum field theories which have elementary scalars, and is referred to as the *hierarchy problem*.

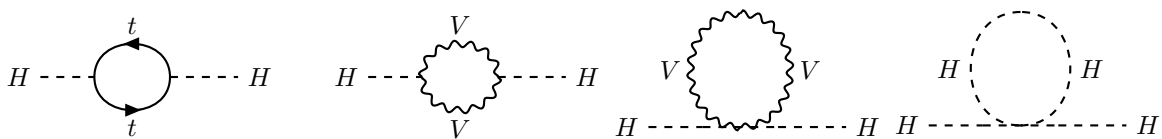


Figure 2.1: One-loop SM corrections to the Higgs mass-squared. The label ‘t’ represents the top quark and ‘V’ represents vector bosons

The hierarchy problem in the SM can be more precisely stated in terms of the squared mass of the Higgs boson. If the SM is considered as an effective theory having some cutoff Λ , the quantum correction to the Higgs boson mass-squared involve a term proportional to Λ^2 . This can be seen from an approximate calculation of the Feynman diagrams listed in Fig. 2.1. The dominant contribution is expected to come from the top quark, since it has by far the largest coupling y_t with the Higgs boson. Taking the leading contribution from the top loop, then,

the Higgs mass-squared is given by

$$M_H^2 = (M_H^2)_{\text{bare}} + \delta M_h^2 = (M_H^2)_{\text{bare}} + \frac{y_t^2}{8\pi^2} \left(\Lambda^2 - 6m_t^2 \ln \frac{\Lambda}{m_t} + 2m_t^2 \right) \quad (2.2.10)$$

Obviously, if the value of Λ is several orders of magnitude above the electroweak scale, then the theory will predict $M_H \approx \Lambda \gg 125$ GeV, which is contrary to the experimental result. In the extreme case that there is no new physics between the electroweak scale and the Planck scale, the Higgs boson mass will be predicted to be of the order of $M_{\text{Pl}} \simeq 10^{19}$ GeV, which is quite absurd, for, apart from its empirical abnegation, it would drive the Higgs quartic coupling $\lambda = M_H^2/4v^2$ to impossibly non-perturbative values.

It may seem that it is simple to arrange for a mass of 125 GeV by choosing the bare mass-squared $(M_H^2)_{\text{bare}}$ as a large negative quantity, and thus arrange a highly delicate cancellation of $\sim \mathcal{O}(10^{34})$ GeV between it and the divergent correction to the mass squared. This is highly unnatural, but not more so than the cancellations envisaged in the original renormalisation programme for QED and other quantum field theories. However, the problem for the Higgs boson is that even if we arrange such a cancellation at the one-loop level, the quadratic (and logarithmic) divergences reappear at the two-loop level, when we have no more free parameters left to tune. We could, of course, redefine the bare mass to have the cancellation at the two-loop level, but then there will be a divergence at the one-loop level. Similar arguments can be applied to every order in perturbation theory, making nonsense of the very notion of a perturbation expansion. This is the naturalness or fine-tuning problem [64–67], in the sense of Dirac that a small number – the Higgs boson mass – is unstable under quantum corrections.

One may take the extreme view that the hierarchy problem is just an artefact of perturbation theory and the fact that we calculate only a few orders in the perturbation theory. In the exact SM, which exists in principle, there is just one cancellation which gives us the Higgs boson mass of 125 GeV. However, in this case, one would have to explain why the perturbation theoretic calculations for Higgs contributions to electroweak precision observables as well as the Higgs boson decay widths provide results which are closely corroborated by experiment. For this reason, it is widely believed that the hierarchy problem can be solved within the framework of perturbation theory.

The earliest attempt to solve the hierarchy problem within perturbation theory was made by Veltman [68], where he proposed that the entire quadratic divergence in the Higgs boson mass cancels. This proposal made sense before the masses of the top quark and the Higgs boson were known, but now it is negated by the experimental results. Nevertheless, the author of Ref [69] revives the idea and proposes that the cancellation does indeed occur at a very high scale, where the renormalisation group evolution of the SM parameters makes this possible. This is, in principle, possible, but the jury is still out on this idea.

Many other attempts to solve the hierarchy problem and save the Higgs boson mass from receiving impossibly large radiative corrections have been made in the forty-five years since

it was discovered. All of these involve new physics beyond the SM. Some of these ideas are discussed in Section 2.3.

B. Stability of the Electroweak (EW) Vacuum

Other than the hierarchy problem, another problem induced by the discovery that the Higgs boson has a mass as light as 125 GeV is that of the stability of the electroweak vacuum. We may recall that the Higgs potential is given by

$$V(S) = -\mu^2 (S^\dagger S) + \lambda (S^\dagger S)^2; \quad \mu^2 > 0 \quad (2.2.11)$$

These values are known at the electroweak scale (see Eqn. 2.2.6) and the quartic coupling λ is positive, ensuring that the potential is bounded from below. However, for $M_H < 170$ GeV, it is known that the beta function of λ is negative and thus, with the knowledge that $M_H \simeq 125$ GeV tells us that the running of the quartic coupling λ decreases its value at high energy scales. At a scale where it becomes zero (or negative), the electroweak vacuum becomes unbounded from below and the current value $V(v) = \mu^2 v^2 + \lambda v^4 \simeq -2.34 \times 10^8 \text{ GeV}^4$ becomes unstable. This would be a disaster, for then any hot spot in the Universe above the threshold energy would see all the matter losing energy and heating up the neighbourhood, which would in turn cross the instability threshold and also start losing energy. In a fraction of a second, then, the Universe would disappear in an enormous explosion, known as a *fiery death*. However, the proof that this does not happen is provided by the fact that the Universe immediately after the Big Bang was at a higher temperature, and then it cooled down rather than undergoing a fiery death.

Based on the zero-crossing of λ , the SM vacuum can either be stable, unstable or metastable. The vacuum is stable if the quartic coupling remains positive all the way up to $M_{\text{Pl}} \sim 10^{19}$ GeV. If the quartic coupling becomes negative before reaching this scale, the vacuum can be either unstable or metastable. If the value is only slightly negative, such that the lifetime of the vacuum is larger than the age of the universe, the vacuum is regarded as metastable. Otherwise, it is unstable.

Assuming only the SM field content, it was shown in [70], using a state-of-the-art calculation involving a set of full 2-loop NNLO gauge couplings and 3-loop NNLO RGE precision, that the SM is near-critical and not necessarily stable. It lies on the phase transition boundary between a stable configuration and a metastable one. The results crucially depend on the measured masses of the Higgs and the top quark. The authors calculate that the stability condition on the Higgs mass can be well-approximated by

$$M_h > 129.6 \text{ GeV} + 2.0 (m_t - 173.34 \text{ GeV}) - 0.5 \text{ GeV} \frac{\alpha_3(M_Z) - 0.1184}{0.0007} \pm 0.3 \text{ GeV} \quad (2.2.12)$$

With the experimental bounds on the Higgs mass from Run-I being at $M_H = 125.09 \pm 0.24$ GeV [71], the stability condition is excluded at 2.8σ . The lifetime of the vacuum is

greater than the age of the universe if [72]

$$M_h > 111 \text{ GeV} + 2.8 \text{ GeV} \left(\frac{m_t - 173.2 \text{ GeV}}{0.9 \text{ GeV}} \right) - 0.9 \text{ GeV} \left(\frac{\alpha_S(M_Z) - 0.1184}{0.0007} \right) \pm 3 \text{ GeV} \quad (2.2.13)$$

indicating that if we take central values, we will certainly get a metastable Universe. The regions of instability, metastability and stability of the EW vacuum are given in Fig. 3 of Ref. [70],

As is obvious from Eqn. 2.2.12 and 2.2.13, precise measurements of the mass of the Higgs boson and, more importantly, of the top quark are of paramount importance in determining the stability condition of the SM vacuum.

C. The Axial Anomaly and Strong CP Problem

The third and perhaps the most intractable problem with the SM as a quantum field theory is the so-called *strong CP problem*. This is described briefly in this section, based mainly on the treatment of Refs. [73–75].

If one considers the classical theory only, then in the limit of vanishing quark masses, the QCD Lagrangian of Eqn. 1.2.24 ought to have a large global symmetry, viz. $U(N)_V \times U(N)_A$, with V and A indicating vector and pseudovector (axial vector) respectively. For the first generation quarks, in fact, $m_u, m_d \ll \Lambda_{\text{QCD}}$, so the corresponding symmetry ought to be found. While the vector part is indeed exhibited in the form of isospin and baryon number ($U(2)_V \equiv SU(2)_I \times U(1)_B$), the axial vector symmetry $U(1)_A$ is not seen. This can be explained by claiming that the axial vector symmetry is spontaneously broken by the quark condensates $\langle \bar{u}u \rangle = \langle \bar{d}d \rangle \neq 0$. However, we would then expect four Nambu-Goldstone bosons corresponding to the four broken generators of $U(2)_A$, which cannot be removed by a gauge choice since these are global symmetries. In fact, the three pions π^0, π^\pm are good candidates for these Nambu-Goldstone bosons, but there is no fourth light state in the mass spectrum, since the only other possible candidate, the η , is far too heavy. This absence was recognised as the $U(1)_A$ problem.

The problem was resolved by the recognition of the multiple vacuum structure of QCD. In QCD, there is a chiral anomaly because of which axial currents are not conserved, viz.

$$\partial_\mu J_5^\mu = \frac{g_s^2 n_f}{32\pi^2} F_{\mu\nu}^a \tilde{F}^{a\mu\nu}; \quad \tilde{F}^{a\mu\nu} = \frac{1}{2} \epsilon^{\mu\nu\alpha\beta} F_{\alpha\beta}^a \quad (2.2.14)$$

where n_f is the number of quarks and the $F_{\mu\nu}^a$ are the $SU(3)_c$ field strength tensors. However, the above operator can be written as a total derivative

$$F_{\mu\nu}^a \tilde{F}^{a\mu\nu} = \partial_\mu K^\mu \quad (2.2.15)$$

with

$$K_\mu = \epsilon_{\mu\nu\alpha\beta} A^{\alpha\nu} \left(F^{a\alpha\beta} - \frac{g}{3} f^{abc} A^{b\alpha} A^{c\beta} \right) \quad (2.2.16)$$

It follows that under the transformation of the quark field $q_f \rightarrow \exp\left(\frac{1}{2}i\alpha\gamma_5\right)q_f$, the chiral anomaly changes the action by

$$\begin{aligned}\delta S = \alpha \int_V d^4x \partial_\mu J_5^\mu &= \alpha \frac{g^2 n_f}{32\pi^2} \int_V d^4x F^{a\mu\nu} \tilde{F}_{\mu\nu}^a \\ &= \alpha \frac{g^2 n_f}{32\pi^2} \int_V d^4x \partial_\mu K^\mu = \alpha \frac{g^2 n_f}{32\pi^2} \int_S ds_\mu K^\mu\end{aligned}\quad (2.2.17)$$

The surface integral in the last step suggests that if we were to set $A_\mu^a = 0$ at spatial infinity, the integral would vanish and the anomaly with it. The axial symmetry would then be a good symmetry. However, as t'Hooft showed [76], in a non-Abelian gauge theory like QCD there exist multiple vacua, and tunneling between them permits the construction of non-trivial gauge configurations for which the integrand does not vanish at infinity, i.e. the anomaly exists. This explains why $U(1)_A$ is not a good symmetry of QCD.

However, this resolution of the $U(1)_A$ puzzle immediately leads to another problem of the QCD Lagrangian and that is the existence of non-trivial anomaly-like terms such as

$$\mathcal{L}_\theta = \frac{g^2}{32\pi^2} \theta F_{\mu\nu}^a \tilde{F}^{a\mu\nu} \quad (2.2.18)$$

which are known as θ terms. This would lead to CP -violating effects in the strong sector — but such effects have not been observed. For example, the θ term leads to a non-zero neutron dipole moment, which has been estimated [77] to be $d_n = 5.2 \times 10^{-16} \theta$ cm. The experimental upper bound [78] on the electric dipole moment of the neutron is $d_n \simeq 10^{-26}$, giving us an upper bound of $\theta \leq 10^{-9} - 10^{-10}$. Obviously, such a small parameter in the Lagrangian is an acute fine-tuning problem, and this is referred to as the *Strong CP problem*.

While several ideas beyond the SM have been proposed to solve this problem, the most widely-accepted explanation is the Peccei-Quinn (PQ) theory, which predicts the existence of new particles called *axions*. This is discussed in Section 2.3.4.

2.2.3 Phenomenological Problems

In the previous two sections we have discussed the internal problems with the SM, both in its classical and quantum versions. However, it is not enough for the SM merely to be internally self-consistent, but it must also explain the observed phenomena and measurements. This leads to a class of problems which we may call *phenomenological*, in the sense that they are directly related to empirical data. While potentially every new measurement confronts the SM, the major problem areas lie in studies of extra-terrestrial physics. These are

- A. Baryogenesis at the observed level.
- B. The Dark Matter problem.
- C. The Dark Energy problem.

A. Baryogenesis

In this section, we discuss the problem of baryogenesis, i.e. the question of what causes the overwhelming dominance of matter over antimatter in our present Universe. This section closely follows the treatment of Refs. [79–82].

Our very existence proves that, at least in our immediate neighbourhood in the Universe, the amount of matter overwhelmingly dominates the amount of antimatter. There is, moreover, extensive observational evidence that matter does indeed dominate antimatter in the Universe as a whole. This is quantified by a quantity called the *baryon number asymmetry*

$$\eta = \frac{n_B - n_{\bar{B}}}{n_\gamma} \quad (2.2.19)$$

where n_B , $n_{\bar{B}}$ and n_γ are the number of baryons, antibaryons and photons, respectively, in the Universe. Obviously, this would vanish if the Universe was matter-antimatter symmetric, but, in fact it does not. In the SM, we have a prediction of $\eta \sim 10^{-26}$, but observations tell us that, in fact, $\eta \sim 10^{-10}$. This huge discrepancy is a major drawback of the SM.

How can one explain such a phenomenon? The first, and most naive, explanation would be to say that the Universe was always baryon-asymmetric and all that we are observing is its manifestation. However, as all the basic equations governing matter and radiation are baryon-number symmetric (at least in the SM), this is an unnatural starting point and is a solution by fiat rather than a satisfactory explanation. Alternatively, one could assume that there are indeed equal amounts of matter and anti-matter in the Universe, but they exist in different spatial zones. If this were the case, however, we would expect γ -rays arising from the annihilation of matter and anti-matter at the interface of the zones, which would lead to an isotropic haze of gamma radiation. No such effect has, however, been found. Keeping the zones separate with an intervening vacuum is not possible with the present theories of cosmological evolution. We are, then forced to the third, and most likely hypothesis, viz. that the Universe started out as baryon symmetric, but developed a non-zero asymmetry during its evolution. This is the idea of *baryogenesis*.

The necessary conditions for baryogenesis were enunciated by Andrei Sakharov in 1967 [83]. These are

1. *Baryon number violation*: This is an obvious requirement, or else $n_B = n_{\bar{B}}$. If baryon number is violated, we could have baryons produced through a heavy boson X which decays as $X \rightarrow Y + B$, where B is a baryon and X, Y do not carry any baryon number.
2. *C and CP violation*: If C (or charge) is conserved, the charge-conjugate reaction would produce equal numbers of antibaryons, since

$$\Gamma(X \rightarrow Y + B) = \Gamma(\bar{X} \rightarrow \bar{Y} + \bar{B}) \quad (2.2.20)$$

However, even if C is not conserved, X could decay to two left-chiral baryons or to two right-chiral baryons. If CP were an exact symmetry, we would have $\Gamma(X \rightarrow b_L b_L) =$

$\Gamma(\bar{X} \rightarrow \bar{b}_R \bar{b}_R)$, even if $\Gamma(X \rightarrow b_L b_L) \neq \Gamma(\bar{X} \rightarrow \bar{b}_L \bar{b}_L)$. Thus, when an X boson decays, we will have

$$\Gamma(X \rightarrow b_L b_L) + \Gamma(X \rightarrow b_R b_R) = \Gamma(\bar{X} \rightarrow \bar{b}_R \bar{b}_R) + \Gamma(\bar{X} \rightarrow \bar{b}_L \bar{b}_L) \quad (2.2.21)$$

which would wipe out the baryon asymmetry. It follows, then, that both C and CP should be violated.

3. *Out-of-thermal-equilibrium interactions:* At thermal equilibrium with high temperatures, the rate at which the particle X decays and the rate at which it is created are equal, i.e. $\Gamma(X \rightarrow Y + B) = \Gamma(Y + B \rightarrow X)$. One cannot, then have a stable population of either baryons or antibaryons.

However, if the particle X decays at a time when the temperature of the Universe, $T < M_X$, the final state with an energy of $\mathcal{O}(T)$ cannot produce the particle X back. The rate of creation of X is then Boltzmann-suppressed $\Gamma(Y + B \rightarrow X) \sim e^{-M_X/T}$. This will ensure that the baryon population survives through the cooling of the Universe.

It is now interesting to discuss the SM and see if the Sakharov conditions can be realised within its framework.

- *Baryon Number Violation in the SM:*

Naively speaking, the SM at zero temperature conserves baryon number, so this may seem to immediately preclude baryogenesis in the SM. However, matters are not so simple at finite temperatures, especially the very high temperatures in the early Universe. This is discussed below, following the classic treatment of Ref. [85].

In the SM, baryon number can be violated through the triangle anomaly since

$$\partial_\mu J_5^\mu \propto F_{\mu\nu}^a \tilde{F}^{a\mu\nu} \neq 0 \quad (2.2.22)$$

where the $F_{\mu\nu}^a$ are the $SU(2)_L$ field strength tensors. As this is a total derivative, the corresponding terms in the Lagrangian may vanish if the gauge fields vanish at the surface, just as we have argued in the case of the strong CP problem. As in that case, it can be shown [76] showed that these gauge fields do not actually vanish at infinity. This is because the classical electroweak vacuum field configuration comprises an infinite number of equivalent vacua which are related to each other by “large” gauge transformations. This is often referred to as the θ -vacuum of non-Abelian gauge theories. Each vacuum state is associated with a winding number ν_i .

In $SU(N)$ theories with spontaneously broken symmetries, we can define a Chern-Simons number [86]

$$N_{\text{CS}} = \int d^3x J^0; \quad \text{with} \quad J^\mu = \frac{g^2}{32\pi^2} \epsilon^{\mu\nu\rho\sigma} \left(F_{\nu\rho}^a A_\sigma^a - \frac{g}{3} \epsilon_{abc} A_\nu^a A_\rho^b A_\sigma^c \right) \quad (2.2.23)$$

The Chern-Simons number is topological and labels each vacuum state. It changes by integral values. If a state is a vacuum state at time t_0 and is at another vacuum state

at time t_1 , we have

$$N_{\text{CS}}(t_1) - N_{\text{CS}}(t_0) = \int_{t_0}^{t_1} dt \int d^3x \partial_\mu J^\mu = \nu \equiv \text{integer} \quad (2.2.24)$$

and then the change in baryon number is

$$\Delta B = \Delta L = \nu n_f \quad (2.2.25)$$

where n_f is the number of fermion fields.

Continuous transformations around a vacuum cannot change N_{CS} , however. That can only occur by a transition from one vacuum to another either by tunnelling or by going over the barrier. The solution of the state at the top of the barrier between two consecutive vacua is called the *sphaleron*. This saddle point solution was first proposed by Klinkhammer and Manton [87]. At zero temperature, the probability of tunnelling from one vacuum state to the next is found to be exceedingly small.

$$P \sim \exp\left(-\frac{8\pi^2}{g^2}\right) \sim 10^{-173} \quad (2.2.26)$$

which explains the conservation of baryon number in the SM at zero temperature. However, Kuzmin *et al.* [88] showed that at high temperatures, the transitions are much less suppressed. At $T \gtrsim 100$ GeV, these processes have significant amplitudes. The calculations for the probability at finite temperature are complicated and require to be done numerically. State-of-the-art computations [89] give the transition time between two successive vacua as

$$\tau^{-1} \equiv \frac{\Gamma}{V} = C \alpha_W^5 T^4; \quad \alpha_W = \frac{\alpha}{\sin^2 \theta_W} \quad (2.2.27)$$

Lattice calculations [90] are used to obtain the value of C . Recent results show that

$$C = 25.4 \pm 2.0 \quad (2.2.28)$$

With these numbers, one can predict a finite probability for the transition from one vacuum to the other and hence of a non-zero winding number, which, by Eqn. 2.2.25 corresponds to a finite amount of baryon-number violation. Thus, finite temperatures are the key to baryon number violation in the SM.

- *Out of equilibrium interactions in the SM:*

This condition of Sakharov can be met in the SM by the electroweak phase transition (EWPT), which presumably happened in the early Universe. The electroweak vacuum near criticality can develop domains, inside which the Higgs vev and therefore particle masses are non-zero in the symmetry-broken phase, while outside these domains the symmetry is unbroken and all the masses are zero. Thus, baryogenesis can occur outside the domains, and such baryons can propagate inside the domains, but the corresponding antibaryons cannot be generated inside the domains due to the nonvanishing masses. As

the Universe cools below the electroweak transition temperature, these domains expand and join, eventually encapsulating the entire Universe. Thus, any baryogenesis taking place at the domain walls freezes out and remains fixed for the rest of the evolution process.

- *CP violation:*

From the basis-independent measure of *CP*-violation in the SM given by the Jarlskog invariant (Eqn. 1.1.3), it is seen that the quantitative level of *CP* violation is extremely small, essentially because of the near-diagonal nature of the CKM matrix. It is especially small when compared to what is required for baryogenesis to occur. This is a clear failure of the SM, which has no other source of *CP* violation. It is therefore widely believed that extra sources of *CP* violation are needed, and this can only happen in theories which go beyond the SM.

B. Dark Matter

Perhaps the greatest shortcoming of the SM is that it does not have any explanation for the phenomenon of *dark matter* in the Universe. Dark matter (DM) is, in fact, one of the most important mysteries in Science today, and the subject of intensive research by cosmologists, astrophysicists and elementary particle physicists. The present discussion has been referenced mainly from [91–93].]

DM was first proposed by Zwicky in 1937 to explain the unexpectedly large proper velocities of galaxies in the Coma cluster. However, the idea was universally expected only after the work of Rubin in 1973 on the velocity distribution of stars in the arms of spiral galaxies. If we assume the mass M of such a galaxy to be concentrated in the central luminous region, then Newtonian dynamics establishes that the transverse velocity of a star in the highly tenuous spiral arms at a distance R from the galactic centre would be

$$v(R) = \sqrt{\frac{GM}{R}} \quad (2.2.29)$$

i.e. it would fall as R increased. Rubin's observations, and a host of later results, suggest that instead of having $v(R) \propto R^{-1/2}$, it appears that $v(R)$ is approximately constant, even showing a slight tendency to increase (see Fig. 2.2). To explain this, Rubin revived Zwicky's idea that the luminous galaxy is immersed in a halo of non-luminous, but transparent, dark matter, whose gravitational attraction can be used to explain the observed effect. Thus, if the matter within a sphere of radius R is $M(R)$, then $v(R)$ would be constant if $M(R) \propto R$, i.e. the matter density distribution is $\rho \propto R^{-2}$. This is a sharply rising curve towards the centre of the galaxy, and is likely to be mostly due to dark matter. The fact that the constancy of the velocity curves is also applicable to isolated stars out far beyond the luminous region suggests that the bulk of the matter in the galaxy is dark. This phenomenon has now been established for hundreds of galaxies and is believed to be universal. For remote galaxies where it is difficult to measure rotation curves of individual stars, the existence of dark matter halos

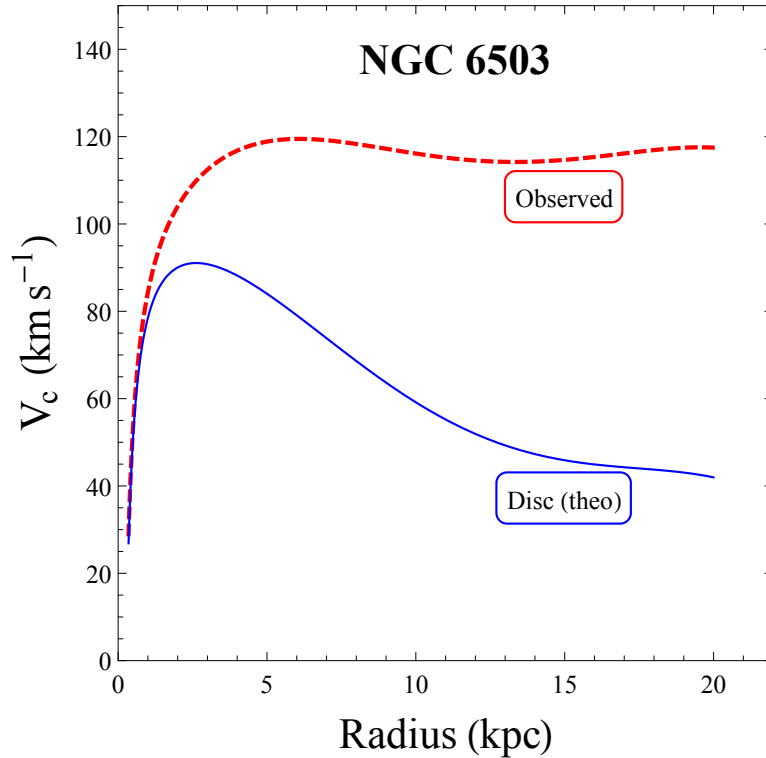


Figure 2.2: Rotation curve for NGC 6503, which shows the observed rotation curve (red) and the theoretically expected rotation curve (blue), if the observed luminous matter made up the entire mass of the galaxy. The data for the red curve is taken from hep-ph/9710467.

has been conclusively established by observing gravitational lensing by these galaxies and galaxy clusters.

The question naturally arises as to the nature of this dark matter. Clearly it has gravitational but no electromagnetic interactions. However, it is not immediately clear if it is distributed or clumpy or if it has strong or weak interactions. A major clue arises from the of the so-called *Bullet Cluster* (1E 0657-558) by the Chandra X-ray observatory [94]. This is an irregular cluster (by optical and X-ray imagery) of galaxies which appears to have been formed by the collision of two roughly spherical clusters (see Fig. 2.3). However, it is flanked on both sides by roughly spherical dark halos which are revealed by gravitational lensing effects on distant sources behind the halos [95], leading to the obvious conjecture that the two roughly spherical dark halos have simply passed through each other, while the luminous baryonic components have collided and merged into the observed irregular shape. This proves rather conclusively that the dark matter is non-baryonic in nature and does not have strong interactions. The hypothesis that dark matter could consist of massive compact halo objects (MACHOs) is thus laid to rest. What is left is the possibility that dark matter consists of a new form of elementary particle which has gravitational and possibly weak interactions, and not strong or electromagnetic interactions.

The final piece in the puzzle comes from observation of fluctuations in the cosmic microwave

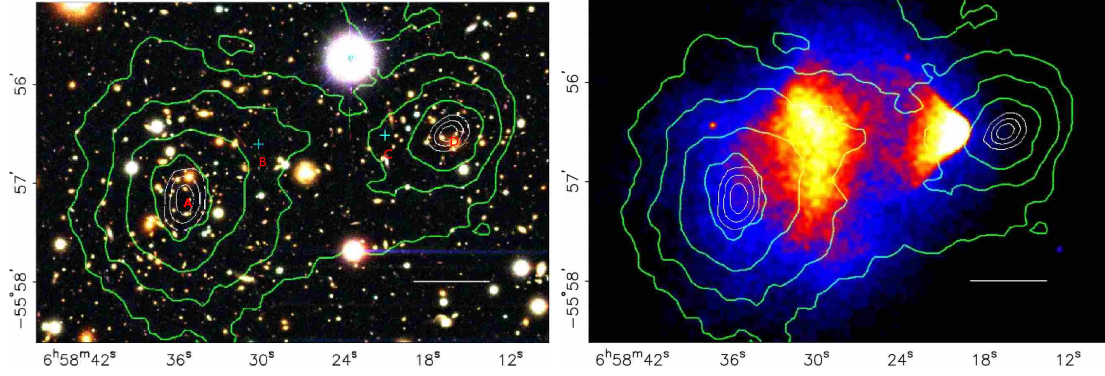


Figure 2.3: The bullet cluster: The figure shows the merging galaxy cluster 1E0657-558, where the left image is an image from Magellan and the right image is an x-ray image by the Chandra X-Ray Telescope. The contours show the distribution of mass reconstructed using weak gravitational lensing methods. The image is reproduced with permission from Dai *et. al.* 10.1103/PhysRevD.78.104004, Vol 78 Issue 10, 2008. Copyright (2008) by the American Physical Society

background radiation (CMBR), where data from the Planck experiment [96] suggests that baryonic matter comprises 4.9% of the total energy-mass content of the Universe, DM comprises 26.8%, and the rest is a mysterious things called Dark Energy (see next section). The relic density of DM in our Universe is calculated to be

$$\Omega_{\text{DM}} h^2 = 0.1198 \pm 0.0026 \quad (2.2.30)$$

where $\Omega_{\text{DM}} = \rho_{\text{DM}}/\rho_{\text{crit}}$ and $h = H_0/100 \text{ kms}^{-1} \text{ Mpc}^{-1}$. The relic density bounds constitute an important constraint for any DM model.

It is important to note that given current models of cosmological evolution, it would not be possible to generate so high a relic density from gravitational interactions alone. The DM particles must, then, have been produced through weak interactions, and this gives us a handle for their possible experimental detection. In fact, it is widely believed today that the dark matter components are weakly-interacting massive particles (WIMPs). Moreover, their masses must be comparable to the electroweak scale if the cosmological evolution is to be explained by the current Λ CDM model. It is a remarkable coincidence that ~ 100 GeV WIMPs interacting with the SM particles with the weak interaction coupling strength provides just the right amount of relic density without any unnatural tuning of the values of the parameters. This is known as the ‘WIMP miracle’.

Experiments and bounds: As mentioned above, the fact that DM particles must have weak interactions provides a way to detect them in terrestrial experiments, much in the same way as neutrinos (which also have only weak and gravitational interactions) can be detected by experiments of sufficient sensitivity.

- Direct DM detection experiments mainly focus on WIMP searches. Non-relativistic WIMPs hitting nuclei now and then in an underground detector produce recoil and this can be measured accurately. Several versions of this idea have been implemented for the different nature of couplings, one being dependent on the spin of the nuclei and the

other being independent of it. The different experiments like CoGeNT (using ^{73}Ge), XENON100 (using ^{131}Xe) even have different threshold energies and help establish independent limits for different WIMP velocity distributions.

- Indirect DM detection can be done in two ways. The relative abundance of DM is indicated by the CMBR data, when the fluctuations are expanded in terms of spherical harmonics. The ratio of the strengths of the second and the third harmonics gives the ratio of the baryonic matter to the dark matter abundances (See Refs. [97]). Alternatively, assuming that the DM consists of WIMPs, they can be searched for in accelerator machines where they could be produced in weak decays of strongly-produced particles, and would leave a characteristic missing-energy-and-momentum signature.

A detailed review of the experimental searches are given in Refs. [98, 99]. It hardly needs to be said that all DM detection experiments till date have yielded negative results, indicating that if the WIMP hypothesis is correct, then the DM particles must be either too heavy or too weakly-interacting to leave any traces in the current experiments. There is every possibility, however, that the next round of experiments or the next round of data-taking at current experiments would reveal signs of DM.

Constituents of Dark Matter: We have already seen that the SM does not contain any WIMPs, except neutrinos, which are far too light to be DM candidates. However, there are several possible candidates in theories beyond the SM, of which a few are

- *Sterile neutrinos:* It is possible that there exist heavy neutrinos which have no gauge interactions, but mix with the light neutrino species through an extended PMNS matrix. These heavy eigenstates can be produced through their mixing angles and create the DM relic density observed. This is the hypothesis which involves minimum addition to the SM.
- *Axions:* The solution to the Strong CP-problem (Sections 2.2.2 and 2.3.4) may also provide a viable DM candidate in the axion. Most models place the axion mass in the range of μeV and they can be detected by their oscillations to photons. Though all current results are negative, experiments like ADMX [100] and CARRACK [101] are actively searching for axion DM.
- *Supersymmetric particles:* Supersymmetry (SUSY) provides a good natural option for WIMPs in the lightest neutralino (see Section 2.4). If SUSY particles are prevented from decaying to any SM particle by the imposition of a \mathbb{Z}_2 symmetry between the SUSY and SM particles, neutralinos produced in the early Universe survive to the present day after the “freeze-out” temperature is reached, and they might interact weakly with SM fields. The masses and coupling strengths of the lightest neutralino are expected to lie in the very range where the ‘WIMP miracle’ occurs.

In some models of SUSY which include gravity, it is the lightest gravitino rather than the lightest neutralino which are the DM candidates. Such gravitinos would be the end product of decays of weakly-interacting particles produced in the early Universe.

However, detection of these will be a real challenge, as they have only gravitational interactions.

- *Other Candidates:* Other DM candidates which have been occasionally proposed include the lightest Kaluza-Klein modes of the photon in models with a universal extra dimension (UED), and a heavy photon in little Higgs models with T -parity conservation.

Problems with the DM hypothesis: Despite the strength of the DM hypothesis, it still suffers from certain problems, most notably its inability to explain small scale observations such as the following.

1. *Core-versus-Cusp problem:* This refers to the disagreement between the N -body simulations using Cold Dark Matter (CDM) and observations. The Navarro-Frenk-White (NFW) density profile for DM is [102]

$$\rho(R) = \rho_0 \frac{R_s}{R} \left(1 + \frac{R}{R_s} \right)^{-2} \quad (2.2.31)$$

where R_s is the scale radius and ρ_0 is a density scale, both characteristics of the DM halo being considered. This predicts a sharply increasing density at smaller radii (a ‘cuspy’ distribution) in line with the naive calculation mentioned above, while the observed data suggests more flat central density profiles (the ‘cores’). A detailed discussion may be found in Ref. [103].

2. *Missing satellites problem:* Simulations involving the CDM model predict that every galaxy ought to have a large number of DM sub-halos, and each sub-halo can be associated with a satellite galaxy. For example, the CDM model predicts thousands of satellite galaxies for the Milky Way, whereas the Local Group comprises only ~ 50 satellite galaxies. One could try to explain away these missing satellites by arguing that they do not contain enough luminous matter to be detected. However, this idea runs into the ‘too big to fail’ problem discussed below. More details on this can be found in Ref. [92].
3. *Too-big-to-fail problem:* In continuation of the missing satellites problem. detailed simulations within CDM models indicates that a large number of the missing satellite galaxies would be too massive to not have stars. i.e. they are too big to fail to produce visible stars. For the Local Group, then, there are several large satellite galaxies predicted which are simply not seen.

Before concluding this discussion on DM, it is worth mentioning that there is a class of theories called Modified Newtonian Dynamics (MOND) theories [104, 105] which deny the existence of DM altogether and suggest that modification of Newton’s law of gravitation over long distances provides the explanation of the observed effects. MOND theories are not very popular but they have proved rather difficult to rule out in any conclusive manner.

C. Dark Energy

The largest and most mysterious component of the Universe, as evidenced by the Planck data, is Dark Energy. This is briefly discussed in this section, based on Refs. [106, 107].

The simple form of Hubble's law gives us a uniformly expanding Universe, but the Friedman equations tell us that if the Universe consists of gravitating matter with a positive density and pressure, then the expansion rate must gradually slow down. However, in 1998, a momentous discovery in cosmology came from the observation of Type Ia supernovae in distant galaxies which are considered to be standard candles, their apparent luminosities telling us the distances of those galaxies, while a study of the redshift in their spectra tells us their velocity of recession. It was found that the rate of expansion of the Universe is accelerating instead of slowing down [108, 109]. Studies from CMBR [110] and large scale structure [111] independently support this observation. It follows that about 70% of the energy-mass of the Universe is an unknown form which exerts negative pressure, leading to repulsion rather than attraction — unlike gravitation. Most recent data from the Planck satellite studying the CMB also confirm the overwhelming dominance of this unknown entity, which has been dubbed 'dark energy'. A naive representation of dark energy is to simply add a constant term with the cosmological constant Λ to the Einstein equation, yielding

$$R_{\mu\nu} - \frac{1}{2}g_{\mu\nu}R = 8\pi G T_{\mu\nu} + \Lambda g_{\mu\nu} \quad (2.2.32)$$

In a Friedmann-Robertson-Walker (FRW) Universe, the force law can be then written as

$$F = -\frac{GM}{R^2} + \frac{\Lambda}{3}R \quad (2.2.33)$$

where R is the scale factor in the FRW metric. A positive value of Λ [112] means that at sufficiently large distances the gravitational force is repulsive, rather than attractive. This would explain the accelerated expansion of the Universe.

The Cosmological Constant Problem: A Λ term also contributes to the positive curvature of the Universe. Our Universe has been observed to be very close to flatness and any positive curvature must be tiny, which means that Λ itself must be extremely small. Why Λ is small but not zero is a fundamental question in cosmology, because no known symmetry forces it to be zero.

The existence of the cosmological constant means that the vacuum energy is non-zero. To match the observations, the vacuum energy density needed is

$$\Lambda \sim \rho_{\text{vac}}^{\text{obs}} = (10^{-3}\text{eV})^4 \quad (2.2.34)$$

However, the introduction of the SM fields and the Planck scale brings with itself the zero point fluctuations of the quantum fields. For the Planck scale, the vacuum energy is

$$\Lambda \sim \rho_{\text{vac}}^{\text{Planck}} \sim (10^{27}\text{eV})^4 \quad (2.2.35)$$

which is a discrepancy with the data by an intolerable 120 orders of magnitude — far worse than the hierarchy problem discussed earlier. This is known as the *cosmological constant problem*.

Several ingenious proposals to mitigate this problem may be found in the literature [113,114], although no proposal has been accepted as completely satisfactory to date. However, issues linked with dark energy are not discussed further as they form no part of the research work in this thesis.

2.3 Beyond Standard Model Physics

As we have seen above, there are several problems and questions to which the SM has no solution. It is natural, therefore, to assume that the SM is not the ultimate theory, but an effective low-energy limit of a deeper underlying theory whose effects would become manifest at higher energy scales than have been probed till the present. Many different versions of this underlying theory have been proposed. Most of these address a limited set of the problems in the SM — often just a single one — and it may be expected that eventually some combination of these theories may prove to be the candidate for the ultimate ‘theory of everything’.

2.3.1 Hierarchy Problem

In the wake of the Higgs boson discovery, perhaps the most pressing question is the explanation of its low mass, which we have described as the hierarchy problem. As we have seen, this arises from the large quadratic divergences (Λ^2) in the radiative corrections to the Higgs boson mass, which are caused by the high cutoff scale Λ for the SM. There are two main ways in which this problem can be tackled, viz.

- A. Arranging for cancellation of the quadratic divergence between different radiative corrections, i.e. realising the Veltman condition in a new physics scenario.
- B. Arranging for the cutoff scale Λ for the SM to lie in the range of a few TeV to a few tens of TeV, in which case a low Higgs boson mass does not call for much fine tuning.

In either case, one requires the introduction of new fields and new interactions beyond the SM.

A. Cancellation of quadratic divergences

In such theories, one introduces extra fields and interactions with some underlying symmetry ensuring that the radiative corrections from these extra fields are equal and opposite to the SM contributions, at least so far as the quadratically divergent term goes. There are two major classes of these theories.

- *Supersymmetric theories:* Supersymmetry is a symmetry which keeps the action of the theory invariant under transformations which take a boson to a fermion and vice versa. In the limit of unbroken supersymmetry, this requires every bosonic degree of the SM to be paired with an extra fermionic degree of freedom, and every fermionic degree of the SM to be paired with an extra fermionic degree of freedom. These extra fields are called *superpartners*. In the limit of unbroken supersymmetry the SM particles and the corresponding superpartners have the same masses and couplings. As a result, when radiative corrections to the mass of the Higgs boson are calculated, one gets contributions of equal magnitude from every boson-fermion pair of degrees of freedom. Cancellation is then automatic, for it is well known that closed fermion loops and closed boson loops differ by an extra negative sign.



Figure 2.4: One-loop SUSY corrections to the Higgs mass squared. \tilde{t} represents the scalar superpartner to a SM top t

To be more concrete, we consider the dominant top quark contributions to the Higgs boson mass corrections discussed in 2.2.2A. In a supersymmetric theory we will have scalar superpartners of the left- and right-chiral top quarks, which are called left- and right-scalar tops (or stops) respectively. The leading contribution of the stop loops given in Fig. 2.4 are given by [115]

$$\delta M_h^2 = \frac{\lambda^2}{16\pi^2} \left(\Lambda^2 - 2m_{\tilde{t}}^2 \text{Log} \frac{\Lambda}{m_{\tilde{t}}} \right) + \frac{\lambda^2 v^2}{16\pi^2} \left(1 - 2 \text{Log} \frac{\Lambda}{m_{\tilde{t}}} \right) \quad (2.3.1)$$

where λ^2 and λv are the quartic and trilinear couplings between the Higgs and the stop fields respectively, while $m_{\tilde{t}}$ is the stop mass. Given that there are two stops in the theory, a summation of the results in Eqn. 2.2.10 and 2.3.1 cancels out the quadratic divergence if $y_t = \lambda$, a condition that is guaranteed by supersymmetry. The summation of the two leading contributions is, then

$$\delta M_h^2 = \frac{y_t^2}{4\pi^2} \left[(m_t^2 - m_{\tilde{t}}^2) \text{Log} \frac{\Lambda}{m_{\tilde{t}}} + 3m_{\tilde{t}}^2 \text{Log} \frac{m_{\tilde{t}}}{m_t} \right] \quad (2.3.2)$$

which is free from quadratic divergences, the offending terms having cancelled exactly. Thus, the hierarchy problem is solved in the framework of supersymmetry.

In the limit of unbroken supersymmetry, $m_{\tilde{t}} = m_t$, and thus the entire radiative correction in Eqn. 2.3.2 cancels. However, as is elaborated in the next section, the superpartners must generally be heavier than their SM counterparts – since they have not been observed, which corresponds to broken supersymmetry. Thus $m_{\tilde{t}} > m_t$, and thus there is a non-vanishing radiative correction, which can be used to put limits on the mass of the stops. We note however, that the quadratic divergence cancels, irrespective of whether supersymmetry is exact or broken.

- *Little Higgs models:* Another popular proposal to tackle the hierarchy problem is the class of Little Higgs models [116, 117]. The basic idea of these models is that the Higgs boson is a pseudo Nambu-Goldstone boson (pNGB) of a global symmetry which is broken at some high energy scale. This is analogous to the breaking of chiral symmetry of the light quarks, where the pions play the role of the pNGBs. The general ideas are briefly discussed below, based on the treatment of Ref. [29].

In Little Higgs models, a global gauge group G is broken to a subgroup H at a scale f . The subgroup H contains the SM electroweak gauge group $\mathcal{G}_{\text{EW}} \equiv \text{SU}(2) \times \text{U}(1)$ (where the subscripts ‘ L ’ and ‘ Y ’ have been omitted for brevity). The Goldstone bosons, including the SM Higgs, of the global symmetry breaking (at scale f) reside in the coset space G/H . Various models have been invented to implement this idea using various choices for G and H .

One of the simplest cases for Little Higgs can be constructed in analogy with the low-energy sigma models. These assume a global symmetry group $G \equiv \text{SU}(3)_V \times \text{SU}(3)_A$, where the labels ‘ V ’ and ‘ A ’ are arbitrary. In such a toy construction, the global groups each break to a $\text{SU}(2)$ group. Thus, from the initial $(8 + 8 =)16$ generators of the two $\text{SU}(3)$ groups, only $(3 + 3 =)6$ survive and 10 are broken, giving 10 massless Goldstone bosons. However, gauging $\text{SU}(3)_V$ eliminates five of the Goldstone bosons (they are ‘eaten’ up as the gauge group breaks to $\text{SU}(2)$). Introducing two copies of pNGBs Φ_1 and Φ_2 , both of which transform as triplets under the gauged $\text{SU}(3)_V$, we have

$$\Phi_1 = e^{i\theta_A/f} \begin{pmatrix} 0 \\ 0 \\ \phi_1 + f \end{pmatrix}, \quad \Phi_2 = e^{-i\theta_A/f} \begin{pmatrix} 0 \\ 0 \\ \phi_2 + f \end{pmatrix} \quad (2.3.3)$$

where the vevs of the two triplets are $f_1 = f_2 = f$ and ϕ_1, ϕ_2 are real scalar fields whose mass is $m_\phi \sim f$. Moreover, the 5 Goldstone bosons are $\theta_A = \sum_{i=4}^8 \theta_A^a \tau^a$, $\tau^a = \lambda^a/2$ are the $\text{SU}(3)$ generators and the sum extends only over the broken generators. The Lagrangian is given by

$$\mathcal{L}_\Phi = |D_\mu \Phi_1|^2 + |D_\mu \Phi_2|^2 \quad (2.3.4)$$

The calculation of Feynman diagrams such as Fig 2.5 (a) and (b) yields

$$\sim \frac{g^2}{16\pi^2} \Lambda^2 (|\Phi_1|^2 + |\Phi_2|^2) \quad (2.3.5)$$

which doesn’t break the global $\text{SU}(3)_A$ symmetry. The term which breaks the symmetry is the cross-term, which can arise from the Feynman diagram in Fig. 2.5(c)

$$\frac{g^4}{16\pi^2} \text{Ln} \left(\frac{\Lambda^2}{f^2} \right) |\Phi_1^\dagger \Phi_2|^2 \quad (2.3.6)$$

Using the definitions for the Φ fields as given in Eqn. 2.3.3 and

$$\theta_A = \frac{1}{\sqrt{2}} \begin{pmatrix} 0 & 0 & h^+ \\ 0 & 0 & h^0 \\ h^- & h^{0*} & 0 \end{pmatrix} \quad (2.3.7)$$

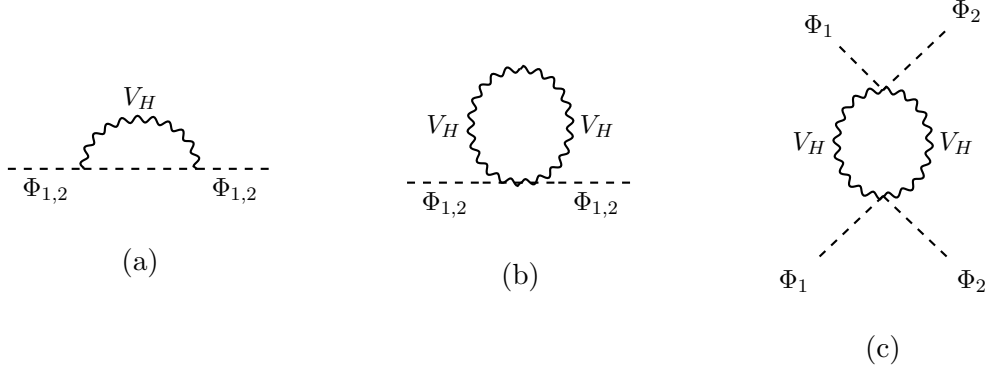


Figure 2.5: The different loop diagrams. Diagrams in (a) and (b) are propagator corrections and do not contribute to the potential of the Φ . Diagram given in (c) does contribute to the potential.

we find that

$$\left| \Phi_1^\dagger \Phi_2 \right|^2 = -4f^2 \left(H^\dagger H \right) + \frac{9}{2} \left(H^\dagger H \right)^2 + \dots \quad \text{where} \quad H = \frac{1}{\sqrt{2}} \begin{pmatrix} h^+ \\ h^0 \end{pmatrix} \quad (2.3.8)$$

The mass term for the Higgs boson, generated after symmetry breaking is then

$$m_H^2 \sim \frac{g^4}{16\pi^2} f^2 \text{Ln} \left(\frac{\Lambda^2}{f^2} \right) \quad (2.3.9)$$

giving us $m_H^2 \sim 100 \text{ GeV}$ if the value of the weak coupling is chosen for g and $f \sim 1 \text{ TeV}$. This is a remarkable result and unlike anything found in the SM, since naively we might expect the mass-squared to be proportional to $\Lambda^2/16\pi^2$, where Λ is some extremely high scale acting as the cutoff for the theory. However, that it is instead proportional to $f^2/16\pi^2$ tells us that the quadratic divergences cancel off. The cancellation happens between the heavy gauge bosons of the bigger symmetry group and the massless $SU(2)$ gauge bosons. Furthermore, unlike in SUSY, in this case, the cancellation happens between fields of same spin, an example of what is called ‘same statistics cancellation’. A similar calculation can be performed with the fermion loops, yielding the same remarkable cancellation of quadratic divergences, where the heavy top quark loop cancels the contribution from the SM top.

Besides the toy model described above, the simplest viable model was constructed by Arkani-Hamed, Cohen and Georgi, called the *Littlest Higgs* [118] and was based on the $SU(5)$ group. However, the model is disfavoured by electroweak precision data. An extension of the model [218] which involves enlarging the group with a discrete symmetry, called “T-symmetry”, helps the model evade the electroweak precision constraints [219, 220]. Additionally, the presence of the T-symmetry provides a natural lightest T-odd particle (LTP), generally the T-odd heavy photon, which can act as a dark matter candidate [221].

B. Theories with a low cut-off

In such theories, the SM is superseded by a new physics theory at fairly low energy scales, such as a few TeV, or a few tens of TeV. In that case, the presence of a Λ^2 term does not drive the Higgs boson mass to extraordinary values, since a minor tuning of the couplings could reduce it to the 125 GeV level. There are again two major classes of these theories.

- *Compositeness models*; In view of the fact that mesons and baryons, which were once thought to be elementary particles, are actually composites made up of quarks, the idea can easily be extended to the quarks and leptons, and especially the Higgs boson, which is the only elementary scalar. One possibility is that the Higgs boson is not elementary but a composite of two unknown fermions bound together by a hitherto unknown force [119–122]. Following the analogue of QCD, one can model this force as a $SU(N)_{TC}$ gauge theory, in which it is called a *technicolour* theory, and the unknown fermions are called *technifermions*. Since the force is non-Abelian in nature, we may expect a Landau pole in the interaction strength just as we do in QCD, and this will set the energy scale up to which we can treat the Higgs boson as an elementary particle, i.e. the SM is valid. Above this energy, the technicolour interactions will have to be considered in addition to the SM interactions. If we set the technicolour scale to a few TeV, the hierarchy problem disappears.

While technicolour is, in principle, a simple and attractive idea (and is supported by historical trends), in practice, it has proved to be very difficult to construct a technicolour model which is consistent with the experimental data already available. For example, to generate Yukawa couplings of the composite Higgs boson with the quarks and leptons it is necessary to embed the $SU(3)_c$ and $SU(N)_{TC}$ gauge groups in a larger gauge group called *extended technicolour* (ETC). However, in ETC models, the electroweak couplings run to large values at lower energies, and result in too large values of K^0 - \bar{K}^0 mixing and the electroweak precision variable S . This can be ameliorated by including some extra fields which suppress the beta functions in a model called *walking* (as opposed to running) technicolour. However, this then fails to explain the large top quark mass, for which one has to extend the gauge group and postulate some kind of mixing phenomena between the Higgs and a top quark condensate. There are serious problems even with these *topcolour-assisted* technicolour models.

One can go beyond technicolour and postulate that all the elementary particles, including leptons and gauge bosons, are composites of more elementary particles called *preons*. The best known models are the *haplon* and *rishon* models [123–125]. However, these theories are highly speculative in nature and we do not have properly falsifiable predictions from them as of now. All this has led to the virtual abandonment of composite models as a solution to the hierarchy problem.

- *Extra dimensions*: Theories with extra dimensions provide an economical solution to the hierarchy problem. In the simplest Kaluza-Klein models [129,130], any dimension

beyond our observable four spacetime dimension is assumed to be finite and compactified to a circle of radius R below the threshold observable in gravity experiments [126]. This gives rise to the $\mathbb{R}_4 \times \mathbb{S}_1$ topology where \mathbb{S}_1 is the circle of radius R . This was brilliantly used to create the first unified field theory, but this could not permit particle masses between zero and the Planck mass.

The basic idea of Kaluza and Klein was revived by Arkani-Hamed, Dimopoulos and Dvali(ADD) [131] to explain the hierarchy problem. They postulate a world in which a (1+3) dimensional spacetime (a D_3 brane) is embedded in a (1+3+D) dimensional toroidal spacetime (called the ‘bulk’). The SM fields are all contained on the brane, but gravity cannot be confined since it arises from the geometry of spacetime. For interactions on the brane, the bulk effects can be integrated out of the action, and hence it can be shown that

$$(M_{\text{Pl}})^2 = \left(M_{\text{Pl}}^{(1+3+D)}\right)^{D+2} V_D = \left(M_{\text{Pl}}^{(1+3+D)}\right)^{D+2} (2\pi R)^D \quad (2.3.10)$$

where M_{Pl} is the usual 4D Planck scale ($\sim 10^{19}$ GeV), $M_{\text{Pl}}^{(1+3+D)}$ is the fundamental Planck scale in the bulk and $V_D = (2\pi R)^D$ is the volume of the compact dimensions. If $R > 1/M_{\text{Pl}}$, the fundamental Planck scale will be much lower than the usual Planck scale. This reduction of the Planck scale sets a cut-off for the SM at a much lower scale and thus one can avoid the hierarchy problem.

An important prediction of the ADD model is the presence on the brane of closely-spaced Kaluza-Klein modes of the graviton field, which could collectively lead to observable effects at high energy experiments such as the LHC. No such signals have, however, been seen till date [127].

Apart from the ADD model, there are other ideas, such as the Randall-Sundrum model, which also solve the hierarchy problem by invoking extra spacetime dimensions [128]. However, as extra dimensional models do not form part of the research work in this thesis, this discussion is not carried any further.

2.3.2 Parity Violation

In sections 2.2.1B it has been mentioned that maximal parity violation is built into the SM by fiat, by placing the left- and right-chiral fermions in different representations of the gauge group $SU(2)_L$. This has intrigued researchers from the beginning, for none of the other interactions distinguish between fermions of different chirality. The neatest of the models which can explain this is the *left-right symmetric* or LRS model, where the idea is that the two chiralities are equivalent at a high scale, but become inequivalent at a low scale through a spontaneous symmetry-breaking mechanism. This is explained below, based mainly on the treatment of Ref. [132].

In the LRS model, the electroweak symmetry group is extended to

$$\mathcal{G}_{\text{LR}} = SU(2)_R \times SU(2)_L \times U(1)_{B-L} \quad (2.3.11)$$

Note that $B - L$, which was an accidental symmetry in the SM, is here elevated to the status of a gauge symmetry. It ensures that fast proton decay cannot happen. Moreover, apart from the usual left-handed fermionic doublets, one also obtains right-handed doublets

$$Q_R \left(2, 1, \frac{1}{6} \right) = \begin{pmatrix} u_R \\ d_R \end{pmatrix}; \quad L_R \left(2, 1, -\frac{1}{2} \right) = \begin{pmatrix} \nu_R \\ l_R \end{pmatrix} \quad (2.3.12)$$

where the numbers in parentheses are the gauge charges under the \mathcal{G}_{LR} gauge group. The electric charge (Q) for the doublets is given by

$$Q = T_{3L} + T_{3R} + \frac{B - L}{2} \quad (2.3.13)$$

The conservation of parity in this model implies that the interactions of the left-handed and the right-handed fermions are identical. With the right-handed weak bosons ($W_{R\mu}$), which belong to the adjoint representation of $SU(2)_R$, the interaction Lagrangian with quark fields is given by

$$\begin{aligned} \mathcal{L}_Q &= \bar{Q}_L i\gamma^\mu \left(\partial_\mu + ig_L \tau \cdot W_{L\mu} + ig' \frac{B-L}{2} B_\mu \right) Q_L \\ &+ \bar{Q}_R i\gamma^\mu \left(\partial_\mu + ig_R \tau \cdot W_{R\mu} + ig' \frac{B-L}{2} B_\mu \right) Q_R \end{aligned} \quad (2.3.14)$$

where g_L and g_R are the left and right gauge charges. A similar Lagrangian can be written for the leptons.

To explain observations, one needs to break the symmetry down to the SM symmetry group. which then breaks to $U(1)_{EM}$. The introduction of a scalar which is a doublet under both the $SU(2)$ groups helps give masses to the quarks via the Yukawa interactions. However, this doesn't break the \mathcal{G}_{LR} gauge group. In order to do so, we require additional scalar triplets $\Delta_L(3, 1, 1)$ and $\Delta_R(1, 3, 1)$. The scalar Lagrangian then becomes

$$\mathcal{L}_{\text{scalar}} = \text{Tr} \left[(D_\mu \phi)^\dagger (D^\mu \phi) + (D_\mu \Delta_L)^\dagger (D^\mu \Delta_L) + (D_\mu \Delta_R)^\dagger (D^\mu \Delta_R) \right] \quad (2.3.15)$$

The vevs can be assigned to the neutral components

$$\langle \phi \rangle_0 = \begin{pmatrix} v & 0 \\ 0 & w \end{pmatrix}; \quad \langle \Delta_{L(R)} \rangle_0 = \frac{1}{\sqrt{2}} \begin{pmatrix} 0 & 0 \\ u_L(u_R) & 0 \end{pmatrix} \quad (2.3.16)$$

The right handed symmetry must be broken at a high scale. Thus, to obtain proper magnitudes of the vevs, we have

$$u_L^2 \ll v^2 + w^2 \ll u_R^2 \quad (2.3.17)$$

which gives the required symmetry-breaking pattern

$$SU(2)_R \times SU(2)_L \times U(1)_{B-L} \xrightarrow{u_R} SU(2)_L \times U(1)_Y \xrightarrow{v,w} U(1)_{EM}$$

2.3.3 Spontaneous CP Violation

Like parity-violation, CP violation is also accommodated in the SM by fiat, as it were, by making the mass matrices complex. Once again, we note that all the other interactions conserve CP . Obviously, then, we can model CP as broken spontaneously [133] just as parity can. The CP -violating phase would then be related to the vev(s) of the Higgs field(s) which would cause the symmetry breaking. Thus, the Lagrangian would be CP -invariant, but the ground state would break the CP symmetry.

It is easy to show that if the vev of a single Higgs doublet has a phase, this can be absorbed in the phases of the Higgs scalars. Thus, more than one Higgs doublet is needed to achieve spontaneous CP violation. In the simplest extension, the most general CP -invariant potential for *two* Higgs doublets (S_1 and S_2) is

$$\begin{aligned} V = & m_1^2|S_1|^2 + m_2^2|S_2|^2 - (m_3^2 S_1 S_2 + H.c) + \lambda_1|S_1|^4 + \lambda_2|S_2|^4 + \lambda_3|S_1|^2|S_2|^2 \\ & + \lambda_4|S_1 S_2|^2 + [\lambda_5(S_1 S_2)^2 + \lambda_6|S_1|^2 S_1 S_2 + \lambda_7|S_2|^2 S_1 S_2 + H.c] \end{aligned} \quad (2.3.18)$$

At the tree level, $\lambda_5 = 0$ because of Natural Flavour Conservation (NFC) which is imposed to tackle the problem of large tree-level FCNCs [135]. However, a non-zero λ_5 might arise from loop corrections. After spontaneous symmetry breaking, we have

$$\langle S_1^0 \rangle = v_1; \quad \langle S_2^0 \rangle = v_2 e^{i\delta} \quad (2.3.19)$$

where only the neutral Higgs components get a vev. The resulting potential (with non-zero λ_5 terms) can be minimized if and only if

$$\lambda_5 > 0; \quad -1 < \cos \delta = \frac{m_3^2 - \lambda_6 v_1^2 - \lambda_7 v_2^2}{4\lambda_5 v_1 v_2} < 1 \quad (2.3.20)$$

Thus, we have a source for CP violation derived from the vevs of the Higgs doublets.

$$\cos \delta = \frac{m_3^2 - \lambda_6 v_1^2 - \lambda_7 v_2^2}{4\lambda_5 v_1 v_2} \quad (2.3.21)$$

Thus, the introduction of an extra scalar doublet is enough to provide a source of spontaneous CP violation. It may be argued, with some justification, that including an extra scalar doublet is no less of a fiat than making the mass matrices complex. However, two Higgs doublets occur naturally in supersymmetric (and other) models, which purport to solve the hierarchy problem, so that we can simultaneously allowing for spontaneous CP violation [134].

2.3.4 Strong CP Problem and Peccei-Quinn symmetry

The Strong CP problem discussed in Section 2.2.2, can be elegantly solved if we assume an extra $U(1)$ symmetry called Peccei-Quinn symmetry [136, 137]. This follows from the realisation that the transformation angle in the quark mass term and in the pseudoscalar gauge field density are related to each other by the chiral anomaly. Thus, in the mass term in the Lagrangian

$$\mathcal{L}_m = m_u \bar{u}u + m_d \bar{d}d + H.c. \quad (2.3.22)$$

we could redefine the quark fields so that the θ dependence of the $F\tilde{F}$ term goes away, in the limit of zero quark masses. In the presence of quark masses, however, we can redefine the quark fields such that there is no $\theta F\tilde{F}$ term in the Lagrangian, but there is a phase in the masses. The Lagrangian can be written as

$$\mathcal{L}_m = (m_u \bar{u}u + m_d \bar{d}d) \cos \frac{\theta}{2} + H.c. \quad (2.3.23)$$

The vacuum expectation value due to the quark condensates is then

$$E(\theta) = (m_u + m_d) e^{i\theta} \langle \bar{q}q \rangle \quad (2.3.24)$$

We can write down the quark condensate in an effective theory language with pions being the only dynamical degrees of freedom.

$$\bar{q}q \equiv \Sigma = \langle \bar{q}q \rangle \exp \left(\frac{i\sigma^a \pi^a}{2f_\pi} \right) \quad (2.3.25)$$

The Lagrangian mass term then becomes

$$\mathcal{L}_m = e^{i\theta} \text{Tr} M_q \Sigma \quad (2.3.26)$$

The pion mass is given (ignoring θ) by

$$m_\pi^2 f_\pi^2 = (m_u + m_d) \langle \bar{q}q \rangle \quad (2.3.27)$$

This can be substituted in Eqn. 2.3.24 to obtain

$$E(\theta) = m_\pi^2 f_\pi^2 \cos(\theta) \quad (2.3.28)$$

Now we assume that there a scalar particle a , called an *axion*, with the Lagrangian

$$\mathcal{L}_a = \partial_\mu a \partial^\mu a + \frac{a/f_a + \theta}{32\pi^2} F_{\mu\nu}^a \tilde{F}^{a\mu\nu} \quad (2.3.29)$$

where f_a is the axion decay constant. If the rest of QCD possesses a symmetry called the Peccei-Quinn symmetry ($U(1)_{\text{PQ}}$) such that it is invariant under a translation

$$\text{PQ} : a \rightarrow a + \alpha \quad (2.3.30)$$

by a constant α , then one can eliminate θ . The minimum of the potential for the axion occurs at $\theta = 0$ and this fixes its value. This solves the Strong CP problem.

The axions are stable particles with mass approximately given by

$$M_a^2 \simeq \frac{f_\pi^2 m_\pi^2}{f_a^2} \quad (2.3.31)$$

If $f_a \sim 10^3$ GeV, $M_a \sim$ keV. Axions are a particularly attractive theoretical proposition since this model provides the economy of solving both the Strong CP problem and providing a natural dark matter candidate.

2.3.5 Fermion Mass Models

There have been several attempts to explain the hierarchy in the fermion masses of the SM by building models which would give a definite structure to the fermion mass matrices (or equivalently, to the Yukawa couplings) in the SM. These may be classified into two types.

1. *Democratic Models:* The simplest democratic model [145, 146] just assumes that the Yukawa couplings are all equal, which can be enforced by adding a S_3 global symmetry to the SM. The Yukawa matrix is, then, of the form

$$Y = k \begin{pmatrix} 1 & 1 & 1 \\ 1 & 1 & 1 \\ 1 & 1 & 1 \end{pmatrix} \quad (2.3.32)$$

This is a completely natural choice, since the couplings of gauge bosons to fermions of a particular charge are all the same. Considering only the quark sector, the up and down sectors are distinguished by the different choices for the value of k (k_u for up type and k_d for down type). The diagonalized mass matrix gives the masses, which are then

$$(m_1, m_2, m_3) = (0, 0, 3k) \quad (2.3.33)$$

Although this reflects the hierarchy between the third (heavy) generation and the first two (light) generations, it does not provide masses for the first generations. In order to obtain non-zero masses for the first two generations, attempts to break the democratic S_3 symmetry or perturb the democratic Yukawa matrices have been pursued in the literature [138, 139]. None of these models are quite convincing, however, since their assumptions are rather ad hoc, and moreover, it is not clear how much of the mass of the first generation quarks comes from the Lagrangian and how much comes from the electromagnetic and other self-energy corrections.

2. *Textures:* The opposite point of view to the democratic model is to assume that some of the terms in the Yukawa matrix are actually zero, i.e. they are presumably forbidden by some symmetry. One of the first ansätze, made by Fritzsch [140], for the quark mass matrix was

$$M_u = \begin{pmatrix} 0 & A_u & 0 \\ A_u^* & 0 & B_u \\ 0 & B_u^* & C_u \end{pmatrix}; \quad M_d = \begin{pmatrix} 0 & A_d & 0 \\ A_d^* & 0 & B_d \\ 0 & B_d^* & C_d \end{pmatrix} \quad (2.3.34)$$

This however fails to explain the quark mixing data as it cannot faithfully reproduce the CKM matrix [141]. The Fritzsch model has been generalised into the texture models where a model is called an ' n -zero texture model' if for the mass matrix the number of zeros along the diagonal added to half of the symmetric off-diagonal zeros equals n . Thus, each of M_u and M_d above is a 3-zero texture model while the two taken together makes the Fritzsch model a 6-zero texture model. There is a family of such models, but modern quark mixing data generally rules them out [142]. Analysis of 5-zero

texture models have not yielded any success at explaining the observed quark masses and mixings either [142]. However, 4-zero texture models have been quite successful [143, 144].

In conclusion, we may say that though there exist different models which try to explain the flavour-mixing and CP -violation in the SM, none of them is completely convincing, and hence, this sector of the SM remains as much of a mystery as ever.

2.3.6 Neutrino Masses

The main issue in neutrino masses is their smallness, which, as we have seen, would require Yukawa couplings of 10^{-13} or less, which would be difficult to sustain under radiative corrections. However, there is a saving grace. Neutrinos, being the only neutral fermions in the SM, can be Majorana in nature, which means that a neutrino is its own CP -conjugate particle. This allows one to write down a mass term for the left-handed neutrinos ($LH\nu$ s) alone without invoking the right-handed neutrinos. However, the mass parameter would still be intolerably small.

To get around this, an ingenious mechanism called the *seesaw mechanism* was invented by introducing the right handed neutrinos ($RH\nu$ s) in the theory with their own Majorana mass term in the Lagrangian [149], viz.

$$\mathcal{L}_m^\nu = m_{LL}\overline{\nu}_L\nu_L^C + M_{RR}\overline{\nu}_R\nu_R^C \quad (2.3.35)$$

The introduction of the $RH\nu$ s also allow us to write down a Dirac-type mass term $m_{LR}\overline{\nu}_L\nu_R$ giving us the mass matrix

$$\begin{pmatrix} \overline{\nu}_L & \overline{\nu}_R^C \end{pmatrix} \begin{pmatrix} 0 & m_{LR} \\ m_{LR}^T & M_{RR} \end{pmatrix} \begin{pmatrix} \nu_L^C \\ \nu_R \end{pmatrix} \quad (2.3.36)$$

Since $RH\nu$ s are singlets in the theory, their Majorana masses can be very large, even several orders of magnitude higher than the electroweak scale. Under such an approximation, the diagonalisation of this matrix gives

$$m_{LL} \simeq -m_{LR}M_{RR}^{-1}m_{LR}^T \quad (2.3.37)$$

If $m_{LR} \sim 100$ GeV then $M_{RR} \sim 10^{16}$ GeV, $m_{LL} \sim 10^{-3}$ eV, fits solar neutrino data quite well.

The model described above is called ‘Type I seesaw’. There are other ways to implement a seesaw mechanism, e.g., by including a heavy weak triplet scalar field (‘Type II seesaw’) or two fermionic weak triplet fields (‘Type III seesaw’). More details can be found in Refs. [147, 148].

2.4 Grand Unified Theories

Unification of interactions previously thought to be fundamental has always been a major objective of physics. Two great advances in this direction have been the unification of electricity

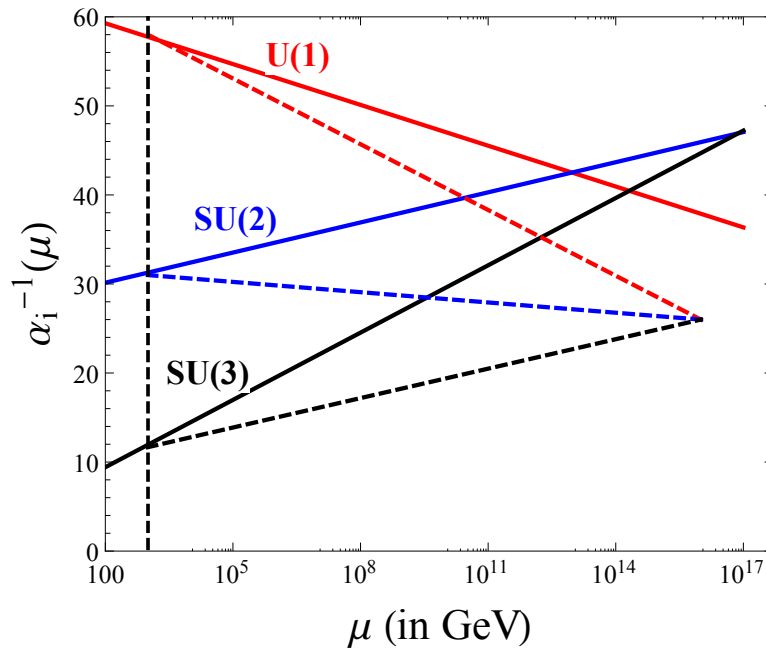


Figure 2.6: The running of the couplings of the different gauge groups. The dashed lines represent the running of the coupling constants in the framework of the SM and the unbroken lines are plotted in the framework of a SU(5) GUT. New particles are assumed to occur at the TeV scale, indicated by the dashed vertical line.

with magnetism by Maxwell in the nineteenth century [150], and the unification of electromagnetism with weak interactions by Glashow, Salam and Weinberg in the twentieth [3, 5, 6]. Thus, the SM consists of two fundamental interactions, viz. strong and electroweak, with gravitation as a third fundamental force. Though gravitation is well explained at the classical level by Einstein's equations its true nature still remains a mystery, since no wholly satisfactory means has been found to quantise it. There are also alternative views which treat gravitation as a classical background field [151] or as an emergent force [152, 153]. However, when we come to the two forces in the SM, it is natural to ask if they can also be unified at some higher energy scale, in a repetition of the triumph of the electroweak theory [124]. This has given rise to a class of unified gauge-theoretic models known as *Grand Unified Theories* (GUTs).

The main hypothesis of all GUTs is that there is a single gauge interaction above a sufficiently high scale called the GUT scale (Λ_{GUT}) (see Fig. 2.6). The corresponding gauge group, called the GUT group \mathcal{G}_{GUT} , breaks spontaneously at this scale to the SM gauge group

$$\mathcal{G}_{\text{GUT}} \xrightarrow{\Lambda_{\text{GUT}}} \mathcal{G}_{\text{SM}} = SU(3)_c \times SU(2)_L \times U(1)_Y \xrightarrow{v_{\text{EW}}} U(1)_{\text{em}}$$

of which the electroweak component, in turn, breaks spontaneously to the electromagnetic gauge group at the electroweak scale v_{EW} . We note that the main challenge of GUT is not only to be able to unify the forces in the SM, but also to reproduce the observed fermion

masses and mixing. There have been very many proposals for GUTs over the decades, only a few of which have stood the test of time. As an example, however, we describe only the simplest one.

GUT based on SU(5): This theory was originally due to Georgi and Glashow [154], but this section mainly follows the discussion in Refs. [155–157]. The SM gauge group \mathcal{G}_{SM} is embedded within $SU(5)$ and the spontaneous symmetry-breaking happens at the GUT scale. The fields in this theory are all left-handed; the right-handed fields are related to them by a CP -conjugation. The fermions are in the fundamental $\mathbf{5} + \bar{\mathbf{5}}$ representation, which makes the theory anomaly-free. The 24 generators of the group are given by a generalization of the Gell-Mann matrices, λ_a , $a = 1, \dots, 24$ (listed in Ref. [155]), with the first eight generators identified with the generators of $SU(3)_C$. The $SU(2)_L$ generators are associated the last three generators of the list. Thus,

$$T_a^{(3)} = \frac{\lambda_a}{2} \quad (a = 1, \dots, 8); \quad T_1^{(2)} = \frac{\lambda_{22}}{2}, \quad T_2^{(2)} = \frac{\lambda_{23}}{2}, \quad T_3^{(2)} = \frac{\sqrt{10}\lambda_{24} - \sqrt{6}\lambda_{15}}{6} \quad (2.4.1)$$

where the superscripts refer either to the group $SU(3)_C$ or $SU(2)_L$. The generator of electric charge is identified with

$$Q = -\sqrt{\frac{2}{3}}\lambda_{15} \quad (2.4.2)$$

Thus, using $Q = T_3^L + Y$, we can identify the generator associated with the hypercharge

$$Y = -\frac{1}{8} \left(\sqrt{10}\lambda_{24} + \frac{5\sqrt{6}}{3}\lambda_{15} \right) \quad (2.4.3)$$

The gauge fields, written as $A^\mu = A_a^\mu T_a$, $a = 1, \dots, 24$. There are a set of new fields which get introduced as well. These are the *leptoquarks* — vector bosons which interact with a quark and a lepton. They are given by

$$\begin{aligned} X_1^\mu &= \frac{1}{\sqrt{2}} (A_9^\mu + iA_{10}^\mu) & X_2^\mu &= \frac{1}{\sqrt{2}} (A_{11}^\mu + iA_{12}^\mu) & X_3^\mu &= \frac{1}{\sqrt{2}} (A_{13}^\mu + iA_{14}^\mu) \\ Y_1^\mu &= \frac{1}{\sqrt{2}} (A_{16}^\mu + iA_{17}^\mu) & Y_2^\mu &= \frac{1}{\sqrt{2}} (A_{18}^\mu + iA_{19}^\mu) & Y_3^\mu &= \frac{1}{\sqrt{2}} (A_{20}^\mu + iA_{21}^\mu) \end{aligned} \quad (2.4.4)$$

The left-handed fermions fit into $\bar{\mathbf{5}}$ of $SU(5)$, ψ_L^i , and a $\mathbf{10}$ of $SU(5)$, ψ_{Lij} along with a singlet neutrino. It is given by

$$\psi_L^i = \begin{pmatrix} d_R^C \\ d_B^C \\ d_G^C \\ e \\ \nu_e \end{pmatrix}_L; \quad \psi_{Lij} = \begin{pmatrix} 0 & u_G^C & -u_B^C & -u_R & -d_R \\ -u_G^C & 0 & u_R^C & -u_B & -d_B \\ u_B^C & -u_R^C & 0 & -u_G & -d_G \\ u_R & u_B & u_G & 0 & -e^C \\ d_R & d_B & d_G & e^C & 0 \end{pmatrix}_L \quad (2.4.5)$$

The RH antiparticles can be similarly represented in a $\mathbf{5} + \bar{\mathbf{10}}$ of $SU(5)$.

Spontaneous Symmetry Breaking: There are two widely different scales involved in GUT — one is the GUT scale and the other is the electroweak (EW) scale. This requires us to include

two separate Higgs multiplets with two different vacuum expectation values (vevs). A Higgs represented as a 24-plet in the adjoint representation breaks $SU(5)$ to the SM gauge group and another Higgs in the 5-plet breaks the SM gauge symmetry. The vevs of the **24** Higgs give masses of $\sim 10^{15}$ GeV and that of the **5** Higgs provide EW-scale masses. The two Higgses ($\Phi \equiv \mathbf{24}$ of Higgs; $H \equiv \mathbf{5}$ of Higgs) are written as

$$\Phi \equiv \sum_{a=1}^{24} S_a T_a; \quad H \equiv \begin{pmatrix} H_1 \\ H_2 \\ H_3 \\ H_4 \\ H_5 \end{pmatrix} \quad (2.4.6)$$

The potential for the two Higgses are

$$\begin{aligned} V_\Phi &= m_1^2 \text{Tr} \Phi^2 + \lambda_1 (\text{Tr} \Phi^2)^2 + \lambda_2 \text{Tr} \Phi^4 \\ V_H &= \frac{m_2^2}{2} H^\dagger H + \frac{\lambda_3}{4} (H^\dagger H)^2 \end{aligned} \quad (2.4.7)$$

The minimum can be calculated to obtain the vev.

$$v_\Phi^2 = -\frac{m_1^2}{\lambda_1 + 7\lambda_2/30}; \quad v_H^2 = -\frac{m_2^2}{\lambda_3} \quad (2.4.8)$$

Since the Φ field provides mass to the leptoquarks which are supposed to have masses of the order of Λ_{GUT} , we have

$$m_X, m_Y \simeq g_G (\Lambda_{\text{GUT}}) v_\Phi \quad (2.4.9)$$

It can be estimated using $\alpha_S(M_Z)$ that $g_G \sim 10^{-2}$, which gives

$$v_\Phi \simeq \frac{\Lambda_{\text{GUT}}}{g_G} \simeq \frac{10^{14} \text{ GeV}}{10^{-2}} = 10^{16} \text{ GeV} \quad (2.4.10)$$

This is a rough estimate and other numerical factors might change it by an order or so. The electroweak transition happens due to the H field and thus $v_H \sim 10^2$ GeV. Thus there is a large hierarchy between the two vevs.

Problems with GUTs: The scale of unification varies somewhat between different GUTs, but it is always a few orders of magnitude below the Planck scale. For $SU(5)$, e.g., $\Lambda_{\text{GUT}} \simeq 10^{14}$ GeV. However, calculations show that the value of $\sin^2 \theta_W(M_Z) = 0.206$, which is different from the experimentally established value of $\sin^2 \theta_W(M_Z) = 0.229 \pm 0.004$ [22]. Thus, the initial intention of uniting the three forces at a scale ends up short when compared with electroweak measurement.

Another more-or-less universal prediction of GUTs is proton decay due to the leptoquark gauge bosons in the theory which couple to both leptons and quarks. The lifetime of the proton predicted by most GUTs is in the range of $10^{30} - 10^{33}$ years, which is lower than the lower limit of 10^{34} years established by experiments [158]. This rules out these theories, including the minimal $SU(5)$ model described above. Some of the models which can survive

the proton decay constraint are based on the flipped $SU(5)$ [159], $SO(10)$ [160] and E_6 [161] gauge groups.

It is worth mentioning that the introduction of Λ_{GUT} , which acts as a cutoff for the SM, and lies far above the electroweak scale, exacerbates the hierarchy problem in GUTs. For this reason, most modern GUTs are embedded in supersymmetric theories, to which we now turn.

2.5 Supersymmetry

It has already been explained above how the hierarchy problem is ameliorated in models with *supersymmetry*. In this section, we describe supersymmetric models in some more detail. Most of this material is referenced from the multiple lectures, reviews and books available in the literature, such as [162–169].

A supersymmetry (SUSY) transformation turns bosons (b) into fermions (f) and vice versa. The Haag-Lopuszanski-Sohnius theorem [170] shows how to bypass the no-go theorem of Coleman and Mandula [171] by making the SUSY transformation spinorial and Grassmann-valued in nature. Its generators Q and Q^\dagger are, therefore, anti-commutating spinor (fermionic) operators which act as

$$Q|f\rangle = |b\rangle; \quad Q|b\rangle = |f\rangle \quad (2.5.1)$$

where $|b\rangle$ and $|f\rangle$ are bosonic and fermionic states respectively. The SUSY algebra is given by

$$\begin{aligned} \{Q, Q^\dagger\} &= P^\mu \\ \{Q, Q\} &= \{Q^\dagger, Q^\dagger\} = 0 \\ \{P^\mu, Q\} &= \{P^\mu, Q^\dagger\} = 0 \end{aligned}$$

where P^μ is the generator of spacetime translations, i.e. the four-momentum. Furthermore, the SUSY generators commute with all the generators of gauge transformations. In principle, there could be N copies of the SUSY generators Q and Q^\dagger , in which case the model is called N -SUSY. However, it has been shown that only $N = 1$ SUSY theories survive the test of experimental evidence (E.g. see Sec. 3.1 of Ref. [164]).

A supersymmetric multiplet comprises a SM field and its superpartners, as well as some unphysical ‘auxiliary’ fields (F and D fields) which disappear in on-shell terms. Each left-chiral and each right-chiral fermion has a scalar partner, while each gauge boson has a corresponding Majorana fermion as a partner. The scalar superpartners of SM fermions are called sfermions (squarks and sleptons, or more specifically, selectrons, smuons, stops, etc.). The fermionic partners of gauge bosons are called gauginos, e.g. the SUSY partner of a W boson is a wino and that of a gluon is a gluino. Additionally, the Higgs sector has two scalar doublets and their superpartners are called Higgsinos. The additional Higgs doublet must be present because the superpotential, being a holomorphic function of chiral superfields, does not permit a single Higgs doublet to provide mass to both up and down type quarks.

The above constitute the complete set of fields in the so-called *minimal* supersymmetric Standard Model (MSSM). A summary of all these MSSM fields is given in Table 2.1.

SM field	SUSY partner	$SU(3)_C \times SU(2)_L \times U(1)_Y$
Scalar superpartners		
<i>Squarks</i>		
Q_L	$\tilde{Q} = \begin{pmatrix} \tilde{u}_L \\ \tilde{d}_L \end{pmatrix}$	(3, 2, 1/6)
u_R	\tilde{u}_R	(3, 1, 2/3)
d_R	\tilde{d}_R	(3, 1, -1/3)
<i>Sleptons</i>		
L_L	$\tilde{L} = \begin{pmatrix} \tilde{\nu}_L \\ \tilde{e}_L \end{pmatrix}$	(1, 2, -1/2)
e_R	\tilde{e}_R	(1, 1, -1)
Fermionic superpartners		
<i>Bino</i>		
B^0	\tilde{B}^0	(1,1,0)
<i>Wino</i>		
W_3^0 W_3^\pm	\tilde{W}_3^0 \tilde{W}_3^\pm	(1,3,0)
<i>Gluino</i>		
g	\tilde{g}	(8, 1, 0)
<i>Higgsino</i>		
$H_1 = \begin{pmatrix} H_1^0 \\ H_1^- \end{pmatrix}$	$\tilde{H}_1 = \begin{pmatrix} H_1^0 \\ H_1^- \end{pmatrix}$	(1, 2, -1/2)
$H_2 = \begin{pmatrix} H_2^+ \\ H_2^0 \end{pmatrix}$	$\tilde{H}_2 = \begin{pmatrix} \tilde{H}_2^+ \\ H_2^0 \end{pmatrix}$	(1, 2, 1/2)

Table 2.1: The different supermultiplets in the MSSM

The MSSM Lagrangian can then be constructed in analogy with the SM, taking care that it remains invariant under SUSY transformations.

2.5.1 SUSY breaking

As mentioned before, if SUSY is exact, the superpartners would have the same masses and couplings as the SM fields, and if this were so, they should have been observed in the same set of experiments as the SM fields. Since this is not the case, clearly the superpartners must *all* be heavier than their SM counterparts – heavy enough to have evaded discovery at all experiments done till date. This would require SUSY to be broken in the MSSM Lagrangian, with the higher masses of the superpartners arising from the SUSY-breaking parameter(s).

The most obvious notion would be to assume that SUSY breaks spontaneously, just as the gauge symmetries do. However, the energy of the vacuum state in a SUSY theory is non-

negative

$$\langle 0|H|0\rangle = \frac{1}{4} \left(|Q_1|0\rangle|^2 + |Q_1^\dagger|0\rangle|^2 + |Q_2|0\rangle|^2 + |Q_2^\dagger|0\rangle|^2 \right) \geq 0 \quad (2.5.2)$$

and therefore, it has a unique minimum at zero. It follows that SUSY cannot be spontaneously broken and hence some other mode of SUSY breaking is called for. Moreover, spontaneous breaking of SUSY would lead to the ‘supertrace’ mass formula

$$\mathcal{STr} \mathcal{M}^2 \equiv \sum_i (-1)^{2s_i} m_i^2 = 0 \quad (2.5.3)$$

where m_i and s_i are the mass and spin of all the MSSM fields. Separating out terms with opposite signs shows that the sum of all SM particle masses must equal the sum of all superpartner masses, which is clearly not possible if *all* the superpartners are heavier than their SM counterparts.

Since SUSY cannot be spontaneously broken, it is necessary to explicitly break it by introducing soft SUSY-breaking terms

$$\mathcal{L}_{\text{soft}}^{\text{MSSM}} = \mathcal{L}_{\text{soft}}^{\text{Gauginos}} + \mathcal{L}_{\text{soft}}^{\text{sleptons}} + \mathcal{L}_{\text{soft}}^{\text{squarks}} + \mathcal{L}_{\text{soft}}^{\text{Higgs}} + \mathcal{L}_{\text{soft}}^{\text{trilinear}} \quad (2.5.4)$$

where

$$\mathcal{L}_{\text{soft}}^{\text{Gauginos}} = -\frac{1}{2} \left(M_1 \tilde{B} \tilde{B} + M_2 \tilde{W} \tilde{W} + M_3 \tilde{g} \tilde{g} \right) + c.c. \quad (2.5.5)$$

$$\mathcal{L}_{\text{soft}}^{\text{sleptons}} = -\tilde{L}^\dagger \mathbf{m}_{\tilde{L}}^2 \tilde{L} - \tilde{e}^2 \mathbf{m}_{\tilde{e}}^2 e^\dagger \quad (2.5.6)$$

$$\mathcal{L}_{\text{soft}}^{\text{squarks}} = -\tilde{Q}^\dagger \mathbf{m}_{\tilde{Q}}^2 \tilde{Q} - \tilde{u} \mathbf{m}_{\tilde{u}}^2 \tilde{u}^\dagger - \tilde{d} \mathbf{m}_{\tilde{d}}^2 \tilde{d}^\dagger \quad (2.5.7)$$

$$\mathcal{L}_{\text{soft}}^{\text{Higgs}} = -m_{H_u}^2 H_u^* H_u - m_{H_d}^2 H_d^* H_d - (B H_u H_d + \text{H.c.}) \quad (2.5.8)$$

$$\mathcal{L}_{\text{soft}}^{\text{trilinear}} = -\mathbf{A}_u \tilde{u} \tilde{Q} H_u + \mathbf{A}_d \tilde{d} \tilde{Q} H_d + \mathbf{A}_e \tilde{e} \tilde{L} H_d + \text{H.c.} \quad (2.5.9)$$

These terms are called ‘soft’ because when they are used to calculate radiative corrections, one only gets ‘soft’ i.e. logarithmic divergences, and not the quadratic divergences which create the hierarchy problem. Thus, breaking SUSY through soft terms does not re-generate a hierarchy problem.

Of course, the inclusion of a whole set of new terms in the Lagrangian calls for an explanation. The soft terms can then be thought of as generated by the spontaneous breaking of SUSY in a *hidden* sector, i.e. a set of fields which do not have any interaction terms with the SM fields (as shown schematically in Fig. 2.7). The breaking of SUSY is then communicated to the (potentially) visible SUSY sector by certain interactions. Depending on the nature of these interactions, the SUSY-breaking can be gravity-mediated (SUGRA) or gauge-mediated (GMSB) or anomaly (AMSB) or gravitino-mediated. In this section, we discuss only gravity mediation, while gauge mediation is described briefly in Chapter 6.

Gravity Mediation: This is the most obvious option since gravity couples universally. The effect of the new physics in the hidden sector can be parametrised by higher-order operators suppressed by the Planck scale mass, M_{Pl} . A hidden sector chiral superfield has a non-vanishing F term which gets a vev, such that

$$\langle \hat{X} \rangle = 0; \quad \langle F_X \rangle \neq 0 \quad (2.5.10)$$

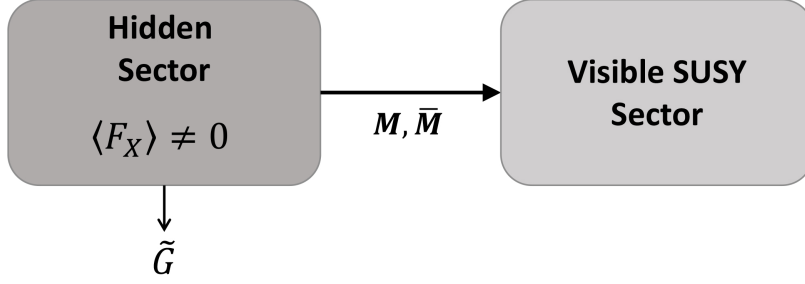


Figure 2.7: In the standard paradigm of SUSY breaking, SUSY is broken in the hidden sector, which produces a goldstino. The goldstino is ‘eaten’ by the gravitino \tilde{G} . The breaking is communicated to the visible SUSY sector by means of messenger fields M, \bar{M} .

The interaction Lagrangian between the hidden sector superfield \hat{X} and the visible SUSY superfields is

$$\begin{aligned} \mathcal{L}_{\text{int}} = & \int d^2\theta d^2\bar{\theta} \left(\frac{c}{M_{\text{Pl}}^2} \hat{X}^\dagger \hat{X} \hat{Q}_i^\dagger \hat{Q}_i + \frac{b'}{M_{\text{Pl}}^2} \hat{X}^\dagger \hat{X} \hat{H}_u \hat{H}_d + \frac{b}{M_{\text{Pl}}} \hat{X}^\dagger \hat{H}_u \hat{H}_d + H.c. \right) \\ & + \int d^2\theta \left(\frac{s}{M_{\text{Pl}}} \hat{X} \hat{W}_a^\alpha \hat{W}_a^\alpha + \frac{a}{M_{\text{Pl}}} \hat{X} \hat{Q}_i \hat{H}_u \hat{Q}_i + H.c. \right) \end{aligned} \quad (2.5.11)$$

where $\alpha, a = 1, 2, 3$ and the carets indicate superfields. The soft masses are then roughly given by

$$m_{\text{soft}} \sim \frac{\langle F_X \rangle}{M_{\text{Pl}}} \quad (2.5.12)$$

If we assume that $m_{\text{soft}} \sim \text{TeV}$, we get the intermediate scale

$$M_I = \sqrt{\langle F_X \rangle} \sim \sqrt{m_{\text{soft}} M_{\text{Pl}}} \sim 10^{11} \text{GeV} \quad (2.5.13)$$

From the Lagrangian in Eqn. 2.5.11, we get a B -term given by

$$\int d^2\theta d^2\bar{\theta} \frac{b}{M_{\text{Pl}}} \hat{X}^\dagger \hat{H}_u \hat{H}_d = b \frac{\langle F_X \rangle}{M_{\text{Pl}}} \int d^2\theta \hat{H}_u \hat{H}_d \quad (2.5.14)$$

There is however a term in the SUSY potential generated from the unbroken MSSM Lagrangian

$$\hat{W}_\mu = \mu H_u H_d \quad (2.5.15)$$

Since this is not related to any dynamical supersymmetry breaking mechanism, μ can have any magnitude, not necessarily one related to m_{soft} . In gravity mediation, however, that is not a problem. One can impose a discrete symmetry such that at the tree level $\mu = 0$ and then both μ and B are generated radiatively and are thus of the same order of magnitude.

Gravity mediation, elegant as it is, has a problem in the flavour sector, as it can potentially lead to large FCNCs at the tree level. These are severely constrained from experimental data, and difficult to fit in with the predictions of gravity-mediation. This is referred to as the *flavour problem* in SUSY theories.

2.5.2 The Higgs Sector in the MSSM:

It has already been explained that at least two Higgs doublets are needed in SUSY. In the MSSM, there are exactly two Higgs doublets. After spontaneous breaking of the electroweak symmetry, three of these become Goldstone modes ‘eaten up’ by the weak gauge bosons, leaving five physical Higgs bosons, viz. the h^0 (light Higgs), the H^0 (heavy Higgs), the H^\pm (charged Higgses) and the A^0 (CP-odd Higgs).

The two Higgs doublets may be written

$$H_1 = \begin{pmatrix} H_1^0 \\ H_1^- \end{pmatrix} \quad \text{with} \quad Y_{H_1} = -1; \quad H_2 = \begin{pmatrix} H_2^+ \\ H_2^0 \end{pmatrix} \quad \text{with} \quad Y_{H_2} = +1 \quad (2.5.16)$$

The Higgs potential is given by

$$\begin{aligned} V_H &= (\mu^2 + m_{H_1}^2) H_1^\dagger H_1 + (\mu^2 + m_{H_2}^2) H_2^\dagger H_2 - \mu B(\epsilon_{ab} H_1^a H_2^b + H.c.) \\ &+ \frac{g_1^2 + g_2^2}{8} (H_1^\dagger H_1 - H_2^\dagger H_2)^2 + \frac{g^2}{2} |H_1^\dagger H_2|^2 \end{aligned} \quad (2.5.17)$$

The neutral component of the two Higgs doublets can acquire a vev each such that

$$\langle H_1 \rangle = \begin{pmatrix} v_1 \\ 0 \end{pmatrix} \quad \langle H_2 \rangle = \begin{pmatrix} 0 \\ v_2 \end{pmatrix} \quad (2.5.18)$$

The ratio of the vevs is defined as $\tan \beta = v_2/v_1$. The mass of the CP-odd Higgs, given by

$$M_A^2 = \mu B(\tan \beta + \cot \beta), \quad (2.5.19)$$

is another parameter. In fact, all the masses and mixing angles in the MSSM Higgs sector can be expressed in terms of $\tan \beta$ and M_A . For example, the tree-level masses of the charged and the neutral Higgs bosons are given by

$$\begin{aligned} M_{H^\pm}^2 &= M_{A^0}^2 + M_W^2 \\ M_{H^0, h^0}^2 &= \frac{1}{2} \left(M_{A^0}^2 + M_Z^2 \pm \sqrt{(M_{A^0}^2 + M_Z^2)^2 - 4M_Z^2 M_{A^0}^2 \cos^2 2\beta} \right) \end{aligned} \quad (2.5.20)$$

The second of the equations tells us that at tree level $M_{h^0} \leq M_Z$, which would be contrary to the observations. However, loop corrections are very important for the mass of the light Higgs boson. The one-loop result is

$$M_{h^0}^2 \simeq M_Z^2 \cos^2 2\beta + \frac{3g^2}{8\pi^2} \frac{m_t^4}{M_W^2} \log \left(\frac{m_{\tilde{t}_1}^2 + m_{\tilde{t}_2}^2}{2m_t^2} \right) \quad (2.5.21)$$

This correction, which drives M_{h^0} above M_Z , is very sensitive to the mass of the top quark, which appears as a fourth power. In the MSSM, two-loop calculations have been done for the neutral CP-even Higgs bosons and the upper limit for the mass of the light Higgs has been found to be about 135 GeV [172, 173] — which is perfectly consistent with the 125 GeV scalar found at CERN. This, in fact, is the only experimental fact that supports SUSY models, as of date. Of course, while this is encouraging, it is far from being in any way conclusive.

2.5.3 Mixing between SUSY particles

Sfermions: We have seen that every fermion in the SM is partnered by two sfermions. These can mix with each other since they have the same quantum numbers. The flavour eigenstates – the right- and left-handed sfermions – mix with each other to give two mass eigenstates. Thus, in the third generation, $(\tilde{t}_L, \tilde{t}_R)$ mix to give the two mass states $(\tilde{t}_1, \tilde{t}_2)$, while $(\tilde{b}_L, \tilde{b}_R)$ mix to give $(\tilde{b}_1, \tilde{b}_2)$ and $(\tilde{\tau}_L, \tilde{\tau}_R)$ mix to give $(\tilde{\tau}_1, \tilde{\tau}_2)$. The stop mass matrix in the flavour basis $(\tilde{t}_L, \tilde{t}_R)$ is given by

$$m_{\tilde{t}}^2 = \begin{pmatrix} m_{\tilde{Q}_3}^2 + m_t^2 + \left(\frac{1}{2} - \frac{2}{3} \sin^2 \theta_W\right) M_Z^2 \cos 2\beta & m_t \left(A_t - \frac{\mu}{\tan \beta}\right) \\ m_t \left(A_t - \frac{\mu}{\tan \beta}\right) & m_{\tilde{u}_3}^2 + m_t^2 + \frac{2}{3} M_Z^2 \sin^2 \theta_W \cos 2\beta \end{pmatrix} \quad (2.5.22)$$

The mass eigenstates are then

$$\begin{pmatrix} \tilde{t}_1 \\ \tilde{t}_2 \end{pmatrix} = \begin{pmatrix} \cos \theta_{\tilde{t}} & -\sin \theta_{\tilde{t}} \\ \sin \theta_{\tilde{t}} & \sin \theta_{\tilde{t}} \end{pmatrix} \begin{pmatrix} \tilde{t}_L \\ \tilde{t}_R \end{pmatrix} \quad (2.5.23)$$

where obviously $\theta_{\tilde{t}}$ is substantial because m_t is large. The analogous mass matrices in the $(\tilde{b}_L, \tilde{b}_R)$ and the $(\tilde{\tau}_L, \tilde{\tau}_R)$ basis are

$$\begin{aligned} m_{\tilde{b}}^2 &= \begin{pmatrix} m_{\tilde{Q}_3}^2 + m_b^2 - \left(\frac{1}{2} - \frac{1}{3} \sin^2 \theta_W\right) M_Z^2 \cos 2\beta & m_b(A_b - \mu \tan \beta) \\ m_b(A_b - \mu \tan \beta) & m_{\tilde{d}_3}^2 + m_b^2 + \frac{1}{3} M_Z^2 \sin^2 \theta_W \cos 2\beta \end{pmatrix} \\ m_{\tilde{\tau}}^2 &= \begin{pmatrix} m_{\tilde{L}_3}^2 + m_{\tau}^2 - \left(\frac{1}{2} - \sin^2 \theta_W\right) M_Z^2 \cos 2\beta & m_{\tau}(A_{\tau} - \mu \tan \beta) \\ m_{\tau}(A_{\tau} - \mu \tan \beta) & m_{\tilde{e}_3}^2 + m_{\tau}^2 + M_Z^2 \sin^2 \theta_W \cos 2\beta \end{pmatrix} \end{aligned} \quad (2.5.24)$$

and here too, there is mixing, though not at the same level as the stop mixing because of the smaller masses of the b and the τ^{\pm} .

The RG evolution of some of the squared-mass parameters is given by

$$\begin{aligned} \frac{d}{dt} m_{\tilde{Q}_3}^2 &= \frac{1}{16\pi^2} \left(X_t + X_b - \frac{2}{15} g_1^2 |M_1|^2 - 6g_2^2 |M_2|^2 - \frac{32}{3} g_3^2 |M_3|^2 + \frac{1}{5} g_1^2 S \right) \\ \frac{d}{dt} m_{\tilde{u}_3}^2 &= \frac{1}{16\pi^2} \left(2X_t - \frac{32}{15} g_1^2 |M_1|^2 - \frac{32}{3} g_3^2 |M_3|^2 - \frac{4}{5} g_1^2 S \right) \\ \frac{d}{dt} m_{\tilde{d}_3}^2 &= \frac{1}{16\pi^2} \left(2X_b - \frac{8}{15} g_1^2 |M_1|^2 - \frac{32}{3} g_3^2 |M_3|^2 + \frac{2}{5} g_1^2 S \right) \end{aligned} \quad (2.5.25)$$

where

$$\begin{aligned} X_t &= 2|y_t|^2 (m_{H_u}^2 + m_{\tilde{Q}_3}^2 + m_{\tilde{u}_3}^2) + 2|a_t|^2 \\ X_b &= 2|y_b|^2 (m_{H_d}^2 + m_{\tilde{Q}_3}^2 + m_{\tilde{d}_3}^2) + 2|a_b|^2 \\ S &= m_{H_u}^2 - m_{H_d}^2 + \text{Tr} \left(\mathbf{m}_{\tilde{Q}}^2 - \mathbf{m}_{\tilde{L}}^2 - 2\mathbf{m}_{\tilde{u}}^2 + \mathbf{m}_{\tilde{d}}^2 + \mathbf{m}_{\tilde{e}}^2 \right) \end{aligned}$$

The mixing of these squarks is controlled by the $\tan \beta$ term in the off-diagonal elements. If $\tan \beta$ is small, the effect of the mixing is very small and the mass eigenstates will be very

nearly the flavour eigenstates. This means that both the staus and the right handed sbottom and stop will be nearly degenerate with the first two generations. However, the left-handed bottom squark can receive large contributions from the fact that it is in the same doublet as the left handed stop. It is seen from Eqns. 2.5.25 that the effect of X_t and X_b is to drive the value of $m_{Q_3}^2$ towards smaller values as one goes down in energy. However, X_t is much higher than X_b because of the Yukawa coupling and thus it is much more efficient at driving the value down than X_b . This reduces the mass squared of the stop and thus the lighter stop can be much lighter than the up-type squarks of the first two generations. As for the \tilde{b}_L , it is also affected by the same factor of X_t as it is in the same doublet as the stop. Thus it too is generally much lighter than the \tilde{d}_L and \tilde{s}_L .

For the first two generations, the mass coefficients in the off-diagonal terms will be the masses of the corresponding fermions, and these are relatively small, so that mixing in the first two generations is well-nigh negligible.

Gauginos and Higgsinos: Electroweak symmetry-breaking, which mixes the W_3 and B fields in the SM, also mixes the corresponding wino and bino states, as well as the higgsinos. These neutral gauginos \tilde{W}_3^0 and \tilde{B}^0 mix with neutral Higgsinos \tilde{H}_u^0 and \tilde{H}_d^0 to provide four mass eigenstates – the *neutralinos*, $\chi_i^0, (i = 1, \dots, 4)$. The neutralino mass matrix in the flavour basis is given by:

$$M_{\tilde{\chi}^0} = \begin{pmatrix} M_1 & 0 & -M_Z \cos \beta \sin \theta_W & M_Z \sin \beta \sin \theta_W \\ 0 & M_2 & M_Z \cos \beta \cos \theta_W & -M_Z \sin \beta \cos \theta_W \\ -M_Z \cos \beta \sin \theta_W & M_Z \cos \beta \cos \theta_W & 0 & -\mu \\ M_Z \sin \beta \sin \theta_W & -M_Z \sin \beta \cos \theta_W & -\mu & 0 \end{pmatrix} \quad (2.5.26)$$

which can be diagonalised to give the masses of the neutralinos. The mass hierarchy of these Majorana fermions is $m_{\tilde{\chi}_1^0} < m_{\tilde{\chi}_2^0} < m_{\tilde{\chi}_3^0} < m_{\tilde{\chi}_4^0}$. The lightest neutralino is often the lightest SUSY particle (LSP) and this is an attractive proposition as it can act as a dark matter candidate, since it is colour and charge neutral.

In a similar way, the charged gauginos \tilde{W}^\pm and the charged Higgsinos \tilde{H}^\pm can mix to give two chargino states, $\chi_i^\pm, (i = 1, 2)$. The chargino mass matrix in the flavour basis is given by

$$M_{\tilde{\chi}^\pm} = \begin{pmatrix} M_2 & \sqrt{2}M_W \cos \beta \\ \sqrt{2}M_W \sin \beta & \mu \end{pmatrix} \quad (2.5.27)$$

and again, after diagonalisation, one obtains two Dirac fermions with $m_{\tilde{\chi}_1^\pm} < m_{\tilde{\chi}_2^\pm}$.

The *gluinos* form a colour octet and thus do not mix with any other MSSM particle. In most SUSY breaking schemes, the gluino is much heavier than the electroweak gauginos. In SUSY theories which incorporate gravity, one also has a *gravitino*, which is a spin- $\frac{3}{2}$ particle.

2.5.4 R-parity and its violation

In SUSY models, one can define a \mathbb{Z}_2 symmetry corresponding to a conserved quantum number called R-parity, which is

$$R_p = (-1)^{3(B-L)+2s} \quad (2.5.28)$$

for a field having B, L, s as the baryon number, lepton number and spin respectively. Like all \mathbb{Z}_2 quantum numbers, R-parity is multiplicative and its conservation prevents any baryon or lepton number-violating terms arising in the superpotential. As both are observed to be conserved in Nature, R-parity is an obvious symmetry to impose on a SUSY theory. Furthermore, R_p helps distinguish between SUSY and SM particles – while SUSY particles have an $R_p = -1$, SM particles have $R_p = +1$. Thus, at any SUSY vertex there must be an even number of SUSY particles. This implies that the LSP is stable and a viable DM candidate.

R_p can also be violated and this leads to terms in the superpotential such as

$$\hat{W}_{\mathcal{R}_p} = \frac{1}{2}\lambda^{ijk}\hat{L}_i\hat{L}_j\hat{E}_k^c + \lambda^{ijk}\hat{L}_i\hat{Q}_j\hat{D}_k^c + \frac{1}{2}\lambda^{ijk}\hat{U}_i^c\hat{D}_j\hat{D}_k^c + \mu^i\hat{L}_iH_u \quad (2.5.29)$$

where the first term (LLE) violates lepton number by $\Delta L = 2$, the second term (LQD) violates lepton number by $\Delta L = 1$ and the third term (UDD) violates baryon number by $\Delta B = 0$. In general, due to stringent bounds from proton decay either of LQD and UDD is considered non-zero, but not both simultaneously. Other aspects of R-parity and bounds on the couplings are discussed more elaborately in Chapter 3.

2.5.5 Decay of SUSY particles

The superpartners in the MSSM, being heavy, may be expected to undergo fast decays, and the study of such decay chains has been a major part of SUSY studies, especially in the context of collider studies. In this section, we consider decays of SUSY particles with the assumption that R-parity is conserved and a spectrum is such that $\tilde{\chi}_1^0$ is the LSP. R-parity then ensures that the LSP will be stable and very weakly interacting, like neutrinos, so that it will be observable only through missing energy and momentum signals in collider events.

- *Sleptons, Squarks and Sneutrinos:* Charged sleptons, squarks and sneutrinos can decay through their weak interactions. A sample of such decays is

$$\tilde{l} \rightarrow \nu\tilde{\chi}_i^\pm; \quad \tilde{l} \rightarrow l\tilde{\chi}_i^0; \quad \tilde{\nu} \rightarrow l\tilde{\chi}_i^\pm; \quad \tilde{\nu} \rightarrow \nu\tilde{\chi}_i^0; \quad \tilde{q} \rightarrow q\tilde{\chi}_i^0; \quad \tilde{q} \rightarrow q'\tilde{\chi}_i^\pm \quad (2.5.30)$$

The right handed sleptons decay via the bino-like $\tilde{\chi}_1^0$ because they lack the $SU(2)_L$ charge and cannot couple to weak gauginos. Even though weak squark decay as indicated above is kinematically feasible, it remains subdominant if $\tilde{q} \rightarrow q\tilde{g}$ is also allowed because of the relative strength of the couplings. Decays of stops are particularly interesting. If the stop is too light, $\tilde{t} \rightarrow t\tilde{\chi}_1^0$ and $\tilde{t} \rightarrow t\tilde{g}$ may both be forbidden. In that case, the stop will undergo a 3-body decay $\tilde{t} \rightarrow bW\tilde{\chi}_1^0$. This is an important search channel for a stop which is almost degenerate with the top quark.

- *Neutralinos and Charginos:* Several decay modes are possible for neutralinos and charginos. For example a heavier neutralino and chargino can decay to the lightest neutralino

$$\tilde{\chi}_2^0 \rightarrow \tilde{\chi}_1^0 Z \quad \tilde{\chi}_2^0 \rightarrow \tilde{\chi}_1^0 h^0 \quad \tilde{\chi}_1^\pm \rightarrow \tilde{\chi}_1^0 W^\pm$$

As with the squarks, if two neutralino masses are very close to each other, the next to lightest neutralino would undergo a 3-body decay, e.g. $\tilde{\chi}_2^0 \rightarrow f \bar{f} \tilde{\chi}_1^0$.

- *Gluino Decay:* Gluinos will decay to a quark and an (on-shell or off-shell) squark. The squark then decays to a quark and a neutralino, or a quark and a chargino, which itself then decays to a neutralino.

$$\begin{aligned} \tilde{g} &\rightarrow q\bar{q} \rightarrow q\bar{q}\tilde{\chi}_1^0 \\ \text{or } \tilde{g} &\rightarrow q\bar{q} \rightarrow q\bar{q}'\tilde{\chi}_1^\pm \rightarrow q\bar{q}'W^\pm\tilde{\chi}_1^0 \rightarrow q\bar{q}'l\nu_l\tilde{\chi}_1^0 \end{aligned}$$

A generic feature of R-parity conserving SUSY decays is a cascade-like structure with a lot of sources of missing energy. For example one can easily imagine a slepton decay such as

$$\begin{aligned} \tilde{l} &\rightarrow l\tilde{\chi}_2^0 \rightarrow lZ\tilde{\chi}_1^0 \rightarrow ljj\tilde{\chi}_1^0 \\ \text{or } \tilde{l} &\rightarrow \nu\tilde{\chi}_1^- \rightarrow lW^-\tilde{\chi}_1^0 \rightarrow l'l'\nu_l\tilde{\chi}_1^0 \end{aligned}$$

Thus a prominent feature of SUSY search strategies is looking for large missing energy. However, if R_p is violated, many more modes of decay open up and those decay chains typically involve very little missing energy.

Before concluding this section it is worth mentioning that though searches for supersymmetric particles have been and are being vigorously pursued, till date there is no evidence for any of them. In fact, the lower mass bounds for the gluinos and the squarks of the first two generations are now near 2 TeV. Bounds on the others are somewhat model dependent, but these have also been slowly going up with time. For these reasons, the status of SUSY — acquired in the 1980s and 1990s — as the ‘standard’ theory beyond the SM is gradually being eroded. However, any new discovery at the LHC could immediately change the situation quite drastically.

Flavour-changing Decays of Top Quarks

3.1 Introduction : FCNC portal to new physics

The Run-I of the CERN Large Hadron Collider (LHC) has already led to the discovery of the long-sought Higgs boson [174], and, probably, the elusive pentaquark [175] as well. As the LHC has now commenced its crucial Run-II, the eyes of the whole world are focussed on CERN with the hope that there will be startling discoveries at this machine, which is designed to probe an energy regime hitherto inaccessible to terrestrial experiments.

It is natural, at this stage, to inquire into the different possibilities, and ask how sure we are that any such discovery will be made. Unfortunately, it turns out that there is no really *compelling* reason to expect a new discovery at the LHC Run-2 – though it is certainly possible. This is because the whole range of experiments done at low, intermediate and the highest available energies are beautifully explained by the Standard Model (SM), a portmanteau theory which incorporates three or four disparate ideas and holds them together with a set of phenomenological parameters. Ad hoc as it may seem, this clumsy model has been remarkably successful – perhaps too successful – in explaining every known measurement, sometimes to four or five decimal places. Ironically, it is the LHC, in its Run-I, which has put the strongest stamp of authenticity on the SM by discovering the missing Higgs boson, measuring its properties to be consistent with the SM predictions and, at the same time, failing to find any significant deviations from the SM in a host of highly precise measurements. The recent discoveries of the different hadronic and mesonic bound states, and that of exotics like the pentaquark are as consistent with the SM as any of the other results.

When we extend our consideration beyond purely terrestrial experiments to the cosmos at large, we immediately realise that the SM fails to explain several outstanding problems. These include the problems of dark matter [178], dark energy [179] and ultra-high energy cosmic rays above the Greisen-Zatsepin-Kuzmin (GZK) bound [180]. In particular, if the Earth is immersed in a distribution of dark matter, as appears to be the case, there must be some way to detect this fact. This is a subject of intense experimental investigation around

the world [181–184]. It is also hoped that discoveries at the LHC could shed light on the problem of dark matter, which, if particulate, would appear in a collision as missing energy and momentum. Some of the theoretical deficiencies of the SM are addressed in theories which extend or go beyond it to postulate new structures and symmetries at higher energy scales – these are generically referred to as ‘new physics’. A few of these models also have dark matter candidates. The great hope of the present moment is that unambiguous signals for such new physics will be discovered in Run-II of the LHC.

There are two ways in which new physics can be discovered at the LHC. The first – and simplest – way is to ‘directly’ discover evidence for new particles, which could appear either as resonances or pairs, or be produced in association with SM particles. Denoting a ‘new’ particle by P , the simplest tree-level processes are:

$$pp \rightarrow P \text{ or } P^* \rightarrow X + Y \qquad pp \rightarrow P + \bar{P} \qquad pp \rightarrow P + X \qquad (3.1.1)$$

where X and Y stand for SM particles. Taking into account the fact that a ‘new’ particle will either decay into SM particles, or, if it is a component of dark matter, lead to missing energy and momentum signals, one can enumerate the possible final states and then analyse the LHC data to see if there is any evidence for such signals. An answer in the affirmative would, of course, be very exciting, and hopefully this is what will occur in the near future.

While we have no wish to pour cold water on optimistic predictions of the above nature, one cannot ignore the possibility that the mass of the ‘new’ particle(s) may very well lie outside the kinematic reach of the LHC. Curiously, the last undiscovered particle for whose mass we had a theoretical *upper* bound was the Higgs boson, and, in fact, the LHC was designed to find it within the entire range of possibilities¹. For ‘new’ particles, however, all that we have are experimental lower bounds [185–191] – which are more a measure of the failure of experimental searches than a reflection of any physical principle. Thus, future failures to find any signals of new physics can always be explained away as due to higher and higher masses of the ‘new’ particle(s). In such a case, there would arise a serious problem in falsifying the theories in question.

There does, however, exist an escape route, and this happens when we consider the quantum effects of the ‘new’ physics. When we consider, say, tree-level decays of a SM particle which have been mediated by a heavy ‘new’ particle P , e.g. a decay of the form

$$Q \rightarrow X + P^* \rightarrow X + Y + Z$$

where the Q, X, Y, Z are all SM particles, then these are generally subject to a propagator suppression by a factor M_Q^2/M_P^2 — which can be quite severe if $M_Q \ll M_P$, which is usually the case. However, if, instead of a decaying particle, we have a scattering experiment

$$Q + \bar{X} \rightarrow P^* \rightarrow Y + Z$$

¹As it happens, the Higgs boson was found rather soon, and that too, near its lower mass bound rather than the upper.

conducted at an energy $\sqrt{s} < M_P$, the corresponding ‘suppression’ factor will be s/M_P^2 — which may be orders of magnitude larger than the earlier factor since it is possible to make $\sqrt{s} \gg M_Q$. Even then, it could very well be that M_P is so large that even with the effective values $\sqrt{s} \sim 1 - 2$ TeV available at the LHC, the propagator suppression will still make the process unobservable at the LHC, especially if there are large backgrounds arising from purely SM production of $Y + Z$ final states.

What we need to find, therefore, is a process which, for some reason, is severely suppressed in the SM, but, for some equally valid reason, is not so severely suppressed in the new physics sector. Here we are lucky, for there exists a whole class of SM processes which are severely suppressed by the unitarity constraints of the Cabibbo-Kobayashi-Maskawa (CKM) matrix. These are the so-called flavour-changing neutral current (FCNC) processes involving at least two generations of fermions in the initial and final states, and all the generations in the loop. Though this suppression, commonly called the Glashow-Iliopoulos-Maiani (GIM) mechanism [30], is described in any textbook on the SM [37], it is worthwhile to take a quick look at the main argument, since it will form the crux of some of the discussions in this article. The idea is that if we have an initial quark flavour q and a final quark flavour q' of the same charge, and the only flavour-changing couplings we have are due to the charged currents coupling to the W -boson, then the transition amplitude must have the form

$$M_{qq'} = \sum_{i=1}^3 V_{qi}^* V_{q'i} A(x_i, M_W) = \sum_{i=1}^3 \lambda_i A(x_i, M_W) \quad (3.1.2)$$

where $x_i \equiv m_i^2/M_W^2$ carries the generation dependence and M_W sets the mass scale for charged-current interactions. Moreover, $\lambda_i = V_{qi}^* V_{q'i}$, and the unitarity of the CKM matrix ensures that if $q \neq q'$, then $\sum_i \lambda_i = 0$. Obviously, we can expand the $A(x_i, M_W)$ in a Maclaurin series

$$A(x_i, M_W) = A_0(M_W) + x_i A'_i(M_W) + \frac{1}{2} x_i^2 A''_i(M_W) + \dots \quad (3.1.3)$$

where

$$A_0(M_W) = A(0, M_W), \quad A'_i(M_W) = \left[\frac{\partial A}{\partial x_i} \right]_{x_i=0}, \quad A''_i(M_W) = \left[\frac{\partial^2 A}{\partial x_i^2} \right]_{x_i=0}$$

and so on, where we make the assumption that $x_i \ll 1$. The leading term in $M_{qq'}$ cancels out and what is left is therefore suppressed by x_i . Obviously, this will work nicely if we take the quarks q, q' to have charge $+2/3$, for then we automatically get a suppression in the probability by $x_b = (m_b/M_W)^2 \sim 10^{-3}$, or by even smaller factors for the other generations².

If we now assume that the ‘new’ particle(s) P make(s) contributions of the form

$$M_{qq'}^{\text{new}} = \sum_{i=1}^3 \lambda_i \eta_i \tilde{A}(y_i, M_P) \quad (3.1.4)$$

²For FCNC decays of the b quark, we need to expand about x_t rather than $x_i = 0$, since $x_t > 1$. However, this article focusses only on decays of the t quark.

where the $y_i \equiv m_i^2/M_P^2$ are similar to the x_i and the η_i are arbitrary flavour-dependent factors, then we immediately see that the leading order contribution stays, for $\sum_i \lambda_i \eta_i \neq 0$. Such contributions are unaffected by the GIM suppression, and, therefore, could, in principle, be three orders of magnitude larger than the SM contributions.

The beauty of the above argument lies in the fact that in the above process, all that we need to observe is the transition of a t quark to a quark of a different flavour but the same charge, i.e. a u or a c . There is no requirement to produce heavy ‘new’ particles on-shell. Thus, in the disappointing situation that all direct searches for ‘new’ physics at the LHC fail, one can fall back upon GIM-suppressed processes as a portal through which we can still peer into that otherwise-inaccessible new world.

The major loop-induced FCNC processes involving the top quark which have been studied in the literature are:

1. the decays $t \rightarrow q + S$, where $q = u, c$ and S is a scalar – either the Higgs boson H^0 or its counterpart(s) in new physics models; and
2. the decays $t \rightarrow q + V$, where $q = u, c$ and V is a vector gauge boson – which can be a photon or a gluon or a Z^0 -boson or any counterpart(s) in new physics models;

In the SM, we have well known results for the branching ratio

$$B(t \rightarrow c + H^0) \sim 10^{-15} \qquad B(t \rightarrow c + Z^0) \sim 10^{-13} \qquad (3.1.5)$$

These are many, many orders of magnitude too small to be measured at Run-2 of the LHC, where estimates are that at best branching ratios at the level of 10^{-5} may become accessible when enough data are eventually collected (see Figure 8). There have been several predictions in the literature that new physics processes could provide the necessary enhancement and predict branching ratios at this level. The purpose of this article is to investigate these claims critically and try to determine the model requirements which could lead to an actual discovery of new physics at the LHC through the top quark FCNC portal.

Before proceeding further, we address the question of the rare decay $t \rightarrow q + \gamma$, which is bound to happen if its counterpart $t \rightarrow q + Z$ is possible. Electromagnetic gauge invariance demands that $t \rightarrow q + \gamma$ be mediated only by the magnetic dipole moment operator [192]. This process, however, turns out to be less interesting for two reasons. In the first place, one loop contributions to $t \rightarrow q + \gamma$ are suppressed by about an order of magnitude compared to the corresponding process with a final-state Z . This turns out to be essentially because the coupling of a photon to d_i -quark pairs is suppressed by their fractional charge of $-1/3$. A more serious hurdle is that experimental measurement of the rare decay $t \rightarrow q + \gamma$ is plagued with much larger backgrounds because of the ease with which photons can be radiated at tree-level. For this reason, experiments [193] can only achieve an accuracy for $t \rightarrow c + \gamma$ which is an order of magnitude poorer than that for $t \rightarrow c + Z$. Taken together, these two factors ensure that the search for $t \rightarrow q + Z$ should clearly take precedence³ over that for

³As we will see in the final section, the process $t \rightarrow c + Z$ is somewhat marginal at the LHC. This makes the case hopeless for $t \rightarrow c + \gamma$. Replacing c by u leads to even smaller decay widths.

$t \rightarrow q + \gamma$. Hence, we do not discuss the latter process further. For similar reasons, we do not consider the process $t \rightarrow q + g$ either.

This article is organised as follows. In the following section, we consider generic FCNC decays of the top quark [194], taking a toy model, and determine the conditions required to have maximal contributions to an FCNC process like $t \rightarrow c + B$, where B is a scalar or a vector boson. As an example we take up, in the next section, a supersymmetric model which is quite likely to evade direct searches at the LHC. The following section extends this to the case of a supersymmetric model with R -parity violation, which relies on non-CKM sources of FCNC. Finally we present a summary of our results and a conclusion. In the interests of smooth reading, most of the more cumbersome formulae are relegated to the Appendix B.

3.2 Generic FCNC Decays of the top quark in a toy model

In this section, we investigate a toy model which could be taken as a prototype for FCNC decays for the top quark. Let us assume there are a pair of charged scalars ω^\pm with couplings of the form

$$\begin{aligned} \mathcal{L}_{\text{int}} &= \xi \omega^+ \omega^- H \\ &+ \sum_{i,j=1}^3 (\eta V_{ij} \bar{u}_{iL} d_{jR} \omega^+ + \text{H.c.}) \end{aligned} \quad (3.2.1)$$

where H is the SM Higgs boson and ξ, η are unknown couplings. These ω^\pm 's are rather like scalar versions of the W^\pm -bosons. The choice of scalars

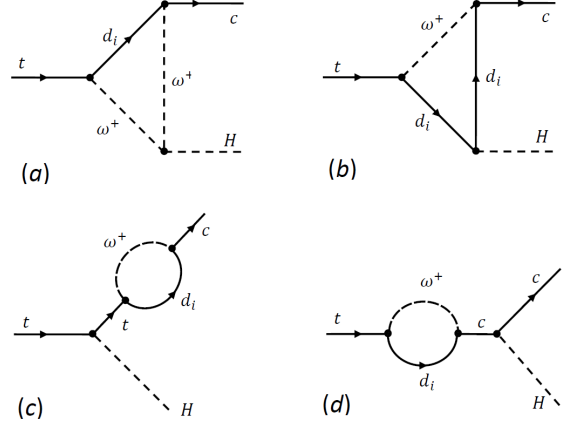


Figure 3.1: Set of Feynman Diagrams leading to the decay $t \rightarrow c + H$ in our toy model.

makes the calculation simple and sidesteps complications due to gauge choice which arise with the W^\pm . For this part we stay within the minimal flavour violation (MFV) paradigm (see for example, Ref. [195]) insofar as the only flavour-changing effects happen through the ‘CKM’ matrix elements V_{ij} .

Let us now consider the decay $t \rightarrow c + H$ as predicted in this model. Using the SM Yukawa couplings for the H -boson and Feynman rules for ω^\pm (which can quite easily be read off from the above Lagrangian), we obtain four diagrams, shown in Figure 1. It is then a straightforward matter to calculate the helicity amplitudes for the decay $t \rightarrow c + H$. In terms of the $\lambda_i = V_{ti}^* V_{ci}$, these can be written in the generic form

$$\mathcal{M}_{hcHt} = \sum_{i=1}^3 \lambda_i \mathcal{A}_i(h_c, h_t) \quad (3.2.2)$$

where h_c and h_t are the helicities of the c and the t quarks respectively, and $\lambda_1 + \lambda_2 + \lambda_3 = 0$ by unitarity of the CKM-like matrix V . Explicit expressions for these in terms of Passarino-'tHooft-Veltman functions [196] are given in Appendix B.1. We require to calculate only two non-vanishing amplitudes

$$(a) \quad \mathcal{M}_{++} = \sum_{i=1}^3 \lambda_i \mathcal{A}_i(+1, +1) \quad (b) \quad \mathcal{M}_{--} = \sum_{i=1}^3 \lambda_i \mathcal{A}_i(-1, -1) \quad (3.2.3)$$

which become analogues of the SM amplitudes if we put $\xi = gM_W$ and $\eta = g/\sqrt{2}$. To calculate the branching ratio, we note that the squared and spin-summed/averaged matrix element, in terms of the helicity amplitudes of Eqn. (3.2.3), is

$$\overline{|\mathcal{M}|^2} = \frac{1}{2} \left[|\mathcal{M}_{++}|^2 + |\mathcal{M}_{--}|^2 \right] \quad (3.2.4)$$

The partial width can now be written as

$$\Gamma(t \rightarrow c + H) = \frac{1}{16\pi m_t} \left(1 - \frac{M_H^2}{m_t^2} \right) \overline{|\mathcal{M}|^2} \quad (3.2.5)$$

and (if necessary) the branching ratio is easily obtained by dividing by the total decay width $\Gamma_t \simeq 1.29 \text{ GeV}$.

At this point we pause to make a rough numerical estimate of the above quantities. As may be seen from Eqn. (3.2.5), the helicity amplitudes must have a mass dimension $+1$. Since these arise from one-loop computations, and if M_ω is close to M_W , a crude approximation for the amplitude factor will be

$$\overline{|\mathcal{M}|^2} \approx \left(\frac{m_t}{16\pi^2} \right)^2 \quad (3.2.6)$$

Substituting this into Eqn. (3.2.5), leads to a numerical estimate

$$\Gamma(t \rightarrow c + H) \approx 5.9 \times 10^{-5} \text{ GeV} \quad (3.2.7)$$

which is ten orders of magnitude larger than the SM prediction.

It is natural to ask why the SM prediction is so much smaller than what one would naively have expected. The answer is that the SM amplitude is suppressed by a combination of three different effects, each reducing the amplitude by a few orders of magnitude. These are explained below.

1. The first of these suppression effects is, of course, the GIM cancellation, which we have already shown to lead to suppression by a factor

$$\left[\frac{m_b(m_t)}{M_W} \right]^2 = \left[\frac{2.6 \text{ GeV}}{80.4 \text{ GeV}} \right]^2 \simeq 1.0 \times 10^{-3}$$

in the decay amplitude.

2. In this toy model, we have taken the flavour-violating coupling to be ηV_{ij} (or $\eta_i V_{ij}$), where the flavour-violation arises exactly as in the SM – from the off-diagonal terms

in the ‘CKM’ matrix. This makes it a model with *minimal* flavour violation (MFV). Since the CKM matrix exhibits a strong hierarchy as we move away from the diagonal, this results in a further suppression in all MFV models – which may not hold in a new physics model which deviates from the MFV paradigm. To make matters explicit, we have $\lambda_i = V_{2i}V_{3i}^*$ for $i = 1, 2, 3$. If we choose the η_i as in Eqn. (3.2.10), the only relevant one is $\lambda_3 = V_{23}V_{33}^* \simeq V_{23}$ since $V_{33} \simeq 1$. Now, $|V_{23}| \approx 0.04$ [346]. This gives us a suppression by two orders of magnitude.

There is a subtle issue, however. If we consider the flavour mixing in a model of new physics to be arbitrary and of unknown origin, it is perfectly fine to set $\lambda_3 = 1$ and thereby obtain an enhancement factor of $1/0.04 = 25$. In fact, this is what we shall assume in Section 5 of this paper. However, in a large class of non-MFV models, flavour mixing does arise from mixing effects of the quarks, and there exists some *unitary* matrix V'_{ij} which is not the measured CKM matrix. To get a maximal value of V'_{23} , we take

$$V' = \begin{pmatrix} 1 & 0 & 0 \\ 0 & \cos \theta & \sin \theta \\ 0 & -\sin \theta & \cos \theta \end{pmatrix} \quad (3.2.8)$$

so that $\lambda'_3 = \sin \theta \cos \theta = \frac{1}{2} \sin 2\theta$. Obviously, the maximum occurs for $\theta = \pi/4$ and the corresponding value of λ_3 is 0.5 — an enhancement by a factor of 12.5 instead of 25. Thus, what we can achieve by abandoning the MFV paradigm is an enhancement by half of what we would get by discarding the CKM-type mechanism altogether.

3. Finally, in a model of new physics, there is always the possibility that the actual couplings may be enhanced over the SM ones. To see this, we put⁴ $\xi = M_\omega$ instead of gM_W and $\eta_3 = 1$ instead of $g/\sqrt{2}$, and recalculate the amplitudes, thereby achieving a modest enhancement by a factor of $2/g^3 \simeq 7.3$, assuming that $M_\omega \simeq M_W$. This means that the ‘SM’ amplitude is suppressed by a factor $1/7.3 \simeq 0.14$.

If we now combine the three effects, then the amplitude will have an overall suppression factor

$$(1.0 \times 10^{-3}) \times 0.04 \times 0.14 \simeq 5.6 \times 10^{-6} \quad (3.2.9)$$

Multiplying the amplitude by this factor and squaring leads to a suppression of the estimated partial decay width in Eqn. (3.2.7) by ten orders of magnitude to 1.85×10^{-15} — which is in the right ballpark.

Now that we have a clear understanding of the nature of the FCNC suppression in the SM (or a SM-like model), we can remove these effects one by one to see how much the amplitude can be enhanced in a new physics model. In order to predict really significant deviations from the SM branching ratio any new physics model requires to meet the following conditions:

A. Frustration of the GIM cancellation.

⁴Strictly speaking, the couplings can be taken up to $\sqrt{4\pi} \approx 3.5$, but then we will have to worry about higher-order effects.

B. Non-MFV pattern of flavour mixing.

C. Enhanced couplings.

To illustrate these in a concrete manner, we perform detailed numerical computations of the helicity amplitudes of Eqn. (3.2.3) using the formulae of Appendix B.1.1. The loop integrals in these formulae are evaluated using the well-known package FF [197], and our numerical results are given in Figure 3.2.

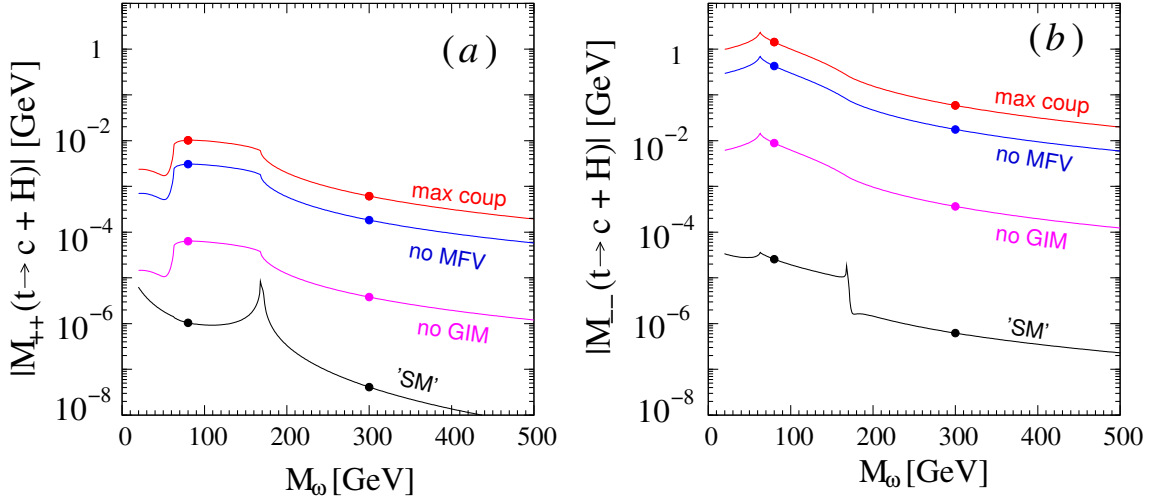


Figure 3.2: The two non-vanishing helicity amplitudes for the decay $t \rightarrow c + H$, as calculated in our toy model as a function of the mass M_ω of the scalar field ω . The legends next to each curve are explained in the text. The small solid circles indicate the values $M_\omega = 80, 300$ GeV used in Table 1.

The ‘normal case’, when the couplings in Eqn. (3.2.2) are exactly like those in the SM corresponds to the black curves marked ‘SM’ in Figure 2. The dots correspond to the values $M_\omega = 80, 300$ GeV (see Table 1). These amplitudes are suppressed due to a combination of all the three effects described above⁵ (see below).

We can disrupt the GIM cancellation partially or wholly by replacing the coupling constant η in Eqn. (3.2.2) by a generation-dependent factor η_i . The maximal effect will be obtained if, for example, we consider

$$\eta_1 = \eta_2 = 0 \quad \eta_3 = \frac{g}{\sqrt{2}} \quad (3.2.10)$$

The corresponding numerical curves are shown in Figure 2 in magenta, and labelled ‘no GIM’. It is immediately obvious that the amplitude increases by 2 – 3 orders of magnitude, exactly as expected.

Next, we eschew MFV and consider the case $\lambda_3 = 1$. This gives an enhancement by a factor of 25. The blue lines marked ‘no MFV’ in Figure 2 represent the case in question. Finally, we set the couplings to the maximal values $\xi = M_\omega$ and $\eta_3 = 1$ and obtain a further enhancement

⁵It may be seen in Appendix B.1.1 that the form factors $F_{1i}^{(b)}$ and $F_{2i}^{(b)}$ would violate the GIM cancellation. This is indeed true, and arises from the helicity-flipping nature of the scalar ω interaction. However, the contributions of $F_{1i}^{(b)}$ and $F_{2i}^{(b)}$ are very small, and hence, for all practical purposes, may be ignored in the numerical evaluation.

illustrated by the curves shown in red in Figure 2 and marked ‘max coup’. This, as predicted, is enhanced by one order of magnitude.

If we consider the combination of all these effects, as we have done in Figure 2, we get an enhancement factor around 2.04×10^4 (5.43×10^4) for $|\mathcal{M}_{++}|$ ($|\mathcal{M}_{--}|$) taking $M_\omega = 80$ GeV. This is a more modest enhancement than estimated in Eqn. (3.2.9), but that is not surprising, given the fact that the earlier estimate was made under a very crude approximation to the decay amplitude. The actual enhancements available are made explicit in Table 1, where we list the partial widths for $t \rightarrow c + H$ in the toy model for $M_\omega = 80, 300$ GeV, for the SM-like case as well as with the three suppression mechanisms successively disabled.

M_ω	‘SM’	\oplus no GIM	\oplus no MFV	\oplus max coup
80	1.81×10^{-14}	2.04×10^{-9}	4.74×10^{-6}	5.31×10^{-5}
300	4.31×10^{-18}	5.12×10^{-11}	1.19×10^{-7}	1.33×10^{-6}

Table 3.1: Partial decay widths for the decay $t \rightarrow c + H$ in the toy model, with successive application of the three enhancement conditions. All numerical values are in units of GeV.

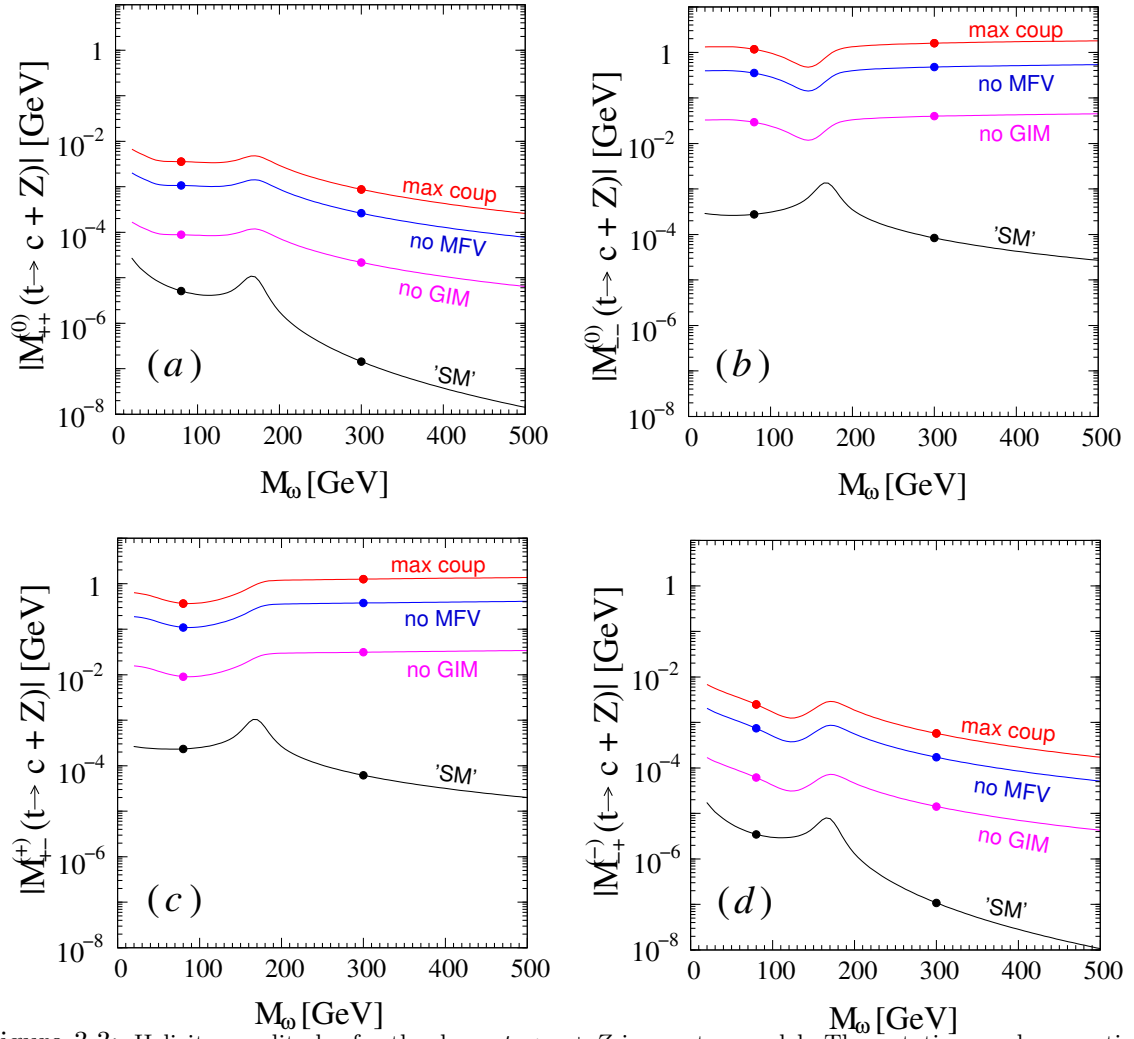


Figure 3.3: Helicity amplitudes for the decay $t \rightarrow c + Z$ in our toy model. The notations and conventions follow those of Figure 3.2.

Another process of interest at the LHC is the decay $t \rightarrow c + Z$. The diagrams for this are identical to those in Figure 1, except that the scalar H line must be replaced by a wiggly Z line. We do not exhibit these diagrams in the interest of brevity, though we keep the same configuration and numbering. In this case, the computation is rendered a little more complicated because of the vector nature of the Z boson. The toy Lagrangian will be

$$\mathcal{L}_{\text{int}} = i\xi\omega^+ \overleftrightarrow{\partial}_\mu \omega^- Z^\mu + \sum_{i,j=1}^3 (\eta V_{ij} \bar{u}_{iL} d_{jR} \omega^+ + \text{H.c.}) \quad (3.2.11)$$

where ξ, η are unknown couplings, as before. We can now compute the partial width for the decay $t \rightarrow c + Z$. The Feynman amplitude will assume the form

$$\mathcal{M}_{hc\bar{t}}^{(h_Z)} = \sum_{i=1}^3 \lambda_i \mathcal{A}_i(h_Z; h_c, h_t) \quad (3.2.12)$$

where the sum over h_Z runs over the longitudinal polarisation $\varepsilon_L = \varepsilon(h_Z)|_{h_Z=0}$ and the transverse polarisations $\varepsilon_T^\pm = \varepsilon(h_Z)|_{h_Z=\pm 1}$. The only non-vanishing amplitudes are

$$\begin{aligned} (a) \quad \mathcal{M}_{-+}^{(+)} &= \sum_{i=1}^3 \lambda_i \mathcal{A}_i(+1; -1, +1) & (b) \quad \mathcal{M}_{+-}^{(-)} &= \sum_{i=1}^3 \lambda_i \mathcal{A}_i(-1; +1, -1) \\ (c) \quad \mathcal{M}_{++}^{(0)} &= \sum_{i=1}^3 \lambda_i \mathcal{A}_i(0; +1, +1) & (d) \quad \mathcal{M}_{--}^{(0)} &= \sum_{i=1}^3 \lambda_i \mathcal{A}_i(0; -1, -1) \end{aligned} \quad (3.2.13)$$

and these may be regarded as ‘SM’ amplitudes, if we take $\xi = gM_\omega$ and $\eta = g/\sqrt{2}$ as before. Once again, we plot these amplitudes in Figure 3.3 as a function of M_ω and relegate the detailed formulae to Appendix B.

In Figure 3.3, the four panels marked (a)–(d) correspond to the four amplitudes (a)–(d) indicated in Eqn. (3.2.13). The colour coding and conventions for this figure are identical to those in Figure 3.2. It is not difficult to see that once again, we get enhancement factors for these amplitudes which are very similar to those for the $t \rightarrow c + H$ case, when we successively (a) relax the GIM cancellation, (b) abandon the minimal flavour-violation paradigm and (c) enhance the couplings. This enables us to predict much larger partial widths, as shown in Table 2.

For this calculation, we require the squared and spin-summed/averaged matrix element, which is

$$|\overline{\mathcal{M}}|^2 = \frac{1}{2} \left[|\mathcal{M}_{-+}^{(+)}|^2 + |\mathcal{M}_{+-}^{(-)}|^2 + |\mathcal{M}_{++}^{(0)}|^2 + |\mathcal{M}_{--}^{(0)}|^2 \right] \quad (3.2.14)$$

in terms of the helicity amplitudes of Eqn. (3.2.13). The partial width can now be written

$$\Gamma(t \rightarrow c + Z) = \frac{1}{16\pi m_t} \left(1 - \frac{M_Z^2}{m_t^2} \right) |\overline{\mathcal{M}}|^2 \quad (3.2.15)$$

as before, with M_Z replacing M_H . In this case, of course, the partial width in more enhanced cases far exceeds the measured top quark width of 1.29 GeV, but this is not a serious matter, since this is, after all, a toy model. The enhancement in this case due to, successively, frustration of the GIM mechanism, saturation of the flavour off-diagonal terms and saturation

of the coupling constant, have the same magnitudes as in the case of the top decaying through a scalar H boson. We may, therefore, apply the same insights to both cases.

In general, the summed amplitudes for the decay $t \rightarrow c + Z^0$ are about an order of magnitude larger than the similar summed amplitudes for the decay $t \rightarrow c + H^0$. This is principally because a major contribution comes from the diagram with a $\omega^+\omega^-Z$ or $\omega^+\omega^-Z$ vertex, which are proportional to $g \cos \theta_W$ and λ respectively, other factors being equal or similar. Since the measurement of the Higgs boson mass tells us that $\lambda \simeq 0.12$ it follows that $g \cos \theta_W / \lambda \simeq 5$. A further factor of around 2 is obtained because of the four non-vanishing helicity amplitudes for $t \rightarrow c + Z^0$ as opposed to the two obtained for $t \rightarrow c + H^0$. Thus, we get an enhancement of around 10, which becomes around 10^2 when we consider the partial decay width. As this is a generic feature of the SM and most new physics models, it is obvious that the decay mode $t \rightarrow c + Z^0$ is more promising for discovery than the $t \rightarrow c + H^0$ mode.

M_ω	'SM'	no GIM	no MFV	max coup
80	4.23×10^{-11}	3.55×10^{-4}	5.15×10^{-2}	0.58
300	8.16×10^{-12}	8.32×10^{-3}	1.21	13.5

Table 3.2: Partial widths for the decay $t \rightarrow c + Z$ in the toy model, with successive application (L to R) of the three enhancement conditions. All numerical values are in units of GeV.

3.3 FCNC decays of the top quark in the SM

We are now in a position to explore the decays $t \rightarrow c + H$ and $t \rightarrow c + Z$ in the Standard Model, using insights from the toy model in the previous section. We start with $t \rightarrow c + H$. This time, of course, we have to take into account the exchange of the weak gauge bosons W^\pm in the loops, and this requires a choice of gauge in which to work. For loop diagrams, it is convenient to choose the 'tHooft-Feynman gauge, since that keeps the ultraviolet divergences at a manageable level. Of course, this comes at the cost of having extra diagrams with unphysical Higgs bosons, and hence, in the SM, the four diagram topologies of Figure 3.1. The Feynman diagrams for this can be obtained from those of Fig. 3.4 by replacing the dashed lines for H by wiggly lines for Z and changing the labels accordingly. We then go on to calculate the helicity amplitudes of Eqn. (3.2.13) in terms of four form factors, which are given in Appendix B.2. Most of the arguments given in the case of $t \rightarrow c + H$ above hold for this case as well, except that the presence of four separate helicity amplitudes leads to a somewhat larger branching ratio, $\mathcal{O}(10^{-13})$ as quoted in Eq. (3.1.5). The most important thing we learn from this exercise has already been stated in the Introduction – the branching ratios for flavour-changing t -quark decays in the SM are severely suppressed, being far too small to be detected at the LHC, or even the most ambitious futuristic machine that can be conceived. This has the effect of making these decays a very sensitive probe of new physics, for any enhancement to measurable levels must arise from new physics beyond the SM.

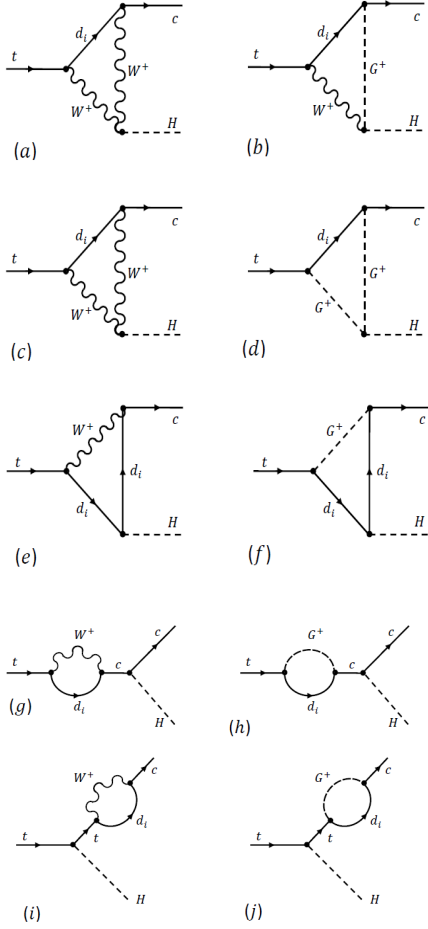


Figure 3.4: Feynman Diagrams leading to the decay $t \rightarrow c + H$ in the SM.

become the ten diagrams in Fig. 3.4. There is a small catch in using the 'tHooft-Feynman gauge, however, and that lies in the appearance of the unphysical Higgs bosons. The couplings of these to quarks depend on the d -quark masses m_i , and hence, would apparently lead to frustration of the GIM mechanism. However, these contributions cancel out when all the diagrams are added, as may be expected, since after all, they constitute a gauge artefact. The largest contributions to the amplitudes from individual diagrams (once the singularities are isolated) are of the order of 10^{-3} – this already contains the suppression of one order due to the electroweak couplings and the factor $1/16\pi^2$ which appears in all loop diagrams. When all the contributions are summed-up, the GIM cancellation becomes manifest, and there is a reduction by $\mathcal{O}(m_b^2/m_t^2) \approx 6 \times 10^{-4}$. This brings down the amplitude to $\mathcal{O}(10^{-7})$ and hence, its square to $\mathcal{O}(10^{-14})$. Another order is lost in kinematics, and thus we get the final result 5.8×10^{-15} , as quoted in Eq. (3.1.5). When we turn to the decay $t \rightarrow c + Z$, we have a situation similar to the toy model in the previous section.

3.4 FCNC decays of the top quark in the cMSSM

When we turn to new physics beyond the SM, the very first option must be the one which has captivated the imagination of high energy physicists for the last few decades, viz., supersymmetry (SUSY). The merits and demerits of SUSY have been exhaustively discussed in the literature [198] and do not require to be repeated here. Instead, we focus on the effects of SUSY on the flavour-changing processes $t \rightarrow c + H$ and $t \rightarrow c + Z$ which are the subject of this work.

Apart from the fact that every SM field has a supersymmetric partner differing from it in spin by one half, one of the most significant new features of SUSY models is the fact that they all require the existence of two scalar Higgs doublets. Thus, after the electroweak symmetry-breaking, these models contain five physical scalar fields, viz. a pair of charged Higgs bosons H^\pm and a triplet of neutral Higgs bosons, of which two (h^0, H^0) are even under CP and one (A^0) is odd under CP . The lighter one h^0 of the CP -even pair can be identified with the near-125 GeV scalar state found at the LHC in recent times. All the other states, H^\pm, H^0 and A^0 , are presumed to be heavier, and, in fact, too heavy to have been detected in any experiments

so far, including the LHC. As we shall see, it is likely that these states are all heavier than the t -quark, and hence, the only kinematically-permitted decay will be $t \rightarrow c + h^0$, which is analogous to the SM decay.

The more important difference from the SM in SUSY models arises because of the contributions of new particles in the loops. The most important of these are the contributions due to the charged Higgs bosons H^\pm , which have flavour-changing coupling like the W -boson. However, since these couplings originate from the Yukawa sector, they are proportional to the quark masses and hence will frustrate the GIM mechanism. Then there are contributions where the SM particles are replaced by their SUSY partners, viz. squarks and charginos. Here the flavour-changing effects will arise from the mixing matrices for squarks. In the so-called minimal flavour violation (MFV) models, the squark mixing matrices are aligned with the quark mixing matrix, i.e. the CKM matrix. This is the paradigm we shall adopt in the present study. Non-MFV models have been studied in the literature and we shall have occasion to discuss them in the final section.

gauginos :	$\tilde{\chi}_1^\pm$	$\tilde{\chi}_2^\pm$	$\tilde{\chi}_1^0$	$\tilde{\chi}_2^0$	$\tilde{\chi}_3^0$	$\tilde{\chi}_4^0$	\tilde{g}	
mass bound (GeV) :	94	94	46	63	100	116	520	
squarks :	\tilde{u}_1	\tilde{u}_2	\tilde{d}_1	\tilde{d}_2	\tilde{t}_1	\tilde{t}_2	\tilde{b}_1	\tilde{b}_2
mass bound (GeV) :	1100	1100	1100	1100	96	96	89	247
gauginos :	\tilde{e}_1	\tilde{e}_2	$\tilde{\tau}_1$	$\tilde{\tau}_2$	$\tilde{\nu}_e$	$\tilde{\nu}_{\tau 1}$		
mass bound (GeV) :	82	82	73	94	94	94		
Higgs bosons :	H^0	A^0	H^\pm					
mass bound (GeV) :	500	0	80					

Table 3.3: Experimental lower bounds on new particle masses relevant to SUSY models. The results for the second generation of quarks and leptons are the same as those shown for the first generation. The most conservative bounds have been taken. The numbers shown in this Table correspond to the case when R -parity is conserved, but they do not change very much when R -parity is violated.

Though there are many SUSY versions of the SM and its extensions, the minimal version of this is the so-called constrained minimal supersymmetric SM, or cMSSM [198]. This is the SUSY model which has the minimum number of extra parameters (four parameters and a sign), when compared with all the others. Not surprisingly, it is also the SUSY model which is most constrained by experiment. However, since a light Higgs boson h^0 is a common feature of all SUSY models, including the cMSSM, the only features which will be affected will be the couplings and the super-partner masses. As we have seen, this is not too serious a constraint on loop-induced processes, so it is sensible to use the cMSSM as a paradigm case for FCNC processes in SUSY. This is adopted in our work and it fixes the particle content and the vertex factors, though there will be large variations in the latter as the model parameters change.

In the cMSSM, the process $t \rightarrow c + h^0$ will be mediated by the 10 diagrams of the SM listed earlier in Fig. 3.4 as well as the 12 additional one-loop diagrams listed in Fig. 3.5. These

diagrams have not only charged Higgs bosons but also charginos and squarks in the loops. The details for calculating all these 22 diagrams are given in Appendix B.2, in terms of the

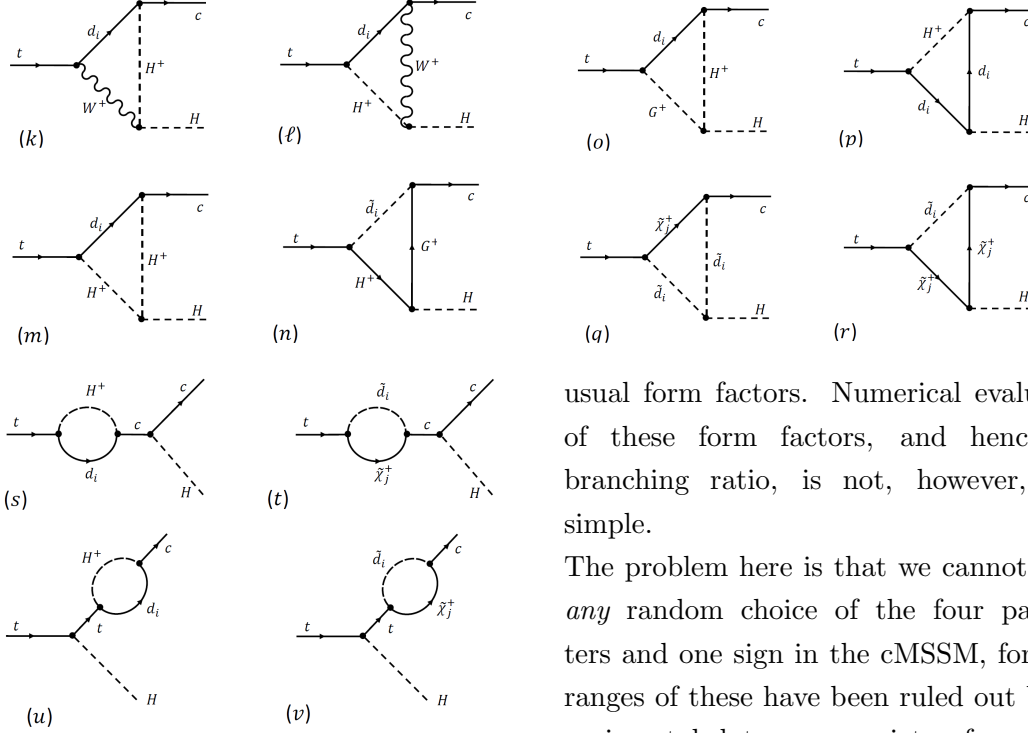


Figure 3.5: Additional Feynman diagrams leading to the decay $t \rightarrow c + H$ in the cMSSM.

usual form factors. Numerical evaluation of these form factors, and hence the branching ratio, is not, however, very simple.

The problem here is that we cannot make *any* random choice of the four parameters and one sign in the cMSSM, for large ranges of these have been ruled out by experimental data on a variety of measured processes.

We, therefore, must evaluate the branching ratio for $t \rightarrow c + h^0$ *only* for points in the parameter space which are permitted by all the experimental constraints [199]. At a first glance, this is a daunting prospect, given the wide range and diverse nature of experimental data which impact the cMSSM, but the task is made much easier by the presence of public domain software which do most of the computation automatically. We have, therefore, made free use of these software to constrain the cMSSM parameter space. The exact procedure followed is described as follows.

1. A set of random choices is made of the four parameters of the cMSSM, viz. the universal scalar mass m_0 , the universal fermion mass $m_{1/2}$, the universal trilinear coupling A_0 and the ratio of Higgs boson vevs $\tan \beta$, within the ranges

$$\begin{aligned} 100 \text{ GeV} &\leq m_0 \leq 10 \text{ TeV} & 100 \text{ GeV} &\leq m_{1/2} \leq 10 \text{ TeV} \\ -10 \text{ TeV} &\leq A_0 \leq 10 \text{ TeV} & 2 &\leq \tan \beta \leq 50 \end{aligned}$$

The sign of the μ parameter is chosen positive, since it is known that the negative sign is disfavoured by measurements of the muon anomalous magnetic moment.

2. Given a choice of the above parameters, we find the low-energy cMSSM mass spectrum by using the software SUSPECT [200], which takes these values at the scale of grand unification and uses the renormalisation group equations to evolve them down to the

electroweak scale, and also calculates mixing induced by the electroweak symmetry-breaking.

3. We eliminate parameter sets which are inconsistent with the observed h^0 mass 125 ± 2 GeV. This turns out to be a very severe constraint for low values of m_0 , $m_{1/2}$ and A_0 .
4. Of the surviving parameter sets, we eliminate those that are inconsistent with the results of direct searches for SUSY, i.e. which yield masses for the SUSY particles which are smaller than the experimental lower bounds given in Table 3 below [185–191, 201, 346].
5. With the remaining parameter sets, we calculate a clutch of low-energy variables measured in K and B decays, using the software SUPERISO [202]. We then eliminate parameter sets which are inconsistent with the 95% C.L. experimental data on these variables, as given in Table 4.

The most restrictive of these are the branching ratios $\mathcal{B}(B \rightarrow X_s \gamma)$ and $\mathcal{B}(B_s \rightarrow \mu^+ \mu^-)$. The former is known to be highly sensitive to low values of the charged Higgs boson mass and the latter is important for precluding very large values of $\tan \beta$. Once a parameter set survives all the above filters, we consider it acceptable and use it to evaluate the $t \rightarrow c + h^0$ branching ratio. Our results are then set out in Figure 3.6.

Variable	Lower Bound	Upper Bound
$\mathcal{B}(B \rightarrow X_s \gamma)$	2.766×10^{-4}	4.094×10^{-4}
$\Delta_0(B \rightarrow K^* \gamma)$	-3.8×10^{-2}	1.0×10^{-1}
$\mathcal{B}(B_s \rightarrow \mu^+ \mu^-)$	7.261×10^{-10}	6.173×10^{-9}
$\mathcal{B}(B_d \rightarrow \mu^+ \mu^-)$	4.0×10^{-11}	6.8×10^{-10}
$\mathcal{B}(B \rightarrow X_s \mu^+ \mu^-)$ (low Q^2)	2.4×10^{-7}	2.96×10^{-6}
$\mathcal{B}(B \rightarrow X_s \mu^+ \mu^-)$ (high Q^2)	1.48×10^{-7}	6.88×10^{-7}
$\mathcal{B}(B \rightarrow \tau^+ \nu_\tau)$	7.388×10^{-5}	2.993×10^{-4}
$R[\mathcal{B}(B \rightarrow \tau^+ \nu_\tau)]$	5.5×10^{-1}	2.71
$\mathcal{B}(B \rightarrow D \tau \nu)$	5.2×10^{-3}	1.02×10^{-2}
$\mathcal{B}(D_s \rightarrow \tau \nu)$	5.06×10^{-2}	5.7×10^{-2}
$\mathcal{B}(D_s \rightarrow \mu \nu)$	4.95×10^{-3}	6.67×10^{-3}
$\mathcal{B}(D \rightarrow \mu^+ \mu^-)$	3.49×10^{-4}	4.15×10^{-4}
$R[\mathcal{B}(K \rightarrow \mu \nu)]$	6.325×10^{-1}	6.391×10^{-1}
R_μ^{23}	9.92×10^{-1}	1.006
$\delta(a_\mu)$	-6.5×10^{-10}	5.75×10^{-9}

Table 3.4: Experimental bounds [202–211] at 95% C.L. on low energy parameters calculable in the software SUPERISO. For detailed definitions, see [202].

The left panel in Figure 3.6 shows a scatter plot indicating the allowed regions in the m_0 – $m_{1/2}$ plane, which is probably the best way to indicate constraints on the cMSSM. We note that every point on this plane corresponds to all possible random choices of the other parameters in the model, which accounts for the fuzziness in shapes. The black regions are disallowed by ‘theory’ constraints, which include the proper shape of the electroweak potential [212, 213] and the requirement that the lightest supersymmetric particle – a prime dark matter candidate

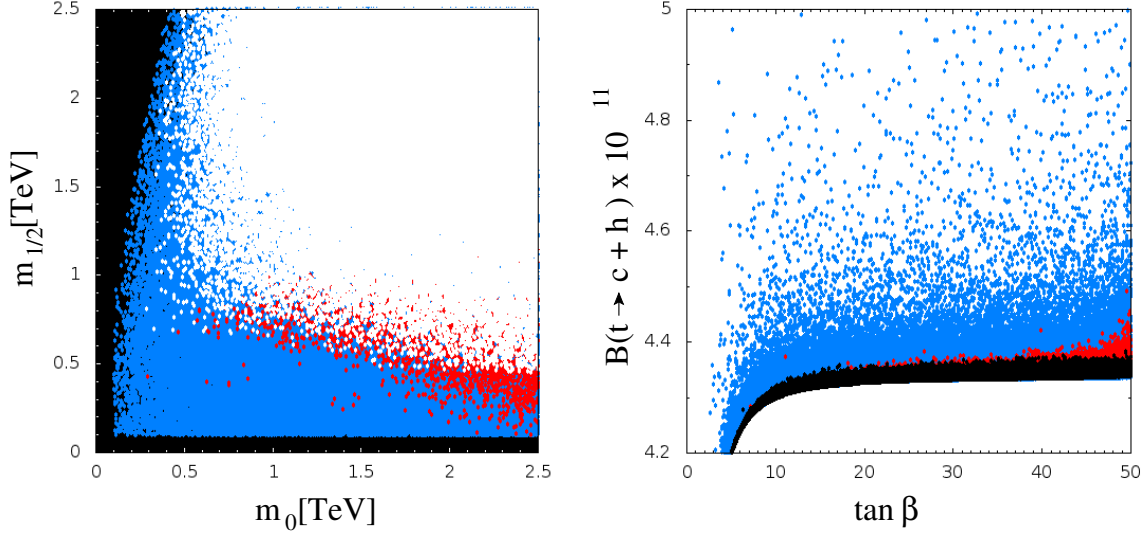


Figure 3.6: The panel on the left shows the parts of the m_0 - $m_{1/2}$ plane in the cMSSM which are ruled out for all chosen values of A_0 and $\tan\beta$. In the left panel, the black region is ruled out by theory constraints, the blue dots by the Higgs boson mass constraints, and the red dots by all low-energy constraints. In the right panel, blue and red dots follow the same convention as in the left panel, while the black dots are *allowed* by all constraints.

– should be electrically neutral and have no colour quantum numbers. The extensive region in blue is ruled out by a combination of the h^0 mass constraint and the direct searches for supersymmetry, while the comparatively limited red regions are ruled out by constraints from low-energy measurements. Points falling in the white region are all allowed, and it is for these that we can legitimately try to evaluate top FCNC processes. It is important to note that almost the entire region for m_0 and $m_{1/2}$ within a TeV is ruled out – this is another way of stating that there are no light squarks, unless we consider the third generation, where a seesaw-type mechanism can give us one lighter squark state.

The panel on the right in Figure 3.6 contains our actual results. The scale on the y -axis, where we have plotted the branching ratio of $t \rightarrow c + h^0$ immediately tells that this always comes of the order of 10^{-11} , which is just two-orders of magnitude above the SM prediction. On the x -axis we have plotted the $\tan\beta$ variable, even though the actual branching ratio is not a very sensitive function of this, except when $\tan\beta$ is around 5. As before, the blue points are ruled out by Higgs mass constraints and direct constraints, and the red points are ruled out by low-energy measurements. Unlike the left panel, however, the *black* points are the ones which represent the allowed parameter sets. It is immediately obvious, therefore, that the cMSSM prediction for $B(t \rightarrow c + h)$ is around 4.3×10^{-11} , and this holds for almost all the points in the allowed parameter space.

Why is this branching ratio so small in the cMSSM, when there exist charged Higgs bosons to frustrate the GIM mechanism, as well as a wide range of possible couplings? The reason is quite simple. We do indeed have contributions which frustrate the GIM mechanism. This raises the branching ratio from the SM value of $\mathcal{O}(10^{-15})$ to $\mathcal{O}(10^{-11})$. However, if the factor had been as large as $m_W^2/m_b^2 \simeq 5 \times 10^5$, we should have expected the prediction to be one

order larger. That this does not happen is a phenomenon rather peculiar to the cMSSM, which is more constrained than other SUSY models. The requirement of a light Higgs boson with a mass as high as 125 GeV above the tree-level value, which is M_Z , requires most of the SUSY partners in this model to be very heavy, and this, being essentially a logarithmic effect, leads to the additional suppression of one order of magnitude in the $t \rightarrow c + Z$ branching ratio. Once this is understood, we cannot get the other enhancements, since (a) we have adopted the MFV paradigm, and (b) the couplings in SUSY closely resemble the gauge couplings. The Yukawa couplings of the charged Higgs boson are, indeed, dependent on $\tan \beta$, but they are proportional to

$$\frac{m_t}{M_W} \cot \beta + \frac{m_b}{M_W} \tan \beta$$

and hence do not grow very large in the range $3 \leq \tan \beta \leq 50$.

As shown in the right panel in Figure 3.6, the application of the Higgs mass and direct search constraints pushes the branching ratio down by a factor around 3, which is expected since these are known to push up the SUSY partner masses from the 100 GeV to the TeV range. The application of low-energy constraints (especially $B_s \rightarrow \mu^+ \mu^-$) further kills the feeble enhancement due to large $\tan \beta$, leading to the somewhat disappointing prediction of 4.3×10^{-11} .

When we come to the process $t \rightarrow c + Z^0$, this will be mediated by the whole set of diagrams in Figures 3.4 and 3.5 where, as in the previous case, the h^0 is replaced by the Z^0 and the corresponding broken line by a wiggly line. As in the previous section, we can calculate the four helicity amplitudes in terms of F_1 – F_4 form factors which are listed in Appendix B.2.2 and make a numerical evaluation. As in the case of the toy model, we predict branching ratios which are about two orders of magnitude greater than the branching ratios for $t \rightarrow c + h^0$, i.e. we get $\mathcal{B}(t \rightarrow c + Z^0) \sim 10^{-9}$, which is still far too small to be accessed by experiment. The reason is, of course, the same – breakdown of the GIM mechanism leads to a value about four orders of magnitude greater than the SM prediction, but so long as we stay within the MFV paradigm and have couplings which are not significantly greater than gauge coupling, no further enhancements will be obtained.

We see, therefore, that not only does the cMSSM fail to produce enough enhancement of the top FCNC decays for observation, but this will be a generic feature of any MSSM variant which follows the MFV paradigm. Not much can be gained, therefore, by relaxing the universality constraints on the SUSY-breaking parameters, as is done in, for example, the so-called phenomenological MSSM or pMSSM models. However, it is possible to break the MFV paradigm by choosing squark mixing matrices which are not aligned with the CKM matrix [214]. This provides some enhancement of the branching ratios for top FCNC decay, but only to the level of about 10^{-7} , partly because the squarks are already constrained to be rather heavy.

3.5 Beyond the MFV paradigm : R-parity violation

In the preceding section we have discussed how the cMSSM and its variants fail to produce top FCNC effects at a measurable level. Within SUSY, however, there exists another scenario which can provide the necessary enhancements, and that is the scenario when R -parity is violated. It is well-known that the conservation of the Z_2 quantum number $R = (-1)^{L+2S+3B}$, where L , S and B stand for lepton number, spin and baryon number of a particle, is a condition which must be imposed by hand on all SUSY models if we want the lightest SUSY particle, or LSP, to be a candidate for cold dark matter. Thus, when we consider a scenario in which the R -parity is not conserved, we abandon the idea of explaining dark matter in a SUSY model – a feature which has contributed to making such models far less popular than the opposite variant. It is important to note, however, that R -parity conservation is not demanded by SUSY at all – it is an add-on which was originally believed to be necessary to explain the long lifetime of the proton [215]. However, ever since it was pointed out that this can be done be separately conserving either lepton number L or baryon number B , it has been known that one can easily have R -parity violating models which are consistent with both exact and broken SUSY. In that case, R -parity loses its special position, for the way in which R -parity produces a dark matter candidate is no different from any other Z_2 symmetry imposed by hand on a new physics model, such as, for example, the KK-parity imposed in models with a universal extra dimension [216] and the T -parity imposed in the littlest Higgs models [217]. Thus, at the cost of decoupling SUSY from the search for an explanation of dark matter in terms of new particles, it is legitimate to consider models where R -parity is violated.

Once we allow R -parity violation, it is straightforward to write down the extra interactions allowed. These will arise from a superpotential term [318]

$$\widehat{W}_R = \sum_{i,j,k=1}^3 \left(\frac{1}{2} \lambda_{ijk} \widehat{L}_i \widehat{L}_j \widehat{E}_k^c + \lambda'_{ijk} \widehat{L}_i \widehat{Q}_j \widehat{D}_k^c + \frac{1}{2} \lambda''_{ijk} \widehat{U}_i^c \widehat{D}_j^c \widehat{D}_k^c \right) \quad (3.5.1)$$

where the \widehat{L} and \widehat{Q} superfields are SU(2) doublets (suitably combined) and the \widehat{E}^c , \widehat{U}^c and \widehat{D}^c are SU(2) singlets. The indices i , j and k run over the three matter generations. It is immediately clear that the λ_{ijk} are antisymmetric in i and j , i.e. there are 9 independent λ_{ijk} 's and the λ''_{ijk} are antisymmetric in j and k , i.e. there are 9 independent λ''_{ijk} 's. The λ'_{ijk} have no such symmetry properties and hence there will be 27 independent λ'_{ijk} 's, bringing the total number of independent parameters to 45. However, to avoid fast proton decay, we must either conserve lepton number and set all the λ_{ijk} 's and λ'_{ijk} 's to zero, or conserve baryon number and set all the λ''_{ijk} 's to zero. Either alternative leads to FCNC processes, including, when the third generation is considered, the top quark. In this work, all RPV couplings will be considered real.

Constraints on the R -parity violating couplings from various low-energy FCNC processes have been industriously studied in the literature [223–228, 318] and a first look would lead to the conclusion that the λ , λ' and λ'' couplings must be rather small. Such constraints depend, however, on two crucial assumptions, viz.,

- Only one (or at most two) of the R -parity couplings are substantial and all the others are zero or of negligible value. This makes a phenomenological analysis simple, but its virtue ends there. The oft-repeated analogy with a similar pattern observed in the SM Yukawa couplings is not a very convincing argument.
- Most of the bounds used to be presented with scaling factors depending on the mass of the exchanged squark, which was assumed to be around 100 GeV. Today, most of the lower bounds on the squark masses (at least in the first two generations) are an order of magnitude higher, leading to considerable relaxation in the constraints on the R -parity violating couplings.

Once we realise that the R -parity violating couplings can, in fact, be very large, we also note that they have no need to be aligned with the CKM matrix or even satisfy unitarity constraints, for these are parameters of the Lagrangian, and do not arise from the mixing of fields. The R -parity violating scenario, therefore, can satisfy all the conditions required for

	Strongest Constraint arises from	Scales		Upper bound (100 GeV)	Sfermion mass (GeV)	Current upper bound
		as mass of	Scaling Exponent			
λ'_{121}	Atomic Parity Violation [223]	\tilde{q}_L	1	0.035	1350 [230]	0.473
λ'_{122}	ν_e mass bound [231]	\tilde{d}_R	$1/2$	0.004	1100 [346]	0.013
λ'_{123}	CC Universality [223]	\tilde{b}_1	$1/2$	0.02	620 [232]	0.05
λ'_{131}	Atomic parity violation [229]	\tilde{t}_L	1	0.019	300 [233]	0.057
λ'_{132}	FB asymmetry (e^+e^-) [229] [318]	\tilde{t}_L	1	0.28	300 [233]	0.84
λ'_{133}	ν_e mass bound [231]	\tilde{b}_1	$1/2$	0.0002	620 [232]	0.0005
λ'_{221}	Bounds on $R_{\mu e}$ [234]	\tilde{d}_R	1	0.18	1100 [346]	1.98
λ'_{222}	ν_μ mass bound [231]	\tilde{d}_R	$1/2$	0.015	1100 [346]	0.05
λ'_{223}	D_s meson decay [234]	\tilde{b}_1	1	0.18	620 [232]	1.1
λ'_{231}	ν_μ DIS [223, 318]	$\tilde{\nu}_\tau$	1	0.22	1700 [235]	2.00
λ'_{232}	Bounds on $R_\mu(Z)$ [236, 342]	\tilde{s}	1	0.39	1000 [346]	2.00
		$\tilde{\mu}$	-1		100 [346]	
λ'_{233}	ν_μ mass bound [231]	\tilde{d}_R	$1/2$	0.001	1100 [346]	0.003
λ'_{321}	D_s decays [318]	\tilde{d}_R	1	0.52	1100 [346]	0.66
λ'_{322}	ν_τ mass bound [231]	\tilde{d}_R	$1/2$	0.02	1100 [346]	0.07
λ'_{323}	D_s decay [318]	\tilde{b}_1	1	0.52	620 [232]	2.00
λ'_{331}	Bounds on $R_\tau(Z)$ [236]	\tilde{d}	1,	0.22	1000 [346]	2.00
λ'_{332}		$\tilde{\tau}$	-1	0.22	100 [346]	2.00
λ'_{333}	ν_τ mass bound [231]	\tilde{b}_1	$1/2$	0.001	620 [232]	0.003

Table 3.5: Showing the experimental constraints on the R -parity-violating couplings λ'_{ij} and λ'_{i3j} relevant for FCNC decays of the top quark. The abbreviations used in the second column are as follows: charged current (CC), forward-backward (FB), deep inelastic scattering (DIS), branching ratio (BR). The upper bounds on the λ' and λ'' couplings scale as the masses of the sfermions listed in the third column, raised to the powers given in the fourth column. The fifth column records the upper bounds when these masses are uniformly set to 100 GeV (except for the gluino, whose mass is set to 1000 GeV). The sixth column gives the current lower bound on the relevant sparticle masses and the last column gives the corresponding (scaled) upper bound on the R -parity-violating couplings.

FCNC enhancement, viz. frustration of the GIM mechanism, non-MFV mixing terms and almost unconstrained coupling constants. We therefore choose, in this section, the R -parity violating model (RPV-MSSM) as a paradigm to illustrate how large top FCNC effects can be obtained.

As a first step to this study, we note that the λ_{ijk} , while interesting enough in their own right, are not relevant for the processes of interest in this article, since they do not appear with operators involving quark fields. We do not discuss them further in this article. The couplings of interest are the λ'_{ijk} or the λ''_{ijk} – but obviously not both. We therefore list, in Table 5 below, the constraints on the R -parity violating couplings relevant for the processes under consideration, taking into account the current constraints on the masses of the sleptons and squarks. These, of course, still assume that one (or at most two) coupling(s) at a time is dominant.

Strongest Constraint arises from	Scales		Upper bound (100 GeV)	Sfermion mass (GeV)	Current upper bound
	as mass of	Scaling Exponent			
λ''_{212} λ''_{213} λ''_{223}	Perturbativity [339]	–	1.24	–	1.24
λ''_{312} λ''_{313}					
λ''_{323}					
$n - \bar{n}$ oscillation [239, 240]	\tilde{d}_R	2	10^{-3}	1100 [346]	0.1
	\tilde{g}	$1/2$		1000 [201]	0.1
Bounds on $R_b(Z)$ [338]	\tilde{b}	1	1.89	500 [232]	1.89
	$\tilde{\tau}$	-1	1.89	80 [346]	

Table 3.6: Showing the experimental constraints on the R -parity-violating couplings λ''_{2jk} and λ''_{3jk} relevant for FCNC decays of the top quark. The notations and abbreviations follow the conventions of Table 3.5.

A glance at the last column of Tables 3.5 and 3.6 will make it clear that with the current values of sfermion masses, the constraints on most of the R -parity-violating couplings are very weak. These couplings can be as large as gauge couplings, or, in specific cases, much larger. Top FCNC processes will typically involve

1. the products $\lambda'_{i2k}\lambda'_{i3k}$ for the decays $t \rightarrow c + h^0/Z$, where i denotes the leptonic flavour in the loop and k denotes the d -type quark flavour in the loop. For decays to $t \rightarrow u + h^0/Z$, we would get the products $\lambda'_{i1k}\lambda'_{i3k}$, but these have not been considered in this work.
2. the products $\lambda''_{2jk}\lambda''_{3jk}$ for the decays $t \rightarrow c + h^0/Z$, where j denotes a quark flavour of the u -type and k denotes a d -type quark flavour. As in the previous case, for the decays $t \rightarrow u + h^0/Z$, we would get products like $\lambda''_{1jk}\lambda''_{3jk}$, which are not considered in this work.

In Table 3.7, we list the pairs of R -parity-violating couplings which can lead to top FCNC processes, together with their maximum values corresponding to the last column of Tables 3.5 and 3.6. Some of the products are rather large, though staying well within the perturbative limit of 4π .

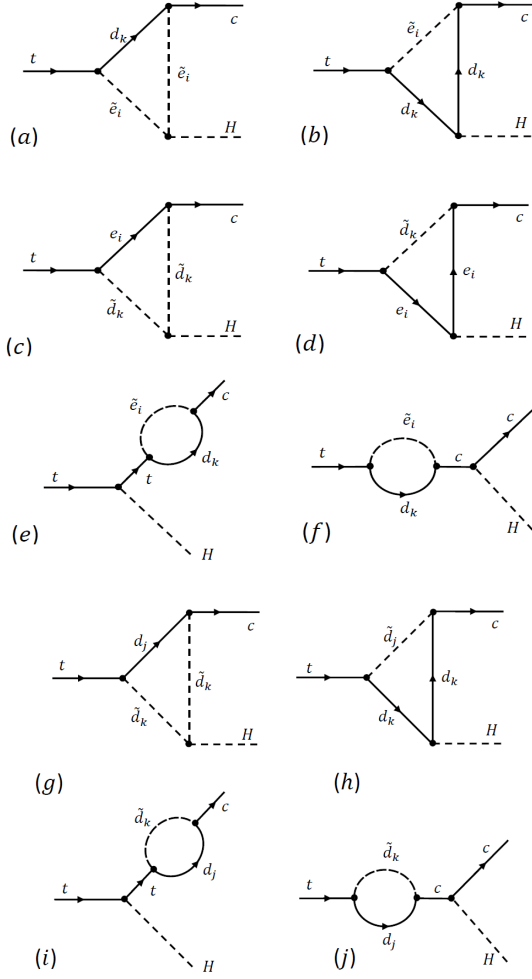


Figure 3.7: Further Feynman Diagrams leading to the decay $t \rightarrow c + H$ in the RPV MSSM.

The Feynman diagrams which contribute to the FCNC decay $t \rightarrow c + h^0$ in the RPV-MSSM have been listed in Fig. 3.7. Of course, since the R -parity violating superpotential is added to the MSSM terms, we will also have contributions from all the diagrams in Figs. 3.4 and 3.5. However, these are always small – as we have seen – and hence the dominant contribution will arise from R -parity-violating terms alone.

As before, the details of the calculation are given in Appendix B.3. It is important to note that we have presented the diagrams mediated by λ' couplings and the diagrams mediated by λ'' couplings in the same framework. The former include diagrams labelled (a)–(f), while the latter are labelled (g)–(j). The corresponding amplitudes will be added, as described in Appendix B.3. However, there is no harm done, so long as we keep all the λ'' zero when the λ' are non-zero, and vice versa. The variation of the branching ratios for $t \rightarrow c + h^0$ and $t \rightarrow c + Z$ as a function of the sfermion mass are given in Figure 3.8. The panels on the left, carrying the header LQ \bar{D} , correspond to the λ' couplings and show values proportional to $(\lambda'_{i2k}\lambda'_{i3k})^2$. The relevant values of ik are marked alongside each curve.

To illustrate the variation with the sfermion masses, we have set these couplings to the experimental upper bounds in the last column of Table 5, and consequently, the products to the values in Table 7. These, of course, will be relaxed further if the concerned sfermion masses are taken higher, and would lead to even greater branching ratios, as may be imagined. However, we have chosen to keep the couplings fixed to the values given in Table 7. In a similar way, the panels on the right, carrying the header UD \bar{D} , correspond to the λ'' couplings, and show values proportional to the products $(\lambda''_{2jk}\lambda''_{3jk})^2$. Here, too, we have marked the values of jk next to the relevant curves.

In Figure 3.8, the left panels illustrate the behaviour of the respective branching ratios with respect to variations in the mass of the slepton \tilde{e}_{Li} . Each curve starts on the left from the current lower bound on the mass of this slepton and goes up to a TeV. The variation of the branching ratio as the mass of the squark \tilde{d}_{Rk} varies from 1 – 2 TeV is represented by the

$\lambda'_{121}\lambda'_{131}$	$\lambda'_{122}\lambda'_{132}$	$\lambda'_{123}\lambda'_{133}$	$\lambda'_{221}\lambda'_{231}$	$\lambda'_{222}\lambda'_{232}$	$\lambda'_{223}\lambda'_{233}$
0.0269	0.0109	2.5×10^{-5}	3.96	0.1	0.0033
\tilde{e}_L, \tilde{d}_R	\tilde{e}_L, \tilde{s}_R	\tilde{e}_L, \tilde{b}_R	$\tilde{\mu}_L, \tilde{d}_R$	$\tilde{\mu}_L, \tilde{s}_R$	$\tilde{\mu}_L, \tilde{b}_R$
$\lambda'_{321}\lambda'_{331}$	$\lambda'_{322}\lambda'_{332}$	$\lambda'_{323}\lambda'_{333}$	$\lambda''_{212}\lambda''_{312}$	$\lambda''_{213}\lambda''_{313}$	$\lambda''_{223}\lambda''_{323}$
1.32	0.14	0.006	0.124	0.124	2.3436
$\tilde{\tau}_L, \tilde{d}_R$	$\tilde{\tau}_L, \tilde{s}_R$	$\tilde{\tau}_L, \tilde{b}_R$	\tilde{s}_R	\tilde{b}_R	\tilde{b}_R

Table 3.7: Showing upper limits on the products of pairs of R -parity-violating couplings relevant for the decays $t \rightarrow c + h^0/Z$, as well as the sparticles exchanged in the loops for each combination.

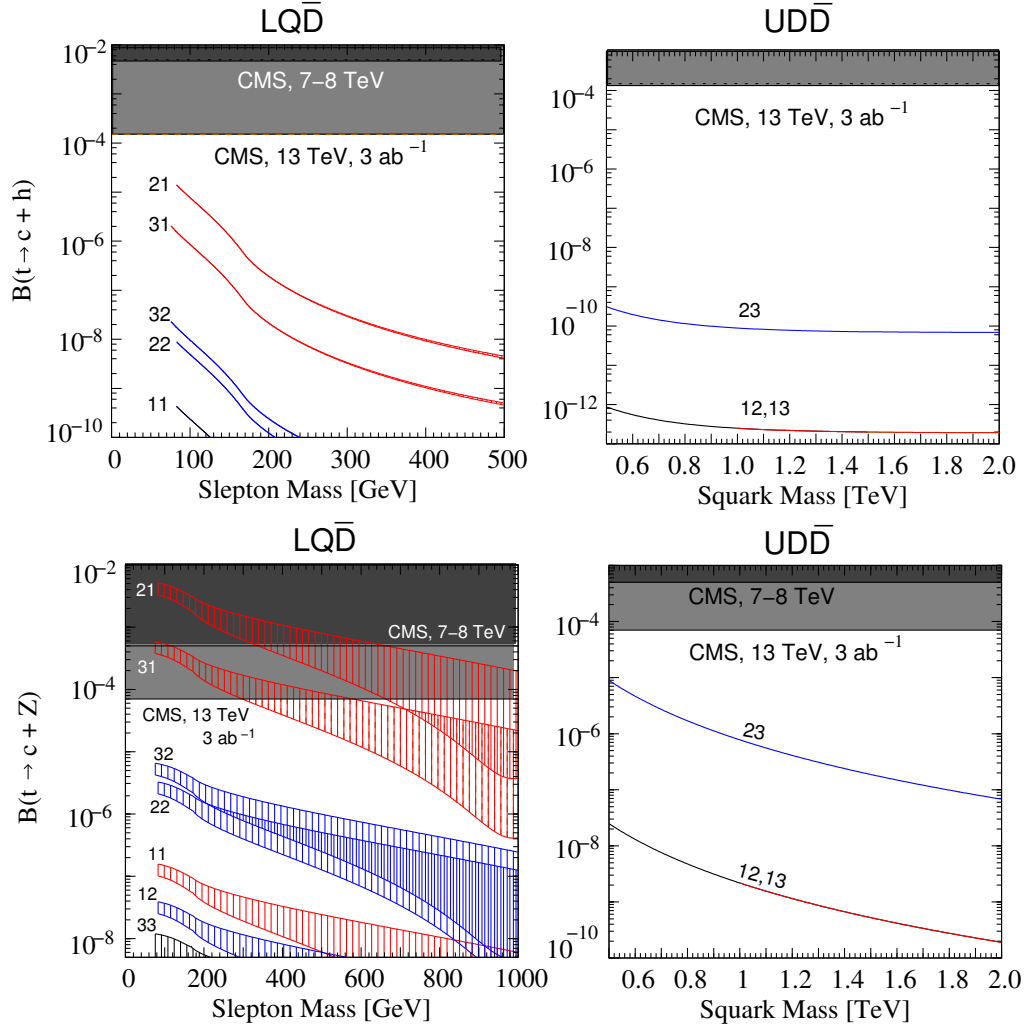


Figure 3.8: Illustrating the variation in the branching ratios $\mathcal{B}(t \rightarrow c + h^0)$ (upper panels) and $\mathcal{B}(t \rightarrow c + Z^0)$ (lower panels) with increase in the sfermion masses. For the panels on the left, which show branching ratios proportional to $(\lambda'_{i2k}\lambda'_{i3k})^2$ with the values of ik marked next to each curve, the mass of the slepton \tilde{e}_{Li} is plotted along the abscissa, and the mass of the squark \tilde{d}_{Rk} is responsible for the thickness of the lines in the upper panel and the hatched region in the lower panel. For the panels on the right, which show branching ratios proportional to $(\lambda''_{2jk}\lambda''_{3jk})^2$ with the values of jk marked next to each curve, the mass of the squark \tilde{d}_{Rk} is plotted along the abscissa. The dark (light) grey shaded regions represent the experimental bounds (discovery limits) from the LHC, operating at 7–8 TeV (13 TeV, projected).

thickness of the lines in the upper panel, and by the hatched regions on the lower panel (with the upper boundary indicating a squark mass of 1 TeV). Quite obviously, the branching ratio $\mathcal{B}(t \rightarrow c + h^0)$ is hardly affected by changes in the squark mass, whereas the branching ratio $\mathcal{B}(t \rightarrow c + Z^0)$ can vary by as much as an order of magnitude as the squark grows heavier.

The panels on the right in Figure 3.8 illustrate the variation in the respective branching ratios with change in the mass of the squark \tilde{d}_{Rk} , which is the b -squark for $jk = 13, 23$ and the c -squark for $jk = 12$. The black and blue curves correspond to the former two cases and the red curves to the latter. In all the panels, the upper region shaded dark grey corresponds to bounds on the relevant branching ratios as set by the CMS Collaboration [242], while the regions shaded light grey corresponds to the projected discovery limits at the 13 TeV LHC, assuming an integrated luminosity of 3000 fb^{-1} . It is immediately obvious, that even with all the enhancements available to us in a model with R -parity violation, the FCNC branching ratios of the t -quark are rather small. For λ'' couplings, in fact, these are hopelessly small – in fact, so small, that even if we take the couplings to their perturbative limits, detection at the LHC will become a touch-and-go affair. The situation is better for λ' couplings, largely because the sleptons can still be quite light. However, as the sleptons become heavier, the FCNC branching ratios fall rather fast and become unobservable. The best case arises for $\mathcal{B}(t \rightarrow c + Z^0)$ when we have the couplings $\lambda'_{221}\lambda'_{231}$ and $\lambda'_{321}\lambda'_{331}$, with exchange of $\tilde{\mu}_L$ or $\tilde{\tau}_L$ in the loops. In the former case, the data already available from the LHC constrains the slepton mass to be greater than about 350 GeV. In either case, a discovery at the 13 TeV run is possible for a wide range of slepton and squark masses. For other combinations of the λ' couplings, the branching ratios are too small to be accessible at the LHC, even at the end of its run.

Before concluding this section, we may take up the issue mentioned before, that if the experimental bounds on the sfermion masses increase, the upper bounds on the R -parity-violating couplings can be relaxed still further. This may lead to higher values of the branching ratios in question, if the sfermion in the FCNC loop is not the same one which leads to relaxation of the bound. However, if we consider the only products which lead to sizable results as shown in Figure 3.8, viz. $\lambda'_{221}\lambda'_{231}$, $\lambda'_{321}\lambda'_{331}$ and $\lambda''_{223}\lambda''_{323}$, we can see from Table 7 that the values are, respectively, 3.96, 1.32 and 2.34. The maximum value that we can push these to is, of course, 4π , and that would provide enhancements in the branching ratios at the level of one or two orders of magnitude. This might just make it possible to observe the decay $t \rightarrow c + Z$ if it is mediated by $\lambda''_{223}\lambda''_{323}$, with more optimistic results for the λ' couplings. However, only if some sign of R -parity-violating SUSY is found at the LHC will it be worthwhile to investigate further details in this regard.

3.6 Summary and Conclusions

This work was undertaken with a definite view, viz. to investigate FCNC decays of the t quark which involve heavy particles that cannot be discovered directly at the LHC. Several such

claims exist in the literature, but the results obtained are not always mutually consistent (see Table 8 below). By starting with a toy model which closely resembles the SM, we have shown that the extremely low values of FCNC branching ratios of the t -quark in the SM arise from three different sources. These are (i) the GIM cancellation between one-loop diagrams with different d -type quarks in the loop, (ii) the MFV paradigm, i.e. the choice of the hierarchical CKM matrix as the only source of flavour violation, and (iii) the choice of gauge couplings or their equivalent for the new particles. These result in suppression factors of the order 10^{-5} , 10^{-4} and 10^{-1} respectively, driving the loop-induced branching ratios from their naive values around 10^{-4} to tiny values in the neighbourhood of 10^{-14} . It follows, therefore, that a new physics model will be able to predict enhanced rates of these FCNC decays only to the extent that one or more of these conditions is violated. We then illustrate this set of conditions by considering (a) the cMSSM – a model where GIM cancellation is frustrated, but MFV holds and the couplings can be modestly enhanced, and (b) the R -parity-violating extension of the cMSSM, where all three conditions can be broken. In vindication of the general principles enunciated above, the branching ratios in the cMSSM do not exceed 10^{-10} for $t \rightarrow c + h^0$ and 10^{-8} for $t \rightarrow c + Z^0$, whereas, for the case when R -parity is violated, we can predict them to be as large as 10^{-5} and 10^{-3} respectively. The last-mentioned values are well within the range of accessibility at the LHC, as illustrated in Figure 3.8 above.

Reference	Model	GIM	MFV	g	$t \rightarrow ch^0$	$t \rightarrow cZ^0$
T.-J. Gao <i>et al.</i> [243]	\mathcal{B}, \mathcal{L}	×	×	×	$10^{-4(5)}$	–
J.-J. Cao <i>et al.</i> [244]	MSSM	×	✓	×	$10^{-5(9)}$	$10^{-6(7)}$
B. Mele [245]	MSSM	×	✓	×	$10^{-5(9)}$	$10^{-8(7)}$
S. Bejar <i>et al.</i> [246]	2HDM Type-II	×	✓	×	$10^{-4(9)}$	–
G. Eilam <i>et al.</i> [229]	\mathcal{R} SUSY	×	×	✓	$10^{-5(5)}$	–
C. Yue <i>et al.</i> [247]	Non-universal Z'	×	×	×	–	$10^{-6(4)}$
I. Baum <i>et al.</i> [248]	t -quark 2HDM	×	✓	×	$10^{-6(6)}$	–
A. Dedes <i>et al.</i> [214]	SUSY	×	×	×	$10^{-7(7)}$	–

Table 3.8: A few of the earlier calculations of FCNC decays of the top quark. Some of the results are in agreement with our predictions, given in parentheses. Those which are not are generally due to choice of vastly different parameters, which were allowed when these calculations were performed.

The utility of identifying the three suppression principles is well illustrated in Table 8, where some of the different models considered in the literature are classified according to the conditions which hold (✓) or are violated (×). It is, then, easy to utilise the suppression levels quoted above to understand/criticise the branching ratios predicted by these authors. Moreover, we now have a quick rule of thumb to predict the branching ratios for FCNC decays of the top quark for *any* new physics model, for all that we need is to ask ourselves is which of these three conditions are applicable.

The appendices of this article present a collection of the formulae needed to perform the computations given in the text, in an explicit and user-friendly form, using the 'tHooft-Veltman and Passarino-Veltman formalism for one-loop integrals. The formulae are given in

terms of certain generic couplings, so as to be easily usable to carry out similar computations in almost any new model of physics beyond the SM.

Finally, a word about the phenomenological implications of this work. It turns out that the use of the FCNC decays of the top quark is not such a ready handle to new physics at the LHC (and other high energy machines) as one might naively think, since the corresponding branching ratios are generally rather small. Even when we deviate almost completely from the SM, as exemplified in the R -parity-violating couplings, we require to be lucky to have just the right masses and pairing(s) of couplings in order to predict an observable effect. This is something which only the future can tell, and it is certain that the eyes of the entire high energy community will be turned to the results of the LHC, as they slowly unfold over the years to come.

A closer look at the R_D and R_{D^*} anomalies

4.1 Introduction

The third generation quarks are thought to be important probes of New Physics. As a counterpart to the up-type third generation quark – the top – we have seen that in recent years, a number of experimental measurements involving B meson decays have shown interesting deviations from their SM expectations. Deviations have been seen both in the neutral current $b \rightarrow s$ decays [249, 250]¹ as well as the charged current $b \rightarrow c$ processes. The most statistically significant deviation, at the 4σ level [358], is seen in the combination of R_D and R_{D^*} which are defined as,

$$R_{D^{(*)}} = \frac{\mathcal{B}(\overline{B} \rightarrow D^{(*)} \tau \bar{\nu}_\tau)}{\mathcal{B}(\overline{B} \rightarrow D^{(*)} l \bar{\nu}_l)}, \quad (4.1.1)$$

where $l = e$ or μ . In Table 4.1, we collect all the relevant experimental results related to the $\overline{B} \rightarrow D^{(*)} \ell \nu_\ell$ decay processes.

Note that, we have used the notation ℓ to denote any lepton (e , μ or τ) and l to denote only the light leptons, e and μ .

The large statistical significance of the anomaly in R_D and R_{D^*} has spurred a lot of interest in this decay modes in the last few years [272, 277–311] and various possible theoretical explanations have been proposed.

The main purpose of this work is to identify observables which can help distinguish the different NP Lorentz structures that can potentially solve the R_D and R_{D^*} anomalies. We first perform an operator analysis of these potential NP signals by considering all the dimension-6 operators that are consistent with SM gauge invariance. We compute the values of the relevant Wilson coefficients (WCs) that explain the experimental measurements within their 1σ ranges. It is important to note that we consider the presence of NP only in the tau-channel

¹For theoretical implications, see for example [251–264] and the references therein.

List of Observables			
Observable	Experimental Results		SM Prediction
	Experiment	Measured value	
R_D	Belle	$0.375 \pm 0.064 \pm 0.026$ [266]	0.299 ± 0.011 [267]
	BaBar	$0.440 \pm 0.058 \pm 0.042$ [268, 269]	0.300 ± 0.008 [270]
	HFAG average	$0.397 \pm 0.040 \pm 0.028$ [358]	0.299 ± 0.003 [271] 0.300 ± 0.011
R_{D^*}	Belle	$0.293 \pm 0.038 \pm 0.015$ [266]	0.252 ± 0.003 [272] 0.254 ± 0.004
	Belle	$0.302 \pm 0.030 \pm 0.011$ [273]	
	BaBar	$0.332 \pm 0.024 \pm 0.018$ [268, 269]	
	LHCb	$0.336 \pm 0.027 \pm 0.030$ [274]	
	HFAG average	$0.316 \pm 0.016 \pm 0.010$ [358]	
	Belle	$0.276 \pm 0.034^{+0.029}_{-0.026}$ [275]	
	Our average	0.310 ± 0.017	
$\mathcal{B}(\bar{B} \rightarrow D\tau\bar{\nu}_\tau)$	BaBar	$1.02 \pm 0.13 \pm 0.11$ % [268]	0.633 ± 0.014 %
$\mathcal{B}(\bar{B} \rightarrow D^*\tau\bar{\nu}_\tau)$	BaBar	$1.76 \pm 0.13 \pm 0.12$ % [268]	1.28 ± 0.09 %
$\mathcal{B}(\bar{B} \rightarrow D\ell\bar{\nu}_\ell)$	HFAG average	$2.13 \pm 0.03 \pm 0.09$ % [358]	$2.11^{+0.12}_{-0.10}$ %
$\mathcal{B}(\bar{B} \rightarrow D^*\ell\bar{\nu}_\ell)$	HFAG average	$4.93 \pm 0.01 \pm 0.11$ % [358]	$5.04^{+0.44}_{-0.42}$ %
$P_\tau(\bar{B} \rightarrow D\tau\bar{\nu}_\tau)$			0.325 ± 0.009 [276] 0.325 ± 0.012
$P_\tau(\bar{B} \rightarrow D^*\tau\bar{\nu}_\tau)$	Belle	$-0.44 \pm 0.47^{+0.20}_{-0.17}$ [275]	-0.497 ± 0.013 [275, 277] -0.497 ± 0.008
\mathcal{A}_{FB}^D			$-0.360^{+0.002}_{-0.001}$
$\mathcal{A}_{FB}^{D^*}$			0.064 ± 0.014

Table 4.1: The relevant observables, their experimental measurements and the SM predictions are shown. While computing the branching ratios, we have used $V_{cb} = 0.04$. As HFAG has not yet included the latest Belle measurement of R_{D^*} in their global average, we have taken a naive weighted average of the latest Belle result and the average given by HFAG. However, since the recent Belle result has a large uncertainty, it does not affect the previous world average in any significant way. The values given in boldface are our results for the SM predictions. Note that, for the $\bar{B} \rightarrow D^*\ell\bar{\nu}_\ell$ SM predictions, the uncertainties correspond to 2σ uncertainties in the form factor parameters, see section 4.5 for more details.

and not for the electron or the muon channels. Thus, in our calculations of R_D and R_{D^*} , we use the SM values of the WCs in the denominator. For these values of the WCs, we compute the predictions for a few observables that have the potential to distinguish between the various NP operators. Although we provide numerical results only for the operators that are consistent with SM gauge invariance, we provide the analytical expressions for the double differential decay rates for the individual τ helicities for all the 10 independent dimension-6 operators contributing to these decays. To our knowledge, we are the first in the literature to provide the full expressions.

As we show later, R_D and R_{D^*} are in general theoretically independent observables and the anomalies can exist independently. A future measurement might reveal a greater anomaly in one of them without affecting the other. Hence, in this paper, we attempt to explain each without worrying about the other initially, but then also point out how both can be explained together.

Very recently, the Belle collaboration reported the first measurement of the τ -polarisation in the decay $\bar{B} \rightarrow D^* \tau \bar{\nu}_\tau$ [275]. While the uncertainty in this measurement is rather large now, motivated by the possibility of more precise measurements in the future, we investigate how such a measurement can distinguish the various NP explanations of R_D and R_{D^*} . Furthermore, we show that measurements of R_{D^*} in bins of q^2 can provide important information about the nature of short distance physics. In fact, a combination of binwise R_{D^*} and more precise measurements (that can be done in Belle II, for example) of τ polarisation in both the $\bar{B} \rightarrow D \tau \bar{\nu}_\tau$ and $\bar{B} \rightarrow D^* \tau \bar{\nu}_\tau$ decays can completely distinguish all the different NP operators. Moreover, we show that the forward-backward asymmetry of the τ lepton (in the $\tau - \nu_\tau$ rest frame) also has the potential to differentiate the various NP Lorentz structures.

The paper is organised as follows: In section 4.2 we write down all the operators relevant for this study and define the notations for the corresponding WCs. The various observables of our interest are defined in section 4.3. The sections 4.4 and 4.5 discuss the form factors required for the calculation of the decay amplitudes. The analytic expressions for the double differential decay widths for the individual lepton helicities are shown in sections 4.6 and 4.7. In the following section (section 4.8), we present all our numerical results. Finally, we summarise our findings in section 6.6.

The full expressions for the double differential decay widths are shown in the appendices C.1 and C.2, and the contribution of the tensor operator \mathcal{O}_{TL} is discussed in appendix C.3. In appendix C.4, we show how our operators are related to the dimension-6 operators of [42]. The renormalisation group equations for the WCs are computed in appendix C.5.

4.2 Operator basis

The effective Lagrangian for the $b \rightarrow c \ell \bar{\nu}$ process at the dimension 6 level is given by,

$$\begin{aligned} \mathcal{L}_{\text{eff}}^{b \rightarrow c \ell \nu} = \frac{2G_F V_{cb}}{\sqrt{2}} \left(\begin{aligned} &C_9^{cbl} \mathcal{O}_9^{cbl} + C_9^{cbl'} \mathcal{O}_9^{cbl'} + C_{10}^{cbl} \mathcal{O}_{10}^{cbl} + C_{10}^{cbl'} \mathcal{O}_{10}^{cbl'} + C_s^{cbl} \mathcal{O}_s^{cbl} + C_s^{cbl'} \mathcal{O}_s^{cbl'} \\ &+ C_p^{cbl} \mathcal{O}_p^{cbl} + C_p^{cbl'} \mathcal{O}_p^{cbl'} + C_T^{cbl} \mathcal{O}_T^{cbl} + C_{T5}^{cbl} \mathcal{O}_{T5}^{cbl} \end{aligned} \right) \end{aligned} \quad (4.2.1)$$

where \mathcal{O}_i^{cbl} constitute a complete basis of 6-dimensional operators and C_i^{cbl} are the corresponding Wilson coefficients defined at the renormalization scale $\mu = m_b$. In the SM, $C_9^{cbl} = -C_{10}^{cbl} = 1$ and all the other WCs vanish. The full set of operators is given by:

$$\begin{aligned} \mathcal{O}_9^{cbl} &= [\bar{c} \gamma^\mu P_L b][\bar{\ell} \gamma_\mu \nu] \\ \mathcal{O}_{10}^{cbl} &= [\bar{c} \gamma^\mu P_L b][\bar{\ell} \gamma_\mu \gamma_5 \nu] \\ \mathcal{O}_s^{cbl} &= [\bar{c} P_L b][\bar{\ell} \nu] \\ \mathcal{O}_p^{cbl} &= [\bar{c} P_L b][\bar{\ell} \gamma_5 \nu] \\ \mathcal{O}_T^{cbl} &= [\bar{c} \sigma^{\mu\nu} b][\bar{\ell} \sigma_{\mu\nu} \nu] \end{aligned}$$

$$\begin{aligned}
\mathcal{O}_9^{cbl\ell'} &= [\bar{c} \gamma^\mu P_R b][\bar{\ell} \gamma_\mu \nu] \\
\mathcal{O}_{10}^{cbl\ell'} &= [\bar{c} \gamma^\mu P_R b][\bar{\ell} \gamma_\mu \gamma_5 \nu] \\
\mathcal{O}_s^{cbl\ell'} &= [\bar{c} P_R b][\bar{\ell} \nu] \\
\mathcal{O}_p^{cbl\ell'} &= [\bar{c} P_R b][\bar{\ell} \gamma_5 \nu] \\
\mathcal{O}_{T5}^{cbl\ell} &= [\bar{c} \sigma^{\mu\nu} b][\bar{\ell} \sigma_{\mu\nu} \gamma_5 \nu]
\end{aligned} \tag{4.2.2}$$

The other possible tensor structures are related to $\mathcal{O}_T^{cbl\ell}$ and $\mathcal{O}_{T5}^{cbl\ell}$ in the following way,

$$\epsilon_{\mu\nu\alpha\beta}[\bar{c} \sigma^{\mu\nu} b][\bar{\ell} \sigma^{\alpha\beta} \nu] = -2i\mathcal{O}_{T5}^{cbl\ell} \tag{4.2.3}$$

$$[\bar{c} \sigma^{\mu\nu} \gamma_5 b][\bar{\ell} \sigma_{\mu\nu} \gamma_5 \nu] = \mathcal{O}_T^{cbl\ell} \tag{4.2.4}$$

$$[\bar{c} \sigma^{\mu\nu} \gamma_5 b][\bar{\ell} \sigma_{\mu\nu} \nu] = \mathcal{O}_{T5}^{cbl\ell}. \tag{4.2.5}$$

Note that the above basis of operators is different from the one used in some earlier literature [279, 284]. For example, the reference [279] uses the following set of operators,

$$\begin{aligned}
\mathcal{O}_{VL}^{cbl\ell} &= [\bar{c} \gamma^\mu b][\bar{\ell} \gamma_\mu P_L \nu] & \mathcal{O}_{VR}^{cbl\ell} &= [\bar{c} \gamma^\mu b][\bar{\ell} \gamma_\mu P_R \nu] \\
\mathcal{O}_{AL}^{cbl\ell} &= [\bar{c} \gamma^\mu \gamma_5 b][\bar{\ell} \gamma_\mu P_L \nu] & \mathcal{O}_{AR}^{cbl\ell} &= [\bar{c} \gamma^\mu \gamma_5 b][\bar{\ell} \gamma_\mu P_R \nu] \\
\mathcal{O}_{SL}^{cbl\ell} &= [\bar{c} b][\bar{\ell} P_L \nu] & \mathcal{O}_{SR}^{cbl\ell} &= [\bar{c} b][\bar{\ell} P_R \nu] \\
\mathcal{O}_{PL}^{cbl\ell} &= [\bar{c} \gamma_5 b][\bar{\ell} P_L \nu] & \mathcal{O}_{PR}^{cbl\ell} &= [\bar{c} \gamma_5 b][\bar{\ell} P_R \nu] \\
\mathcal{O}_{TL}^{cbl\ell} &= [\bar{c} \sigma^{\mu\nu} b][\bar{\ell} \sigma_{\mu\nu} P_L \nu] & \mathcal{O}_{TR}^{cbl\ell} &= [\bar{c} \sigma^{\mu\nu} b][\bar{\ell} \sigma_{\mu\nu} P_R \nu]
\end{aligned} \tag{4.2.6}$$

The Wilson coefficients of these two basis of operators are related through the following equations,

$$\begin{aligned}
C_{VL}^{cbl\ell} &= \frac{1}{2} (C_9^{cbl\ell} - C_{10}^{cbl\ell} + C_9^{cbl\ell'} - C_{10}^{cbl\ell'}) & C_{SR}^{cbl\ell} &= \frac{1}{2} (C_s^{cbl\ell} + C_p^{cbl\ell} + C_s^{cbl\ell'} + C_p^{cbl\ell'}) \\
C_{AL}^{cbl\ell} &= \frac{1}{2} (-C_9^{cbl\ell} + C_{10}^{cbl\ell} + C_9^{cbl\ell'} - C_{10}^{cbl\ell'}) & C_{PR}^{cbl\ell} &= \frac{1}{2} (-C_s^{cbl\ell} - C_p^{cbl\ell} + C_s^{cbl\ell'} + C_p^{cbl\ell'}) \\
C_{SL}^{cbl\ell} &= \frac{1}{2} (C_s^{cbl\ell} - C_p^{cbl\ell} + C_s^{cbl\ell'} - C_p^{cbl\ell'}) & C_{VR}^{cbl\ell} &= \frac{1}{2} (C_9^{cbl\ell} + C_{10}^{cbl\ell} + C_9^{cbl\ell'} + C_{10}^{cbl\ell'}) \\
C_{PL}^{cbl\ell} &= \frac{1}{2} (-C_s^{cbl\ell} + C_p^{cbl\ell} + C_s^{cbl\ell'} - C_p^{cbl\ell'}) & C_{AR}^{cbl\ell} &= \frac{1}{2} (-C_9^{cbl\ell} - C_{10}^{cbl\ell} + C_9^{cbl\ell'} + C_{10}^{cbl\ell'}) \\
C_{TL}^{cbl\ell} &= (C_T^{cbl\ell} - C_{T5}^{cbl\ell}) & C_{TR}^{cbl\ell} &= (C_T^{cbl\ell} + C_{T5}^{cbl\ell})
\end{aligned} \tag{4.2.7}$$

We now assume the neutrino in the final state to be left handed. This implies that the WCs in eq. (4.2.1) satisfy the following relations,

$$C_9^{cbl\ell} = -C_{10}^{cbl\ell} \tag{4.2.8}$$

$$C_9^{cbl\ell'} = -C_{10}^{cbl\ell'} \tag{4.2.9}$$

$$C_s^{cbl\ell} = -C_p^{cbl\ell} \tag{4.2.10}$$

$$C_s^{cbl\ell'} = -C_p^{cbl\ell'} \tag{4.2.11}$$

$$C_T^{cbl\ell} = -C_{T5}^{cbl\ell}. \tag{4.2.12}$$

Consequently, all the WCs in the right hand column of eq. 4.2.7 vanish. Note that, the operators on the left hand column of eq. 4.2.7 are the only ones that are consistent with the full gauge invariance of the SM. In appendix C.4, we show how these WCs are related to the 6-dimensional operators listed in [42]. Moreover, since many microscopic models do not generate the tensor operator, we neglect them in the main text and study its effect only in the appendix (see appendix C.3).

Although, we do not study the effects of the operators with a right handed neutrino (the ones in the right hand column of eq. 4.2.7), we compute the full analytic expressions considering all the 10 operators for the first time in the literature. The results are presented in appendices C.1 and C.2.

4.3 Observables

The double differential branching fractions for the decays $\bar{B} \rightarrow D\ell\bar{\nu}_\ell$ and $\bar{B} \rightarrow D^*\ell\bar{\nu}_\ell$ can be written as

$$\frac{d^2\mathcal{B}_\ell^{D^{(*)}}}{dq^2 d(\cos\theta)} = \mathcal{N} |p_{D^{(*)}}| \left(a_\ell^{D^{(*)}} + b_\ell^{D^{(*)}} \cos\theta + c_\ell^{D^{(*)}} \cos^2\theta \right). \quad (4.3.1)$$

The normalisation factor, \mathcal{N} and the absolute value of the $D^{(*)}$ -meson momentum, $|p_{D^{(*)}}|$ are given by,

$$\mathcal{N} = \frac{\tau_B G_F^2 |V_{cb}|^2 q^2}{256\pi^3 M_B^2} \left(1 - \frac{m_\ell^2}{q^2} \right)^2 \quad (4.3.2)$$

$$|p_{D^{(*)}}| = \frac{\sqrt{\lambda(M_B^2, M_{D^{(*)}}^2, q^2)}}{2M_B}, \quad (4.3.3)$$

where $\lambda(a, b, c) = a^2 + b^2 + c^2 - 2(ab + bc + ca)$. The angle θ is defined as the angle between the lepton and $D^{(*)}$ -meson in the lepton-neutrino centre-of-mass frame, and q^2 is the invariant mass squared of the lepton-neutrino system.

The total branching fraction is given by,

$$\mathcal{B}_\ell^{D^{(*)}} = \int \mathcal{N} |p_{D^{(*)}}| \left(2a_\ell^{D^{(*)}} + \frac{2}{3}c_\ell^{D^{(*)}} \right) dq^2 \quad (4.3.4)$$

The observables R_D and R_{D^*} have already been defined in eq. (4.1.1). We now define binned $R_{D^{(*)}}$ in the following way,

$$R_{D^{(*)}}[q^2 \text{ bin}] = \frac{\mathcal{B}_\tau^{D^{(*)}}[q^2 \text{ bin}]}{\mathcal{B}_\ell^{D^{(*)}}[q^2 \text{ bin}]} \quad (4.3.5)$$

For the decays with τ lepton in the final state, the polarisation of the τ also constitutes an useful observable and can potentially be used to distinguish the NP Lorentz structures. The τ polarisation fraction is defined in the following way,

$$P_\tau(D^{(*)}) = \frac{\Gamma_\tau^{D^{(*)}}(+)-\Gamma_\tau^{D^{(*)}}(-)}{\Gamma_\tau^{D^{(*)}}(+)+\Gamma_\tau^{D^{(*)}}(-)} \quad (4.3.6)$$

where, $\Gamma_\tau^{D^{(*)}}(+)$ and $\Gamma_\tau^{D^{(*)}}(-)$ are the decay widths for positive and negative helicity τ leptons respectively.

The τ forward-backward asymmetry, $\mathcal{A}_{FB}^{D^{(*)}}$ is defined as

$$\begin{aligned}\mathcal{A}_{FB}^{D^{(*)}} &= \frac{\int_0^{\pi/2} \frac{d\Gamma^{D^{(*)}}}{d\theta} d\theta - \int_{\pi/2}^\pi \frac{d\Gamma^{D^{(*)}}}{d\theta} d\theta}{\int_0^{\pi/2} \frac{d\Gamma^{D^{(*)}}}{d\theta} d\theta + \int_{\pi/2}^\pi \frac{d\Gamma^{D^{(*)}}}{d\theta} d\theta} \\ &= \frac{\int b_\tau^{D^{(*)}}(q^2) dq^2}{\Gamma^{D^{(*)}}}\end{aligned}\quad (4.3.7)$$

where $\Gamma^{D^{(*)}}$ is the total decay width of $D^{(*)}$ and the angle θ has already been defined above. Note that, while the branching fractions depend on the functions $a_\ell^{D^{(*)}}$ and $c_\ell^{D^{(*)}}$, the forward-backward asymmetry depends only on $b_\ell^{D^{(*)}}$. Hence, they provide complementary information on the nature of the short distance physics.

4.4 $\bar{B} \rightarrow D$ form factors

The hadronic matrix elements for $\bar{B} \rightarrow D$ transition are parametrised by²

$$\begin{aligned}\langle D(p_D, M_D) | \bar{c} \gamma^\mu b | \bar{B}(p_B, M_B) \rangle &= F_+(q^2) \left[(p_B + p_D)^\mu - \frac{M_B^2 - M_D^2}{q^2} q^\mu \right] \\ &\quad + F_0(q^2) \frac{M_B^2 - M_D^2}{q^2} q^\mu\end{aligned}\quad (4.4.1)$$

$$\langle D(p_D, M_D) | \bar{c} \gamma^\mu \gamma_5 b | \bar{B}(p_B, M_B) \rangle = 0 \quad (4.4.2)$$

$$\langle D(p_D, M_D) | \bar{c} b | \bar{B}(p_B, M_B) \rangle = F_0(q^2) \frac{M_B^2 - M_D^2}{m_b - m_c} \quad (4.4.3)$$

$$\langle D(p_D, M_D) | \bar{c} \gamma_5 b | \bar{B}(p_B, M_B) \rangle = 0 \quad (4.4.4)$$

$$\langle D(p_D, M_D) | \bar{c} \sigma^{\mu\nu} b | \bar{B}(p_B, M_B) \rangle = -i(p_B^\mu p_D^\nu - p_B^\nu p_D^\mu) \frac{2F_T(q^2)}{M_B + M_D} \quad (4.4.5)$$

$$\langle D(p_D, M_D) | \bar{c} \sigma^{\mu\nu} \gamma_5 b | \bar{B}(p_B, M_B) \rangle = \varepsilon^{\mu\nu\rho\sigma} p_{B\rho} p_{D\sigma} \frac{2F_T(q^2)}{M_B + M_D} \quad (4.4.6)$$

Note that Eq. (4.4.3) and Eq. (4.4.6) are not independent equations and follow from Eq. (4.4.1) and Eq. (4.4.5) respectively. Multiplying the left hand side of Eq. (4.4.1) by q_μ one gets

$$\begin{aligned}q_\mu \langle D(p_D, m_D) | \bar{c} \gamma^\mu b | \bar{B}(p_B, M_B) \rangle &= \text{Inverse Fourier transform of } \langle D | i \partial_\mu (\bar{c} \gamma^\mu b) | B \rangle \\ &= \text{Inverse Fourier transform of } \langle D | (i \partial_\mu \bar{c} \gamma^\mu b + \bar{c} \gamma^\mu i \partial_\mu b) | B \rangle \\ &= (m_b - m_c) \langle D(p_D, M_D) | \bar{c} b | \bar{B}(p_B, M_B) \rangle\end{aligned}\quad (4.4.7)$$

Similarly, the term proportional to F_+ in the right hand side of Eq. (4.4.1) vanishes upon multiplication by q_μ and gives

$$\text{RHS} = F_0(q^2) (M_B^2 - M_D^2). \quad (4.4.8)$$

²We use the convention $\epsilon^{0123} = 1$. This implies $\epsilon_{0123} = -1$.

Thus, Eq. (4.4.7) and Eq. (4.4.8) taken together give us Eq. (4.4.3).

In order to get Eq. (4.4.6) from Eq. (4.4.5) one has to use the identity,

$$\sigma^{\mu\nu}\gamma_5 = \frac{i}{2}\varepsilon^{\mu\nu\alpha\beta}\sigma_{\alpha\beta}. \quad (4.4.9)$$

Substituting the above identity into the left hand side of Eq. (4.4.6) one gets,

$$\langle D(p_D, M_D) | \bar{c}\sigma^{\mu\nu}\gamma_5 b | \bar{B}(p_B, M_B) \rangle = \frac{i}{2}\varepsilon^{\mu\nu\alpha\beta} \langle D(p_D, M_D) | \bar{c}\sigma_{\alpha\beta} b | \bar{B}(p_B, M_B) \rangle \quad (4.4.10)$$

$$= \frac{i}{2}\varepsilon^{\mu\nu\alpha\beta} \left(-i(p_{B\alpha}p_{D\beta} - p_{B\beta}p_{D\alpha}) \frac{2F_T(q^2)}{M_B + M_D} \right) \quad (4.4.11)$$

$$= \varepsilon^{\mu\nu\alpha\beta} p_{B\alpha} p_{D\beta} \frac{2F_T(q^2)}{M_B + M_D} \quad (4.4.12)$$

The form factors $F_0(q^2)$ and $F_+(q^2)$ have been calculated using lattice QCD techniques in [267]³. They are given by the following expressions,

$$F_+(z) = \frac{1}{\phi_+(z)} \sum_{k=0}^3 a_k^+ z^k, \quad (4.4.13)$$

$$F_0(z) = \frac{1}{\phi_0(z)} \sum_{k=0}^3 a_k^0 z^k, \quad (4.4.14)$$

where

$$z \equiv z(q^2) = \frac{\sqrt{(M_B + M_D)^2 - q^2} - \sqrt{4M_B M_D}}{\sqrt{(M_B + M_D)^2 - q^2} + \sqrt{4M_B M_D}}.$$

The functions $\phi_+(z)$ and $\phi_0(z)$ are given by,

$$\phi_+(z) = 1.1213 \frac{(1+z)^2(1-z)^{1/2}}{[(1+r)(1-z) + 2\sqrt{r}(1+z)]^5}, \quad (4.4.15)$$

$$\phi_0(z) = 0.5299 \frac{(1+z)(1-z)^{3/2}}{[(1+r)(1-z) + 2\sqrt{r}(1+z)]^4}, \quad (4.4.16)$$

where, $r = M_D/M_B$.

The central values, uncertainties, and correlation matrix for the parameters a_k^0 and a_k^+ are shown in tables 4.2 and 4.3.

	a_0^+	a_1^+	a_2^+	a_3^+	a_0^0	a_1^0	a_2^0	a_3^0
Values	0.01261	-0.0963	0.37	-0.05	0.01140	-0.0590	0.19	-0.03
Uncertainties	0.00010	0.0033	0.11	0.90	0.00009	0.0028	0.10	0.87

Table 4.2: The central values and uncertainties for the parameters a_k^0 and a_k^+ from ref. [267] (table XI of their arXiv version 1).

³There has been another Lattice calculation of these form factors with similar results [270].

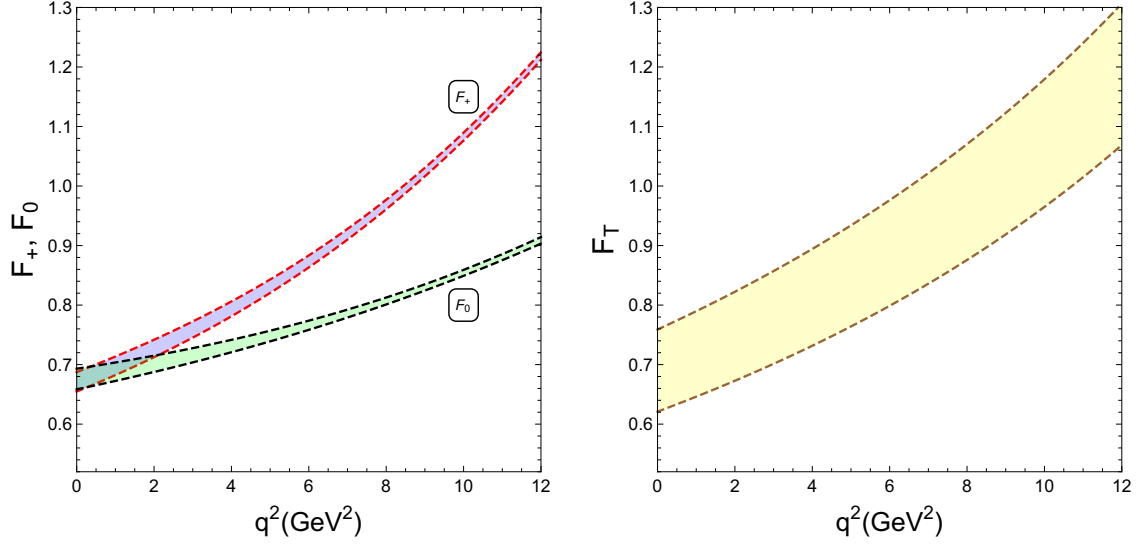


Figure 4.1: The q^2 dependence of the form factors F_0 , F_+ and F_T . The uncertainty bands for F_0 and F_+ correspond to a $\chi^2 \leq 1.646$ where the χ^2 is computed using the expression $\chi^2(\mathbf{x}) = (\mathbf{x} - \mathbf{x}_0)^T \mathbf{V}^{-1} (\mathbf{x} - \mathbf{x}_0)$ where $\mathbf{x} = (a_0^+, a_1^+, a_2^+, a_3^+, a_0^0, a_1^0, a_2^0, a_3^0)$ and x_0 consists of the central values given in table 4.2. The covariance matrix V is computed from the correlation matrix ρ_{ij} given in table 4.3 using the formula $V_{ij} = \sigma_i(\mathbf{x}) \rho_{ij} \sigma_j(\mathbf{x})$ where $\sigma(\mathbf{x})$ is the vector of uncertainties given in tables 4.2. The uncertainty band for F_T is obtained by simply taking a $\pm 10\%$ uncertainty on the central value.

	a_0^+	a_1^+	a_2^+	a_3^+	a_0^0	a_1^0	a_2^0	a_3^0
a_0^+	1.00000	0.24419	-0.08658	0.01207	0.00000	0.23370	0.03838	-0.05639
a_1^+		1.00000	-0.57339	0.25749	0.00000	0.80558	-0.25493	-0.15014
a_2^+			1.00000	-0.64492	0.00000	-0.44966	0.66213	0.05120
a_3^+				1.00000	0.00000	0.11311	-0.20100	0.23714
a_0^0					1.00000	0.00000	0.00000	0.00000
a_1^0						1.00000	-0.44352	0.02485
a_2^0							1.00000	-0.46248
a_3^0								1.00000

Table 4.3: The correlation matrix for the parameters a_k^0 and a_k^+ from ref. [267] (table XI of their arXiv version 1).

As the tensor form factor F_T has not been computed from lattice QCD, we have taken them from [312]. Following [312], we write $F_T(q^2)$ as,

$$F_T(q^2) = \frac{0.69}{\left(1 - \frac{q^2}{(6.4\text{GeV})^2}\right) \left(1 - 0.56 \frac{q^2}{(6.4\text{GeV})^2}\right)}. \quad (4.4.17)$$

In fig. 4.1, we show the q^2 dependences of F_0 , F_+ and F_T following the above expressions.

4.5 $\bar{B} \rightarrow D^*$ form factors

The hadronic matrix elements for $\bar{B} \rightarrow D^*$ transition are parametrised by

$$\langle D^*(p_{D^*}, M_{D^*}) | \bar{c} \gamma_\mu b | \bar{B}(p_B, M_B) \rangle = i \varepsilon_{\mu\nu\rho\sigma} \epsilon^{\nu*} p_B^\rho p_{D^*}^\sigma \frac{2V(q^2)}{M_B + M_{D^*}} \quad (4.5.1)$$

$$\begin{aligned} \langle D^*(p_{D^*}, M_{D^*}) | \bar{c} \gamma_\mu \gamma_5 b | \bar{B}(p_B, M_B) \rangle &= 2M_{D^*} \frac{\epsilon^* \cdot q}{q^2} q_\mu A_0(q^2) + (M_B + M_{D^*}) \left[\epsilon_\mu^* - \frac{\epsilon^* \cdot q}{q^2} q_\mu \right] A_1(q^2) \\ &\quad - \frac{\epsilon^* \cdot q}{M_B + M_{D^*}} \left[(p_B + p_{D^*})_\mu - \frac{M_B^2 - M_{D^*}^2}{q^2} q_\mu \right] A_2(q^2) \end{aligned} \quad (4.5.2)$$

$$\langle D^*(p_{D^*}, M_{D^*}) | \bar{c} b | \bar{B}(p_B, M_B) \rangle = 0 \quad (4.5.3)$$

$$\langle D^*(p_{D^*}, M_{D^*}) | \bar{c} \gamma_5 b | \bar{B}(p_B, M_B) \rangle = -\epsilon^* \cdot q \frac{2M_{D^*}}{m_b + m_c} A_0(q^2) \quad (4.5.4)$$

$$\begin{aligned} \langle D^*(p_{D^*}, M_{D^*}) | \bar{c} \sigma_{\mu\nu} b | \bar{B}(p_B, M_B) \rangle &= -\varepsilon_{\mu\nu\alpha\beta} \left[-\epsilon^{\alpha*} (p_{D^*} + p_B)^\beta T_1(q^2) \right. \\ &\quad \left. + \frac{M_B^2 - M_{D^*}^2}{q^2} \epsilon^{\alpha*} q^\beta (T_1(q^2) - T_2(q^2)) \right. \\ &\quad \left. + 2 \frac{\epsilon^* \cdot q}{q^2} p_B^\alpha p_{D^*}^\beta \left(T_1(q^2) - T_2(q^2) - \frac{q^2}{M_B^2 - M_{D^*}^2} T_3(q^2) \right) \right] \end{aligned} \quad (4.5.5)$$

$$\langle D^*(p_{D^*}, M_{D^*}) | \bar{c} \sigma_{\mu\nu} q^\nu b | \bar{B}(p_B, M_B) \rangle = -2\varepsilon_{\mu\nu\rho\sigma} \epsilon^{\nu*} p_B^\rho p_{D^*}^\sigma T_1(q^2) \quad (4.5.6)$$

None of the form factors $V, A_0, A_1, A_2, T_1, T_2, T_3$ has been calculated in Lattice QCD. We used the heavy quark effective theory (HQET) form factors based on [313]. These form factors can be written in terms of the HQET form factors in the following way [284, 313],

$$\begin{aligned} V(q^2) &= \frac{M_B + M_{D^*}}{2\sqrt{M_B M_{D^*}}} h_V(w(q^2)), \\ A_1(q^2) &= \frac{(M_B + M_{D^*})^2 - q^2}{2\sqrt{M_B M_{D^*}}(M_B + M_{D^*})} h_{A_1}(w(q^2)) \\ A_2(q^2) &= \frac{M_B + M_{D^*}}{2\sqrt{M_B M_{D^*}}} \left[h_{A_3}(w(q^2)) + \frac{M_{D^*}}{M_B} h_{A_2}(w(q^2)) \right] \\ A_0(q^2) &= \frac{1}{2\sqrt{M_B M_{D^*}}} \left[\frac{(M_B + M_{D^*})^2 - q^2}{2M_{D^*}} h_{A_1}(w(q^2)) \right. \\ &\quad \left. - \frac{M_B^2 - M_{D^*}^2 + q^2}{2M_B} h_{A_2}(w(q^2)) - \frac{M_B^2 - M_{D^*}^2 - q^2}{2M_{D^*}} h_{A_3}(w(q^2)) \right] \\ T_1(q^2) &= \frac{1}{2\sqrt{M_B M_{D^*}}} [(M_B + M_{D^*}) h_{T_1}(w(q^2)) - (M_B - M_{D^*}) h_{T_2}(w(q^2))] \\ T_2(q^2) &= \frac{1}{2\sqrt{M_B M_{D^*}}} \left[\frac{(M_B + M_{D^*})^2 - q^2}{M_B + M_{D^*}} h_{T_1}(w(q^2)) - \frac{(M_B - M_{D^*})^2 - q^2}{M_B - M_{D^*}} h_{T_2}(w(q^2)) \right] \\ T_3(q^2) &= \frac{1}{2\sqrt{M_B M_{D^*}}} [(M_B - M_{D^*}) h_{T_1}(w(q^2)) - (M_B + M_{D^*}) h_{T_2}(w(q^2)) \\ &\quad - 2 \frac{M_B^2 - M_{D^*}^2}{M_B} h_{T_3}(w(q^2))] \end{aligned}$$

where,

$$\begin{aligned}
h_V(w) &= R_1(w) h_{A_1}(w) \\
h_{A_2}(w) &= \frac{R_2(w) - R_3(w)}{2r_{D^*}} h_{A_1}(w) \\
h_{A_3}(w) &= \frac{R_2(w) + R_3(w)}{2} h_{A_1}(w) \\
h_{T_1}(w) &= \frac{1}{2(1 + r_{D^*}^2 - 2r_{D^*}w)} \left[\frac{m_b - m_c}{M_B - M_{D^*}} (1 - r_{D^*})^2 (w + 1) h_{A_1}(w) \right. \\
&\quad \left. - \frac{m_b + m_c}{M_B + M_{D^*}} (1 + r_{D^*})^2 (w - 1) h_V(w) \right] \\
h_{T_2}(w) &= \frac{(1 - r_{D^*}^2)(w + 1)}{2(1 + r_{D^*}^2 - 2r_{D^*}w)} \left[\frac{m_b - m_c}{M_B - M_{D^*}} h_{A_1}(w) - \frac{m_b + m_c}{M_B + M_{D^*}} h_V(w) \right]
\end{aligned} \tag{4.5.7}$$

$$\begin{aligned}
h_{T_3}(w) &= -\frac{1}{2(1 + r_{D^*})(1 + r_{D^*}^2 - 2r_{D^*}w)} \left[2 \frac{m_b - m_c}{M_B - M_{D^*}} r_{D^*} (w + 1) h_{A_1}(w) \right. \\
&\quad - \frac{m_b - m_c}{M_B - M_{D^*}} (1 + r_{D^*}^2 - 2r_{D^*}w) (h_{A_3}(w) - r_{D^*} h_{A_2}(w)) \\
&\quad \left. - \frac{m_b + m_c}{M_B + M_{D^*}} (1 + r_{D^*})^2 h_V(w) \right]
\end{aligned} \tag{4.5.8}$$

$$\begin{aligned}
h_{A_1}(w) &= h_{A_1}(1) [1 - 8\rho_{D^*}^2 z + (53\rho_{D^*}^2 - 15)z^2 - (231\rho_{D^*}^2 - 91)z^3] \\
R_1(w) &= R_1(1) - 0.12(w - 1) + 0.05(w - 1)^2 \\
R_2(w) &= R_2(1) + 0.11(w - 1) - 0.06(w - 1)^2 \\
R_3(w) &= 1.22 - 0.052(w - 1) + 0.026(w - 1)^2
\end{aligned} \tag{4.5.9}$$

Here, $r_{D^*} = M_{D^*}/M_B$, $w(q^2) = (M_B^2 + M_{D^*}^2 - q^2)/2M_B M_{D^*}$ and $z(w) = (\sqrt{w + 1} - \sqrt{2})/(\sqrt{w + 1} + \sqrt{2})$.

The numerical values of the relevant parameters of the form factors along with their respective 1σ errors are given by

$$\begin{aligned}
R_1(1) &= 1.406 \pm 0.033, \quad R_2(1) = 0.853 \pm 0.020, \quad \rho_{D^*}^2 = 1.207 \pm 0.026 \quad [358] \\
h_{A_1}(1) &= 0.906 \pm 0.013 \quad [314].
\end{aligned} \tag{4.5.10}$$

In Fig. 4.2 we show the q^2 dependence of the form factors using these numerical values. As there have been no lattice calculations of these form factors, in order to be conservative, we use two times larger uncertainties than those quoted above.

4.6 Expressions for a_ℓ^D , b_ℓ^D and c_ℓ^D for $\overline{B} \rightarrow D\ell\bar{\nu}_\ell$

The quantities a_ℓ^D , b_ℓ^D and c_ℓ^D for positive helicity lepton are given by:

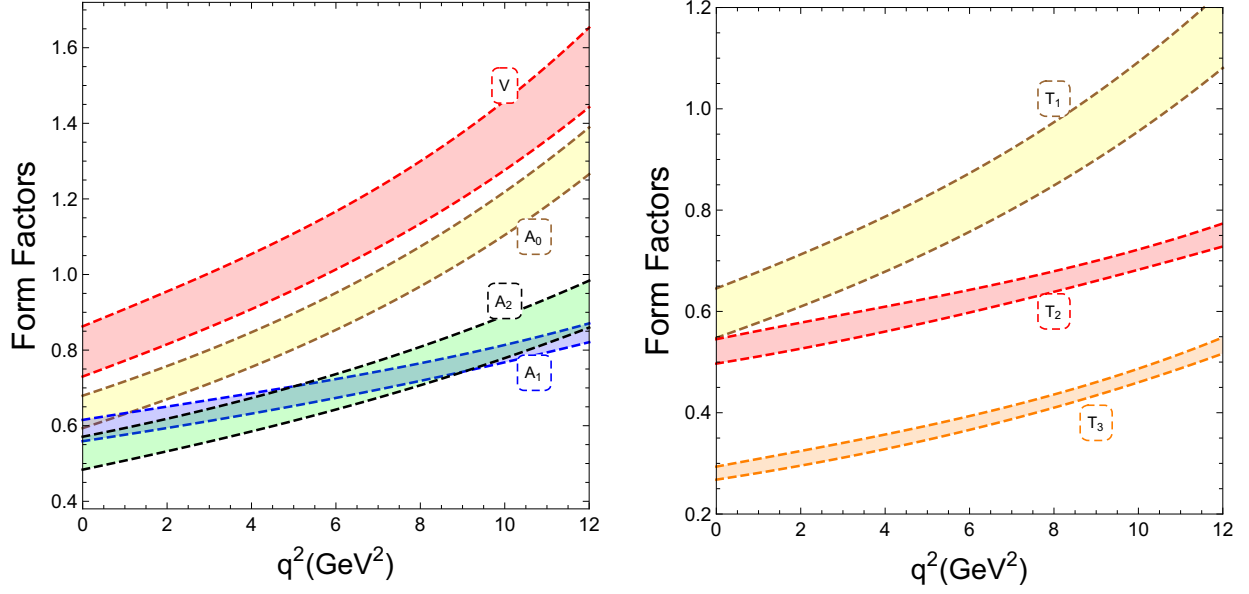


Figure 4.2: The q^2 dependence of the $B \rightarrow D^*$ form factors. The bands correspond to two times the uncertainties given in Eq. 4.5.10 .

$$\begin{aligned}
 a_\ell^D(+) &= \frac{2(M_B^2 - M_D^2)^2}{(m_b - m_c)^2} |\mathbf{C}_{\text{SL}}^\ell|^2 \mathbf{F}_0^2 \\
 &+ m_\ell \left[\frac{4(M_B^2 - M_D^2)^2}{q^2(m_b - m_c)} \mathcal{R}(\mathbf{C}_{\text{VL}}^\ell \mathbf{C}_{\text{SL}}^{\ell*}) \mathbf{F}_0^2 \right] \\
 &+ m_\ell^2 \left[\frac{2(M_B^2 - M_D^2)^2}{q^4} |\mathbf{C}_{\text{VL}}^\ell|^2 \mathbf{F}_0^2 \right]
 \end{aligned} \tag{4.6.1}$$

$$\begin{aligned}
 b_\ell^D(+) &= -m_\ell \left[\frac{8|p_D| M_B (M_B^2 - M_D^2)}{q^2(m_b - m_c)} \mathcal{R}(\mathbf{C}_{\text{SL}}^\ell \mathbf{C}_{\text{VL}}^{\ell*}) \mathbf{F}_0 \mathbf{F}_+ \right] \\
 &- m_\ell^2 \left[\frac{8|p_D| M_B (M_B^2 - M_D^2)}{q^4} |\mathbf{C}_{\text{VL}}^\ell|^2 \mathbf{F}_0 \mathbf{F}_+ \right]
 \end{aligned} \tag{4.6.2}$$

$$c_\ell^D(+) = m_\ell^2 \left[\frac{8|p_D|^2 M_B^2}{q^4} |\mathbf{C}_{\text{VL}}^\ell|^2 \mathbf{F}_+^2 \right] \tag{4.6.3}$$

Their expressions for the negative helicity lepton are,

$$a_\ell^D(-) = \frac{8M_B^2 |p_D|^2}{q^2} |\mathbf{C}_{\text{VL}}^\ell|^2 \mathbf{F}_+^2 \tag{4.6.4}$$

$$b_\ell^D(-) = 0 \tag{4.6.5}$$

$$c_\ell^D(-) = -\frac{8M_B^2 |p_D|^2}{q^2} |\mathbf{C}_{\text{VL}}^\ell|^2 \mathbf{F}_+^2 \tag{4.6.6}$$

Note that, the WCs C_{AL}^ℓ and C_{PL}^ℓ do not contribute to this decay. This is because the corresponding QCD matrix elements vanish, as can be seen from eqs. (4.4.2) and (4.4.4).

The lepton mass dependence of the various terms can also be understood easily. As the vector operators do not change the chirality of the fermion line, because of the left chiral nature of the neutrino, the outgoing (negatively charged) lepton also has negative chirality (and hence negative helicity in the massless limit). Thus the production of a left-handed lepton through the vector operator does not need a mass insertion. By a similar argument, one can see that the production of a right-handed lepton through the scalar operator does not need any mass insertion. The amplitude for the production of a right-handed lepton through a vector operator, on the other hand, clearly requires a mass insertion in order to flip the lepton helicity. This explains why the terms proportional to $|C_{VL}^\ell|^2$ in Eqs. 4.6.1-4.6.3 have m_ℓ^2 and the interference terms proportional to $\mathcal{R}(C_{SL}^\ell C_{VL}^{\ell*})$ have m_ℓ in front, while there is no such dependence in Eqs. 4.6.4-4.6.6.

The full expressions for a_ℓ^D , b_ℓ^D and c_ℓ^D including all the operators in Eq. (4.2.6) are shown in appendix C.1.

4.7 Expressions for a_ℓ^{D*} , b_ℓ^{D*} and c_ℓ^{D*} for $\bar{B} \rightarrow D^* \ell \bar{\nu}_\ell$

The quantities a_ℓ^{D*} , b_ℓ^{D*} and c_ℓ^{D*} for positive and negative helicity leptons are given by,

$$\begin{aligned} a_\ell^{D*}(-) &= \frac{8M_B^2 |p_{D^*}|^2}{(M_B + M_{D^*})^2} |C_{VL}^\ell|^2 \mathbf{V}^2 + \frac{(M_B + M_{D^*})^2 (8M_{D^*}^2 q^2 + \lambda)}{2M_{D^*}^2 q^2} |C_{AL}^\ell|^2 \mathbf{A}_1^2 \\ &\quad + \frac{8M_B^4 |p_{D^*}|^4}{M_{D^*}^2 (M_B + M_{D^*})^2 q^2} |C_{AL}^\ell|^2 \mathbf{A}_2^2 \\ &\quad - \frac{4 |p_{D^*}|^2 M_B^2 (M_B^2 - M_{D^*}^2 - q^2)}{M_{D^*}^2 q^2} |C_{AL}^\ell|^2 (\mathbf{A}_1 \mathbf{A}_2) \end{aligned} \quad (4.7.1)$$

$$b_\ell^{D*}(-) = -16 |p_{D^*}| M_B \mathcal{R}(C_{VL}^\ell C_{AL}^{\ell*}) (\mathbf{V} \mathbf{A}_1) \quad (4.7.2)$$

$$\begin{aligned} c_\ell^{D*}(-) &= \frac{8 |p_{D^*}|^2 M_B^2}{(M_B + M_{D^*})^2} |C_{VL}^\ell|^2 \mathbf{V}^2 - \frac{(M_B + M_{D^*})^2 \lambda}{2M_{D^*}^2 q^2} |C_{AL}^\ell|^2 \mathbf{A}_1^2 \\ &\quad - \frac{8 |p_{D^*}|^4 M_B^4}{(M_B + M_{D^*})^2 M_{D^*}^2 q^2} |C_{AL}^\ell|^2 \mathbf{A}_2^2 \\ &\quad + \frac{4 |p_{D^*}|^2 M_B^2 (M_B^2 - M_{D^*}^2 - q^2)}{M_{D^*}^2 q^2} |C_{AL}^\ell|^2 (\mathbf{A}_1 \mathbf{A}_2) \end{aligned} \quad (4.7.3)$$

$$\begin{aligned} a_\ell^{D*}(+) &= \frac{8 |p_{D^*}|^2 M_B^2}{(m_b + m_c)^2} |C_{PL}^\ell|^2 \mathbf{A}_0^2 \\ &\quad - m_\ell \left[\frac{16 |p_{D^*}|^2 M_B^2}{(m_b + m_c) q^2} \mathcal{R}(C_{AL}^\ell C_{PL}^{\ell*}) \mathbf{A}_0^2 \right] \\ &\quad + m_\ell^2 \left[\frac{8 |p_{D^*}|^2 M_B^2}{q^4} |C_{AL}^\ell|^2 \mathbf{A}_0^2 + \frac{8 |p_{D^*}|^2 M_B^2}{(M_B + M_{D^*})^2 q^2} |C_{VL}^\ell|^2 \mathbf{V}^2 \right. \\ &\quad \left. + \frac{2 (M_B + M_{D^*})^2}{q^2} |C_{AL}^\ell|^2 \mathbf{A}_1^2 \right] \end{aligned} \quad (4.7.4)$$

$$\begin{aligned}
b_\ell^{D^*}(+) &= m_\ell \left[\frac{4|p_{D^*}|M_B(M_B + M_{D^*})(M_B^2 - M_{D^*}^2 - q^2)}{M_{D^*}(m_b + m_c)q^2} \mathcal{R}(\mathbf{C}_{\text{AL}}^\ell \mathbf{C}_{\text{PL}}^{\ell*}) \mathbf{A}_0 \mathbf{A}_1 \right. \\
&\quad \left. - \frac{16}{(m_b + m_c)(M_B + M_{D^*})M_{D^*}q^2} \mathcal{R}(\mathbf{C}_{\text{AL}}^\ell \mathbf{C}_{\text{PL}}^{\ell*}) \mathbf{A}_0 \mathbf{A}_2 \right] \\
&\quad + m_\ell^2 \left[-\frac{4|p_{D^*}|M_B(M_B + M_{D^*})(M_B^2 - M_{D^*}^2 - q^2)}{M_{D^*}q^4} |\mathbf{C}_{\text{AL}}^\ell|^2 \mathbf{A}_0 \mathbf{A}_1 \right. \\
&\quad \left. + \frac{16|p_{D^*}|^3 M_B^3}{(M_B + M_{D^*})M_{D^*}q^4} |\mathbf{C}_{\text{AL}}^\ell|^2 \mathbf{A}_0 \mathbf{A}_2 \right] \quad (4.7.5)
\end{aligned}$$

$$\begin{aligned}
c_\ell^{D^*}(+) &= m_\ell^2 \left[-\frac{8|p_{D^*}|^2 M_B^2}{(M_B + M_{D^*})^2 q^2} |\mathbf{C}_{\text{VL}}^\ell|^2 \mathbf{V}^2 + \frac{(M_B + M_{D^*})^2 \lambda}{2M_{D^*}^2 q^4} |\mathbf{C}_{\text{AL}}^\ell|^2 \mathbf{A}_1^2 \right. \\
&\quad \left. + \frac{8|p_{D^*}|^4 M_B^4}{M_{D^*}^2 (M_B + M_{D^*})^2 q^4} |\mathbf{C}_{\text{AL}}^\ell|^2 \mathbf{A}_2^2 \right. \\
&\quad \left. - \frac{4|p_{D^*}|^2 M_B^2}{M_{D^*}^2 q^4} (M_B^2 - M_{D^*}^2 - q^2) |\mathbf{C}_{\text{AL}}^\ell|^2 (\mathbf{A}_1 \mathbf{A}_2) \right] \quad (4.7.6)
\end{aligned}$$

The WC C_{SL}^ℓ does not contribute to this decay because the corresponding QCD matrix element vanishes as can be seen from eq. (4.5.3). The lepton mass dependence of the various terms can be understood in the same way as the $\bar{B} \rightarrow D\ell\bar{\nu}_\ell$ decay. Note also the absence of interference terms proportional to $\mathcal{R}(C_{VL}^\ell C_{PL}^{\ell*})$ in the above expressions.

We provide the completely general result taking into account all the operators in Eq. (4.2.6) in appendix C.2.

4.8 Results

4.8.1 Explaining R_D alone

As mentioned in sec. 4.6, the $\bar{B} \rightarrow D\tau\bar{\nu}_\tau$ amplitude depends only on the WCs C_{VL}^τ and C_{SL}^τ . In Fig. 4.3, we show R_D as function of C_{VL}^τ and C_{SL}^τ . In the right plot, we set C_{VL}^τ to its SM value $C_{VL}^\tau|_{\text{SM}} = 1$ and vary C_{SL}^τ , while in the left plot, we hold C_{SL}^τ fixed at its SM value $C_{SL}^\tau|_{\text{SM}} = 0$ and change C_{VL}^τ . The red and brown shades correspond to the experimentally allowed 1σ and 2σ ranges (see Table 4.1), for which we have added the statistical and systematic uncertainties in quadrature.

The ranges of C_{VL}^τ and C_{SL}^τ that are consistent with R_D at 1σ are shown in the second row of Table 4.4. The ranges for C_{SL}^τ are slightly asymmetric about zero because of its interference with C_{VL}^τ . In the rows 3, 4 and 5-8, we also show the predictions for $P_\tau(D)$, \mathcal{A}_{FB}^D and R_D in four different bins for the allowed ranges of C_{VL}^τ and C_{SL}^τ . Note that, \mathcal{A}_{FB}^D and the polarisation fraction $P_\tau(D)$ are independent of C_{VL}^τ if C_{SL}^τ is set to zero. This is because, in this case the differential decay rate is proportional to $|C_{VL}^\tau|^2$ and hence, the dependence on C_{VL}^τ drops out in $P_\tau(D)$ and \mathcal{A}_{FB}^D . This is why the ranges for $P_\tau(D)$ and \mathcal{A}_{FB}^D in the third and fourth columns are identical. The binwise R_D values are also graphically represented in

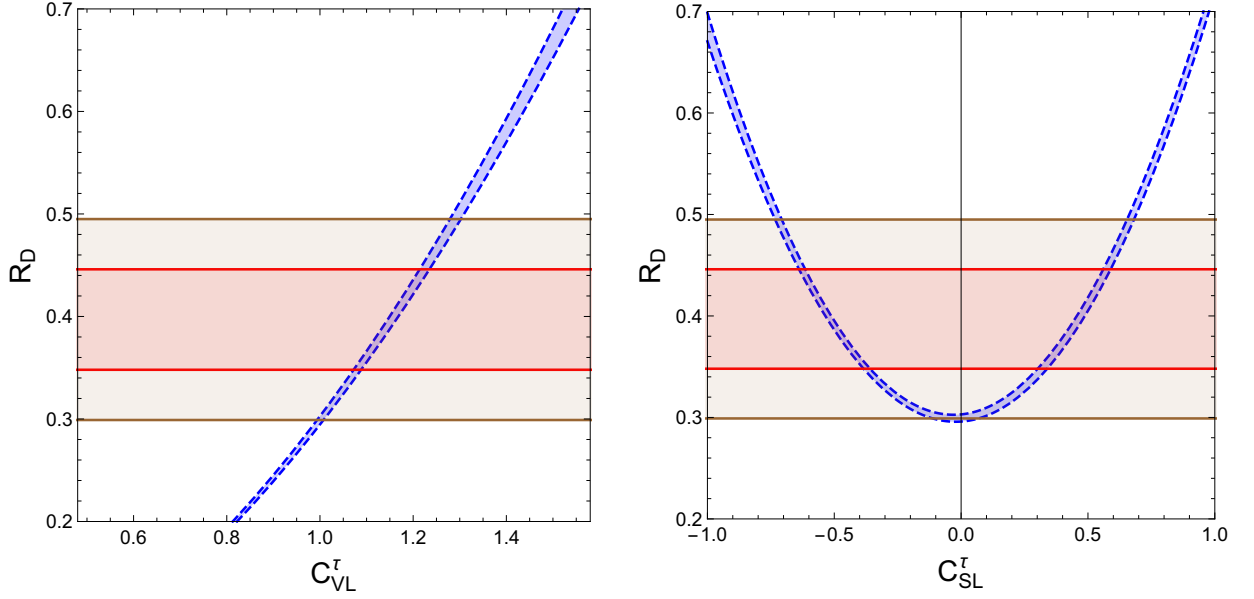


Figure 4.3: The dependence of R_D with respect to the variation of the WCs C_{VL}^τ (left) and C_{SL}^τ (right).

Fig. 4.4. The left and the right panels correspond to the WCs C_{VL}^τ and C_{SL}^τ respectively. The SM predictions are shown in red. One can conclude from Fig. 4.4 that the binwise R_D does not help distinguish the two WCs C_{VL}^τ and C_{SL}^τ .

		SM	$\mathbf{C_{VL}}$ ($\mathbf{C_{SL}} = 0$)	$\mathbf{C_{SL}}$ ($\mathbf{C_{VL}} = 1$)
	1σ range of the WC		[1.073, 1.222]	$[-0.656, -0.342]$ [0.296, 0.596]
	$P_\tau(D)$	[0.313, 0.336]	[0.313, 0.336]	[0.408, 0.556]
	\mathcal{A}_{FB}^D	$[-0.361, -0.358]$	$[-0.361, -0.358]$	$[-0.168, -0.022]$ $[-0.450, -0.428]$
R_D [bin]	$[m_\tau^2 - 5] \text{ GeV}^2$	[0.154, 0.158]	[0.178, 0.236]	[0.161, 0.181]
	$[5 - 7] \text{ GeV}^2$	[0.578, 0.593]	[0.665, 0.888]	[0.626, 0.752]
	$[7 - 9] \text{ GeV}^2$	[0.980, 1.003]	[1.127, 1.505]	[1.125, 1.502]
	$[9 - (M_B - M_D)^2] \text{ GeV}^2$	[1.776, 1.823]	[2.049, 2.741]	[2.294, 3.669]

Table 4.4: The values of the WCs consistent with the 1σ experimental range for R_D are shown in the second row. The subsequent rows show the predictions for $P_\tau(D)$, \mathcal{A}_{FB}^D and R_D in four q^2 bins for the WC ranges shown in the second row.

The predictions for $P_\tau(D)$, \mathcal{A}_{FB}^D are pictorially presented in the left and middle panel of Fig. 4.5. As mentioned earlier, in the absence of C_{SL}^τ , $P_\tau(D)$ and \mathcal{A}_{FB}^D are completely independent of C_{VL}^τ . Hence, neither measurement can distinguish between $C_{VL}^\tau = 1$ and other values of C_{VL}^τ . However, the predictions are very different for C_{SL}^τ . Therefore, a measurement

of $P_\tau(D)$ will tell us whether NP in the form of scalar operator $\mathcal{O}_{SL}^{cb\tau}$ exists or not. Moreover, the two separate ranges of C_{SL}^τ which satisfy the experimental bounds give very different values of \mathcal{A}_{FB}^D , indicated by the subscripts “+” and “-” in the middle figure.

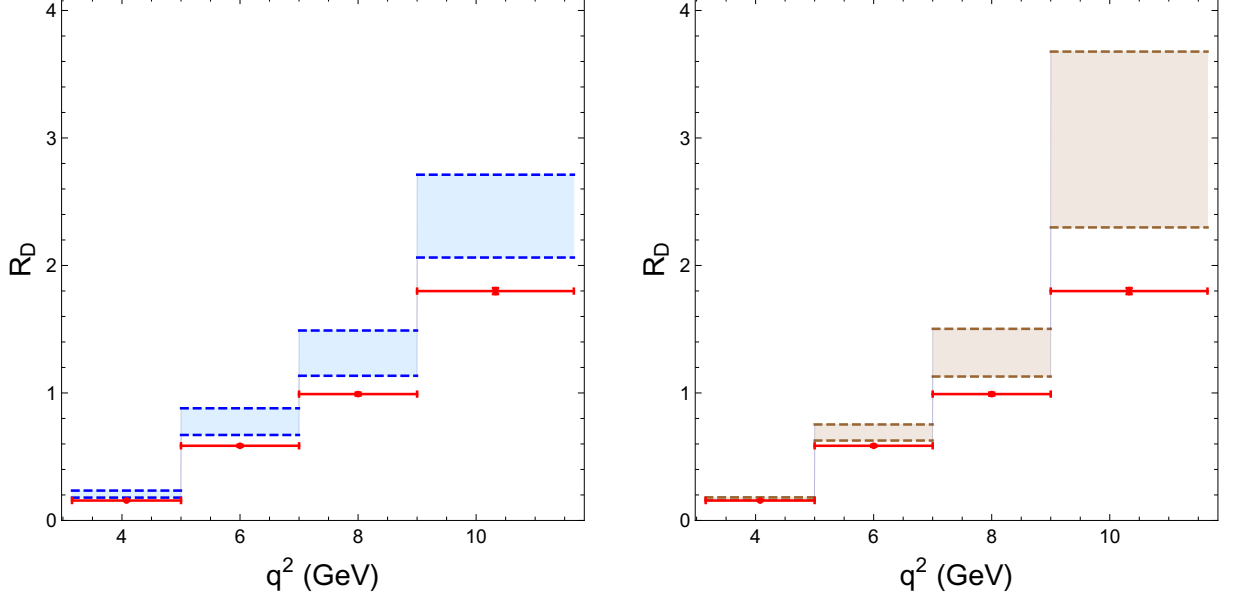


Figure 4.4: The binwise R_D for four q^2 bins. On the left, C_{VL}^τ is varied, while on the right, C_{SL}^τ is varied within their 1σ allowed ranges.

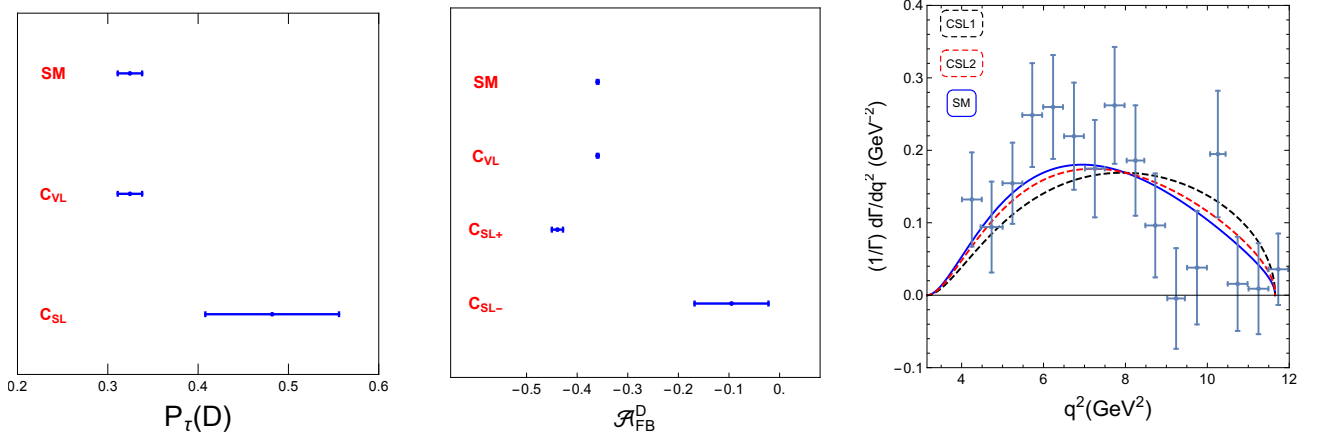


Figure 4.5: Predictions for the polarisation fraction $P_\tau(D)$ (left), \mathcal{A}_{FB}^D (middle) and the differential decay width (right). The subscripts “+” and “-” in the middle figure correspond to the two ranges of C_{SL}^τ that satisfy the experimental bounds of R_D . In the right graph showing the normalised differential decay width, the solid blue line is the SM prediction. The dashed black and red lines correspond to $C_{SL}^\tau = -0.650$ and 0.310 respectively. The data points shown on the right plot are due to the BaBar collaboration and are taken from [269].

In the right panel of Fig. 4.5, we also show the normalised differential decay width as a function of q^2 . As for the case of $P_\tau(D)$ and \mathcal{A}_{FB}^D , the normalised differential decay width is

independent of C_{VL}^τ for $C_{SL}^\tau = 0$. The blue solid line is the SM prediction, and the black and red dashed lines are the predictions for two representative values of C_{SL}^τ , $C_{SL}^\tau = -0.650$ and 0.310 respectively. While producing these plots, we have used the central values of the form factors. The blue data points are from the BaBar measurement reported in [269]. It is clear that the differential decay width is not a good discriminant of the various NP operators.

4.8.2 Explaining R_{D^*} alone

The $\bar{B} \rightarrow D^* \tau \bar{\nu}_\tau$ decay amplitude depends on three WCs, C_{VL}^τ , C_{AL}^τ and C_{PL}^τ . In Fig. 4.6, we show R_{D^*} as function of these WCs. In each of the plots, the WCs that are not varied are all set to their SM values. The red and brown shades correspond to the experimentally allowed 1σ and 2σ ranges respectively (see table 4.1).

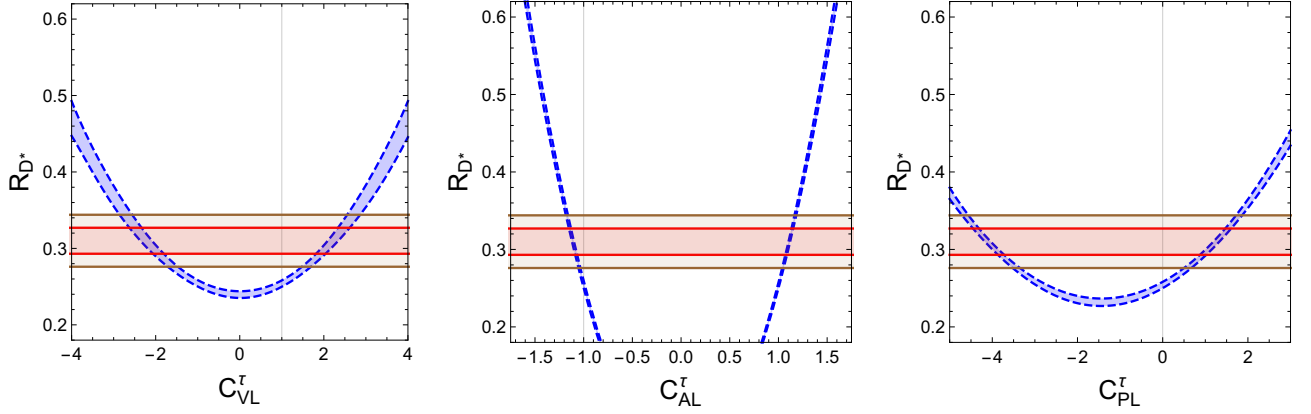


Figure 4.6: The dependence of R_{D^*} with respect to the variation of the WCs C_{VL}^τ (left), C_{AL}^τ (middle) and C_{PL}^τ (right). A thin vertical line shows the SM values of the WCs.

The ranges of C_{VL}^τ , C_{AL}^τ and C_{PL}^τ that are consistent with the experimental value of R_{D^*} at 1σ are shown in the second row of Table 4.5. We only show the ranges that are closest to the SM values of the WCs. In the rows 3, 4 and 5-8, we also show the predictions for $P_\tau(D^*)$, $\mathcal{A}_{FB}^{D^*}$ and R_{D^*} in four different bins for these allowed ranges of C_{VL}^τ , C_{AL}^τ and C_{PL}^τ .

The binwise R_{D^*} values are also plotted in Fig. 4.7. The left, middle and the right panels correspond to the variation of WCs C_{VL}^τ , C_{AL}^τ and C_{SL}^τ respectively. The 1σ and 2σ experimental values are shown in red and brown respectively. It can be seen that R_{D^*} in the last bin can be used to distinguish between C_{VL}^τ (or C_{PL}^τ) and C_{AL}^τ .

The predictions for $P_\tau(D^*)$ are pictorially presented in the left panel of Fig. 4.8. We do not show the recent Belle measurements in this figure because the uncertainties are rather large. Instead, we show a projection for Belle II 20 ab^{-1} (which is expected to be collected by the end of 2021 [315]) assuming that the systematic uncertainty will go down by a factor of two compared to that in the recent Belle measurement. It is then possible to distinguish C_{PL}^τ from the other WCs. The middle panel of Fig. 4.8 shows the predictions of $\mathcal{A}_{FB}^{D^*}$ pictorially. It can

		SM	$\mathbf{C_{VL}}$ $\mathbf{C_{AL,PL} = -1, 0}$	$\mathbf{C_{AL}}$ $\mathbf{C_{VL,PL} = 1, 0}$	$\mathbf{C_{PL}}$ $\mathbf{C_{VL,AL} = 1, -1}$
	Range in WC		[1.856, 2.569]	[-1.149, -1.073]	[0.890, 1.583]
	$P_\tau(D^*)$	[-0.505, -0.490]	[-0.530, -0.509]	[-0.505, -0.488]	[-0.322, -0.144]
	$\mathcal{A}_{FB}^{D^*}$	[0.050, 0.078]	[0.191, 0.297]	[0.028, 0.062]	[-0.078, -0.007]
R_{D^*} [bin]	$[m_\tau^2 - 5] \text{ GeV}^2$	[0.103, 0.105]	[0.120, 0.140]	[0.116, 0.132]	[0.124, 0.148]
	$[5 - 7] \text{ GeV}^2$	[0.331, 0.336]	[0.387, 0.457]	[0.373, 0.425]	[0.390, 0.465]
	$[7 - 9] \text{ GeV}^2$	[0.475, 0.479]	[0.535, 0.613]	[0.535, 0.613]	[0.534, 0.610]
	$[9 - (M_B - M_{D^*})^2] \text{ GeV}^2$	[0.554, 0.556]	[0.577, 0.619]	[0.621, 0.710]	[0.571, 0.611]

Table 4.5: The values of the WCs consistent with the 1σ experimental range for R_{D^*} are shown in the second row. We only show the ranges that are closest to the SM values of the WCs. The subsequent rows show the predictions for $P_\tau(D^*)$, $\mathcal{A}_{FB}^{D^*}$ and R_{D^*} in four q^2 bins for the WC ranges shown in the second row.

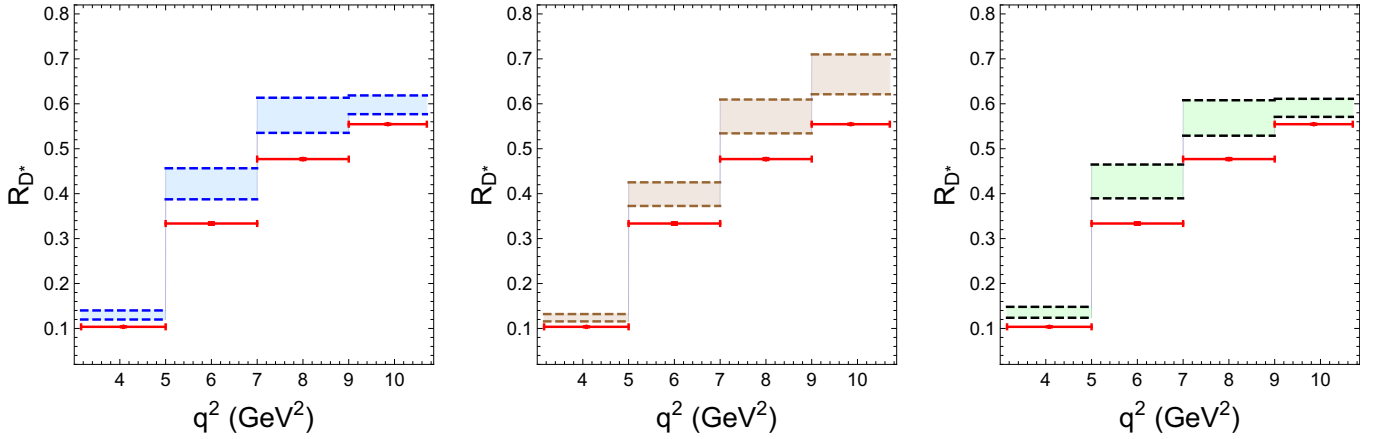


Figure 4.7: The binwise R_{D^*} for four q^2 bins. On the left, C_{VL}^τ is varied, in the middle C_{AL}^τ is varied, and on the right, C_{PL}^τ is varied within their 1σ allowed ranges. The SM predictions are shown in red.

be seen that a measurement of $\mathcal{A}_{FB}^{D^*}$ can also potentially differentiate the various operators. In the right panel of Fig. 4.8, we show the normalised differential decay width as a function of q^2 for some representative values of the WCs from Table 4.5. It can be seen that the shape of the distribution does not change dramatically across the various NP explanations of R_{D^*} .

In Fig. 4.9, we show the predictions for $P_\tau(D^*)$, R_{D^*} in the last bin and $\mathcal{A}_{FB}^{D^*}$ in three different planes for the three WCs C_{VL}^τ , C_{AL}^τ and C_{PL}^τ when their values are restricted to the ranges shown in Table 4.5. Interestingly, we find that each of the three pairs of observables can potentially distinguish between the WCs unambiguously. Hence, the measurements of these observables by the experimental collaborations ought to be very much on the cards in their future runs.

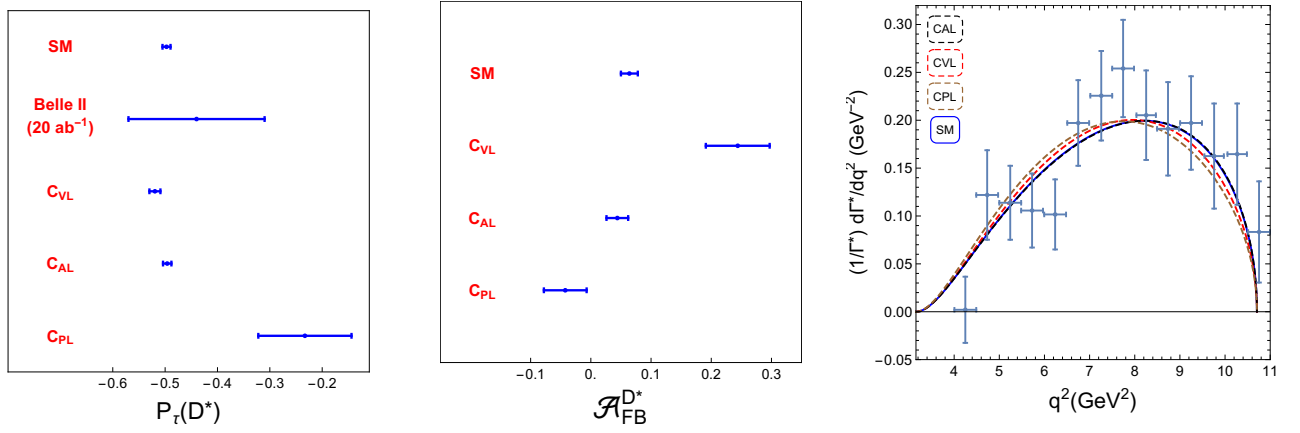


Figure 4.8: Predictions for the polarisation fraction $P_\tau(D^*)$ (left), $\mathcal{A}_{FB}^{D^*}$ (middle) and the differential decay width (right). In the left plot, the Belle II 20 ab^{-1} projection is obtained by i) scaling down the statistical uncertainty of the recent Belle measurement by the ratio of the luminosities i.e., $\sqrt{20/0.71}$ ii) assuming the systematic uncertainty to go down by a factor of two, and adding them in quadrature. The central value is assumed to remain unchanged. On the right plot, The solid blue line is the SM prediction. The dashed black, red and brown lines correspond to $C_{AL}^\tau = -1.12$, $C_{VL}^\tau = 1.9$ and $C_{PL}^\tau = 1.5$ respectively, where in each case every other WC is set to their SM values. Note that the black dashed curve is indistinguishable from the SM curve. The data is due to a BaBar measurement reported in [269].

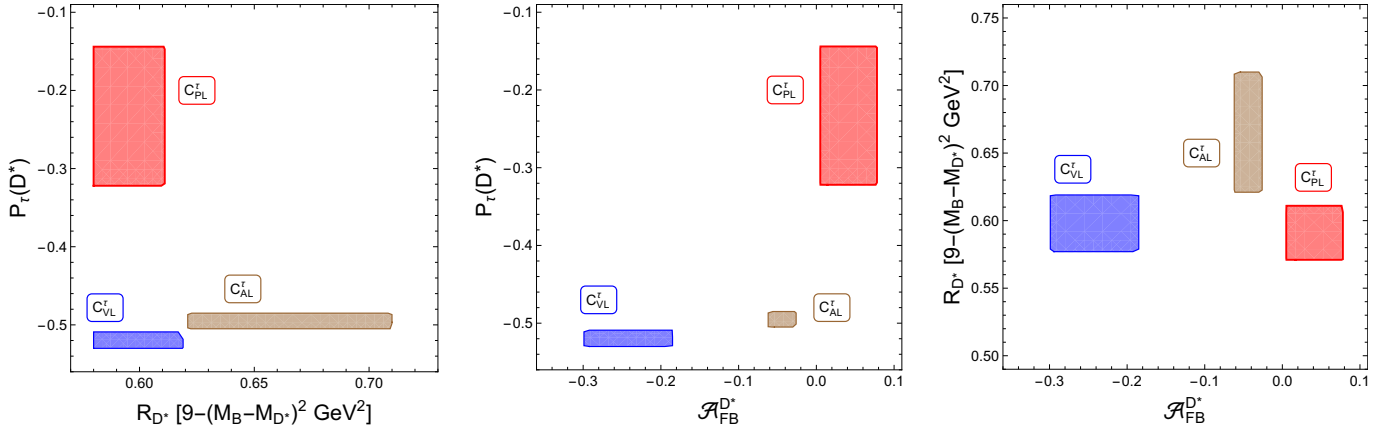


Figure 4.9: The predictions for $P_\tau(D^*)$, R_{D^*} in the last bin and $\mathcal{A}_{FB}^{D^*}$ are shown in three different planes for the ranges of the three WCs C_{VL}^τ , C_{AL}^τ and C_{PL}^τ given in Table 4.5. We remind the readers that, we have inflated the uncertainties in the form factor parameters in Eq. (4.5.10) by a factor of two. Hence, the ranges of $P_\tau(D^*)$ and R_{D^*} shown here are rather conservative.

4.8.3 Explaining R_D and R_{D^*} together

We have seen from section 4.8.1 and 4.8.2 that while R_D gets contributions from C_{VL}^τ and C_{SL}^τ , R_{D^*} is affected by C_{VL}^τ , C_{AL}^τ and C_{PL}^τ . Therefore, in general, these two observables are theoretically independent. In the basis of WCs defined by $\{C_{VL}^\tau, C_{AL}^\tau, C_{SL}^\tau, C_{PL}^\tau\}$, the C_{VL}^τ direction is the only direction that affects both. However, as can be seen from tables 4.4 and 4.5, the range of C_{VL}^τ (i.e., $[1.073, 1.222]$) that explains R_D within 1σ is different from the

range (i.e., $[1.849, 2.648]$) that explains R_{D^*} successfully within 1σ . Thus R_D and R_{D^*} can not be explained simultaneously by invoking NP only of type C_{VL}^τ . Fig. 4.10 shows the allowed region in the $C_{VL}^\tau - C_{AL}^\tau$ plane by the R_D and R_{D^*} measurements. As C_{AL}^τ does not contribute to the $\bar{B} \rightarrow D\tau\bar{\nu}_\tau$ decay, the allowed region for C_{VL}^τ from R_D (the red region) is independent of the value of C_{AL}^τ . On the other hand, both the WCs C_{VL}^τ and C_{AL}^τ contribute to the $\bar{B} \rightarrow D^*\tau\bar{\nu}_\tau$ decay and hence the values of these WCs allowed by R_{D^*} measurement are correlated. The overlap of the red and the green regions correspond to $C_{VL}^\tau \in [1.073, 1.222]$ and $C_{AL}^\tau \in [-1.144, -1.062]$.

Hence, a minimum value of $C_{VL}^\tau \approx -C_{AL}^\tau \approx 1.07$ which translates to $\Delta(C_9 - C_{10}) \approx 0.15$ (i.e., 15% shift from the SM values) can explain both R_D and R_{D^*} successfully. This correspond to the operator $[\bar{c}\gamma^\mu P_L b][\bar{\ell}\gamma_\mu P_L \nu]$ with a coefficient g_{NP}^2/Λ^2 where Λ is given by $\Lambda \approx g_{NP} 2.25 \text{ TeV}$.

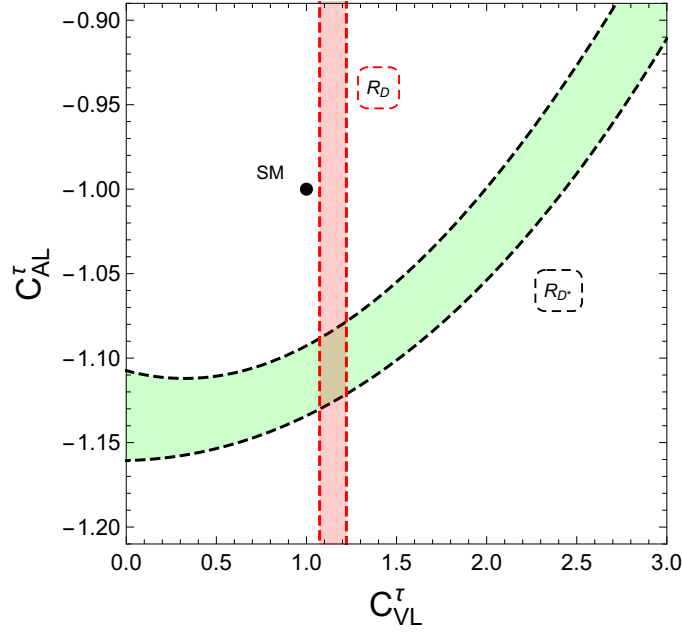


Figure 4.10: Allowed region in the $C_{VL}^\tau - C_{AL}^\tau$ plane by R_D and R_{D^*} measurements .

The predictions for $P_\tau(D^*)$, $\mathcal{A}_{FB}^{D^*}$ and binwise R_{D^*} for the above ranges of C_{VL}^τ and C_{AL}^τ are given in table 4.6.

C_{VL}^τ $\in [1.073, 1.222]$	$P_\tau(D^*)$ $\in [-0.507, -0.489]$	R_{D^*} [bin]			
		$[m_\tau^2 - 5] \text{ GeV}^2$	$[5 - 7] \text{ GeV}^2$	$[7 - 9] \text{ GeV}^2$	$[9 - (M_B - M_{D^*})^2] \text{ GeV}^2$
C_{AL}^τ $\in [-1.144, -1.067]$	$\mathcal{A}_{FB}^{D^*}$ $\in [0.055, 0.092]$	[0.116, 0.131]	[0.373, 0.426]	[0.535, 0.609]	[0.616, 0.706]

Table 4.6: Predictions for $P_\tau(D^*)$, $\mathcal{A}_{FB}^{D^*}$ and binwise R_{D^*} for the values of WCs satisfying both the observations simultaneously. The 1σ range of the WCs is given in the first column.

4.9 Summary

In this paper we have performed a model independent analysis of the R_D and R_{D^*} anomalies using dimension-6 operators that arise in a gauge invariant way. Among the four WCs C_{VL}^τ , C_{AL}^τ , C_{SL}^τ and C_{PL}^τ , only C_{VL}^τ and C_{SL}^τ contribute to R_D . On the other hand, R_{D^*} gets contributions from C_{VL}^τ , C_{AL}^τ and C_{PL}^τ . Thus, C_{VL}^τ is the only WC that affects both (barring tensor operator that is discussed in appendix C.3) and hence, these two observables are in general theoretically independent. In view of this, initially we studied the solutions of R_D and R_{D^*} anomalies independent of each other. We obtained the ranges of the WCs that are allowed by the R_D and R_{D^*} measurements at 1σ . We also discussed the possibility of simultaneous solutions of these two anomalies.

For the allowed ranges of the WCs, we computed the predictions for both R_D and R_{D^*} in four different q^2 bins, the forward-backward asymmetry, $\mathcal{A}_{FB}^{D^{(*)}}$ and the polarisation fraction of the final state τ lepton. We show that measuring the τ polarisation in $\bar{B} \rightarrow D^* \tau \bar{\nu}_\tau$ decays along with the value of R_{D^*} in the last q^2 bin can distinguish between the three WCs which contribute to this process. This is graphically presented in Fig. 4.9. Similarly, as seen in Fig. 4.5, the measurement of the τ polarisation in $\bar{B} \rightarrow D \tau \bar{\nu}_\tau$ decay can in principle be used to distinguish the two WCs C_{VL}^τ and C_{SL}^τ . Furthermore, we find that the forward-backward asymmetry of the τ lepton is also a powerful discriminant of the various WCs (see Figs. 4.5 and 4.9). Unlike $P_\tau(D)$, it can even distinguish the sign of the scalar operator for the $\bar{B} \rightarrow D \tau \bar{\nu}_\tau$ decay. We hope that the experimental collaborations will take a note of this and make these measurements in near future.

Additionally, in the appendix we also provide the analytic expressions for the double differential decay widths for individual τ helicities taking into account all the 10 dimension-6 operators listed out in section 4.2. To our knowledge, we are the first to provide the full expressions in the literature.

Although we have not considered the tensor operator \mathcal{O}_{TL} in the main text, we have explored its effects on the R_D and R_{D^*} anomalies in appendix C.3. We have shown that there exists a small range of C_{TL} that is consistent with both the anomalies.

Bottom squarks in B-number violating MSSM

5.1 Introduction

Since the discovery of the Higgs by the LHC in its first run [62,63], the searches for signatures for BSM physics have intensified. One of the most sought after theories of BSM physics has been supersymmetry (SUSY) and a vast number of searches strategies have been developed keeping the theory in mind. However, the majority of the SUSY search strategies at the LHC assume that ‘R-parity’, a multiplicative quantum number defined as $R = (-1)^{3B+L+2s}$ with B , L and s in terms of the baryon number (B), the lepton number (L) and the spin (S) of the particle, is conserved. Conservation of R-parity implies that SUSY particles will always be pair produced and that a heavy SUSY particle will decay into an odd number of lighter SUSY particles, with or without other SM particles¹. This ensures that the lightest SUSY particle (LSP) is stable. A characteristic signature of an R-parity conserving SUSY scenario is a final state with large missing transverse energy (\cancel{E}_T) due to the presence of the LSP. Since, in the SM, neutrinos are the only real sources of missing energy apart from detector acceptance and resolution effects, \cancel{E}_T can be used as a standard candle to search for these SUSY particles. Besides, in supersymmetric theories with conserved R-parity, the lightest SUSY particle, if colourless and electrically neutral, can always act as a good dark matter candidate.

However, the conservation of R-parity is not guaranteed, and, if one allows for its violation, an sfermion can decay to a pair of SM fermions², giving rise to signatures with, at best, only a small missing transverse energy [318]. This negation of one of the standard features of SUSY searches would, immediately, negate much of the collider constraints on the SUSY spectrum. Welcome consequences of this are the easing of fine-tuning on the one hand [319],

¹In most popular models, the decays are into a single lighter SUSY particle and one or two (and, only rarely three) SM particles.

²Similarly, the gauginos and higgsinos would decay into three SM fermions.

and, on the other, the possibility of facilitating electroweak baryogenesis [320–322] through the accommodation of a top-squark lighter than what the R -conserving scenarios can allow. From its very definition, one can see that the violation of R -parity can be achieved in three ways: violation of either L or B , or both. However, if we allow both L and B to be violated, nothing prevents the proton from decaying into a meson and a lepton, and, thus, the lower limit on the proton decay lifetime [323] places severe constraints on their products. It is, of course, more natural to ensure proton stability by insisting on one of the symmetries (B or L) being unbroken, and this is the route that we take. Interestingly, such R -violating scenarios can be easily motivated from supergravity models [324]. And while violating R -parity implies that we lose the DM candidate, the dark matter content of the universe can appear from other sources [325].

In this paper, we study a R -violating (RPV) SUSY scenario in the presence of baryon number (UDD-type) violating operators alone. Contrary to naive expectations, such a scenario can be well-accommodated within a GUT-framework [326], thereby preserving one of the successes of SUSY. A further ramification is that, unlike in the case of the L -violating couplings, the lack of any excess in the multilepton channel at the LHC does not impose any worthwhile constraint on the squark/gluino masses [327–332]. We are faced, instead, with a multijet signal [333–336] and it has been argued that the large irreducible QCD background would result in much weaker sensitivity. Performing a collider analysis of the lightest scalar superpartner of the bottom quark, namely the sbottom (\tilde{b}), subsequently decaying to a top quark and a light down-type quark through non-zero λ'' couplings, we show that it is not necessarily so. Depending on the decay of the top quark, the final state can consist of only hadronic elements (jets), or may contain at least one lepton. The latter semi-leptonic case is easier to study at a hadronic collider environment like that of the LHC, since we can tag on the lepton. Our analysis will take into account the very different nature of these two possible final states and is thus done in two parts: first, for a final state with at least one lepton, and second, for a fully hadronic final state. To study the semi-leptonic final state, we shall use both the traditional cut-based analysis and multivariate analysis, while in the hadronic final state, we shall rely solely on the multivariate analysis.

The rest of the paper is arranged as follows: in Section II, we briefly introduce R -parity violating SUSY, noting down the couplings relevant for our analysis. In Section III, we introduce our simplified model detailing all the parameters used. The analysis of a final state with a lepton is presented in Section IV and in Section V, we perform the analysis for a completely hadronic final state. Finally, we conclude in Section VI.

5.2 The R -parity violating MSSM

In terms of lepton, quark and Higgs superfields one can write down the R -parity violating superpotential in the following form [318]: either bilinear terms or by Yukawa-like trilinear

terms. The most generic RPV superpotential is given by:

$$W_{\mathcal{R}_p} = \mu_i \hat{H}_u \hat{L}_i + \frac{1}{2} \lambda_{kij} \hat{L}_i \hat{L}_j \hat{E}_k^c + \lambda'_{ijk} \hat{L}_i \hat{Q}_j \hat{D}_k^c + \frac{1}{2} \lambda''_{ijk} \hat{U}_i^c \hat{D}_j^c \hat{D}_k^c \quad (5.2.1)$$

where the first three sets of operators violate L while the last set violates B . Here, i, j and k are generation indices, whereas both $SU(2)$ and $SU(3)$ indices have been suppressed. Clearly, the couplings λ_{kij} and λ''_{ijk} are antisymmetric in the last two indices and, thus, there are a total of $(3 + 9 + 27 =) 39$ L - and 9 B -violating interactions. Switching off the first three sets, and concentrating only on the last, we have, in terms of the quark and squark fields:

$$\mathcal{L}_{UDD} = -\frac{1}{2} \lambda''_{ijk} \left(\tilde{u}_{iR}^* \bar{d}_{jR} d_{kL}^c + \tilde{d}_{kR}^* \bar{u}_{iR} d_{jL}^c + \tilde{d}_{jR}^* \bar{u}_{iR} d_{kL}^c \right) . \quad (5.2.2)$$

The bounds on the couplings λ''_{ijk} are varied. Some of them are strongly constrained from $n - \bar{n}$ oscillations [337] or the LEP data on Z -decays [338]. The others are only weakly restricted, for example, through the requirement of their perturbative under renormalization group flows [339]. Compendia of such constraints can be found in Refs. [318, 324, 340–346]. It should be noted that many of the low-energy constraints emanate from effective four-fermi interactions, and in quoting them a reference squark mass is used; these bounds need to be scaled appropriately when the squark mass differs.

As we are interested in the \tilde{b} , one of j, k in λ''_{ijk} must be 3. Similarly, if we demand that the sbottom should decay into a top, we must have $i = 3$. In other words, we are left with just two choices, namely λ''_{313} and λ''_{323} , leading to $\tilde{b}^* \rightarrow t + d$ and $\tilde{b}^* \rightarrow t + s$ respectively. Since the simultaneous presence of two such couplings lead to too large a size for flavour changing neutral currents (FCNC) [347, 348], we assume that only one of the two is non-zero and real. For the mass range (of the squarks) that we are interested in, the strongest constraints are $\lambda''_{313} < 0.1$ [346] and $\lambda''_{323} < 1.89$ [338] respectively. Even without saturating these bounds, it is obvious that, once produced, the sbottom may decay promptly, thereby eliminating the possibility of recognizably displaced vertices [349, 350]. We shall assume that while the R-violating couplings are small enough to be both consistent with low energy phenomenology as well as having at best marginal effect on squark-production, they are large enough to prevent displaced vertices, thereby removing tell-tale signatures.

In the presence of ‘UDD’-type couplings, the decays (direct or cascades) of squarks and gluinos (the dominantly produced SUSY particles at the LHC) would, typically, result in multi-jet configurations with very little missing momentum. As these are very difficult to detect (especially in the absence of hard leptons) in the messy hadronic environment of the LHC, the strong limits on squark/gluino masses, derived in the context of R-conserving models (or, even for R-violating, but B -conserving ones) do not hold. In particular, if a pair-produced squark decays directly into a pair of quarks, the resultant four-jet sample is likely to be overwhelmed by the QCD background. The situation is ameliorated somewhat if some of the quarks (rather, the corresponding jets) can be tagged as this would allow us not only to eliminate much of the background, but also to use invariant mass combinations to increase the signal-to-noise ratio. This was used in Refs. [351, 352] and, subsequently, by

the ATLAS collaboration [334], to investigate the pair-production of stops and their decays, through the very same couplings that we are considering here, to a b -quark and a light quark each. Here, we investigate the complementary scenario, namely where the sbottom (rather than the stop) is the LSP.

5.3 The Simplified Model Spectrum and Simulation

As we are primarily interested in the lighter bottom squark, we simplify the spectrum by considering it to be the LSP with the other SUSY partners being much heavier. In particular, we do not include gluino production despite the fact that, for similar masses, $\sigma(\tilde{g}\tilde{g}) \gg \sigma(\tilde{b}\tilde{b}^*)$ and that the gluino could easily decay into a $\tilde{b}\tilde{b}$ pair, thereby adding to the signal strength. Indeed, gluino pair-production, with each decaying into three quarks has been used [336] to set a limit of $m_{\tilde{g}} > 1.08$ TeV and, hence, by making the \tilde{g} heavy, we deliberately preclude this contribution altogether. Our assumption about the spectrum obviously means that decays through R-conserving channels are no longer possible and that the sbottom is forced to decay to two SM quarks with 100% branching ratio. For the choice of the RPV coupling λ''_{313} (λ''_{323}), the daughters are the top and a light-quark (d or s , as the case may be). The top quark can decay either leptonically or hadronically; thus giving rise to the following final states :

- $2\ell\ell' + b\bar{b} + \text{jets} + \cancel{E}_T; \ell, \ell' = e, \mu,$
- $1\ell + b\bar{b} + \text{jets} + \cancel{E}_T,$
- $0\ell + b\bar{b} + \text{jets} + \cancel{E}_T.$

It should be noted that all these channels will be associated with only a small missing transverse energy, if any. Final states with multiple jets are very challenging in the LHC environment and thus require dedicated studies. Several SM processes which provide similar final state signatures have been treated as background, particularly, $t\bar{t} + \text{jets}$ (upto 2), $t\bar{t}b\bar{b}$, $t\bar{t}Z$, $t\bar{t}W$ and $t\bar{t}H$, constitute the dominant SM background; QCD multijet events constitute huge background for the purely hadronic case.

Before we delve into the discussion of signals and backgrounds, let us examine the parameter space that leads to the spectrum that we consider. The gaugino mass parameters M_1 and M_2 , as well as the higgsino mass parameter, μ are set to 1 TeV, while the value of $\tan\beta$, the ratio of the vacuum expectation values of the two Higgs doublets H_u^0 and H_d^0 , is fixed at 10. The masses of the first two generations of squarks and all the three generations of sleptons lie around 3 TeV and the mass of the right-handed stop is set to ~ 1 TeV. The left-handed third generation squark mass is set to about 1.5 TeV. While the tri-linear couplings A_t is set to -2 TeV, the other tri-linear couplings A_b and A_τ are set to zero. We also fix the gluino mass parameter (M_3) at 2 TeV, while varying only the right-handed sbottom mass parameter (m_{b_R}) to obtain different sbottom masses. In our analysis we consider six representative benchmark points with sbottom masses 500 GeV (BP-1), 600 GeV (BP-2), 700 GeV (BP-3), 800 GeV (BP-4), 900 GeV (BP-5) and 1000 GeV (BP-6).

	BP - 1	BP - 2	BP - 3	BP - 4	BP - 5	BP - 6
$m_{\tilde{b}_1}$ (GeV)	500	600	700	800	900	1000
$\mathcal{B}(B_s \rightarrow \mu^+ \mu^-)$	4.27×10^{-9}					
$\mathcal{B}(b \rightarrow s \gamma)$	3.19×10^{-4}					
$\Delta m_{B_s}(\text{ps}^{-1})$	18.01					
$\Delta m_{B_d}(\text{ps}^{-1})$	0.403					

Table 5.1: The first row presents the masses of the bottom squark for the different benchmark points. In the bottom part of the table, the values of the low-energy flavour observables are presented. These remain identical for the different benchmark points.

The particle spectrum has been generated using SPheno v-3.3.8 [353, 354] with the trilinear R-parity violating model as implemented in SARAH v-4.4.6 [355, 356]. FlavorKit [357] is used to calculate the low energy flavour observables $b \rightarrow s \gamma$ and $B_s \rightarrow \mu^+ \mu^-$ and care has been taken to ensure that the benchmark points are consistent with the flavour physics data [358] at better than 95% C.L. In particular, the mass differences Δm_{B_d} (Δm_{B_s}) associated with B_0 - and B_s -mixing (see Table 5.1) are very close to the experimental measurements [346]. We further ensure that the spectrum we use at each benchmark point is consistent with the latest measurements of Higgs mass, Higgs couplings and Higgs signal strength at the LHC.

It is worth noting that for our analysis, lighter squarks, consistent with the present bounds, would not be a problem. Since the contribution to various flavour processes from RPV, typically, are proportional to $(\lambda''^2/m_{\tilde{q}}^2)$, it is possible to accommodate a smaller squark mass, provided the couplings are reduced accordingly. In this scenario, we would, for example, receive additional contribution to our signal events from, say the sstrange. If the sstrange were only slightly heavier than the sbottom, it would decay to the sbottom along with a bottom and a strange quark, via an off-shell gluino³. Owing to only a small difference in the masses, the sbottom would be produced almost at rest with the two other jets being very soft; this would be indistinguishable from the sbottom pair production scenario and would thus add to our signal events. We do not consider this, and, thus, the analysis in this paper is quite conservative.

The signal and background events are generated using MADGRAPH (version 2.2.2) [359], properly interfaced with PYTHIA8 (version 8.210) [360, 361] for parton showering and hadronization. Event sets are then passed through DELPHES (version 3.2.0) [362] in order to simulate the detector response. Jets are reconstructed using FASTJET (version 3.1.3) [363], with $R = 0.4$ using the anti- k_t algorithm [364] in the leptonic case. For the hadronic case, we intend to tag the boosted top quarks in the final state, which will necessarily be a fat jet; thus, we use $R = 1.8$ using the C/A algorithm [365] which is optimized for tagging moderately boosted tops [366].

³The only other channel available to it would be the RPV channel to the top and the bottom, which would, again, be largely indistinguishable from that we consider here.

Jets are selected with $p_T > 30$ GeV and $|\eta| < 2.5$. Leptons (electron and muon) are selected with $p_T > 20$ GeV and $|\eta| < 2.4$. To reduce the background contribution of electrons or muons from semileptonic decays of heavy flavours, a relative isolation criteria is imposed. The relative isolation parameter, I_{rel} , defined as,

$$I_{\text{rel}} = \frac{\sum_{i \neq P} p_T(i)}{p_T(P)} \quad (5.3.1)$$

with P being the particle of interest (here electron or muon), is calculated as the sum of transverse energy of all the charged and neutral particles measured in the tracker and calorimeters in an isolation cone⁴ $\Delta R < 0.3$ around the lepton direction divided by the lepton transverse momentum. In our analysis, we demand $I_{\text{rel}} < 0.15$.

In the semi-leptonic decays of the top, the final state contains multiple leptons and a significant amount of missing transverse energy, calculated using the p_T of all the visible particles. Our signal topology also includes multiple b-jet candidates and in order to tag them as ‘b-jets’, we require the angular distance ΔR between the parton level b-quark and the jet to be less than 0.4, as implemented in DELPHES. A p_T dependent b-tagging efficiency (ϵ_b) for $|\eta| < 2.5$, following the CMS collaboration [367], is used to make our analysis more robust:

$$\epsilon_b = \begin{cases} 0.75 & \text{for } p_T^b \leq 30 \text{ GeV} \\ 0.85 & \text{for } 30 \text{ GeV} < p_T^b \leq 400 \text{ GeV} \\ 0.95 - 0.00025 p_T & \text{for } 400 \text{ GeV} < p_T^b \leq 800 \text{ GeV} \\ 0.65 & \text{for } p_T > 800 \text{ GeV.} \end{cases} \quad (5.3.2)$$

Throughout the entire p_T range, following the CMS card, a mistagging rate of 1% is assumed for the non b-jets. Note that, the b-tagging efficiency obtained by the ATLAS collaboration [368] is comparable with that of the CMS collaboration.

The cross-section of the $t\bar{t}$ + jets (upto 2) process is taken from the LHC Top Quark Working Group [369], while that of the $t\bar{t}H$ is taken from the LHC Higgs Cross-Section Working Group report [370]. The NLO cross-section for $t\bar{t}W$ and $t\bar{t}Z$ are taken from [371], where the results have been computed using MSTW2008 parton distribution functions (PDFs). We use PYTHIA to calculate the cross-section for the $t\bar{t}b\bar{b}$ process, where the PDF used in the calculation is CTEQ6L [372] and the factorization scale has been chosen to be M_Z , the mass of the Z-boson. For the signal processes, we use the sbottom pair production cross-sections at the 13 TeV LHC calculated including the resummation of soft-gluon emission at next-to-leading logarithmic accuracy matched to next-to-leading order supersymmetric QCD corrections [373].

⁴Here, and henceforth, $\Delta R \equiv \sqrt{(\Delta\eta)^2 + (\Delta\phi)^2}$ is the usual distance measure in the rapidity(η)–azimuthal angle (ϕ) plane.

5.4 Leptonic Final State

In this section we consider the final state in which there is at least one lepton; thus this analysis includes both leptonic and semi-leptonic decays of the top quarks. We first perform a cut-based analysis on the data sets and then supplement it with a multivariate analysis.

In Fig. 5.1, we present the jet multiplicity and the p_T distribution of the two leading non b-tagged jets. Additionally, in Fig. 5.2, the distributions for H_T and M_{T2} , both defined shortly, are also shown. All the distributions include three representative benchmark points - BP-1, corresponding to $m_{\tilde{b}_1} = 500$ GeV, BP-4, corresponding to $m_{\tilde{b}_1} = 800$ GeV, and BP-6, corresponding to $m_{\tilde{b}_1} = 1000$ GeV - along with the dominant SM backgrounds. Following these distributions, we can discuss the optimization of our selection cuts in order to improve the signal to background ratio.

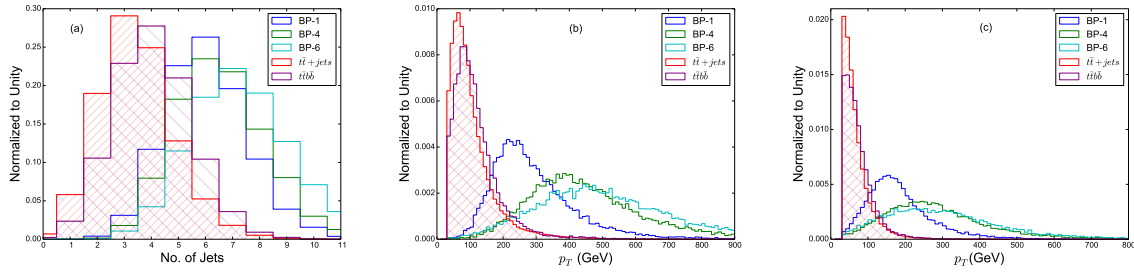


Figure 5.1: In (a) we show the distribution of the number of jets, (b) the p_T distribution of the hardest non b-tagged jet, while in (c) the same for the second hardest non b-tagged jet. For the sake of clarity, just the two dominant SM background processes are shown, viz. $t\bar{t} + \text{jets}$ and $t\bar{t}b\bar{b}$.

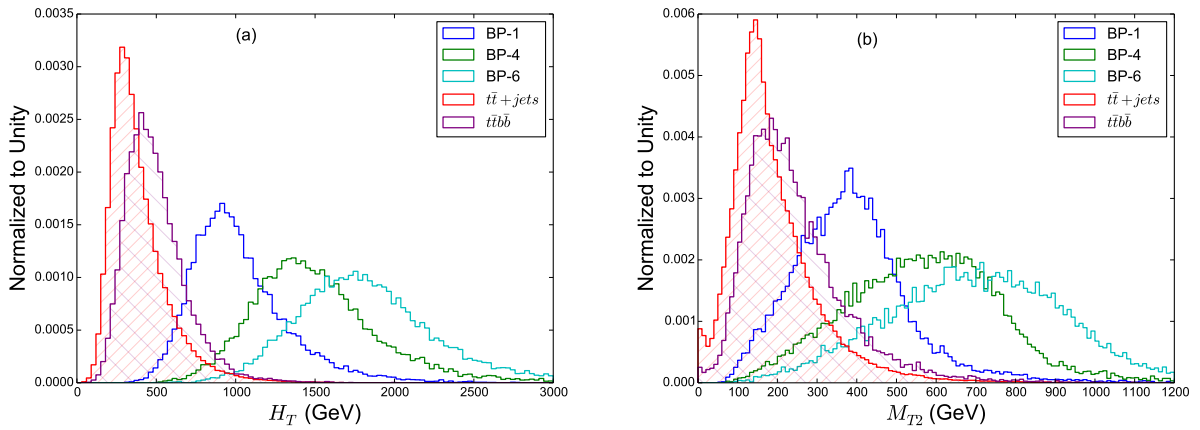


Figure 5.2: Distribution of the (a) scalar H_T and (b) Stransverse mass variable, M_{T2} , are displayed.

5.4.1 Cut-based Analysis

Our cut optimization prescription resembles the one adopted by the CMS collaboration [376] in order to distinguish a $t\bar{t}b\bar{b}$ sample from a background sample of $t\bar{t} + \text{jets}$ (upto 2). In this

section, we consider only leptonic events, i.e. events which have at least one lepton. In order to distinguish the signal from background, we make use of five discriminating variables: the number of jets, the p_T of the hardest and the second hardest jets in each event, the scalar H_T and the transverse mass variable, M_{T2} . The individual variables and the cuts imposed on them are discussed below:

- **C1** : We demand that each signal event contain at least one lepton. This particular choice of signal topology will substantially remove the most severe SM background coming from the pure QCD multijet processes.
- **C2** : In any process with multiple jets in the final state, the number of jets (including both the b-jets and the light jets) plays a very crucial role as a discriminatory variable. Due to the large mass-splitting between the sbottom and the top, both the latter and the other daughter would, often, carry a large p_T , and, hence, we expect a higher multiplicity of large- p_T jets as compared to the SM backgrounds which, typically, have a significant number of softer jet-progenitors. Consequently, we demand that the number of jets be greater than four.
- **C3** : Since we expect the non b-tagged jets coming from the sbottom decay to have a high p_T , we can place a p_T cut on such a jet. We demand that the leading non b-tagged jet have a $p_T > 250$ GeV.
- **C4** : Since the sbottom pair decay produces two light jets, we expect that the second hardest non b-tagged jet will also be very energetic. We put a cut of $p_T > 150$ GeV on the sub-leading non b-tagged jet. The light jets, if any, from the background processes are not expected to have such a high p_T .
- **C5** : We calculate H_T , the scalar sum of p_T of all the visible particles, namely jets, leptons and photons. It is defined as follows:

$$H_T = \sum_{i=e,\mu,j,\gamma} |\vec{p}_T(i)|. \quad (5.4.1)$$

The importance of this variable as a signal discriminator is very well reflected in Fig 5.2. If we demand that our signal events should have substantially large value of $H_T \sim 1000$ GeV then most of the $t\bar{t}jj$ and $t\bar{t}b\bar{b}$ events are removed. This is again taking advantage of the fact that the large mass of the sbottom results in jets and leptons with a p_T typically much higher than those emerging from SM processes.

- **C6** : Finally, we put a cut on the transverse mass variable $M_{T2} > 360$ GeV. The variable is defined as [377]:

$$M_{T2}(\vec{p}_T^{\mathcal{V}1}, \vec{p}_T^{\mathcal{V}2}, \vec{p}_T) = \min_{\vec{p}_T^1 + \vec{p}_T^2 = \vec{p}_T} \left[\max \left\{ M_T(\vec{p}_T^{\mathcal{V}1}, \vec{p}_T^1), M_T(\vec{p}_T^{\mathcal{V}2}, \vec{p}_T^2) \right\} \right] \quad (5.4.2)$$

where, \vec{p}_T^1 and \vec{p}_T^2 are two hypothetical subdivisions of the total missing transverse momentum \vec{p}_T . The separation of the visible particles into two sets with associated transverse momenta $\vec{p}_T^{\mathcal{V}1}$ and $\vec{p}_T^{\mathcal{V}2}$, is done so that the invariant masses of the two parts are as close to each other as possible.

In general, the transverse mass $M_T(\vec{p}_1, \vec{p}_2)$ of the (\vec{p}_1, \vec{p}_2) system is defined as

$$M_T(\vec{p}_1, \vec{p}_2) = \sqrt{m_1^2 + 2|\vec{p}_1||\vec{p}_2|(1 - \cos\phi)} . \quad (5.4.3)$$

Here, ϕ is the azimuthal angle between the \vec{p}_1 and \vec{p}_2 vectors with \vec{p}_2 corresponding to a massless particle (neutrino) and $m_1^2 \equiv p_1^2$. For the process under consideration, the visible part comprises of a b-quark, a light quark and a lepton coming from each of the bottom squarks. Given the symmetry of the system, we group the visible entities such that the two visible parts are nearly identical in invariant mass. For calculating M_{T2} , we use the Cheng and Han Bisection algorithm [378]. From the distribution shown in Fig. 5.2, we can easily see that this variable too has a good discriminatory power.

The event summary for the signal and backgrounds after individual selection cuts is presented in Table 5.2. The numbers in the table denote the resulting cross-sections after each selection cut is applied to both signal and background events. The first row in the table, denoted by ‘C0’, refers to the NLO production cross-section for each process.

The numbers on the subsequent rows relate to the surviving cross-section for each of the cases after the relevant cut (indicated as bullet points earlier) has been imposed.

Cuts	$t\bar{t} + jets$	$t\bar{t}b\bar{b}$	$t\bar{t}Z$	$t\bar{t}H$	$t\bar{t}W$	BP1	BP2	BP3	BP4	BP5	BP6
C0:	8.3×10^5	1.7×10^4	8.7×10^2	5.1×10^2	6.5×10^2	5.2×10^2	1.8×10^2	67.0	28.3	12.9	6.2
C1:	1.8×10^5	3.3×10^3	2.7×10^2	1.0×10^2	2.3×10^2	90.6	29.6	10.9	4.4	1.9	0.8
C2:	3.8×10^4	1.2×10^3	1.4×10^2	63.4	89.4	76.8	25.8	9.7	3.9	1.7	0.8
C3:	3.9×10^3	65.2	20.3	6.8	10.5	43.3	19.3	8.2	3.6	1.6	0.7
C4:	1.6×10^3	27.2	11.0	3.2	2.1	33.4	16.1	7.2	3.2	1.5	0.6
C5:	9.6×10^2	16.3	7.7	2.1	3.1	26.1	14.3	6.9	3.2	1.4	0.6
C6:	7.6×10^2	13.9	5.5	1.6	1.9	17.4	10.9	5.6	2.7	1.3	0.6

Table 5.2: The surviving cross-section (in fb) for the different processes after each of the cuts. For $t\bar{t} + jets$, we consider up to 2 jets.

We can now estimate the signal significance corresponding to each benchmark point at the 13 TeV LHC assuming 300 fb^{-1} of integrated luminosity. We are interested in the cross-section after the cut ‘C6’ is imposed (last row of Table 5.2). The number of signal (background) events, denoted by S (B), is given by the product of this cross-section and the integrated luminosity. In Table 5.3, we tabulate the signal significance \mathcal{S} given by

$$\mathcal{S} = \frac{S}{\sqrt{S+B}} .$$

It is evident from the table that, for an integrated luminosity of 300 fb^{-1} , the LHC stands in extremely good stead to detect the sbottom should its mass be 600 GeV or below. The LHC will graze past the exclusion limit of 95% C.L. for masses around $\sim 750 \text{ GeV}$. Given 3000 fb^{-1} integrated luminosity, we find that the discovery reach (i.e. 5σ significance) will exceed 800 GeV and the exclusion bounds might be extended to beyond the 900 GeV mass point.

	Background	BP1	BP2	BP3	BP4	BP5	BP6
$m_{\tilde{b}_1}$ (GeV)		500	600	700	800	900	1000
\mathcal{N}	2.3×10^5	5.2×10^3	3.3×10^3	1.7×10^3	8.2×10^2	3.9×10^2	1.7×10^2
$\mathcal{S} = \frac{S}{\sqrt{S+B}}$		10.7	6.7	3.5	1.7	0.8	0.4

Table 5.3: Number of background and signal events for a integrated luminosity of 300 fb^{-1} , along with the significances for the different benchmark points. See text for details.

5.4.2 Multivariate Analysis

To achieve a better discrimination between the signal and the SM background, we perform a multivariate analysis (MVA) using the Boosted Decision Tree (BDT) algorithm as implemented in the Toolkit for Multivariate Data Analysis (TMVA) [374] with ROOT [375]. We briefly describe the procedure, the details of which may be found in Ref. [374], along with the parameters for our analysis below.

Decision trees are used to classify events as either signal-like or background-like. Each node in a decision tree uses a single discriminating variable, along with a certain cut value imposed on it, to provisionally classify events as either signal-like or background-like depending on the purity of the sample. The decision tree needs to be ‘trained’ and that starts with the root node. We can think of the process as two bins originating from the root node (i.e., the zeroth node), one having events classified as signal-like and the other as background-like. At the next level, each of these bins can be treated in exactly the same way as the root node, using a variable of choice and a particular value of cut on it, giving us two bins—one signal-like and the other background-like—for each node. A tree is built up to a depth either determined by the remaining number of background events, or by the depth specified by the user. The final leaf nodes contain background-like and signal-like events from the training sample. Generally half of the provided sample is used for training and the other half is then used for testing.

Decision trees, however, are unstable under statistical fluctuations and cannot be used as good classifiers. Instead, the technique of boosting can be used to combine several classifiers into a single one, such that the latter is more stable under such fluctuations and, hence, has a smaller error than the individual ones. Boosting modifies the weights of individual events and creates a new decision tree. Higher weights are preferentially assigned to the incorrectly classified events. Previously assigned weights are modified by α , given by

$$\alpha = \frac{1 - \epsilon}{\epsilon}, \quad \text{where } \epsilon = \sqrt{\frac{p(1-p)}{N}}, \quad (5.4.4)$$

where N is the total number of training events in the node and $p = S/(S+B)$, called the purity of the sample. The number of decision trees in the forest we use is given by `NTrees` = 400, the maximum depth of the decision tree allowed is `MaxDepth` = 5 and the minimum percentage of training events in each leaf node is given by `MinNodeSize` = 2.5%. We choose Adaptive Boost, proven to be effective with weak classifiers and implemented as `AdaBoost` in TMVA, as the method for boosting the decision trees in the forest with the boost parameter

Set-1	$(p_T)_{j1}, (p_T)_{j2}, (p_T)_{j3}, (p_T)_{j4}, (p_T)_{bj1}, (p_T)_{bj2}, (p_T)_{bj3}, (p_T)_{bj4},$ $H_T, \cancel{E}_T, \text{nJets}, \text{nbJets}, M_{T2}, m_{b_1}^h, m_{b_1}^\ell$
Set-2	$(p_T)_{j1}, (p_T)_{j2}, (p_T)_{j3}, (p_T)_{j4}, (p_T)_{bj1}, (p_T)_{bj2}, H_T,$ $\cancel{E}_T, \text{nJets}, M_{T2}, m_{b_1}^h, m_{b_1}^\ell$
Set-3	$(p_T)_{j1}, (p_T)_{j2}, (p_T)_{bj1}, (p_T)_{bj2}, H_T, \cancel{E}_T, \text{nJets}, M_{T2}$
Set-4	$(p_T)_{j1}, (p_T)_{j2}, H_T, \cancel{E}_T, \text{nJets}, M_{T2}$

Table 5.4: Different sets of variables that can be considered for the multivariate analysis. We choose Set-2 for our analysis.

$\beta \equiv \text{AdaBoostBeta} = 0.5$. This parameter adjusts the learning rate of the algorithm simply by changing the weights $\alpha \rightarrow \alpha^\beta$. We have used the default values of the BDT parameters, viz. `NTrees`, `MaxDepth` and `MinNodeSize`.

A challenge endemic to TMVA is finding an optimal set of observables that would lead to the best possible discrimination between signal and background events. It is important to note that a larger set of variables need not always provide better discrimination, especially if it is mostly filled with irrelevant observables. We tried four sets comprising of 15 (Set-1), 12 (Set-2), 8 (Set-3) and 6 (Set-4) variables respectively as detailed in Table 5.4. We then plot the ROC (Receiver's Operative Characteristic) Curve for these sets. The ROC curves signify the efficiency of the signal (ϵ_S) with respect to the efficiency of rejecting the background ($1 - \epsilon_B$), with ϵ_B being the efficiency of the background. This is exemplified by the left panel of Fig.5.3, wherein we plot these ROCs for the benchmark point BP-4. Whereas the use of Set-1 and Set-2 offers some improvement over Sets 3 and 4, the former are virtually indistinguishable in their efficacy. In other words, the extra variables in Set-1 are of very little relevance. Given this, we choose the largest set of variables without keeping any irrelevant variables, namely Set-2 for the rest of the analysis in this section.

The variables chosen as BDT inputs have already been introduced in the previous section (see the cut-based analysis) except for the two new variables, namely $m_{b_1}^h$ and $m_{b_1}^\ell$, which represent the reconstructed sbottom mass using the hadronically (h) and leptonically (ℓ) decaying top quarks respectively. We select events with exactly one isolated lepton (electron or muon) with two or more b-tagged jets, utilising only the two hardest b-tagged jets in our reconstruction. Additionally, we work with the four hardest light (i.e., non-b-tagged) jets in the event.

We could have also attempted to reconstruct the sbottom for events with two isolated leptons originating from the leptonic decay of the two top quarks. However, the presence of two neutrinos, the only source of missing energy here, renders the reconstruction non-trivial and makes it a highly involved task. With the dileptonic branching fraction being only 5% (compared to 30% for the semileptonic one), and with the pair production cross-section falling rapidly with the sbottom mass, this channel is likely to be important only in the very high luminosity run of the LHC. In this work, we thus focus only the semi-leptonic case when

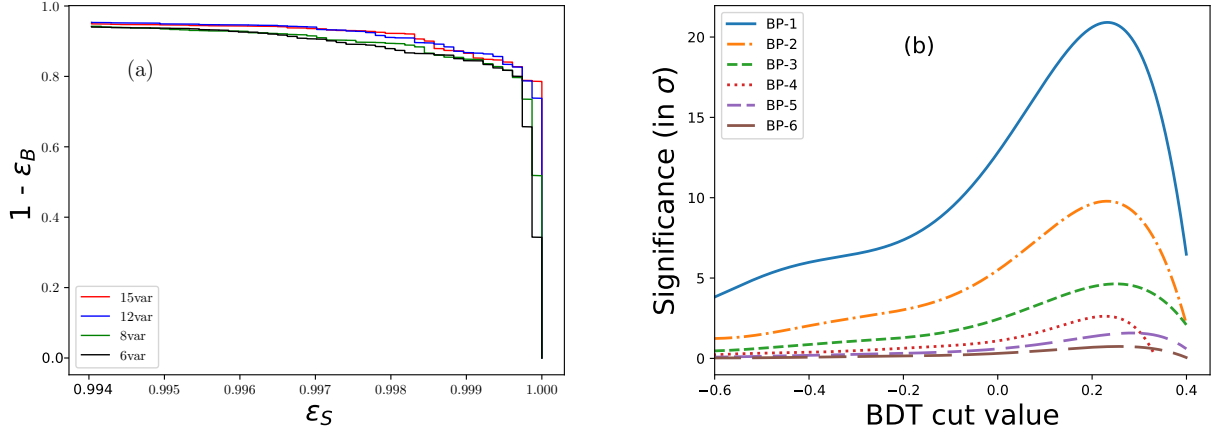


Figure 5.3: On the left (a), the ROC plot is shown for BP-4 with the four sets of variables and on the right (b), the plot for the signal significance against different BDT cut-values is shown.

events contain exactly one isolated lepton with b-tagged and light jets and missing transverse energy. The interested reader can refer to [379, 380] for the detailed implementation of the reconstruction of $t\bar{t}$ and heavy resonances using dileptonic modes.

Before we proceed to reconstruct the top quark, we must reconstruct the W bosons. The hadronically decaying W boson is reconstructed by choosing the pair of light non b-tagged jets which give an invariant mass closest to the actual W boson mass with a further demand that the thus reconstructed mass lies within $M_W \pm 30$ GeV. The leptonically decaying W boson in the decay of the top quark is reconstructed, within a quadratic ambiguity, from the four momentum of the lepton, p_ℓ and the missing transverse momentum $\vec{p}_T \equiv (p_x^\ell, p_y^\ell)$, by imposing the condition that the invariant mass $M_{\ell\nu} = M_W$. Note that, here it is assumed that the only source of missing energy is the neutrino originating from the leptonic decay of W . Using the 4-vector of the isolated lepton $p^\mu = (E^\ell, p_x^\ell, p_y^\ell, p_z^\ell)$, arising from the decay of the W , one can construct the longitudinal component (and, hence, the energy) of the missing momentum as follows:

$$p_z^\ell = \frac{1}{2(E^{\ell 2} - p_z^{\ell 2})} \left[p_z^\ell \left(2p_x^\ell p_x^\ell + 2p_y^\ell p_y^\ell - m_\ell^2 + M_W^2 \right) \pm \sqrt{\Delta} \right], \quad (5.4.5)$$

where the quantity Δ is given by

$$\Delta = E^{\ell 2} \left[\left(2p_x^\ell p_x^\ell + 2p_y^\ell p_y^\ell - m_\ell^2 + M_W^2 \right)^2 - 4p_T^2 \left(E^{\ell 2} - p_z^{\ell 2} \right) \right], \quad (5.4.6)$$

with m_ℓ being the mass of the lepton and M_W being the input mass for the W boson. This provides us with two values of p_z^ℓ corresponding to the two signs of the square root. For certain configurations, however, one may obtain $\Delta < 0$, rendering the calculated p_z^ℓ complex and thus unphysical. In these cases, one can re-calculate the missing energy by finding those values of p_T^ℓ for which $\Delta \geq 0$:

$$p_T^\ell = \frac{1}{2(E^{\ell 2} - p_z^{\ell 2} - (p_x^\ell \cos \phi + p_y^\ell \sin \phi)^2)} \left[-(p_x^\ell \cos \phi + p_y^\ell \sin \phi)(m_\ell^2 - M_W^2) \pm \sqrt{(m_\ell^2 - M_W^2)^2(E^{\ell 2} - p_z^{\ell 2})} \right]. \quad (5.4.7)$$

For each sign of the square root in Eqn. 5.4.7, we get a value of \not{p}_T , which when substituted in Eqn. 5.4.5 give two values of \not{p}_z for every value of \not{p}_T . Thus, we end up with four values of \not{p}_z in this case, instead of just two as in the earlier case.

For each value of the z-component of the MET (i.e. \not{p}_z), we can reconstruct the leptonically decaying top quark mass by combining the 4-momenta of the lepton, b-jets and the missing energy. Several reconstructed mass combinations can exist, depending on the number of solutions of \not{p}_z and since there are two b-tagged jets to choose from.

To obtain the optimal values of the leptonic and hadronic top quark masses in each event, a minimum- χ^2 approach is adopted with the χ^2 defined as:

$$\chi^2 = \frac{(m_{tH} - m_t)^2}{\sigma_{m_{tH}}^2} + \frac{(m_{tL} - m_t)^2}{\sigma_{m_{tL}}^2}, \quad (5.4.8)$$

where $\sigma_{m_{tL}}$ and $\sigma_{m_{tH}}$ represent the uncertainty in top quark mass measurement for leptonically and hadronically decaying tops respectively at the LHC. We consider $\sigma_{m_{tL}} = 2.7$ GeV and $\sigma_{m_{tH}} = 1.15$ GeV [381, 382]. Using the 4-momentum information of the isolated lepton and missing transverse energy along with the two b-tagged jets and the leading four non b-tagged jets, we reconstruct the leptonic and hadronic top quark masses. The combination which leads to the lower χ^2 value is chosen. Nice resonance peaks around top quark mass are observed for both the leptonically and hadronically decaying tops for all the benchmark points.

After the reconstruction of two top quarks, we are now left with the final reconstruction of the sbottom mass using these two reconstructed top quarks and the two remaining light quark jets originating from the decay of the two sbottoms. For each reconstructed top mass, there are two possible choice to combine the light jets for the reconstruction of the sbottom mass. We select the combination which leads to the least difference between the reconstructed mass of the leptonically decaying sbottom and the hadronically decaying sbottom. The plot for the reconstructed sbottom for BP-1 (corresponding to a 500 GeV sbottom) and for BP-4 (corresponding to a 800 GeV sbottom) are shown in Fig. 5.4, where the left and right panels denote the reconstruction method involving the leptonically and hadronically decaying top quarks. The reconstructed sbottom masses peak at the truth masses for the two benchmark points, while for $t\bar{t}$ events it peaks near the truth top quark mass. The peaks corresponding to the signal events are significantly distinct from that of the backgrounds, and this motivates us to consider the reconstructed masses as the BDT inputs.

	BP-1	BP-2	BP-3	BP-4	BP-5	BP-6
$m_{\tilde{b}_1}$ (GeV)	500	600	700	800	900	1000
BDT cut	0.231	0.234	0.258	0.230	0.311	0.294
$\mathcal{S} = \frac{S}{\sqrt{S+B}}$	20.9	9.9	4.7	2.7	1.6	0.9

Table 5.5: Signal significances for the benchmark points with the choice of BDT cuts with $\mathcal{L} = 300 \text{ fb}^{-1}$ of integrated luminosity.

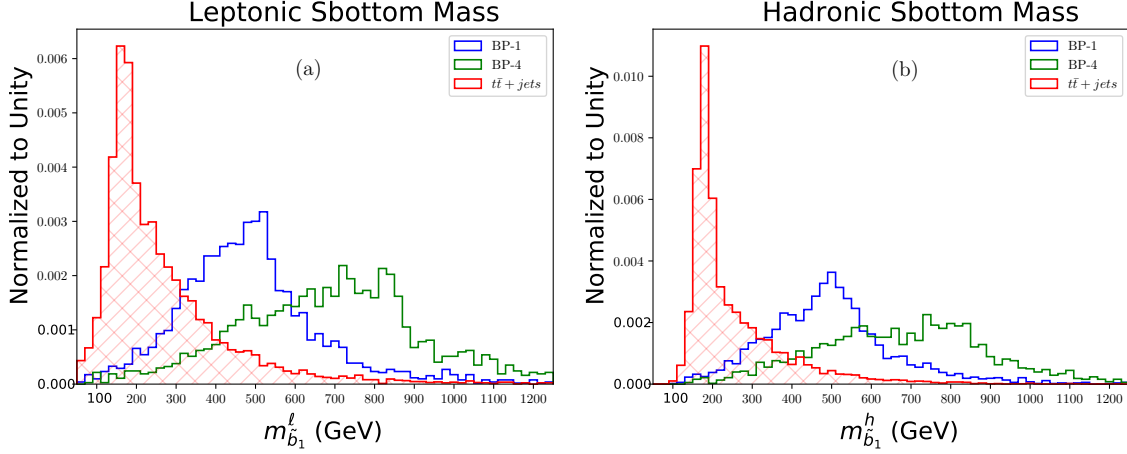


Figure 5.4: Reconstructed sbottom masses for BP-1, BP-4 and the $t\bar{t}$ events, left (a) denotes the case when the top quark decays leptonically while the right (b) signifies the hadronically decaying top quark scenario. For details, see the text.

For each benchmark point, the variation of signal significance with the BDT cut value has been shown in plot (b) of Fig. 5.3 and Table 5.5 shows the best signal significance with the corresponding BDT cut values assuming $\mathcal{L} = 300 \text{ fb}^{-1}$. Clearly, the MVA improves the reach of the search compared to the cut-based analysis, e.g. signal significance improves from 10.7 to 20.9 for BP-1, resulting in an increase of the discovery reach of $\sim 100 \text{ GeV}$ in the mass of the \tilde{b}_1 . The variation of signal significance with integrated luminosity is shown in Fig. 5.5, solid lines for the cut-based analysis and the dashed lines for the MVA. One can observe that with 2000 fb^{-1} data, \tilde{b}_1 mass of upto 1 TeV can be explored at the High Luminosity run of LHC.

5.5 The Hadronic Final State

We now consider the case where both the top-quarks decay fully hadronically. The fully hadronic final state is difficult to investigate at the LHC because of the overwhelming QCD background. However, in our signal events, the top quarks are expected to be boosted, such that the three quarks from its decay form a ‘fatjet’ with substructure. Our plan is to exploit the substructure of such a fatjet to identify a top quark and investigate the reach for sbottom using 13 TeV data from the LHC.

Our final state will contain only reclustered fatjets and we shall attempt to tag some of these jets as tops. The background should ideally have contributions from all the SM processes we considered in the leptonic counterpart— $t\bar{t} + \text{jets}$ (upto two), $t\bar{t}b\bar{b}$, $t\bar{t}Z$, $t\bar{t}W$ and $t\bar{t}H$ —in addition to the QCD multijet, but for all practical purposes the QCD multijet processes and $t\bar{t} + \text{jets}$ (upto two) contribute so overwhelmingly to the background (even after cuts) that we really need not consider the other processes. In this section, we work with this simplifying assumption about the background. It is to be noted that while simulating the QCD multijet

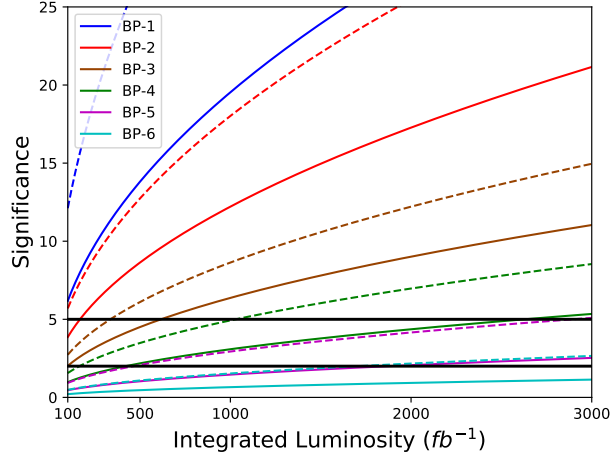


Figure 5.5: Plot of significance versus the integrated luminosity. While the inset legend shows the colour for the different benchmark points, the solid line corresponds to the significance corresponding to the cut-based analysis and the dashed line to that provided by the multivariate analysis. Horizontal lines at 2σ and 5σ indicate the potential for exclusion and discovery.

events, we restrict ourselves up to four jets at the parton level (light quarks and gluons only) due to our computational limitations. However, once parton showering is switched on, the jet multiplicity can and does become larger.

Our strategy is to tag at least one top quark in each signal event. For this purpose, we use **HEPTopTagger** [383], which is quite efficient for tagging tops with moderate boosts ($p_T \gtrsim 200$ GeV). We avail of the energy flow of the particles, provided in the **EFlow** branch of the **DELPHES** generated **ROOT** file to obtain the particle information. We use **FASTJET** to construct fat jets of $R = 1.8$ using the anti- k_T jet algorithm with a minimum p_T of 30 GeV. The jets with $p_T > 200$ GeV and $|\eta| < 3$ are then selected to pass through the **HEPTopTagger**. Before they enter the toptagger, these jets are reclustered exclusively with the Cambridge-Aachen (C/A) algorithm with the same jet radius (viz. $R = 1.8$). The default settings of **HEPTopTagger** were used: the mass drop required for jet splitting was set at $\min(m_{j_1}, m_{j_2})/m_j = \mu < 0.8$ with the minimum mass of a subjet $m_{sub}^{min} = 30$ GeV, where j_1 and j_2 are the subjets of the fatjet j . The top- and W-masses are reconstructed on a set of filtered subjets numbering no more than $N_{filt} = 5$. Tops are tagged with masses in the range between $m_{top}^{min} = 140$ GeV and $m_{top}^{max} = 200$ GeV. We achieve an efficiency of about 30% using these conditions for moderate (~ 200 GeV) to high (say 600 GeV or more) p_T regime. The choice of large jet radius indicates that we are required to incorporate some jet grooming technique in order to get rid of soft and large angle radiations as well as underlying events. In our analysis, we use a particular technique, named Jet Trimming [384] which has been found to be very effective in grooming large R jets. This grooming technique involves two independent parameters, namely R_{trim} and p_T^{frac} . The prescription is to essentially recluster the constituents of a given jet with a smaller jet radius R_{trim} and then keep those subjets with p_T greater than a fixed fraction, p_T^{frac} of the input jet p_T . In our analysis, we optimize these two parameters and choose $R_{trim} = 0.4$

and $p_T^{\text{frac}} = 1\%$. These trimmed jets, obtained after trimming the original anti- k_T jets, are used for further analysis.

5.5.1 Multivariate Analysis

After passing the jets to the `HEPTopTagger`, we select the events containing at least one top-tagged jet. The complete event information is used to construct different observables, and these, in turn, are used to perform a multivariate analysis using the TMVA framework.

Once we have successfully described the full event information in terms of jets, we classify the different types of jets as top-tagged jets, b-tagged jets and “light” jets (non top-tagged, non b-tagged jets). For b-tagging, we calculate the angular distance between a jet and the b-hadron, and make sure that the separation $\Delta R < 0.5$. Furthermore, we also take into account a p_T dependent b-tagging efficiency given by [368]:

$$\epsilon_b = \begin{cases} 0.5 & \text{for } p_T^b \leq 50 \text{ GeV} \\ 0.75 & \text{for } 50 \text{ GeV} < p_T^b \leq 400 \text{ GeV} \\ 0.5 & \text{for } p_T > 400 \text{ GeV} \end{cases} \quad (5.5.1)$$

Note that the above-mentioned efficiencies are conservative estimates; with more data and improved algorithms we expect significant improvement in b-tagging efficiencies. Finally, jets which are not tagged either as ‘top-jets’ or ‘b-jets’ are called ‘light jets’.

Not only are the light-jets in the signal sample often harder than those in the background, an analogous statement also holds for the respective top-jet constituent (especially for heavier sbottoms). To utilize these characteristic differences, between the signal and background events, we consider the p_T of the hardest top jet and the p_T of the hardest and second hardest light jets as BDT input variables. Like the leptonic analysis, one of the most important variables is H_T (see eqn.5.4.1), with the sum, obviously, running over all the jets. Being closely associated with the center-of-mass energy of the process, it too is an important discriminator. It is important to remind our readers here that we use only trimmed jets to construct the jet observables. We use the number of b-tagged jets as a discriminator by passing it as a variable for MVA, as QCD decreases vastly if a b-tag is demanded. We could, instead, have put a cut on it before the MVA—a pre-MVA cut—but as this would decrease the background a lot, making the BDT analysis somewhat unreliable, we desist. In Fig. 5.6, we plot the distributions in the p_T of the hardest light jet, that of the hardest top tagged jet and H_T . The QCD multijet sample was generated with an imposed cut of 1 TeV on the H_T and after demanding that the two hardest jets in the sample be harder than 100 GeV. With the center of mass energy of the sbottom pair production process being ~ 1 TeV, this ensures ample, yet relevant statistics for the QCD multijet process. The variable H_T turns out to be a good discriminator as the peak of higher mass benchmarks lies to the right of the QCD peak, the tail of the distribution only contributes to the signal peaks.

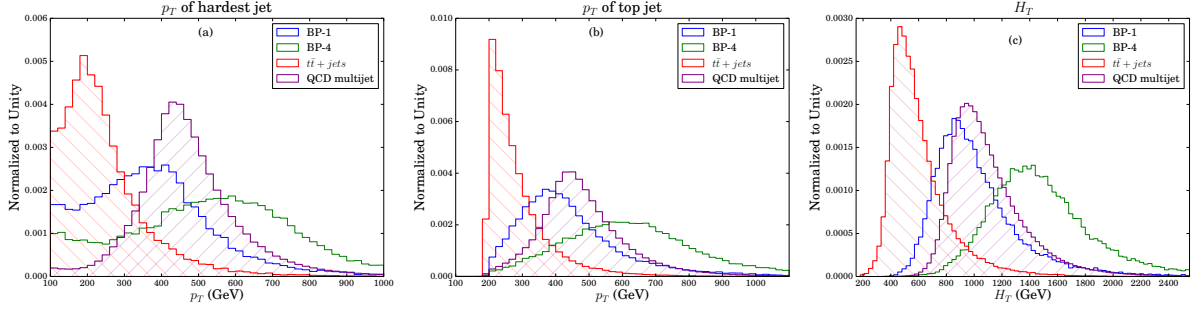


Figure 5.6: The plots for a few of the variables used in the analysis. The left plot (a) shows the p_T of the hardest light jet (non top-tagged, non b-tagged jet), while the plot in the middle (b) shows the p_T of the hardest top-tagged jet. The rightmost figure (c) is that of the H_T , which is the scalar sum of all the jets. In all of these, only two benchmark points (BP-1 and BP-4) have been shown and the histograms for the background processes are hatched.

Restricting ourselves to events with a tagged-top and at least four jets overall⁵ two more useful observables are obtained by partitioning an event such that one subset contains the tagged top and a single non-b jet, while the other contains the rest of the jets. Denoting the invariant masses of the two sets by m_{tj} and m_{jets} , we retain these variables for the pairing that minimizes the difference

$$\Delta M \equiv |m(j_t, j_i) - m(j_k, j_l, \dots)| \quad (5.5.2)$$

Ideally, ΔM should vanish. However, owing to the vagaries of jet reconstruction algorithms as well as detector effects, this would rarely occur. Note that the requirement of the top's partner above being a non-b jet helps get rid of significant amount of the QCD background in the signal peak region. Note that, among the two invariant masses m_{tj} and m_{jets} and the mass difference ΔM , only two are independent parameters. In the MVA analysis, however, we use all the three parameters simultaneously as BDT inputs. In Fig. 5.7, we plot the two invariant masses we talked about earlier. These seem to have moderate discriminatory powers. Furthermore, In Fig. 5.8, we also show the correlations in the $m_{tj} - m_{jets}$ plane for the QCD multijets (left plot), and for two benchmark points - BP-4 (middle) and BP-6 (right). For the QCD, the points are dense in the region around the (500,500) point while for the signal it is dense around (800,800) for BP-4 and around (1000,1000) for BP-6. It is interesting to note that this feature, in principle, can be used for probing heavier bottom squarks.

Nsubjettiness [385] is an inclusive jet shape variable which takes into account the energy distribution within a fat jet. It is defined as

$$\tau_N = \frac{\sum_k p_{T,k} \min(\Delta R_{1,k}, \Delta R_{2,k} \dots \Delta R_{N,k})}{\sum_k p_{T,k} R_0} \quad (5.5.3)$$

⁵Our primary event selection criteria includes at least one toptagged jet, however for the reconstruction of invariant masses we restrict ourselves to exactly one toptagged event. In principle, two or more toptagged samples would give better mass peaks with negligible QCD events, however we find a very few signal events surviving the two or more toptagged jet selection criteria.

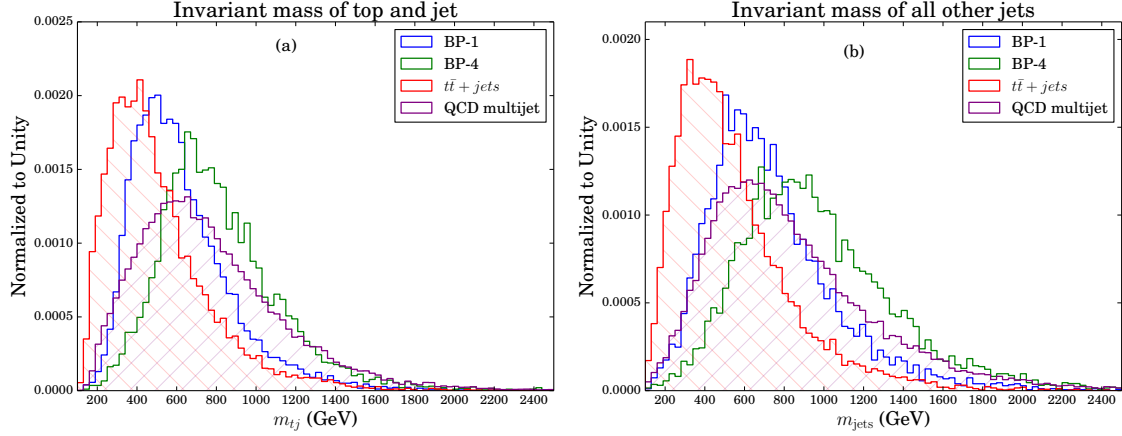


Figure 5.7: The reconstructed masses that we used for the multivariate analysis. The plot on the left (a) is the invariant mass of the top with one of the light jets (in short, ‘tj’ set), while that on the right (b) is the invariant mass of all the other jets in that event which do not correspond to the ‘tj’ set. The invariant mass reconstruction technique has been discussed in the text in detail. Only two benchmarks (BP-1 and BP-4) are plotted and the background histograms are hatched.

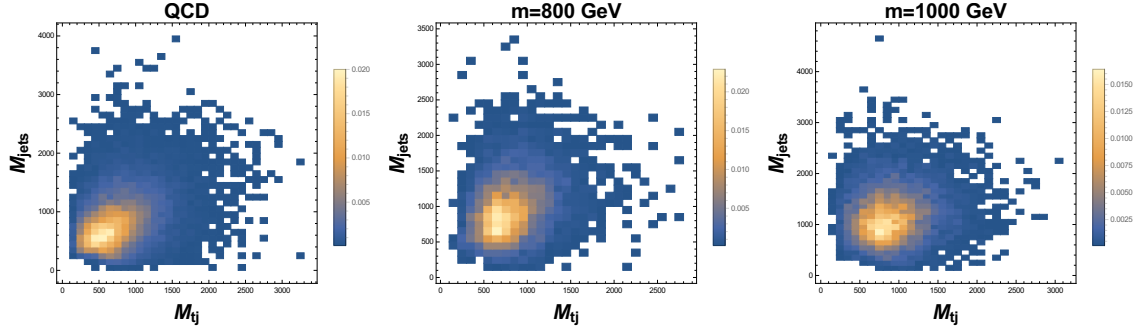


Figure 5.8: Colour plots showing correlation between the m_{tj} and m_{jets} variables in the case of QCD (left), BP-4 (middle) and BP-6 (right). Strong correlation can clearly be seen around the (500, 500) point for QCD, (800, 800) for BP-4 and (1000, 1000) for BP-6. This can be exploited to probe heavier sbottoms as well.

where $\Delta R_{j,k}$ is the angular separation between the j^{th} candidate jet and the k^{th} constituent particle, $p_{T,k}$ is the p_T of the k^{th} constituent and R_0 is the jet radius of the fatjet under consideration. Normalisation ensures that $0 \leq \tau_N \leq 1$. If $\tau_N \approx 0$, it indicates that all the radiation in the jet is aligned with the subjet directions and that there is a maximum of N subjets in the considered jet. On the other hand, if $\tau_N \gg 0$, it indicates the presence of more subjets and that the radiation is distributed far from the candidate subjets. It turns out that the ratio between two Nsubjettiness variables might have higher discriminatory power than the variables themselves. For events with at least one toptagged jet, we calculate three such ratios, τ_{21} , τ_{31} and τ_{32} , where $\tau_{ij} = \tau_i/\tau_j$, associated to the leading toptagged jet. The ideal toptagged jet should have a three-prong structure, and thus τ_{31} and τ_{32} are expected to be small, while this would not be true for the QCD background. Thus, these can be used as good discriminating variables. In Table 5.6, we list all the above-mentioned variables that are passed to the BDT for the MVA.

Variable	Definition
1. nlJet	The number of light jets in the event
2. nbJet	The number of b-tagged jets in the event
3. ntJet	The number of top-tagged jets in the event
4. $(p_T)_{j_1}$	p_T of the hardest light jet
5. $(p_T)_{j_2}$	p_T of the second hardest light jet
6. $(p_T)_{j_t^{(1)}}$	p_T of the hardest top tag jet
7. H_T	scalar sum of the p_T of all the jets
8. m_{tj}	the invariant mass of the top and jet system
9. m_{jets}	the invariant mass of all the other jets
10. $\Delta M = m_{tj} - m_{\text{jets}} $	the mass difference of the two reconstructed invariant masses
11. $\tau_{21} = \tau_2/\tau_1$	Ratio of the Nsubjettiness variables
12. $\tau_{31} = \tau_3/\tau_1$	Ratio of the Nsubjettiness variables
13. $\tau_{32} = \tau_3/\tau_2$	Ratio of the Nsubjettiness variables
14. $\rho = \frac{(p_T)_{j_t^{(1)}}}{(p_T)_{j_\ell^{(1)}}}$	Ratio of the hardest top-jet p_T and light jet p_T
15. $\Phi(t, j)$	Azimuthal angle separation between the toptagged jet and the leading light jet.

Table 5.6: List of all the variables used in the multivariate analysis. Note that, the variable ρ_2 is calculated only only for events with two or more tagged tops.

	QCD	$t\bar{t} + \text{jets}$	BP-1	BP-2	BP-3	BP-4	BP-5	BP-6
σ_0 (fb)	1.9×10^7	8.3×10^5	5.2×10^2	1.8×10^2	6.7×10^1	2.8×10^1	1.3×10^1	6.2
$\sigma_{\text{top tag}}$ (fb)	2.6×10^6	6.7×10^4	1.4×10^2	5.0×10^1	2.0×10^1	8.6	4.0	2.0

Table 5.7: Showing the initial cross-section (σ_0) and surviving cross-section after at least one top is tagged ($\sigma_{\text{top tag}}$) for the background and all the signal benchmarks. The QCD multijet sample is generated after a cut on the H_T variable of 800 GeV and cut of 100 GeV on the p_T of the two hardest jets.

Two further observables, namely ρ and $\Phi(t, j)$, are used as BDT inputs, with the former being defined as

$$\rho = \frac{(p_T)_{j_t^{(1)}}}{(p_T)_{j_\ell^{(1)}}} \quad (5.5.4)$$

where $(p_T)_{j_t^{(i)}}$ is the p_T of the i^{th} top jet, while $(p_T)_{j_\ell^{(i)}}$ is the p_T of the i^{th} light jet (i.e. a non top-tagged, non b-tagged jet). The quantity $\Phi(t, j)$ measures the azimuthal angular separation between the top-tagged jet and the leading light jet.

5.5.2 Results

We now proceed to discuss the details of the multivariate analysis using the BDT method implemented in the TMVA ROOT framework. The fifteen variables discussed earlier and

listed in Table 5.6), each of which we expect to have some discrimination power, are used as the BDT inputs. The BDT parameters are same as in the leptonic case, viz. $\text{NTrees} = 400$, $\text{MaxDepth} = 5$ and $\text{MinNodeSize} = 2.5\%$ with $\text{AdaBoostBeta} = 0.5$. In Table 5.7, we show the initial cross-sections (σ_0) and the cross-section after at least one top is tagged ($\sigma_{\text{top tag}}$). The top tagged events in the QCD samples are due to misidentification of fat jets as top jets; the corresponding ‘fake rate’ is about 10% for the QCD sample. The advantage of using the multivariate analysis is that we can translate a complicated multi-dimensional optimisation problem over all input variables into that involving a one parameter function which is much easier to handle. We can now choose the BDT cut value such that it maximizes the signal significances. The results of the multivariate analysis are presented in Table 5.8 and Fig. 5.9.

	BP-1	BP-2	BP-3	BP-4	BP-5	BP-6
$m_{\tilde{b}_1}$ (GeV)	500	600	700	800	900	1000
BDT cut	0.186	0.167	0.245	0.238	0.266	0.280
$\mathcal{S} = \frac{S}{\sqrt{S+B}}$	3.50	1.21	0.57	0.32	0.20	0.16

Table 5.8: Signal significances for the benchmark points with the choice of BDT cuts with $\mathcal{L} = 300 \text{ fb}^{-1}$ of integrated luminosity.

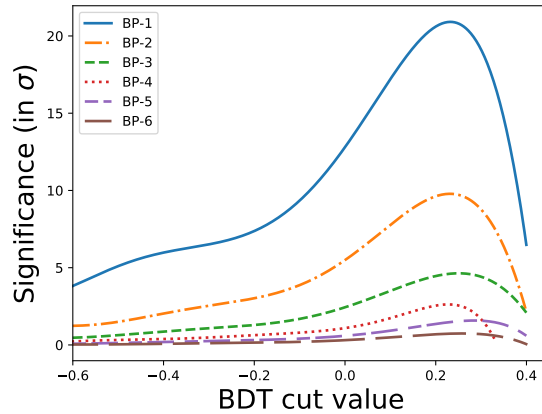


Figure 5.9: Plot showing the significance of the different benchmark points with variation of the BDT cut value. All figures for for 300 fb^{-1}

From Table 5.8, it is evident that the signal significances for the benchmark points diminish rapidly as we proceed from BP-1 to BP-6. The primary reason is the rapid decrease of the sbottom pair production cross-section with the increase of sbottom mass. Even though we expect to tag the top quarks originating from the heavier sbottoms more efficiently, the impact is negligible compared to the drastic fall in the production cross-section. Improved toptagging with smaller fake rate for the QCD multijet events is essential for better signal-background discrimination. State-of-the-art jet grooming techniques, namely Pruning [386] and SoftDrop [387] may help in reducing QCD multijet events and, thus, enhancing the signal significance.

It is thus clear that the hadronic channel is not the most favourable one for the discovery of the sbottom. The exclusion limit is barely reached, for 300 fb^{-1} integrated luminosity, for the first benchmark point (500 GeV). A higher integrated luminosity of 3000 fb^{-1} from a futuristic collider like the High Luminosity LHC will be able to push the exclusion limit to about 650 GeV. However, here we would like to suggest an interesting extension of this analysis which combines our leptonic and hadronic analyses, a successful marriage of the boosted and non-boosted analyses with semi-leptonic final states. We will leave this very interesting avenue for our future work.

5.6 Summary and Outlook

In this paper, we analyze the discovery potential of the LHC for a bottom-squark (the LSP) which decays, with a 100% branching ratio, to the top and a light quark via R -parity violating UDD couplings. While relatively heavy squarks allow for large couplings, thereby opening up the possibility of significant resonance production (such as $d + b \rightarrow \tilde{t}^*$), we eschew this possibility altogether, assuming the couplings are small enough for them to be unimportant in production processes (whether resonance or pair), yet large enough to preclude recognizably displaced vertices.

Based on the final state, we devise two strategies, one for a final state which has at least one isolated lepton (electron or muon) and the other for a fully hadronic final state. For the leptonic state, two independent investigations have been performed: first, using the traditional cut-based analysis and then using a multivariate analysis (MVA). The backgrounds considered for the leptonic analysis are $t+\bar{j}$ ets, $t\bar{t}b\bar{b}$, $t\bar{t}W$, $t\bar{t}H$ and $t\bar{t}Z$. After demanding an isolated lepton tag, we consider cuts on various observables, like H_T and M_{T2} among others, in order to separate signal from background. We also reconstruct the sbottom mass with exactly one isolated lepton with two or more b-tagged jets and four hardest light (i.e., non-b-tagged) jets in the event. We use these reconstructed sbottom masses, namely $m_{\tilde{b}_1}^h$ and $m_{\tilde{b}_1}^\ell$ representing the reconstructed masses using the hadronically and leptonically decaying top quarks respectively, as BDT inputs. While the cut-based analysis reveals an exclusion of $\sim 750 \text{ GeV}$ of the sbottom mass, the MVA extends that range to $\sim 850 \text{ GeV}$ with 300 fb^{-1} of data.

For the fully hadronic final state, we perform the MVA directly as we find through our leptonic analysis that it helps to improve the reach for heavy resonance. The dominant QCD multijet and the $(t\bar{t} + \text{jets})$ backgrounds drown out all other sources of SM backgrounds. We consider events in which we can tag at least one top jet using the **HEPTopTagger** framework. Furthermore, in order to reduce the effect of underlying events and soft radiation, we groom the large R anti- k_T jets using the “Trimming” technique. Several observables are then constructed using these trimmed jets and then passed to the MVA. The results, unfortunately, are not as good as in the leptonic channel, with the exclusion limit barely crossing 500 GeV.

The sensitivity that our analyses project can be further improved upon the inclusion of other aspects. We list a few here:

- Incorporating tracker information such as number of soft-tracks [388], not associated with the reconstructed objects, is likely to help in improving the sensitivity, especially for the most challenging case, viz. the fully hadronic final state.
- As we have already mentioned, the very couplings that we have investigated here also lead to the stop decaying to a bottom and a light quark. Although the background processes to the corresponding final state (two $b + d/s$ pairs) have larger production rates than the one here, the simpler nature of the final state, especially the ability to reconstruct the masses [351, 352] allows for a higher experimental sensitivity [334]. In this work, we have deliberately avoided this channel, assuming the stop to be much heavier. If it is not so, but is comparable to the sbottom in mass, the sensitivities need to be compounded.
- The very same coupling will also lead to decays like $\tilde{d}(\tilde{s}) \rightarrow \bar{t} + \bar{b}$ (depending on the identity of the coupling). Once again, we have not included this assuming that the $\tilde{d}(\tilde{s})$ is much heavier. This assumption was partly motivated by the need to keep large FCNCs at bay. However, a second solution exists if the squark masses are relatively degenerate [389–391]. This can be motivated if the soft-supersymmetry breaking masses for the right-handed squarks are similar, and so are the small trilinear terms A_d, A_s, A_b . As can be readily appreciated, this solution is more natural than the one we have considered here.

Direct two-body decays of $\tilde{d}(\tilde{s})$ that are nearly degenerate with the \tilde{b} would lead to configurations very similar to that we have considered here, with the added advantage that the non-top jets here originate from b -quarks and, thus, can be tagged. This would severely curtail the SM backgrounds (with the biggest effect being seen in the fully hadronic state), resulting in much improved sensitivity.

- Indeed, even if the $\tilde{d}(\tilde{s})$ are sufficiently heavier than the \tilde{b} (on account of a possibly large A_b , the effects due to $A_{d,s}$ of similar magnitudes being smaller) so as to open up their R-conserving three-body decays (into \tilde{b} accompanied by a pair of quarks), the associated quarks would lead to only soft jets. Thus, for such a cascade, one essentially comes back to the configuration that we have analysed here.
- Finally, both stops and sbottoms (and, similarly, the other squarks) can originate from gluinos. If the gluino is not much heavier than the quark, its production cross section is much larger. Such a gluino would decay into the squark-quark pair. The latter would lead to a soft jet, with the first suffering a R-violating decay leading to a configuration very similar to the one under consideration. This is quite analogous to the ATLAS study [336] (that set a limit of $m_{\tilde{g}} > 1.08$ TeV), except for the fact that, in the present context, some of the jets would be rather soft.

On the other hand, if the gluino is very heavy, the produced squarks will be highly boosted, providing highly boosted tops in turn. This suits top tagger algorithms favorably and has been analyzed in [392].

In view of these obvious improvements to the sensitivity that can be effected, it is quite apparent that the conclusions reached by us are only conservative.

The Sgoldstino as a 750 GeV diphoton resonance

6.1 Introduction

Discovery through direct searches has remained a gold standard in particle physics and the LHC holds promise of fulfilling such aspirations. Till date, however, there haven't been any signs of a new particle. Towards the end of 2015, there was a lot of excitement in the community over a tantalising signal of an excess in the diphoton channel. The excess, initially reported by both the ATLAS and the CMS collaborations, have since disappeared and is now thought to be a statistical fluctuation.

The ATLAS and the CMS collaborations had reported the excess of events in the diphoton invariant mass ($m_{\gamma\gamma}$) distribution based on 3.2 and 2.6 fb⁻¹ of proton-proton collision data respectively collected at a center-of-mass energy of 13 TeV. ATLAS observed the most significant deviation from the background hypothesis at $m_{\gamma\gamma} \approx 750$ GeV, corresponding to a local (global) significance of 3.6 (2.0)¹ [393]. The largest excess in the CMS data was seen around the 760 GeV mass bin with a local (global) significance of 2.6 ($\lesssim 1.2$) standard deviations [394]. This excess is also found consistent with the constraints from the run 1 data [396]. It was also reported by ATLAS that the properties of the events in the signal region were found to be compatible with those in the invariant mass regions above and below the excess. As suggested by many authors, the most simple-minded explanation of this excess is to propose the existence of a resonance (\mathcal{S}) of mass ~ 750 GeV. In order to generate the correct amount of signal, the resonance must have couplings that produce $\sigma^{\text{signal}} \equiv \sigma(pp \rightarrow \mathcal{S})\text{Br}(\mathcal{S} \rightarrow \gamma\gamma)$ about 5 fb [396, 445, 446].

¹This was obtained using a narrow width of the signal component. The statistical significance increases slightly once the possibility of larger width is taken into account. See [395] for more details.

In this article, we consider the possibility of this resonance being an sgoldstino², the “superpartner” of the goldstino, the goldstone fermion of spontaneous global supersymmetry (SUSY) breaking. This possibility has been discussed by [405–408, 418] using an effective description of how the SUSY breaking is mediated to the MSSM sector. In this article, we scrutinise the viability of this proposal when realistic models for the mediation of SUSY breaking are considered. But before we start discussing that, we would like to make a few general comments about SUSY breaking in order to put things in perspective.

Unlike other symmetries, there are some interesting limitations on the possibility of spontaneous global SUSY breaking. For example, neither a pure super Yang-Mills (SYM) nor a SYM theory with massive matter in real representations of the gauge group breaks SUSY spontaneously³. In particular, global $N = 2$ SYM theories (that have matter in real representations) cannot have SUSY spontaneously broken. This is one of the reasons why one needs global $N = 1$ SUSY with complex representation for phenomenology (i.e., MSSM) as there is a hope that SUSY can be spontaneously broken as required by experiments.

However, even in MSSM, it turns out to be impossible to break SUSY spontaneously. In fact, with the minimal field content of MSSM both the SUSY and the EW symmetry remain unbroken⁴. Hence, adding more fields to the MSSM is unavoidable. However, even after adding many heavy fields, the gaugino masses cannot arise in a renormalisable SUSY theory at tree-level. This is because SUSY does not contain any (gaugino)-(gaugino)-(scalar) coupling that could give rise to a gaugino mass term when the scalar gets a vacuum expectation value (VEV). Moreover, the tree level supertrace rules do not allow a phenomenologically acceptable spectrum.

Hence, one possibility for breaking SUSY spontaneously in the MSSM is to have tree level SUSY breaking in a so-called “hidden sector” and radiatively mediate the information of SUSY breaking to the MSSM sector⁵. This also helps in finding a solution of the SUSY flavour problem. As the pattern of SUSY breaking interactions in the visible MSSM sector is determined by the interactions of the messenger particles with the MSSM, a natural way to avoid additional flavour violation in the MSSM is to have flavour symmetries in the messenger interactions. The models of gauge mediation, where the information of SUSY breaking is communicated to the MSSM sector by gauge interactions, achieve this goal in a natural way⁶. In the gauge mediation scenarios, one assumes the existence of “messenger fields” that are charged both under the SM gauge group as well as the hidden sector quantum numbers. The mass scale of these messengers is arbitrary and, in principle, can be as low as ~ 10 TeV. These models are often called “low scale SUSY breaking” scenarios and, as we will see later, are the only ones (among the different SUSY breaking scenarios) relevant for the diphoton excess.

²To our knowledge, the name “sgoldstino” was first used in [422].

³This follows from the fact that Witten Index of these theories is non-zero [419]. See also [420, 421].

⁴A Fayet-Iliopoulos D -term breaking also turns out to be phenomenologically unacceptable [167].

⁵Note that, in four space-time dimensions, if supersymmetry is not broken spontaneously at the tree level, then it can not be broken by radiative Coleman-Weinberg mechanism [443]

⁶This is however not true in general, as the messenger fields can have renormalisable superpotential couplings to the MSSM [403, 432–435, 444]

In the following section, we review the general framework that leads to the sgoldstino explanation of the diphoton excess and present the necessary formulae to study the phenomenology. In section 6.3, we will discuss the ordinary gauge mediation (OGM) scenario and point out the various theoretical issues it confronts in connection to the diphoton excess. The generalisation of the OGM framework, called the extraordinary gauge mediation (EOGM), will be discussed in section 6.4. In section 6.5, we will investigate whether there is some way out of the difficulties raised in the previous sections. We will conclude in section 6.6.

6.2 Generalities

6.2.1 Theoretical framework

In order to parameterise the effect of SUSY breaking in the visible sector, it is usually assumed that SUSY is broken in the hidden sector by the VEV of the F component of a chiral superfield X . In particular, the gaugino masses are generated by the following terms,

$$\begin{aligned} \mathcal{L} \subset & -\frac{1}{2} \frac{c_1}{M_1} \int d^2\theta X W^{1\alpha} W_\alpha^1 - \frac{1}{2} \frac{c_2}{M_2} \int d^2\theta X W^{2\alpha A} W_\alpha^{2A} \\ & - \frac{1}{2} \frac{c_3}{M_3} \int d^2\theta X W^{3\alpha A} W_\alpha^{3A} + \text{h.c.} \end{aligned} \quad (6.2.1)$$

where the superscripts $\{1,2,3\}$ refer to the $U(1)$, $SU(2)$ and $SU(3)$ gauge groups respectively (the adjoint indices for both the gauge groups $SU(2)$ and $SU(3)$ are denoted by A), and α is the spinor index. The scale M_i denotes the mass scale of the messenger fields which have been integrated out to get the above Lagrangian terms⁷. The chiral superfield X and W_α have the following expansion in terms of the ordinary fields,

$$X = \mathcal{S} + \sqrt{2}\theta\xi(y) + \theta\theta F_x(y) \quad (6.2.2)$$

$$= \frac{1}{\sqrt{2}}(\phi(y) + ia(y)) + \sqrt{2}\theta\xi(y) + \theta\theta F_x(y) \quad (6.2.3)$$

$$W_\alpha^A = -i\lambda_\alpha^A(y) + D^A(y)\theta_\alpha - (\sigma^{\mu\nu}\theta)_\alpha F_{\mu\nu}^A(y) - \theta\theta\sigma_{\alpha\dot{\beta}}^\mu D_\mu^{(y)}\lambda^{\dagger A\dot{\beta}}(y), \quad (6.2.4)$$

where, $y^\mu = x^\mu - i\theta\sigma^\mu\theta^\dagger$.

Once the F term of X gets a VEV, say $\langle F_x \rangle$, the above Lagrangian terms generate the following Majorana masses for the gauginos,

$$m_i = c_i \frac{\langle F_x \rangle}{M_i}. \quad (6.2.5)$$

The Lagrangian of Eq. (6.2.1) also generates couplings of the scalar components of X to the

⁷In models of gravity mediation, the scale M_i is of the order of the planck scale. It is then clear that gravity mediation models are not relevant for the diphoton excess.

gauge bosons,

$$\mathcal{L}_{gg} = \frac{1}{2\sqrt{2}} \frac{c_3}{M_3} \left(\phi G_{\mu\nu}^a G^{\mu\nu a} - a G_{\mu\nu} \tilde{G}^{\mu\nu} \right) \quad (6.2.6)$$

$$\mathcal{L}_{WW} = \frac{1}{2\sqrt{2}} \frac{2c_2}{M_2} \left(\phi W_{\mu\nu}^+ W^{-\mu\nu} - a W_{\mu\nu}^+ \tilde{W}^{-\mu\nu} \right) \quad (6.2.7)$$

$$\mathcal{L}_{\gamma\gamma} = \frac{1}{2\sqrt{2}} \left(\frac{c_1}{M_1} c_W^2 + \frac{c_2}{M_2} s_W^2 \right) \left(\phi F_{\mu\nu} F^{\mu\nu} - a F_{\mu\nu} \tilde{F}^{\mu\nu} \right) \quad (6.2.8)$$

$$\mathcal{L}_{ZZ} = \frac{1}{2\sqrt{2}} \left(\frac{c_1}{M_1} s_W^2 + \frac{c_2}{M_2} c_W^2 \right) \left(\phi Z_{\mu\nu} Z^{\mu\nu} - a Z_{\mu\nu} \tilde{Z}^{\mu\nu} \right) \quad (6.2.9)$$

$$\mathcal{L}_{Z\gamma} = \frac{1}{2\sqrt{2}} 2s_W c_W \left(\frac{c_2}{M_2} - \frac{c_1}{M_1} \right) \left(\phi Z_{\mu\nu} F^{\mu\nu} - a Z_{\mu\nu} \tilde{F}^{\mu\nu} \right). \quad (6.2.10)$$

The scalars ϕ and a can decay to the gauge bosons through these couplings. The corresponding partial decay rates are given by (see appendix D.1 for details)⁸

$$\Gamma_{\gamma\gamma} \equiv \Gamma(\phi \rightarrow \gamma\gamma) = \left[\frac{1}{2m_\phi} \right] \left[\frac{1}{8\pi} \right] \left[\frac{1}{8} \left(\frac{c_1}{M_1} c_W^2 + \frac{c_2}{M_2} s_W^2 \right)^2 \right] [8m_\phi^4] \left[\frac{1}{2} \right] \quad (6.2.11)$$

$$\Gamma_{gg} \equiv \Gamma(\phi \rightarrow gg) = \left[\frac{1}{2m_\phi} \right] \left[\frac{1}{8\pi} \right] \left[\frac{1}{8} \left(\frac{c_3}{M_3} \right)^2 \right] [64m_\phi^4] \left[\frac{1}{2} \right] \quad (6.2.12)$$

$$\begin{aligned} \Gamma_{z\gamma} \equiv \Gamma(\phi \rightarrow Z\gamma) &= \left[\frac{1}{2m_\phi} \right] \left[\frac{1}{8\pi} \left(1 - \frac{m_Z^2}{m_\phi^2} \right) \right] \left[\frac{1}{8} \left(\frac{c_2}{M_2} - \frac{c_1}{M_1} \right)^2 4s_W^2 c_W^2 \right] \\ &\times \left[2m_\phi^4 \left(1 - \frac{m_Z^2}{m_\phi^2} \right)^2 \right] \end{aligned} \quad (6.2.13)$$

$$\begin{aligned} \Gamma_{zz} \equiv \Gamma(\phi \rightarrow ZZ) &= \left[\frac{1}{2m_\phi} \right] \left[\frac{1}{8\pi} \left(1 - 4 \frac{m_Z^2}{m_\phi^2} \right)^{1/2} \right] \left[\frac{1}{8} \left(\frac{c_1}{M_1} s_W^2 + \frac{c_2}{M_2} c_W^2 \right)^2 \right] \\ &\times \left[8m_\phi^4 \left(1 - 4 \frac{m_Z^2}{m_\phi^2} + 6 \frac{m_Z^4}{m_\phi^4} \right) \right] \left[\frac{1}{2} \right] \end{aligned} \quad (6.2.14)$$

$$\begin{aligned} \Gamma_{ww} \equiv \Gamma(\phi \rightarrow WW) &= \left[\frac{1}{2m_\phi} \right] \left[\frac{1}{8\pi} \left(1 - 4 \frac{m_W^2}{m_\phi^2} \right)^{1/2} \right] \left[\frac{1}{8} \left(\frac{2c_2}{M_2} \right)^2 \right] \\ &\times \left[8m_\phi^4 \left(1 - 4 \frac{m_W^2}{m_\phi^2} + 6 \frac{m_W^4}{m_\phi^4} \right) \right] \end{aligned} \quad (6.2.15)$$

Here s_W and c_W denote the sine and cosine of the Weinberg angle respectively. The partial decay rates for the scalar a can be obtained from the above expressions by replacing m_ϕ by m_a . There is slight difference between the decay rates of $\phi \rightarrow ZZ(W^+W^-)$ and $a \rightarrow ZZ(W^+W^-)$; however, that is numerically insignificant (see appendix D.1).

⁸Signatures of sgoldstino at the e^+e^- and hadron colliders were first studied in [447,448] where the formulae for the decay rates can also be found.

6.2.2 Explaining the excess

The total cross section for the diphoton production via the resonance \mathcal{S} is given by⁹,

$$\begin{aligned}\sigma_{\text{LHC energy}} &= \sigma(pp \rightarrow \mathcal{S})_{\text{LHC energy}} \text{Br}(\mathcal{S} \rightarrow \gamma\gamma) \\ &= \sum_i \mathcal{A}_{\text{LHC energy}}^{ii} \Gamma(\mathcal{S} \rightarrow p_i p_i) \frac{\Gamma(\mathcal{S} \rightarrow \gamma\gamma)}{\Gamma_{\mathcal{S}}},\end{aligned}\quad (6.2.16)$$

where $\{p_i p_i\}$ refers to the initial state partons i.e., $\{gg\}$, $\{\bar{u}u\}$, $\{\bar{d}d\}$ and so on. The total width of \mathcal{S} is denoted by $\Gamma_{\mathcal{S}}$. The numerical values of the quantities $\mathcal{A}_{\text{LHC energy}}^{ii}$ are calculated in appendix D.2 and are given by,

$$\begin{aligned}\mathcal{A}_{13}^{gg} &\equiv \mathcal{A}_{13 \text{ TeV LHC}}^{gg} = \frac{5.44 \text{ pb}}{\text{GeV}} & \mathcal{A}_8^{gg} &\equiv \mathcal{A}_{8 \text{ TeV LHC}}^{gg} = \frac{1.15 \text{ pb}}{\text{GeV}} \\ \mathcal{A}_{13}^{\bar{u}u} &\equiv \mathcal{A}_{13 \text{ TeV LHC}}^{\bar{u}u} = \frac{2.94 \text{ pb}}{\text{GeV}} & \mathcal{A}_8^{\bar{u}u} &\equiv \mathcal{A}_{8 \text{ TeV LHC}}^{\bar{u}u} = \frac{1.2 \text{ pb}}{\text{GeV}} \\ \mathcal{A}_{13}^{\bar{d}d} &\equiv \mathcal{A}_{13 \text{ TeV LHC}}^{\bar{d}d} = \frac{1.73 \text{ pb}}{\text{GeV}} & \mathcal{A}_8^{\bar{d}d} &\equiv \mathcal{A}_{8 \text{ TeV LHC}}^{\bar{d}d} = \frac{0.66 \text{ pb}}{\text{GeV}}\end{aligned}\quad (6.2.17)$$

In order to explain the signal, $\sigma_{13 \text{ TeV}}$ must be approximately in the range 3 – 8 fb, assuming that the resonance has a small width \lesssim few GeV [396]. A larger width of ~ 40 GeV requires $\sigma_{13 \text{ TeV}}$ to be slightly higher: $\sigma_{13 \text{ TeV}} \approx 5 - 14 \text{ fb}$ [396]. As the sgoldstino typically has a narrow width, in our estimates we will use the range 3 – 8 fb for the required cross section.

We will first consider the production by gluon fusion only, as the production by $u\bar{u}$ and $d\bar{d}$ initial states is slightly disfavoured [396, 445, 446]. In section 6.5.3, we will comment on the possibility of quark initiated production.

6.3 Ordinary gauge mediation

In the OGM framework, the hidden sector is parameterised by a single chiral superfield X . Both the scalar and auxiliary components of X are assumed to get VEVs that are denoted by $\langle \mathcal{S} \rangle$ and $\langle F_x \rangle$ respectively. In addition to this, OGM also includes N_5 vector like pairs of messenger fields, $(\Phi_i, \tilde{\Phi}_i)$, transforming under $\mathbf{5} + \bar{\mathbf{5}}$ of $SU(5)$ ¹⁰. The corresponding superpotential reads,

$$W_{\text{OGM}} = \lambda_{ij} X \tilde{\Phi}_i \Phi_j, \quad (6.3.1)$$

where the indices $\{i, j\}$ run from 1 to N_5 . Note that the matrix λ_{ij} can always be brought to a diagonal form with real entries by independent unitary rotations on Φ and $\tilde{\Phi}$ (the Kähler

⁹Here we use the approximation that $\Gamma_{\mathcal{S}}/m_{\mathcal{S}}$ is small. This is a very good approximation even for the case when $\Gamma = 45 \text{ GeV}$, which gives $\Gamma_{\mathcal{S}}/m_{\mathcal{S}} = 0.06$.

¹⁰Complete representations of a GUT group are normally used in order to keep the unification of the gauge couplings intact. However, in general, complete representations are not necessary. The use of incomplete representations often also have interesting phenomenology, see for example, [409] and the references therein.

potential remain unchanged). Hence, in the rest of this section, we will assume that λ_{ij} is diagonal with $\lambda_{ii} \equiv \lambda_i$.

The fermions of each $\{\Phi_i, \tilde{\Phi}_i\}$ pair has a Dirac mass $m_F^i = \lambda_i \langle \mathcal{S} \rangle$. The mass eigenstates of the complex scalars, on the other hand, have squared masses $m_{\pm}^2 = \lambda_i^2 \langle \mathcal{S} \rangle^2 \pm \lambda_i \langle F_x \rangle$. The gaugino masses are generated at the one loop level and are given by [398],

$$m_a = \frac{\alpha_a}{4\pi} \sum_{i=1}^{N_5} d_i^a \frac{\lambda_i \langle F_x \rangle}{m_F^i} g(x_i) \quad (a = 1, 2, 3) \quad (6.3.2)$$

where, $x_i = \frac{\lambda_i \langle F_x \rangle}{(m_F^i)^2}$ and the function $g(x)$ is given by [398],

$$g(x) = \frac{1}{x^2} [(1+x)\text{Log}(1+x) + (1-x)\text{Log}(1-x)]. \quad (6.3.3)$$

The symbol d_i denotes twice the Dynkin index for a particular representation. For example, in the case of $\mathbf{5} + \bar{\mathbf{5}}$ of $SU(5)$, $d = 1$. In Eq. 6.3.2, we have used the GUT normalisation of the hypercharge gauge coupling.

Note that the SUSY breaking F -term VEV $\langle F_x \rangle$ must satisfy $\langle F_x \rangle \leq \lambda_i \langle \mathcal{S} \rangle^2, \forall i$ in order to avoid the messenger scalar masses from becoming tachyonic. For simplicity, we assume all the λ_i couplings to be equal and set them to a common value λ . We define the ratio $\lambda \langle F_x \rangle / m_F^2$ to be κ . With these definitions, the formula for the gaugino mass takes the form (for messengers in $\mathbf{5} + \bar{\mathbf{5}}$ of $SU(5)$),

$$m_a = \frac{\alpha_a}{4\pi} \kappa m_F N_5 g(\kappa) \quad (a = 1, 2, 3). \quad (6.3.4)$$

The c_a couplings (see Eq. 6.2.5) which control the signal strength are given by,

$$\frac{c_a}{M_a} = \frac{m_a}{\langle F_x \rangle} = \frac{\alpha_a}{4\pi} \frac{\lambda}{m_F} N_5 g(\kappa) \quad (a = 1, 2, 3). \quad (6.3.5)$$

Similarly, the scalar masses can be written as [416, 417],

$$\tilde{m}_a^2 = 2N_5 \kappa^2 m_F^2 \left[C_3^a \left(\frac{\alpha_3}{4\pi} \right)^2 + C_2^a \left(\frac{\alpha_2}{4\pi} \right)^2 + C_1^a \left(\frac{\alpha_1}{4\pi} \right)^2 \right] f(\kappa) \quad (6.3.6)$$

where C^a are the quadratic Casimirs and the function $f(x)$ is given by [398],

$$f(x) = \frac{1+x}{x^2} \left[\text{Log}(1+x) - 2\text{Li}_2 \left(\frac{x}{1+x} \right) + \frac{1}{2} \text{Li}_2 \left(\frac{2x}{1+x} \right) \right] + (x \rightarrow -x). \quad (6.3.7)$$

In order to calculate the gaugino masses at the \sim TeV scale, we use the values of α_a at 1 TeV, which we compute using the one loop SM running equations,

$$\frac{1}{\alpha_a(\mu)} \simeq \frac{1}{\alpha_a(m_Z)} + \frac{b_a}{\pi} \text{Ln} \left(\frac{\mu}{m_Z} \right) \quad (6.3.8)$$

$$\left\{ \frac{1}{\alpha_1(m_Z)}, \frac{1}{\alpha_2(m_Z)}, \frac{1}{\alpha_3(m_Z)} \right\} = \{59, 30, 8.5\} \quad (6.3.9)$$

$$\{b_1^{\text{SM}}, b_2^{\text{SM}}, b_3^{\text{SM}}\} = \left\{ -\frac{41}{20}, \frac{19}{12}, \frac{7}{2} \right\}$$

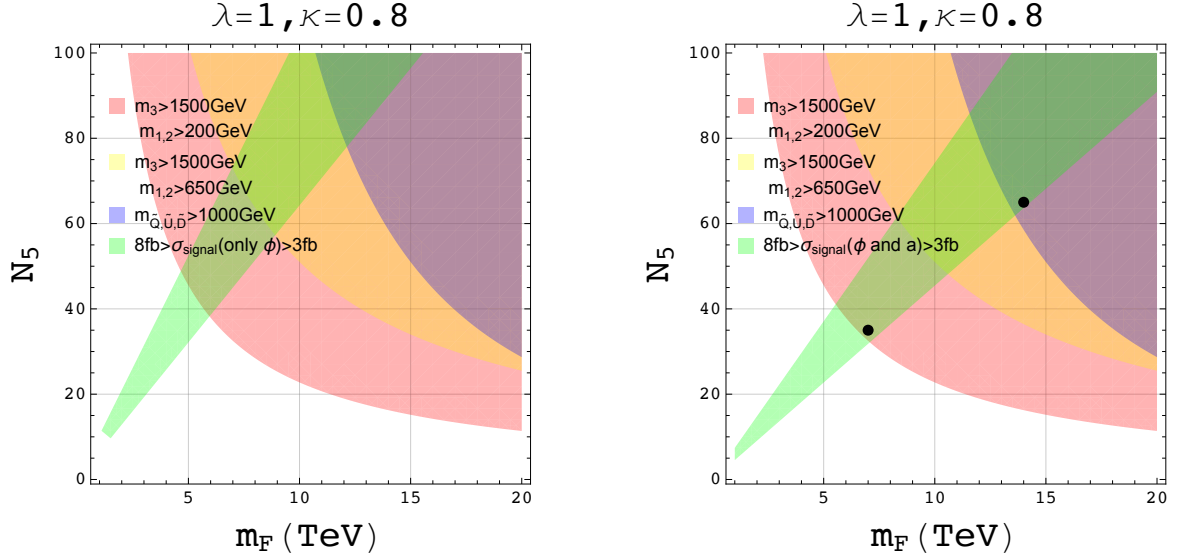


Figure 6.1: Allowed region in the OGM parameter space that successfully explains the signal and satisfy LHC bounds on squark and gaugino masses. While in the left panel the contribution from only ϕ is considered, the right panel takes into account both ϕ and a contributions.

We now examine the requirements on m_F , $\langle F_x \rangle$ and N_5 in order to generate the correct cross section for the excess. In order to have a feeling for the messenger mass scale required for the excess, we first consider a single pair of $SU(5)$ messengers $\{\mathbf{5} + \bar{\mathbf{5}}\}$ i.e., $N_5 = 1$ and also set $\lambda = 1$. Following the discussion of the previous section, the explanation of the diphoton excess requires¹¹,

$$\mathcal{A}_{13}^{gg} \frac{\Gamma_{gg} \Gamma_{\gamma\gamma}}{\Gamma_{gg} + \Gamma_{\gamma\gamma} + \Gamma_{ww} + \Gamma_{zz} + \Gamma_{z\gamma}} \gtrsim 3 \text{ fb}. \quad (6.3.10)$$

This gives,

$$m_F \lesssim 175 \text{ GeV}. \quad (6.3.11)$$

The messenger scale can be raised if the number of messenger fields is increased. In Fig. 6.1 we show the allowed region in the $m_F - N_5$ plane for $\lambda = 1$ and $\kappa = 0.8$. In the left panel, only the contribution of ϕ to the signal is considered, while in the upper right panel contributions from both ϕ and a are taken into account. As discussed before, κ should satisfy $\kappa \leq 1$ to avoid tachyonic states in the messenger sector. For κ very close to unity, one of the complex scalars in every pair of messenger fields becomes too light (its squared mass is $m_F^2(1 - \kappa)$). Also, the function $f(\kappa)$ decreases rapidly for $\kappa \gtrsim 0.8$ [398] reducing the MSSM squark masses. Hence, we have chosen a value $\kappa = 0.8$ in Fig. 6.1.

The light green shaded region reproduces the correct amount of signal to explain the excess. In the light red shaded region, the gaugino masses are what is required by the exclusion limits

¹¹Here we have neglected any decay mode other than the gauge boson final states. However, existence of other decay modes will increase the total width of the resonance, hence adding an extra contribution to the denominator of Eq. 6.3.10. This means that the required signal cross section will be even higher, as pointed out also in the end of section 6.2.2. Thus our estimate is on the conservative side.

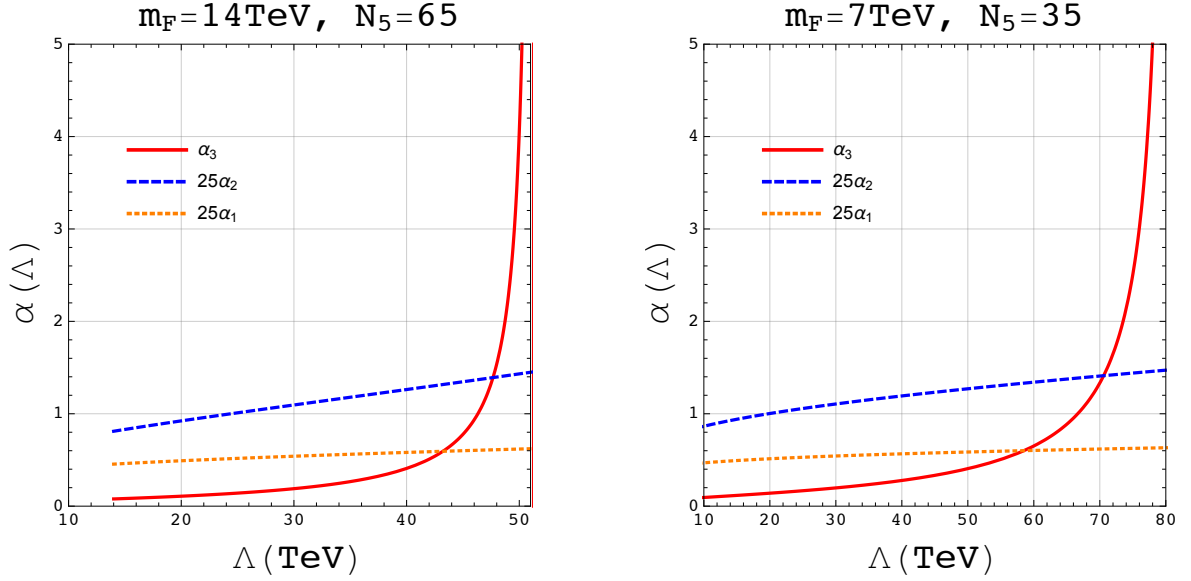


Figure 6.2: RG running of the SM gauge couplings above m_F for the two representative sets of values of $\{m_F, N_5\}$ shown as black dots in Fig. 6.1, see text for more details. The values of the couplings at the scale m_F is obtained using the SM evolution from m_Z to 2 TeV and the MSSM evolution from 2 TeV to m_F .

of the LHC. In particular, the gluino mass is set to more than 1.5 TeV and a conservative lower bound of 200 GeV is considered for the bino and wino masses (we also show the region satisfying a stricter lower bound of 650 GeV on the bino and wino masses [451]). Similarly, in the light blue region the squarks are heavier than a TeV. It can be seen that a very large number of messengers $\gtrsim 60$ is required in order to both successfully explain the signal as well as produce sufficiently large gaugino and squark masses.

However, for such a large number of messenger fields, the gauge couplings lose asymptotic freedom. The one-loop running of the gauge couplings above the messenger fermion mass m_F is shown in Fig. 6.2 for two sets of values of $\{m_F, N_5\}$, shown as black dots in Fig. 6.1. The point $\{m_F, N_5\} = \{14 \text{ TeV}, 65\}$ is chosen such that all the requirements namely, correct amount of the signal cross section and heavy enough gaugino and squark masses are satisfied. It can be seen from the left panel of Fig. 6.2 that the $SU(3)$ gauge coupling in this case hits a one-loop Landau pole below $\sim 50 \text{ TeV}$. The right panel of Fig. 6.2 shows the renormalisation group (RG) running for $\{m_F, N_5\} = \{7 \text{ TeV}, 35\}$ i.e., when the constraint from the squark masses is relaxed. This is relevant for example, in models where the squark masses are generated at the tree level [423, 424]. However, even in this case, the required number of messenger pairs is $\gtrsim 35$ and the one-loop Landau pole is encountered below $\sim 80 \text{ TeV}$.

Before concluding this section, we would like to make two final comments:

- i) Although we have presented our results for messengers transforming under $\{\mathbf{5} + \bar{\mathbf{5}}\}$ of $SU(5)$, our general conclusions hold for other representations also and even in the case when the possibility of doublet-triplet splitting is considered (this will be more clear in section 6.5.3).
- ii) The formula in Eq. 6.3.5 is strictly valid only if the SUSY breaking VEV is small namely,

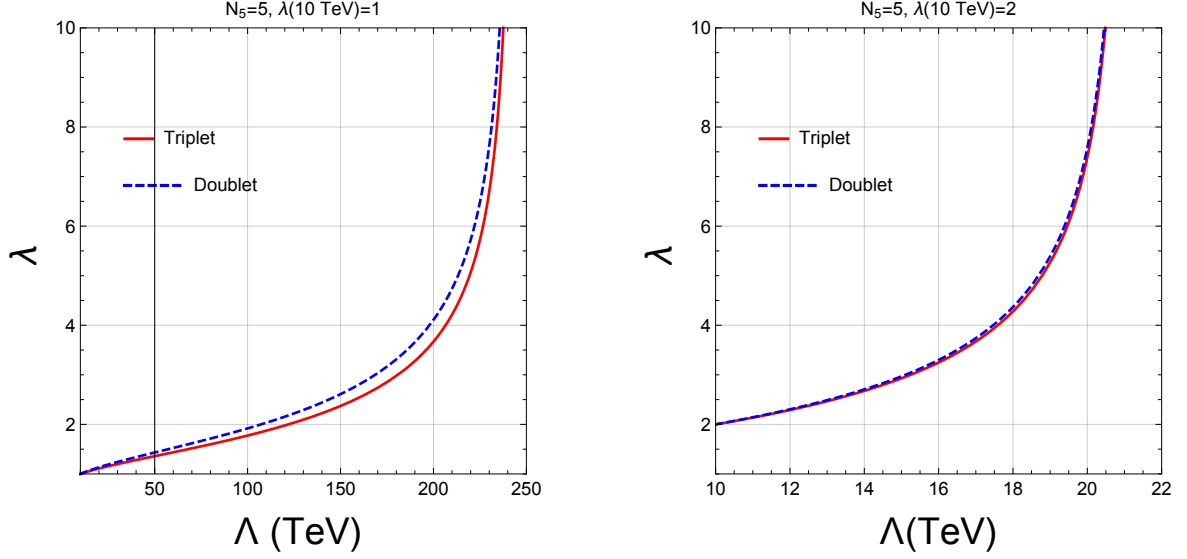


Figure 6.3: RG evolution of λ for $N_5 = 5$ and for two initial values of λ : $\lambda(10 \text{ TeV}) = 1$ (left) and $\lambda(10 \text{ TeV}) = 2$ (right).

$\kappa \ll 1$. For $\kappa \sim 1$, one has to compute the separate loop contributions from the messenger scalar with masses $m_{\pm}^2 = m_F^2(1 \pm \kappa)$. This gives a correction factor $\sim \left(\frac{1 - 2/3 \kappa^2}{1 - \kappa^2} \right)^2$ in the decay rates for the scalar ϕ (here we have assumed $\lambda = 1$ for simplicity). This factor is only ≈ 2.5 for $\kappa = 0.8$ which we use for our analysis¹² and is absent for a . Hence, this does not affect our numerical analysis.

6.3.1 Possibility of larger λ

It can be seen from Eq. 6.3.5 that, for a given gaugino mass, the c_i coefficients (hence, diphoton signal cross section) can be increased by increasing λ . However, one should first check the RG running of λ in order to see the maximum value of λ that is safe.

As the fundamental representation of $SU(5)$ can be decomposed into representations of $SU(3) \otimes SU(2) \otimes U(1)$ in the following way,

$$\mathbf{5} \rightarrow (\mathbf{3}, 1)_{-1/3} \oplus (\mathbf{1}, 2)_{1/2} \quad (6.3.12)$$

the superpotential can be rewritten as,

$$W = \lambda_i^{D^c} X \Phi_i^{D^c} \tilde{\Phi}_i^{D^c} + \lambda_i^L X \Phi_i^L \tilde{\Phi}_i^L \quad (6.3.13)$$

Note that, the notation D^c and L have been used just for notational convenience and they

¹²The paper [395] which appeared *after* the first version of our paper considered the very fine tuned possibility of κ being extremely close to unity which may somewhat mitigate the problem, however, at the cost of very large trilinear coupling between the sgoldstino and some of the light messenger scalars. We do not consider this extremely fine-tuned possibility in this paper.

do not represent the MSSM fields. The beta functions of these couplings are given by

$$\beta_{\lambda_i^{D^c}} = \lambda_i^{D^c} \left(\gamma(\Phi_i^{D^c}) + \gamma(\tilde{\Phi}_i^{D^c}) + \gamma(X) \right), \quad (6.3.14)$$

$$\beta_{\lambda_i^L} = \lambda_i^L \left(\gamma(\Phi_i^L) + \gamma(\tilde{\Phi}_i^L) + \gamma(X) \right), \quad (6.3.15)$$

where

$$\gamma(\Phi_i^{D^c}) = \gamma(\tilde{\Phi}_i^{D^c}) = \frac{1}{4\pi} \left(-\frac{2\alpha_1}{15} + \alpha_{di} - \frac{8\alpha_3}{3} \right) \quad (6.3.16)$$

$$\gamma(\Phi_i^L) = \gamma(\tilde{\Phi}_i^L) = \frac{1}{4\pi} \left(-\frac{3\alpha_1}{10} + \alpha_{li} - \frac{3\alpha_2}{2} \right) \quad (6.3.17)$$

$$\gamma(X) = \sum_i \frac{1}{4\pi} (3\alpha_{di} + 2\alpha_{li}) \quad (6.3.18)$$

We have used the notation, $\alpha_{di} \equiv \frac{(\lambda_i^{D^c})^2}{4\pi}$ and $\alpha_{li} \equiv \frac{(\lambda_i^L)^2}{4\pi}$.

Hence, the RG equations for the λ couplings are,

$$\frac{d\lambda_i^{D^c}}{dt} = \frac{1}{16\pi^2} \lambda_i^{D^c} \left[(3N+2) (\lambda_i^{D^c})^2 - \frac{16}{3} g_3^2 - \frac{4}{15} g_1^2 + 2N(\lambda_i^L)^2 \right], \quad (6.3.19)$$

$$\frac{d\lambda_i^L}{dt} = \frac{1}{16\pi^2} \lambda_i^L \left[(2N+2) (\lambda_i^L)^2 - 3g_2^2 - \frac{3}{5} g_1^2 + 3N(\lambda_i^{D^c})^2 \right], \quad (6.3.20)$$

In Fig. 6.3 we show the running of these λ couplings for five pairs of $\{\mathbf{5} + \bar{\mathbf{5}}\}$ messengers and for two initial values of λ at the scale 10 TeV, $\lambda(10 \text{ TeV}) = 1$ and 2. It can be seen from the right panel of Fig. 6.3 that even for $\lambda(10 \text{ TeV}) = 2$, it grows very fast and hits a one-loop Landau-pole below $\sim 25 \text{ TeV}$. Needless to say, the situation gets worse if a larger number of messenger pairs is considered. Hence, we conclude from this analysis that values of λ much larger than unity at the messenger scale is not a possibility.

6.3.2 Estimate of the mass of S

It was shown in [413] that in renormalizable Wess-Zumino models with canonical Kähler potential, the existence of a massless fermion implies that the complex scalar in the same chiral multiplet remains massless at the tree level even if SUSY is spontaneously broken. As the fermion component of X is the goldstino in our case (which is exactly massless even at loop level), the scalar component of X , the sgoldstino will be massless at the tree level. However, in general, the sgoldstino is expected to acquire non-zero mass when loop corrections are included.

In our scenario, the sgoldstino mass gets contribution from the loops of messenger fields (apart from possible contributions from the hidden sector). The messenger contribution is computed in appendix D.3. The final result is given by (for N_5 pairs of $\mathbf{5} + \bar{\mathbf{5}}$ of $SU(5)$),

$$\Pi(p^2 = 0) = - \left(\frac{\lambda}{g_3^2} \right)^2 \left(4\pi \sqrt{\frac{5}{N_5}} F(x) \right)^2 m_g^2 \quad (6.3.21)$$

Hence, the potential for the sgoldstino gets a one-loop negative quadratic contribution from the messenger fields and this contribution is considerably larger in magnitude than the squared gluino mass¹³. This means that a large contribution from the hidden sector is required to stabilise the sgoldstino potential and somehow generate a small mass ~ 750 GeV for the sgoldstino.

At this point, we would like to remind the readers that, in our discussions till now, we have completely ignored specifying the details of the hidden sector and how SUSY is broken there. We just assumed that the chiral superfield X gets a SUSY breaking F -term VEV from the dynamics of the hidden sector without specifying the hidden sector at all. However, in order to understand whether a light sgoldstino can be obtained without too much tuning, we are now forced to consider the hidden sector as part of our model and think about the problem in its entirety. We postpone any further investigation of this issue to section 6.5.

6.4 Extra Ordinary Gauge Mediation

We have seen in the previous section that the OGM framework needs a very large number of messengers in order to explain the diphoton signal and avoid the strong constraints on the gluino and squark masses from LHC. We have also seen that such a large number of messengers renders the theory non-perturbative at scales as low as ~ 50 TeV, much below the GUT scale.

In this section we will consider a generalisation of the OGM framework namely, the Extra Ordinary Gauge Mediation (EOGM) where the OGM Lagrangian (Eq. 6.3.1) is supplemented with vector-like mass terms for the chiral superfields $\tilde{\Phi}_i$ and Φ_j [400]. Hence, we now have the EOGM superpotential

$$W_{\text{EOGM}} = (\lambda_{ij}X + m_{ij})\tilde{\Phi}_i\Phi_j, \quad (6.4.1)$$

where, λ_{ij} and m_{ij} are arbitrary complex matrices. As in the OGM scenario, the auxiliary field of X is assumed to get a VEV to break SUSY spontaneously. The fermion components of the messenger fields have the Dirac mass matrix,

$$m_F = \lambda_{ij}\langle\mathcal{S}\rangle + m_{ij}. \quad (6.4.2)$$

Without loss of generality, one can always go to the basis of $\tilde{\Phi}$ and Φ (by independent unitary rotations on them that do not affect their Kähler potential) where m_F is diagonal with real eigenvalues $(m_F)_i$. Hence, from now on we will assume that the matrix m_F is diagonal and the matrices λ_{ij} and m_{ij} are defined in the basis where m_F is diagonal. The scalar mass-squared matrix in this basis can now be written as,

$$\tilde{m}^2 = \begin{pmatrix} m_F^2 & -\lambda\langle F_x \rangle \\ -\lambda\langle F_x \rangle & m_F^2 \end{pmatrix}. \quad (6.4.3)$$

¹³Note that, models with non-polynomial superpotential can give rise to tree level sgoldstino mass. We compute the sgoldstino mass in one such model [442] in appendix D.3.3, however, again it turns out to be in general much larger than the gluino mass.

We will assume the matrix λ to be real and symmetric in order to impose invariance under CP and messenger parity (i.e., $\Phi_i \rightarrow \tilde{\Phi}_i$ in the basis where m_F is diagonal) in the messenger sector [402, 404].

The matrix \tilde{m}^2 can be block diagonalised by a suitable change of basis of the scalar fields, the block diagonalised matrix being,

$$\mathcal{M}^2 = \begin{pmatrix} m_+^2 & 0 \\ 0 & m_-^2 \end{pmatrix}, \quad (6.4.4)$$

where $m_\pm^2 = m_F^2 \pm \lambda \langle F_x \rangle$. Now assuming that the matrices m_\pm^2 are diagonalised by the unitary matrices U_\pm , the gaugino masses can be written as [410],

$$m_a = \frac{\alpha_a}{4\pi} \sum_{\pm} \sum_{i,j=1}^N (\pm) (U_\pm^\dagger)_{ij} (U_\pm)_{ji} m_j \frac{m_{\pm i}^2 \text{Log}(m_{\pm i}^2/m_j^2)}{m_{\pm i}^2 - m_j^2}. \quad (6.4.5)$$

Let us now consider only one pair of messengers to simplify the discussion. In this case the expressions of the gaugino masses and couplings c_a take the same form as the OGM case,

$$m_a = \frac{\alpha_a}{4\pi} \kappa m_F g(\kappa) \quad (6.4.6)$$

$$\frac{c_a}{M_a} = \frac{\alpha_a}{4\pi} \frac{\lambda}{m_F} g(\kappa) \quad (6.4.7)$$

the only difference being in the definition of m_F which now has the form,

$$m_F = \lambda \langle \mathcal{S} \rangle + m. \quad (6.4.8)$$

Hence, for fixed values of the messenger fermion masses, the situation is exactly the same as OGM. In the presence of many pair of messengers, if $[m_F, \lambda] = 0$ then the matrix λ can be diagonalised simultaneously with m_F and hence, the situation is again exactly the same as OGM with many messenger fields. In the case when $[m_F, \lambda] \neq 0$, in general, one has to analyse the situation numerically. Analytic results are known even in this case for $\lambda \langle F_x \rangle \ll m_F^2$ [400, 415]:

- The R charge for the field X , $R(X) \neq 0$: In this case the expression of the gaugino mass can be written as,

$$m_a = \frac{\alpha_a}{4\pi} n_{\text{eff}} \frac{\langle F_x \rangle}{\langle \mathcal{S} \rangle} \quad (6.4.9)$$

where,

$$n_{\text{eff}} = \frac{1}{R(X)} \sum_i \left(2 - R(\Phi_i) - R(\tilde{\Phi}_i) \right). \quad (6.4.10)$$

As n_{eff} is less than the total number of messengers, the gaugino mass in this case is always less than that in the OGM case.

- $R(X) = 0$, even in this case the expression of the gaugino mass simplifies to,

$$m_a = \frac{\alpha_a}{4\pi} \langle F_x \rangle \sum_i \frac{\lambda_{ii}}{m_F^i}, \quad (6.4.11)$$

If $\min(m_F^i) = m$, then

$$m_a \leq \frac{\alpha_a}{4\pi} \frac{\langle F_x \rangle}{m} \text{Tr} \lambda. \quad (6.4.12)$$

Hence, the situation is again the same as the OGM case.

We have checked numerically that the situation does not improve for the case when $\lambda \langle F_x \rangle \sim m_F^2$.

6.5 Way out?

We have seen in the previous sections that an sgoldstino explanation of the diphoton excess faces two major issues: i) the gaugino masses, and in particular the gluino mass, turn out to be rather low unless a very large number of messenger fields is considered; ii) the messenger particles yield a large negative one loop contribution to the sgoldstino potential. In this section, our goal is to look for potential solutions of the above problems.

6.5.1 D -term contribution to the gaugino mass

We have only considered F -term contribution to the gaugino mass in the previous sections. We will now assume that the messenger fields are also charged under some new $U(1)$ gauge group. The Φ fields have charge $+1$ and the $\tilde{\Phi}$ fields carry a charge -1 under this new $U(1)$. The relevant part of the Lagrangian is given by,

$$\mathcal{L} \subset \int d^4\theta \left(\Phi_i^\dagger e^{gV} \Phi_i + \tilde{\Phi}_i^\dagger e^{-gV} \tilde{\Phi}_i \right) + \int d^2\theta (\lambda_{ij} X + m_{ij}) \tilde{\Phi}_i \Phi_j + \text{h.c.} \quad (6.5.1)$$

The F -term of the chiral superfield X and the D -term of the vector superfield V are assumed to have VEVs $\langle F_x \rangle$ and $\langle D \rangle$ respectively¹⁴. However, since the above Lagrangian possesses an $U(1)$ R -symmetry, the charges being $R(\Phi) = 1, R(\tilde{\Phi}) = 1, R(X) = 0$ and $R(V) = 0$, it follows that the F -term and the D -term have the R -charges $R(F) = 2$ and $R(D) = 0$. Hence, $\langle F_x \rangle \neq 0$ breaks R -symmetry spontaneously, while $\langle D \rangle \neq 0$ does not. It is then clear that the gaugino masses must be associated with non-zero $\langle F_x \rangle$.

As we discussed previously, the leading F -term contribution to the gaugino mass comes from the term

$$-\frac{1}{2} \frac{c_F}{\Lambda} X W_A W^A. \quad (6.5.2)$$

¹⁴Note that the existence of non-zero $\langle D \rangle$ breaks the messenger parity spontaneously.

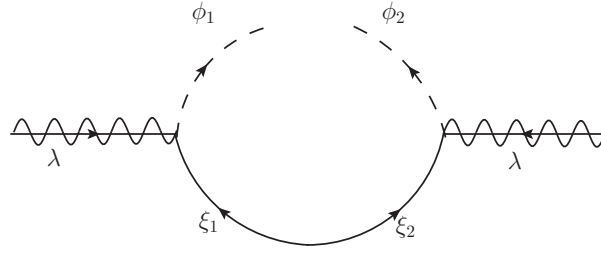


Figure 6.4: Diagram showing that a D -term does not contribute to the Majorana gaugino mass at the leading order in the F -term VEV.

As the gaugino mass is always associated with $\langle F_x \rangle$, the D -term contribution must always be suppressed by higher powers of Λ and hence, subdominant compared to the leading F -term contribution. That there is no D -term contribution at the leading order in the F -term VEV can also be understood diagrammatically. It can be seen from Fig. 6.4 that, in order to join the scalar lines, one needs a term $\phi_1\phi_2$ in the Lagrangian (refer to appendix D.3 for the notation) which does not arise from the D -term.

In models with explicitly broken R -symmetry, the lowest dimensional operators that can give rise to the gaugino mass should be,

$$-\frac{1}{2} \frac{c_D}{\Lambda_D^3} \widetilde{W} \widetilde{W} W_A W^A \quad (6.5.3)$$

which generates a contribution,

$$m_\lambda = c_D \frac{\langle D_{\widetilde{W}} \rangle^2}{\Lambda_D^3}, \quad (6.5.4)$$

which is subleading compared to (6.5.2). The chiral superfield \widetilde{W} belongs to the hidden sector and corresponds to either an abelian or a non-abelian gauge group. Note that, as mentioned before, the term in (6.5.3) breaks R -symmetry explicitly. We thus conclude that D -term contribution can not enhance the gaugino mass considerably.

We would like to comment in passing on the problem of vanishing leading order (in SUSY breaking F term VEV) gaugino masses in models of direct gauge mediation [428,429] and semi-direct gauge mediation [430], regardless of how the R -symmetry is broken. The authors of [413] proved this in generalised renormalizable O’Raifeartaigh models assuming a locally stable pseudomoduli space. This problem can be avoided with non-polynomial superpotential which naturally appears in many models of dynamical/non-perturbative SUSY breaking (DSB) [439–441]. Hence, the gaugino mass to leading order in $\langle F_x \rangle$ that were considered in the previous sections should indeed be thought in the framework of DSB models.

6.5.2 Metastable SUSY breaking

Before going to the discussion of metastable SUSY breaking, it is worth reviewing briefly the relation between R -symmetry and spontaneous SUSY breaking.

Consider a generic model of gauge mediated supersymmetry breaking in which a *Hidden* sector (HS) consisting of the superfields (Y_a, X) breaks supersymmetry and then *messenger* fields $(\Phi_i, \tilde{\Phi}_i)$ communicate the supersymmetry breaking to the *visible* MSSM sector via loop effects. The hidden sector fields are neutral under the Standard Model gauge group but could have its own gauge dynamics while the messenger fields $(\Phi_i, \tilde{\Phi}_i)$ transform in a vector like representation of SM gauge group and could also be charged under the HS gauge group.

Let us write the full superpotential of the theory as follows

$$W = W_{\text{HS}}(\{Y_a\}, X) + W_{\text{M}}(X, \Phi_i, \tilde{\Phi}_i) + W_{\text{MSSM}}, \quad (6.5.5)$$

with $W_{\text{M}} = \lambda_{ij} X \Phi_i \tilde{\Phi}_j + m_{ij} \Phi_i \tilde{\Phi}_j$.

Here W_{MSSM} is the MSSM superpotential and W_{HS} is hidden sector superpotential which spontaneously breaks SUSY¹⁵.

What can one say about the R -symmetry in W_{HS} ? Note that, for generic superpotential without R -symmetry, Nelson and Seiberg showed that a supersymmetric vacuum always exists [411]. In other words, R -symmetry is a necessary (but not sufficient) condition for spontaneous breaking of supersymmetry. However, unbroken R -symmetry forbids (Majorana) masses for the gauginos. Thus, it must be broken spontaneously which, in turn, would lead to a massless R -axion that may be dangerous for phenomenology¹⁶.

Another possibility is to break R -symmetry explicitly in hidden sector (W_{HS}). Now it is possible to write down models with no R -symmetry which break SUSY spontaneously but these models have a non-generic superpotential in the sense that it doesn't allow all renormalisable terms allowed by symmetries. As superpotential couplings are protected from renormalisation and hence are not generated at loop levels, a non generic superpotential is technically natural. However, it is tuned and not satisfactory.

One scenario which avoids these problems is metastable supersymmetry breaking [412]. It is based on the idea that though the true vacuum is supersymmetric, our universe lies in a metastable vacuum. In this picture, there is no need to keep R -symmetry but one does need to worry about decay rates from the metastable vacuum to the true vacuum and arrange for a long lived universe.

As mentioned in the previous section, the problem of vanishing leading order (in SUSY breaking F -term) gaugino masses can be avoided in models of DSB. Hence, DSB in a metastable vacuum is an attractive phenomenological possibility. In fact, some of these models can potentially solve the problem mentioned in section 6.3.2 and give rise to a light sgoldstino [425–427]. However, detailed exploration of these models is necessary to see whether they can indeed serve as natural models for a light sgoldstino and avoid the problems mentioned in section 6.3.

¹⁵Note that the R -parity conserving MSSM has three parameter worth of R -symmetries. However, R -symmetry has gauge anomalies in the MSSM.

¹⁶ R -symmetry may be broken by Gravity effects, thus giving mass to the R -axion [397]

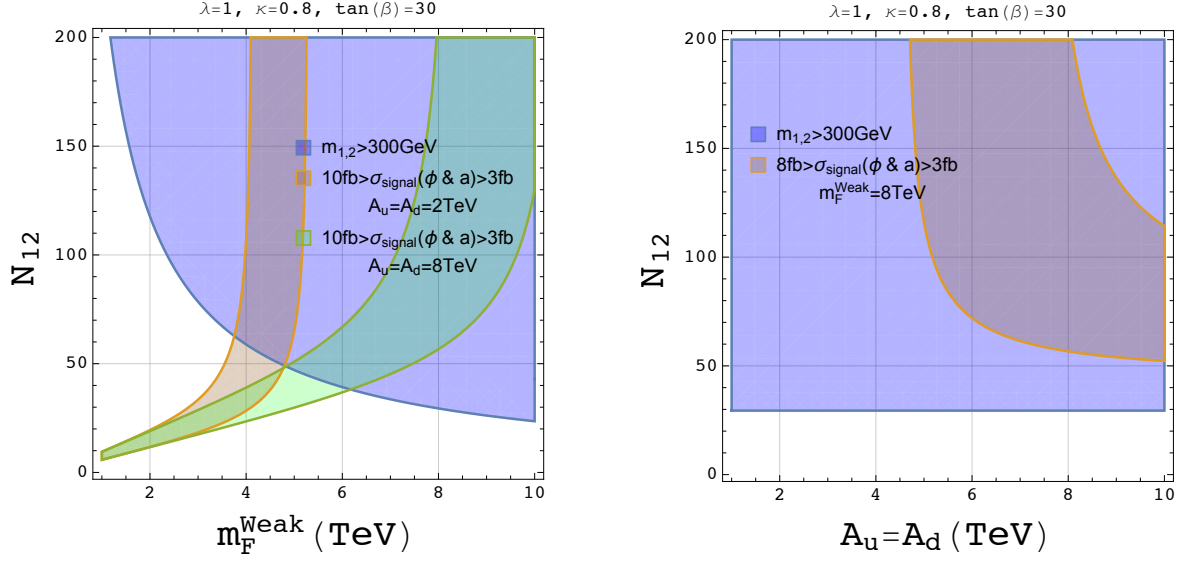


Figure 6.5: Allowed region in the case of quark anti-quark initiated production of the sgoldstino. See text for more details.

6.5.3 Quark anti-quark initiated production of the sgoldstino

In this section, we consider the possibility that the production cross section of sgoldstino has a significant contribution from quark anti-quark initial state. The coupling of the sgoldstino to the quark anti-quark pair can arise from the same effective Lagrangian that generates the trilinear A -terms namely,

$$\mathcal{L}_{\text{trilinear}} \subset \frac{A_u}{\langle F_x \rangle} \int d^2\theta X H_u Q U^c + \frac{A_d}{\langle F_x \rangle} \int d^2\theta X H_d Q D^c + \text{h.c.} \quad (6.5.6)$$

which generates following couplings for the sgoldstino,

$$\frac{v \sin \beta A_u}{\sqrt{2} \langle F_x \rangle} \mathcal{S} \bar{u} P_L u, \quad \frac{v \cos \beta A_d}{\sqrt{2} \langle F_x \rangle} \mathcal{S} \bar{d} P_L d. \quad (6.5.7)$$

The decay rates $\Gamma(\phi \rightarrow \bar{u} u)$ and $\Gamma(\phi \rightarrow \bar{d} d)$ can now be calculated from the above Lagrangian and read,

$$\Gamma(\phi \rightarrow \bar{u} u) = \left[\frac{1}{2m_\phi} \right] \left[\frac{1}{8\pi} \right] \left[\left(\frac{v \sin \beta A_u}{\sqrt{2} \langle F_x \rangle} \right)^2 3m_\phi^2 \right], \quad (6.5.8)$$

$$\Gamma(\phi \rightarrow \bar{d} d) = \left[\frac{1}{2m_\phi} \right] \left[\frac{1}{8\pi} \right] \left[\left(\frac{v \cos \beta A_d}{\sqrt{2} \langle F_x \rangle} \right)^2 3m_\phi^2 \right], \quad (6.5.9)$$

where we have neglected the quark masses. In this limit, the corresponding decay rates of a have the same expressions with m_ϕ replaced by m_a .

We now assume that the production of sgoldstino is mostly by the $\bar{u} u$ and $\bar{d} d$ initial states so that a large coupling to gluons is not necessary. We define the number of messengers with quantum numbers $(1, 2)_{1/2}$ to be N_{12} . Their mass will be denoted by m_F^{Weak} . In the

left panel of Fig. 6.5 we show the allowed region in the $N_{12} - m_F^{\text{weak}}$ plane when two sets of values for A_u and A_d are chosen¹⁷. Similarly, in the right panel the allowed region in the $N_{12} - A_u/A_d$ plane is shown for $m_F^{\text{weak}} = 8 \text{ TeV}$. It can be seen that even for very large value of $A_u = A_d \sim 10 \text{ TeV}$ ¹⁸, quite low masses for the electroweak messenger fields $m_F^{\text{weak}} \lesssim 10 \text{ TeV}$ with a very large multiplicity $\gtrsim 50$ are necessary. Consequently, the $SU(2)$ and $U(1)$ couplings (i.e., $g_i^2/4\pi$) hit Landau poles typically below few hundred TeV. For example, for $m_F^{\text{weak}} = 8 \text{ TeV}$ and $N_{12} = 100$, the one loop Landau poles for $SU(2)$ and $U(1)$ appear around 50 TeV and 200 TeV respectively.

As the SUSY breaking F -term VEV $\langle F_x \rangle$ must be less than $(m_F^{\text{weak}})^2$ in order to avoid tachyons in the messenger sector, it also turns out that a gluino mass of more than 1.5 TeV again requires a very large number of $SU(3)$ messengers, exactly as in the OGM scenario discussed earlier.

However, one could consider a scenario where the X superfields that couple to the $SU(3)$ messengers (denoted by Φ_3 and $\tilde{\Phi}_3$ below) are different from the X superfields that couple to the $SU(2)$ messengers (denoted by Φ_2 and $\tilde{\Phi}_2$ below) so that,

$$W = (X_2 + m_2)\tilde{\Phi}_2\Phi_2 + (X_3 + m_3)\tilde{\Phi}_3\Phi_3, \quad (6.5.10)$$

The X_2 and X_3 superfields get VEVs given by,

$$\langle X_2 \rangle = \langle \mathcal{S}_2 \rangle + \theta\theta\langle F_2 \rangle, \quad (6.5.11)$$

$$\langle X_3 \rangle = \langle \mathcal{S}_3 \rangle + \theta\theta\langle F_3 \rangle. \quad (6.5.12)$$

One can define two complex scalars that are linear combinations of \mathcal{S}_2 and \mathcal{S}_3 ,

$$\mathcal{S}_h = \frac{F_2\mathcal{S}_2 + F_3\mathcal{S}_3}{\sqrt{F_2^2 + F_3^2}} \quad (6.5.13)$$

$$\mathcal{S}_l = \frac{-F_3\mathcal{S}_2 + F_2\mathcal{S}_3}{\sqrt{F_2^2 + F_3^2}} \quad (6.5.14)$$

In the limit of $F_3 \gg F_2$, $\mathcal{S}_h \approx \mathcal{S}_3$ and $\mathcal{S}_l \approx \mathcal{S}_2$. If we now assume that the scalar \mathcal{S}_l is actually the 750 GeV resonance and the other scalar \mathcal{S}_h is much heavier then the diphoton signal can be explained. Moreover, as F_3 is now assumed to be much large than F_2 , large gluino mass can also be easily obtained.

However, it should be mentioned that the scalar \mathcal{S}_l is actually not the sgoldstino. It is actually \mathcal{S}_h which appears in the goldstino multiplet, hence, \mathcal{S}_h should be identified as the sgoldstino. In this sense, we have not solved the original problem with sgoldstino being the candidate for the 750 GeV resonance.

¹⁷In general, A -terms are generated at 1-loop level in the models of messenger matter interactions. Thus they are of same order of the gaugino masses. Larger A -terms can be obtained from model where A -terms are generated at the tree level [401]. These models have the advantage of being free from A/m^2 problem [403].

¹⁸Note that very large A -terms may give rise to electric charge and $SU(3)$ colour breaking minima in the potential [449, 450], thus we restrict them to 10 TeV in our analysis.

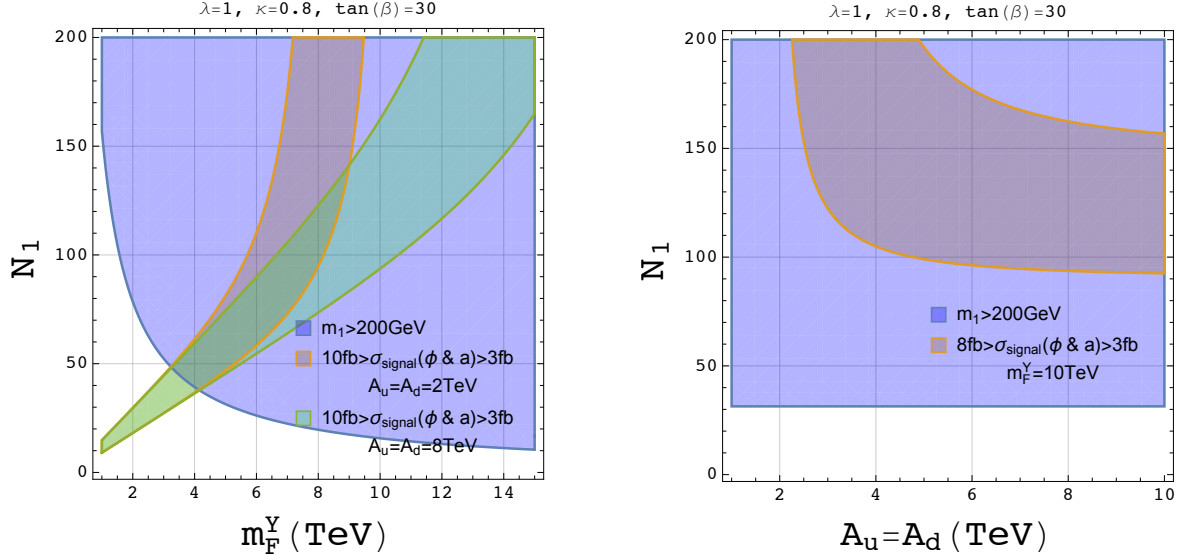


Figure 6.6: Allowed region in the case of quark anti-quark initiated production of the sgoldstino with only light hypercharge messengers.

Before concluding this section, we would also like to point out that one can also consider the extreme case when there are three different superfields X_1 , X_2 and X_3 that couple to the $U(1)$, $SU(2)$ and $SU(3)$ messengers respectively. In this case, both the $SU(2)$ and $SU(3)$ messenger masses can be very high. In Fig. 6.6 we show the number of $U(1)$ messengers (N_1) and their mass (m_F^Y) required for the correct amount of signal and also mass of Bino more than 200 GeV. It can be seen that for $m_F^Y \sim 5 \text{ TeV}$ one needs $N_1 \gtrsim 50$. The Landau pole in the $U(1)$ gauge coupling only appears around 2000 TeV in this case.

6.6 Conclusion

In this paper we have carefully studied the possibility of an sgoldstino being a candidate for the signal of a possible new resonance with mass $\sim 750 \text{ GeV}$ recently reported by the ATLAS and CMS collaborations. We have found that the explanation of the signal is in tension with the lower bound on masses from direct searches of gauginos, in particular, the gluino. In order to achieve a large enough gluino mass, a very large number of messenger fields is required, which, in turn, renders the theory non-perturbative at a rather low scale of order few tens of TeV. Moreover, we find that the one-loop messenger contribution to the sgoldstino potential is negative and large in magnitude (larger than the gluino mass squared). Hence, a large positive contribution from the hidden sector is required to tune this away and get a small mass $\sim 750 \text{ GeV}$ for the sgoldstino.

While there exist examples of models with dynamically broken SUSY where a light sgoldstino can, in principle, be achieved, perhaps without large tuning, getting both the correct amount of signal cross-section and also large enough gluino and squark masses (without spoiling the calculability of the theory at a rather low scale) seems to be a stubborn problem. It would

be interesting to find explicit models where these problems can be overcome in a satisfactory way. We postpone investigation in this direction to future studies.

We have also considered the possibility of the resonance being produced by quark anti-quark initial state. While in this case the problem of Landau poles can be delayed beyond few thousand TeV, the scalar resonance can not be the sgoldstino.

Conclusion

The work presented in this thesis aims to highlight some aspects of the search for physics beyond the Standard Model (BSM) using both direct and indirect search strategies. With the LHC running at peak potential, this is the ripe time for a successful hunt for BSM physics. The studies presented in this thesis focus on the different aspects of such a search.

The scope of direct searches at colliders is naturally limited by the centre-of-mass energy of the collisions. While the LHC is expected to probe the range up to about 2-3 TeV quite well, BSM physics might well lie beyond this energy range. A theoretical tool which allows one to probe regions beyond this energy range is looking at virtual effects of heavy particles. Any existent heavy BSM particle will contribute to a process in excess over the Standard Model (SM) contribution and thereby modify experimentally-measurable quantities like branching ratios. To actually see these effects we must choose a process for which the SM contribution is known to be extremely small so that BSM physics would be able to modify it significantly.

Decay processes of interest for such a study are decays via flavour-changing neutral currents in the quark sector, which are known to be absent at tree level in the SM. Of particular interest are the flavour-changing neutral current decays of the top quark, since they are easy to identify in the final states at a hadronic collider like the LHC. We showed in our work that since the branching ratios of $t \rightarrow cH$ and $t \rightarrow cZ$ in the SM are exceedingly small, they are good processes to consider for BSM effects. In order to understand the process, we took a toy model which possesses the essential features of the SM weak sector. Our analysis serves to highlight the three possible sources of suppression of the branching ratio of the process in the SM, and thus the possible avenues for enhancement. This provides a useful ready reckoner to check if a new model with BSM physics can enhance top quark FCNC decays at all. We concluded that a model like the cMSSM cannot contribute enough to the branching ratio so as to bring it to the projected reach of the LHC, but, under certain conditions, R-parity-violating SUSY might be able to fulfill the requirements.

Apart from studying flavour-changing processes via neutral currents, we also focussed on flavour changes in the quark sector via charged currents. From a theoretical standpoint, one of the most exciting results have been observed in this regime are the charged current decay processes of $B^0 \rightarrow D\ell\nu$ and $B^0 \rightarrow D^*\ell\nu$, where ℓ is any of the three leptons. Recent measurements of ratios such as R_D and R_{D^*} have shown deviations from the SM and have hinted at possible lepton non-universality. Approaching the problem from a model-independent effective theory point of view, we computed the values of the different Wilson coefficients required to explain the discrepancy, assuming that BSM physics affects the third leptonic generation alone. Several numerical calculations relating to the different observables of the decays were performed. Additionally, for the first time in literature, we provided completely general formulae for the matrix elements, considering all relevant six-dimensional operators, including the tensorial operators. The formulae are listed in the Appendix of this thesis.

Direct searches, of course, precede rather than accompany indirect searches. We therefore performed a collider study for a certain simplified model in R-parity-violating SUSY. Given that the third generation squarks can be light and might be probed by the LHC, the lighter sbottom is the lightest supersymmetric particle in the simplified spectrum of our choice. It decays to a top quark along with a light quark. State-of-the-art multivariate analysis techniques were employed to study this decay both in the leptonic and in the hadronic channel. Investigations confirm our expectations that the leptonic channel is more promising than the hadronic channel in terms of discovery or exclusion.

Towards the end of 2015, there was much excitement because both the CMS and ATLAS collaborations of the LHC seemed to be seeing a resonance at ~ 750 GeV in the diphoton channel. This created huge interest in the high energy physics community, as it would be a clear BSM signal, if confirmed. Many candidates for this kind of a resonance were proposed. One interesting suggestion was that it was a sgoldstino, the scalar partner of the Goldstino associated with the spontaneous-breaking of supersymmetry. We investigated various aspects of the proposal and found that such a model would be quite untenable. In fact, later, by the middle of 2016, the erstwhile signal disappeared and it is now thought to be a mere fluctuation. The negative conclusion of our work thus, in a way, stands vindicated for that particular proposal, and moreover, tells us what to expect if there is indeed a sgoldstino and its signals are seen. Our analysis may be treated as a example of how a proposal for the candidate of a reported excess might be investigated. It demonstrates that a holistic approach to an analysis of a reported excess is important and that consequences of the suggestion, including the effect of messenger particles on the coupling constant, the mass of the sgoldstino, etc., are to be considered beyond the obvious branching ratio.

There are a number of ways in which the work presented in this thesis could remain relevant and useful in the future.

- The analysis methods for the top rare decays are independent of the model used and can be used for a generic analysis in the future. For a model to predict a branching ratio for the top rare decays to the Higgs or Z boson, which would be observable either

at the LHC or a future collider, it would have to satisfy the level of enhancements as found from our study. This provides a quick check of the viability of such models.

- Similar statements can be made about the model-independent flavour physics results. Furthermore, a generic numerical treatment of the process will greatly benefit from the general formulae provided in the Appendix.
- Our analysis of signals for decaying squarks of the third generation, even if not the final word on the subject (which can only come with increasing data), does set out a paradigm for such analyses.
- The evaluation of a sgoldstino candidate for the CERN 750 GeV resonance can form a useful caveat for the future, that any explanation of an observed experimental anomaly should be consistent with all the observations, and not just the one in question.

There is, of course, scope for further work following what has been done in the thesis. Future studies may focus on the limitations of a completely model independent study in flavour physics using six-dimensional operators. This could shed more light on the various assumptions which are involved in the study of charged current and neutral current decays of mesons, especially those containing the b -quark. Furthermore, one may be interested in the effects of different operators in the context of neutral B -meson decays, the study of which compliments the neutral current decays of the B -meson, especially in the context of BSM physics. As it is increasingly becoming evident that the LHC might be able to probe only third generation squarks, more sophisticated collider analyses of such particles will serve as blueprints for future studies.

Plans to run the LHC at its current energy till the year 2035 seem to be on firm footing now, and the experimental collaborations are expected to steadily collect more and more data as the run proceeds. The quantum of flavour data for B -mesons will also rise in volume as B -factories like Belle-II and LHCb promise to deliver very high luminosity in the very near future. This new data might soon indicate a direction for the departure from the SM. It is hoped that the contents of this thesis, in their own humble way, would further the cause of this global scientific pursuit of BSM physics over the next two decades.

Appendix A

FCNC Processes in the SM: CP Violation

A.1 CKM Matrix and Unitarity Triangles

The CKM matrix, as stated above, is written defined as

$$\mathbf{V}_{\text{CKM}} \equiv \mathbf{V} = \mathbf{V}_L^u \mathbf{V}_L^{d\dagger}$$

The matrices \mathbf{V}_L^u and \mathbf{V}_L^d being unitary makes \mathbf{V} unitary as well. The unitarity of the CKM matrix is mathematically given by the two following equations:

$$\sum_{i=1}^3 |V_{ij}|^2 = 1 \quad j = 1, 2, 3 \quad (1.1.1)$$

$$\sum_{i=1}^3 V_{ji} V_{ki}^* = \sum_{i=1}^3 V_{ij} V_{ik}^* = 0 \quad j, k = 1, 2, 3 \quad (1.1.2)$$

Eqn. 1.1.1 expresses weak universality since it says that the sum of the couplings of any up-type quark to all the down-type quark is the same regardless of the quark generation. Eqn. 1.1.2 provides a constraint on the size of the CKM matrix elements. It represents six triangles in a complex plane, each of which has equal area, given as $J_{CP}/2$, where

$$J_{CP} = |\Im(V_{ik}^* V_{jk} V_{il} V_{jl}^*)|; \quad i, j, k, l = 1, 2, 3 \quad (1.1.3)$$

is called the Jarlskog invariant [21] and is true for any value of i, j, k, l . These six triangles are called unitary triangles.

There are, in principle, an infinite number of ways to represent the CKM matrix and all are mathematically equivalent to each other. A standard representation is given by the Particle Data Group (PDG) [22]

$$V = \begin{pmatrix} c_{12}c_{13} & s_{12}c_{13} & s_{13}e^{-i\delta} \\ -s_{12}c_{23} - c_{12}s_{23}s_{13}e^{i\delta} & c_{12}c_{23} - s_{12}s_{23}s_{13}e^{i\delta} & s_{23}c_{13} \\ s_{12}s_{23} - c_{12}c_{23}s_{13}e^{i\delta} & -c_{12}s_{23} - s_{12}c_{23}s_{13}e^{i\delta} & c_{23}c_{13} \end{pmatrix} \quad (1.1.4)$$

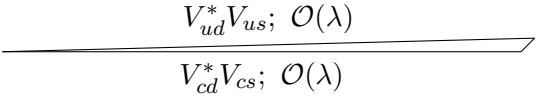
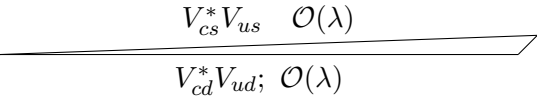
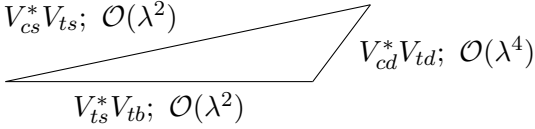
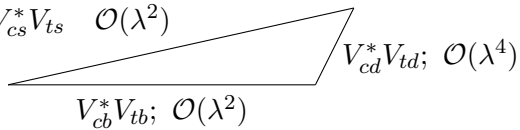
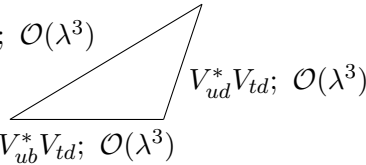
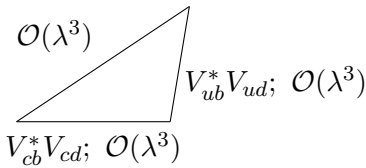
Unitary relation	Triangle representation
$V_{cd}^* V_{cs} + V_{td}^* V_{ts} + V_{ud}^* V_{us} = 0$	
$V_{cd}^* V_{ud} + V_{cb}^* V_{ub} + V_{us}^* V_{cs} = 0$	
$V_{ts}^* V_{tb} + V_{cd}^* V_{td} + V_{cs}^* V_{ts} = 0$	
$V_{cb}^* V_{tb} + V_{cb}^* V_{ub} + V_{cs}^* V_{ts} = 0$	
$V_{ub}^* V_{td} + V_{cb}^* V_{ub} + V_{us}^* V_{ts} = 0$	
$V_{cb}^* V_{cd} + V_{cb}^* V_{ub} + V_{tb}^* V_{td} = 0$	

Table A.1: The six different unitary triangles of the CKM matrix.

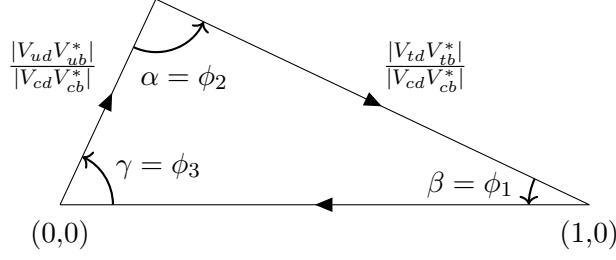


Figure A.1: Angles in the unitary triangle

Phenomenologically, however, it makes sense to exploit the observation that

$$|V_{ub}| \ll |V_{cb}| \ll |V_{us}| \ll 1; \quad |V_{ud}| \simeq |V_{tb}| = 1 \quad (1.1.5)$$

In order to accommodate this information, we can express the matrix as an expansion in $\lambda = |V_{us}| = \sin \theta_C \simeq 0.23$ (where θ_C is called the Cabibbo angle [23]). Up to $\mathcal{O}(\lambda^4)$, the CKM matrix can be written as

$$V = \begin{pmatrix} 1 - \frac{1}{2}\lambda^2 & \lambda & A\lambda^3(\rho - i\eta + \frac{i}{2}\eta\lambda^2) \\ -\lambda & 1 - \frac{1}{2}\lambda^2 - i\eta A^2\lambda^4 & A\lambda^2(1 + i\eta\lambda^2) \\ A\lambda^3(1 - \rho - i\eta) & -A\lambda^2 & 1 \end{pmatrix} \quad (1.1.6)$$

This is called the Wolfenstein parametrisation of the CKM matrix [24]. The four parameters of the CKM matrix are replaced by four real numbers $-\lambda, A, \rho, \eta$. In this parameterisation, the diagonal elements are almost (or exactly) unity and the magnitude falls off as one moves away from the diagonal due to increasing powers of λ . Furthermore, the matrix is nearly symmetric. Both these features accurately represent experimental observations. The edges of the six unitary triangles can be expressed as powers of λ and is shown in Table A.1, along with the corresponding constraint relations. Depending on the magnitudes of the sides of the triangles, two of the triangles (listed as the first two in the table) are highly squashed, while the next two are somewhat less squashed. The last two triangles have sides of nearly equal length and are thus expected to have large angles, which allows for easier measurements at colliders. These two triangles have factors which determine bottom transitions. In Section A.4, it will be shown that the amount of CP asymmetry in the b-system is dependent on the value of an angle in this triangle; the angle being large produces a large CP asymmetry in b-systems.

The angles of the last unitarity triangle are indicated in Figure A.1 and they are (according to two equivalent naming conventions) given by

$$\alpha = \phi_2 = \arg\left(-\frac{V_{td}V_{tb}^*}{V_{ud}V_{ub}^*}\right); \quad \beta = \phi_1 = \arg\left(-\frac{V_{cd}V_{cb}^*}{V_{td}V_{tb}^*}\right); \quad \gamma = \phi_3 = \arg\left(-\frac{V_{ud}V_{ub}^*}{V_{cd}V_{cb}^*}\right) \quad (1.1.7)$$

A.2 Oscillations of Neutral Mesons: Formalism

A neutral meson, generically called P^0 in this section and in the next, can oscillate between P^0 and \bar{P}^0 states. The particle can in the meanwhile also undergo decay and thus the Hamiltonian describing this process is not Hermitian. It can be written as a sum of Hermitian and anti-Hermitian pieces :

$$\mathcal{H} = \mathbf{M} - \frac{i}{2}\mathbf{\Gamma} = \begin{pmatrix} M_{11} & M_{12} \\ M_{12}^* & M_{11} \end{pmatrix} - \frac{i}{2} \begin{pmatrix} \Gamma_{11} & \Gamma_{12} \\ \Gamma_{12}^* & \Gamma_{11} \end{pmatrix} \quad (1.2.1)$$

where \mathbf{M} and $\mathbf{\Gamma}$ are Hermitian. We have already assumed that the two interaction states have equal masses and have the same decay widths (i.e. $M_{22} = M_{11}$ and $\Gamma_{22} = \Gamma_{11}$ (as demanded by CPT invariance) and that $M_{21} = M_{12}^*$, $\Gamma_{21} = \Gamma_{12}^*$ by the condition of hermiticity. P^0 and \bar{P}^0 are the interaction eigenstates and there exist two mass eigenstates misaligned with the interaction eigenstates – P_L and P_H , for light and heavy states. At the initial time ($t = 0$)

$$|P_L(0)\rangle = p|P^0\rangle + q|\bar{P}^0\rangle \quad |P_H(0)\rangle = p|P^0\rangle - q|\bar{P}^0\rangle \quad (1.2.2)$$

which gives

$$|P^0\rangle = \frac{1}{2p} (|P_L(0)\rangle + |P_H(0)\rangle) \quad (1.2.3)$$

Under time evolution due to the Hamiltonian in Eqn. 1.2.1, we have

$$\begin{aligned} |P^0(t)\rangle &= \frac{1}{2p} (|P_L(t)\rangle + |P_H(t)\rangle) \\ &= \frac{1}{2p} \left(e^{-i(M_L - \frac{i}{2}\Gamma_L)t} |P_L(0)\rangle + e^{-i(M_H - \frac{i}{2}\Gamma_H)t} |P_H(0)\rangle \right) \\ &= \frac{1}{2p} \left(e^{-i(M_L - \frac{i}{2}\Gamma_L)t} (p|P^0\rangle + q|\bar{P}^0\rangle) + e^{-i(M_H - \frac{i}{2}\Gamma_H)t} (p|P^0\rangle - q|\bar{P}^0\rangle) \right) \\ &= g_+(t) |P^0\rangle + \frac{q}{p} g_-(t) |\bar{P}^0\rangle \end{aligned} \quad (1.2.4)$$

where we have inverted in the second last step using Eqn. 1.2.2 and

$$g_{\pm} = \frac{1}{2} \left(e^{-i(M_L - \frac{i}{2}\Gamma_L)t} \pm e^{-i(M_H - \frac{i}{2}\Gamma_H)t} \right) \quad (1.2.5)$$

Similarly, the state starting out as $|\bar{P}^0\rangle$ at $t = 0$, evolves to a state $|\bar{P}^0(t)\rangle$ given by

$$|\bar{P}^0(t)\rangle = \frac{p}{q} g_-(t) |P^0\rangle + g_+(t) |\bar{P}^0\rangle \quad (1.2.6)$$

Oscillation between the states $|P^0\rangle$ and $|\bar{P}^0\rangle$ will give rise to CP violation if the two states are the two conjugate CP eigenstates, i.e. $\text{CP} |P^0\rangle = e^{i\delta} |\bar{P}^0\rangle \implies \text{CP} |\bar{P}^0\rangle = e^{-i\delta} |P^0\rangle$.

A.3 Measuring CP Violation: Formalism

The first detection of CP violation happened in 1964 due to Cronin and Fitch. The experiment involved neutral kaons and their decay. The two flavour eigenstates for the kaons K^0 and \bar{K}^0

are misaligned from the CP eigenstates K_S (CP = +1) and K_L (CP = -1) (called K -short and K -long respectively). The names have been chosen because K_S decays quite rapidly compared to K_L and thus if a beam of kaons is fired along a beam pipe, the K_L would preferably survive after a certain length. Thus, with a longer beam length, one is expected to end up with an arbitrarily pure K_L state. It happens to be that K_S can decay to two pions whereas K_L to three pions, which is a fortunate kinematic accident. Thus, if after a sufficiently long distance, if one were to see 2π decay, representing the presence of K_S , it would mean that the CP of the state flipped from -1 to +1 and is thus not conserved. The experimentalists measured 2π decays even at the end of the 17m beamline at a rate of about 1 in 500, much higher than that expected if CP were conserved.

It beckons us to understand CP violation more formally. Consider the final state f and its CP conjugate \bar{f} . Using the evolution equations in Eqns. 1.2.4 and 1.2.6, the matrix element for the decay of P^0 to f is given by

$$\begin{aligned}\mathcal{M}(|P^0(t)\rangle \rightarrow |f\rangle) &= g_+ \langle f | \mathcal{H} | P^0 \rangle + \frac{q}{p} g_- \langle f | \mathcal{H} | \bar{P}^0 \rangle \\ &= g_+(t)A(f) + \frac{q}{p} g_-(t)\bar{A}(f)\end{aligned}\quad (1.3.1)$$

Thus, for calculating the decay width, we get

$$\begin{aligned}\Gamma(|P^0(t)\rangle \rightarrow |f\rangle) &\propto |\mathcal{M}(|P^0(t)\rangle \rightarrow |f\rangle)|^2 \\ &\propto |A(f)|^2 \left[|g_+(t)|^2 + 2\Re\left(\frac{q}{p}g_+g_-\bar{\rho}(f)\right) + \left|\frac{q}{p}\right|^2 |g_-(t)|^2 |\bar{\rho}(f)|^2 \right]\end{aligned}\quad (1.3.2)$$

where

$$\bar{\rho}(f) = \frac{\bar{A}(f)}{A(f)} = \frac{1}{\rho(f)} \quad (1.3.3)$$

Similarly, one can compute the following

$$\begin{aligned}\Gamma(|\bar{P}^0(t)\rangle \rightarrow |f\rangle) &\propto |\bar{A}(f)|^2 \left[|g_+(t)|^2 + 2\Re\left(\frac{p}{q}g_+g_-\rho(f)\right) + \left|\frac{p}{q}\right|^2 |g_-(t)|^2 |\rho(f)|^2 \right] \\ \Gamma(|P^0(t)\rangle \rightarrow |\bar{f}\rangle) &\propto |A(\bar{f})|^2 \left[|g_+(t)|^2 + 2\Re\left(\frac{q}{p}g_+g_-\bar{\rho}(\bar{f})\right) + \left|\frac{q}{p}\right|^2 |g_-(t)|^2 |\bar{\rho}(\bar{f})|^2 \right] \\ \Gamma(|\bar{P}^0(t)\rangle \rightarrow |\bar{f}\rangle) &\propto |\bar{A}(\bar{f})|^2 \left[|g_+(t)|^2 + 2\Re\left(\frac{p}{q}g_+g_-\rho(\bar{f})\right) + \left|\frac{p}{q}\right|^2 |g_-(t)|^2 |\rho(\bar{f})|^2 \right]\end{aligned}\quad (1.3.4)$$

CP asymmetry is then measured to be

$$\mathcal{A}_{\text{CP}} = \frac{\Gamma(|P^0(t)\rangle \rightarrow |f\rangle) - \Gamma(|\bar{P}^0(t)\rangle \rightarrow \bar{f})}{(\Gamma(|P^0(t)\rangle \rightarrow |f\rangle) + \Gamma(|\bar{P}^0(t)\rangle \rightarrow \bar{f}))} \quad (1.3.5)$$

CP violation in mesonic systems can be of three different types. For each of the cases, we use Eqns. (1.3.2 and 1.3.4) to calculate the CP violation.

1. *Through Decay*: There is (almost) no oscillation between the two CP eigenstates, but the magnitude of the amplitude of the decay of a neutral meson P to a final state f is not the same as the CP conjugate of the process, i.e.

$$|A(f)| \neq |\bar{A}(\bar{f})| \quad (1.3.6)$$

In this case, $M_L = M_H$ and $\Gamma_L = \Gamma_H = \Gamma$, which gives $g_- = 0$ and $|g_+|^2 = e^{-\Gamma t}$. Thus,

$$\mathcal{A}_{\text{CP}} = \frac{|A(f)|^2 - |\bar{A}(\bar{f})|^2}{|A(f)|^2 + |\bar{A}(\bar{f})|^2} \quad (1.3.7)$$

which is non-zero only because the amplitudes for the two processes are different. This is also called CP violation through decay or Direct CP violation.

2. *Flavour specific decays*: This occurs when P can decay to a final state f , whereas the CP conjugate cannot decay to the same state. By the analysis of the final state, the identity of the decaying meson can be ascertained. Thus,

$$P \rightarrow f \quad \text{but} \quad \bar{P} \not\rightarrow f \quad (1.3.8)$$

The P meson can oscillate to a \bar{P} which can then decay to a \bar{f} . Even if the $|A(P \rightarrow f)| = |\bar{A}(\bar{P} \rightarrow \bar{f})|$, the mixing between the two CP states gives a measure of CP violation. In the scenario when the two amplitudes are equal in magnitude, the CP asymmetry is given by

$$\mathcal{A}_{\text{CP}} = \frac{1 - |p/q|^4}{1 + |p/q|^4} \quad (1.3.9)$$

3. *Flavour non-specific decays*: This occurs when both the meson P and its CP conjugate state \bar{P} go to the same final state f . There are two different scenarios to consider :

- (a) When $|A(f)| = |\bar{A}(f)|$ – This holds when f is a CP eigenstate. CP asymmetry will occur solely through neutral meson oscillations. Thus, with $|A(P \rightarrow f)| = |\bar{A}(\bar{P} \rightarrow f)|$ and $|q/p| = 1$,

$$\begin{aligned} \mathcal{A}_{\text{CP}} &= \frac{\Gamma(|P^0(t)\rangle \rightarrow |f\rangle) - \Gamma(|\bar{P}^0(t)\rangle \rightarrow |f\rangle)}{\Gamma(|P^0(t)\rangle \rightarrow |f\rangle) + \Gamma(|\bar{P}^0(t)\rangle \rightarrow |f\rangle)} \\ &= \frac{\Re\left(\frac{q}{p}g_+^*g_- \bar{\rho}(f)\right) - \Re\left(\frac{p}{q}g_+^*g_- \rho(f)\right)}{|g_+|^2 + |g_-|^2 + \Re\left(\frac{q}{p}g_+^*g_- \bar{\rho}(f)\right) + \Re\left(\frac{q}{p}g_+^*g_- \bar{\rho}(f)\right)} \\ &= \frac{-2 \sin(\arg(q/p) + \arg(\bar{\rho}(f))) e^{\frac{1}{2}\Delta\Gamma t} \sin(\Delta M t)}{1 + e^{\Delta\Gamma t} + \cos(\arg(q/p) + \arg(\bar{\rho}(f))) (1 - e^{\Delta\Gamma t})} \end{aligned} \quad (1.3.10)$$

since one can write $g_+^*g_- = \frac{1}{4}e^{-\Gamma_L t} \left(1 + e^{\Delta\Gamma t} - 2ie^{\frac{1}{2}\Delta\Gamma t} \sin(\Delta M t)\right)$ with $\Delta M = M_H - M_L$ and $\Delta\Gamma = \Gamma_L - \Gamma_H$. It is noteworthy that both (q/p) , which is an oscillation parameter, and $\bar{\rho}(f)$, which is a decay parameter, contribute to the CP asymmetry.

- (b) When $|A(f)| \neq |\bar{A}(f)|$ – This is the more general case for a CP eigenstate. In this case,

$$\begin{aligned} \mathcal{A}_{\text{CP}} &= \frac{\Gamma(|P^0(t)\rangle \rightarrow |f\rangle) - \Gamma(|\bar{P}^0(t)\rangle \rightarrow |f\rangle)}{\Gamma(|P^0(t)\rangle \rightarrow |f\rangle) + \Gamma(|\bar{P}^0(t)\rangle \rightarrow |f\rangle)} \\ &= C_f \cos(\Delta Mt) - S_f \sin(\Delta Mt) \end{aligned} \quad (1.3.11)$$

with

$$C_f = \frac{1 - |\bar{\rho}(f)|^2}{1 + |\bar{\rho}(f)|^2} \quad ; \quad S_f = \frac{2\Im((q/p)\bar{\rho}(f))}{1 + |\bar{\rho}(f)|^2} \quad (1.3.12)$$

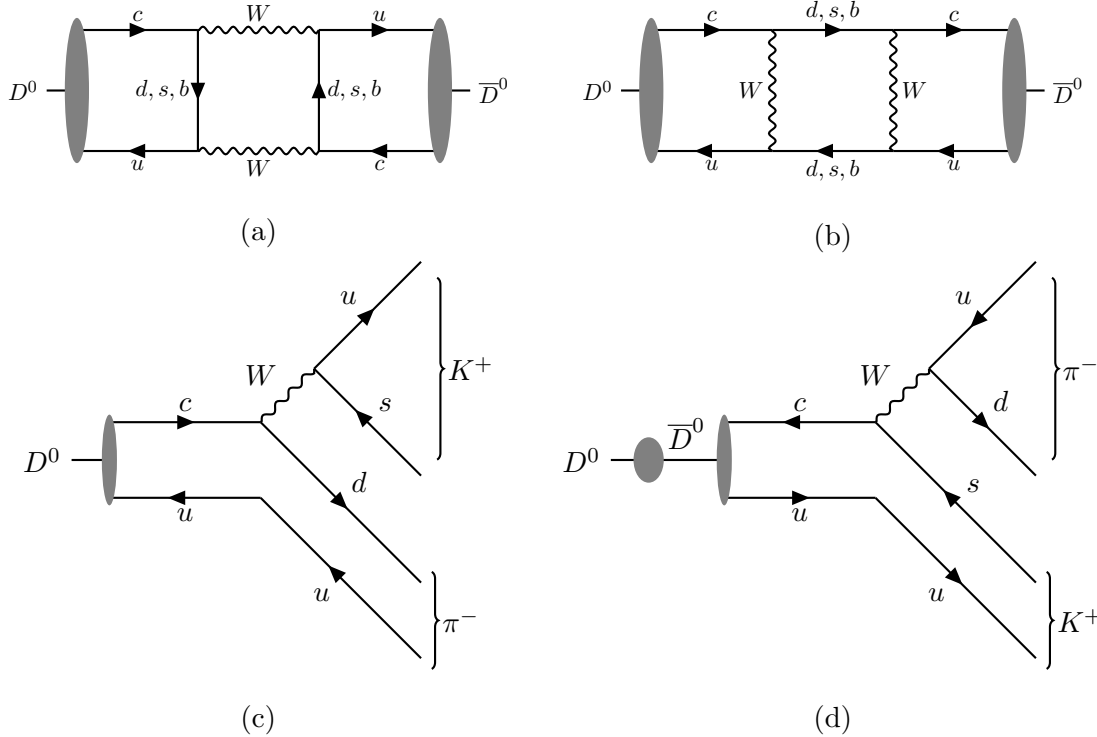


Figure A.2: Feynman diagrams for the $D^0 - \bar{D}^0$ oscillation are shown in (a) and (b), and the decay of D^0 and \bar{D}^0 to the $K^+\pi^-$ channel are given in (c) and (d).

A.4 Measuring CP violation in Mesons

Among the mesons with the dominant quark being the up-type quarks, only charm mesons allow for a whole range of experimental observations. This is because the top quark doesn't form mesons and thus $T - \bar{T}$ oscillation does not exist, limiting our avenues of searches for the CP asymmetry in top decay. Mesons built out of u and \bar{u} quarks, like π^0 are their own anti-particles and thus there are no oscillations. Furthermore they possess very few decay channels and so measuring CP asymmetry is a difficult process.

$D^0 - \bar{D}^0$ oscillations have been quite extensively studied. The Feynman diagrams for the process are shown in diagram (a) and (b) of Fig. A.2. One of the oft-looked at channels in

the search for CP violation is the $D^0 \rightarrow K^-\pi^+$ channel. The CP conjugate final state of the channel (i.e. $D^0 \rightarrow K^+\pi^-$) can occur from either $c \rightarrow d\bar{s}u$ transition or from $D^0 - \bar{D}^0$ (diagram (c) and (d) in Fig. A.2). The decay rate evolution as a function of time can help in distinguishing between the two contributions to the final state (and their interference).

For the down-type quarks, a rich repertoire of experimental results exists in both the K^0 and the B^0 system. We shall only concentrate on the bottom mesons. B^0 (\bar{B}^0) mesons survive

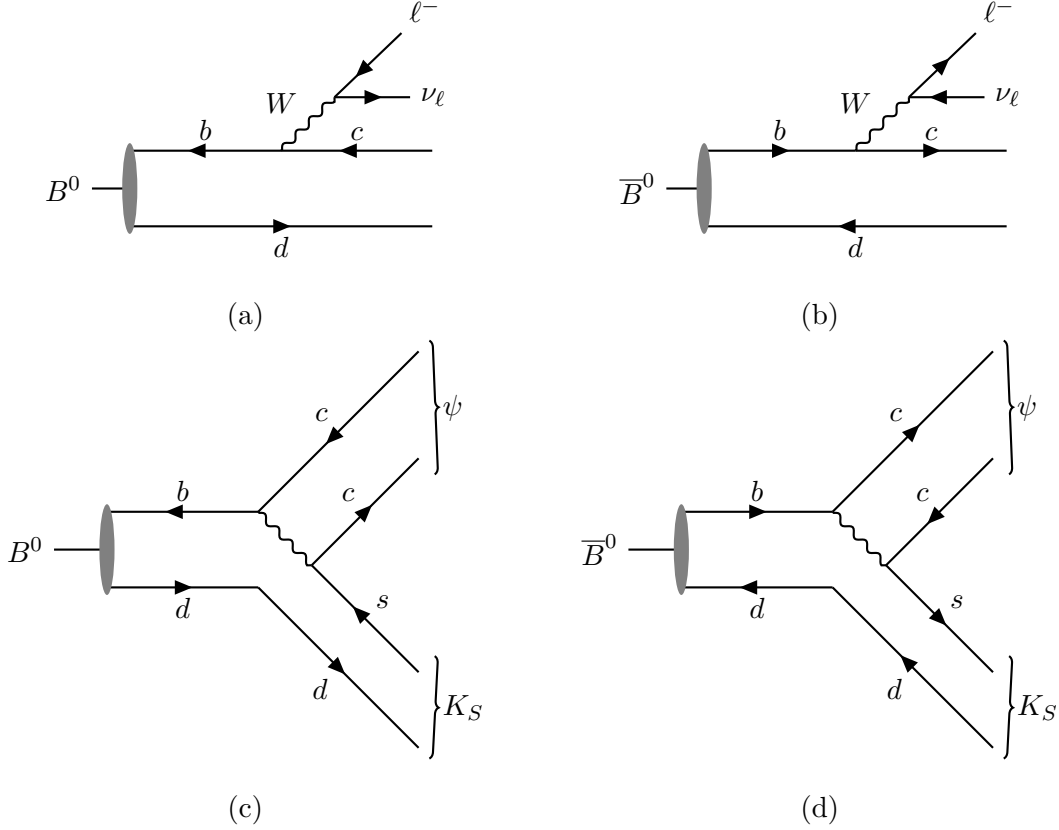


Figure A.3: The presence of a lepton or an anti-lepton in the final state identifies whether the initial state is a B^0 or a \bar{B}^0 as shown in (a) and (b). The decay to $J/\psi K_S$ are shown in (c) and (d).

long enough to be detected by Silicon Vertex Detector (SVD) in modern B-factories like Belle and BaBar. The lifetime of the B^- mesons is $\sim 10^{-12}$ s, which allows for a secondary vertex to form about a hundred microns away from the primary vertex. Tracks from the decay vertex (secondary) do not coincide with the primary vertex when they are extrapolated back. This non-zero value of displacement is key to the measurement of the lifetime of the bottom meson. Early studies were carried out by ALEPH, DELPHI and OPAL at LEP which had the resolution of $\sim 25\mu m$ [34]. Modern detectors at the B-factories like Belle with a SVD resolution of $12\mu m$ [35] have helped achieve sub-picosecond accuracy for the B-meson lifetimes.

The B-system is important for the measurement of CP violation, primarily because the effect in the B-system is about three orders of magnitude higher than in the K-system. However, unlike the K-system, the decay widths of the two B-meson mass eigenstates are almost equal.

The measurement is an exemplary experimental achievement. A collider like KEK produces $e^+e^- \rightarrow \Upsilon(4S) \rightarrow B^0\bar{B}^0$ events. These two B^0 mesons are correlated in the EPR fashion, i.e. the oscillation of the two B^0 's are such that at any point of time one of them is a B^0 and the other is a \bar{B}^0 . When one of them, say a \bar{B}^0 decays and is tagged from its semi-leptonic decay $\bar{B}^0 \rightarrow \ell^- + X^+$ at some time t_1 , we know that the other meson is a B^0 at that moment. It then decays at t_2 ($t_2 > t_1$) into a CP eigenstate f . During this time interval $\Delta t (= t_2 - t_1)$, the B^0 might oscillate to the \bar{B}^0 meson (shown in Fig. A.3).

The amplitude for the process is given by

$$A(f, t_1, \Delta t) = e^{-\frac{1}{2}\Gamma(t_1+\Delta t) - \frac{i}{2}(M_1+M_2)(t_1+\Delta t)} \left[A(f) \cos\left(\frac{1}{2}\Delta M_B \Delta t\right) + i\frac{q}{p}\bar{A}(f) \sin\left(\frac{1}{2}\Delta M_B \Delta t\right) \right] \quad (1.4.1)$$

where the different quantities are all defined in the previous section. The decay widths for the B^0 (\bar{B}^0) going to the state f and the other decaying to a charged lepton (l^- or l^+) are given by

$$\begin{aligned} \Gamma(B^0\bar{B}^0 \rightarrow [l^+ X]_t f_{l+\Delta t}) &\propto e^{-\Gamma(2t+\Delta t)} |A(l^+)|^2 |A(f)|^2 \left[1 + \Im\left(\frac{q}{p}\bar{\rho}(f)\right) \sin(\Delta M_B \Delta t) \right] \\ \Gamma(B^0\bar{B}^0 \rightarrow [l^- X]_t f_{l+\Delta t}) &\propto e^{-\Gamma(2t+\Delta t)} |\bar{A}(l^-)|^2 |A(f)|^2 \left[1 - \Im\left(\frac{q}{p}\bar{\rho}(f)\right) \sin(\Delta M_B \Delta t) \right] \end{aligned} \quad (1.4.2)$$

The CP eigenstate of choice, often used by the Belle and BaBar collaborations, is $J/\psi K_S$. The decays of the B^0 and \bar{B}^0 to the $J/\psi K_S$ is shown in Fig.A.3, we have

$$\frac{q}{p}\bar{\rho}(J/\psi K_S) = \frac{q}{p} \frac{\bar{A}(J/\psi K_S)}{A(J/\psi K_S)} = \frac{\mathbf{V}_{tb}^* \mathbf{V}_{td}}{\mathbf{V}_{tb} \mathbf{V}_{td}^*} \cdot \frac{\mathbf{V}_{cb} \mathbf{V}_{cs}^*}{\mathbf{V}_{cb}^* \mathbf{V}_{cs}} = e^{-2i\phi_1} \quad (1.4.3)$$

Thus,

$$\Im\left(\frac{q}{p}\bar{\rho}(J/\psi K_S)\right) = \sin(2\phi_1) \quad (1.4.4)$$

Thus, the CP asymmetry is

$$\mathcal{A}_{\text{CP}} = \frac{\Gamma(B^0 \rightarrow J/\psi K_S) - \Gamma(\bar{B}^0 \rightarrow J/\psi K_S)}{\Gamma(B^0 \rightarrow J/\psi K_S) + \Gamma(\bar{B}^0 \rightarrow J/\psi K_S)} = \sin(\Delta M_B \Delta t) \sin 2\phi_1 \quad (1.4.5)$$

FCNC Decays of the Top Quark

(Pertaining to Chapter 3)

B.1 Toy model amplitudes

B.1.1 The decay $t \rightarrow c + H$

We consider the decay $t(k) \rightarrow c(p) + H(q)$. In the rest frame of the t quark, we have $k = (m_t, \vec{0})$ and

$$u(k, h_t) = \sqrt{\frac{m_t}{2}} \begin{pmatrix} 1 + h_t & 1 - h_t & 0 & 0 \end{pmatrix}^T \quad (2.1.1)$$

where $h_t = \pm 1$ is the helicity of the t quark. Now, the three-momenta \vec{p} and \vec{q} will be back-to-back, and we can choose this as the z -axis. In this case, we can write

$$p = \begin{pmatrix} E_c & 0 & 0 & |\vec{p}| \end{pmatrix} \quad q = \begin{pmatrix} E_H & 0 & 0 & -|\vec{p}| \end{pmatrix} \quad (2.1.2)$$

where

$$|\vec{p}| \simeq E_c \simeq \frac{m_t^2 - M_H^2}{2m_t} \quad E_H \simeq \frac{m_t^2 + M_H^2}{2m_t} \quad (2.1.3)$$

taking $m_c \ll m_t, M_H$. In the approximation, the c -quark wave function is

$$u(p, h_c) \simeq \sqrt{\frac{m_t^2 - M_H^2}{8m_t}} \begin{pmatrix} 1 + h_c & 1 - h_c & 1 + h_c & -1 + h_c \end{pmatrix}^T \quad (2.1.4)$$

The helicity amplitudes $\mathcal{M}(h_c, h_t)$ now have the explicit form

$$\mathcal{M}(h_c, h_t) = \sum_{i=1}^3 \lambda_i \mathcal{A}_i(h_c, h_t) \quad (2.1.5)$$

where i runs over the three d -type quarks in the loop, $\lambda_i = V_{2i}V_{3i}^*$, and we parametrise

$$\mathcal{A}_i(h_c, h_t) = \bar{u}(p, h_c) i (F_{1i} P_L + F_{2i} P_R) u(k, h_t) \quad (2.1.6)$$

where P_L, P_R are the chiral projection operators

$$P_L = \frac{1}{2}(1 - \gamma_5) \quad P_R = \frac{1}{2}(1 + \gamma_5) \quad (2.1.7)$$

and F_{1i} and F_{2i} are form factors given below. Four helicity amplitudes are possible, but the only non-vanishing ones are

$$\begin{aligned} \mathcal{A}_i(+1, +1) &\simeq \sqrt{m_t^2 - M_H^2} F_{1i} \\ \mathcal{A}_i(-1, -1) &\simeq \sqrt{m_t^2 - M_H^2} F_{2i} \end{aligned} \quad (2.1.8)$$

Each of the form factors F_{1i} and F_{2i} can be written

$$F_{ni} = F_{ni}^{(a)} + F_{ni}^{(b)} + F_{ni}^{(c)} + F_{ni}^{(d)} \quad (2.1.9)$$

where $n = 1, 2$ and the superscripts refer to the graphs (a)–(d) shown in Figure 1. These can be written in terms of the Passarino-'tHooft-Veltman functions, defined as Euclidean space integrals

$$\begin{aligned} B_0(m_1, m_2; M) &= \int \frac{d^4k}{\pi^2} \frac{1}{(k^2 + m_1^2)\{(k+p)^2 + m_2^2\}} \\ p_\mu B_1(m_1, m_2; M) &= \int \frac{d^4k}{\pi^2} \frac{k_\mu}{(k^2 + m_1^2)\{(k+p)^2 + m_2^2\}} \end{aligned} \quad (2.1.10)$$

where $p^2 = -M^2$. In the $\overline{\text{MS}}$ scheme, we can write

$$\begin{aligned} B_0(m_1, m_2; M) &= \Delta + \hat{B}_0(m_1, m_2; M) \\ B_1(m_1, m_2; M) &= -\frac{1}{2}\Delta + \hat{B}_1(m_1, m_2; M) \end{aligned} \quad (2.1.11)$$

where the $\hat{B}_{0,1}$ are finite. The divergent quantity is $\Delta = 2/\varepsilon - \gamma + \ln 4\pi$ where $\varepsilon \rightarrow 0$ and γ is the Euler-Mascheroni constant. We also have

$$\begin{aligned} C_0(m_1, m_2, m_3; M_1, M_2, M_3) &= \int \frac{d^4k}{\pi^2} \frac{1}{(k^2 + m_1^2)\{(k+p_2)^2 + m_2^2\}\{(k+p_2+p_3)^2 + m_3^2\}} \\ C_{11}p_{2\mu} + C_{12}p_{3\mu} &= \int \frac{d^4k}{\pi^2} \frac{k_\mu}{(k^2 + m_1^2)\{(k+p_2)^2 + m_2^2\}\{(k+p_2+p_3)^2 + m_3^2\}} \end{aligned} \quad (2.1.12)$$

where $p_1 = p_2 + p_3$ and $p_i^2 = -M_i^2$ for $i = 1, 2, 3$ and the C_0, C_{11} and C_{12} are naturally finite. In fact, the GIM cancellation ensures that all the form factors are finite and hence, we keep only the finite parts of the B and C functions. In terms of these, we can now compute the F_1 form factors

$$\begin{aligned} F_{1i}^{(a)} &= -\frac{\xi\eta^2}{16\pi^2} m_c C_{12}^{(a)} \\ F_{1i}^{(b)} &= \frac{y_i m_i \eta^2}{16\pi^2} m_t \{2(C_{11}^{(b)} - C_{12}^{(b)}) + C_0^{(b)}\} \\ F_{1i}^{(c)} &= \frac{y_c \eta^2 m_t}{16\pi^2 (m_t^2 - m_c^2)} m_t \tilde{B}_1(m_i, M_\omega; m_t) \\ F_{1i}^{(d)} &= -\frac{y_t \eta^2 m_c}{16\pi^2 (m_t^2 - m_c^2)} m_c \tilde{B}_1(m_i, M_\omega; m_c) \end{aligned} \quad (2.1.13)$$

and the F_2 form factors

$$\begin{aligned}
F_{2i}^{(a)} &= -\frac{\xi\eta^2}{16\pi^2}m_t \left(C_{11}^{(a)} - C_{12}^{(a)} \right) \\
F_{2i}^{(b)} &= \frac{y_i m_i \eta^2}{16\pi^2}m_c \left(C_0^{(b)} + 2C_{12}^{(b)} \right) \\
F_{2i}^{(c)} &= \frac{y_c \eta^2 m_t}{16\pi^2(m_t^2 - m_c^2)}m_c \tilde{B}_1(m_i, M_\omega; m_t) \\
F_{2i}^{(d)} &= -\frac{y_t \eta^2 m_c}{16\pi^2(m_t^2 - m_c^2)}m_t \tilde{B}_1(m_i, M_\omega; m_c)
\end{aligned} \tag{2.1.14}$$

where

$$\begin{aligned}
C_X^{(a)} &= C_X(m_i, M_\omega, M_\omega; m_c, m_t, M_H) \\
C_X^{(b)} &= C_X(M_\omega, m_i, m_i; m_c, m_t, M_H)
\end{aligned} \tag{2.1.15}$$

for $X = 0, 11, 12, 22$. These are evaluated using the public domain software FF [197].

The Yukawa couplings y are the SM ones, i.e.

$$y_i = \frac{gm_i}{2M_\omega} \quad y_t = \frac{gm_t}{2M_\omega} \quad y_c = \frac{gm_c}{2M_\omega} . \tag{2.1.16}$$

The above form factors can be used to evaluate the total form factors appearing in Eqn. (2.1.9), which then enables us to compute the helicity amplitudes in Eqn. (2.1.8). These are then convoluted with the λ factors in Eqn. (3.2.3) and used to generate the squared and spin-summed/ averaged matrix element in Eqn. (3.2.4). Plugging this into Eqn. (3.2.5) then produces the desired result.

B.1.2 The decay $t \rightarrow c + Z$

We now consider the decay $t(k) \rightarrow c(p) + Z(q)$. The kinematics is similar to the previous case, with M_Z in place of M_H . Accordingly, the helicity spinor for the c -quark, in the approximation $m_c \ll m_t, M_Z$, is

$$u(p, h_c) \simeq \sqrt{\frac{m_t^2 - M_Z^2}{8m_t}} \begin{pmatrix} 1 + h_c & 1 - h_c & 1 + h_c & -1 + h_c \end{pmatrix}^T \tag{2.1.17}$$

while the helicity spinor for the t -quark is identical with that in Eqn. (2.1.1). In this case, we also have to consider the polarisation vector of the Z boson, which, for the three helicity choices $h_Z = 0, \pm 1$, has the form

$$\varepsilon(q, h_Z) = \begin{pmatrix} -\frac{(1-|h_Z|)|\vec{p}|}{M_Z} & \mp \frac{h_Z}{\sqrt{2}} & -\frac{i|h_Z|}{\sqrt{2}} & \frac{(1-|h_Z|)E_Z}{M_Z} \end{pmatrix} \tag{2.1.18}$$

where, as in Eqn. (2.1.3),

$$|\vec{p}| \simeq E_c \simeq \frac{m_t^2 - M_Z^2}{2m_t} \quad E_Z \simeq \frac{m_t^2 + M_Z^2}{2m_t} \tag{2.1.19}$$

The helicity amplitudes $\mathcal{M}(h_Z; h_c, h_t)$ now have the explicit form

$$\mathcal{M}(h_Z; h_c, h_t) = \sum_{i=1}^3 \lambda_i \mathcal{A}_i(h_Z; h_c, h_t) \tag{2.1.20}$$

where i runs over the three d -type quarks in the loop, $\lambda_i = V_{2i}V_{3i}^*$, and we parametrise

$$\begin{aligned}\mathcal{A}_i(h_Z; h_c, h_t) &= \bar{u}(p, h_c) i\Gamma^\mu u(k, h_t) \varepsilon_\mu^*(q) \\ \Gamma^\mu &= F_{1i}\gamma^\mu P_L + F_{2i}\gamma^\mu P_R + iF_{3i}\sigma^{\mu\nu} q_\nu P_L + iF_{4i}\sigma^{\mu\nu} q_\nu P_R\end{aligned}\quad (2.1.21)$$

Of the 12 possible helicity amplitudes, the only nonvanishing ones are

$$\begin{aligned}\mathcal{A}_i(+1; -1, +1) &= -\sqrt{2(m_t^2 - M_Z^2)} [F_{1i} - F_{4i}(E_Z + |\vec{p}|)] \\ \mathcal{A}_i(-1; +1, -1) &= -\sqrt{2(m_t^2 - M_Z^2)} [F_{2i} - F_{3i}(E_Z + |\vec{p}|)] \\ \mathcal{A}_i(0; +1, +1) &= -\sqrt{m_t^2 - M_Z^2} \left[F_{2i} \sqrt{\frac{E_Z + |\vec{p}|}{E_Z - |\vec{p}|}} - F_{3i} M_Z \right] \\ \mathcal{A}_i(0; -1, -1) &= -\sqrt{m_t^2 - M_Z^2} \left[F_{1i} \sqrt{\frac{E_Z + |\vec{p}|}{E_Z - |\vec{p}|}} - F_{4i} M_Z \right]\end{aligned}\quad (2.1.22)$$

Each of the form factors can be written

$$F_{ni} = F_{ni}^{(a)} + F_{ni}^{(b)} + F_{ni}^{(c)} + F_{ni}^{(d)} \quad (2.1.23)$$

where $n = 1, 2, 3, 4$ and the superscripts refer to the graphs (a)–(d) shown in Figure 1 (with H replaced by Z). These can be written, as before, in terms of the Passarino-'tHooft-Veltman functions. We thus obtain the F_1 form factors

$$\begin{aligned}F_{1i}^{(a)} &= \frac{\xi\eta^2}{16\pi^2} [m_t^2(C_{11}^{(a)} - C_{12}^{(a)} + C_{21}^{(a)} - C_{23}^{(a)}) + m_c m_t (C_{12}^{(a)} + C_{23}^{(a)}) - C_{24}^{(a)}] \\ F_{1i}^{(b)} &= \frac{\eta^2}{16\pi^2} [\alpha_i m_i^2 C_0^{(b)} + \beta_i (B_0 - M_\omega^2 C_0^{(b)} + m_t^2 (C_{21}^{(b)} - C_{23}^{(b)}) - m_c^2 C_{12}^{(b)} - 2C_{24}^{(b)}) \\ &\quad + \beta_i m_c m_t \left(\frac{3}{2} (C_0^{(b)} + C_{11}^{(b)}) + C_{12}^{(b)} + C_{23}^{(b)} \right)] \\ F_{1i}^{(c)} &= -\frac{\eta^2}{16\pi^2 (m_t^2 - m_c^2)} [\alpha m_c^2 B_1(m_i, M_\omega; m_c) + \beta m_c m_t B_1(m_i, M_\omega; m_c)] \\ F_{1i}^{(d)} &= \frac{\eta^2}{16\pi^2 (m_t^2 - m_c^2)} [\alpha m_i^2 B_1(m_i, M_\omega; m_t) + \beta m_c m_t B_1(m_i, M_\omega; m_t)]\end{aligned}\quad (2.1.24)$$

the F_2 form factors

$$\begin{aligned}F_{2i}^{(a)} &= -\frac{\xi\eta^2}{16\pi^2} [m_t^2 (C_{11}^{(a)} - C_{12}^{(a)} + C_{21}^{(a)} - C_{23}^{(a)}) - m_c m_t (C_{12}^{(a)} + C_{23}^{(a)}) - C_{24}^{(a)}] \\ F_{2i}^{(b)} &= -\frac{\eta^2}{16\pi^2} [\alpha_i m_i^2 C_0^{(b)} + \beta_i (B_0 - M_\omega^2 C_0^{(b)} + m_t^2 (C_{21}^{(b)} - C_{23}^{(b)}) - m_c^2 C_{12}^{(b)} - 2C_{24}^{(b)}) \\ &\quad - \beta_i m_c m_t \left(\frac{3}{2} (C_0^{(b)} + C_{11}^{(b)}) + C_{12}^{(b)} + C_{23}^{(b)} \right)] \\ F_{2i}^{(c)} &= \frac{\eta^2}{16\pi^2 (m_t^2 - m_c^2)} [\alpha m_c^2 B_1(m_i, M_\omega; m_c) - \beta m_c m_t B_1(m_i, M_\omega; m_c)] \\ F_{2i}^{(d)} &= -\frac{\eta^2}{16\pi^2 (m_t^2 - m_c^2)} [\alpha m_i^2 B_1(m_i, M_\omega; m_t) - \beta m_c m_t B_1(m_i, M_\omega; m_t)]\end{aligned}\quad (2.1.25)$$

the nonvanishing F_3 form factors

$$\begin{aligned}F_{3i}^{(a)} &= -\frac{\xi\eta^2}{16\pi^2} [m_t (C_{11}^{(a)} - C_{12}^{(a)} + C_{21}^{(a)} - C_{23}^{(a)}) + m_c (C_{12}^{(a)} + C_{23}^{(a)})] \\ F_{3i}^{(b)} &= -\frac{\eta^2}{16\pi^2} \beta_i [m_t (C_{11}^{(b)} - C_{12}^{(b)} + C_{21}^{(b)} - C_{23}^{(b)}) + m_c \left(\frac{1}{2} (C_0^{(b)} + C_{11}^{(b)}) + C_{12}^{(b)} + C_{23}^{(b)} \right)]\end{aligned}\quad (2.1.26)$$

and the nonvanishing F_4 form factors

$$\begin{aligned} F_{4i}^{(a)} &= -\frac{\xi\eta^2}{16\pi^2} \left[m_t (C_{11}^{(a)} - C_{12}^{(a)} + C_{21}^{(a)} - C_{23}^{(a)}) - m_c (C_{12}^{(a)} + C_{23}^{(a)}) \right] \\ F_{4i}^{(b)} &= -\frac{\eta^2}{16\pi^2} \beta_i \left[m_t \left(C_{11}^{(b)} - C_{12}^{(b)} + C_{21}^{(b)} - C_{23}^{(b)} \right) - m_c \left(\frac{1}{2} (C_0^{(b)} + C_{11}^{(b)}) + C_{12}^{(b)} + C_{23}^{(b)} \right) \right] \end{aligned} \quad (2.1.27)$$

In the above,

$$\begin{aligned} B_0 &= B_0(m_i, m_i; M_Z) \\ C_X^{(a)} &= C_X(m_i, M_\omega, M_\omega; m_c, m_t, M_Z) \\ C_X^{(b)} &= C_X(M_\omega, m_i, m_i; m_c, m_t, M_Z) \end{aligned}$$

where $X = 0, 11, 12, 21, 23, 24$. The $Zd_i\bar{d}_i$ couplings are $\alpha = -\frac{1}{2} - 2Q\sin^2\theta_W$ and $\beta = \frac{1}{2}$ where $Q = -1/3$ is the charge of the down-type quark.

Once we have these form factors, we sum them up using Eqn. (2.1.23) and use them to calculate the helicity amplitudes in Eqn. (2.1.23). These are then convoluted with the λ_i factors in Eqn. (3.2.13) and used to calculate the squared spin-summed/ averaged matrix element in Eqn. (3.2.14). Finally this is used in Eqn. (3.2.15) to produce the partial width.

B.2 SM and cMSSM amplitudes

B.2.1 The decay $t \rightarrow c + H$

In the Standard Model, as in the toy model, the decay $t \rightarrow c + H$ can be parametrised in terms of the two nonvanishing helicity amplitudes of Eqn. (2.1.8). The calculation follows the lines of the toy model, except that the diagrams are those of Figure 3.4 instead of Figure 3.1. Thus, in this Appendix, we only require to list the form factors, diagram-wise.

It is convenient, in evaluating these diagrams, to define a set of general vertices:

$$\begin{aligned} \bar{u}_i u_i h &: ig(A_{ui}^h P_L + B_{ui}^h P_R) \\ \bar{d}_i d_i h &: ig(A_{di}^h P_L + B_{di}^h P_R) \\ h(-q)\phi^+(p)W_\mu^- &: ig\alpha_\phi^h(p+q)_\mu \\ h\phi^+\phi'^- &: igM_W\beta_{\phi\phi'}^h \\ hW_\mu^+W_\nu^- &: igM_W\omega_h g_{\mu\nu} \\ \bar{u}_i d_j \phi^+ &: ig\left(X_{ij}^\phi P_L + Y_{ij}^\phi P_R\right) \end{aligned}$$

in terms of a set of coupling constants $A_{ui}^h, B_{ui}^h, A_{di}^h, B_{di}^h, \alpha_\phi^h, \beta_{\phi\phi'}^h, \omega_h, X_{ij}^\phi$ and Y_{ij}^ϕ . In order to obtain numerical values in the SM, we need to substitute the coupling constants according to the table given below.

coupling:	A_{ui}^h	B_{ui}^h	A_{di}^h	B_{di}^h	α_ϕ^h	$\beta_{\phi\phi'}^h$	ω_h	X_{ij}^ϕ	Y_{ij}^ϕ
SM value :	$\frac{m_i}{2M_W}$	$\frac{m_i}{2M_W}$	$\frac{m_i}{2M_W}$	$\frac{m_i}{2M_W}$	$-\frac{1}{2}$	$-\frac{m_h^2}{M_W^2}$	1	$\frac{m_i}{\sqrt{2}M_W}$	$-\frac{m_j}{\sqrt{2}M_W}$

In terms of these, the form factors of type F_1 are

$$\begin{aligned}
F_{1i}^{(a)} &= \frac{ig^3 M_W \omega_h}{16\pi^2} m_c C_{12}^{(a)} \\
F_{1i}^{(b)} &= \frac{ig^3 \alpha_{G+}^h}{16\sqrt{2}\pi^2} \left[X_{ci}^G \left((m_t^2 - 2M_h^2)(C_{11}^{(b)} - C_{12}^{(b)}) - B_0(2, 3) + m_t^2 C_0^{(b)} + 2m_c^2 C_{11}^{(b)} \right) - m_i m_c Y_{ci}^G (C_{12}^{(b)} + 2C_0^{(b)}) \right] \\
F_{1i}^{(c)} &= \frac{ig^3 \alpha_{G+}^h}{16\sqrt{2}\pi^2} \left[X_{ti}^G \left(2m_t^2 C_{11}^{(c)} - 2m_s^2 C_{12}^{(c)} + m_c^2 C_{12}^{(c)} - B_0(2, 3) + m_t^2 C_0^{(c)} \right) - m_i m_t Y_{ti}^G (C_{11}^{(c)} - C_{12}^{(c)} + 2C_0^{(c)}) \right] \\
F_{1i}^{(d)} &= -\frac{ig^3 M_W \beta_{GG}^h}{16\pi^2} \left[m_t X_{ci}^G X_{ti}^G (C_{11}^{(d)} - C_{12}^{(d)}) - m_i X_{ci}^G Y_{ti}^G C_0^{(d)} + m_c Y_{ci}^G Y_{ti}^G C_{12}^{(d)} \right] \\
F_{1i}^{(e)} &= \frac{ig^3 m_i}{16\pi^2} m_c \left[(A_{di}^h + B_{di}^h) C_{12}^{(e)} + B_{di}^h C_0^{(e)} \right] \\
F_{1i}^{(f)} &= -\frac{ig^3}{16\pi^2} \left[z_1 \left(B_0(2, 3) - M_W^2 C_0^{(f)} \right) - z_3 C_0^{(f)} - m_t z_5 \frac{X_{ti}^G}{Y_{ti}^G} (C_{11}^{(f)} - C_{12}^{(f)}) - m_c z_2 C_{12}^{(f)} \right] Y_{ti}^G \\
F_{1i}^{(g)} &= \frac{ig^3}{16\pi^2 (m_t^2 - m_c^2)} m_t^2 A_{uc}^h B_1^{(g)} \\
F_{1i}^{(h)} &= \frac{ig^3}{16\pi^2 (m_t^2 - m_c^2)} \left[m_t \left(m_t A_{uc}^h Y_{ci}^G + m_c A_{uc}^h \frac{X_{ti}^G}{Y_{ti}^G} X_{ci}^G \right) B_1^{(h)} - m_i \left(m_t A_{uc}^h Y_{ci}^G \frac{X_{ti}^G}{Y_{ti}^G} + m_c A_{uc}^h X_{ci}^G \right) B_0^{(h)} \right] Y_{ti}^G \\
F_{1i}^{(i)} &= -\frac{ig^3}{16\pi^2 (m_t^2 - m_c^2)} m_c m_t A_{ut}^h B_1^{(i)} \\
F_{1i}^{(j)} &= -\frac{ig^3}{16\pi^2 (m_t^2 - m_c^2)} \left[m_c X_{ti}^G (m_c X_{ci}^G B_1^{(j)} - m_i Y_{ci}^G B_0^{(j)}) + m_t Y_{ti}^G (m_c Y_{ci}^G B_1^{(j)} - m_i X_{ci}^G B_0^{(j)}) \right] A_{ut}^h \quad (2.2.1)
\end{aligned}$$

and the form factors of type F_2 are

$$\begin{aligned}
F_{2i}^{(a)} &= \frac{ig^3 M_W \omega_h}{16\pi^2} m_t (C_{11}^{(a)} - C_{12}^{(a)}) \\
F_{2i}^{(b)} &= \frac{ig^3 \alpha_{G+}^h}{16\sqrt{2}\pi^2} \left[X_{ci}^G m_c m_t (C_{12}^{(b)} - 2C_{11}^{(b)}) + Y_{ci}^G m_i m_t (C_0^{(b)} - C_{11}^{(b)} + C_{12}^{(b)}) \right] \\
F_{2i}^{(c)} &= \frac{-ig^3 \alpha_{G+}^h}{16\sqrt{2}\pi^2} \left[X_{ti}^G m_c m_t (C_{12}^{(c)} - 2C_{11}^{(c)}) + Y_{ti}^G m_i m_t (C_0^{(c)} - C_{11}^{(c)} + C_{12}^{(c)}) \right] \\
F_{2i}^{(d)} &= -\frac{ig^3 M_W \beta_{GG}^h}{16\pi^2} \left[m_t Y_{ci}^G Y_{ti}^G (C_{11}^{(d)} - C_{12}^{(d)}) - m_i X_{ti}^G Y_{ci}^G C_0^{(d)} + m_c X_{ci}^G X_{ti}^G C_{12}^{(d)} \right] \\
F_{2i}^{(e)} &= \frac{ig^3 m_i}{16\pi^2} m_t \left[(A_{di}^h + B_{di}^h) (C_{11}^{(e)} - C_{12}^{(e)}) + A_{di}^h C_0^{(e)} \right] \\
F_{2i}^{(f)} &= -\frac{ig^3}{16\pi^2} \left[z_4 \left(B_0(2, 3) - M_W^2 C_0^{(f)} \right) - z_6 C_0^{(f)} - m_t z_2 \frac{Y_{ti}^G}{X_{ti}^G} (C_{11}^{(f)} - C_{12}^{(f)}) - m_c z_5 C_{12}^{(f)} \right] X_{ti}^G \\
F_{2i}^{(g)} &= \frac{ig^3}{16\pi^2 (m_t^2 - m_c^2)} m_c m_t B_{uc}^h B_1^{(g)} \\
F_{2i}^{(h)} &= \frac{ig^3}{16\pi^2 (m_t^2 - m_c^2)} \left[m_t \left(m_t B_{uc}^h X_{ci}^G + m_c B_{uc}^h \frac{Y_{ti}^G}{X_{ti}^G} Y_{ci}^G \right) B_1^{(h)} - m_i \left(m_t B_{uc}^h X_{ci}^G \frac{Y_{ti}^G}{X_{ti}^G} + m_c B_{uc}^h Y_{ci}^G \right) B_0^{(h)} \right] X_{ti}^G \\
F_{2i}^{(i)} &= -\frac{ig^3}{16\pi^2 (m_t^2 - m_c^2)} m_c^2 B_{ut}^h B_1^{(i)} \\
F_{2i}^{(j)} &= -\frac{ig^3}{16\pi^2 (m_t^2 - m_c^2)} \left[m_c Y_{ti}^G (m_c Y_{ci}^G B_1^{(j)} - m_i X_{ci}^G B_0^{(j)}) + m_t X_{ti}^G (m_c X_{ci}^G B_1^{(j)} - m_i Y_{ci}^G B_0^{(j)}) \right] B_{ut}^h \quad (2.2.2)
\end{aligned}$$

As in the previous section, the superscripts refer to the diagrams marked (a)–(j) in Figure 3.4.

In the above, we have used the functions

$$\begin{aligned}
C_X^{(a)} &= C_X(m_i, M_W, M_W; m_c, m_t, M_h) & B_1^{(g)} &= B_1(m_i, M_W; m_t) \\
C_X^{(b)} &= C_X(m_i, M_W, M_W; m_c, m_t, M_h) & B_1^{(h)} &= B_1(m_i, M_W; m_t) \\
C_X^{(c)} &= C_X(m_i, M_W, M_W; m_c, m_t, M_h) & B_0^{(h)} &= B_0(m_i, M_W; m_t) \\
C_X^{(d)} &= C_X(m_i, M_W, M_W; m_c, m_t, M_h) & B_1^{(i)} &= B_1(m_i, M_W; m_c) \\
C_X^{(e)} &= C_X(M_W, m_i, m_i; m_c, m_t, M_h) & B_1^{(j)} &= B_1(m_i, M_W; m_c) \\
C_X^{(f)} &= C_X(M_W, m_i, m_i; m_c, m_t, M_h) & B_0^{(j)} &= B_0(m_i, M_W; m_c)
\end{aligned} \tag{2.2.3}$$

where $X = 0, 11, 12, 21, 23, 24$, as before, and defined a set of effective couplings

$$\begin{aligned}
z_1 &= X_{ci}^G B_{di}^h \\
z_2 &= m_t Y_{ci}^G \frac{X_{ti}^G}{Y_{ti}^G} A_{di}^h + m_c X_{ci}^G B_{di}^h + m_i Y_{ci}^G B_{di}^h + m_i Y_{ci}^G A_{di}^h \\
z_3 &= m_t \frac{X_{ti}^G}{Y_{ti}^G} A_{di}^h (m_i X_{ci}^G + m_c Y_{ci}^G) + m_i^2 A_{di}^h X_{ci}^G + m_i m_c A_{di}^h Y_{ci}^G \\
z_4 &= Y_{ci}^G A_{di}^h \\
z_5 &= m_t X_{ci}^G \frac{Y_{ti}^G}{X_{ti}^G} B_{di}^h + m_c Y_{ci}^G A_{di}^h + m_i X_{ci}^G A_{di}^h + m_i X_{ci}^G B_{di}^h \\
z_6 &= m_t \frac{Y_{ti}^G}{X_{ti}^G} B_{di}^h (m_i Y_{ci}^G + m_c X_{ci}^G) + m_i^2 B_{di}^h Y_{ci}^G + m_i m_c B_{di}^h X_{ci}^G
\end{aligned} \tag{2.2.4}$$

These form factors can now be combined, using $F_{ni} = \sum_{A=a}^j F_{ni}^A$ for $n = 1, 2$ and the results substituted into Eqn. (2.1.8) as before.

When we come to consider the cMSSM, the SM contributions will not only involve modifications of the SM couplings given above, but will also be enhanced by contributions from the additional eight diagrams in Figure 3.5, which involve superparticles in the loops. These involve some additional couplings which are parametrised in a general way as

$$\begin{aligned}
\chi_i^+ \chi_j^- h &: ig \left(A_{ij}^h P_L + B_{ij}^h P_R \right) \\
\chi_i^+ \chi_j^- Z^\mu &: ig \gamma^\mu \left(A_{ij}^Z P_L + B_{ij}^Z P_R \right) \\
\tilde{d}^* \tilde{d} h &: ig M_W \beta_{\tilde{d}\tilde{d}}^h \\
\tilde{d}(p) \tilde{d}^*(q) Z^\mu &: ig \alpha_{\tilde{d}}^{\tilde{d}} (p+q)^\mu \\
\tilde{d}_i^* \bar{u}_k \chi_j^+ &: ig \left(X_{kj}^i P_L + Y_{kj}^i P_R \right)
\end{aligned}$$

in terms of an additional set of coupling constants $A_{ij}^h, B_{ij}^h, A_{ij}^Z, B_{ij}^Z, \beta_{\tilde{d}\tilde{d}}^h, \alpha_{\tilde{d}}^{\tilde{d}}, X_{kj}^i, Y_{kj}^i$. For a numerical analysis, we require to take the full set of coupling constants as given in the table below.

where, in terms of the chargino mixing matrices U and V ,

$$\begin{aligned}
Q_{ij} &= \frac{1}{\sqrt{2}} U_{i2} V_{j1}; \quad S_{ij} = \frac{1}{\sqrt{2}} U_{i1} V_{j2} \\
Q_{ij}^U &= -U_{i1} U_{j1}^* - \frac{1}{2} U_{i2} U_{j2}^* + \delta_{ij} \sin^2 \theta_W; \quad Q_{ij}^V = -V_{i1} V_{j1}^* - \frac{1}{2} V_{i2} V_{j2}^* + \delta_{ij} \sin^2 \theta_W
\end{aligned}$$

coupling :	A_{ui}^h	B_{ui}^h	A_{di}^h	B_{di}^h
cMSSM :	$-\frac{m_i \cos \alpha}{2M_W \sin \beta}$	$-\frac{m_i \cos \alpha}{2M_W \sin \beta}$	$\frac{m_i \sin \alpha}{2M_W \cos \beta}$	$\frac{m_i \sin \alpha}{2M_W \cos \beta}$
coupling:	$\alpha_{G^+}^h$	$\alpha_{h^+}^h$	$\beta_{G^+G^-}^h$	$\beta_{G^+h^+}^h$
cMSSM :	$-\frac{1}{2} \sin(\beta - \alpha)$	$-\frac{1}{2} \cos(\beta - \alpha)$	$\frac{\cos 2\beta \sin(\alpha + \beta)}{2 \cos^2 \theta_W}$	$\frac{\cos(\beta - \alpha)(m_{h^+}^2 - m_{h^0}^2)}{2M_W^2}$
coupling:	$\beta_{h^+h^-}^h$	ω_h	$X_{ij}^{G^+}$	$Y_{ij}^{G^+}$
cMSSM value :	$-\sin(\beta - \alpha)$ $-\frac{\cos 2\beta \sin(\alpha + \beta)}{2 \cos^2 \theta_W}$	$\sin(\beta - \alpha)$	$\frac{m_i}{\sqrt{2}M_W}$	$-\frac{m_j}{\sqrt{2}M_W}$
coupling:	$X_{ij}^{h^+}$	$Y_{ij}^{h^+}$		
cMSSM value :	$\frac{m_i \cot \beta}{\sqrt{2}M_W}$	$\frac{m_j \tan \beta}{\sqrt{2}M_W}$		
coupling:	A_{ij}^h	B_{ij}^h	A_{ij}^Z	B_{ij}^Z
cMSSM value :	$Q_{ij}^* \sin \alpha - S_{ij}^* \cos \alpha$	$Q_{ji} \sin \alpha - S_{ji} \cos \alpha$	Q_{ij}^V	Q_{ij}^U
coupling:	$\beta_{\tilde{d}\tilde{d}}^h$	$\alpha_{\tilde{d}}^{\tilde{d}}$	X_{kj}^i	Y_{kj}^i
cMSSM value :	$-\left(\frac{1}{2} - \frac{\sin^2 \theta_W}{3}\right)$ $+\frac{\sin(\alpha + \beta)}{\cos^2 \theta_W}$	$\frac{1 - \frac{2}{3} \sin^2 \theta_W}{2 \cos \theta_W}$	0	U_{j1}

Evaluating the Feynman diagrams of Figs. 3.4 and 3.5 now leads to the F_1 form factors

$$\begin{aligned}
F_{1i}^{(k)} &= \frac{ig^3 \alpha_{h^+}^h}{16\sqrt{2}\pi^2} \left[X_{ci}^{h^+} \left((m_t^2 - 2M_{h^+}^2)(C_{11}^{(k)} - C_{12}^{(k)}) - B_0(2, 3) + m_i^2 C_0^{(k)} + 2m_c^2 C_{11}^{(k)} \right) - m_i m_c Y_{ci}^{h^+} (C_{12}^{(k)} + 2C_0^{(k)}) \right] \\
F_{1i}^{(l)} &= \frac{ig^3 \alpha_{h^+}^h}{16\sqrt{2}\pi^2} \left[X_{ti}^{h^+} \left(2m_t^2 C_{11}^{(l)} - 2M_{h^+}^2 C_{12}^{(l)} + m_c^2 C_{12}^{(l)} - B_0(2, 3) + m_i^2 C_0^{(l)} \right) - m_i m_t Y_{ti}^{h^+} (C_{11}^{(l)} - C_{12}^{(l)} + 2C_0^{(l)}) \right] \\
F_{1i}^{(m)} &= -\frac{ig^3 M_W \beta_{G^+h^-}^h}{16\pi^2} \left[m_t X_{ci}^{h^+} X_{ti}^{h^+} (C_{11}^{(m)} - C_{12}^{(m)}) - m_i X_{ci}^{h^+} Y_{ti}^{h^+} C_0^{(m)} + m_c Y_{ci}^{h^+} Y_{ti}^{h^+} C_{12}^{(m)} \right] \\
F_{1i}^{(n)} &= -\frac{ig^3 M_W \beta_{G^+h^-}^h}{16\pi^2} \left[m_t X_{ci}^G X_{ti}^{h^+} (C_{11}^{(n)} - C_{12}^{(n)}) - m_i X_{ci}^G Y_{ti}^{h^+} C_0^{(n)} + m_c Y_{ci}^G Y_{ti}^{h^+} C_{12}^{(n)} \right] \\
F_{1i}^{(o)} &= -\frac{ig^3 M_W \beta_{G^+h^-}^S}{16\pi^2} \left[m_t X_{ci}^{h^+} X_{ti}^G (C_{11}^{(o)} - C_{12}^{(o)}) - m_i X_{ci}^{h^+} Y_{ti}^G C_0^{(o)} + m_c Y_{ci}^{h^+} Y_{ti}^G C_{12}^{(o)} \right] \\
F_{1i}^{(p)} &= -\frac{ig^3}{16\pi^2} \left[z_1 \left(B_0^{(p)} - M_{h^+}^2 C_0^{(p)} \right) - z_3 C_0^{(p)} - m_t z_5 \frac{X_{ti}^{h^+}}{Y_{ti}^{h^+}} (C_{11}^{(p)} - C_{12}^{(p)}) - m_c z_2 C_{12}^{(p)} \right] Y_{ti}^{h^+} \\
F_{1i}^{(q)} &= -\frac{ig^3 M_W \beta_{\tilde{d}\tilde{d}}^h}{16\pi^2} \left[m_t X_{cj}^i X_{tj}^i (C_{11}^{(q)} - C_{12}^{(q)}) - m_i X_{cj}^i Y_{tj}^i C_0^{(q)} + m_c Y_{cj}^i Y_{tj}^i C_{12}^{(q)} \right] \\
F_{1i}^{(r)} &= -\frac{ig^3}{16\pi^2} \left[z_1 \left(B_0^{(r)} - M_{\tilde{d}_i}^2 C_0^{(r)} \right) - z_3 C_0^{(r)} - m_t z_5 \frac{X_{tj}^i}{Y_{tj}^i} (C_{11}^{(r)} - C_{12}^{(r)}) - m_c z_2 C_{12}^{(r)} \right] Y_{tj}^i \\
F_{1i}^{(s)} &= \frac{ig^3}{16\pi^2(m_t^2 - m_c^2)} \left[m_t \left(m_t A_{uc}^h Y_{ci}^{h^+} + m_c A_{uc}^h \frac{X_{ti}^{h^+}}{Y_{ti}^{h^+}} X_{ci}^{h^+} \right) B_1^{(s)} \right. \\
&\quad \left. - m_i \left(m_t A_{uc}^h Y_{ci}^{h^+} \frac{X_{ti}^{h^+}}{Y_{ti}^{h^+}} + m_c A_{uc}^h X_{ci}^{h^+} \right) B_0^{(s)} \right] Y_{ti}^{h^+} \\
F_{1i}^{(t)} &= \frac{ig^3}{16\pi^2(m_t^2 - m_c^2)} \left[m_t \left(m_t A_{uc}^h Y_{cj}^i + m_c A_{uc}^h \frac{X_{ti}^{h^+}}{Y_{ti}^{h^+}} X_{cj}^i \right) B_1^{(t)} - m_i \left(m_t A_{uc}^h Y_{cj}^i \frac{X_{ti}^{h^+}}{Y_{ti}^{h^+}} + m_c A_{uc}^h X_{cj}^i \right) B_0^{(t)} \right] Y_{ti}^{h^+} \\
F_{1i}^{(u)} &= -\frac{ig^3}{16\pi^2(m_t^2 - m_c^2)} \left[m_c X_{ti}^{h^+} \left(m_c X_{ci}^{h^+} B_1^{(u)} - m_i Y_{ci}^{h^+} B_0^{(u)} \right) + m_t Y_{ti}^{h^+} \left(m_c Y_{ci}^{h^+} B_1^{(u)} - m_i X_{ci}^{h^+} B_0^{(u)} \right) \right] A_{ut}^h \\
F_{1i}^{(v)} &= -\frac{ig^3}{16\pi^2(m_t^2 - m_c^2)} \left[m_c X_{tj}^i \left(m_c X_{cj}^i B_1^{(v)} - m_i Y_{cj}^i B_0^{(v)} \right) + m_t Y_{tj}^i \left(m_c Y_{cj}^i B_1^{(v)} - m_i X_{cj}^i B_0^{(v)} \right) \right] A_{ut}^h \quad (2.2.5)
\end{aligned}$$

and the F_2 form factors

$$\begin{aligned}
F_{2i}^{(k)} &= \frac{ig^3 \alpha_{h+}^h}{16\sqrt{2}\pi^2} \left[X_{ci}^{h+} m_c m_t (C_{12}^{(k)} - 2C_{11}^{(k)}) + Y_{ci}^{h+} m_i m_t (C_0^{(k)} - C_{11}^{(k)} + C_{12}^{(k)}) \right] \\
F_{2i}^{(l)} &= \frac{-ig^3 \alpha_{h+}^h}{16\sqrt{2}\pi^2} \left[X_{ti}^{h+} m_c m_t (C_{12}^{(l)} - 2C_{11}^{(l)}) + Y_{ti}^{h+} m_i m_t (C_0^{(l)} - C_{11}^{(l)} + C_{12}^{(l)}) \right] \\
F_{2i}^{(m)} &= -\frac{ig^3 M_W \beta_{h+h-}^h}{16\pi^2} \left[m_t Y_{ci}^{h+} Y_{ti}^{h+} (C_{11}^{(m)} - C_{12}^{(m)}) - m_i X_{ti}^{h+} Y_{ci}^{h+} C_0^{(m)} + m_c X_{ci}^{h+} X_{ti}^{h+} C_{12}^{(m)} \right] \\
F_{2i}^{(n)} &= -\frac{ig^3 M_W \beta_{G+h-}^h}{16\pi^2} \left[m_t Y_{ci}^G Y_{ti}^{h+} (C_{11}^{(n)} - C_{12}^{(n)}) - m_i X_{ti}^{h+} Y_{ci}^G C_0^{(n)} + m_c X_{ci}^G X_{ti}^{h+} C_{12}^{(n)} \right] \\
F_{2i}^{(o)} &= -\frac{ig^3 M_W \beta_{G+h-}^S}{16\pi^2} \left[m_t Y_{ci}^{h+} Y_{ti}^G (C_{11}^{(o)} - C_{12}^{(o)}) - m_i X_{ti}^G Y_{ci}^{h+} C_0^{(o)} + m_c X_{ci}^{h+} X_{ti}^G C_{12}^{(o)} \right] \\
F_{2i}^{(p)} &= -\frac{ig^3}{16\pi^2} \left[z_4 \left(B_0^{(p)} - M_{h+}^2 C_0^{(p)} \right) - z_6 C_0^{(p)} - m_t z_2 \frac{Y_{ti}^{h+}}{X_{ti}^{h+}} (C_{11}^{(p)} - C_{12}^{(p)}) - m_c z_5 C_{12}^{(p)} \right] X_{ti}^{h+} \\
F_{2i}^{(q)} &= -\frac{ig^3 M_W \beta_{dd}^h}{16\pi^2} \left[m_t Y_{cj}^i Y_{tj}^i (C_{11}^{(q)} - C_{12}^{(q)}) - m_i X_{tj}^i Y_{cj}^i C_0^{(q)} + m_c X_{cj}^i X_{tj}^i C_{12}^{(q)} \right] \\
F_{2i}^{(r)} &= -\frac{ig^3}{16\pi^2} \left[z_4 \left(B_0^{(r)} - M_{di}^2 C_0^{(r)} \right) - z_6 C_0^{(r)} - m_t z_2 \frac{Y_{tj}^i}{X_{tj}^i} (C_{11}^{(r)} - C_{12}^{(r)}) - m_c z_5 C_{12}^{(r)} \right] X_{tj}^i \\
F_{2i}^{(s)} &= \frac{ig^3}{16\pi^2 (m_t^2 - m_c^2)} \left[m_t \left(m_t B_{uc}^h X_{ci}^{h+} + m_c B_{uc}^h \frac{Y_{ti}^{h+}}{X_{ti}^{h+}} Y_{ci}^{h+} \right) B_1^{(s)} \right. \\
&\quad \left. - m_i \left(m_t B_{uc}^h X_{ci}^{h+} \frac{Y_{ti}^{h+}}{X_{ti}^{h+}} + m_c B_{uc}^h Y_{ci}^{h+} \right) B_0^{(s)} \right] X_{ti}^{h+} \\
F_{2i}^{(t)} &= \frac{ig^3}{16\pi^2 (m_t^2 - m_c^2)} \left[m_t \left(m_t B_{uc}^h X_{cj}^i + m_c B_{uc}^h \frac{Y_{ti}^{h+}}{X_{ti}^{h+}} Y_{cj}^i \right) B_1^{(t)} - m_i \left(m_t B_{uc}^h X_{cj}^i \frac{Y_{ti}^{h+}}{X_{ti}^{h+}} + m_c B_{uc}^h Y_{cj}^i \right) B_0^{(t)} \right] X_{ti}^{h+} \\
F_{2i}^{(u)} &= -\frac{ig^3}{16\pi^2 (m_t^2 - m_c^2)} \left[m_c Y_{ti}^{h+} \left(m_c Y_{ci}^{h+} B_1^{(u)} - m_i X_{ci}^{h+} B_0^{(u)} \right) + m_t X_{ti}^{h+} \left(m_c X_{ci}^{h+} B_1^{(u)} - m_i Y_{ci}^{h+} B_0^{(u)} \right) \right] B_{ut}^h \\
F_{2i}^{(v)} &= -\frac{ig^3}{16\pi^2 (m_t^2 - m_c^2)} \left[m_c Y_{tj}^i \left(m_c Y_{cj}^i B_1^{(v)} - m_i X_{cj}^i B_0^{(v)} \right) + m_t X_{tj}^i \left(m_c X_{cj}^i B_1^{(v)} - m_i Y_{cj}^i B_0^{(v)} \right) \right] B_{ut}^h \quad (2.2.6)
\end{aligned}$$

where

$$\begin{aligned}
C_X^{(k)} &= C_X(m_i, M_W, M_{h+}; m_c, m_t, M_h) & B_X^{(s)} &= B_X(m_{\tilde{\chi}_i^+}, M_{\tilde{d}_j}; m_t) \\
C_X^{(l)} &= C_X(m_i, M_{h+}, M_W; m_c, m_t, M_h) & B_X^{(t)} &= B_X(m_i, M_{h+}; m_t) \\
C_X^{(m)} &= C_X(m_i, M_{h+}, M_{h+}; m_c, m_t, M_h) & B_X^{(u)} &= B_X(m_{\tilde{\chi}_i^+}, M_{\tilde{d}_j}; m_c) \\
C_X^{(n)} &= C_X(m_i, M_{h+}, M_W; m_c, m_t, M_h) & B_X^{(v)} &= B_X(m_i, M_{h+}; m_c) \\
C_X^{(o)} &= C_X(m_i, M_W, M_{h+}; m_c, m_t, M_h) & C_X^{(p)} &= C_X(M_{h+}, m_i, m_i; m_c, m_t, M_h) \\
C_X^{(q)} &= C_X(m_{\tilde{\chi}_i^+}, M_{\tilde{d}_j}, M_{\tilde{d}_j}; m_c, m_t, M_h) & C_X^{(r)} &= C_X(M_{\tilde{d}_j}, m_{\tilde{\chi}_i^+}, m_{\tilde{\chi}_i^+}; m_c, m_t, M_h)
\end{aligned} \quad (2.2.7)$$

where $X = 0, 11, 12, 21, 23, 24$, as before, and defined two sets of effective couplings

$$\begin{aligned}
z_1^{(p)} &= X_{ci}^h B_{di}^h \\
z_2^{(p)} &= m_t Y_{ci}^h \frac{X_{ti}^h}{Y_{ti}^h} A_{di}^h + m_c X_{ci}^h B_{di}^h + m_i Y_{ci}^h B_{di}^h + m_i Y_{ci}^h A_{di}^h \\
z_3^{(p)} &= m_t \frac{X_{ti}^h}{Y_{ti}^h} A_{di}^h (m_i X_{ci}^h + m_c Y_{ci}^h) + m_i^2 A_{di}^h X_{ci}^h + m_i m_c A_{di}^h Y_{ci}^h \\
z_4^{(p)} &= Y_{ci}^h A_{di}^h
\end{aligned}$$

$$\begin{aligned}
z_5^{(p)} &= m_t X_{ci}^h \frac{Y_{ti}^h}{X_{ti}^h} B_{di}^h + m_c Y_{ci}^h A_{di}^h + m_i X_{ci}^h A_{di}^h + m_i X_{ci}^h B_{di}^h \\
z_6^{(p)} &= m_t \frac{Y_{ti}^h}{X_{ti}^h} B_{di}^h (m_i Y_{ci}^h + m_c X_{ci}^h) + m_i^2 B_{di}^h Y_{ci}^h + m_i m_c B_{di}^h X_{ci}^h
\end{aligned} \tag{2.2.8}$$

and

$$\begin{aligned}
z_1^{(r)} &= X_{cj}^i B_{ij}^h \\
z_2^{(r)} &= m_t Y_{cj}^i \frac{X_{tj}^i}{Y_{tj}^i} A_{ij}^h + m_c X_{cj}^i B_{ij}^h + m_i Y_{cj}^i B_{ij}^h + m_i Y_{cj}^i A_{ij}^h \\
z_3^{(r)} &= m_t \frac{X_{tj}^i}{Y_{tj}^i} A_{ij}^h (m_i X_{cj}^i + m_c Y_{cj}^i) + m_i^2 A_{ij}^h X_{cj}^i + m_i m_c A_{ij}^h Y_{cj}^i \\
z_4^{(r)} &= Y_{cj}^i A_{ij}^h \\
z_5^{(r)} &= m_t X_{cj}^i \frac{Y_{tj}^i}{X_{tj}^i} B_{ij}^h + m_c Y_{cj}^i A_{ij}^h + m_i X_{cj}^i A_{ij}^h + m_i X_{cj}^i B_{ij}^h \\
z_6^{(r)} &= m_t \frac{Y_{tj}^i}{X_{tj}^i} B_{ij}^h (m_i Y_{cj}^i + m_c X_{cj}^i) + m_i^2 B_{ij}^h Y_{cj}^i + m_i m_c B_{ij}^h X_{cj}^i
\end{aligned} \tag{2.2.9}$$

As before, these form factors can now be combined, using $F_{ni} = \sum_{A=a}^j F_{ni}^A$ for $n = 1, 2$ and the results substituted into Eqn. (2.1.8) to get the final amplitude.

B.2.2 The decay $t \rightarrow c + Z$

When we turn to the decay process $t \rightarrow c + Z$, then, as in the toy model, we have to calculate four helicity amplitudes in terms of four form factors F_1 , F_2 , F_3 and F_4 . For the Standard Model, we then evaluate the diagrams of Figure 3.4, replacing the H everywhere by a Z . In order to do this, we set up the following general vertices.

$$\begin{aligned}
\bar{u}_i u_i Z^\mu &: ig\gamma^\mu (A_{ui}^Z P_L + B_{ui}^Z P_R) \\
\bar{d}_i d_i Z^\mu &: ig\gamma^\mu (A_{di}^Z P_L + B_{di}^Z P_R) \\
W^{\mu+} Z^\nu \phi^- &: ig\omega_{WZ}^\phi g^{\mu\nu} \\
Z^\mu \phi(p)^+ \phi'(q)^- &: ig\alpha_{\phi'}^\phi (p+q)^\mu \\
\bar{u}_i d_j \phi^+ &: ig \left(X_{ij}^\phi P_L + Y_{ij}^\phi P_R \right)
\end{aligned}$$

in terms of a set of coupling constants A_{ui}^Z , B_{ui}^Z , A_{di}^Z , B_{di}^Z , ω_{WZ}^ϕ , $\alpha_{\phi'}^\phi$, X_{ij}^ϕ and Y_{ij}^ϕ . In the SM, these have values given in the table below.

where

$$\begin{aligned}
g_L^u &= \frac{1}{2} - \frac{2}{3} \sin^2 \theta_W & g_R^u &= -\frac{2}{3} \sin^2 \theta_W \\
g_L^d &= -\frac{1}{2} + \frac{1}{3} \sin^2 \theta_W & g_R^d &= \frac{1}{3} \sin^2 \theta_W
\end{aligned} \tag{2.2.10}$$

coupling :	A_{ui}^Z	B_{ui}^Z	A_{di}^Z	B_{di}^Z
SM :	$-\frac{g_L^u}{\cos \theta_W}$	$-\frac{g_R^u}{\cos \theta_W}$	$-\frac{g_L^u}{\cos \theta_W}$	$-\frac{g_R^u}{\cos \theta_W}$
coupling :	ω_{WZ}^ϕ	$\alpha_{\phi'}^\phi$	X_{ij}^ϕ	Y_{ij}^ϕ
SM :	$-M_Z \sin^2 \theta_W$	$-\frac{\cos 2\theta_W}{2 \cos \theta_W}$	$\frac{m_i}{\sqrt{2}M_W}$	$-\frac{m_j}{\sqrt{2}M_W}$

As in the previous cases, we can now compute, using the diagrams of Figure 3.4 (with $h^0 \rightarrow Z$) a set of forms factors. The set of F_1 form factors are

$$\begin{aligned}
F_{1i}^{(a)} &= \frac{g^3 \cos \theta_W}{16\pi^2} \left[2m_t^2 (C_{21}^{(a)} - C_{23}^{(a)}) - 2C_{24}^{(a)} + (m_t^2 + m_c^2 - M_Z^2)C_{11}^{(a)} - m_c^2 C_{12}^{(a)} - (B_0^{(a)} - m_i^2 C_0^{(a)}) \right] \\
F_{1i}^{(b)} &= -\frac{g^3 \omega_{WZ}^{G+}}{16\sqrt{2}\pi^2} \left[m_t X_{ti}^G (C_{11}^{(b)} - C_{12}^{(b)}) - m_i Y_{ti}^G C_0^{(b)} \right] \\
F_{1i}^{(c)} &= -\frac{g^3 \omega_{WZ}^{G+}}{16\sqrt{2}\pi^2} \left[m_c X_{ci}^G C_{12}^{(c)} - 2m_i Y_{ci}^G C_0^{(c)} + 2m_t X_{ci}^G (C_{11}^{(c)} - C_{12}^{(c)}) \right] \\
F_{1i}^{(d)} &= -\frac{g^3 \alpha_{G-}^{G+}}{16\sqrt{2}\pi^2} \left[m_t^2 Y_{ci}^G Y_{ti}^G (C_{21}^{(d)} - C_{23}^{(d)}) + m_c m_t X_{ci}^G X_{ti}^G C_{23}^{(d)} - 2Y_{ci}^G Y_{ti}^G C_{24}^{(d)} - m_i m_t Y_{ti}^G X_{ci}^G (C_0^{(d)} + C_{11}^{(d)}) \right] \\
F_{1i}^{(e)} &= \frac{g^3}{32\pi^2} \left[A_{di}^Z \left\{ 2(m_c^2 + m_t^2 - M_Z^2 + m_c m_t)(C_0^{(e)} + C_{11}^{(e)}) + 2m_t^2 (C_{11}^{(e)} - C_{12}^{(e)}) + m_c^2 C_{12}^{(e)} + 2C_{24}^{(e)} \right. \right. \\
&\quad \left. \left. + 2m_i m_t (C_0^{(e)} + C_{11}^{(e)}) - B_0^{(e)} + M_W^2 C_0^{(e)} \right\} + 2m_i B_{di}^Z \left\{ m_t (C_0^{(e)} + C_{11}^{(e)}) - m_i C_0^{(e)} \right\} \right] \\
F_{1i}^{(f)} &= -\frac{g^3}{16\pi^2} \left[X_{ci}^G \left\{ \left(m_i + m_t \frac{Y_{ci}^G}{X_{ci}^G} \right) A_{di}^Z (m_c X_{ci}^G (C_0^{(f)} + C_{12}^{(f)}) + m_i Y_{ci}^G C_0^{(f)}) \right. \right. \\
&\quad \left. \left. - B_{di}^Z (m_c (m_i X_{ci}^G + m_c Y_{ci}^G) C_{12}^{(f)} - Y_{ci}^G (B_0^{(f)} - M_W^2 C_0^{(f)}) - m_t Y_{ci}^G (m_t C_{21}^{(f)} + m_c C_{23}^{(f)}) - 2C_{24}^{(f)}) \right\} \right. \\
&\quad \left. - m_t Y_{ci}^G A_{di}^Z (m_c X_{ci}^G + m_i Y_{ci}^G) C_{11}^{(f)} \right] \\
F_{1i}^{(g)} &= -\frac{g^3}{16\pi^2 (m_t^2 - m_c^2)} m_c^2 A_{ci}^Z B_1^{(g)} \\
F_{1i}^{(h)} &= -\frac{g^3}{16\pi^2 (m_t^2 - m_c^2)} A_{ti}^Z \left[m_t X_{ti}^G (m_c X_{ci}^G B_1^{(h)} - m_i Y_{ci}^G B_0^{(h)}) + m_c Y_{ti}^G (Y_{ci}^G m_c B_1^{(h)} - m_i X_{ci}^G B_0^{(h)}) \right] \\
F_{1i}^{(i)} &= \frac{g^3}{32\pi^2 (m_t^2 - m_c^2)} m_t (m_t A_{ti}^Z + m_c B_{ti}^Z) B_1^{(i)} \tag{2.2.11} \\
F_{1i}^{(j)} &= \frac{g^3}{16\pi^2 (m_t^2 - m_c^2)} A_{ti}^Z Y_{ti}^G \left[m_t Y_{ci}^G \left(m_t + m_c \frac{X_{ti}^G X_{ci}^G}{Y_{ti}^G Y_{ci}^G} \right) B_1^{(j)} - m_i X_{ci}^G \left(m_t \frac{Y_{ci}^G X_{ti}^G}{X_{ci}^G Y_{ti}^G} + m_c \right) B_0^{(j)} \right]
\end{aligned}$$

The nonvanishing F_2 form factors are

$$\begin{aligned}
F_{2i}^{(a)} &= \frac{g^3 \cos \theta_W}{16\pi^2} m_c m_t (C_{11}^{(a)} - C_{12}^{(a)}) \\
F_{2i}^{(b)} &= -\frac{g^3 \omega_{WZ}^{G+}}{16\sqrt{2}\pi^2} (m_t - m_c) X_{ti}^G C_{12}^{(b)} \\
F_{2i}^{(c)} &= \frac{g^3 \omega_{WZ}^{G+}}{16\sqrt{2}\pi^2} m_t X_{ci}^G (C_{11}^{(c)} - C_{12}^{(c)}) \\
F_{2i}^{(d)} &= -\frac{g^3 \alpha_{G-}^{G+}}{16\sqrt{2}\pi^2} \left[m_t^2 X_{ci}^G X_{ti}^G (C_{21}^{(d)} - C_{23}^{(d)}) + m_c m_t Y_{ci}^G Y_{ti}^G C_{23}^{(d)} - 2X_{ci}^G X_{ti}^G C_{24}^{(d)} - m_i m_t X_{ti}^G Y_{ci}^G (C_0^{(d)} + C_{11}^{(d)}) \right] \\
F_{2i}^{(e)} &= -\frac{g^3}{32\pi^2} A_{di}^Z \left[m_t (m_t + m_c) (C_0^{(e)} + C_{11}^{(e)}) + m_t^2 (C_{11}^{(e)} - C_{12}^{(e)}) + m_c m_t C_{12}^{(e)} - m_t^2 C_{21}^{(e)} - m_t (m_t - m_c) C_{23}^{(e)} \right]
\end{aligned}$$

$$\begin{aligned}
F_{2i}^{(f)} &= -\frac{g^3}{16\pi^2} \left[Y_{ci}^G \left\{ \left(m_i + m_t \frac{X_{ci}^G}{Y_{ci}^G} \right) B_{di}^Z \left(m_c Y_{ci}^G (C_0^{(f)} + C_{12}^{(f)}) + m_i X_{ci}^G C_0^{(f)} \right) \right. \right. \\
&\quad \left. \left. - A_{di}^Z \left(m_c (m_i Y_{ci}^G + m_c X_{ci}^G) C_{12}^{(f)} - X_{ci}^G (B_0^{(f)} - M_W^2 C_0^{(f)}) - m_t Y_{ci}^G (m_t C_{21}^{(f)} + m_c C_{23}^{(f)}) - 2C_{24}^{(f)} \right) \right\} \right. \\
&\quad \left. - m_t X_{ci}^G B_{di}^Z (m_c Y_{ci}^G + m_i X_{ci}^G) C_{11}^{(f)} \right] \\
F_{2i}^{(g)} &= -\frac{g^3}{16\pi^2 (m_t^2 - m_c^2)} m_c m_t B_{ci}^Z B_1^{(g)} \\
F_{2i}^{(h)} &= -\frac{g^3}{16\pi^2 (m_t^2 - m_c^2)} B_{ti}^Z \left[m_t Y_{ti}^G \left(m_c Y_{ci}^G B_1^{(h)} - m_i X_{ci}^G B_0^{(h)} \right) + m_c X_{ti}^G \left(m_c X_{ci}^G B_1^{(h)} - m_i Y_{ci}^G B_0^{(h)} \right) \right] \\
F_{2i}^{(j)} &= \frac{g^3}{16\pi^2 (m_t^2 - m_c^2)} B_{ti}^Z X_{ti}^G \left[m_t X_{ci}^G \left(m_t + m_c \frac{Y_{ti}^G Y_{ci}^G}{X_{ti}^G X_{ci}^G} \right) B_1^{(j)} - m_i Y_{ci}^G \left(m_t \frac{X_{ci}^G Y_{ti}^G}{Y_{ci}^G X_{ti}^G} + m_c \right) B_0^{(j)} \right] \quad (2.2.12)
\end{aligned}$$

The nonvanishing F_3 form factors are

$$\begin{aligned}
F_{3i}^{(a)} &= -\frac{g^3 \cos \theta_W}{32\pi^2} m_c \left[C_{11}^{(a)} + 2C_{12}^{(a)} \right] \\
F_{3i}^{(c)} &= \frac{g^3 \omega_{WZ}^{G+}}{16\sqrt{2}\pi^2} X_{ci}^G (C_{11}^{(c)} - C_{12}^{(c)}) \\
F_{3i}^{(d)} &= \frac{g^3 \alpha_{G-}^{G+}}{16\sqrt{2}\pi^2} \left[m_t X_{ci}^G X_{ti}^G (C_{21}^{(d)} - C_{23}^{(d)}) - m_c Y_{ci}^G Y_{ti}^G C_{23}^{(d)} + m_i Y_{ti}^G X_{ci}^G (C_0^{(d)} + C_{11}^{(d)}) \right] \\
F_{3i}^{(e)} &= \frac{g^3}{32\pi^2} A_{di}^Z \left[(m_t + m_c) (C_0^{(e)} + C_{11}^{(e)}) + m_t (C_{11}^{(e)} - C_{12}^{(e)}) + m_c C_{12}^{(e)} - m_t C_{21}^{(e)} - (m_t - m_c) C_{23}^{(e)} \right] \\
F_{3i}^{(f)} &= \frac{g^3}{16\pi^2} X_{ci}^G \left[A_{di}^V \left(m_i + m_t \frac{Y_{ci}^G}{X_{ci}^G} \right) X_{ci}^G (C_{11}^{(f)} - C_{12}^{(f)}) \right. \\
&\quad \left. - B_{di}^Z \left\{ \left(m_i X_{ci}^G + m_c Y_{ci}^G \right) (C_{11}^{(f)} - C_{12}^{(f)}) + (m_i X_{ci}^G + m_c Y_{ci}^G) C_{11}^{(f)} + Y_{ci}^G (m_t C_{21}^{(f)} + m_c C_{23}^{(f)}) \right\} \right] \quad (2.2.13)
\end{aligned}$$

The nonvanishing F_4 form factors are

$$\begin{aligned}
F_{4i}^{(a)} &= \frac{g^3 \cos \theta_W}{16\pi^2} m_t \{ 2(C_{11}^{(a)} - C_{12}^{(a)}) - (C_{21}^{(a)} - C_{23}^{(a)}) \} \\
F_{4i}^{(b)} &= -\frac{g^3 \omega_{WZ}^{G+}}{16\sqrt{2}\pi^2} X_{ti}^G C_{12}^{(b)} \\
F_{4i}^{(d)} &= \frac{g^3 \alpha_{G-}^{G+}}{16\sqrt{2}\pi^2} \left[m_t Y_{ci}^G Y_{ti}^G (C_{21}^{(d)} - C_{23}^{(d)}) - m_c X_{ci}^G X_{ti}^G C_{23}^{(d)} + m_i X_{ti}^G Y_{ci}^G (C_0^{(d)} + C_{11}^{(d)}) \right] \\
F_{4i}^{(e)} &= -\frac{g^3}{16\pi^2} m_i (A_{di}^Z + B_{di}^Z) (C_0^{(e)} + C_{11}^{(e)}) \\
F_{4i}^{(f)} &= \frac{g^3}{16\pi^2} Y_{ci}^G \left[B_{di}^Z \left(m_i + m_t \frac{X_{ci}^G}{Y_{ci}^G} \right) Y_{ci}^G (C_{11}^{(f)} - C_{12}^{(f)}) \right. \\
&\quad \left. - A_{di}^Z \left\{ \left(m_i Y_{ci}^G + m_c X_{ci}^G \right) (C_{11}^{(f)} - C_{12}^{(f)}) + (m_i Y_{ci}^G + m_c X_{ci}^G) C_{11}^{(f)} + X_{ci}^G (m_t C_{21}^{(f)} + m_c C_{23}^{(f)}) \right\} \right] \quad (2.2.14)
\end{aligned}$$

where

$$\begin{aligned}
C_X^{(a)} &= C_X(m_i, M_W, M_W; m_c, m_t, M_Z) & B_0^{(e)} &= B_0(M_W, m_i; M_Z) \\
C_X^{(b)} &= C_X(m_i, M_W, M_W; m_c, m_t, M_Z) & B_1^{(g)} &= B_1(m_i, M_W; m_t) \\
C_X^{(c)} &= C_X(m_i, M_W, M_W; m_c, m_t, M_Z) & B_1^{(h)} &= B_1(m_i, M_W; m_t) \\
C_X^{(d)} &= C_X(m_i, M_W, M_W; m_c, m_t, M_Z) & B_0^{(h)} &= B_0(m_i, M_W; m_t) \\
C_X^{(e)} &= C_X(M_W, m_i, m_i; m_c, m_t, M_Z) & B_1^{(i)} &= B_1(m_i, M_W; m_c) \\
C_X^{(f)} &= C_X(M_W, m_i, m_i; m_c, m_t, M_Z) & B_1^{(j)} &= B_1(m_i, M_W; m_c) \\
B_0^{(a)} &= B_0(M_W, M_W; M_Z) & B_0^{(j)} &= B_0(m_i, M_W; m_c) \quad (2.2.15)
\end{aligned}$$

where $X = 0, 11, 12, 21, 23, 24$, as usual. We then calculate the total form factors using $F_{ni} = \sum_{A=a}^j F_{ni}^A$ for $n = 1, 2, 3, 4$ and substitute the results into Eqn. (2.1.23) to get the final SM amplitude.

In the cMSSM, we require to evaluate all the diagrams which contribute in the SM, i.e. those which are listed in Figure 3.4. This will involve all the vertices we have defined for the SM, but the coupling constants will be somewhat different. These are listed in the table below.

coupling :	A_{ui}^Z	B_{ui}^Z	A_{di}^Z	B_{di}^Z
SM :	$-\frac{g_L^u}{\cos \theta_W}$	$-\frac{g_R^u}{\cos \theta_W}$	$-\frac{g_L^u}{\cos \theta_W}$	$-\frac{g_R^u}{\cos \theta_W}$
coupling :	$\omega_{WZ}^{G^+}$	$\alpha_{G^-}^{G^+}$	$X_{ij}^{H^+}$	$Y_{ij}^{H^+}$
SM :	$-M_Z \sin^2 \theta_W$	$-\frac{\cos 2\theta_W}{2 \cos \theta_W}$	$\frac{m_i \cot \beta}{\sqrt{2} M_W}$	$\frac{m_j \tan \beta}{\sqrt{2} M_W}$

Due to the absence of a $W^\pm H^\mp Z$ vertex (whereas there is a $W^\pm H^\mp h^0$ vertex, the list of additional diagrams in the cMSSM can be obtained by changing the H lines in Figure 3.5 to Z lines, provided we discard the diagrams marked (k) , (ℓ) , (n) and (o) . Evaluating the remaining ones we get the F_1 form factors

$$\begin{aligned}
F_{1i}^{(m)} &= -\frac{g^3 \alpha_{h^+}^-}{16\sqrt{2}\pi^2} \left[m_t^2 (C_{21}^{(m)} - C_{23}^{(m)}) Y_{ci}^h Y_{ti}^h + m_c m_t C_{23}^{(m)} X_{ci}^h X_{ti}^h - 2C_{24}^{(m)} Y_{ci}^h Y_{ti}^h - m_i m_t (C_0^{(m)} + C_{11}^{(m)}) Y_{ti}^h X_{ci}^h \right] \\
F_{1i}^{(p)} &= -\frac{g^3}{16\pi^2} \left[X_{ci}^h \left\{ \left(m_i + m_t \frac{Y_{ci}^h}{X_{ci}^h} \right) A_{di}^Z \left(X_{ci}^h m_c (C_0^{(p)} + C_{12}^{(p)}) + m_i Y_{ci}^h C_0^{(p)} \right) \right. \right. \\
&\quad \left. \left. - B_{di}^Z \left((m_i X_{ci}^h + m_c Y_{ci}^h) m_c C_{12}^{(p)} - Y_{ci}^h (B_0^{(p)} - M_{h^+}^2 + C_0^{(p)}) - m_t Y_{ci}^h (m_t C_{21}^{(p)} + m_c C_{23}^{(p)}) - 2C_{24}^{(p)} \right) \right\} \right. \\
&\quad \left. - m_t A_{di}^Z Y_{ci}^h (m_i Y_{ci}^h + m_c X_{ci}^h) C_{11}^{(p)} \right] \\
F_{1i}^{(q)} &= -\frac{g^3 \alpha_d^{\tilde{d}}}{16\sqrt{2}\pi^2} \left[m_t^2 Y_{ci}^j Y_{ti}^j (C_{21}^{(q)} - C_{23}^{(q)}) + m_c m_t X_{ci}^j X_{ti}^j C_{23}^{(q)} - 2Y_{ci}^j Y_{ti}^j C_{24}^{(q)} - m_i m_t Y_{ti}^j X_{ci}^j (C_0^{(m)} + C_{11}^{(q)}) \right] \\
F_{1i}^{(r)} &= -\frac{g^3}{16\pi^2} \left[X_{ci}^j \left\{ \left(m_i + m_t \frac{Y_{ci}^j}{X_{ci}^j} \right) A_{di}^Z \left(X_{ci}^j m_c (C_0^{(r)} + C_{12}^{(r)}) + m_i Y_{ci}^j C_0^{(r)} \right) \right. \right. \\
&\quad \left. \left. - B_{di}^Z \left((m_i X_{ci}^j + m_c Y_{ci}^j) m_c C_{12}^{(r)} - Y_{ci}^j (B_0^{(r)} - M_{d_j}^2 + C_0^{(r)}) - Y_{ci}^j (m_t C_{21}^{(r)} + m_c C_{23}^{(r)}) m_t - 2C_{24}^{(r)} \right) \right\} \right. \\
&\quad \left. - m_t A_{di}^Z Y_{ci}^j (m_i Y_{ci}^j + m_c X_{ci}^j) C_{11}^{(r)} \right] \\
F_{1i}^{(s)} &= \frac{g^3}{16\pi^2 (m_t^2 - m_c^2)} A_{ci}^Z Y_{ti}^h \left[m_t Y_{ci}^h \left(m_t + m_c \frac{X_{ti}^h X_{ci}^h}{Y_{ti}^h Y_{ci}^h} \right) B_1^{(s)} - m_i X_{ci}^h \left(m_t \frac{Y_{ci}^h X_{ti}^h}{X_{ci}^h Y_{ti}^h} + m_c \right) B_0^{(s)} \right] \\
F_{1i}^{(t)} &= \frac{g^3}{16\pi^2 (m_t^2 - m_c^2)} A_{ci}^Z Y_{ti}^j \left[m_t Y_{ci}^j \left(m_t + m_c \frac{X_{ti}^j X_{ci}^j}{Y_{ti}^j Y_{ci}^j} \right) B_1^{(t)} - m_i X_{ci}^j \left(m_t \frac{Y_{ci}^j X_{ti}^j}{X_{ci}^j Y_{ti}^j} + m_c \right) B_0^{(t)} \right] \\
F_{1i}^{(u)} &= -\frac{g^3}{16\pi^2 (m_t^2 - m_c^2)} A_{ti}^Z \left[m_c Y_{ti}^h \left(m_c Y_{ci}^h B_1^{(u)} - m_i X_{ci}^h B_0^{(u)} \right) + m_t X_{ti}^h \left(m_c X_{ci}^h B_1^{(u)} - m_i Y_{ci}^h B_0^{(u)} \right) \right] \\
F_{1i}^{(v)} &= -\frac{g^3}{16\pi^2 (m_t^2 - m_c^2)} A_{ti}^Z \left[m_c Y_{ti}^j \left(m_c Y_{ci}^j B_1^{(r)} - m_i X_{ci}^j B_0^{(r)} \right) + m_t X_{ti}^j \left(m_c X_{ci}^j B_1^{(r)} - m_i Y_{ci}^j B_0^{(r)} \right) \right] \quad (2.2.16)
\end{aligned}$$

The F_2 form factors are

$$\begin{aligned}
F_{2i}^{(m)} &= -\frac{g^3 \alpha_{h^+}^-}{16\sqrt{2}\pi^2} \left[m_t^2 X_{ci}^h X_{ti}^h (C_{21}^{(m)} - C_{23}^{(m)}) + m_c m_t Y_{ci}^h Y_{ti}^h C_{23}^{(m)} - 2X_{ci}^h X_{ti}^h C_{24}^{(m)} - m_i m_t X_{ti}^h Y_{ci}^h (C_0^{(m)} + C_{11}^{(m)}) \right] \\
F_{2i}^{(p)} &= -\frac{g^3}{16\pi^2} \left[Y_{ci}^h \left\{ \left(m_i + m_t \frac{X_{ci}^h}{Y_{ci}^h} \right) B_{di}^Z \left(Y_{ci}^h m_c (C_0^{(p)} + C_{12}^{(p)}) + m_i X_{ci}^h C_0^{(p)} \right) \right. \right. \\
&\quad \left. \left. - A_{di}^Z \left((m_i Y_{ci}^h + m_c X_{ci}^h) m_c C_{12}^{(p)} - X_{ci}^h (B_0^{(p)} - M_{h^+}^2 + C_0^{(p)}) - m_t X_{ci}^h (m_t C_{21}^{(p)} + m_c C_{23}^{(p)}) - 2C_{24}^{(p)} \right) \right\} \right. \\
&\quad \left. - m_t B_{di}^Z X_{ci}^h (m_i X_{ci}^h + m_c Y_{ci}^h) C_{11}^{(p)} \right] \\
F_{2i}^{(q)} &= -\frac{g^3 \alpha_d^{\tilde{d}}}{16\sqrt{2}\pi^2} \left[m_t^2 X_{ci}^j X_{ti}^j (C_{21}^{(q)} - C_{23}^{(q)}) + m_c m_t Y_{ci}^j Y_{ti}^j C_{23}^{(q)} - 2X_{ci}^j X_{ti}^j C_{24}^{(q)} - m_i m_t X_{ti}^j Y_{ci}^j (C_0^{(m)} + C_{11}^{(q)}) \right]
\end{aligned}$$

$$\begin{aligned}
F_{2i}^{(r)} &= -\frac{g^3}{16\pi^2} \left[Y_{ci}^j \left\{ \left(m_i + m_t \frac{X_{ci}^j}{Y_{ci}^j} \right) B_{di}^Z \left(Y_{ci}^j m_c (C_0^{(r)} + C_{12}^{(r)}) + m_i X_{ci}^j C_0^{(r)} \right) \right. \right. \\
&\quad \left. \left. - B_{di}^Z \left(\left(m_i Y_{ci}^j + m_c X_{ci}^j \right) m_c C_{12}^{(r)} - X_{ci}^j \left(B_0^{(r)} - M_{d_j}^2 C_0^{(r)} \right) - X_{ci}^j (m_t C_{21}^{(r)} + m_c C_{23}^{(r)}) m_t - 2C_{24}^{(r)} \right) \right\} \right. \\
&\quad \left. - m_t B_{di}^Z X_{ci}^j (m_i X_{ci}^j + m_c Y_{ci}^j) C_{11}^{(r)} \right] \quad (2.2.17) \\
F_{2i}^{(s)} &= \frac{g^3}{16\pi^2 (m_t^2 - m_c^2)} B_{ci}^Z X_{ti}^h \left[m_t X_{ci}^h \left(m_t + m_c \frac{Y_{ti}^h Y_{ci}^h}{X_{ti}^h X_{ci}^h} \right) B_1^{(s)} - m_i Y_{ci}^h \left(m_t \frac{X_{ci}^h Y_{ti}^h}{Y_{ci}^h X_{ti}^h} + m_c \right) B_0^{(s)} \right] \\
F_{2i}^{(t)} &= \frac{g^3}{16\pi^2 (m_t^2 - m_c^2)} B_{ci}^Z X_{ti}^j \left[m_t X_{ci}^j \left(m_t + m_c \frac{Y_{ti}^j Y_{ci}^j}{X_{ti}^j X_{ci}^j} \right) B_1^{(t)} - m_i Y_{ci}^j \left(m_t \frac{X_{ci}^j Y_{ti}^j}{Y_{ci}^j X_{ti}^j} + m_c \right) B_0^{(t)} \right] \\
F_{2i}^{(u)} &= -\frac{g^3}{16\pi^2 (m_t^2 - m_c^2)} B_{ti}^Z \left[m_c X_{ti}^h \left(m_c X_{ci}^h B_1^{(u)} - m_i Y_{ci}^h B_0^{(u)} \right) + m_t Y_{ti}^h \left(m_c Y_{ci}^h B_1^{(u)} - m_i X_{ci}^h B_0^{(u)} \right) \right] \\
F_{2i}^{(v)} &= -\frac{g^3}{16\pi^2 (m_t^2 - m_c^2)} B_{ti}^Z \left[m_c X_{ti}^j \left(m_c X_{ci}^j B_1^{(r)} - m_i Y_{ci}^j B_0^{(r)} \right) + m_t Y_{ti}^j \left(m_c Y_{ci}^j B_1^{(r)} - m_i X_{ci}^j B_0^{(r)} \right) \right] \quad (2.2.18)
\end{aligned}$$

The nonvanishing F_3 form factors are

$$\begin{aligned}
F_{3i}^{(m)} &= \frac{g^3 \alpha_{h+}^-}{16\sqrt{2}\pi^2} \left[m_t X_{ci}^h X_{ti}^h (C_{21}^{(m)} - C_{23}^{(m)}) - m_c Y_{ci}^h Y_{ti}^h C_{23}^{(m)} + m_i Y_{ti}^h X_{ci}^h (C_0^{(m)} + C_{11}^{(m)}) \right] \\
F_{3i}^{(p)} &= \frac{g^3}{16\pi^2} X_{ci}^h \left[A_{di}^Z \left(m_i + m_t \frac{Y_{ci}^h}{X_{ci}^h} \right) X_{ci}^h (C_{11}^{(p)} - C_{12}^{(p)}) \right. \\
&\quad \left. - B_{di}^Z \left\{ \left(m_i X_{ci}^h + m_c Y_{ci}^h \right) (C_{11}^{(p)} - C_{12}^{(p)}) + (m_i X_{ci}^h + m_c Y_{ci}^h) C_{11}^{(p)} + Y_{ci}^h (m_t C_{21}^{(p)} + m_c C_{23}^{(p)}) \right\} \right] \\
F_{3i}^{(q)} &= \frac{g^3 \alpha_d^{\tilde{d}}}{16\sqrt{2}\pi^2} \left[m_t X_{ci}^j X_{ti}^j (C_{21}^{(q)} - C_{23}^{(q)}) - m_c Y_{ci}^j Y_{ti}^j C_{23}^{(q)} + m_i Y_{ti}^j X_{ci}^j (C_0^{(q)} + C_{11}^{(q)}) \right] \\
F_{3i}^{(r)} &= \frac{g^3}{16\pi^2} X_{ci}^j \left[A_{di}^Z \left(m_i + m_t \frac{Y_{ci}^j}{X_{ci}^j} \right) X_{ci}^j (C_{11}^{(r)} - C_{12}^{(r)}) \right. \\
&\quad \left. - B_{di}^Z \left\{ \left(m_i X_{ci}^j + m_c Y_{ci}^j \right) (C_{11}^{(r)} - C_{12}^{(r)}) + (m_i X_{ci}^j + m_c Y_{ci}^j) C_{11}^{(r)} + Y_{ci}^j (m_t C_{21}^{(r)} + m_c C_{23}^{(r)}) \right\} \right] \quad (2.2.19)
\end{aligned}$$

Finally, the nonvanishing F_4 form factors are

$$\begin{aligned}
F_{4i}^{(m)} &= \frac{g^3 \alpha_{h+}^-}{16\sqrt{2}\pi^2} \left[m_t Y_{ci}^h Y_{ti}^h (C_{21}^{(m)} - C_{23}^{(m)}) - m_c X_{ci}^h X_{ti}^h C_{23}^{(m)} + m_i X_{ti}^h Y_{ci}^h (C_0 + C_{11}^{(m)}) \right] \\
F_{4i}^{(p)} &= \frac{g^3}{16\pi^2} X_{ci}^h \left[B_{di}^Z \left(m_i + m_t \frac{X_{ci}^h}{Y_{ci}^h} \right) Y_{ci}^h (C_{11}^{(p)} - C_{12}^{(p)}) \right. \\
&\quad \left. - A_{di}^Z \left\{ \left(m_i Y_{ci}^h + m_c X_{ci}^h \right) (C_{11}^{(p)} - C_{12}^{(p)}) + (m_i Y_{ci}^h + m_c X_{ci}^h) C_{11}^{(p)} + X_{ci}^h (m_t C_{21}^{(p)} + m_c C_{23}^{(p)}) \right\} \right] \\
F_{4i}^{(q)} &= \frac{g^3 \alpha_d^{\tilde{d}}}{16\sqrt{2}\pi^2} \left[m_t Y_{ci}^j Y_{ti}^j (C_{21}^{(q)} - C_{23}^{(q)}) - m_c X_{ci}^j X_{ti}^j C_{23}^{(q)} + m_i X_{ti}^j Y_{ci}^j (C_0 + C_{11}^{(q)}) \right] \\
F_{4i}^{(r)} &= \frac{g^3}{16\pi^2} X_{ci}^j \left[B_{di}^Z \left(m_i + m_t \frac{X_{ci}^j}{Y_{ci}^j} \right) Y_{ci}^j (C_{11}^{(r)} - C_{12}^{(r)}) \right. \\
&\quad \left. - A_{di}^Z \left\{ \left(m_i Y_{ci}^j + m_c X_{ci}^j \right) (C_{11}^{(r)} - C_{12}^{(r)}) + (m_i Y_{ci}^j + m_c X_{ci}^j) C_{11}^{(r)} + X_{ci}^j (m_t C_{21}^{(r)} + m_c C_{23}^{(r)}) \right\} \right] \quad (2.2.20)
\end{aligned}$$

where we have used

$$\begin{aligned}
C_X^{(m)} &= C_X(m_i, M_{h+}, M_{h+}; m_c, m_t, M_Z) & B_0^{(m)} &= B_0(M_{h+}, M_{h+}; M_Z) \\
C_X^{(p)} &= C_X(M_{h+}, m_i, m_i; m_c, m_t, M_Z) & B_0^{(q)} &= B_X(M_{\tilde{d}_j}, M_{\tilde{d}_j}; M_Z) \\
C_X^{(q)} &= C_X(m_{\tilde{\chi}_i^+}, M_{\tilde{d}_j}, M_{\tilde{d}_j}; m_c, m_t, M_Z) & B_X^{(s)} &= B_X(m_i, M_{h+}; m_t) \\
C_X^{(r)} &= C_X(M_{\tilde{d}_j}, m_{\tilde{\chi}_i^+}, m_{\tilde{\chi}_i^+}; m_c, m_t, M_Z) & B_X^{(t)} &= B_X(m_{\tilde{\chi}_i^+}, M_{\tilde{d}_j}; m_t) \\
B_X^{(u)} &= B_X(m_i, M_{h+}; m_t) & B_X^{(v)} &= B_X(m_{\tilde{\chi}_i^+}, M_{\tilde{d}_j}; m_c) \quad (2.2.21)
\end{aligned}$$

for $X = 0, 11, 12, 21, 23, 24$, as usual. It is now a simple matter to calculate the total form factors using $F_{ni} = \sum_{A=a}^j F_{ni}^A$ for $n = 1, 2, 3, 4$ and substitute the results into Eqn. (2.1.23) to get the final cMSSM amplitude.

B.3 RPV-MSSM amplitudes

B.3.1 The decay $t \rightarrow c + H$

Since the RPV-MSSM is merely an extension of the MSSM, it will contain all the diagrams of Figures 3.4 and 3.5. However, as we have seen in the text, these contributions are small, and the R -parity violating contributions can be much larger. It is sensible, therefore, to calculate these alone. To have a unified picture, we include both λ'_{ijk} and λ''_{ijk} couplings when listing the diagrams in Figure 3.7, though only one set at a time can contribute. In terms of these, the F_1 form factors are

$$\begin{aligned}
F_{1ik}^{1a} &= gM_W \beta_{\tilde{e}_i \tilde{e}_i}^h \frac{\lambda'_{i2k} \lambda'_{i3k}}{16\pi^2} m_c C_{12}^{(a)} \\
F_{1ik}^{1b} &= \frac{y_{d_k} \lambda'_{i2k} \lambda'_{i3k}}{16\pi^2} m_c M_{\tilde{d}_k} \left[C_0^{(b)} + 2C_{12}^{(b)} \right] \\
F_{1ik}^{1c} &= gM_W \beta_{\tilde{d}_k \tilde{d}_k}^h \frac{\lambda'_{i2k} \lambda'_{i3k}}{16\pi^2} m_c C_{12}^{(c)} \\
F_{1ik}^{1d} &= \frac{y_{l_i} \lambda'_{i2k} \lambda'_{i3k}}{16\pi^2} m_c m_{l_i} \left[C_0^{(d)} + 2C_{12}^{(d)} \right] \\
F_{1ik}^{1e} &= -\frac{y_t \lambda'_{i2k} \lambda'_{i3k}}{16\pi^2 (m_t^2 - m_c^2)} m_c m_t B_1^{(e)} \\
F_{1ik}^{1f} &= \frac{y_c \lambda'_{i2k} \lambda'_{i3k}}{16\pi^2 (m_t^2 - m_c^2)} m_t (m_t + m_c) B_1^{(f)} \\
F_{1jk}^{1g} &= gM_W \beta_{\tilde{d}_k \tilde{d}_k}^h \frac{\lambda''_{2jk} \lambda''_{3jk}}{16\pi^2} m_t \left[C_{11}^{(g)} - C_{12}^{(g)} \right] \\
F_{1jk}^{1h} &= \frac{y_{d_k} \lambda''_{2jk} \lambda''_{3jk}}{16\pi^2} m_t m_{d_i} \left[C_0^{(h)} + 2 \left(C_{11}^{(h)} - C_{12}^{(h)} \right) \right] \\
F_{1jk}^{1i} &= \frac{y_t \lambda''_{2jk} \lambda''_{3jk}}{16\pi^2 (m_t^2 - m_c^2)} m_c m_t B_1^{(i)} \\
F_{1jk}^{1j} &= -\frac{y_c \lambda''_{2jk} \lambda''_{3jk}}{16\pi^2 (m_t^2 - m_c^2)} m_t (m_t + m_c) B_1^{(j)}
\end{aligned} \tag{2.3.1}$$

and the F_2 form factors are

$$\begin{aligned}
F_{1ik}^{2a} &= gM_W \beta_{\tilde{e}_i \tilde{e}_i}^h \frac{\lambda'_{i2k} \lambda'_{i3k}}{16\pi^2} m_t \left[C_{11}^{(a)} - C_{12}^{(a)} \right] \\
F_{1ik}^{2b} &= \frac{y_{d_k} \lambda'_{i2k} \lambda'_{i3k}}{16\pi^2} m_t m_{d_k} \left[C_0^{(b)} + 2(C_{11}^{(b)} - C_{12}^{(b)}) \right] \\
F_{1ik}^{2c} &= gM_W \beta_{\tilde{d}_k \tilde{d}_k}^h \frac{\lambda'_{i2k} \lambda'_{i3k}}{16\pi^2} m_t \left[C_{11}^{(c)} - C_{12}^{(c)} \right] \\
F_{1ik}^{2d} &= \frac{y_{l_i} \lambda'_{i2k} \lambda'_{i3k}}{16\pi^2} m_t m_{l_i} \left[C_0^{(d)} + 2 \left(C_{11}^{(d)} - C_{12}^{(d)} \right) \right] \\
F_{1ik}^{2e} &= -\frac{y_t \lambda'_{i2k} \lambda'_{i3k}}{16\pi^2 (m_t^2 - m_c^2)} m_c^2 B_1^{(e)} \\
F_{1jk}^{2g} &= gM_W \beta_{\tilde{d}_k \tilde{d}_k}^h \frac{\lambda''_{2jk} \lambda''_{3jk}}{16\pi^2} m_c C_{12}^{(g)} \\
F_{1jk}^{2h} &= \frac{y_{d_k} \lambda''_{2jk} \lambda''_{3jk}}{16\pi^2} m_c M_{\tilde{d}_k} \left[C_0^{(h)} + 2C_{12}^{(h)} \right] \\
F_{1jk}^{2i} &= \frac{y_t \lambda''_{2jk} \lambda''_{3jk}}{16\pi^2 (m_t^2 - m_c^2)} m_c^2 B_1^{(i)}
\end{aligned} \tag{2.3.2}$$

in terms of

$$\begin{aligned}
C_X^{(a)} &= C_X(m_k, M_{\tilde{e}_i}, M_{\tilde{e}_i}; m_c, m_t, M_h) & B_1^{(e)} &= B_1(m_k, M_{\tilde{e}_i}; m_c) \\
C_X^{(b)} &= C_X(M_{\tilde{e}_i}, m_k, m_k; m_c, m_t, M_h) & B_1^{(f)} &= B_1(m_k, M_{\tilde{e}_i}; m_c) \\
C_X^{(c)} &= C_X(m_i, M_{\tilde{d}_k}, M_{\tilde{d}_k}; m_c, m_t, M_h) & B_1^{(i)} &= B_1(m_j, M_{\tilde{d}_k}; m_t) \\
C_X^{(d)} &= C_X(M_{\tilde{d}_k}, m_{e_i}, m_{e_i}; m_c, m_t, M_h) & B_1^{(j)} &= B_1(m_j, M_{\tilde{d}_k}; m_t) \\
C_X^{(g)} &= C_X(m_j, M_{\tilde{d}_k}, M_{\tilde{d}_k}; m_c, m_t, M_h) & C_X^{(h)} &= C_X(M_{\tilde{d}_k}, m_j, m_j; m_c, m_t, M_h)
\end{aligned} \tag{2.3.3}$$

where, as usual, $X = 0, 11, 12, 21, 23, 24$. As before, we go on to compute total form factors using $F_{ni} = \sum_{A=a}^j F_{ni}^A$ for $n = 1, 2$ and substitute the results into Eqn. (2.1.8) to get the amplitude in the RPV-MSSM.

B.3.2 The decay $t \rightarrow c + Z$

The Feynman diagrams for the decay $t \rightarrow c + Z$ are the same as those in Figure 3.7, with $h^0 \rightarrow Z$, as we have seen before. As before, we present the amplitudes for the λ' and λ'' couplings together, though either one or the other must be zero.

The F_1 form factors are

$$\begin{aligned}
F_{1ik}^{1a} &= \frac{gZe\lambda'_{i2k}\lambda'_{i3k}}{16\pi^2} \left[m_t^2 (C_{11}^{(a)} - C_{12}^{(a)} + C_{21}^{(a)} - C_{23}^{(a)}) - 2C_{24}^{(a)} \right] \\
F_{1ik}^{1b} &= \frac{\lambda'_{i2k}\lambda'_{i3k}}{16\pi^2} \left[g_{dR} (m_t^2 (C_{21}^{(b)} - C_{23}^{(b)}) - 2C_{24}^{(b)} + B_0^{(b)} - M_{\tilde{e}_i}^2 C_0^{(b)}) + g_{dL} m_k^2 C_0^{(b)} \right] \\
F_{1ik}^{1c} &= \frac{gZd\lambda'_{i2k}\lambda'_{i3k}}{16\pi^2} \left[m_t^2 (C_{11}^{(c)} - C_{12}^{(c)} + C_{21}^{(c)} - C_{23}^{(c)}) - 2C_{24}^{(c)} \right] \\
F_{1ik}^{1d} &= \frac{\lambda'_{i2k}\lambda'_{i3k}}{16\pi^2} \left[g_{eR} (m_t^2 (C_{21}^{(d)} - C_{23}^{(d)}) - 2C_{24}^{(d)} + B_0^{(d)} - M_{\tilde{d}_k}^2 C_0^{(d)}) + g_{eL} m_i^2 C_0^{(d)} \right] \\
F_{1ik}^{1e} &= -\frac{\lambda'_{i2k}\lambda'_{i3k}}{16\pi^2(m_t^2 - m_c^2)} g_{uL} m_t^2 B_1^{(e)} \\
F_{1ik}^{1f} &= \frac{\lambda'_{i2k}\lambda'_{i3k}}{16\pi^2(m_t^2 - m_c^2)} g_{uL} m_c^2 B_1^{(f)} \\
F_{1jk}^{1g} &= \frac{gZd\lambda''_{2jk}\lambda''_{3jk}}{16\pi^2} m_t m_c (C_{12}^{(g)} + C_{23}^{(g)}) \\
F_{1jk}^{1h} &= \frac{\lambda''_{2jk}\lambda''_{3jk}}{16\pi^2} g_{dL} \left[m_c m_t C_{23}^{(h)} + m_t (m_t (C_{11}^{(h)} - C_{12}^{(h)}) + m_c C_{12}^{(h)}) + m_c m_t C_{11}^{(h)} \right] \\
F_{1jk}^{1i} &= -\frac{\lambda''_{2jk}\lambda''_{3jk}}{16\pi^2(m_t^2 - m_c^2)} g_{uL} m_c m_t B_1^{(i)} \\
F_{1jk}^{1j} &= \frac{\lambda''_{2jk}\lambda''_{3jk}}{16\pi^2(m_t^2 - m_c^2)} g_{uL} m_c m_t B_1^{(j)}
\end{aligned} \tag{2.3.4}$$

The F_2 form factors are

$$\begin{aligned}
F_{1ik}^{2a} &= \frac{gZe\lambda'_{i2k}\lambda'_{i3k}}{16\pi^2} m_t m_c (C_{12}^{(a)} + C_{23}^{(a)}) \\
F_{1ik}^{2b} &= \frac{\lambda'_{i2k}\lambda'_{i3k}}{16\pi^2} g_{dR} (m_t^2 (C_{11}^{(b)} - C_{12}^{(b)}) + m_c m_t (C_{11}^{(b)} + C_{12}^{(b)} + C_{23}^{(b)})) \\
F_{1ik}^{2c} &= \frac{gZd\lambda'_{i2k}\lambda'_{i3k}}{16\pi^2} m_t m_c (C_{12}^{(c)} + C_{23}^{(c)}) \\
F_{1ik}^{2d} &= \frac{\lambda'_{i2k}\lambda'_{i3k}}{16\pi^2} g_{eR} \left[m_c m_t C_{23}^{(d)} + m_t (m_t (C_{11}^{(d)} - C_{12}^{(d)}) + m_c C_{12}^{(d)}) + m_c m_t C_{11}^{(d)} \right]
\end{aligned} \tag{2.3.5}$$

$$\begin{aligned}
F_{1ik}^{2e} &= -\frac{\lambda'_{i2k}\lambda'_{i3k}}{16\pi^2(m_t^2 - m_c^2)} g_{uR} m_c m_t B_1^{(e)} \\
F_{1ik}^{2f} &= \frac{\lambda'_{i2k}\lambda'_{i3k}}{16\pi^2(m_t^2 - m_c^2)} g_{uR} m_c m_t B_1^{(f)} \\
F_{1jk}^{2g} &= \frac{g_{Zd}\lambda''_{2jk}\lambda''_{3jk}}{16\pi^2} \left[m_t^2 \left(C_{11}^{(g)} - C_{12}^{(g)} + C_{21}^{(g)} - C_{23}^{(g)} \right) - 2C_{24}^{(g)} \right] \\
F_{1jk}^{2h} &= \frac{\lambda''_{2jk}\lambda''_{3jk}}{16\pi^2} \left[g_{dL} \left(m_t^2 (C_{21}^{(h)} - C_{23}^{(h)}) - 2C_{24}^{(h)} + B_0^{(h)} - M_{d_k}^2 C_0^{(h)} \right) + g_{dR} m_j^2 C_0^{(h)} \right] \\
F_{1jk}^{2i} &= -\frac{\lambda''_{2jk}\lambda''_{3jk}}{16\pi^2(m_t^2 - m_c^2)} g_{uR} m_t^2 B_1^{(i)} \\
F_{1jk}^{2j} &= \frac{\lambda''_{2jk}\lambda''_{3jk}}{16\pi^2(m_t^2 - m_c^2)} g_{uR} m_c^2 B_1^{(j)}
\end{aligned} \tag{2.3.6}$$

The F_3 form factors are

$$\begin{aligned}
F_{1ik}^{3a} &= -\frac{g_{Ze}\lambda'_{i2k}\lambda'_{i3k}}{16\pi^2} m_c \left(C_{12}^{(a)} + C_{23}^{(a)} \right) \\
F_{1ik}^{3b} &= -\frac{\lambda'_{i2k}\lambda'_{i3k}}{16\pi^2} g_{dL} m_c \left(C_{11}^{(b)} + C_{23}^{(b)} \right) \\
F_{1ik}^{3c} &= -\frac{g_{Zd}\lambda'_{i2k}\lambda'_{i3k}}{16\pi^2} m_c \left(C_{12}^{(c)} + C_{23}^{(c)} \right) \\
F_{1ik}^{3d} &= -\frac{\lambda'_{i2k}\lambda'_{i3k}}{16\pi^2} g_{eL} m_c \left(C_{11}^{(d)} + C_{23}^{(d)} \right) \\
F_{1jk}^{3g} &= -\frac{g_{Zd}\lambda''_{2jk}\lambda''_{3jk}}{16\pi^2} m_t \left(C_{11}^{(g)} - C_{12}^{(g)} + C_{21}^{(g)} - C_{23}^{(g)} \right) \\
F_{1jk}^{3h} &= -\frac{\lambda''_{2jk}\lambda''_{3jk}}{16\pi^2} g_{dL} m_t \left(C_{21}^{(h)} - C_{23}^{(h)} \right)
\end{aligned} \tag{2.3.7}$$

and, finally the F_4 form factors are

$$\begin{aligned}
F_{1ik}^{4a} &= -\frac{g_{Ze}\lambda'_{i2k}\lambda'_{i3k}}{16\pi^2} m_t \left(C_{11}^{(a)} - C_{12}^{(a)} + C_{21}^{(a)} - C_{23}^{(a)} \right) \\
F_{1ik}^{4b} &= \frac{\lambda'_{i2k}\lambda'_{i3k}}{16\pi^2} g_{dR} m_c \left(C_{21}^{(b)} - C_{23}^{(b)} \right) \\
F_{1ik}^{4c} &= -\frac{g_{Zd}\lambda'_{i2k}\lambda'_{i3k}}{16\pi^2} m_t \left(C_{11}^{(c)} - C_{12}^{(c)} + C_{21}^{(c)} - C_{23}^{(c)} \right) \\
F_{1ik}^{4d} &= -\frac{\lambda'_{i2k}\lambda'_{i3k}}{16\pi^2} g_{eR} m_t \left(C_{21}^{(d)} - C_{23}^{(d)} \right) \\
F_{1jk}^{4g} &= -\frac{g_{Zd}\lambda''_{2jk}\lambda''_{3jk}}{16\pi^2} m_c \left(C_{12}^{(g)} + C_{23}^{(g)} \right) \\
F_{1jk}^{4h} &= -\frac{\lambda''_{2jk}\lambda''_{3jk}}{16\pi^2} g_{dR} m_c \left(C_{11}^{(h)} + C_{23}^{(h)} \right)
\end{aligned} \tag{2.3.8}$$

where

$$\begin{aligned}
C_X^{(a)} &= C_X(m_k, M_{\bar{e}_i}, M_{\bar{e}_i}; m_c, m_t, M_Z) & B_0^{(b)} &= B_0(m_k, m_k; M_Z) \\
C_X^{(b)} &= C_X(M_{\bar{e}_i}, m_k, m_k; m_c, m_t, M_Z) & B_0^{(d)} &= B_0(m_i, m_i; M_Z) \\
C_X^{(c)} &= C_X(m_i, M_{\bar{d}_k}, M_{\bar{d}_k}; m_c, m_t, M_Z) & B_1^{(e)} &= B_1(m_k, M_{\bar{e}_i}; m_c) \\
C_X^{(d)} &= C_X(M_{\bar{d}_k}, m_i, m_i; m_c, m_t, M_Z) & B_1^{(f)} &= B_1(m_k, M_{\bar{e}_i}; m_t) \\
C_X^{(g)} &= C_X(m_i, M_{\bar{d}_k}, M_{\bar{d}_k}; m_c, m_t, M_Z) & B_0^{(h)} &= B_0(m_j, m_j; M_Z) \\
C_X^{(h)} &= C_X(M_{\bar{d}_k}, m_j, m_j; m_c, m_t, M_Z) & B_1^{(i)} &= B_1(m_j, M_{\bar{d}_k}; m_c) \\
B_1^{(j)} &= B_1(m_j, M_{\bar{d}_k}; m_t)
\end{aligned} \tag{2.3.9}$$

and we have defined effective couplings

$$\begin{aligned}
g_{Zd} &= -\frac{\sin^2 \theta_W}{6 \cos \theta_W} & g_{Ze} &= \frac{1 - 2 \sin^2 \theta_W}{2 \cos \theta_W} \\
g_{uL} &= -\frac{1 - 2q_u \sin^2 \theta_W}{2 \cos \theta_W} & g_{uR} &= \frac{q_u \sin^2 \theta_W}{\cos \theta_W} \\
g_{dL} &= \frac{1 + 2q_d \sin^2 \theta_W}{2 \cos \theta_W} & g_{dR} &= \frac{q_d \sin^2 \theta_W}{\cos \theta_W} \\
g_{eL} &= \frac{1 - 2 \sin^2 \theta_W}{2 \cos \theta_W} & g_{eR} &= -\frac{\sin^2 \theta_W}{\cos \theta_W}
\end{aligned} \tag{2.3.10}$$

It is now a straightforward matter to calculate the total form factors using $F_{ni} = \sum_{A=a}^j F_{ni}^A$ for $n = 1, 2, 3, 4$ and substitute the results into Eqn. (2.1.23) to get the final RPV-MSSM amplitude.

The R_D and R_{D^*} Anomalies

C.1 Full expressions for a_ℓ^D , b_ℓ^D and c_ℓ^D

For the negative helicity of the lepton:

$$\begin{aligned}
\frac{1}{8}a_\ell^D(-) &= \frac{M_B^2|p_D|^2}{q^2} \boxed{|\mathbf{C}_{\mathbf{VL}}^\ell|^2 \mathbf{F}_+^2} + \frac{(M_B^2 - M_D^2)^2}{4(m_b - m_c)^2} |\mathbf{C}_{\mathbf{SR}}^\ell|^2 \mathbf{F}_0^2 \\
&+ m_\ell \left[\frac{(M_B^2 - M_D^2)^2}{2q^2(m_b - m_c)} \mathcal{R}(\mathbf{C}_{\mathbf{SR}}^\ell \mathbf{C}_{\mathbf{VR}}^{\ell*}) \mathbf{F}_0^2 + \frac{4M_B^2|p_D|^2}{q^2(M_B + M_D)} \mathcal{R}(\mathbf{C}_{\mathbf{TL}}^\ell \mathbf{C}_{\mathbf{VL}}^{\ell*}) \mathbf{F}_+ \mathbf{F}_\mathbf{T} \right] \\
&+ m_\ell^2 \left[\frac{(M_B^2 - M_D^2)^2}{4q^4} |\mathbf{C}_{\mathbf{VR}}^\ell|^2 \mathbf{F}_0^2 + \frac{4|p_D|^2 M_B^2}{q^2(M_B + M_D)^2} |\mathbf{C}_{\mathbf{TL}}^\ell|^2 \mathbf{F}_\mathbf{T}^2 \right] \tag{3.1.1}
\end{aligned}$$

$$\begin{aligned}
\frac{1}{8}b_\ell^D(-) &= \left[-2|p_D|M_B \frac{M_B - M_D}{m_b - m_c} \mathcal{R}(\mathbf{C}_{\mathbf{SR}}^\ell \mathbf{C}_{\mathbf{TR}}^{\ell*}) \mathbf{F}_0 \mathbf{F}_\mathbf{T} \right] \\
&- m_\ell \left[\frac{2|p_D|M_B(M_B - M_D)}{q^2} \mathcal{R}(\mathbf{C}_{\mathbf{VR}}^\ell \mathbf{C}_{\mathbf{TR}}^{\ell*}) \mathbf{F}_0 \mathbf{F}_\mathbf{T} \right. \\
&+ \left. \frac{|p_D|M_B(M_B^2 - M_D^2)}{q^2(m_b - m_c)} \mathcal{R}(\mathbf{C}_{\mathbf{SR}}^\ell \mathbf{C}_{\mathbf{VR}}^{\ell*}) \mathbf{F}_0 \mathbf{F}_+ \right] \\
&- m_\ell^2 \left[\frac{|p_D|M_B(M_B^2 - M_D^2)}{q^4} |\mathbf{C}_{\mathbf{VR}}^\ell|^2 \mathbf{F}_0 \mathbf{F}_+ \right] \tag{3.1.2}
\end{aligned}$$

$$\begin{aligned}
\frac{1}{8}c_\ell^D(-) &= \left[\frac{4M_B^2|p_D|^2}{(M_B + M_D)^2} |\mathbf{C}_{\mathbf{TR}}^\ell|^2 \mathbf{F}_\mathbf{T}^2 - \frac{M_B^2|p_D|^2}{q^2} \boxed{|\mathbf{C}_{\mathbf{VL}}^\ell|^2 \mathbf{F}_+^2} \right] \\
&- m_\ell \left[\frac{4|p_D|^2 M_B^2}{q^2(M_B + M_D)} (\mathcal{R}(\mathbf{C}_{\mathbf{VL}}^\ell \mathbf{C}_{\mathbf{TL}}^{\ell*}) \mathbf{F}_+ \mathbf{F}_\mathbf{T} - \mathcal{R}(\mathbf{C}_{\mathbf{VR}}^\ell \mathbf{C}_{\mathbf{TR}}^{\ell*}) \mathbf{F}_+ \mathbf{F}_\mathbf{T}) \right] \\
&+ m_\ell^2 \left[\frac{|p_D|^2 M_B^2}{q^4} |\mathbf{C}_{\mathbf{VR}}^\ell|^2 \mathbf{F}_+^2 - \frac{4|p_D|^2 M_B^2}{(M_B + M_D)^2 q^2} |\mathbf{C}_{\mathbf{TL}}^\ell|^2 \mathbf{F}_\mathbf{T}^2 \right]. \tag{3.1.3}
\end{aligned}$$

For the positive helicity of the lepton:

$$\begin{aligned}
\frac{1}{8}a_\ell^D(+) &= \frac{M_B^2|p_D|^2}{q^2}|\mathbf{C}_{\mathbf{VR}}^\ell|^2\mathbf{F}_+^2 + \frac{(M_B^2 - M_D^2)^2}{4(m_b - m_c)^2}|\mathbf{C}_{\mathbf{SL}}^\ell|^2\mathbf{F}_0^2 \\
&+ m_\ell \left[\frac{(M_B^2 - M_D^2)^2}{2q^2(m_b - m_c)}\mathcal{R}(\mathbf{C}_{\mathbf{SL}}^\ell\mathbf{C}_{\mathbf{VL}}^{\ell*})\mathbf{F}_0^2 + \frac{4M_B^2|p_D|^2}{q^2(M_B + M_D)}\mathcal{R}(\mathbf{C}_{\mathbf{VR}}^\ell\mathbf{C}_{\mathbf{TR}}^{\ell*})\mathbf{F}_+\mathbf{F}_\mathbf{T} \right] \\
&+ m_\ell^2 \left[\frac{(M_B^2 - M_D^2)^2}{4q^4}\boxed{|\mathbf{C}_{\mathbf{VL}}^\ell|^2\mathbf{F}_0^2} + \frac{4M_B^2|p_D|^2}{q^2(M_B + M_D)^2}|\mathbf{C}_{\mathbf{TR}}^\ell|^2\mathbf{F}_\mathbf{T}^2 \right] \quad (3.1.4)
\end{aligned}$$

$$\begin{aligned}
\frac{1}{8}b_\ell^D(+) &= \left[-2M_B|p_D|\frac{M_B - M_D}{m_b - m_c}\mathcal{R}(\mathbf{C}_{\mathbf{SL}}^\ell\mathbf{C}_{\mathbf{TL}}^{\ell*})\mathbf{F}_0\mathbf{F}_\mathbf{T} \right] \\
&- m_\ell \left[\frac{2|p_D|(M_B - M_D)M_B}{q^2}\mathcal{R}(\mathbf{C}_{\mathbf{VL}}^\ell\mathbf{C}_{\mathbf{TL}}^{\ell*})\mathbf{F}_0\mathbf{F}_\mathbf{T} \right. \\
&+ \left. \frac{|p_D|M_B(M_B^2 - M_D^2)}{q^2(m_b - m_c)}\mathcal{R}(\mathbf{C}_{\mathbf{SL}}^\ell\mathbf{C}_{\mathbf{VL}}^{\ell*})\mathbf{F}_0\mathbf{F}_+ \right] \\
&- m_\ell^2 \left[\frac{|p_D|M_B(M_B^2 - M_D^2)}{q^4}\boxed{|\mathbf{C}_{\mathbf{VL}}^\ell|^2\mathbf{F}_0\mathbf{F}_+} \right] \quad (3.1.5)
\end{aligned}$$

$$\begin{aligned}
\frac{1}{8}c_\ell^D(+) &= \left[\frac{4|p_D|^2M_B^2}{(M_B + M_D)^2}|\mathbf{C}_{\mathbf{TL}}^\ell|^2\mathbf{F}_\mathbf{T}^2 - \frac{|p_D|^2M_B^2}{q^2}|\mathbf{C}_{\mathbf{VR}}^\ell|^2\mathbf{F}_+^2 \right] \\
&- m_\ell \left[\frac{4|p_D|^2M_B^2}{(M_B + M_D)q^2}\mathcal{R}(\mathbf{C}_{\mathbf{VR}}^\ell\mathbf{C}_{\mathbf{TR}}^{\ell*})\mathbf{F}_+\mathbf{F}_\mathbf{T} - \frac{4M_B^2|p_D|^2}{(M_B + M_D)q^2}\mathcal{R}(\mathbf{C}_{\mathbf{VL}}^\ell\mathbf{C}_{\mathbf{TL}}^{\ell*})\mathbf{F}_+\mathbf{F}_\mathbf{T} \right] \\
&+ m_\ell^2 \left[\frac{|p_D|^2M_B^2}{q^4}\boxed{|\mathbf{C}_{\mathbf{VL}}^\ell|^2\mathbf{F}_+^2} - \frac{4|p_D|^2M_B^2}{(M_B + M_D)^2q^2}|\mathbf{C}_{\mathbf{TR}}^\ell|^2\mathbf{F}_\mathbf{T}^2 \right] \quad (3.1.6)
\end{aligned}$$

C.2 Full expressions for $a_\ell^{D^*}$, $b_\ell^{D^*}$ and $c_\ell^{D^*}$

$$\begin{aligned}
a_\ell^{D^*}(-) &= \frac{8M_B^2|p_{D^*}|^2}{(M_B + M_{D^*})^2}|\mathbf{C}_{\mathbf{VL}}^\ell|^2\mathbf{V}^2 + \frac{(M_B + M_{D^*})^2(8M_{D^*}^2q^2 + \lambda)}{2M_{D^*}^2q^2}|\mathbf{C}_{\mathbf{AL}}^\ell|^2\mathbf{A}_1^2 \\
&+ \frac{8M_B^4|p_{D^*}|^4}{M_{D^*}^2(M_B + M_{D^*})^2q^2}|\mathbf{C}_{\mathbf{AL}}^\ell|^2\mathbf{A}_2^2 \\
&- \frac{4|p_{D^*}|^2M_B^2(M_B^2 - M_{D^*}^2 - q^2)}{M_{D^*}^2q^2}|\mathbf{C}_{\mathbf{AL}}^\ell|^2\mathbf{A}_1\mathbf{A}_2 \\
&+ \frac{32M_B^2|p_{D^*}|^2}{q^2}|\mathbf{C}_{\mathbf{TR}}^\ell|^2\mathbf{T}_1^2 + \frac{8(M_B^2 - M_{D^*}^2)^2}{q^2}|\mathbf{C}_{\mathbf{TR}}^\ell|^2\mathbf{T}_2^2 \\
&+ m_\ell \left[\frac{32M_B^2|p_{D^*}|^2}{q^2(M_B + M_{D^*})}\mathcal{R}(\mathbf{C}_{\mathbf{VL}}^\ell\mathbf{C}_{\mathbf{TL}}^{\ell*})\mathbf{V}\mathbf{T}_1 \right. \\
&+ \left. \frac{8(M_B + M_{D^*})\left(2M_{D^*}^2(M_B^2 - M_{D^*}^2) + M_B^2|p_{D^*}|^2\right)}{q^2M_{D^*}^2}\mathcal{R}(\mathbf{C}_{\mathbf{AL}}^\ell\mathbf{C}_{\mathbf{TL}}^{\ell*})\mathbf{A}_1\mathbf{T}_2 \right. \\
&- \left. \frac{8M_B^2(M_B^2 - M_{D^*}^2 - q^2)|p_{D^*}|^2}{q^2(M_B - M_{D^*})M_{D^*}^2}\mathcal{R}(\mathbf{C}_{\mathbf{AL}}^\ell\mathbf{C}_{\mathbf{TL}}^{\ell*})\mathbf{A}_1\mathbf{T}_3 \right. \\
&- \left. \frac{8M_B^2(M_B^2 + 3M_{D^*}^2 - q^2)|p_{D^*}|^2}{q^2(M_B + M_{D^*})M_{D^*}^2}\mathcal{R}(\mathbf{C}_{\mathbf{AL}}^\ell\mathbf{C}_{\mathbf{TL}}^{\ell*})\mathbf{A}_2\mathbf{T}_2 \right. \\
&+ \left. \frac{32M_B^4|p_{D^*}|^4}{q^2M_{D^*}^2(M_B + M_{D^*})(M_B^2 - M_{D^*}^2)}\mathcal{R}(\mathbf{C}_{\mathbf{AL}}^\ell\mathbf{C}_{\mathbf{TL}}^{\ell*})\mathbf{A}_2\mathbf{T}_3 \right]
\end{aligned}$$

$$\begin{aligned}
& + \frac{32M_B^2 |p_{D^*}|^2}{(M_B + M_{D^*})q^2} \mathcal{R}(\mathbf{C}_{\mathbf{VR}}^\ell \mathbf{C}_{\mathbf{TR}}^{\ell*}) \mathbf{V} \mathbf{T}_1 \\
& - \frac{8(M_B - M_{D^*})(M_B + M_{D^*})^2}{q^2} \mathcal{R}(\mathbf{C}_{\mathbf{AR}}^\ell \mathbf{C}_{\mathbf{TR}}^{\ell*}) \mathbf{A}_1 \mathbf{T}_2 \Big] \\
& + m_\ell^2 \left[\frac{32M_B^2 |p_{D^*}|^2}{q^4} |\mathbf{C}_{\mathbf{TL}}^\ell|^2 \mathbf{T}_1^2 \right. \\
& + \frac{2(8M_{D^*}^2(2(M_B^2 + M_{D^*}^2) - q^2)q^2 + (4M_{D^*}^2 + q^2)\lambda)}{q^4 M_{D^*}^2} |\mathbf{C}_{\mathbf{TL}}^\ell|^2 \mathbf{T}_2^2 \\
& + \frac{32M_B^4 |p_{D^*}|^4}{q^2 M_{D^*}^2 (M_B^2 - M_{D^*}^2)^2} |\mathbf{C}_{\mathbf{TL}}^\ell|^2 \mathbf{T}_3^2 - \frac{16M_B^2 |p_{D^*}|^2 (M_B^2 + 3M_{D^*}^2 - q^2)}{q^2 M_{D^*}^2 (M_B^2 - M_{D^*}^2)} |\mathbf{C}_{\mathbf{TL}}^\ell|^2 \mathbf{T}_2 \mathbf{T}_3 \Big] \\
b_\ell^{D*}(-) = & -16|p_{D^*}| M_B \mathcal{R}(\mathbf{C}_{\mathbf{VL}}^\ell \mathbf{C}_{\mathbf{AL}}^{\ell*}) \mathbf{V} \mathbf{A}_1 \\
& + \frac{32M_B^3 |p_{D^*}|^3}{(m_b + m_c)(M_B^2 - M_{D^*}^2)M_{D^*}} \mathcal{R}(\mathbf{C}_{\mathbf{PR}}^\ell \mathbf{C}_{\mathbf{TR}}^{\ell*}) \mathbf{A}_0 \mathbf{T}_3 \\
& - \frac{8M_B |p_{D^*}| (M_B^2 + 3M_{D^*}^2 - q^2)}{(m_b + m_c)M_{D^*}} \mathcal{R}(\mathbf{C}_{\mathbf{PR}}^\ell \mathbf{C}_{\mathbf{TR}}^{\ell*}) \mathbf{A}_0 \mathbf{T}_2 \\
& - m_\ell \left[\frac{32M_B (M_B - M_{D^*}) |p_{D^*}|}{q^2} \mathcal{R}(\mathbf{C}_{\mathbf{VL}}^\ell \mathbf{C}_{\mathbf{TL}}^{\ell*}) \mathbf{V} \mathbf{T}_2 \right. \\
& + \frac{32M_B (M_B + M_{D^*}) |p_{D^*}|}{q^2} \mathcal{R}(\mathbf{C}_{\mathbf{AL}}^\ell \mathbf{C}_{\mathbf{TL}}^{\ell*}) \mathbf{A}_1 \mathbf{T}_1 \\
& + \frac{8M_B |p_{D^*}| (M_B^2 + 3M_{D^*}^2 - q^2)}{M_{D^*} q^2} \mathcal{R}(\mathbf{C}_{\mathbf{AR}}^\ell \mathbf{C}_{\mathbf{TR}}^{\ell*}) \mathbf{A}_0 \mathbf{T}_2 \\
& - \frac{32M_B^3 |p_{D^*}|^3}{(M_B - M_{D^*})M_{D^*}(M_B + M_{D^*})q^2} \mathcal{R}(\mathbf{C}_{\mathbf{AR}}^\ell \mathbf{C}_{\mathbf{TR}}^{\ell*}) \mathbf{A}_0 \mathbf{T}_3 \Big] \\
& - m_\ell^2 \left[\frac{64M_B (M_B^2 - M_{D^*}^2) |p_{D^*}|}{q^4} |\mathbf{C}_{\mathbf{TL}}^\ell|^2 \mathbf{T}_1 \mathbf{T}_2 \right] \tag{3.2.2} \\
c_\ell^{D*}(-) = & \frac{8|p_{D^*}|^2 M_B^2}{(M_B + M_{D^*})^2} |\mathbf{C}_{\mathbf{VL}}^\ell|^2 \mathbf{V}^2 - \frac{(M_B + M_{D^*})^2 \lambda}{2M_{D^*}^2 q^2} |\mathbf{C}_{\mathbf{AL}}^\ell|^2 \mathbf{A}_1^2 \\
& - \frac{8|p_{D^*}|^4 M_B^4}{(M_B + M_{D^*})^2 M_{D^*}^2 q^2} |\mathbf{C}_{\mathbf{AL}}^\ell|^2 \mathbf{A}_2^2 \\
& + \frac{4|p_{D^*}|^2 M_B^2 (M_B^2 - M_{D^*}^2 - q^2)}{M_{D^*}^2 q^2} |\mathbf{C}_{\mathbf{AL}}^\ell|^2 \mathbf{A}_1 \mathbf{A}_2 \\
& - \frac{32M_B^2 M_{D^*}^2 (M_B^2 - M_{D^*}^2)^2 |p_{D^*}|^2}{(-M_B^2 M_{D^*} + M_{D^*}^3)^2 q^2} |\mathbf{C}_{\mathbf{TR}}^\ell|^2 \mathbf{T}_1^2 \\
& - \frac{2(M_B^2 - M_{D^*}^2)^2}{M_{D^*}^2} |\mathbf{C}_{\mathbf{TR}}^\ell|^2 \mathbf{T}_2^2 \\
& - \frac{4(-M_B^2 + M_{D^*}^2)(-M_B^4 + M_{D^*}^4 + 4M_B^2 |p_{D^*}|^2)}{M_{D^*}^2 q^2} |\mathbf{C}_{\mathbf{TR}}^\ell|^2 \mathbf{T}_2^2 \\
& + \frac{32M_B^4 |p_{D^*}|^4}{(-M_B^2 M_{D^*} + M_{D^*}^3)^2} |\mathbf{C}_{\mathbf{TR}}^\ell|^2 \mathbf{T}_3^2 \\
& + \frac{16M_B^2 |p_{D^*}|^2 (M_B^2 + 3M_{D^*}^2 - q^2)}{-M_B^2 M_{D^*}^2 + M_{D^*}^4} |\mathbf{C}_{\mathbf{TR}}^\ell|^2 \mathbf{T}_2 \mathbf{T}_3 \\
& + m_\ell \left[\frac{32M_B^2 |p_{D^*}|^2}{q^2 (M_B + M_{D^*})} \mathcal{R}(\mathbf{C}_{\mathbf{VL}}^\ell \mathbf{C}_{\mathbf{TL}}^{\ell*}) \mathbf{V} \mathbf{T}_1 \right. \\
& - \frac{8M_B^2 (M_B + M_{D^*}) |p_{D^*}|^2}{q^2 M_{D^*}^2} \mathcal{R}(\mathbf{C}_{\mathbf{AL}}^\ell \mathbf{C}_{\mathbf{TL}}^{\ell*}) \mathbf{A}_1 \mathbf{T}_2 \\
& + \frac{8M_B^2 (M_B^2 - M_{D^*}^2 - q^2) |p_{D^*}|^2}{q^2 M_{D^*}^2 (M_B - M_{D^*})} \mathcal{R}(\mathbf{C}_{\mathbf{AL}}^\ell \mathbf{C}_{\mathbf{TL}}^{\ell*}) \mathbf{A}_1 \mathbf{T}_3
\end{aligned}$$

$$\begin{aligned}
& + \frac{8M_B^2 (M_B^2 + 3M_{D^*}^2 - q^2) |p_{D^*}|^2}{q^2 M_{D^*}^2 (M_B + M_{D^*})} \mathcal{R}(\mathbf{C}_{\text{AL}}^\ell \mathbf{C}_{\text{TL}}^{\ell*}) \mathbf{A}_2 \mathbf{T}_2 \\
& - \frac{32M_B^4 |p_{D^*}|^4}{q^2 M_{D^*}^2 (M_B + M_{D^*}) (M_B^2 - M_{D^*}^2)} \mathcal{R}(\mathbf{C}_{\text{AL}}^\ell \mathbf{C}_{\text{TL}}^{\ell*}) \mathbf{A}_2 \mathbf{T}_3 \\
& - \frac{32M_B^2 |p_{D^*}|^2}{(M_B + M_{D^*}) q^2} \mathcal{R}(\mathbf{C}_{\text{VR}}^\ell \mathbf{C}_{\text{TR}}^{\ell*}) \mathbf{V} \mathbf{T}_1 \\
& + \frac{8M_B^2 (M_B + M_{D^*}) |p_{D^*}|^2}{M_{D^*}^2 q^2} \mathcal{R}(\mathbf{C}_{\text{AR}}^\ell \mathbf{C}_{\text{TR}}^{\ell*}) \mathbf{A}_1 \mathbf{T}_2 \\
& - \frac{8M_B^2 |p_{D^*}|^2 (-M_B^2 + M_{D^*}^2 + q^2)}{(M_B - M_{D^*}) M_{D^*}^2 q^2} \mathcal{R}(\mathbf{C}_{\text{VR}}^\ell \mathbf{C}_{\text{TR}}^{\ell*}) \mathbf{A}_1 \mathbf{T}_3 \\
& + \frac{8M_B^2 |p_{D^*}|^2 (M_B^2 + 3M_{D^*}^2 - q^2)}{M_{D^*}^2 (M_B + M_{D^*}) q^2} \mathcal{R}(\mathbf{C}_{\text{VR}}^\ell \mathbf{C}_{\text{TR}}^{\ell*}) \mathbf{A}_2 \mathbf{T}_2 \\
& - \frac{32M_B^4 |p_{D^*}|^4}{(M_B - M_{D^*}) M_{D^*}^2 (M_B + M_{D^*})^2 q^2} \mathcal{R}(\mathbf{C}_{\text{VR}}^\ell \mathbf{C}_{\text{TR}}^{\ell*}) \mathbf{A}_2 \mathbf{T}_3 \Big] \\
& + m_\ell^2 \left[\frac{32M_B^2 |p_{D^*}|^2}{q^4} |\mathbf{C}_{\text{TL}}^\ell|^2 \mathbf{T}_1^2 + \frac{2(4M_{D^*}^2 - q^2) \lambda}{M_{D^*}^2 q^4} |\mathbf{C}_{\text{TL}}^\ell|^2 \mathbf{T}_2^2 \right. \\
& - \frac{32M_B^4 |p_{D^*}|^4}{q^2 M_{D^*}^2 (M_B^2 - M_{D^*}^2)^2} |\mathbf{C}_{\text{TL}}^\ell|^2 \mathbf{T}_3^2 \\
& \left. + \frac{16M_B^2 |p_{D^*}|^2 (M_B^2 + 3M_{D^*}^2 - q^2)}{q^2 M_{D^*}^2 (M_B^2 - M_{D^*}^2)} |\mathbf{C}_{\text{TL}}^\ell|^2 \mathbf{T}_2 \mathbf{T}_3 \right] \\
a_\ell^{D^*}(+) = & \frac{8 |p_{D^*}|^2 M_B^2}{(m_b + m_c)^2} |\mathbf{C}_{\text{PL}}^\ell|^2 \mathbf{A}_0^2 + \frac{32M_B^2 |p_{D^*}|^2}{q^2} |\mathbf{C}_{\text{TL}}^\ell|^2 \mathbf{T}_1^2 + \frac{8(M_B^2 - M_{D^*}^2)^2}{q^2} |\mathbf{C}_{\text{TL}}^\ell|^2 \mathbf{T}_2^2 \\
& - m_\ell \left[\frac{16 |p_{D^*}|^2 M_B^2}{(m_b + m_c) q^2} \mathcal{R}(\mathbf{C}_{\text{AL}}^\ell \mathbf{C}_{\text{PL}}^{\ell*}) \mathbf{A}_0^2 - \frac{32M_B^2 |p_{D^*}|^2}{q^2 (M_B + M_{D^*})} \mathcal{R}(\mathbf{C}_{\text{VL}}^\ell \mathbf{C}_{\text{TL}}^{\ell*}) \mathbf{V} \mathbf{T}_1 \right. \\
& - \frac{8(M_B + M_{D^*}) (M_B^2 - M_{D^*}^2)}{q^2} \mathcal{R}(\mathbf{C}_{\text{AL}}^\ell \mathbf{C}_{\text{TL}}^{\ell*}) \mathbf{A}_1 \mathbf{T}_2 - \frac{32M_B^2 |p_{D^*}|^2}{(M_B + M_{D^*}) q^2} \mathcal{R}(\mathbf{C}_{\text{VR}}^\ell \mathbf{C}_{\text{TR}}^{\ell*}) \mathbf{V} \mathbf{T}_1 \\
& + \frac{8(M_B + M_{D^*}) (-2M_{D^*}^4 + M_B^2 (2M_{D^*}^2 + |p_{D^*}|^2))}{M_{D^*}^2 q^2} \mathcal{R}(\mathbf{C}_{\text{AR}}^\ell \mathbf{C}_{\text{TR}}^{\ell*}) \mathbf{A}_1 \mathbf{T}_2 \\
& + \frac{8M_B^2 |p_{D^*}|^2 (-M_B^2 + M_{D^*}^2 + q^2)}{(M_B - M_{D^*}) M_{D^*}^2 q^2} \mathcal{R}(\mathbf{C}_{\text{AR}}^\ell \mathbf{C}_{\text{TR}}^{\ell*}) \mathbf{A}_1 \mathbf{T}_3 \\
& - \frac{8M_B^2 |p_{D^*}|^2 (M_B^2 + 3M_{D^*}^2 - q^2)}{M_{D^*}^2 (M_B + M_{D^*}) q^2} \mathcal{R}(\mathbf{C}_{\text{AR}}^\ell \mathbf{C}_{\text{TR}}^{\ell*}) \mathbf{A}_2 \mathbf{T}_2 \\
& + \frac{32M_B^4 |p_{D^*}|^4}{(M_B - M_{D^*}) M_{D^*}^2 (M_B + M_{D^*})^2 q^2} \mathcal{R}(\mathbf{C}_{\text{AR}}^\ell \mathbf{C}_{\text{TR}}^{\ell*}) \mathbf{A}_2 \mathbf{T}_3 \Big] \\
& + m_\ell^2 \left[\frac{8 |p_{D^*}|^2 M_B^2}{q^4} |\mathbf{C}_{\text{AL}}^\ell|^2 \mathbf{A}_0^2 + \frac{8 |p_{D^*}|^2 M_B^2}{(M_B + M_{D^*})^2 q^2} |\mathbf{C}_{\text{VL}}^\ell|^2 \mathbf{V}^2 \right. \\
& + \frac{2(M_B + M_{D^*})^2}{q^2} |\mathbf{C}_{\text{AL}}^\ell|^2 \mathbf{A}_1^2 \\
& + \frac{32M_B^2 |p_{D^*}|^2}{q^4} |\mathbf{C}_{\text{TR}}^\ell|^2 \mathbf{T}_1^2 + 8 \frac{M_B^2 |p_{D^*}|^2}{M_{D^*}^2 q^2} |\mathbf{C}_{\text{TR}}^\ell|^2 \mathbf{T}_2^2 \\
& + \frac{16(M_B^4 + M_{D^*}^4 - 2M_B^2 (M_{D^*}^2 + |p_{D^*}|^2))}{q^4} |\mathbf{C}_{\text{TR}}^\ell|^2 \mathbf{T}_2^2 \\
& + \frac{32M_B^4 |p_{D^*}|^4}{(-M_B^2 M_{D^*} + M_{D^*}^3)^2 q^2} |\mathbf{C}_{\text{TR}}^\ell|^2 \mathbf{T}_3^2 \\
& \left. + \frac{16M_B^2 |p_{D^*}|^2 (M_B^2 + 3M_{D^*}^2 - q^2)}{M_{D^*}^2 (-M_B^2 + M_{D^*}^2) q^2} |\mathbf{C}_{\text{TR}}^\ell|^2 \mathbf{T}_2 \mathbf{T}_3 \right] \tag{3.2.3}
\end{aligned}$$

$$\begin{aligned}
b_\ell^{D*}(+) &= \frac{8M_B(M_B^2 + 3M_{D^*}^2 - q^2)|p_{D^*}|}{(m_b + m_c)M_{D^*}} \mathcal{R}(\mathbf{C}_{\text{PL}}^\ell \mathbf{C}_{\text{TL}}^{\ell*}) \mathbf{A}_0 \mathbf{T}_2 \\
&\quad - \frac{32M_B^3|p_{D^*}|^3}{(m_b + m_c)M_{D^*}(M_B^2 - M_{D^*}^2)} \mathcal{R}(\mathbf{C}_{\text{PL}}^\ell \mathbf{C}_{\text{TL}}^{\ell*}) \mathbf{A}_0 \mathbf{T}_3 \\
&\quad + m_\ell \left[\frac{4|p_{D^*}|M_B(M_B + M_{D^*})(M_B^2 - M_{D^*}^2 - q^2)}{M_{D^*}(m_b + m_c)q^2} \mathcal{R}(\mathbf{C}_{\text{AL}}^\ell \mathbf{C}_{\text{PL}}^{\ell*}) \mathbf{A}_0 \mathbf{A}_1 \right. \\
&\quad - \frac{16}{(m_b + m_c)} \frac{|p_{D^*}|^3 M_B^3}{(M_B + M_{D^*})M_{D^*}q^2} \mathcal{R}(\mathbf{C}_{\text{AL}}^\ell \mathbf{C}_{\text{PL}}^{\ell*}) \mathbf{A}_0 \mathbf{A}_2 \\
&\quad - \frac{8M_B(M_B^2 + 3M_{D^*}^2 - q^2)|p_{D^*}|}{M_{D^*}q^2} \mathcal{R}(\mathbf{C}_{\text{AL}}^\ell \mathbf{C}_{\text{TL}}^{\ell*}) \mathbf{A}_0 \mathbf{T}_2 \\
&\quad + \frac{32M_B^3|p_{D^*}|^3}{q^2 M_{D^*}(M_B^2 - M_{D^*}^2)} \mathcal{R}(\mathbf{C}_{\text{AL}}^\ell \mathbf{C}_{\text{TL}}^{\ell*}) \mathbf{A}_0 \mathbf{T}_3 \\
&\quad + \frac{32M_B(-M_B + M_{D^*})|p_{D^*}|}{q^2} \mathcal{R}(\mathbf{C}_{\text{VR}}^\ell \mathbf{C}_{\text{TR}}^{\ell*}) \mathbf{V} \mathbf{T}_2 \\
&\quad \left. + \frac{32M_B(M_B + M_{D^*})|p_{D^*}|}{q^2} \mathcal{R}(\mathbf{C}_{\text{AR}}^\ell \mathbf{C}_{\text{TR}}^{\ell*}) \mathbf{A}_1 \mathbf{T}_1 \right] \\
&\quad + m_\ell^2 \left[-\frac{4|p_{D^*}|M_B(M_B + M_{D^*})}{M_{D^*}q^4} (M_B^2 - M_{D^*}^2 - q^2) |\mathbf{C}_{\text{AL}}^\ell|^2 \mathbf{A}_0 \mathbf{A}_1 \right. \\
&\quad + \frac{16|p_{D^*}|^3 M_B^3}{(M_B + M_{D^*})M_{D^*}q^4} |\mathbf{C}_{\text{AL}}^\ell|^2 \mathbf{A}_0 \mathbf{A}_2 \\
&\quad \left. + \frac{64M_B(-M_B^2 + M_{D^*}^2)|p_{D^*}|}{q^4} |\mathbf{C}_{\text{TR}}^\ell|^2 \mathbf{T}_1 \mathbf{T}_2 \right] \tag{3.2.4} \\
c_\ell^{D*}(+) &= -\frac{32M_B^2|p_{D^*}|^2}{q^2} |\mathbf{C}_{\text{TL}}^\ell|^2 \mathbf{T}_1^2 - \frac{2(4M_{D^*}^2 - q^2)\lambda}{M_{D^*}^2 q^2} |\mathbf{C}_{\text{TL}}^\ell|^2 \mathbf{T}_2^2 + \frac{32M_B^4|p_{D^*}|^4}{M_{D^*}^2(M_B^2 - M_{D^*}^2)^2} |\mathbf{C}_{\text{TL}}^\ell|^2 \mathbf{T}_3^2 \\
&\quad - \frac{16M_B^2|p_{D^*}|^2(M_B^2 + 3M_{D^*}^2 - q^2)}{M_{D^*}^2(M_B^2 - M_{D^*}^2)} |\mathbf{C}_{\text{TL}}^\ell|^2 \mathbf{T}_2 \mathbf{T}_3 \\
&\quad - m_\ell \left[\frac{32M_B^2|p_{D^*}|^2}{q^2(M_B + M_{D^*})} \mathcal{R}(\mathbf{C}_{\text{VL}}^\ell \mathbf{C}_{\text{TL}}^{\ell*}) \mathbf{V} \mathbf{T}_1 \right. \\
&\quad - \frac{8M_B^2(M_B + M_{D^*})|p_{D^*}|^2}{q^2 M_{D^*}^2} \mathcal{R}(\mathbf{C}_{\text{AL}}^\ell \mathbf{C}_{\text{TL}}^{\ell*}) \mathbf{A}_1 \mathbf{T}_2 \\
&\quad + \frac{8M_B^2(M_B^2 - M_{D^*}^2 - q^2)|p_{D^*}|^2}{q^2 M_{D^*}^2(M_B - M_{D^*})} \mathcal{R}(\mathbf{C}_{\text{AL}}^\ell \mathbf{C}_{\text{TL}}^{\ell*}) \mathbf{A}_1 \mathbf{T}_3 \\
&\quad + \frac{8M_B^2(M_B^2 + 3M_{D^*}^2 - q^2)|p_{D^*}|^2}{q^2 M_{D^*}^2(M_B + M_{D^*})} \mathcal{R}(\mathbf{C}_{\text{AL}}^\ell \mathbf{C}_{\text{TL}}^{\ell*}) \mathbf{A}_2 \mathbf{T}_2 \\
&\quad - \frac{32M_B^4|p_{D^*}|^4}{q^2 M_{D^*}^2(M_B + M_{D^*})(M_B^2 - M_{D^*}^2)} \mathcal{R}(\mathbf{C}_{\text{AL}}^\ell \mathbf{C}_{\text{TL}}^{\ell*}) \mathbf{A}_2 \mathbf{T}_3 \\
&\quad + \frac{32M_B^2|p_{D^*}|^2}{(M_B + M_{D^*})q^2} \mathcal{R}(\mathbf{C}_{\text{VR}}^\ell \mathbf{C}_{\text{TR}}^{\ell*}) \mathbf{V} \mathbf{T}_1 \\
&\quad + \frac{8M_B^2(M_B + M_{D^*})|p_{D^*}|^2}{M_{D^*}^2 q^2} \mathcal{R}(\mathbf{C}_{\text{AR}}^\ell \mathbf{C}_{\text{TR}}^{\ell*}) \mathbf{A}_1 \mathbf{T}_2 \\
&\quad - \frac{8M_B^2|p_{D^*}|^2(-M_B^2 + M_{D^*}^2 + q^2)}{(M_B - M_{D^*})M_{D^*}^2 q^2} \mathcal{R}(\mathbf{C}_{\text{AR}}^\ell \mathbf{C}_{\text{TR}}^{\ell*}) \mathbf{A}_1 \mathbf{T}_3 \\
&\quad + \frac{8M_B^2|p_{D^*}|^2(M_B^2 + 3M_{D^*}^2 - q^2)}{M_{D^*}^2(M_B + M_{D^*})q^2} \mathcal{R}(\mathbf{C}_{\text{AR}}^\ell \mathbf{C}_{\text{TR}}^{\ell*}) \mathbf{A}_2 \mathbf{T}_2 \\
&\quad \left. - \frac{32M_B^4|p_{D^*}|^4}{(M_B - M_{D^*})M_{D^*}^2(M_B + M_{D^*})^2 q^2} \mathcal{R}(\mathbf{C}_{\text{AR}}^\ell \mathbf{C}_{\text{TR}}^{\ell*}) \mathbf{A}_2 \mathbf{T}_3 \right]
\end{aligned}$$

$$\begin{aligned}
& +m_\ell^2 \left[-\frac{8|p_{D^*}|^2 M_B^2}{(M_B + M_{D^*})^2 q^2} |\mathbf{C}_{\text{VL}}^\ell|^2 \mathbf{V}^2 + \frac{(M_B + M_{D^*})^2 \lambda}{2M_{D^*}^2 q^4} |\mathbf{C}_{\text{AL}}^\ell|^2 \mathbf{A}_1^2 \right. \\
& + \frac{8|p_{D^*}|^4 M_B^4}{M_{D^*}^2 (M_B + M_{D^*})^2 q^4} |\mathbf{C}_{\text{AL}}^\ell|^2 \mathbf{A}_2^2 \\
& - \frac{4|p_{D^*}|^2 M_B^2}{M_{D^*}^2 q^4} (M_B^2 - M_{D^*}^2 - q^2) |\mathbf{C}_{\text{AL}}^\ell|^2 \mathbf{A}_1 \mathbf{A}_2 \\
& + \frac{32M_B^2 |p_{D^*}|^2}{q^4} |\mathbf{C}_{\text{TR}}^\ell|^2 \mathbf{T}_1^2 + \frac{8M_B^2 |p_{D^*}|^2 (4M_{D^*}^2 - q^2)}{M_{D^*}^2 q^4} |\mathbf{C}_{\text{TR}}^\ell|^2 \mathbf{T}_2^2 \\
& - \frac{32M_B^4 |p_{D^*}|^4}{(-M_B^2 M_{D^*} + M_{D^*}^3)^2 q^2} |\mathbf{C}_{\text{TR}}^\ell|^2 \mathbf{T}_3^2 \\
& \left. + \frac{16M_B^2 |p_{D^*}|^2 (M_B^2 + 3M_{D^*}^2 - q^2)}{M_{D^*}^2 (M_B^2 - M_{D^*}^2) q^2} |\mathbf{C}_{\text{TR}}^\ell|^2 \mathbf{T}_2 \mathbf{T}_3 \right] \quad (3.2.5)
\end{aligned}$$

C.3 Contribution of the Tensor operator $\mathcal{O}_{\text{TL}}^{cb\ell}$

C.3.1 $\bar{B} \rightarrow D\tau\bar{\nu}_\tau$

In this section we investigate the effect of the tensor operator $\mathcal{O}_{\text{TL}}^{cb\ell}$ on the $\bar{B} \rightarrow D\tau\bar{\nu}_\tau$ decay. In the first column of table C.1, we show the range of C_{TL}^τ that explains R_D within 1σ . In the subsequent columns, we show the predictions of $P_\tau(D)$, \mathcal{A}_{FB}^D and binwise R_D for the allowed range of C_{TL}^τ that is closest to zero (i.e., $C_{TL}^\tau \in [0.240, 0.796]$). A comparison with the left plot of Fig. 4.6 reveals that $P_\tau(D)$ in this case is quite different from the other cases and thus, can completely distinguish the tensor operator from the vector or scalar operators. Similarly, \mathcal{A}_{FB}^D can also be used to distinguish the tensor from the vector operator, however, there exists some degeneracy with the scalar operator.

The variation of R_D as a function of C_{TL}^τ is also shown in the left plot of Fig. C.1. The predictions for binwise R_D for the tensor operators are graphically presented in the right plot of Fig. C.1.

C.3.2 $\bar{B} \rightarrow D^*\tau\bar{\nu}_\tau$

The range of C_{TL}^τ that explains R_D^* within 1σ is shown in the first column of table C.2. The resulting values for $P_\tau(D^*)$, $\mathcal{A}_{FB}^{D^*}$ and binwise R_D^* are shown in the subsequent columns. In

C_{TL}^τ	$P_\tau(D)$	R_D [bin]			
$\in [0.240, 0.796]$	$\in [0.125, 0.254]$	$[m_\tau^2 - 5] \text{ GeV}^2$	$[5 - 7] \text{ GeV}^2$	$[7 - 9] \text{ GeV}^2$	$[9 - (M_B - M_D)^2] \text{ GeV}^2$
C_{TL}^τ	\mathcal{A}_{FB}^D				
$\in [-3.500, -3.052]$	$\in [-0.451, -0.404]$	$[0.178, 0.233]$	$[0.673, 0.907]$	$[1.135, 1.533]$	$[1.989, 2.508]$

Table C.1: Predictions for $P_\tau(D)$, \mathcal{A}_{FB}^D and binwise values of R_D for a range of C_{TL}^τ for which R_D is experimentally satisfied within 1σ . The range of the WCs is given in the first column. The values in the subsequent columns are only for the range of C_{TL}^τ closest to the SM value of 0, viz. the positive range.

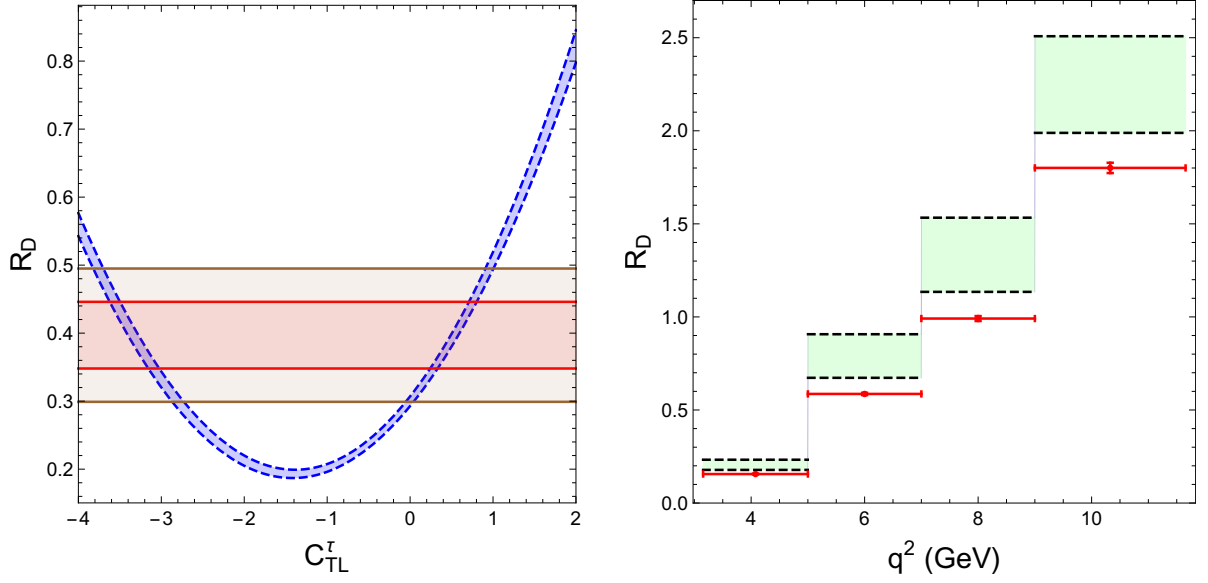


Figure C.1: The left panel shows the dependence of R_D with respect to the variation of the WCs C_{TL}^T and the right panel shows the prediction for R_D in four different bins of q^2 from table C.1.

C_{TL}^T	$P_\tau(D^*)$	R_{D^*} [bin]			
$\in [-0.120, -0.058]$	$\in [-0.481, -0.441]$	$[m_\tau^2 - 5] \text{ GeV}^2$	$[5 - 7] \text{ GeV}^2$	$[7 - 9] \text{ GeV}^2$	$[9 - (M_B - M_{D^*})^2] \text{ GeV}^2$
C_{TL}^T	$\mathcal{A}_{FB}^{D^*}$				
$\in [0.709, 0.834]$	$\in [-0.016, 0.034]$	$[0.113, 0.129]$	$[0.368, 0.423]$	$[0.531, 0.610]$	$[0.620, 0.715]$

Table C.2: Predictions for $P_\tau(D^*)$, $\mathcal{A}_{FB}^{D^*}$ and binwise values of R_{D^*} for a range of C_{TL}^T for which R_{D^*} is experimentally satisfied within 1σ . The corresponding range of the WCs is given in the first column. The values in the subsequent columns are only for the range of C_{TL}^T closest to the SM value of 0, viz. the negative range.

the left plot of Fig. C.2 we also show the dependence of R_D^* as a function of C_{TL}^T . The right plot shows the binwise R_D^* graphically.

A quick look at the allowed ranges for C_{TL} in the $B \rightarrow D$ (Table C.1) and the $B \rightarrow D^*$ (Table C.2) cases shows that there is a region of overlap, around 0.7-0.8, which allows one to explain both the anomalies simultaneously.

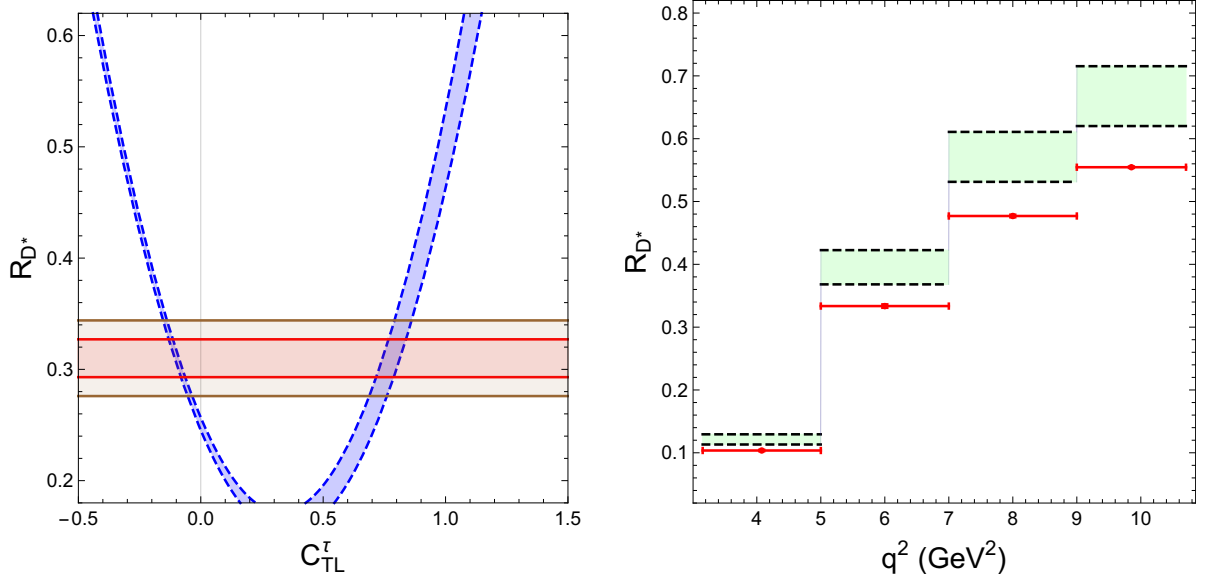


Figure C.2: The left panel shows the dependence of R_{D^*} with respect to the variation of the WCs C_{TL}^T and the right panel shows the prediction for R_{D^*} in four different bins of q^2 from table C.2.

C.4 $SU(3)_C \times SU(2)_L \times U(1)_Y$ gauge invariance

In table C.3, we show how the WCs of the operators in this paper are related to the WCs of the gauge invariant dimension 6 operators of [42]. We use the following set of notations:

- Greek letters μ, ν, \dots are used to denote Lorentz indices.
- $SU(2)$ fundamental indices are denoted by a, b, \dots and I, J, \dots will be used to denote adjoint indices.
- To represent quark (lepton) flavors, we use i, j, k, \dots (m, n, \dots).
- A tilde (e.g. \tilde{C}) is used to denote high energy Wilson coefficients.
- The notation for the operators is as given in [42].
- definition of the quark mixing matrices (f and m denote flavour and mass bases)

$$\begin{aligned}
 u_L^f &= V_L^u u_L^m \\
 u_R^f &= V_R^u u_R^m \\
 d_L^f &= V_L^d d_L^m \\
 d_R^f &= V_R^d d_R^m
 \end{aligned} \tag{3.4.1}$$

C.5 RG Running of Wilson Coefficients

In this section, we note the renormalisation group (RG) running of the couplings and the Wilson coefficients. The QCD coupling above the m_b scale is given by $\alpha_s^{(5)}$ and that above

WCs in this work	WCs in [42]	Operator structure
$\frac{2G_F V_{cb}}{\sqrt{2}} \times \left\{ \begin{array}{l} \Delta C_9^{cb\tau^*} = -\Delta C_{10}^{cb\tau^*} \\ C_9^{cb\tau'^*} = -C_{10}^{cb\tau'^*} \\ C_s^{cb\tau^*} = -C_p^{cb\tau^*} \\ C_s^{cb\tau'^*} = -C_p^{cb\tau'^*} \\ C_T^{cb\tau^*} = -C_{T5}^{cb\tau^*} \end{array} \right\}$	$= \begin{array}{l} \frac{1}{2} [V_L^{d\dagger}]_{3i} \left[-\frac{g^2 v^2}{2M_W^2} \left(\tilde{C}_{\phi q}^{(3)ij,33\dagger} + \right. \right. \\ \left. \left. \tilde{C}_{\phi \ell}^{(3)33,ij} \right) + 2\tilde{C}_{\ell q}^{(3)ij,33} \right] [V_L^u]_{j2} \\ -\frac{1}{2} [V_R^{u\dagger}]_{2i} \frac{g^2 v^2}{2M_W^2} \tilde{C}_{\phi ud}^{ij,33\dagger} [V_R^d]_{j3} \\ \frac{1}{2} [V_L^{d\dagger}]_{3i} \tilde{C}_{\ell equ}^{(1)ij,33} [V_R^u]_{j2} \\ \frac{1}{2} [V_R^{u\dagger}]_{3i} \tilde{C}_{\ell edq}^{ij,33} [V_L^u]_{j2} \\ \frac{1}{2} [V_L^{d\dagger}]_{3i} \tilde{C}_{\ell equ}^{(3)ij,33} [V_R^u]_{j2} \end{array}$	$\begin{array}{l} [\phi^\dagger i \overleftrightarrow{D}_\mu^I \phi] [\bar{q}_i^2 \frac{\sigma^I}{2} \gamma^\mu q_j^1] \\ [\phi^\dagger i \overleftrightarrow{D}_\mu^I \phi] [\bar{\ell}_i^1 \frac{\sigma^I}{2} \gamma^\mu \ell_j^2] \\ [\bar{q}_i^2 \gamma^\mu q_j^1] [\bar{\ell}_3^1 \gamma_\mu \ell_3^2] \\ [i \tilde{\phi}^\dagger D_\mu \phi] [\bar{u}_p \gamma^\mu d_r] \\ (\bar{\ell}_3^1 e_3) (\bar{q}_i^2 u_j) \\ (\bar{\ell}_3^1 e_3) (\bar{d}_i q_j^1) \\ (\bar{\ell}_3^1 \sigma_{\mu\nu} e_3) \epsilon_{12} (\bar{q}_i^2 \sigma^{\mu\nu} u_j) \end{array}$

Table C.3: Correspondence of our operators with those in reference [42]. The mixing of different lepton flavours are ignored.

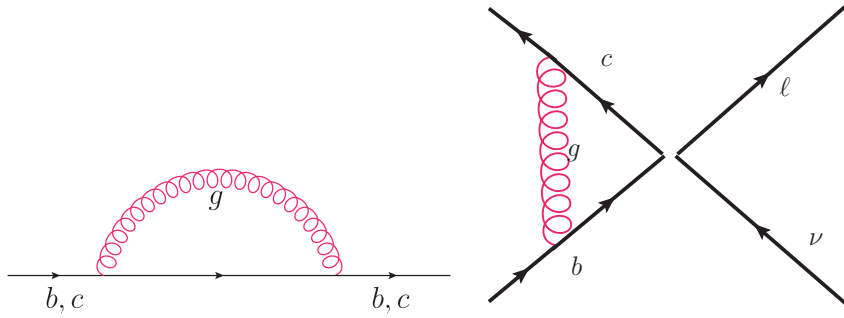


Figure C.3: Vertex Correction and self energy diagrams.

the m_t scale is given by $\alpha_s^{(6)}$. These are given by

$$\alpha_s^{(5)}(\mu) = \frac{\alpha_s(m_b)}{1 + \beta_0^{(5)} \frac{\alpha_s(m_b)}{2\pi} \ln\left(\frac{\mu}{m_b}\right)} \quad \alpha_s^{(6)}(\mu) = \frac{\alpha_s(m_t)}{1 + \beta_0^{(6)} \frac{\alpha_s(m_t)}{2\pi} \ln\left(\frac{\mu}{m_t}\right)} \quad (3.5.1)$$

where $\beta_0^{(n_f)} = 11 - \frac{2n_f}{3}$.

In order to calculate the running of the Wilson Coefficients to a high scale M , we need to calculate the beta functions for the different operators - the scalar, vector and tensor operators. The calculation is sketched below (for a good review on the subject, see [316])

Firstly, we need to consider the self-energy correction for the b or c quarks (left diagram in

Fig. C.3). This is given by

$$\begin{aligned}\Sigma(p) &= i \int \frac{d^4 k}{(2\pi)^4} (ig_s \gamma^\mu T^a) \frac{i(\not{p} + \not{k} + m_{b/c})}{(p+k)^2 - m_{b/c}^2} (ig_s \gamma^\nu T^b) \frac{(-ig_{\mu\nu} \delta_{ab})}{k^2} \\ &= \frac{4}{3} \left(-\frac{\alpha_s}{4\pi} \not{p} + \underbrace{\frac{\alpha_s m_{b/c}}{\pi}}_{\text{dropped}} \right) \frac{1}{\epsilon} + \text{finite}\end{aligned}\quad (3.5.2)$$

where p is the momentum of the incoming (or outgoing) quark.

From Feynman diagram on the right of Fig. C.3, we find that the vertex correction in d dimensions ($d = 4 - 2\epsilon$) is given by

$$\begin{aligned}\Gamma_{\text{Had}}(p, p') &= i \int \frac{d^d k}{(2\pi)^d} (ig_s \gamma^\lambda T^a) \frac{i}{\not{p} + \not{k} - m_b} i\mathcal{F} \frac{i}{\not{p}' + \not{k} - m_c} (ig_s \gamma^\sigma T^b) (-i\delta_{ab} g_{\lambda\sigma}) \frac{1}{k^2} \\ &= ig_s^2 C_2(3) \int \frac{d^d k}{(2\pi)^d} \frac{\gamma_\lambda (\not{p} + \not{k} + m_b) \mathcal{F} (\not{p}' + \not{k} + m_c) \gamma^\lambda}{k^2 ((p+k)^2 + m_b^2) ((p'+k)^2 + m_c^2)}\end{aligned}\quad (3.5.3)$$

where $C_2(3) = \frac{4}{3}$ and $\mathcal{F} = 1, \gamma_\mu, \sigma_{\mu\nu}$ for scalar, vector and tensor operators and p (p') is the on-shell momentum of the b (c) quark. A few things are noteworthy and enlisted below:

- As the denominator has mass dimension 6, divergence will appear only when the numerator is a function of loop momentum with mass dimension greater than and equals to two.
- The general form of the numerator is

$$\begin{aligned}N &= \gamma_\lambda (\not{p}' + \not{k} + m_b) \mathcal{F} (\not{p} + \not{k} + m_c) \gamma^\lambda \\ &= \gamma_\lambda \not{k} \mathcal{F} \not{k} \gamma^\lambda + \text{finite}\end{aligned}\quad (3.5.4)$$

– For scalar

$$N = 4k^2 \quad (3.5.5)$$

– For vector

$$N = \gamma_\lambda \not{k} \gamma_\mu \not{k} \gamma^\lambda = -k^2 \gamma_\lambda \gamma_\mu \gamma^\lambda + 2k_\mu \gamma_\lambda \not{k} \gamma^\lambda = 2k^2 \gamma_\mu - 4k_\mu \not{k}$$

Using

$$\int d^4 k k^\mu k^\nu f(k^2) = \frac{1}{4} g^{\mu\nu} \int d^4 k k^2 f(k^2)$$

we get

$$N = k^2 \gamma_\mu \quad (3.5.6)$$

– For tensor

$$N = \gamma_\lambda \not{k} \sigma_{\mu\nu} \not{k} \gamma^\lambda \rightarrow k^2 \frac{1}{4} \gamma_\lambda \gamma_\rho \sigma_{\mu\nu} \gamma^\rho \gamma^\lambda = 0 \quad (3.5.7)$$

where we used the previous integral formula in the second step.

Putting this back and using Feynman parameterisation and neglecting quark masses, we have the following formula

$$\begin{aligned}
\Gamma_{\text{Had}} &= i g_s^2 C_2(3) \mathcal{N} \mathcal{F} \int_0^1 d\zeta \int \frac{d^d k}{(2\pi)^d} \frac{1}{\left[\zeta (p+k)^2 + (1-\zeta) (p'+k)^2 \right]^2} \\
&= i \frac{16\pi}{3} \alpha_s \mathcal{N} \mathcal{F} \int_0^1 d\zeta \int \frac{d^d \ell}{(2\pi)^d} \frac{1}{(\ell^2 + \Delta)^2} \\
&\quad \text{where } \ell = k + p + (1-\zeta)(p' - p) \text{ and } \Delta = \zeta(1-\zeta)(p' - p)^2 \\
&= i \frac{16\pi}{3} \alpha_s \mathcal{N} \mathcal{F} \int_0^1 d\zeta \frac{i}{(4\pi)^2} \left(\frac{2}{\epsilon} + \text{finite} \right) \\
&= -\frac{\alpha_s}{4\pi} \frac{8\mathcal{N}}{3} \mathcal{F} \frac{1}{\epsilon} + \text{finite}
\end{aligned} \tag{3.5.8}$$

where $\mathcal{N} = 4, 1, 0$ for $\mathcal{F} = 1, \gamma^\mu, \sigma^{\mu\nu}$ respectively. The bare effective Lagrangian to the lowest power in derivatives is

$$\mathcal{L}_{\text{eff}}^{\text{bare}} = i \bar{\psi}_0 \not{\partial} \psi_0 + \mathcal{C} \bar{c}_0 \mathcal{F} b_0 \bar{\ell}_0 \mathcal{F}' \nu_{\ell 0} \tag{3.5.9}$$

where ψ_0 is any bare quark or lepton field, \mathcal{C} is the Wilson coefficient to the six-dimensional operator and $\mathcal{F}, \mathcal{F}'$ are Dirac operators.

We redefine the quantities in the bare Lagrangian as

$$\psi_0 = \sqrt{Z_\psi} \psi; \quad \mathcal{C}_0 = \mu^{2\epsilon} Z_C \mathcal{C} \tag{3.5.10}$$

where ψ represents any quark field. The QCD contributions to the different quark fields will be equal to each other. Then Eqn. 3.5.9 can then be written as

$$\begin{aligned}
\mathcal{L}_{\text{eff}}^{\text{ren}} &= i Z_\psi \bar{\psi} \not{\partial} \psi + \mathcal{C} Z_C Z_\psi^2 \mu^{2\epsilon} \bar{c} \mathcal{F} b \bar{\ell} \mathcal{F}' \nu_\ell \\
&= i \bar{\psi} \not{\partial} \psi + i(Z_\psi - 1) \bar{\psi} \not{\partial} \psi + \mathcal{C} \mu^{2\epsilon} \bar{c} \mathcal{F} b \bar{\ell} \mathcal{F}' \nu_\ell + \mathcal{C} (Z_C Z_\psi^2 - 1) \mu^{2\epsilon} \bar{c} \mathcal{F} b \bar{\ell} \mathcal{F}' \nu_\ell
\end{aligned}$$

Absorbing the divergences in Eqn. 3.5.2 and Eqn. 3.5.8 in the counter terms, we find that

$$Z_\psi = 1 - \frac{4}{3} \frac{\alpha_s}{4\pi} \frac{1}{\epsilon} \text{ and } Z_C = 1 - \frac{8}{3} \frac{\alpha_s}{4\pi} (\mathcal{N} - 1) \frac{1}{\epsilon} \tag{3.5.11}$$

Using the RG equations, the β -function turns out to be

$$\begin{aligned}
\beta_C &= -2\epsilon \mathcal{C} - \frac{\mu}{Z_C} \mathcal{C} \frac{d Z_C}{d\mu} \\
&= \frac{8}{3} \frac{1}{4\pi} (\mathcal{N} - 1) \mathcal{C} \frac{\mu}{Z_C} \frac{d \alpha_s}{d\mu} \frac{1}{\epsilon} \\
&= -\frac{8}{3} \frac{\alpha_s}{4\pi} (\mathcal{N} - 1) \mathcal{C}
\end{aligned} \tag{3.5.12}$$

Thus,

$$\beta_C^S = -8 \frac{\alpha_s}{4\pi} \mathcal{C}, \quad \beta_C^V = \mathbf{0}, \text{ and } \beta_C^T = \frac{8}{3} \frac{\alpha_s}{4\pi} \mathcal{C} \tag{3.5.13}$$

where the superscripts S, V and T on the β denote scalar, vector and tensor couplings. The running of the Wilson Coefficients can be found by solving the β -function equation given in Eqn. 3.5.13. Solving, we get,

$$\tilde{C}(m_b) = \left[\frac{\alpha_s(m_t)}{\alpha_s(m_b)} \right]^{\frac{\gamma}{2\beta_0^{(5)}}} \left[\frac{\alpha_s(M)}{\alpha_s(m_t)} \right]^{\frac{\gamma}{2\beta_0^{(6)}}} \tilde{C}(M) \tag{3.5.14}$$

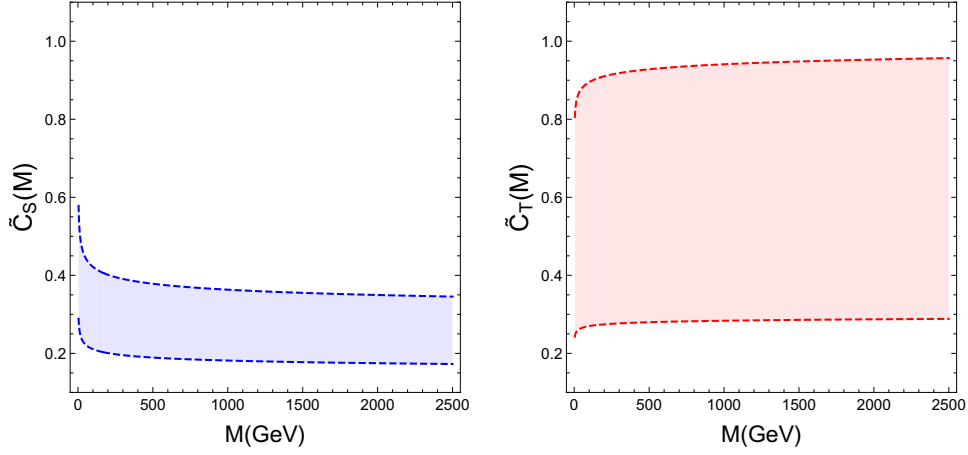


Figure C.4: Plot of the running of the Scalar (left) and Tensor (right) Wilson Coefficients. The range of the running is from m_b to 2.5 TeV. As a demonstration, the range of the initial values used are the ones mentioned in the text for $B \rightarrow D$ decay.

Thus, the scalar and tensor WCs are given by:

$$\tilde{C}_S(M) = \left[\left[\frac{\alpha_s(m_t)}{\alpha_s(m_b)} \right]^{\frac{\gamma_S}{2\beta_0^{(5)}}} \left[\frac{\alpha_s(M)}{\alpha_s(m_t)} \right]^{\frac{\gamma_S}{2\beta_0^{(6)}}} \right]^{-1} \tilde{C}_S(m_b) \quad (3.5.15)$$

$$\tilde{C}_T(M) = \left[\left[\frac{\alpha_s(m_t)}{\alpha_s(m_b)} \right]^{\frac{\gamma_T}{2\beta_0^{(5)}}} \left[\frac{\alpha_s(M)}{\alpha_s(m_t)} \right]^{\frac{\gamma_T}{2\beta_0^{(6)}}} \right]^{-1} \tilde{C}_T(m_b) \quad (3.5.16)$$

where

$$\gamma_S = -8 \quad \gamma_T = \frac{8}{3} \quad (3.5.17)$$

which are simply the boldfaced coefficients in Eqn. 3.5.13. This is plotted in Fig. C.4.

Appendix D

The Sgoldstino as a 750 GeV candidate

D.1 Calculation of the partial decay widths

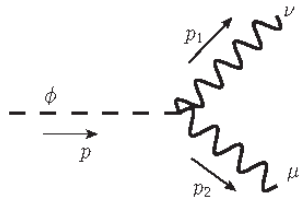
In this appendix we will calculate the partial decay rate of ϕ and a to two vector bosons.

D.1.1 $\phi \rightarrow \gamma\gamma$

We start with the decay $\phi \rightarrow \gamma\gamma$ which arises from the following term in the Lagrangian,

$$\mathcal{L} \subset \frac{1}{\Lambda} \phi F_{\mu\nu} F^{\mu\nu}. \quad (4.1.1)$$

This yields the following Feynman rule,



$$[i] [2!] \left[-\frac{2}{\Lambda} (p_1 \cdot p_2 g_{\mu\nu} - p_{1\mu} p_{2\nu}) \right] \quad (4.1.2)$$

Thus, the matrix element is given by,

$$i\mathcal{M} = -\frac{4}{\Lambda} i (p_1 \cdot p_2 g_{\mu\nu} - p_{1\mu} p_{2\nu}) \epsilon^{*\nu}(p_1) \epsilon^{*\mu}(p_2) \quad (4.1.3)$$

This gives,

$$|\mathcal{M}|^2 = \frac{16}{\Lambda^2} (p_1 \cdot p_2 g_{\mu\nu} - p_{1\mu} p_{2\nu}) (p_1 \cdot p_2 g_{\alpha\beta} - p_{1\alpha} p_{2\beta}) \epsilon^{*\nu}(p_1) \epsilon^{*\mu}(p_2) \epsilon^\beta(p_1) \epsilon^\alpha(p_2) \quad (4.1.4)$$

Summing over the polarizations, i.e.,

$$\sum \epsilon^\mu(p) \epsilon^{*\nu}(p) = -g^{\mu\nu}$$

we get,

$$\begin{aligned} |\mathcal{M}|^2 &= \frac{16}{\Lambda^2} (p_1 \cdot p_2 g_{\mu\nu} - p_{1\mu} p_{2\nu}) (p_1 \cdot p_2 g_{\alpha\beta} - p_{1\alpha} p_{2\beta}) g^{\alpha\mu} g^{\beta\nu} \\ &= \frac{16}{\Lambda^2} (p_1^2 p_2^2 + 4(p_1 \cdot p_2)^2 - 2(p_1 \cdot p_2)^2) \\ &= \frac{32}{\Lambda^2} (p_1 \cdot p_2)^2 \\ &= \frac{32}{\Lambda^2} \left(\frac{m_\phi^2}{2} \right)^2 \\ &= \frac{8m_\phi^4}{\Lambda^2} \end{aligned} \quad (4.1.5)$$

Hence,

$$\Gamma(\phi \rightarrow \gamma\gamma) = \frac{1}{\Lambda^2} \left[\frac{1}{2m_\phi} \right] \left[\frac{1}{8\pi} \right] [8m_\phi^4] \left[\frac{1}{2} \right]. \quad (4.1.6)$$

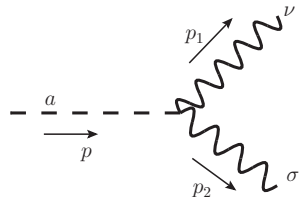
The factor of 1/2 in the end is due to the presence of two identical particles in the final state.

D.1.2 $a \rightarrow \gamma\gamma$

The decay $a \rightarrow \gamma\gamma$ arises from the Lagrangian

$$\mathcal{L} \subset \frac{1}{\Lambda} a F_{\mu\nu} \tilde{F}^{\mu\nu} = \frac{1}{2\Lambda} a F_{\mu\nu} F_{\alpha\beta} \varepsilon^{\mu\nu\alpha\beta} \quad (4.1.7)$$

The Feynman rule for this vertex is given by



$$[i] [2!] \left[-\frac{2}{\Lambda} \varepsilon^{\mu\nu\rho\sigma} p_{1\mu} p_{2\rho} \right] \quad (4.1.8)$$

The matrix element and its square are given by,

$$\begin{aligned} i\mathcal{M} &= -\frac{4}{\Lambda} i \varepsilon^{\mu\nu\rho\sigma} p_{1\mu} p_{2\rho} \epsilon_\nu^*(p_1) \epsilon_\sigma^*(p_2) \\ |\mathcal{M}|^2 &= \frac{16}{\Lambda^2} \varepsilon^{\mu\nu\rho\sigma} \varepsilon^{\alpha\beta\gamma\delta} p_{1\mu} p_{1\alpha} p_{2\rho} p_{2\gamma} \epsilon_\nu^*(p_1) \epsilon_\sigma^*(p_2) \epsilon_\beta(p_1) \epsilon_\delta(p_2) \end{aligned} \quad (4.1.9)$$

Summing over the polarisations we get,

$$\begin{aligned}
\sum |\mathcal{M}|^2 &= \frac{16}{\Lambda^2} \varepsilon^{\mu\nu\rho\sigma} \varepsilon^{\alpha\beta\gamma\delta} p_{1\mu} p_{1\alpha} p_{2\rho} p_{2\gamma} g_{\nu\beta} g_{\sigma\delta} \\
&= \frac{16}{\Lambda^2} \varepsilon^{\mu\rho\sigma} \varepsilon^{\beta\alpha\gamma} p_{1\mu} p_{1\alpha} p_{2\rho} p_{2\gamma} g_{\nu\beta} g_{\sigma\delta} \\
&= \frac{32}{\Lambda^2} (-g^{\mu\alpha} g^{\rho\gamma} + g^{\mu\gamma} g^{\rho\alpha}) p_{1\mu} p_{1\alpha} p_{2\rho} p_{2\gamma} \\
&= \frac{32}{\Lambda^2} (p_1 \cdot p_2)^2 \\
&= \frac{32}{\Lambda^2} \left(\frac{m_a^2}{2} \right)^2 \\
&= \frac{8m_a^4}{\Lambda^2}
\end{aligned} \tag{4.1.10}$$

Hence, finally we get

$$\Gamma(a \rightarrow \gamma\gamma) = \frac{1}{\Lambda^2} \left[\frac{1}{2m_a} \right] \left[\frac{1}{8\pi} \right] [8m_a^4] \left[\frac{1}{2} \right]. \tag{4.1.11}$$

D.1.3 $\phi \rightarrow Z Z$

The relevant part of the Lagrangian is

$$\mathcal{L} \subset \frac{1}{\Lambda} \phi Z_{\mu\nu} Z^{\mu\nu}. \tag{4.1.12}$$

The Feynman rule is same as the decay $\phi \rightarrow \gamma\gamma$ (Eq. 4.1.2).

The squared matrix element is given by,

$$|\mathcal{M}|^2 = \frac{16}{\Lambda^2} (p_1 \cdot p_2 g_{\mu\nu} - p_{1\mu} p_{2\nu}) (p_1 \cdot p_2 g_{\alpha\beta} - p_{1\alpha} p_{2\beta}) \epsilon^{*\nu}(p_1) \epsilon^{*\mu}(p_2) \epsilon^\beta(p_1) \epsilon^\alpha(p_2) \tag{4.1.13}$$

Summation over the polarization vectors,

$$\sum \epsilon^\mu(p) \epsilon^{*\nu}(p) = -g^{\mu\nu} + \frac{p^\mu p^\nu}{m_Z^2}$$

we get,

$$\begin{aligned}
|\mathcal{M}|^2 &= 16 (p_1 \cdot p_2 g_{\mu\nu} - p_{1\mu} p_{2\nu}) (p_1 \cdot p_2 g_{\alpha\beta} - p_{1\alpha} p_{2\beta}) \left(-g^{\mu\alpha} + \frac{p_1^\mu p_1^\alpha}{m_Z^2} \right) \left(-g^{\nu\beta} + \frac{p_2^\nu p_2^\beta}{m_Z^2} \right) \\
&= 16 (p_1 \cdot p_2 g_{\mu\nu} - p_{1\mu} p_{2\nu}) (p_1 \cdot p_2 g_{\alpha\beta} - p_{1\alpha} p_{2\beta}) (-g^{\mu\alpha}) (-g^{\nu\beta}) \\
&= 16 (2(p_1 \cdot p_2)^2 + p_1^2 p_2^2) \\
&= 8m_\phi^4 \left(1 - 4 \frac{m_Z^2}{m_\phi^2} + 6 \frac{m_Z^4}{m_\phi^4} \right)
\end{aligned} \tag{4.1.14}$$

$$\Gamma(\phi \rightarrow Z Z) = \left[\frac{1}{2m_\phi} \right] \left[\frac{\lambda^{1/2}(1, m_Z^2/m_\phi^2, m_Z^2/m_\phi^2)}{8\pi} \right] |\mathcal{M}|^2 \left[\frac{1}{2} \right] \quad (4.1.15)$$

$$(4.1.16)$$

where,

$$\lambda(a, b, c) = a^2 + b^2 + c^2 - 2ab - 2ac - 2bc \quad (4.1.17)$$

$$\Gamma(\phi \rightarrow Z Z) = \frac{1}{\Lambda^2} \left[\frac{1}{2m_\phi} \right] \left[\frac{1}{8\pi} \left(1 - 4 \frac{m_Z^2}{m_\phi^2} \right)^{1/2} \right] |\mathcal{M}|^2 \left[\frac{1}{2} \right] \quad (4.1.18)$$

$$= \frac{1}{\Lambda^2} \left[\frac{1}{2m_\phi} \right] \left[\frac{1}{8\pi} \left(1 - \frac{4m_Z^2}{m_\phi^2} \right)^{1/2} \right] \times \left[8m_\phi^4 \left(1 - 4 \frac{m_Z^2}{m_\phi^2} + 6 \frac{m_Z^4}{m_\phi^4} \right) \right] \left[\frac{1}{2} \right] \quad (4.1.19)$$

D.1.4 $a \rightarrow Z Z$

The relevant part of the Lagrangian is

$$\mathcal{L} \subset \frac{1}{\Lambda} a Z_{\mu\nu} \tilde{Z}^{\mu\nu}. \quad (4.1.20)$$

The Feynman rule is same as the decay $a \rightarrow \gamma\gamma$ (Eq. 4.1.8).

The squared matrix element is given by,

$$|\mathcal{M}|^2 = \frac{16}{\Lambda^2} \varepsilon^{\mu\nu\rho\sigma} \varepsilon^{\alpha\beta\gamma\delta} p_{1\mu} p_{1\alpha} p_{2\rho} p_{2\gamma} \epsilon_\nu^*(p_1) \epsilon_\beta(p_1) \epsilon_\sigma^*(p_2) \epsilon_\delta(p_2) \quad (4.1.21)$$

Summing over the polarisations, we have,

$$|\mathcal{M}|^2 = \frac{16}{\Lambda^2} \varepsilon^{\mu\nu\rho\sigma} \varepsilon^{\alpha\beta\gamma\delta} p_{1\mu} p_{1\alpha} p_{2\rho} p_{2\gamma} \left(-g_{\nu\beta} + \frac{p_{1\nu} p_{1\beta}}{M_Z^2} \right) \left(-g_{\sigma\delta} + \frac{p_{2\sigma} p_{2\delta}}{M_Z^2} \right) \quad (4.1.22)$$

$$= \frac{16}{\Lambda^2} \varepsilon^{\mu\nu\rho\sigma} \varepsilon^{\alpha\beta\gamma\delta} p_{1\mu} p_{1\alpha} p_{2\rho} p_{2\gamma} g_{\nu\beta} g_{\sigma\delta} \quad (4.1.23)$$

where we have used the fact that the second terms in each of the parenthesis vanish due to the antisymmetry of the Levi-civita symbols. We thus have,

$$|\mathcal{M}|^2 = \frac{16}{\Lambda^2} \varepsilon_\beta^{\mu\rho\sigma} \varepsilon_\sigma^{\beta\alpha\gamma} p_{1\mu} p_{1\alpha} p_{2\rho} p_{2\gamma} \quad (4.1.24)$$

Using the relation,

$$\varepsilon_\beta^{\mu\rho\sigma} \varepsilon_\sigma^{\beta\alpha\gamma} = 2(-g^{\mu\alpha} g^{\rho\gamma} + g^{\mu\gamma} g^{\rho\alpha}) \quad (4.1.25)$$

we get,

$$|\mathcal{M}|^2 = \frac{32}{\Lambda^2} (-g^{\mu\alpha} g^{\rho\gamma} + g^{\mu\gamma} g^{\rho\alpha}) p_{1\mu} p_{1\alpha} p_{2\rho} p_{2\gamma} \quad (4.1.26)$$

$$= \frac{32}{\Lambda^2} (-p_1^2 p_2^2 + (p_1 \cdot p_2)^2) \quad (4.1.27)$$

$$= \frac{32}{\Lambda^2} \left(-m_Z^4 + \frac{(m_a^2 - 2m_Z^2)^2}{4} \right) \quad (4.1.28)$$

$$= \frac{8m_a^4}{\Lambda^2} \left(1 - \frac{4m_Z^2}{m_a^2} \right) \quad (4.1.29)$$

$$\Gamma(a \rightarrow Z Z) = \left[\frac{1}{2m_a} \right] \left[\frac{\lambda^{1/2}(1, m_Z^2/m_a^2, m_Z^2/m_a^2)}{8\pi} \right] |\mathcal{M}|^2 \left[\frac{1}{2} \right] \quad (4.1.30)$$

$$= \frac{1}{\Lambda^2} \left[\frac{1}{2m_a} \right] \left[\frac{1}{8\pi} \left(1 - 4 \frac{m_Z^2}{m_a^2} \right)^{1/2} \right] |\mathcal{M}|^2 \left[\frac{1}{2} \right] \quad (4.1.31)$$

$$= \frac{1}{\Lambda^2} \left[\frac{1}{2m_a} \right] \left[\frac{1}{8\pi} \left(1 - \frac{4m_Z^2}{m_a^2} \right)^{1/2} \right] \times \left[8m_a^4 \left(1 - 4 \frac{m_Z^2}{m_a^2} \right) \right] \left[\frac{1}{2} \right] \quad (4.1.32)$$

D.2 Calculation of $\mathcal{A}_{\text{LHC energy}}^{ii}$

In this appendix we will calculate the quantities $\mathcal{A}_{\text{LHC energy}}^{ii}$ defined in section 6.2.2 for two LHC energies 8 TeV and 13 TeV, and for the initial states $\{gg\}$, $\{\bar{u}u\}$ and $\{\bar{d}d\}$.

D.2.1 Production by gluon fusion

The partonic cross section for the process $g(p) g(k) \rightarrow \phi(q)$ is given by

$$\hat{\sigma}(g(p) g(k) \rightarrow \phi(q)) \quad (4.2.1)$$

$$= \frac{1}{2^2} \frac{1}{8^2} \frac{1}{2E_p} \frac{1}{2E_k} \frac{1}{|v_p - v_k|} \int \frac{d^3q}{(2\pi)^3} \frac{1}{2E_q} |\mathcal{M}|^2 (2\pi)^4 \delta^{(4)}(p + k - q) \quad (4.2.2)$$

$$\Rightarrow \text{using the identity } \int dq^0 \delta(q^2 - m_\phi^2) \Theta(q^0) = \frac{1}{2E_q}, \text{ we get} \quad (4.2.3)$$

$$= \frac{1}{2^2} \frac{1}{8^2} \frac{2\pi}{2E_p} \frac{1}{2E_k} \frac{1}{|v_p - v_k|} \int d^4q \delta(q^2 - m_\phi^2) \Theta(q^0) |\mathcal{M}|^2 \delta^{(4)}(p + k - q) \quad (4.2.4)$$

$$= \frac{1}{2^2} \frac{1}{8^2} \frac{2\pi}{2E_p} \frac{1}{2E_k} \frac{1}{|v_p - v_k|} |\mathcal{M}|^2 \delta((p + k)^2 - m_\phi^2) \quad (4.2.5)$$

$$= \frac{1}{2^2} \frac{1}{8^2} \frac{2\pi}{x_1 x_2 S} \frac{1}{2} |\mathcal{M}|^2 \delta(x_1 x_2 S - m_\phi^2) \quad (4.2.6)$$

$$= \frac{\pi}{256} \frac{1}{x_1 x_2 S} |\mathcal{M}|^2 \delta(x_1 x_2 S - m_\phi^2) \quad (4.2.7)$$

where the following definitions have been used,

$$p = x_1 P_1, \quad k = x_2 P_2, \quad P_1 = \frac{\sqrt{S}}{2}(1, 0, 0, 1) \text{ and } P_2 = \frac{\sqrt{S}}{2}(1, 0, 0, -1).$$

Here, P_1 and P_2 are the 4-momenta of the two protons and \sqrt{S} is their centre-of-mass energy.

We now proceed to compute the hadronic cross section which is given by

$$\sigma_{\sqrt{S}} = \int_0^1 dx_1 \int_0^1 dx_2 f_{g/p}(x_1) f_{g/p}(x_2) \hat{\sigma}(x_1, x_2) \quad (4.2.8)$$

\Rightarrow using the change of variables $\{x_1, x_2\} \rightarrow \{x = x_1, z = x_1 x_2\}$, we get

$$= \int_0^1 \frac{dx}{x} \int_0^x dz f_{g/p}(x) f_{g/p}(z/x) \hat{\sigma}(z) \quad (4.2.9)$$

$$= \int_0^1 \frac{dx}{x} \int_0^x dz f_{g/p}(x) f_{g/p}(z/x) \times \frac{\pi}{256} \frac{1}{zS} |\mathcal{M}|^2 \delta(zS - m_\phi^2) \quad (4.2.10)$$

We now use the expression for $\Gamma_{\phi \rightarrow gg}$ (following appendix D.1),

$$\Gamma(\phi \rightarrow gg) = \left[\frac{1}{2m_\phi} \right] \left[\frac{1}{8\pi} \right] |\mathcal{M}|^2 \left[\frac{1}{2} \right], \quad (4.2.11)$$

to get

$$\sigma_{\sqrt{S}} = \frac{\pi}{256} \frac{32\pi m_\phi \Gamma_{\phi \rightarrow gg}}{S} \int_0^1 \frac{dx}{x} \int_0^x dz f_{g/p}(x) f_{g/p}(z/x) \frac{1}{z} \delta(zS - m_\phi^2) \quad (4.2.12)$$

$$= \frac{\pi}{256} \frac{32\pi m_\phi \Gamma_{\phi \rightarrow gg}}{S^2} \int_0^1 \frac{dx}{x} \int_0^x dz f_{g/p}(x) f_{g/p}(z/x) \frac{1}{z} \delta(z - \frac{m_\phi^2}{S}) \quad (4.2.13)$$

$$= \frac{\pi}{256} \frac{32\pi m_\phi \Gamma_{\phi \rightarrow gg}}{S^2} \int_{\frac{m_\phi^2}{S}}^1 \frac{dx}{x} f_{g/p}(x) f_{g/p}(m_\phi^2/Sx) \frac{S}{m_\phi^2} \quad (4.2.14)$$

$$= \frac{\pi^2}{8} \frac{\Gamma_{\phi \rightarrow gg}}{m_\phi S} \int_{\frac{m_\phi^2}{S}}^1 \frac{dx}{x} f_{g/p}(x) f_{g/p}(m_\phi^2/Sx) \quad (4.2.15)$$

Hence,

$$\mathcal{A}_{\text{LHC energy}}^{gg} = \frac{\pi^2}{8} \frac{1}{m_\phi S} \int_{\frac{m_\phi^2}{S}}^1 \frac{dx}{x} f_{g/p}(x) f_{g/p}(m_\phi^2/Sx) \quad (4.2.16)$$

Using the MSTW 2008 LO parton distribution functions (PDF) we get,

$$\mathcal{A}_{13 \text{ TeV}}^{gg} = \frac{5.44 \text{ pb}}{\text{GeV}} \quad (4.2.17)$$

$$\mathcal{A}_{8 \text{ TeV}}^{gg} = \frac{1.15 \text{ pb}}{\text{GeV}}. \quad (4.2.18)$$

D.2.2 Production by quarks

The cross section of the process $\bar{q}q \rightarrow \phi$ can be calculated in the same way as above, except for the following changes,

- The colour factor is different, so we must have $1/3^2$ instead of $1/8^2$ as in the case for gluons

- The symmetry factor (1/2) for identical particle used in Eq. (4.2.11) no longer applies
- The PDF are different - we now have quark PDF instead of the gluon PDF.

Applying the above changes, we finally get,

$$\sigma_{\sqrt{S}} = \frac{4\pi^2}{9} \frac{\Gamma_{\phi \rightarrow q\bar{q}}}{m_\phi S} \int_{\frac{m_\phi^2}{S}}^1 \frac{dx}{x} (f_{q/p}(x) f_{\bar{q}/p}(m_\phi^2/Sx) + f_{\bar{q}/p}(x) f_{q/p}(m_\phi^2/Sx))$$

Hence,

$$\mathcal{A}_{\text{LHC energy}}^{q\bar{q}} = \frac{4\pi^2}{9} \frac{1}{m_\phi S} \int_{\frac{m_\phi^2}{S}}^1 \frac{dx}{x} (f_{q/p}(x) f_{\bar{q}/p}(m_\phi^2/Sx) + f_{\bar{q}/p}(x) f_{q/p}(m_\phi^2/Sx))$$

Using again the MSTW 2008 LO parton distribution functions (PDF) we get,

$$\mathcal{A}_{13}^{\bar{u}u} \equiv \mathcal{A}_{13 \text{ TeV LHC}}^{\bar{u}u} = \frac{2.94 \text{ pb}}{\text{GeV}} \quad \mathcal{A}_8^{\bar{u}u} \equiv \mathcal{A}_{8 \text{ TeV LHC}}^{\bar{u}u} = \frac{1.2 \text{ pb}}{\text{GeV}} \quad (4.2.19)$$

$$\mathcal{A}_{13}^{\bar{d}d} \equiv \mathcal{A}_{13 \text{ TeV LHC}}^{\bar{d}d} = \frac{1.73 \text{ pb}}{\text{GeV}} \quad \mathcal{A}_8^{\bar{d}d} \equiv \mathcal{A}_{8 \text{ TeV LHC}}^{\bar{d}d} = \frac{0.66 \text{ pb}}{\text{GeV}} \quad (4.2.20)$$

$$\mathcal{A}_{13}^{\bar{c}c} \equiv \mathcal{A}_{13 \text{ TeV LHC}}^{\bar{c}c} = \frac{0.11 \text{ pb}}{\text{GeV}} \quad \mathcal{A}_8^{\bar{c}c} \equiv \mathcal{A}_{8 \text{ TeV LHC}}^{\bar{c}c} = \frac{0.03 \text{ pb}}{\text{GeV}} \quad (4.2.21)$$

$$\mathcal{A}_{13}^{\bar{s}s} \equiv \mathcal{A}_{13 \text{ TeV LHC}}^{\bar{s}s} = \frac{0.21 \text{ pb}}{\text{GeV}} \quad \mathcal{A}_8^{\bar{s}s} \equiv \mathcal{A}_{8 \text{ TeV LHC}}^{\bar{s}s} = \frac{0.05 \text{ pb}}{\text{GeV}} \quad (4.2.22)$$

$$\mathcal{A}_{13}^{\bar{b}b} \equiv \mathcal{A}_{13 \text{ TeV LHC}}^{\bar{b}b} = \frac{0.05 \text{ pb}}{\text{GeV}} \quad \mathcal{A}_8^{\bar{b}b} \equiv \mathcal{A}_{8 \text{ TeV LHC}}^{\bar{b}b} = \frac{0.01 \text{ pb}}{\text{GeV}} \quad (4.2.23)$$

D.3 Calculation of the sgoldstino mass

In this appendix, we want to compute the 1-loop contribution to the sgoldstino mass from the term,

$$\mathcal{L} \subset \int d^2\theta \lambda X \Phi_1 \Phi_2 + \text{h.c.} \quad (4.3.1)$$

We will ignore the gauge indices of Φ_1 and Φ_2 for the time being. The following notation will be used for the chiral superfields:

$$X = \mathcal{S} + \sqrt{2}\theta \psi_x + \theta\theta F_x \quad (4.3.2)$$

$$\Phi_1 = \phi_1 + \sqrt{2}\theta \xi_1 + \theta\theta F_1 \quad (4.3.3)$$

$$\Phi_2 = \phi_2 + \sqrt{2}\theta \xi_2 + \theta\theta F_2 \quad (4.3.4)$$

A Dirac fermion Ψ is constructed out of the two Weyl fermions ξ_1 and ξ_2 ,

$$\Psi = \begin{pmatrix} \xi_{1\alpha} \\ \xi_2^{\dagger\dot{\alpha}} \end{pmatrix} \quad (4.3.5)$$

whose Dirac mass will be denoted by $m_\Psi = \lambda \langle \mathcal{S} \rangle$. The scalar mass eigenstates will be denoted by ϕ_+ and ϕ_- with their mass squared given by $m_\pm^2 = m_\Psi^2 \pm \lambda \langle F_x \rangle$.

D.3.1 Diagrammatic calculation

The relevant vertex factors are given by,

$$\mathcal{S} \bar{\Psi} \Psi : -\lambda P_L \quad (4.3.6)$$

$$\mathcal{S}^* \mathcal{S} \phi_+^* \phi_+ : -\lambda^2 \quad (4.3.7)$$

$$\mathcal{S}^* \mathcal{S} \phi_-^* \phi_- : -\lambda^2 \quad (4.3.8)$$

$$\mathcal{S} \phi_+^* \phi_+ : -\lambda m_\Psi \quad (4.3.9)$$

$$\mathcal{S} \phi_-^* \phi_- : -\lambda m_\Psi \quad (4.3.10)$$

The Feynman rules can be obtained by multiplying the above vertex factors by i and appropriate symmetry factors.

The relevant diagrams are,

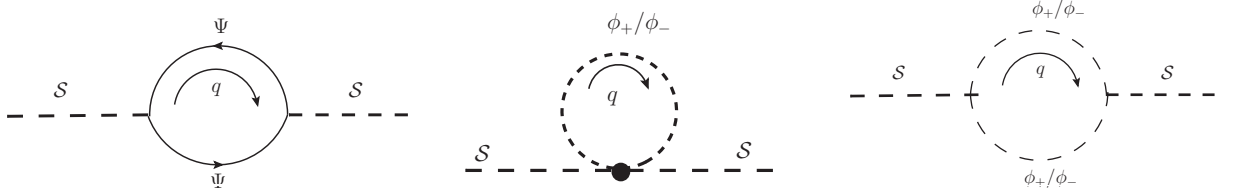


Figure D.1: One loop contributions to the sgoldstino mass from the messengers.

We will now compute the diagrams one-by-one.

Fermion loop

$$\begin{aligned} -i\Pi(p^2=0) &= -(-i\lambda)(-i\lambda) \int \frac{d^4q}{(2\pi)^4} \text{Tr} \left[P_L \frac{i}{\not{q} - m_\Psi} P_R \frac{i}{\not{q} - m_\Psi} \right] \\ &= -2\lambda^2 \int \frac{d^4q}{(2\pi)^4} \frac{q^2}{(q^2 - m_\Psi^2)^2} \\ &= -2\lambda^2 \int \frac{d^4q}{2\pi^4} \left[\frac{1}{q^2 - m_\Psi^2} + \frac{m_\Psi^2}{(q^2 - m_\Psi^2)^2} \right] \end{aligned} \quad (4.3.11)$$

First scalar loop

$$\begin{aligned} -i\Pi(p^2=0) &= (-i\lambda^2) \sum_{\phi=\phi_\pm} \int \frac{d^4q}{(2\pi)^4} \frac{i}{q^2 - m_\phi^2} \\ &= \lambda^2 \int \frac{d^4q}{(2\pi)^4} \left[\frac{1}{q^2 - m_+^2} + \frac{1}{q^2 - m_-^2} \right] \end{aligned} \quad (4.3.12)$$

Second scalar loop

$$-i \Pi(p^2 = 0) = (-i\lambda m_\Psi)(-i\lambda m_\Psi) \sum_{\phi=\phi_\pm} \int \frac{d^4 q}{(2\pi)^4} \frac{i^2}{(q^2 - m_\phi^2)^2} \quad (4.3.13)$$

$$= \lambda^2 m_\Psi^2 \int \frac{d^4 q}{(2\pi)^4} \left[\frac{1}{(q^2 - m_+^2)^2} + \frac{1}{(q^2 - m_-^2)^2} \right] \quad (4.3.14)$$

Note that the sum of the diagrams goes to zero in the limit of equal masses for the scalars and fermions, i.e. when SUSY is unbroken.

We need to evaluate integrals of two the forms:

$$A_0(m) = \int \frac{d^D q}{(2\pi)^D} \frac{1}{q^2 - m^2} \quad ; \quad B_0(0, m, m) = \int \frac{d^D q}{(2\pi)^D} \frac{1}{(q^2 - m^2)^2} \quad (4.3.15)$$

They are given by,

$$A_0(m) = \frac{i}{16\pi^2} m^2 \left[\frac{1}{\hat{\epsilon}} + 1 - \text{Ln} \frac{m^2}{\mu^2} \right] \quad (4.3.16)$$

$$B_0(0, m, m) = \frac{A_0(m)}{m^2} - \frac{i}{16\pi^2} \quad (4.3.17)$$

where,

$$\frac{1}{\hat{\epsilon}} = \frac{2}{4-D} - \gamma_E + \text{Ln}(4\pi), \quad \gamma_E \text{ being the Euler constant.} \quad (4.3.18)$$

Putting all loop contributions in order, we have

$$-i \Pi(p^2 = 0) = -2\lambda^2 \int \frac{d^4 q}{(2\pi)^4} \left[\frac{1}{q^2 - m_\Psi^2} - \frac{1}{2} \frac{1}{q^2 - m_+^2} - \frac{1}{2} \frac{1}{q^2 - m_-^2} \right. \\ \left. + m_\Psi^2 \frac{1}{(q^2 - m_\Psi^2)^2} - \frac{m_\Psi^2}{2} \frac{1}{(q^2 - m_+^2)^2} - \frac{m_\Psi^2}{2} \frac{1}{(q^2 - m_-^2)^2} \right] \quad (4.3.19)$$

$$= -2\lambda^2 \frac{i}{16\pi^2} \left[m_\Psi^2 \left(\frac{1}{\hat{\epsilon}} + 1 - \text{Ln} \frac{m_\Psi^2}{\mu^2} \right) - \frac{m_+^2}{2} \left(\frac{1}{\hat{\epsilon}} + 1 - \text{Ln} \frac{m_+^2}{\mu^2} \right) \right. \\ \left. - \frac{m_-^2}{2} \left(\frac{1}{\hat{\epsilon}} + 1 - \text{Ln} \frac{m_-^2}{\mu^2} \right) + m_\Psi^2 \left(\frac{1}{\hat{\epsilon}} - \text{Ln} \frac{m_\Psi^2}{\mu^2} \right) \right. \\ \left. - \frac{m_\Psi^2}{2} \left(\frac{1}{\hat{\epsilon}} - \text{Ln} \frac{m_+^2}{\mu^2} \right) - \frac{m_\Psi^2}{2} \left(\frac{1}{\hat{\epsilon}} - \text{Ln} \frac{m_-^2}{\mu^2} \right) \right] \quad (4.3.20)$$

$$= -2\lambda^2 \frac{i}{16\pi^2} \left[\frac{m_+^2}{2} \text{Ln} \frac{m_+^2}{\mu^2} + \frac{m_-^2}{2} \text{Ln} \frac{m_-^2}{\mu^2} - m_\Psi^2 \text{Ln} \frac{m_\Psi^2}{\mu^2} \right. \\ \left. + \frac{m_\Psi^2}{2} \text{Ln} \frac{m_+^2}{\mu^2} + \frac{m_\Psi^2}{2} \text{Ln} \frac{m_-^2}{\mu^2} - m_\Psi^2 \text{Ln} \frac{m_\Psi^2}{\mu^2} \right] \quad (4.3.21)$$

$$= -2\lambda^2 \frac{i}{16\pi^2} \left[m_\Psi^2 \text{Ln} \frac{m_+ m_-}{m_\Psi^2} + \lambda \langle F_x \rangle \text{Ln} \frac{m_+}{m_-} + m_\Psi^2 \text{Ln} \frac{m_+ m_-}{m_\Psi^2} \right] \quad (4.3.22)$$

Hence, assuming Φ_1 (Φ_2) to be a $\mathbf{5}$ ($\bar{\mathbf{5}}$) of $SU(5)$, and for N_m pairs of $\{\Phi_1, \Phi_2\}$, we have,

$$\Pi(p^2 = 0) = 5 N_m \frac{2\lambda^2}{16\pi^2} \left[2m_\Psi^2 \text{Ln} \frac{m_+ m_-}{m_\Psi^2} + \lambda \langle F_x \rangle \text{Ln} \frac{m_+}{m_-} \right] \quad (4.3.23)$$

$$= 5 N_m \frac{\lambda^2}{16\pi^2} m_\Psi^2 \left[2 \text{Ln} \frac{m_+^2 m_-^2}{m_\Psi^4} + \frac{\lambda \langle F_x \rangle}{m_\Psi^2} \text{Ln} \frac{m_+^2}{m_-^2} \right] \quad (4.3.24)$$

$$= \left(4\pi \sqrt{5 N_m} \right)^2 \left(\frac{\lambda}{16\pi^2} \right)^2 \frac{\lambda^2 \langle F_x \rangle^2}{m_\Psi^2} G \left(\frac{\lambda \langle F_x \rangle}{m_\Psi^2} \right) \quad (4.3.25)$$

where the function $G(x)$ is given by,

$$G(x) = \frac{1}{x^2} [(2+x)\text{Log}(1+x) + (2-x)\text{Log}(1-x)]. \quad (4.3.26)$$

In terms of gaugino mass, this can be written as,

$$\Pi(p^2 = 0) = - \left(\frac{\lambda}{g_a^2} \right)^2 \left(4\pi \sqrt{\frac{5}{N_m}} F(x) \right)^2 m_a^2 \quad (4.3.27)$$

The behaviour of the function $F(x) \equiv \sqrt{-G(x)/g(x)^2}$ is shown in Fig. D.2.

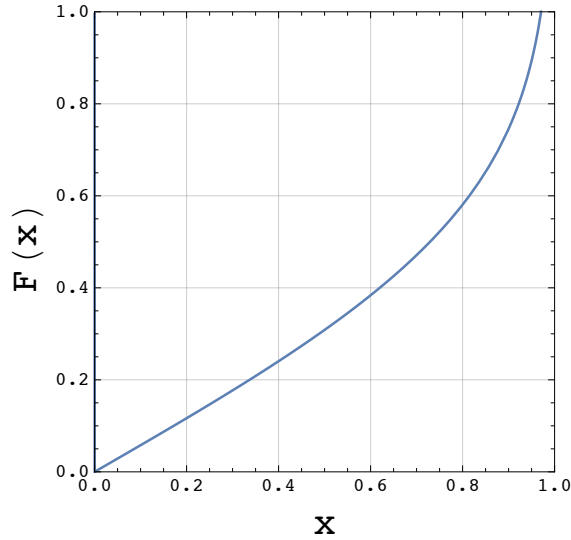


Figure D.2: The behaviour of $F(x)$ as a function of x .

D.3.2 Coleman-Weinberg potential

The Dirac mass for the fermions as a function of \mathcal{S} is given by,

$$m_F(\mathcal{S}) = \lambda \mathcal{S} \quad (4.3.28)$$

and the scalar mass matrix is

$$\tilde{m}^2(\mathcal{S}) = \begin{pmatrix} \lambda^2 \mathcal{S}^* \mathcal{S} & -\lambda \langle F_x \rangle \\ -\lambda \langle F_x \rangle & \lambda^2 \mathcal{S}^* \mathcal{S} \end{pmatrix}, \quad (4.3.29)$$

with the eigenvalues,

$$m_{\pm}^2(\mathcal{S}^* \mathcal{S}) = \lambda^2 \mathcal{S}^* \mathcal{S} \pm \lambda \langle F_x \rangle. \quad (4.3.30)$$

Using the standard formula for the Coleman-Weinberg potential [60],

$$V_{\text{CW}} = \frac{1}{64\pi^2} \text{STr} \left(\mathcal{M}^4 \left[\log \frac{\mathcal{M}^2}{\Lambda_{\text{cut-off}}^2} - \frac{3}{2} \right] \right), \quad (4.3.31)$$

we get,

$$\begin{aligned} V_{\text{CW}} = & \frac{2}{64\pi^2} \left[[m_+^2(\mathcal{S}, \mathcal{S}^*)]^2 \text{Ln} [m_+^2(\mathcal{S}, \mathcal{S}^*)] + [m_-^2(\mathcal{S}, \mathcal{S}^*)]^2 \text{Ln} [m_-^2(\mathcal{S}, \mathcal{S}^*)] \right. \\ & - 2 [m_F(\mathcal{S})^* m_F(\mathcal{S})]^2 \text{Ln} [m_F(\mathcal{S})^* m_F(\mathcal{S})] \\ & \left. - \lambda^2 \langle F_x \rangle^2 \left(\log \Lambda_{\text{cut-off}}^2 + \frac{3}{2} \right) \right] \end{aligned} \quad (4.3.32)$$

After replacing $\mathcal{S} \rightarrow \langle \mathcal{S} \rangle + \mathcal{S}$, we get the coefficient of $\mathcal{S}^* \mathcal{S}$ to be,

$$\Pi(p^2 = 0) = \frac{2\lambda^2}{16\pi^2} \left[2m_{\Psi}^2 \text{Ln} \frac{m_+ m_-}{m_{\Psi}^2} + \lambda \langle F_x \rangle \text{Ln} \frac{m_+}{m_-} \right] \quad (4.3.33)$$

D.3.3 Tree level sgoldstino mass

Here we give an example of a model where the sgoldstino gets tree level mass at the time of SUSY breaking [442]. The model is just an extension of the Affleck-Dine-Seiberg model (ADS) or 3-2 model of [439–441]. The field content of the ADS model is

	$SU(3)$	$SU(2)$	
Q	3	2	
U^c	$\bar{3}$	1	,
D^c	$\bar{3}$	1	
L	1	$\bar{2}$	

and the superpotential is given by,

$$W_{3-2} = W_{\text{cl}} + W_{\text{np}} \quad (4.3.34)$$

$$\text{where,} \quad (4.3.35)$$

$$W_{\text{cl}} = h Q_A^a D_a^c L^A, \quad (4.3.36)$$

$$W_{\text{np}} = \frac{\Lambda_3^7}{\det(QQ^c)}, \quad (4.3.37)$$

where, Q^c is defined as $Q^c \equiv (U^c, D^c)$. In this model $h \ll \tilde{g}_2, \tilde{g}_3$ which are the gauge couplings for the groups $SU(2)$ and $SU(3)$ respectively. Thus, F -term contribution to the

scalar potential is subdominant compared to the D -term contribution. The minimum of the potential can be obtained perturbatively along the D -flat directions,

$$Q = \begin{pmatrix} a & 0 \\ 0 & b \\ 0 & 0 \end{pmatrix} M \quad , \quad Q^c = \begin{pmatrix} a & 0 \\ 0 & b \\ 0 & 0 \end{pmatrix} M \quad , \quad L = \begin{pmatrix} \sqrt{a^2 - b^2} \\ 0 \end{pmatrix} M \quad (4.3.38)$$

where,

$$M \equiv \frac{\Lambda_3}{h^{1/7}} \gg \Lambda_3 \quad , \quad (4.3.39)$$

and $a \approx 1.164$, $b \approx 1.132$.

Note that L_1 (the component of L getting a non-vanishing VEV) is the sgoldstino here. The $\mathcal{SU}(2)$ D -term equation of motion gives,

$$D_2^a = \tilde{g}_2 \sum_f f^\dagger T_2^a f \quad (4.3.40)$$

where $T_2^a = \sigma^a/2$, σ^a being the Pauli matrices. The Eq. 4.3.40 will get contributions from all the fields carrying $\mathcal{SU}(2)$ charge i.e., Q and L ,

$$D^a = \tilde{g}_2 \left(L^\dagger \frac{\sigma^a}{2} L + \sum_r Q_i^{r\dagger} \frac{\sigma^a}{2} Q_i^r \right) \quad (4.3.41)$$

where the index r is the $\mathcal{SU}(3)$ index. This gives, for the scalar potential,

$$V = \frac{1}{2} D^a D_a \quad (4.3.42)$$

$$= \frac{\tilde{g}_2^2}{8} \left(L^\dagger \frac{\sigma^a}{2} L + \sum_r Q_i^{r\dagger} \frac{\sigma^a}{2} Q_i^r \right) \left(L^\dagger \frac{\sigma_a}{2} L + \sum_r Q_i^{r\dagger} \frac{\sigma_a}{2} Q_i^r \right) . \quad (4.3.43)$$

Noting that only the third Pauli matrix contributes, we have,

$$V = \frac{\tilde{g}_2^2}{8} \left[\left(L_1^\dagger L_1 \right)^2 + 2(L_1^\dagger L_1)(Q_1^{r\dagger} Q_1^r - Q_2^{r\dagger} Q_2^r) + \dots \right] , \quad (4.3.44)$$

where the ellipses denote terms unimportant for sgoldstino mass. This generates a mass term for L_1 which is given by,

$$M_{L_1}^2 = \frac{\tilde{g}_2^2}{8} (4(a^2 - b^2)M^2 + 2(a^2 - b^2)M^2) \quad (4.3.45)$$

$$= \frac{3\tilde{g}_2^2}{4} (a^2 - b^2)M^2 . \quad (4.3.46)$$

This is, in general, much larger than the gaugino mass.

D.4 Calculation of the gaugino mass

The relevant part of the Lagrangian is given by

$$\mathcal{L} \subset \int d^4\theta \Phi_1^\dagger e^{2gT^a V^a} \Phi_1 + \int d^4\theta \Phi_2^\dagger e^{2gT^a V^a} \Phi_2 + \left(\int d^2\theta y X \Phi_1 \Phi_2 + \text{h.c.} \right) \quad (4.4.1)$$

where,

$$V^a = \theta \bar{\sigma}^\mu \bar{\theta} A_\mu^a + i\theta^2 \bar{\theta} \lambda^{\dagger a} - i\theta \bar{\theta}^2 \lambda^a + \frac{1}{2} \theta^2 \bar{\theta}^2 D^a \quad (4.4.2)$$

A Majorana fermion Ψ_λ is constructed out of the (Weyl) gaugino field λ_a ,

$$\Psi_\lambda = \begin{pmatrix} \lambda_\alpha \\ \lambda^{\dagger \dot{\alpha}} \end{pmatrix} \quad (4.4.3)$$

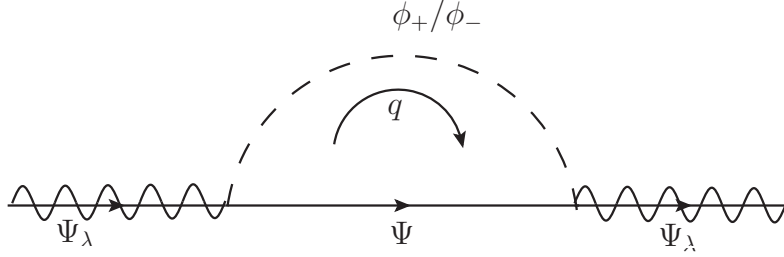


Figure D.3: One-loop contribution to the gaugino mass.

The relevant vertex factors are given by,

$$\alpha \quad \bar{\Psi}_\xi \Psi_\lambda^A \quad : \quad -igT^A \quad (4.4.4)$$

$$\beta \quad \bar{\Psi}_\xi \Psi_\lambda^A \quad : \quad +ig\gamma_5 T^A \quad (4.4.5)$$

The gaugino mass is generated via the one loop diagrams shown in Fig. D.3.

Loop with the scalar α

$$-\frac{i}{2} m_{\Psi_\lambda}^{(\alpha)AB} = \text{Tr}[T^A T^B] \int \frac{d^4 q}{(2\pi)^4} (-g) \frac{-i}{\not{q} + m_\Psi} (+g) \frac{i}{q^2 - m_\alpha^2} \quad (4.4.6)$$

$$= -g^2 \text{Tr}[T^A T^B] \int \frac{d^4 q}{(2\pi)^4} \frac{\not{q} - m_\Psi}{q^2 - m_\Psi^2} \frac{1}{q^2 - m_\alpha^2} \quad (4.4.7)$$

$$= g^2 m_\Psi \text{Tr}[T^A T^B] \int \frac{d^4 q}{(2\pi)^4} \frac{1}{q^2 - m_\Psi^2} \frac{1}{q^2 - m_\alpha^2} \quad (4.4.8)$$

$$= g^2 m_\Psi \text{Tr}[T^A T^B] B_0(0, m_\Psi, m_\alpha) \quad (4.4.9)$$

Loop with the scalar β

$$-\frac{i}{2} m_{\Psi_\lambda}^{(\beta)AB} = \text{Tr}[T^A T^B] \int \frac{d^4 q}{(2\pi)^4} (-g\gamma_5) \frac{-i}{\not{q} + m_\Psi} (-g\gamma_5) \frac{i}{q^2 - m_\beta^2} \quad (4.4.10)$$

$$= g^2 \text{Tr}[T^A T^B] \int \frac{d^4 q}{(2\pi)^4} \gamma_5 \frac{\not{q} - m_\Psi}{q^2 - m_\Psi^2} \gamma_5 \frac{1}{q^2 - m_\beta^2} \quad (4.4.11)$$

$$= g^2 \text{Tr}[T^A T^B] \int \frac{d^4 q}{(2\pi)^4} \frac{(-\not{q} - m_\Psi)}{q^2 - m_\Psi^2} \frac{1}{q^2 - m_\beta^2} \quad (4.4.12)$$

$$= -g^2 m_\Psi \text{Tr}[T^A T^B] B_0(0, m_\Psi, m_\beta) \quad (4.4.13)$$

where, the B_0 function is given by,

$$B_0(0, m_1, m_2) = \frac{A_0(m_1) - A_0(m_2)}{m_1^2 - m_2^2} \quad (4.4.14)$$

$$-\frac{i}{2}m_{\Psi_\lambda}^{AB} = g^2 m_\Psi \text{Tr}[T^A T^B] (B_0(0, m_\Psi, m_\alpha) - B_0(0, m_\Psi, m_\beta)) \quad (4.4.15)$$

$$= -i \frac{g^2 m_\Psi}{16\pi^2} \text{Tr}[T^A T^B] \frac{(1+x) \ln(1+x) + (1-x) \ln(1-x)}{x} \quad (4.4.16)$$

$$= -i \frac{g^2}{16\pi^2} \text{Tr}[T^A T^B] \frac{\langle F_x \rangle}{m_\Psi} \frac{(1+x) \ln(1+x) + (1-x) \ln(1-x)}{x^2} \quad (4.4.17)$$

$$m_{\Psi_\lambda}^{AB} = \frac{g^2}{16\pi^2} 2\text{Tr}[T^A T^B] \frac{\langle F_x \rangle}{m_\Psi} g(x) \quad (4.4.18)$$

$$m_{\Psi_\lambda}^{AB} = \frac{g^2}{16\pi^2} \frac{\langle F_x \rangle}{m_\Psi} g(x) \delta^{AB}. \quad (4.4.19)$$

Bibliography

- [1] C. N. Yang and R. L. Mills, Phys. Rev. **96**, 191 (1954).
- [2] S. L. Glashow, “Partial Symmetries of Weak Interactions,” Nucl. Phys. **22**, 579 (1961).
- [3] S. Weinberg, “A Model of Leptons,” Phys. Rev. Lett. **19**, 1264 (1967).
- [4] S. Weinberg, “Conceptual Foundations of the Unified Theory of Weak and Electromagnetic Interactions,” Rev. Mod. Phys. **52**, 515 (1980) [Science **210**, 1212 (1980)].
- [5] A. Salam, “Gauge Unification of Fundamental Forces,” Rev. Mod. Phys. **52**, 525 (1980) [Science **210**, 723 (1980)].
- [6] S. L. Glashow, “Towards a Unified Theory: Threads in a Tapestry,” Rev. Mod. Phys. **52**, 539 (1980).
- [7] *Lectures on Advanced Mathematical Methods for Physicists* by Sunil Mukhi and N Mukunda, published by World Scientific
- [8] J. S. Schwinger, Annals Phys. **2**, 407 (1957).
- [9] T. D. Lee and C. N. Yang, “Question of Parity Conservation in Weak Interactions,” Phys. Rev. **104**, 254 (1956).
- [10] C. S. Wu, E. Ambler, R. W. Hayward, D. D. Hoppes and R. P. Hudson, “Experimental Test of Parity Conservation in Beta Decay,” Phys. Rev. **105**, 1413 (1957).
- [11] J. H. Christenson, J. W. Cronin, V. L. Fitch and R. Turlay, Phys. Rev. Lett. **13**, 138 (1964).
- [12] R. P. Feynman and M. Gell-Mann, Phys. Rev. **109**, 193 (1958).
- [13] E. C. G. Sudarshan and R. e. Marshak, Phys. Rev. **109**, 1860 (1958).
- [14] J. J. Sakurai, Nuovo Cim. **7**, 649 (1958).
- [15] V. L. Ginzburg and L. D. Landau, Zh. Eksp. Teor. Fiz. **20**, 1064 (1950).
- [16] J. Goldstone, A. Salam and S. Weinberg, Phys. Rev. **127**, 965 (1962).
- [17] G. S. Guralnik, C. R. Hagen and T. W. B. Kibble, Phys. Rev. Lett. **13**, 585 (1964).
- [18] F. Englert and R. Brout, Phys. Rev. Lett. **13**, 321 (1964).
- [19] P. W. Higgs, Phys. Rev. Lett. **13**, 508 (1964).
- [20] M. J. G. Veltman, Phys. Lett. **91B**, 95 (1980).
- [21] C. Jarlskog, Phys. Rev. Lett. **55**, 1039 (1985).
- [22] C. Patrignani *et al.* [Particle Data Group], Chin. Phys. C **40**, no. 10, 100001 (2016).
- [23] N. Cabibbo, Phys. Rev. Lett. **10**, 531 (1963).

- [24] L. Wolfenstein, Phys. Rev. Lett. **51**, 1945 (1983).
- [25] Y. Nir, CERN Yellow Report CERN-2010-001, 279-314 [arXiv:1010.2666 [hep-ph]].
- [26] Y. Grossman, doi:10.5170/CERN-2010-002.111, 10.5170/CERN-2014-003.73 arXiv:1006.3534 [hep-ph].
- [27] K. A. Olive *et al.* [Particle Data Group], Chin. Phys. C **38**, 090001 (2014).
- [28] M. Kobayashi and T. Maskawa, Prog. Theor. Phys. **49**, 652 (1973).
- [29] G. Bhattacharyya, Rept. Prog. Phys. **74**, 026201 (2011) [arXiv:0910.5095 [hep-ph]].
- [30] S. L. Glashow, J. Iliopoulos and L. Maiani, Phys. Rev. D **2**, 1285 (1970).
- [31] Y. Amhis *et al.*, arXiv:1612.07233 [hep-ex].
- [32] J. Charles *et al.* [CKMfitter Group], Eur. Phys. J. C **41**, no. 1, 1 (2005) Updated results and plots available at <http://ckmfitter.in2p3.fr/>
- [33] A. Lazzaro [BaBar Collaboration], SLAC-PUB-12440.
- [34] D. Buskulic *et al.* [ALEPH Collaboration], Nucl. Instrum. Meth. A **360**, 481 (1995).
- [35] Z. Natkaniec *et al.* [BELLE Collaboration], Nucl. Instrum. Meth. A **560** (2006)
- [36] R. Aaij *et al.* [LHCb Collaboration], Phys. Rev. Lett. **115**, no. 3, 031601 (2015)
- [37] T. P. Cheng and L. F. Li, Oxford, Uk: Clarendon (1984) 536 P. (Oxford Science Publications)
- [38] T. Muta, “Foundations of Quantum Chromodynamics: An Introduction to Perturbative Methods in Gauge Theories, (3rd ed.),”
- [39] I. I. Y. Bigi and A. I. Sanda, Camb. Monogr. Part. Phys. Nucl. Phys. Cosmol. **9**, 1 (2000).
- [40] A. J. Buras, hep-ph/9806471.
- [41] M. E. Peskin and D. V. Schroeder, Reading, USA: Addison-Wesley (1995) 842 p
- [42] B. Grzadkowski, M. Iskrzynski, M. Misiak and J. Rosiek, JHEP **1010**, 085 (2010) doi:10.1007/JHEP10(2010)085 [arXiv:1008.4884 [hep-ph]].
- [43] M. R. Krishnaswamy *et al.*, Nuovo Cim. C **9**, 167 (1986) [Conf. Proc. C **850418**, 97 (1985)]. doi:10.1007/BF02514839
- [44] B. Bajc, J. Hisano, T. Kuwahara and Y. Omura, Nucl. Phys. B **910**, 1 (2016) doi:10.1016/j.nuclphysb.2016.06.017 [arXiv:1603.03568 [hep-ph]].
- [45] K. Abe *et al.* [Super-Kamiokande Collaboration], Phys. Rev. D **91**, 072006 (2015) [arXiv:1109.4227 [hep-ex]].
- [46] D. G. Phillips, II *et al.*, Phys. Rept. **612**, 1 (2016) [arXiv:1410.1100 [hep-ex]].

- [47] S. Dell’Oro, S. Marocci, M. Viel and F. Vissani, *Adv. High Energy Phys.* **2016**, 2162659 (2016) [arXiv:1601.07512 [hep-ph]].
- [48] A. M. Baldini *et al.* [MEG Collaboration], *Eur. Phys. J. C* **76**, no. 8, 434 (2016) [arXiv:1605.05081 [hep-ex]].
- [49] Y. Miyazaki *et al.* [Belle Collaboration], *Phys. Lett. B* **660**, 154 (2008) [arXiv:0711.2189 [hep-ex]].
- [50] C. Athanassopoulos *et al.* [LSND Collaboration], *Phys. Rev. C* **54**, 2685 (1996) doi:10.1103/PhysRevC.54.2685 [nucl-ex/9605001].
- [51] Y. Fukuda *et al.* [Super-Kamiokande Collaboration], *Phys. Rev. Lett.* **81**, 1562 (1998) doi:10.1103/PhysRevLett.81.1562 [hep-ex/9807003].
- [52] K. Abe *et al.* [T2K Collaboration], *Phys. Rev. D* **88**, no. 3, 032002 (2013) doi:10.1103/PhysRevD.88.032002 [arXiv:1304.0841 [hep-ex]].
- [53] N. Agafonova *et al.* [OPERA Collaboration], *PTEP* **2014**, no. 10, 101C01 (2014) doi:10.1093/ptep/ptu132 [arXiv:1407.3513 [hep-ex]].
- [54] G. Isidori, *Annales Henri Poincare* **4**, S97 (2003) [hep-ph/0301159].
- [55] O. Gedalia and G. Perez, arXiv:1005.3106 [hep-ph].
- [56] A. Djouadi and A. Lenz, *Phys. Lett. B* **715**, 310 (2012) [arXiv:1204.1252 [hep-ph]].
- [57] V. Khachatryan *et al.* [CMS Collaboration], *Eur. Phys. J. C* **75**, no. 5, 212 (2015) doi:10.1140/epjc/s10052-015-3351-7 [arXiv:1412.8662 [hep-ex]].
- [58] Z. Maki, M. Nakagawa and S. Sakata, *Prog. Theor. Phys.* **28**, 870 (1962). doi:10.1143/PTP.28.870
- [59] <http://pdg.lbl.gov/2017/reviews/rpp2016-rev-neutrino-mixing.pdf>
- [60] S. R. Coleman and E. J. Weinberg, *Phys. Rev. D* **7**, 1888 (1973).
- [61] J. F. Gunion, H. E. Haber, G. L. Kane and S. Dawson, *Front. Phys.* **80**, 1 (2000).
- [62] S. Chatrchyan *et al.* [CMS Collaboration], *Phys. Lett. B* **716**, 30 (2012) [arXiv:1207.7235 [hep-ex]].
- [63] G. Aad *et al.* [ATLAS Collaboration], *Phys. Lett. B* **716**, 1 (2012) [arXiv:1207.7214 [hep-ex]].
- [64] E. Witten, *Nucl. Phys. B* **188**, 513 (1981). doi:10.1016/0550-3213(81)90006-7
- [65] N. Sakai, *Z. Phys. C* **11**, 153 (1981). doi:10.1007/BF01573998
- [66] S. Dimopoulos and H. Georgi, *Nucl. Phys. B* **193**, 150 (1981). doi:10.1016/0550-3213(81)90522-8

- [67] R. K. Kaul and P. Majumdar, Nucl. Phys. B **199**, 36 (1982). doi:10.1016/0550-3213(82)90565-X
- [68] M. J. G. Veltman, Acta Phys. Polon. B **12**, 437 (1981).
- [69] F. Jegerlehner, arXiv:1305.6652 [hep-ph].
- [70] D. Buttazzo, G. Degrassi, P. P. Giardino, G. F. Giudice, F. Sala, A. Salvio and A. Strumia, JHEP **1312**, 089 (2013) doi:10.1007/JHEP12(2013)089 [arXiv:1307.3536 [hep-ph]].
- [71] G. Aad *et al.* [ATLAS and CMS Collaborations], Phys. Rev. Lett. **114**, 191803 (2015) doi:10.1103/PhysRevLett.114.191803 [arXiv:1503.07589 [hep-ex]].
- [72] J. Elias-Miro, J. R. Espinosa, G. F. Giudice, G. Isidori, A. Riotto and A. Strumia, Phys. Lett. B **709**, 222 (2012) doi:10.1016/j.physletb.2012.02.013 [arXiv:1112.3022 [hep-ph]].
- [73] M. Dine, hep-ph/0011376.
- [74] J. E. Kim, AIP Conf. Proc. **1200**, 83 (2010) [arXiv:0909.3908 [hep-ph]].
- [75] R. D. Peccei, Lect. Notes Phys. **741**, 3 (2008) [hep-ph/0607268].
- [76] G. 't Hooft, Phys. Rev. Lett. **37**, 8 (1976). doi:10.1103/PhysRevLett.37.8
- [77] R. J. Crewther, P. Di Vecchia, G. Veneziano and E. Witten, Phys. Lett. **88B**, 123 (1979) Erratum: [Phys. Lett. **91B**, 487 (1980)].
- [78] J. M. Pendlebury *et al.*, Phys. Rev. D **92**, no. 9, 092003 (2015) doi:10.1103/PhysRevD.92.092003 [arXiv:1509.04411 [hep-ex]].
- [79] E. W. Kolb and M. S. Turner, Front. Phys. **69**, 1 (1990).
- [80] J. M. Cline, hep-ph/0609145.
- [81] M. Dine and A. Kusenko, Rev. Mod. Phys. **76**, 1 (2003) doi:10.1103/RevModPhys.76.1 [hep-ph/0303065].
- [82] D. E. Morrissey and M. J. Ramsey-Musolf, New J. Phys. **14**, 125003 (2012) doi:10.1088/1367-2630/14/12/125003 [arXiv:1206.2942 [hep-ph]].
- [83] A. D. Sakharov, Pisma Zh. Eksp. Teor. Fiz. **5**, 32 (1967) [JETP Lett. **5**, 24 (1967)] [Sov. Phys. Usp. **34**, 392 (1991)] [Usp. Fiz. Nauk **161**, 61 (1991)].
- [84] K. S. Babu *et al.*, arXiv:1311.5285 [hep-ph].
- [85] Coleman, S., Aspects of Symmetry. Selected Erice Lectures. Cambridge *et al.*, Cambridge University Press 1985.
- [86] S. S. Chern and J. Simons, Annals Math. **99**, 48 (1974).
- [87] F. R. Klinkhamer and N. S. Manton, Phys. Rev. D **30**, 2212 (1984). doi:10.1103/PhysRevD.30.2212

- [88] V. A. Kuzmin, V. A. Rubakov and M. E. Shaposhnikov, Phys. Lett. **155B**, 36 (1985). doi:10.1016/0370-2693(85)91028-7
- [89] P. B. Arnold, D. Son and L. G. Yaffe, Phys. Rev. D **55**, 6264 (1997) doi:10.1103/PhysRevD.55.6264 [hep-ph/9609481].
- [90] G. D. Moore, C. r. Hu and B. Muller, Phys. Rev. D **58**, 045001 (1998) doi:10.1103/PhysRevD.58.045001 [hep-ph/9710436].
- [91] M. Kamionkowski, arXiv:0706.2986 [astro-ph].
- [92] V. Sahni, Lect. Notes Phys. **653**, 141 (2004) [astro-ph/0403324].
- [93] L. Bergstrom, Annalen Phys. **524**, 479 (2012) doi:10.1002/andp.201200116 [arXiv:1205.4882 [astro-ph.HE]].
- [94] M. Markevitch, ESA Spec. Publ. **604**, 723 (2006) [astro-ph/0511345].
- [95] D. Clowe, M. Bradac, A. H. Gonzalez, M. Markevitch, S. W. Randall, C. Jones and D. Zaritsky, Astrophys. J. **648**, L109 (2006) doi:10.1086/508162 [astro-ph/0608407].
- [96] P. A. R. Ade *et al.* [Planck Collaboration], Astron. Astrophys. **594**, A13 (2016) doi:10.1051/0004-6361/201525830 [arXiv:1502.01589 [astro-ph.CO]].
- [97] W. Hu, arXiv:0802.3688 [astro-ph].
- [98] T. Aramaki *et al.*, Phys. Rept. **618**, 1 (2016) doi:10.1016/j.physrep.2016.01.002 [arXiv:1505.07785 [hep-ph]].
- [99] <http://pdg.lbl.gov/2015/reviews/rpp2015-rev-dark-matter.pdf>
- [100] L. D. Duffy and K. van Bibber, New J. Phys. **11**, 105008 (2009) doi:10.1088/1367-2630/11/10/105008 [arXiv:0904.3346 [hep-ph]].
- [101] K. Yamamoto *et al.*, hep-ph/0101200.
- [102] J. F. Navarro, C. S. Frenk and S. D. M. White, Astrophys. J. **462**, 563 (1996) doi:10.1086/177173 [astro-ph/9508025].
- [103] W. J. G. de Blok, Adv. Astron. **2010**, 789293 (2010) doi:10.1155/2010/789293 [arXiv:0910.3538 [astro-ph.CO]].
- [104] M. Milgrom, Astrophys. J. **270**, 365 (1983). doi:10.1086/161130
- [105] M. Milgrom, Can. J. Phys. **93**, no. 2, 107 (2015) doi:10.1139/cjp-2014-0211 [arXiv:1404.7661 [astro-ph.CO]].
- [106] S. M. Carroll, Living Rev. Rel. **4**, 1 (2001) doi:10.12942/lrr-2001-1 [astro-ph/0004075].
- [107] J. D. Cohn, Astrophys. Space Sci. **259**, 213 (1998) doi:10.1023/A:1001796011627 [astro-ph/9807128].

- [108] A. G. Riess *et al.* [Supernova Search Team], *Astron. J.* **116**, 1009 (1998) doi:10.1086/300499 [astro-ph/9805201].
- [109] S. Perlmutter *et al.* [Supernova Cosmology Project Collaboration], *Astrophys. J.* **517**, 565 (1999) doi:10.1086/307221 [astro-ph/9812133].
- [110] B. D. Sherwin *et al.*, *Phys. Rev. Lett.* **107**, 021302 (2011) [arXiv:1105.0419 [astro-ph.CO]].
- [111] M. Scrimgeour *et al.*, *Mon. Not. Roy. Astron. Soc.* **425**, 116 (2012) [arXiv:1205.6812 [astro-ph.CO]].
- [112] V. Sahni and A. A. Starobinsky, *Int. J. Mod. Phys. D* **9**, 373 (2000) doi:10.1142/S0218271800000542 [astro-ph/9904398].
- [113] S. Weinberg, *Rev. Mod. Phys.* **61**, 1 (1989). doi:10.1103/RevModPhys.61.1
- [114] E. Witten, hep-ph/0002297.
- [115] A. Djouadi, *Phys. Rept.* **459**, 1 (2008) doi:10.1016/j.physrep.2007.10.005 [hep-ph/0503173].
- [116] H. Georgi and A. Pais, *Phys. Rev. D* **12**, 508 (1975). doi:10.1103/PhysRevD.12.508
- [117] M. Schmaltz and D. Tucker-Smith, *Ann. Rev. Nucl. Part. Sci.* **55**, 229 (2005) doi:10.1146/annurev.nucl.55.090704.151502 [hep-ph/0502182].
- [118] N. Arkani-Hamed, A. G. Cohen, E. Katz and A. E. Nelson, *JHEP* **0207**, 034 (2002) doi:10.1088/1126-6708/2002/07/034 [hep-ph/0206021].
- [119] S. Weinberg, *Phys. Rev. D* **13**, 974 (1976). doi:10.1103/PhysRevD.13.974
- [120] L. Susskind, *Phys. Rev. D* **20**, 2619 (1979). doi:10.1103/PhysRevD.20.2619
- [121] S. Dimopoulos and L. Susskind, *Nucl. Phys. B* **155**, 237 (1979). doi:10.1016/0550-3213(79)90364-X
- [122] E. Eichten and K. D. Lane, *Phys. Lett.* **90B**, 125 (1980). doi:10.1016/0370-2693(80)90065-9
- [123] H. Fritzsch and G. Mandelbaum, *Phys. Lett.* **102B**, 319 (1981). doi:10.1016/0370-2693(81)90626-2
- [124] J. C. Pati and A. Salam, *Phys. Rev. D* **10**, 275 (1974) Erratum: [*Phys. Rev. D* **11**, 703 (1975)]. doi:10.1103/PhysRevD.10.275, 10.1103/PhysRevD.11.703.2
- [125] M. A. Shupe, *Phys. Lett.* **86B**, 87 (1979). doi:10.1016/0370-2693(79)90627-0
- [126] D. J. Kapner, T. S. Cook, E. G. Adelberger, J. H. Gundlach, B. R. Heckel, C. D. Hoyle and H. E. Swanson, *Phys. Rev. Lett.* **98**, 021101 (2007) doi:10.1103/PhysRevLett.98.021101 [hep-ph/0611184].

- [127] V. Khachatryan *et al.* [CMS Collaboration], Phys. Lett. B **697**, 434 (2011) doi:10.1016/j.physletb.2011.02.032 [arXiv:1012.3375 [hep-ex]].
- [128] L. Randall and R. Sundrum, Phys. Rev. Lett. **83**, 3370 (1999) doi:10.1103/PhysRevLett.83.3370 [hep-ph/9905221].
- [129] T. Kaluza, Sitzungsber. Preuss. Akad. Wiss. Berlin (Math. Phys.) **1921**, 966 (1921).
- [130] O. Klein, Z. Phys. **37**, 895 (1926) [Surveys High Energ. Phys. **5**, 241 (1986)].
- [131] N. Arkani-Hamed, S. Dimopoulos and G. R. Dvali, Phys. Lett. B **429**, 263 (1998) doi:10.1016/S0370-2693(98)00466-3 [hep-ph/9803315].
- [132] W. Grimus, UWTHPH-1993-10, C92-09-02.2.
- [133] T. D. Lee, Phys. Rev. D **8**, 1226 (1973).
- [134] D. Comelli, M. Pietroni and A. Riotto, In *Valencia 1993, Cosmological dark matter* 283-288
- [135] S. L. Glashow and S. Weinberg, Phys. Rev. D **15**, 1958 (1977).
- [136] R. D. Peccei and H. R. Quinn, Phys. Rev. Lett. **38**, 1440 (1977).
- [137] R. D. Peccei and H. R. Quinn, Phys. Rev. D **16**, 1791 (1977).
- [138] K. Hamaguchi, M. Kakizaki and M. Yamaguchi, Phys. Rev. D **68**, 056007 (2003) doi:10.1103/PhysRevD.68.056007 [hep-ph/0212172].
- [139] A. Kleppe, arXiv:1608.08988 [hep-ph].
- [140] H. Fritzsch, Nucl. Phys. B **155**, 189 (1979). doi:10.1016/0550-3213(79)90362-6
- [141] M. Gupta, P. Fakay, S. Sharma and G. Ahuja, Mod. Phys. Lett. A **30**, 1530024 (2015) doi:10.1142/S0217732315300244 [arXiv:1604.03335 [hep-ph]].
- [142] P. Ramond, R. G. Roberts and G. G. Ross, Nucl. Phys. B **406**, 19 (1993) doi:10.1016/0550-3213(93)90159-M [hep-ph/9303320].
- [143] M. Randhawa and M. Gupta, Phys. Rev. D **63**, 097301 (2001) doi:10.1103/PhysRevD.63.097301 [hep-ph/0011388].
- [144] P. S. Gill and M. Gupta, Phys. Rev. D **57**, 3971 (1998). doi:10.1103/PhysRevD.57.3971
- [145] H. Harari, H. Haut and J. Weyers, Phys. Lett. **78B**, 459 (1978).
- [146] H. Fritzsch, Phys. Lett. **73B**, 317 (1978).
- [147] S. F. King, Rept. Prog. Phys. **67**, 107 (2004) doi:10.1088/0034-4885/67/2/R01 [hep-ph/0310204].
- [148] G. Senjanovic, Riv. Nuovo Cim. **34**, 1 (2011).
- [149] R. N. Mohapatra and G. Senjanovic, Phys. Rev. Lett. **44**, 912 (1980). doi:10.1103/PhysRevLett.44.912

- [150] J. C. Maxwell, Phil. Trans. Roy. Soc. Lond. **155**, 459 (1865). doi:10.1098/rstl.1865.0008
 - [151] S. W. Hawking, Commun. Math. Phys. **43**, 199 (1975) Erratum: [Commun. Math. Phys. **46**, 206 (1976)]. doi:10.1007/BF02345020
 - [152] E. P. Verlinde, JHEP **1104**, 029 (2011) doi:10.1007/JHEP04(2011)029 [arXiv:1001.0785 [hep-th]].
 - [153] E. P. Verlinde, SciPost Phys. **2**, no. 3, 016 (2017) doi:10.21468/SciPostPhys.2.3.016 [arXiv:1611.02269 [hep-th]].
 - [154] H. Georgi and S. L. Glashow, Phys. Rev. Lett. **32**, 438 (1974).
 - [155] D. Bailin and A. Love, Bristol, Uk: Hilger (1986) 348 P. (Graduate Student Series In Physics)
 - [156] <http://pdg.lbl.gov/2016/reviews/rpp2016-rev-guts.pdf>
 - [157] <http://www-fl.ijs.si/~ziherl/Greljo12.pdf>
 - [158] W. W. M. Allison *et al.* [Soudan-2 Collaboration], Phys. Lett. B **427**, 217 (1998) doi:10.1016/S0370-2693(98)00380-3 [hep-ex/9803030].
 - [159] J. L. Lopez and D. V. Nanopoulos, In *Baltimore 1991, Proceedings, Particle physics from underground to heaven* 277-297 and Texas A & M Univ. College Station - CTP-TAMU-91-076 (91/09) 25 p. (114742) [hep-th/9110036].
- SO10
- [160] T. Fukuyama, Int. J. Mod. Phys. A **28**, 1330008 (2013) doi:10.1142/S0217751X13300081 [arXiv:1212.3407 [hep-ph]].
 - [161] P. K. Mohapatra, R. N. Mohapatra and P. B. Pal, Phys. Rev. D **33**, 2010 (1986). doi:10.1103/PhysRevD.33.2010
 - [162] H. Baer and X. Tata,
 - [163] H. E. Haber and G. L. Kane, Phys. Rept. **117**, 75 (1985). doi:10.1016/0370-1573(85)90051-1
 - [164] M. Drees, R. Godbole and P. Roy, Hackensack, USA: World Scientific (2004) 555 p
 - [165] G. L. Kane, Adv. Ser. Direct. High Energy Phys. **21** (2010). doi:10.1142/7763
 - [166] PDG review of SUSY <http://pdg.lbl.gov/2015/reviews/rpp2015-rev-susy-1-theory.pdf>
<http://pdg.lbl.gov/2015/reviews/rpp2015-rev-susy-2-experiment.pdf>
 - [167] S. P. Martin, “A Supersymmetry primer,” Adv. Ser. Direct. High Energy Phys. **21**, 1 (2010) [Adv. Ser. Direct. High Energy Phys. **18**, 1 (1998)] [hep-ph/9709356].
 - [168] SUSY course at SISSA: <http://people.sissa.it/~bertmat/susycourse.pdf>
 - [169] A. Bilal, “Introduction to supersymmetry,” hep-th/0101055.

- [170] R. Haag, J. T. Lopuszanski and M. Sohnius, Nucl. Phys. B **88**, 257 (1975).
- [171] S. R. Coleman and J. Mandula, Phys. Rev. **159**, 1251 (1967).
- [172] G. Degrossi, S. Heinemeyer, W. Hollik, P. Slavich and G. Weiglein, Eur. Phys. J. C **28**, 133 (2003) doi:10.1140/epjc/s2003-01152-2 [hep-ph/0212020].
- [173] S. Heinemeyer, W. Hollik and G. Weiglein, Eur. Phys. J. C **9**, 343 (1999) doi:10.1007/s100529900006, 10.1007/s100520050537 [hep-ph/9812472].
- [174] G. Aad *et al.* [ATLAS Collaboration], Observation of a new particle in the search for the Standard Model Higgs boson with the ATLAS detector at the LHC, Phys. Lett. B **716**, 1 (2012);
S. Chatrchyan *et al.* [CMS Collaboration], Observation of a new boson at a mass of 125 GeV with the CMS experiment at the LHC, Phys. Lett. B **716**, 30 (2012)
- [175] R. Aaij *et al.*, Observation of $J/\psi p$ Resonances Consistent with Pentaquark States in $\Lambda_b^0 \rightarrow J/K^- p$ Decays, [LHCb Collaboration], Phys. Rev. Lett. **115**, 072001 (2015)
- [176] The ATLAS collaboration, Search for resonances decaying to photon pairs in 3.2 fb^{-1} of pp collisions at $\sqrt{s} = 13 \text{ TeV}$ with the ATLAS detector, ATLAS-CONF-2015-081; CMS Collaboration, Search for new physics in high mass diphoton events in proton-proton collisions at 13TeV, CMS-PAS-EXO-15-004.
- [177] See, for example, D. Castelvecchi in *Nature News*, Hint of new boson at LHC sparks flood of papers, doi: 10.1038/nature.2015.19098, December 2015.
- [178] For a comprehensive discussion, see G. Bertone, J. Silk, B. Moore, J. Diemand, J. Bullock, M. Kaplinghat, L. Strigari and Y. Mellier *et al.*, *Particle Dark Matter: Observations, Models and Searches*, (Cambridge University Press, 2010).
- [179] P. J. E. Peebles and B. Ratra, The cosmological constant and dark energy, Rev. Mod. Phys. **75**, 559 (2003) [astro-ph/0207347].
- [180] K. Greisen, End to the cosmic ray spectrum?, Phys. Rev. Lett. **16**, 748 (1966); G. T. Zatsepin and V. A. Kuzmin, Upper limit of the spectrum of cosmic rays, JETP Lett. **4**, 78 (1966), [Pisma Zh. Eksp. Teor. Fiz. **4**, 114 (1966)].
- [181] D. Speller [SuperCDMS Collaboration], Dark matter direct detection with SuperCDMS Soudan, J. Phys. Conf. Ser. **606**, 012003 (2015);
R. F. Lang and W. Seidel, Search for Dark Matter with CRESST, New J. Phys. **11**, 105017 (2009); L. Hehn [EDELWEISS Collaboration], The EDELWEISS-III Dark Matter Search: Status and Perspectives, doi:10.3204/DESY-PROC-2014-04/235; H. Kraus *et al.*, EURECA: The European future of cryogenic dark matter searches, J. Phys. Conf. Ser. **39**, 139 (2006).
- [182] D. Y. Akimov *et al.* [ZEPLIN-III Collaboration], Limits on inelastic dark matter from ZEPLIN-III, Phys. Lett. B **692**, 180 (2010);

- D. S. Akerib *et al.* [LUX Collaboration], First results from the LUX dark matter experiment at the Sanford Underground Research Facility, Phys. Rev. Lett. **112**, 091303 (2014);
- X. Xiao *et al.* [PandaX Collaboration], Low-mass dark matter search results from full exposure of the PandaX-I experiment, Phys. Rev. D **92**, 052004 (2015);
- P. Agnes *et al.* [DarkSide Collaboration], First Results from the DarkSide-50 Dark Matter Experiment at Laboratori Nazionali del Gran Sasso, Phys. Lett. B **743**, 456 (2015);
- M. Felizardo *et al.*, Final Analysis and Results of the Phase II SIMPLE Dark Matter Search, Phys. Rev. Lett. **108**, 201302 (2012);
- S. Archambault *et al.* [PICASSO Collaboration], Constraints on Low-Mass WIMP Interactions on ^{19}F from PICASSO, Phys. Lett. B **711**, 153 (2012).
- [183] M. Ackermann *et al.* [Fermi-LAT Collaboration], Searching for Dark Matter Annihilation from Milky Way Dwarf Spheroidal Galaxies with Six Years of Fermi Large Area Telescope Data, Phys. Rev. Lett. **115**, 231301 (2015);
- AMS Collaboration Collaboration, e. Aguilar, M., First result from the alpha magnetic spectrometer on the international space station: Precision measurement of the positron fraction in primary cosmic rays of 0.5-350 gev, Phys. Rev. Lett. **110** (Apr, 2013) 141102;
- I. Cholis and D. Hooper, Constraining the origin of the rising cosmic ray positron fraction with the boron-to-carbon ratio, Phys. Rev. D **89**, 043013 (2014).
- [184] G. Bertone, D. Hooper and J. Silk, Particle dark matter: Evidence, candidates and constraints, Phys. Rept. **405**, 279 (2005)
- [185] G. Aad *et al.* [ATLAS Collaboration], Summary of the searches for squarks and gluinos using $\sqrt{s} = 8$ TeV pp collisions with the ATLAS experiment at the LHC, JHEP **1510**, 054 (2015)
- [186] G. Aad *et al.* [ATLAS Collaboration], Search for squarks and gluinos with the ATLAS detector in final states with jets and missing transverse momentum using $\sqrt{s} = 8$ TeV proton-proton collision data, JHEP **1409**, 176 (2014)
- [187] G. Aad *et al.* [ATLAS Collaboration], Search for direct production of charginos, neutralinos and sleptons in final states with two leptons and missing transverse momentum in pp collisions at $\sqrt{s} = 8$ TeV with the ATLAS detector, JHEP **1405**, 071 (2014)
- [188] G. Aad *et al.* [ATLAS Collaboration], Search for direct production of charginos and neutralinos in events with three leptons and missing transverse momentum in $\sqrt{s} = 8\text{TeV}$ pp collisions with the ATLAS detector, JHEP **1404**, 169 (2014)
- [189] G. Aad *et al.* [ATLAS Collaboration], Search for supersymmetry in events with four or more leptons in $\sqrt{s} = 8$ TeV pp collisions with the ATLAS detector, Phys. Rev. D **90**, 052001 (2014)
- [190] V. Khachatryan *et al.* [CMS Collaboration], Searches for Supersymmetry using the M_{T2} Variable in Hadronic Events Produced in pp Collisions at 8 TeV, JHEP **1505**, 078

- (2015)
- [191] V. Khachatryan *et al.* [CMS Collaboration], Searches for electroweak production of charginos, neutralinos, and sleptons decaying to leptons and W, Z, and Higgs bosons in pp collisions at 8 TeV, *Eur. Phys. J. C* **74**, 3036 (2014)
 - [192] J. A. Aguilar-Saavedra and B. M. Nobre, Rare top decays $t \rightarrow \bar{c} \gamma$, $t \rightarrow \bar{c} g$ and CKM unitarity, *Phys. Lett. B* **553**, 251 (2003).
 - [193] V. Khachatryan *et al.* [CMS Collaboration], Search for anomalous single top quark production in association with a photon in pp collisions at $\sqrt{s} = 8$ TeV, *JHEP* **1604**, 035 (2016).
 - [194] K. Agashe *et al.* [Top Quark Working Group Collaboration], arXiv:1311.2028 [hep-ph].
 - [195] A. J. Buras, P. Gambino, M. Gorbahn, S. Jager and L. Silvestrini, Universal unitarity triangle and physics beyond the standard model, *Phys. Lett. B* **500**, 161 (2001); G. D'Ambrosio, G. F. Giudice, G. Isidori and A. Strumia, Minimal flavor violation: An Effective field theory *Nucl. Phys. B* **645**, 155 (2002).
 - [196] G. Passarino and M. J. G. Veltman, One Loop Corrections for $e^+ e^-$ Annihilation Into $\mu^+ \mu^-$ in the Weinberg Model, *Nucl. Phys. B* **160**, 151 (1979).
 - [197] G. J. van Oldenborgh, FF: A Package to evaluate one loop Feynman diagrams, *Comput. Phys. Commun.* **66**, 1 (1991).
 - [198] See, for example, S. P. Martin, A Supersymmetry primer, *Adv. Ser. Direct. High Energy Phys.* **21**, 1 (2010) [hep-ph/9709356]; M. Drees, R. Godbole and P. Roy, *Theory and phenomenology of sparticles* (Hackensack, USA: World Scientific, 2004); H. Baer and X. Tata, *Weak scale supersymmetry*, (CUP, Cambridge 2006).
 - [199] J. Cao, C. Han, L. Wu, J. M. Yang and M. Zhang, SUSY induced top quark FCNC decay $t \rightarrow ch$ after Run I of LHC, *Eur. Phys. J. C* **74**, 3058 (2014)
 - [200] A. Djouadi, J. L. Kneur and G. Moultaka, SuSpect: A Fortran code for the supersymmetric and Higgs particle spectrum in the MSSM, *Comput. Phys. Commun.* **176**, 426 (2007)
 - [201] G. Aad *et al.* [ATLAS Collaboration], Search for massive supersymmetric particles decaying to many jets using the ATLAS detector in pp collisions at $\sqrt{s} = 8$ TeV, *Phys. Rev. D* **91**, 112016 (2015).
 - [202] F. Mahmoudi, SuperIso v2.3: A Program for calculating flavor physics observables in Supersymmetry, *Comput. Phys. Commun.* **180**, 1579 (2009).
 - [203] R. Aaij *et al.* [LHCb Collaboration], First Evidence for the Decay $B_s^0 \rightarrow \mu^+ \mu^-$, *Phys. Rev. Lett.* **110**, 021801 (2013).
 - [204] V. Khachatryan *et al.* [CMS and LHCb Collaborations], Observation of the rare $B_s^0 \rightarrow \mu^+ \mu^-$ decay from the combined analysis of CMS and LHCb data, *Nature* **522**, 68 (2015).

- [205] J. P. Lees *et al.* [BaBar Collaboration], Exclusive Measurements of $b \rightarrow s\gamma$ Transition Rate and Photon Energy Spectrum, *Phys. Rev. D* **86**, 052012 (2012)
- [206] D. Ghosh, M. Guchait, S. Raychaudhuri and D. Sengupta, How Constrained is the cMSSM?, *Phys. Rev. D* **86**, 055007 (2012)
- [207] A. Dighe, D. Ghosh, K. M. Patel and S. Raychaudhuri, Testing Times for Supersymmetry: Looking Under the Lamp Post, *Int. J. Mod. Phys. A* **28**, 1350134 (2013)
- [208] J. P. Lees *et al.* [BaBar Collaboration], Evidence of $B^+ \rightarrow \tau^+ \nu$ decays with hadronic B tags, *Phys. Rev. D* **88**, 031102 (2013)
- [209] B. Bhattacharjee, A. Dighe, D. Ghosh and S. Raychaudhuri, Do new data on $B^+ \rightarrow \tau^+ \nu_\tau$ decays point to an early discovery of supersymmetry at the LHC?, *Phys. Rev. D* **83**, 094026 (2011)
- [210] F. Ambrosino *et al.* [KLOE Collaboration], Measurement of the absolute branching ratio for the $K^+ \rightarrow \mu^+ \nu(\gamma)$ decay with the KLOE detector, *Phys. Lett. B* **632**, 76 (2006)
- [211] F. Mahmoudi, Flavour constraints on beyond the Standard Model scenarios, *PoS ICHEP* **2010**, 252 (2010)
- [212] See M. Sher, *Phys. Rept.* **179**, 273 (1989), and references therein, for early work on the subject;
 for more recent work, see J. Ellis, J. R. Espinosa, G. F. Giudice, A. Hoecker and A. Riotto, *Phys. Lett. B* **679**, 369 (2009);
 J. Elias-Miro, J. R. Espinosa, G. F. Giudice, G. Isidori, A. Riotto and A. Strumia, *Phys. Lett. B* **709**, 222 (2012) ;
 G. Degrandi, S. Di Vita, J. Elias-Miro, J. R. Espinosa, G. F. Giudice, G. Isidori and A. Strumia, *JHEP* **1208**, 098 (2012);
 F. Bezrukov, M.Y. Kalmykov, B.A. Kniehl and M. Shaposhnikov, *JHEP* **1210**, 140 (2012);
 M. Holthausen, K.S. Lim and M. Lindner, *JHEP* **1202**, 037 (2012).
- [213] S. Alekhin, A. Djouadi and S. Moch, The top quark and Higgs boson masses and the stability of the electroweak vacuum, *Phys. Lett. B* **716** (2012) 214 [arXiv:1207.0980 [hep-ph]].
- [214] A. Dedes, M. Paraskevas, J. Rosiek, K. Suxho and K. Tamvakis, Rare Top-quark Decays to Higgs boson in MSSM, *JHEP* **1411**, 137 (2014)
- [215] G. Senjanovic, Proton decay and grand unification, *AIP Conf. Proc.* **1200**, 131 (2010)
- [216] C. Macesanu, The Phenomenology of universal extra dimensions at hadron colliders, *Int. J. Mod. Phys. A* **21**, 2259 (2006)
- [217] N. Arkani-Hamed, A. G. Cohen, E. Katz and A. E. Nelson, The Littlest Higgs, *JHEP* **0207**, 034 (2002);

- T. Han, H. E. Logan, B. McElrath and L. T. Wang, Phenomenology of the little Higgs model, *Phys. Rev. D* **67**, 095004 (2003);
M. Perelstein, Little Higgs models and their phenomenology, *Prog. Part. Nucl. Phys.* **58**, 247 (2007)
- [218] H. C. Cheng and I. Low, *JHEP* **0408**, 061 (2004) doi:10.1088/1126-6708/2004/08/061 [hep-ph/0405243].
- [219] J. Hubisz, P. Meade, A. Noble and M. Perelstein, *JHEP* **0601**, 135 (2006) doi:10.1088/1126-6708/2006/01/135 [hep-ph/0506042].
- [220] M. Perelstein, *Pramana* **67**, 813 (2006) doi:10.1007/s12043-006-0094-x [hep-ph/0703138 [HEP-PH]].
- [221] A. Birkedal, A. Noble, M. Perelstein and A. Spray, *Phys. Rev. D* **74**, 035002 (2006) doi:10.1103/PhysRevD.74.035002 [hep-ph/0603077].
- [222] R. Barbier *et al.*, R-parity violating supersymmetry, *Phys. Rept.* **420**, 1 (2005)
- [223] H. K. Dreiner, An Introduction to explicit R-parity violation, *Adv. Ser. Direct. High Energy Phys.* **21**, 565 (2010)
- [224] G. Bhattacharyya, R-parity violating supersymmetric Yukawa couplings: A Minireview, *Nucl. Phys. Proc. Suppl.* **52A**, 83 (1997)
- [225] G. Bhattacharyya, A Brief review of R-parity violating couplings, In *Tegernsee 1997, Beyond the desert 1997* 194-201 [hep-ph/9709395].
- [226] C. Csaki, Y. Grossman and B. Heidenreich, MFV SUSY: A Natural Theory for R-Parity Violation, *Phys. Rev. D* **85**, 095009 (2012)
- [227] Y. Kao and T. Takeuchi, Single-Coupling Bounds on R-parity violating Supersymmetry, an update, arXiv:0910.4980 [hep-ph].
- [228] S. Davidson, M. L. Mangano, S. Perries and V. Sordini, Lepton Flavour Violating top decays at the LHC, *Eur. Phys. J. C* **75**, 450 (2015).
- [229] G. Eilam, A. Gemintern, T. Han, J. M. Yang and X. Zhang, Top quark rare decay $t \rightarrow \tilde{\chi}^0 \chi$ in R-parity violating SUSY, *Phys. Lett. B* **510**, 227 (2001)
- [230] G. Aad *et al.* [ATLAS Collaboration], Search for supersymmetry at $\sqrt{s}=8$ TeV in final states with jets and two same-sign leptons or three leptons with the ATLAS detector, *JHEP* **1406**, 035 (2014)
- [231] G. Bhattacharyya, H. V. Klapdor-Kleingrothaus and H. Pas, Neutrino mass and magnetic moment in supersymmetry without R parity in the light of recent data, *Phys. Lett. B* **463**, 77 (1999);
S. Rakshit, G. Bhattacharyya and A. Raychaudhuri, R-parity violating trilinear couplings and recent neutrino data, *Phys. Rev. D* **59**, 091701 (1999).

- [232] G. Aad *et al.* [ATLAS Collaboration], Search for direct third-generation squark pair production in final states with missing transverse momentum and two b -jets in $\sqrt{s} = 8$ TeV pp collisions with the ATLAS detector, JHEP **1310**, 189 (2013).
- [233] G. Aad *et al.* [ATLAS Collaboration], A search for top squarks with R-parity-violating decays to all-hadronic final states with the ATLAS detector in $\sqrt{s} = 8$ TeV proton-proton collisions, JHEP **1606**, 067 (2016).
- [234] G. Bhattacharyya and D. Choudhury, D and tau decays: Placing new bounds on R-parity violating supersymmetric coupling, Mod. Phys. Lett. A **10**, 1699 (1995)
- [235] G. Aad *et al.* [ATLAS Collaboration], Search for a Heavy Neutral Particle Decaying to $e\mu$, $e\tau$, or $\mu\tau$ in pp Collisions at $\sqrt{s} = 8$ TeV with the ATLAS Detector, Phys. Rev. Lett. **115**, 031801 (2015)
- [236] J. M. Yang, R(b) and R(l) in MSSM without R-parity, Eur. Phys. J. C **20**, 553 (2001)
- [237] G. Bhattacharyya, J. R. Ellis and K. Sridhar, New LEP constraints on some supersymmetric Yukawa interactions that violate R-parity, Mod. Phys. Lett. A **10**, 1583 (1995)
- [238] B. Brahmachari and P. Roy, Constraints on baryon nonconserving Yukawa couplings in a supersymmetric theory, Phys. Rev. D **50**, 39 (1994) [Phys. Rev. D **51**, 3974 (1995)]
- [239] M. Sher and J. L. Goity, Bounds on Delta B = 1 couplings in the supersymmetric standard model, [hep-ph/9503472].
- [240] M. Chemtob, Phenomenological constraints on broken R parity symmetry in supersymmetry models, Prog. Part. Nucl. Phys. **54**, 71 (2005)
- [241] G. Bhattacharyya, D. Choudhury and K. Sridhar, New LEP bounds on B violating scalar couplings: R-parity violating supersymmetry or diquarks, Phys. Lett. B **355**, 193 (1995)
- [242] CMS Collaboration, Physics Analysis Summary CMS-PAS-HIG-13-034 (2014);
S. Chatrchyan *et al.* [CMS Collaboration], Search for Flavor-Changing Neutral Currents in Top-Quark Decays $t \rightarrow Zq$ in pp Collisions at $\sqrt{s} = 8\text{TeV}$, Phys. Rev. Lett. **112**, 171802 (2014).
- [243] T. J. Gao, T. F. Feng, F. Sun, H. B. Zhang and S. M. Zhao, Top quark decay to a 125 GeV Higgs in the BLMSSM, Chin. Phys. C **39**, 073101 (2015)
- [244] J. J. Cao, G. Eilam, M. Frank, K. Hikasa, G. L. Liu, I. Turan and J. M. Yang, SUSY-induced FCNC top-quark processes at the large hadron collider, Phys. Rev. D **75**, 075021 (2007)
- [245] B. Mele, Top quark rare decays in the standard model and beyond, hep-ph/0003064.
- [246] S. Bejar, J. Guasch and J. Sola, FCNC top quark decays beyond the standard model, hep-ph/0101294.

- [247] C. x. Yue, H. j. Zong and L. j. Liu, Nonuniversal gauge bosons Z-prime and rare top decays, *Mod. Phys. Lett. A* **18**, 2187 (2003)
- [248] I. Baum, G. Eilam and S. Bar-Shalom, Scalar flavor changing neutral currents and rare top quark decays in a two Higgs doublet model ‘for the top quark’, *Phys. Rev. D* **77**, 113008 (2008)
- [249] R. Aaij *et al.* [LHCb Collaboration], *Phys. Rev. Lett.* **113**, 151601 (2014) doi:10.1103/PhysRevLett.113.151601 [arXiv:1406.6482 [hep-ex]].
- [250] R. Aaij *et al.* [LHCb Collaboration], *JHEP* **1602**, 104 (2016) doi:10.1007/JHEP02(2016)104 [arXiv:1512.04442 [hep-ex]].
- [251] W. Altmannshofer, P. Ball, A. Bharucha, A. J. Buras, D. M. Straub and M. Wick, *JHEP* **0901**, 019 (2009) doi:10.1088/1126-6708/2009/01/019 [arXiv:0811.1214 [hep-ph]].
- [252] A. K. Alok, A. Dighe, D. Ghosh, D. London, J. Matias, M. Nagashima and A. Szytnkman, *JHEP* **1002**, 053 (2010) doi:10.1007/JHEP02(2010)053 [arXiv:0912.1382 [hep-ph]].
- [253] A. K. Alok, A. Datta, A. Dighe, M. Duraishamy, D. Ghosh and D. London, *JHEP* **1111**, 121 (2011) doi:10.1007/JHEP11(2011)121 [arXiv:1008.2367 [hep-ph]].
- [254] A. K. Alok, A. Datta, A. Dighe, M. Duraishamy, D. Ghosh and D. London, *JHEP* **1111**, 122 (2011) doi:10.1007/JHEP11(2011)122 [arXiv:1103.5344 [hep-ph]].
- [255] S. Descotes-Genon, D. Ghosh, J. Matias and M. Ramon, *JHEP* **1106**, 099 (2011) doi:10.1007/JHEP06(2011)099 [arXiv:1104.3342 [hep-ph]].
- [256] S. Descotes-Genon, J. Matias and J. Virto, *Phys. Rev. D* **88**, 074002 (2013) doi:10.1103/PhysRevD.88.074002 [arXiv:1307.5683 [hep-ph]].
- [257] W. Altmannshofer and D. M. Straub, *Eur. Phys. J. C* **73**, 2646 (2013) doi:10.1140/epjc/s10052-013-2646-9 [arXiv:1308.1501 [hep-ph]].
- [258] A. Datta, M. Duraishamy and D. Ghosh, *Phys. Rev. D* **89**, no. 7, 071501 (2014) doi:10.1103/PhysRevD.89.071501 [arXiv:1310.1937 [hep-ph]].
- [259] D. Ghosh, M. Nardecchia and S. A. Renner, *JHEP* **1412**, 131 (2014) doi:10.1007/JHEP12(2014)131 [arXiv:1408.4097 [hep-ph]].
- [260] R. Mandal, R. Sinha and D. Das, *Phys. Rev. D* **90**, no. 9, 096006 (2014) doi:10.1103/PhysRevD.90.096006 [arXiv:1409.3088 [hep-ph]].
- [261] W. Altmannshofer and D. M. Straub, *Eur. Phys. J. C* **75**, no. 8, 382 (2015) doi:10.1140/epjc/s10052-015-3602-7 [arXiv:1411.3161 [hep-ph]].
- [262] S. Jger and J. Martin Camalich, *Phys. Rev. D* **93**, no. 1, 014028 (2016) doi:10.1103/PhysRevD.93.014028 [arXiv:1412.3183 [hep-ph]].

- [263] S. Descotes-Genon, L. Hofer, J. Matias and J. Virto, JHEP **1606**, 092 (2016) doi:10.1007/JHEP06(2016)092 [arXiv:1510.04239 [hep-ph]].
- [264] M. Ciuchini, M. Fedele, E. Franco, S. Mishima, A. Paul, L. Silvestrini and M. Valli, JHEP **1606**, 116 (2016) doi:10.1007/JHEP06(2016)116 [arXiv:1512.07157 [hep-ph]].
- [265] Y. Amhis *et al.* [Heavy Flavor Averaging Group (HFAG)], arXiv:1412.7515 [hep-ex].
- [266] M. Huschle *et al.* [Belle Collaboration], Phys. Rev. D **92**, no. 7, 072014 (2015) doi:10.1103/PhysRevD.92.072014 [arXiv:1507.03233 [hep-ex]].
- [267] J. A. Bailey *et al.* [MILC Collaboration], Phys. Rev. D **92**, no. 3, 034506 (2015) doi:10.1103/PhysRevD.92.034506 [arXiv:1503.07237 [hep-lat]].
- [268] J. P. Lees *et al.* [BaBar Collaboration], Phys. Rev. Lett. **109**, 101802 (2012) doi:10.1103/PhysRevLett.109.101802 [arXiv:1205.5442 [hep-ex]].
- [269] J. P. Lees *et al.* [BaBar Collaboration], Phys. Rev. D **88**, no. 7, 072012 (2013) doi:10.1103/PhysRevD.88.072012 [arXiv:1303.0571 [hep-ex]].
- [270] H. Na *et al.* [HPQCD Collaboration], Phys. Rev. D **92**, no. 5, 054510 (2015) Erratum: [Phys. Rev. D **93**, no. 11, 119906 (2016)] doi:10.1103/PhysRevD.93.119906, 10.1103/PhysRevD.92.054510 [arXiv:1505.03925 [hep-lat]].
- [271] D. Bigi and P. Gambino, Phys. Rev. D **94**, no. 9, 094008 (2016) doi:10.1103/PhysRevD.94.094008 [arXiv:1606.08030 [hep-ph]].
- [272] S. Fajfer, J. F. Kamenik and I. Nisandzic, Phys. Rev. D **85**, 094025 (2012) doi:10.1103/PhysRevD.85.094025 [arXiv:1203.2654 [hep-ph]].
- [273] A. Abdesselam *et al.* [Belle Collaboration], arXiv:1603.06711 [hep-ex].
- [274] R. Aaij *et al.* [LHCb Collaboration], Phys. Rev. Lett. **115**, no. 11, 111803 (2015) Erratum: [Phys. Rev. Lett. **115**, no. 15, 159901 (2015)] doi:10.1103/PhysRevLett.115.159901, 10.1103/PhysRevLett.115.111803 [arXiv:1506.08614 [hep-ex]].
- [275] A. Abdesselam *et al.*, arXiv:1608.06391 [hep-ex].
- [276] M. Tanaka and R. Watanabe, Phys. Rev. D **82**, 034027 (2010) doi:10.1103/PhysRevD.82.034027 [arXiv:1005.4306 [hep-ph]].
- [277] M. Tanaka and R. Watanabe, Phys. Rev. D **87**, no. 3, 034028 (2013) doi:10.1103/PhysRevD.87.034028 [arXiv:1212.1878 [hep-ph]].
- [278] U. Nierste, S. Trine and S. Westhoff, Phys. Rev. D **78**, 015006 (2008) doi:10.1103/PhysRevD.78.015006 [arXiv:0801.4938 [hep-ph]].
- [279] A. Datta, M. Duraisamy and D. Ghosh, Phys. Rev. D **86**, 034027 (2012) doi:10.1103/PhysRevD.86.034027 [arXiv:1206.3760 [hep-ph]].

- [280] Y. Sakaki and H. Tanaka, Phys. Rev. D **87**, no. 5, 054002 (2013) doi:10.1103/PhysRevD.87.054002 [arXiv:1205.4908 [hep-ph]].
- [281] A. Crivellin, C. Greub and A. Kokulu, Phys. Rev. D **86**, 054014 (2012) doi:10.1103/PhysRevD.86.054014 [arXiv:1206.2634 [hep-ph]].
- [282] D. Choudhury, D. K. Ghosh and A. Kundu, Phys. Rev. D **86**, 114037 (2012) doi:10.1103/PhysRevD.86.114037 [arXiv:1210.5076 [hep-ph]].
- [283] A. Celis, M. Jung, X. Q. Li and A. Pich, JHEP **1301**, 054 (2013) doi:10.1007/JHEP01(2013)054 [arXiv:1210.8443 [hep-ph]].
- [284] Y. Sakaki, M. Tanaka, A. Tayduganov and R. Watanabe, Phys. Rev. D **88**, no. 9, 094012 (2013) doi:10.1103/PhysRevD.88.094012 [arXiv:1309.0301 [hep-ph]].
- [285] I. Dorner, S. Fajfer, N. Konik and I. Niandi, JHEP **1311**, 084 (2013) doi:10.1007/JHEP11(2013)084 [arXiv:1306.6493 [hep-ph]].
- [286] M. Duraisamy and A. Datta, JHEP **1309**, 059 (2013) doi:10.1007/JHEP09(2013)059 [arXiv:1302.7031 [hep-ph]].
- [287] P. Biancofiore, P. Colangelo and F. De Fazio, Phys. Rev. D **87**, no. 7, 074010 (2013) doi:10.1103/PhysRevD.87.074010 [arXiv:1302.1042 [hep-ph]].
- [288] M. Duraisamy, P. Sharma and A. Datta, Phys. Rev. D **90**, no. 7, 074013 (2014) doi:10.1103/PhysRevD.90.074013 [arXiv:1405.3719 [hep-ph]].
- [289] M. Freytsis, Z. Ligeti and J. T. Ruderman, Phys. Rev. D **92**, no. 5, 054018 (2015) doi:10.1103/PhysRevD.92.054018 [arXiv:1506.08896 [hep-ph]].
- [290] A. Greljo, G. Isidori and D. Marzocca, JHEP **1507**, 142 (2015) doi:10.1007/JHEP07(2015)142 [arXiv:1506.01705 [hep-ph]].
- [291] L. Calibbi, A. Crivellin and T. Ota, Phys. Rev. Lett. **115**, 181801 (2015) doi:10.1103/PhysRevLett.115.181801 [arXiv:1506.02661 [hep-ph]].
- [292] S. Bhattacharya, S. Nandi and S. K. Patra, Phys. Rev. D **93**, no. 3, 034011 (2016) doi:10.1103/PhysRevD.93.034011 [arXiv:1509.07259 [hep-ph]].
- [293] C. Hati, G. Kumar and N. Mahajan, JHEP **1601**, 117 (2016) doi:10.1007/JHEP01(2016)117 [arXiv:1511.03290 [hep-ph]].
- [294] M. Bauer and M. Neubert, Phys. Rev. Lett. **116**, no. 14, 141802 (2016) doi:10.1103/PhysRevLett.116.141802 [arXiv:1511.01900 [hep-ph]].
- [295] R. Barbieri, G. Isidori, A. Pattori and F. Senia, Eur. Phys. J. C **76**, no. 2, 67 (2016) doi:10.1140/epjc/s10052-016-3905-3 [arXiv:1512.01560 [hep-ph]].
- [296] M. A. Ivanov, J. G. Krner and C. T. Tran, Phys. Rev. D **92**, no. 11, 114022 (2015) doi:10.1103/PhysRevD.92.114022 [arXiv:1508.02678 [hep-ph]].

- [297] J. M. Cline, Phys. Rev. D **93**, no. 7, 075017 (2016) doi:10.1103/PhysRevD.93.075017 [arXiv:1512.02210 [hep-ph]].
- [298] D. Das, C. Hati, G. Kumar and N. Mahajan, Phys. Rev. D **94**, 055034 (2016) doi:10.1103/PhysRevD.94.055034 [arXiv:1605.06313 [hep-ph]].
- [299] M. Bordone, G. Isidori and D. van Dyk, Eur. Phys. J. C **76**, no. 7, 360 (2016) doi:10.1140/epjc/s10052-016-4202-x [arXiv:1602.06143 [hep-ph]].
- [300] R. Alonso, A. Kobach and J. Martin Camalich, Phys. Rev. D **94**, no. 9, 094021 (2016) doi:10.1103/PhysRevD.94.094021 [arXiv:1602.07671 [hep-ph]].
- [301] S. Nandi, S. K. Patra and A. Soni, arXiv:1605.07191 [hep-ph].
- [302] F. Feruglio, P. Paradisi and A. Pattori, Phys. Rev. Lett. **118**, no. 1, 011801 (2017) doi:10.1103/PhysRevLett.118.011801 [arXiv:1606.00524 [hep-ph]].
- [303] A. K. Alok, D. Kumar, S. Kumbhakar and S. U. Sankar, Phys. Rev. D **95**, no. 11, 115038 (2017) doi:10.1103/PhysRevD.95.115038 [arXiv:1606.03164 [hep-ph]].
- [304] S. M. Boucenna, A. Celis, J. Fuentes-Martin, A. Vicente and J. Virto, Phys. Lett. B **760**, 214 (2016) doi:10.1016/j.physletb.2016.06.067 [arXiv:1604.03088 [hep-ph]].
- [305] S. M. Boucenna, A. Celis, J. Fuentes-Martin, A. Vicente and J. Virto, JHEP **1612**, 059 (2016) doi:10.1007/JHEP12(2016)059 [arXiv:1608.01349 [hep-ph]].
- [306] S. Sahoo, R. Mohanta and A. K. Giri, Phys. Rev. D **95**, no. 3, 035027 (2017) doi:10.1103/PhysRevD.95.035027 [arXiv:1609.04367 [hep-ph]].
- [307] D. A. Faroughy, A. Greljo and J. F. Kamenik, Phys. Lett. B **764**, 126 (2017) doi:10.1016/j.physletb.2016.11.011 [arXiv:1609.07138 [hep-ph]].
- [308] Z. Ligeti, M. Papucci and D. J. Robinson, JHEP **1701**, 083 (2017) doi:10.1007/JHEP01(2017)083 [arXiv:1610.02045 [hep-ph]].
- [309] M. A. Ivanov, J. G. Krner and C. T. Tran, Phys. Rev. D **94**, no. 9, 094028 (2016) doi:10.1103/PhysRevD.94.094028 [arXiv:1607.02932 [hep-ph]].
- [310] I. Dorner, S. Fajfer, A. Greljo, J. F. Kamenik and N. Konik, Phys. Rept. **641**, 1 (2016) doi:10.1016/j.physrep.2016.06.001 [arXiv:1603.04993 [hep-ph]].
- [311] D. Beirevi, S. Fajfer, N. Konik and O. Sumensari, Phys. Rev. D **94**, no. 11, 115021 (2016) doi:10.1103/PhysRevD.94.115021 [arXiv:1608.08501 [hep-ph]].
- [312] D. Melikhov and B. Stech, Phys. Rev. D **62**, 014006 (2000) doi:10.1103/PhysRevD.62.014006 [hep-ph/0001113].
- [313] I. Caprini, L. Lellouch and M. Neubert, Nucl. Phys. B **530**, 153 (1998) doi:10.1016/S0550-3213(98)00350-2 [hep-ph/9712417].
- [314] J. A. Bailey *et al.* [Fermilab Lattice and MILC Collaborations], Phys. Rev. D **89**, no. 11, 114504 (2014) doi:10.1103/PhysRevD.89.114504 [arXiv:1403.0635 [hep-lat]].

- [315] B. Golob. <http://indico.ijs.si/getFile.py/access?contribId=1&resId=0&materialId=slides&confId=801>, Talk given at “Flavour Physics with High-Luminosity Experiments” in Munich.
- [316] W. Skiba, doi:10.1142/97898143271830001 arXiv:1006.2142 [hep-ph].
- [317] CMS SUSY Public Results, ATLAS SUSY Public Results
- [318] R. Barbier *et al.*, Phys. Rept. **420**, 1 (2005)
- [319] L. M. Carpenter, D. E. Kaplan and E. J. Rhee, Phys. Rev. Lett. **99**, 211801 (2007) doi:10.1103/PhysRevLett.99.211801 [hep-ph/0607204].
- [320] C. Balazs, M. Carena and C. E. M. Wagner, Phys. Rev. D **70**, 015007 (2004) doi:10.1103/PhysRevD.70.015007 [hep-ph/0403224].
- [321] M. Carena, M. Quiros, M. Seco and C. E. M. Wagner, Nucl. Phys. B **650**, 24 (2003) doi:10.1016/S0550-3213(02)01065-9 [hep-ph/0208043].
- [322] M. Carena, G. Nardini, M. Quiros and C. E. M. Wagner, Nucl. Phys. B **812**, 243 (2009) doi:10.1016/j.nuclphysb.2008.12.014 [arXiv:0809.3760 [hep-ph]].
- [323] H. Nishino *et al.* [Super-Kamiokande Collaboration], Phys. Rev. Lett. **102**, 141801 (2009) doi:10.1103/PhysRevLett.102.141801 [arXiv:0903.0676 [hep-ex]], V. Takhistov *et al.* [Super-Kamiokande Collaboration], Phys. Rev. Lett. **115**, no. 12, 121803 (2015) doi:10.1103/PhysRevLett.115.121803 [arXiv:1508.05530 [hep-ex]]
- [324] B. C. Allanach, A. Dedes and H. K. Dreiner, Phys. Rev. D **69**, 115002 (2004) [Phys. Rev. D **72**, 079902 (2005)] doi:10.1103/PhysRevD.69.115002, 10.1103/PhysRevD.72.079902 [hep-ph/0309196].
- [325] For example, it has been argued recently that the DM might be largely composed of ultralight axions. See, e.g.,
L. Hui, J. P. Ostriker, S. Tremaine and E. Witten, arXiv:1610.08297 [astro-ph.CO].
- [326] K. Tamvakis, Phys. Lett. B **382**, 251 (1996) doi:10.1016/0370-2693(96)00679-X [hep-ph/9604343].
- [327] The ATLAS collaboration [ATLAS Collaboration], ATLAS-CONF-2016-037.
- [328] The ATLAS collaboration [ATLAS Collaboration], ATLAS-CONF-2016-075.
- [329] M. Aaboud *et al.* [ATLAS Collaboration], arXiv:1607.08079 [hep-ex].
- [330] CMS Collaboration [CMS Collaboration], CMS-PAS-SUS-16-013.
- [331] CMS Collaboration [CMS Collaboration], CMS-PAS-SUS-13-010.
- [332] [CMS Collaboration], CMS-PAS-SUS-13-003.
- [333] CMS Collaboration [CMS Collaboration], CMS-PAS-SUS-14-003.
- [334] The ATLAS collaboration [ATLAS Collaboration], ATLAS-CONF-2016-022.

- [335] The ATLAS collaboration [ATLAS Collaboration], ATLAS-CONF-2016-084
- [336] The ATLAS collaboration [ATLAS Collaboration], ATLAS-CONF-2016-057.
- [337] J. L. Goity and M. Sher, Phys. Lett. B **346**, 69 (1995) Erratum: [Phys. Lett. B **385**, 500 (1996)] doi:10.1016/0370-2693(96)01076-3, 10.1016/0370-2693(94)01688-9 [hep-ph/9412208].
- [338] G. Bhattacharyya, D. Choudhury and K. Sridhar, Phys. Lett. B **355**, 193 (1995) doi:10.1016/0370-2693(95)00701-L [hep-ph/9504314]; D. Bardhan, G. Bhattacharyya, D. Ghosh, M. Patra and S. Raychaudhuri, Phys. Rev. D **94**, no. 1, 015026 (2016) doi:10.1103/PhysRevD.94.015026 [arXiv:1601.04165 [hep-ph]].
- [339] B. Brahmachari and P. Roy, Phys. Rev. D **50**, R39 (1994) [Phys. Rev. D **50**, no. 1, R39 (1994)] Erratum: [Phys. Rev. D **51**, 3974 (1995)] doi:10.1103/PhysRevD.51.3974.2, 10.1103/PhysRevD.50.R39 [hep-ph/9403350].
- [340] J. P. Saha and A. Kundu, Phys. Rev. D **66**, 054021 (2002) doi:10.1103/PhysRevD.66.054021 [hep-ph/0205046]; J. P. Saha and A. Kundu, Phys. Rev. D **69**, 016004 (2004) doi:10.1103/PhysRevD.69.016004 [hep-ph/0307259].
- [341] A. de Gouvea, S. Lola and K. Tobe, Phys. Rev. D **63**, 035004 (2001) doi:10.1103/PhysRevD.63.035004 [hep-ph/0008085]; M. Chaichian and K. Huitu, Phys. Lett. B **384**, 157 (1996) doi:10.1016/0370-2693(96)00787-3 [hep-ph/9603412].
- [342] G. Bhattacharyya, J. R. Ellis and K. Sridhar, Mod. Phys. Lett. A **10**, 1583 (1995) doi:10.1142/S0217732395001708 [hep-ph/9503264].
- [343] G. Bhattacharyya and P. B. Pal, Phys. Rev. D **59**, 097701 (1999) doi:10.1103/PhysRevD.59.097701 [hep-ph/9809493]; A. Abada and M. Losada, Phys. Lett. B **492**, 310 (2000) doi:10.1016/S0370-2693(00)01105-9 [hep-ph/0007041].
- [344] K. Agashe and M. Graesser, Phys. Rev. D **54**, 4445 (1996) doi:10.1103/PhysRevD.54.4445 [hep-ph/9510439].
- [345] D. K. Ghosh, S. Raychaudhuri and K. Sridhar, Phys. Lett. B **396**, 177 (1997) doi:10.1016/S0370-2693(97)00117-2 [hep-ph/9608352]; D. K. Ghosh, X. G. He, B. H. J. McKellar and J. Q. Shi, JHEP **0207**, 067 (2002) doi:10.1088/1126-6708/2002/07/067 [hep-ph/0111106].
- [346] K. A. Olive *et al.* [Particle Data Group Collaboration], Chin. Phys. C **38**, 090001 (2014). doi:10.1088/1674-1137/38/9/090001
- [347] D. Chakraverty and D. Choudhury, Phys. Rev. D **63**, 075009 (2001) doi:10.1103/PhysRevD.63.075009 [hep-ph/0008165].
- [348] D. Chakraverty and D. Choudhury, Phys. Rev. D **63**, 112002 (2001) doi:10.1103/PhysRevD.63.112002 [hep-ph/0012309].
- [349] N. Zwane, arXiv:1505.03479 [hep-ph].

- [350] A. Monteux, JHEP **1603**, 216 (2016) doi:10.1007/JHEP03(2016)216 [arXiv:1601.03737 [hep-ph]].
- [351] D. Choudhury, M. Datta and M. Maity, Phys. Rev. D **73**, 055013 (2006) doi:10.1103/PhysRevD.73.055013 [hep-ph/0508009].
- [352] D. Choudhury, M. Datta and M. Maity, JHEP **1110**, 004 (2011) doi:10.1007/JHEP10(2011)004 [arXiv:1106.5114 [hep-ph]].
- [353] W. Porod, Comput. Phys. Commun. **153**, 275 (2003) doi:10.1016/S0010-4655(03)00222-4 [hep-ph/0301101].
- [354] W. Porod and F. Staub, Comput. Phys. Commun. **183**, 2458 (2012) doi:10.1016/j.cpc.2012.05.021 [arXiv:1104.1573 [hep-ph]].
- [355] F. Staub, arXiv:0806.0538 [hep-ph].
- [356] F. Staub, Adv. High Energy Phys. **2015**, 840780 (2015) doi:10.1155/2015/840780 [arXiv:1503.04200 [hep-ph]].
- [357] W. Porod, F. Staub and A. Vicente, Eur. Phys. J. C **74**, no. 8, 2992 (2014) doi:10.1140/epjc/s10052-014-2992-2 [arXiv:1405.1434 [hep-ph]].
- [358] Y. Amhis *et al.* [Heavy Flavor Averaging Group (HFAG) Collaboration], arXiv:1412.7515 [hep-ex].
- [359] J. Alwall *et al.*, JHEP **1407**, 079 (2014) doi:10.1007/JHEP07(2014)079 [arXiv:1405.0301 [hep-ph]].
- [360] T. Sjöstrand *et al.*, Comput. Phys. Commun. **191**, 159 (2015)
- [361] T. Sjöstrand, S. Mrenna and P. Z. Skands, JHEP **0605**, 026 (2006)
- [362] J. de Favereau *et al.* [DELPHES 3 Collaboration], JHEP **1402**, 057 (2014).
- [363] M. Cacciari, G. P. Salam and G. Soyez, Eur. Phys. J. C **72** (2012) 1896 [arXiv:1111.6097 [hep-ph]].
- [364] M. Cacciari, G. P. Salam and G. Soyez, JHEP **0804**, 063 (2008) doi:10.1088/1126-6708/2008/04/063 [arXiv:0802.1189 [hep-ph]].
- [365] Y. L. Dokshitzer, G. D. Leder, S. Moretti and B. R. Webber, JHEP **9708**, 001 (1997) doi:10.1088/1126-6708/1997/08/001 [hep-ph/9707323].
- [366] C. Anders, C. Bernaciak, G. Kasieczka, T. Plehn and T. Schell, Phys. Rev. D **89**, no. 7, 074047 (2014) doi:10.1103/PhysRevD.89.074047 [arXiv:1312.1504 [hep-ph]].
- [367] CMS Collaboration [CMS Collaboration], CMS-PAS-BTV-13-001.
- [368] The ATLAS collaboration [ATLAS Collaboration], ATLAS-CONF-2014-046
- [369] <https://twiki.cern.ch/twiki/bin/view/LHCPhysics/TtbarNNLO>

- [370] <https://twiki.cern.ch/twiki/bin/view/LHCPhysics/CERNYellowReportPageAt1314TeV2014>
- [371] F. Maltoni, D. Pagani and I. Tsirikos, JHEP **1602**, 113 (2016) doi:10.1007/JHEP02(2016)113 [arXiv:1507.05640 [hep-ph]].
- [372] J. Pumplin, D. R. Stump, J. Huston, H. L. Lai, P. M. Nadolsky and W. K. Tung, JHEP **0207**, 012 (2002) doi:10.1088/1126-6708/2002/07/012 [hep-ph/0201195].
- [373] C. Borschensky, M. Krmer, A. Kulesza, M. Mangano, S. Padhi, T. Plehn and X. Portell, Eur. Phys. J. C **74**, no. 12, 3174 (2014) doi:10.1140/epjc/s10052-014-3174-y [arXiv:1407.5066 [hep-ph]].
- [374] A. Hocker *et al.*, PoS ACAT , 040 (2007) [physics/0703039 [PHYSICS]].
- [375] I. Antcheva *et al.*, Comput. Phys. Commun. **180**, 2499 (2009) doi:10.1016/j.cpc.2009.08.005 [arXiv:1508.07749 [physics.data-an]].
- [376] V. Khachatryan *et al.* [CMS Collaboration], Phys. Lett. B **746**, 132 (2015) doi:10.1016/j.physletb.2015.04.060 [arXiv:1411.5621 [hep-ex]].
- [377] A. Barr, C. Lester and P. Stephens, J. Phys. G **29**, 2343 (2003) doi:10.1088/0954-3899/29/10/304 [hep-ph/0304226].
- [378] H. C. Cheng and Z. Han, JHEP **0812**, 063 (2008) doi:10.1088/1126-6708/2008/12/063 [arXiv:0810.5178 [hep-ph]].
- [379] V. Simk, P. Homola, J. Valenta and R. Leitner, ATL-PHYS-2001-018, ATL-COM-PHYS-99-073, CERN-ATL-PHYS-2001-018.
- [380] Y. Bai and Z. Han, JHEP **0904**, 056 (2009) doi:10.1088/1126-6708/2009/04/056 [arXiv:0809.4487 [hep-ph]].
- [381] M. Aaboud *et al.* [ATLAS Collaboration], arXiv:1702.07546 [hep-ex].
- [382] A. M. Sirunyan *et al.* [CMS Collaboration], arXiv:1701.06228 [hep-ex].
- [383] T. Plehn, G. P. Salam and M. Spannowsky, Phys. Rev. Lett. **104**, 111801 (2010) doi:10.1103/PhysRevLett.104.111801 [arXiv:0910.5472 [hep-ph]], T. Plehn, M. Spannowsky, M. Takeuchi and D. Zerwas, JHEP **1010**, 078 (2010) doi:10.1007/JHEP10(2010)078 [arXiv:1006.2833 [hep-ph]], T. Plehn and M. Spannowsky, J. Phys. G **39**, 083001 (2012) doi:10.1088/0954-3899/39/8/083001 [arXiv:1112.4441 [hep-ph]].
- [384] M. Cacciari, J. Rojo, G. P. Salam and G. Soyez, JHEP **0812**, 032 (2008) doi:10.1088/1126-6708/2008/12/032 [arXiv:0810.1304 [hep-ph]].
- [385] J. Thaler and K. Van Tilburg, JHEP **1103**, 015 (2011) doi:10.1007/JHEP03(2011)015 [arXiv:1011.2268 [hep-ph]].
- [386] S. D. Ellis, C. K. Vermilion and J. R. Walsh, Phys. Rev. D **80**, 051501 (2009) doi:10.1103/PhysRevD.80.051501 [arXiv:0903.5081 [hep-ph]].

- [387] A. J. Larkoski, S. Marzani, G. Soyez and J. Thaler, JHEP **1405**, 146 (2014) doi:10.1007/JHEP05(2014)146 [arXiv:1402.2657 [hep-ph]].
- [388] A. Chakraborty, S. Chakraborty and T. S. Roy, arXiv:1606.07826 [hep-ph]
- [389] D. Choudhury, F. Eberlein, A. Konig, J. Louis and S. Pokorski, Phys. Lett. B **342**, 180 (1995) doi:10.1016/0370-2693(94)01380-U [hep-ph/9408275].
- [390] M. Misiak, S. Pokorski and J. Rosiek, Adv. Ser. Direct. High Energy Phys. **15**, 795 (1998) doi:10.1142/9789812812667_0012 [hep-ph/9703442].
- [391] A. Brignole, L. E. Ibanez and C. Munoz, Adv. Ser. Direct. High Energy Phys. **18**, 125 (1998) doi:10.1142/9789812839657_0003 [hep-ph/9707209].
- [392] B. Bhattacharjee and A. Chakraborty, Phys. Rev. D **89**, no. 11, 115016 (2014) doi:10.1103/PhysRevD.89.115016 [arXiv:1311.5785 [hep-ph]].
- [393] The ATLAS collaboration, “Search for resonances decaying to photon pairs in 3.2 fb⁻¹ of pp collisions at $\sqrt{s} = 13$ TeV with the ATLAS detector,” ATLAS-CONF-2015-081.
- [394] CMS Collaboration [CMS Collaboration], “Search for new physics in high mass diphoton events in proton-proton collisions at 13TeV,” CMS-PAS-EXO-15-004.
- [395] P. Baratella, J. Elias-Miro, J. Penedo and A. Romanino, JHEP **1606**, 086 (2016) doi:10.1007/JHEP06(2016)086 [arXiv:1603.05682 [hep-ph]].
- [396] A. Falkowski, O. Slone and T. Volansky, JHEP **1602**, 152 (2016) doi:10.1007/JHEP02(2016)152 [arXiv:1512.05777 [hep-ph]].
- [397] J. Bagger, E. Poppitz and L. Randall, Nucl. Phys. B **426**, 3 (1994) doi:10.1016/0550-3213(94)90123-6 [hep-ph/9405345].
- [398] G. F. Giudice and R. Rattazzi, Phys. Rept. **322**, 419 (1999) doi:10.1016/S0370-1573(99)00042-3 [hep-ph/9801271].
- [399] A. D. Martin, W. J. Stirling, R. S. Thorne and G. Watt, Eur. Phys. J. C **63**, 189 (2009) doi:10.1140/epjc/s10052-009-1072-5 [arXiv:0901.0002 [hep-ph]].
- [400] C. Cheung, A. L. Fitzpatrick and D. Shih, JHEP **0807**, 054 (2008) doi:10.1088/1126-6708/2008/07/054 [arXiv:0710.3585 [hep-ph]].
- [401] A. Basirnia, D. Egana-Ugrinovic, S. Knapen and D. Shih, JHEP **1506**, 144 (2015) doi:10.1007/JHEP06(2015)144 [arXiv:1501.00997 [hep-ph]].
- [402] S. Dimopoulos and G. F. Giudice, Phys. Lett. B **393**, 72 (1997) doi:10.1016/S0370-2693(96)01513-4 [hep-ph/9609344].
- [403] N. Craig, S. Knapen, D. Shih and Y. Zhao, JHEP **1303**, 154 (2013) doi:10.1007/JHEP03(2013)154 [arXiv:1206.4086 [hep-ph]].
- [404] G. R. Dvali, G. F. Giudice and A. Pomarol, Nucl. Phys. B **478**, 31 (1996) doi:10.1016/0550-3213(96)00404-X [hep-ph/9603238].

- [405] S. V. Demidov and D. S. Gorbunov, JETP Lett. **103**, no. 4, 219 (2016) [Pisma Zh. Eksp. Teor. Fiz. **103**, no. 4, 241 (2016)] doi:10.1134/S0021364016040044 [arXiv:1512.05723 [hep-ph]].
- [406] B. Bellazzini, R. Franceschini, F. Sala and J. Serra, JHEP **1604**, 072 (2016) doi:10.1007/JHEP04(2016)072 [arXiv:1512.05330 [hep-ph]].
- [407] J. A. Casas, J. R. Espinosa and J. M. Moreno, Phys. Lett. B **759**, 159 (2016) doi:10.1016/j.physletb.2016.05.070 [arXiv:1512.07895 [hep-ph]].
- [408] C. Petersson and R. Torre, Phys. Rev. Lett. **116**, no. 15, 151804 (2016) doi:10.1103/PhysRevLett.116.151804 [arXiv:1512.05333 [hep-ph]].
- [409] P. Byakti and D. Ghosh, Phys. Rev. D **86**, 095027 (2012) doi:10.1103/PhysRevD.86.095027 [arXiv:1204.0415 [hep-ph]].
- [410] D. Marques, JHEP **0903**, 038 (2009) doi:10.1088/1126-6708/2009/03/038 [arXiv:0901.1326 [hep-ph]].
- [411] A. E. Nelson and N. Seiberg, Nucl. Phys. B **416**, 46 (1994) doi:10.1016/0550-3213(94)90577-0 [hep-ph/9309299].
- [412] K. A. Intriligator, N. Seiberg and D. Shih, JHEP **0707**, 017 (2007) doi:10.1088/1126-6708/2007/07/017 [hep-th/0703281].
- [413] Z. Komargodski and D. Shih, JHEP **0904**, 093 (2009) doi:10.1088/1126-6708/2009/04/093 [arXiv:0902.0030 [hep-th]].
- [414] G. F. Giudice and R. Rattazzi, Nucl. Phys. B **511**, 25 (1998) doi:10.1016/S0550-3213(97)00647-0 [hep-ph/9706540].
- [415] T. T. Dumitrescu, Z. Komargodski, N. Seiberg and D. Shih, JHEP **1005**, 096 (2010) doi:10.1007/JHEP05(2010)096 [arXiv:1003.2661 [hep-ph]].
- [416] S. Dimopoulos, G. F. Giudice and A. Pomarol, Phys. Lett. B **389**, 37 (1996) doi:10.1016/S0370-2693(96)01241-5 [hep-ph/9607225].
- [417] S. P. Martin, Phys. Rev. D **55**, 3177 (1997) doi:10.1103/PhysRevD.55.3177 [hep-ph/9608224].
- [418] R. Ding, Y. Fan, L. Huang, C. Li, T. Li, S. Raza and B. Zhu, Int. J. Mod. Phys. A **31**, no. 26, 1650151 (2016) doi:10.1142/S0217751X16501517 [arXiv:1602.00977 [hep-ph]].
- [419] E. Witten, Nucl. Phys. B **202**, 253 (1982). doi:10.1016/0550-3213(82)90071-2
- [420] K. I. Izawa and T. Yanagida, Prog. Theor. Phys. **95**, 829 (1996) doi:10.1143/PTP.95.829 [hep-th/9602180].
- [421] K. A. Intriligator and S. D. Thomas, Nucl. Phys. B **473**, 121 (1996) doi:10.1016/0550-3213(96)00261-1 [hep-th/9603158].

- [422] A. Brignole, F. Feruglio and F. Zwirner, *Phys. Lett. B* **438**, 89 (1998) doi:10.1016/S0370-2693(98)00974-5 [hep-ph/9805282].
- [423] M. Nardecchia, A. Romanino and R. Ziegler, *JHEP* **0911**, 112 (2009) doi:10.1088/1126-6708/2009/11/112 [arXiv:0909.3058 [hep-ph]].
- [424] M. Nardecchia, A. Romanino and R. Ziegler, *JHEP* **1003**, 024 (2010) doi:10.1007/JHEP03(2010)024 [arXiv:0912.5482 [hep-ph]].
- [425] A. Givoeon, A. Katz, Z. Komargodski and D. Shih, *JHEP* **0810**, 092 (2008) doi:10.1088/1126-6708/2008/10/092 [arXiv:0808.2901 [hep-th]].
- [426] A. Givoeon, A. Katz and Z. Komargodski, *JHEP* **0907**, 099 (2009) doi:10.1088/1126-6708/2009/07/099 [arXiv:0905.3387 [hep-th]].
- [427] A. Amariti and A. Mariotti, *JHEP* **0907**, 071 (2009) doi:10.1088/1126-6708/2009/07/071 [arXiv:0812.3633 [hep-th]].
- [428] E. Poppitz and S. P. Trivedi, *Phys. Rev. D* **55**, 5508 (1997) doi:10.1103/PhysRevD.55.5508 [hep-ph/9609529].
- [429] N. Arkani-Hamed, J. March-Russell and H. Murayama, *Nucl. Phys. B* **509**, 3 (1998) doi:10.1016/S0550-3213(97)00573-7 [hep-ph/9701286].
- [430] N. Seiberg, T. Volansky and B. Wecht, *JHEP* **0811**, 004 (2008) doi:10.1088/1126-6708/2008/11/004 [arXiv:0809.4437 [hep-ph]].
- [431] M. Huq, *Phys. Rev. D* **14**, 3548 (1976). doi:10.1103/PhysRevD.14.3548
- [432] T. Han and R. J. Zhang, *Phys. Lett. B* **428**, 120 (1998) doi:10.1016/S0370-2693(98)00379-7 [hep-ph/9802422].
- [433] Z. Kang, T. Li, T. Liu, C. Tong and J. M. Yang, *Phys. Rev. D* **86**, 095020 (2012) doi:10.1103/PhysRevD.86.095020 [arXiv:1203.2336 [hep-ph]].
- [434] P. Byakti and T. S. Ray, *JHEP* **1305**, 055 (2013) doi:10.1007/JHEP05(2013)055 [arXiv:1301.7605 [hep-ph]].
- [435] J. A. Evans and D. Shih, *JHEP* **1308**, 093 (2013) doi:10.1007/JHEP08(2013)093 [arXiv:1303.0228 [hep-ph]].
- [436] L. G. Aldrovandi and D. Marques, *JHEP* **0805**, 022 (2008) doi:10.1088/1126-6708/2008/05/022 [arXiv:0803.4163 [hep-th]].
- [437] K. Hamaguchi, M. Ibe, T. T. Yanagida and N. Yokozaki, *Phys. Rev. D* **90**, no. 1, 015027 (2014) doi:10.1103/PhysRevD.90.015027 [arXiv:1403.1398 [hep-ph]].
- [438] T. S. Ray, *Phys. Rev. D* **85**, 035003 (2012) doi:10.1103/PhysRevD.85.035003 [arXiv:1111.4266 [hep-ph]].
- [439] I. Affleck, M. Dine and N. Seiberg, *Nucl. Phys. B* **256**, 557 (1985). doi:10.1016/0550-3213(85)90408-0

- [440] M. E. Peskin, hep-th/9702094.
- [441] E. Poppitz and S. P. Trivedi, Ann. Rev. Nucl. Part. Sci. **48**, 307 (1998) doi:10.1146/annurev.nucl.48.1.307 [hep-th/9803107].
- [442] F. Caracciolo and A. Romanino, JHEP **1212**, 109 (2012) doi:10.1007/JHEP12(2012)109 [arXiv:1207.5376 [hep-ph]].
- [443] S. J. Gates, M. T. Grisaru, M. Rocek and W. Siegel, Front. Phys. **58**, 1 (1983) [hep-th/0108200].
- [444] Y. Shadmi and P. Z. Szabo, JHEP **1206**, 124 (2012) doi:10.1007/JHEP06(2012)124 [arXiv:1103.0292 [hep-ph]].
- [445] R. S. Gupta, S. Jger, Y. Kats, G. Perez and E. Stamou, JHEP **1607**, 145 (2016) doi:10.1007/JHEP07(2016)145 [arXiv:1512.05332 [hep-ph]].
- [446] D. Aloni, K. Blum, A. Dery, A. Efrati and Y. Nir, JHEP **1608**, 017 (2016) doi:10.1007/JHEP08(2016)017 [arXiv:1512.05778 [hep-ph]].
- [447] E. Perazzi, G. Ridolfi and F. Zwirner, Nucl. Phys. B **574**, 3 (2000) doi:10.1016/S0550-3213(00)00055-9 [hep-ph/0001025].
- [448] E. Perazzi, G. Ridolfi and F. Zwirner, Nucl. Phys. B **590**, 287 (2000) doi:10.1016/S0550-3213(00)00504-6 [hep-ph/0005076].
- [449] A. Kusenko, P. Langacker and G. Segre, Phys. Rev. D **54**, 5824 (1996) doi:10.1103/PhysRevD.54.5824 [hep-ph/9602414].
- [450] D. Chowdhury, R. M. Godbole, K. A. Mohan and S. K. Vempati, JHEP **1402**, 110 (2014) doi:10.1007/JHEP02(2014)110 [arXiv:1310.1932 [hep-ph]].
- [451] G. Aad *et al.* [ATLAS Collaboration], Phys. Rev. D **92**, no. 7, 072001 (2015) doi:10.1103/PhysRevD.92.072001 [arXiv:1507.05493 [hep-ex]].